FRIEDRICH-SCHILLER-
UNIVERSITÄT
JENA

Friedrich-Schiller-Universität Jena

Chemisch-Geowissenschaftliche Fakultät

Poly(2-oxazoline)s – Synthesis, self-assembly and biomedical applications

Dissertation

(kumulativ)

zur Erlangung des akademischen Grades

doctor rerum naturalium (Dr. rer. nat.)

vorgelegt dem Rat der Chemisch-Geowissenschaftlichen Fakultät

der Friedrich-Schiller-Universität Jena

von Meike Nicole Leiske

geboren am 09.10.1989 in Delmenhorst

1. Prof. Dr. Ulrich S. Schubert, Friedrich-Schiller-Universität Jena
2. Prof. Dr. Felix H. Schacher, Friedrich-Schiller-Universität Jena
3. Prof. Dr. Stefan Spange, Technische Universität Chemnitz

Tag der öffentlichen Verteidigung: 11. Juli 2018

Table of contents

Documentation of authorship

This election contains a list of the individual authors contribution to the publications reprinted in this thesis.

P1	M. N. Leiske[1], M. Hartlieb[2], F. H. Sobotta[3], R. M. Paulus[4], H. Görls[5], P. Bellstedt[6], U. S. Schubert[7], „Cationic ring-opening polymerization of protected oxazolidine imines resulting in gradient copolymers of poly(2-oxazoline) and poly(urea)", *Polym. Chem.* **2016**, *7*, 4924-4936.							
Author	**1**	**2**	**3**	**4**	**5**	**6**	**7**
Monomer synthesis	×		×				
Monomer characterization	×		×		×		
Polymerization kinetics	×		×				
Polymer synthesis	×		×				
Polymer characterization	×		×	×		×	
Self-assembly	×						
Development of concept	×	×					
Preparation of manuscript	×	×					
Correction of manuscript			×	×	×	×	×
Supervision of M. N. Leiske		×					×
Proposed publication equivalent	1.0						

P2	M. N. Leiske[1], A.-K. Trützschler[2], S. Armoneit[3], P. Sungur[4], S. Hoeppener[5], M. Lehmann[6], A. Traeger[7], U. S. Schubert[8], „Mission ImPOxable – Or the unknown utilization of non-toxic poly(2-oxazoline)s as cryoprotectant and surfactant at the same time", *J. Mater. Chem. B.* **2017**, *5*, 9102-9113.							
Author	**1**	**2**	**3**	**4**	**5**	**6**	**7**	**8**
Polymer synthesis	×	×						
Polymer characterization	×	×						
Nanoparticle preparation	×		×					
Nanoparticle characterization	×		×	×	×			
Biotests							×	
Development of concept	×					×	×	
Preparation of manuscript	×							
Correction of manuscript		×	×	×	×	×	×	×
Supervision of M. N. Leiske							×	×
Proposed publication equivalent	1.0							

P3	M. N. Leiske[1], F. H. Sobotta[2], F. Richter[3], S. Hoeppener[4], J. C. Brendel[5], A. Traeger[6], U. S. Schubert[7], How to tune the gene delivery and biocompatibility of poly(2-(4-aminobutyl)-2-oxazoline) by self and co assembly", *Biomacromolecules* **2018**, *19*, 748-760.

Author	**1**	**2**	**3**	**4**	**5**	**6**	**7**
Polymer synthesis	×	×					
Polymer characterization	×	×					
Self-assembly	×	×					
Characterization of nanostructures	×			×			
In vitro experiments			×			×	
Development of concept	×				×	×	
Preparation of manuscript	×					×	
Correction of manuscript		×	×	×	×		×
Supervision of M. N. Leiske						×	×
Proposed publication equivalent	1.0						

P4	D. Hoelzer[1‡], M. N. Leiske[2‡], M. Hartlieb[3], T. Bus[4], D. Pretzel[5], S. Hoeppener[6], K. Kempe[7], R. Thierbach[8], U. S. Schubert[9], „Tumor targeting with pH-responsive poly(2-oxazoline)-based nanogels for metronomic doxorubicin treatment", *Oncotarget* **2018**, in press.

Author	**1**	**2**	**3**	**4**	**5**	**6**	**7**	**8**	**9**
Polymer and material synthesis		×	×						
Polymer and material characterization		×	×			×			
In vitro experiments and imaging				×					
In vivo experiments	×	×							
Development of concept	×		×		×		×	×	
Preparation of manuscript	×	×	×						
Correction of manuscript				×	×	×	×	×	×
Supervision of M. N. Leiske			×						×
Proposed publication equivalent		1.0							×

P5	D. Hertz[1‡], M. N. Leiske[2‡], T. Wloka[3], A. Traeger[4], M. Hartlieb[5], M. M. Kessels[6], S. Schubert[7], B. Qualmann[8], U. S. Schubert[9], „Comparison of random and gradient amino functionalized poly(2-oxazoline)s: Can the transfection efficiency be tuned by the macromolecular structure?", *J. Polym. Sci., Part A: Polym. Chem*. **2018**, in press. DOI: 10.1002/pola.29000.

Author	**1**	**2**	**3**	**4**	**5**	**6**	**7**	**8**	**9**
Polymerization kinetics			×						
Polymer synthesis		×							
Polymer characterization		×							
In vitro experiments	×								
Development of concept				×			×	×	×
Preparation of manuscript	×	×							
Correction of manuscript			×	×	×	×	×	×	×
Supervision of M. N. Leiske				×	×				×
Proposed publication equivalent		0.75							

P6	M. N. Leiske[1], M. Hartlieb[2], A. Traeger[3], U. S. Schubert[4], Evolution of poly(2-oxazoline)s from *in vitro* and *in vivo* studies to clinical trials, *submitted.*			
Author	**1**	**2**	**3**	**4**
Development of concept	×	×	×	
Preparation of manuscript	×	×		
Correction of manuscript			×	×
Supervision of M. N. Leiske				×
Proposed publication equivalent	0.5			

P7	T. Luehmann[1], M. Schmidt[2], M. N. Leiske[3], V. Spieler[4], T. C. Majdanski[5], M. Grube[6], M. Hartlieb[7], I. Nischang[8], S. Schubert[9], U.S. Schubert[10], L. Meinel[11], „Site-specific POxylation of interleukin-4“, *ACS Biomater. Sci. Eng.* **2017**, *3*, 304-312.										
Author	**1**	**2**	**3**	**4**	**5**	**6**	**7**	**8**	**9**	**10**	**11**
Polymer synthesis			×		×						
Polymer characterization			×		×						
Conjugate preparation		×		×							
MALDI-MS, SDS-PAGE, RP-HPLC and SEC Analysis		×									
Analytical Ultracentrifugation						×		×			
Characterization of conjugate bioactivity				×							
Fluorescence Emission and CD Spectroscopy		×		×							
Development of concept	×						×		×	×	×
Preparation of manuscript	×	×									
Correction of manuscript	×		×	×	×	×	×	×	×	×	×
Supervision of M. N. Leiske							×			×	
Supervision of M. Schmidt	×										
Supervision of V. Spieler											×
Proposed publication equivalent			0.5								

P8	M. Hartlieb[1], T. Bus[2], J. Kübel[3], D. Pretzel[4], S. Hoeppener[5], M. N. Leiske[6], K. Kempe[7], B. Dietzek[8], U. S. Schubert[9], „Tailoring cellular uptake and fluorescence of poly(2-oxazoline)-based nanogels”, *Bioconjugate Chem.* **2017**, *28*, 1229-1235.								
Author	**1**	**2**	**3**	**4**	**5**	**6**	**7**	**8**	**9**
Polymer and material synthesis	×								
Polymer and material characterization	×		×		×				
Biological investigations		×		×					
Development of concept	×								
Preparation of manuscript	×								
Correction of manuscript		×	×	×	×	×	×	×	×
Supervision of M. Hartlieb								×	×
Proposed publication equivalent						0.25			

[‡]Equal contribution of both authors.

Erklärung zu den Eigenanteilen des Promovenden sowie der weiteren Doktoranden/Doktorandinnen als Koautoren an Publikationen und Zweitpublikationsrechten bei einer kumulativen Dissertation

Für alle in dieser kumulativen Dissertation verwendeten Manuskripte liegen die notwendigen Genehmigungen der Verlage („Reprint permissions“) für die Zweitpublikation vor.

Die Co-Autoren der in dieser kumulativen Dissertation verwendeten Manuskripte sind sowohl über die Nutzung als auch über die oben angegebenen Eigenanteile informiert und stimmen dem zu.

Die Anteile der Co-Autoren an den Publikationen sind in den vorausgehenden Tabellen aufgeführt.

Ich bin mit der Abfassung der Dissertation als publikationsbasiert, d.h. kumulativ, einverstanden und bestätige die vorstehenden Angaben. Eine entsprechend begründete Befürwortung mit Angabe des wissenschaftlichen Anteils des Doktoranden an den verwendeten Publikationen werde ich parallel an den Rat der Fakultät der Chemisch-Geowissenschaftlichen Fakultät richten.

Prof. Dr. Ulrich S. Schubert Jena, den _____

Meike N. Leiske Jena, den _____

1. Introduction

Modern nanomedicine is divided into viral, lipoid and polymeric gene- and drug-carrier systems.[1] Herein, viral systems generally suffer from high production costs and upscaling difficulties.[2] Lipoid carriers, such as liposomes or lipoplexes, can be produced more cost-efficiently, however, their storage is challenging.[2] Polymer-based carriers require the utilization of tailored, and biodegradable or biocompatible polymers. During the last years, the utilization of poly(2-oxazoline)s (P(Ox)s) in terms of biomedical applications has increased significantly.[3-4]

The synthesis of P(Ox)s *via* the cationic ring-opening polymerization (CROP) was first developed in the 1960s by four independent research groups.[5-8] The living CROP is divided into three steps: (i) Initiation, (ii) propagation, and (iii) termination.[9] The initiator commonly consists of a labile leaving group, such as a halide, tosylate or triflate, which is bound to a partially positive charged carbon atom.[10] During the initiation, the free electron pair of the nitrogen atom reacts with that carbon atom by a nucleophilic attack. Subsequently, the positively charged oxazolinium ion can be attacked by another monomer, leading to a controlled and living chain growth during the propagation. The reaction can be terminated by the addition of a nucleophile.

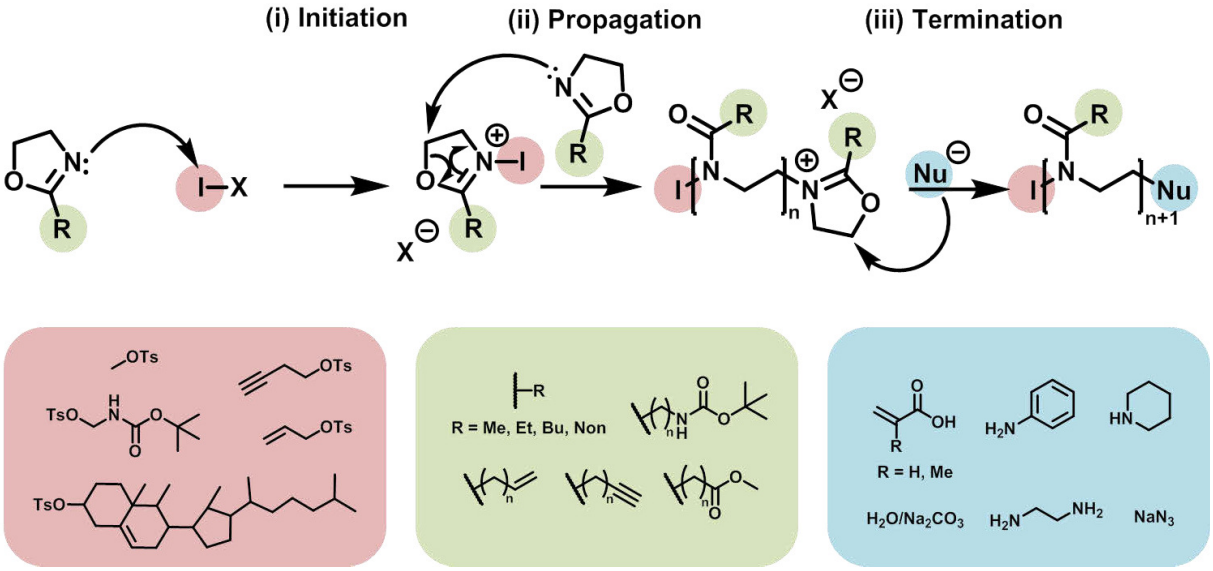

Scheme 1.1. Schematic representation of the living CROP of 2-oxazolines consisting of (i) initiation, (ii) propagation, and (iii) termination as well as examples for functional groups that can be introduced on the α-position (red), ω-position (blue) or in the side-chain (green).

A crucial drawback of the synthesis of P(Ox)s, however, were the rather long reaction times of up to weeks, which could be significantly shortened to several minutes by the utilization of the microwave technique.[11] Since then, many functionalization strategies have been established successfully, resulting in functional P(Ox)s.[10, 12] By choosing functional initiators, the introduction of single modifications, such as alkynes,[13] amines[14] or carboxylic acids[15-16] at the α-position of the polymer is possible. Furthermore, appropriate end-functionalization allows the introduction of azides,[17-18] hydroxyl groups,[15, 19-20] amino

groups,[21-23] or large hydrophobic ω-end-groups.[20, 24-26] In addition, the utilization of 2-substituted monomers can be used for the introduction of multiple (distinct) functionalities into the polymer chain.[10, 27] Common examples for functional side-chains are alkynes,[28-30] azides,[31-33] thiols,[34] carboxylic acids,[35-36] alkenyls,[37-38] aldehydes,[39] and amino groups.[40-41] These numerous modification opportunities enable the preparation of tailored polymers with adjustable properties. The resulting polymers are pseudopeptides, which are biotolerable with respect to their type and amount of functional groups, making P(Ox)s promising candidates for biomedical applications. For this reason, Chapter 2 will provide an overview of the state of the art of P(Ox)s with respect to approaches regarding self-assembly, *in vitro* and *in vivo* experiments as well as the first clinical trial.

In order to correctly evaluate the effects of an applied macromolecular structure on the properties regarding self-assembly as well as drug- or gene-delivery, it is important to evaluate the reactivity ratios of different monomers utilized for the preparation of copolymers. Numerous publications already discussed the effect of the counter-ion of the initiator on the polymerization kinetics.[42-45] Furthermore, the effect of the substituent in 2-position was investigated.[46-48] Copolymerization of different 2-oxazolines resulted in random,[9, 49] gradient[27, 50-51] or quasi block copolymers.[52-53] Herein, differences within the copolymer composition can for instance be caused by length of the alkyl chain in 2-position.[9, 49] In Chapter 3, two amino functionalized monomers are compared directly: (i) 2-(4-((*tert*-Butoxycarbonyl)amino)butyl)-2-oxazoline (BocOx), which is already known from literature[41] and (ii) *tert*-butyl 2-iminooxazolidine-3-carboxylate (BocOI), which was newly synthesized within this thesis.[54] Herein, the synthesis routes of both monomers are shortly compared. Afterwards, polymerization kinetics of BocOI and 2-ethyl-2-oxazoline (EtOx), BocOx and EtOx as well as BocOx and 2-methyl-2-oxazoline (MeOx) are conducted to gain an overview of the reactivity ratios of the different monomers during copolymerization. Since the polymerization of BocOI and the assumed mechanism have been unknown up to this point, a series of BocOI homopolymers and copolymers with EtOx are synthesized and deprotected to yield polymers consisting of poly(urea) and P(Ox). All resulting polymers and *tert*-butyloxycarbonyl (Boc) protected precursors are characterized and compared regarding their properties. Furthermore, BocOx containing statistic and block copolymers are synthesized and characterized. Hereby the acidic deprotection of BocOx containing copolymers yielding 2-(4-aminobutyl)-2-oxazoline (AmOx) groups will be shown.

As already mentioned, possible applications of P(Ox)s are positioned in biomedical applications, such as drug or gene delivery.[3-4] Herein, the utilization of P(Ox)s is versatile, ranging from nano- and microparticles,[50] as well as nanocapsules[55] to crosslinked networks such as hydrogels,[41] surface coatings[56] or nanogels.[51, 57] Herein, the assembly of amphiphilic block copolymers has been described.[53, 58-60] Chapter 4 deals with P(Ox) containing nanostructures. Firstly, the utilization of water-soluble P(Ox)s for the stabilization of hydrophobic nanoparticles consisting of poly(lactide-*co*-glycolide) (PLGA) during preparation, purification and lyophilization, aiming an all-in-one system to replace common particle stabilizers, *i.e.* poly(vinyl alcohol), Pluronic F127, glucose, saccharose and trehalose. Furthermore, amphiphilic block copolymers consisting of P(Ox)s were self- and co-assembled in water as well as characterized regarding their pH responsiveness. In addition to that, AmOx containing block copolymers are self-assembled in chloroform and reversibly core cross-

linked using glutaraldehyde (GA) to form imines. Additionally the covalent attachment of 6-amino-fluorescein (6AF) and doxorubicin (DOX) to the resulting nanogels will be shown.
In addition to the synthesis and assembly of P(Ox)s, their application in biomedical sciences has been widely explored during the last decade.[3-4] Herein, the application of cationic P(Ox)s in terms of gene delivery represents one interesting field of research.[38, 61-62] Chapter 5 describes the utilization of AmOx containing copolymers for gene transfection. Hereby, copolymers containing either EtOx (random), MeOx (gradient) or 2-nonyl-2-oxazoline (NonOx, block) representing the comonomer are compared regarding their cyto- and hemocompatibility, cellular uptake as well as transfection efficiency. A further possible application for functional P(Ox)s is the delivery of conjugated drugs, *e.g.* proteins or small molecules. Hereby, the most important issue concerns the activity of the active pharmaceutical ingredient (API). For this reason, Chapter 6 describes the preparation of two different P(Ox) drug conjugates, *i.e.* the P(Ox)ylation of interleukin-4 (IL-4) to water soluble P(Ox)s using biorthogonal copper catalyzed click chemistry (CuAAC) and the conjugation of doxorubicin (DOX) to AmOx containing nanogels *via* Schiff-base chemistry.
The aim of this thesis is to push forward the potential of 2-oxazolines in terms of synthesis, self-assembly and biomedical utilization. Hereby, the synthesis of two different monomers, namely BocOx and BocOI will be presented. Homo- and copolymerization kinetics with EtOx, respectively MeOx will provide an overview of the monomer distribution within the polymers, which is important for further implementations of the polymers in terms of self-assembly as well as gene- and drug-delivery. Furthermore, the contribution of different P(Ox) regarding the preparation of colloidal nanostructures will be shown. Herein, P(Ox) homopolymers will be utilized as surfactants and cryoprotectants for the stabilization of nanoparticles. It will be demonstrated that different P(Ox) block copolymers can be utilized to form distinct nanostructures, suitable for gene-and drug delivery applications. In addition to that, the usage of cationic, pH responsive nanostructures with respect to gene-delivery will be conducted. Herein, nanostructures will be compared to water soluble cationic random and gradient copolymers. Furthermore, the contribution of P(Ox) to successful and targeted drug delivery will be shown. This thesis contributes to the knowledge of P(Ox) in a wide range, covering not only the synthesis, however, also the preparation and characterization self-assembled structures and their biomedical potential.

2. Poly(2-oxazoline)s in biomedical applications

Parts of this chapter have been published in: **P6**) M. N. Leiske[1], M. Hartlieb[2], A. Traeger[3], U. S. Schubert[4], Evolution of poly(2-oxazoline)s from *in vitro* and *in vivo* studies to clinical trials, *submitted.*

During the last decades, a large range of functionalized P(Ox)s has been reported.[10, 27] Due to their preparation route *via* the CROP, it is possible to introduce different substituents that are feasible for biomedical applications on defined positions along the macromolecule (Scheme 2.1).[4] α- or ω-end-groups can be achieved by the utilization of functional initiators or terminating agents to introduce single functionalities. With respect to biomedical applications, these might be useful for the covalent attachment of targeting ligands or fluorescent dyes as well as the conjugations of single proteins or drugs. Furthermore, the opportunity of side chain functionalization by the utilization of 2-substituted monomers represents an important advantage in comparison to other polymers, *e.g.* poly(ethylene glycol) (PEG). Depending on their reactivity ratios, monomers that are copolymerized can form random or gradient copolymers.[27, 50-51] Thereby, functional units, such as carboxylic acids, amino groups or alkynes can be used for post-polymerization functionalization,[36, 38] polyplex formation[38, 61, 63] or multiple active pharmaceutical ingredient (API) conjugation.[28, 35, 64] Additionally, by using the sequential monomer addition block copolymers can be prepared.[57, 65-66]

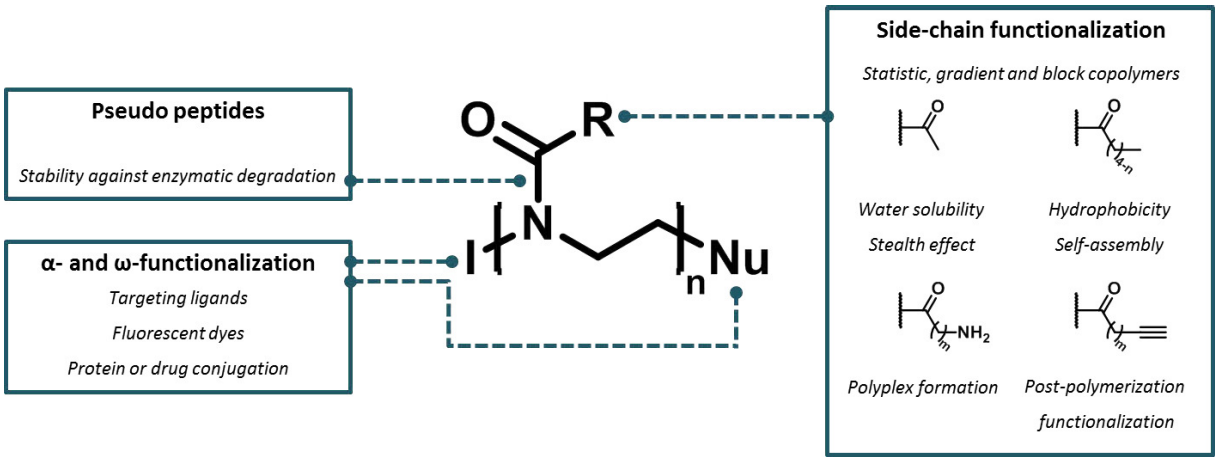

Scheme 2.1. Schematic representation of P(Ox)s and their possibilities of modification useful for biomedical implementations.

Depending on the monomer hydrophilicity, (water) solubility can be adjusted, and the formation of polymersomes, particles, micelles or vesicles can be induced.[50] Consequently, the versatility of P(Ox)s does not halt the level of chemical functionality, however, allows the formation of nano- and microassemblies (Scheme 2.2),[50, 57, 67] which can heavily influence the interaction of polymer therapeutics and biological systems. Hereby, the nanoscopic phase separation can be used for encapsulation of drugs or dyes[22, 65] by either absorption of small molecules into the hydrophobic phase (encapsulation)[21] or the attachment to functional subunits of the polymer (conjugation).[28, 35]

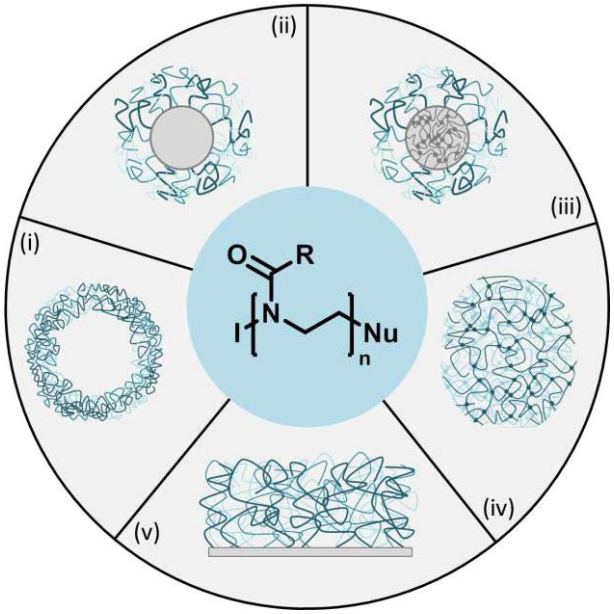

Scheme 2.2. Schematic representation of different assembled P(Ox) structures: (i) Nanocapsules,[55] (ii) micelles,[21] (iii) nanogels,[51] (iv) hydrogels,[51] and (v) surface coatings.[68]

Herein, the hydrohphilic poly(2-ethyl-2-oxazoline) (P(EtOx)) or poly(2-methyl-2-oxazoline) (P(MeOx)) shell induces a shielding towards unspecific interactions with biological matter and prevents undesired protein interactions comparable to PEG.[24-25, 69-70] Furthermore, the preparation of cross-linked materials, such as nanogels,[51, 57] capsules,[55] and hydrogels[41, 51] is possible by either covalent or physical interactions.[51] In general, these materials are utilized, *e.g.* for drug delivery,[35] gene purification[56] or as nano reaction compartment.[71]

2.1. *In vitro* elucidation of the potential of P(Ox)s for biomedical applications

In order to evaluate the potential of P(Ox)s for biomedical applications, *in vitro* investigations (*i.e.* cell tests) are indespensable. Hereby, the initial experiments mainly cover the elucidation of the cytocompatibility, respectively cell viability as well as the hemocompatibility, *i.e.* erythrocyte aggregation and hemolysis experiments (Scheme 2.3). Herein, P(EtOx) and P(MeOx) of varios molar masses did not cause any cytotoxycity, erythrocyte aggregation or hemoglobin release in short-term experiments.[72-73] Long-term experiments revealed a slight decrease of the cell viability dependent on the molar masss of the polymers and the incubation time.[72-73] In addition to that, experiments showed an increase of the cytotoxicity of P(EtOx) in dependence on the degree of hydrolysis.[74] However, investigations on the hydrolysis of P(EtOx) under physiological conditions have shown that a degree of hydrolysis above 10% is unlikely.[75] Furthermore, P(Ox) micelles with a poly(lactic acid) (PLA) or poly(2-butyl-2-oxazoline) core were determined to be non-toxic.[67, 76]

2.1. *In vitro* elucidation of the potential of P(Ox)s for biomedical applications

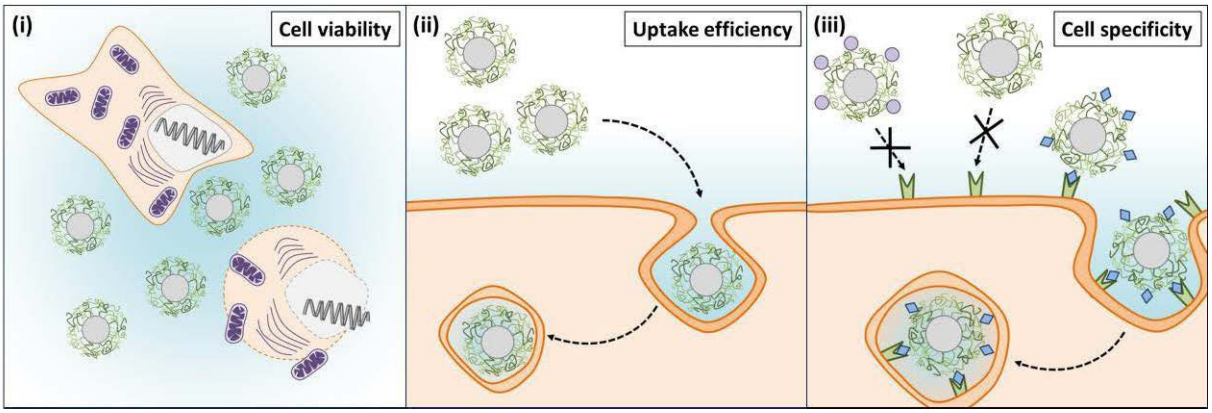

Scheme 2.3. Possibilities of *in vitro* studies in terms of biochemical polymer or carrier systems: (i) Cell viability determination by cytotoxicity, hemoglobin release or cell aggregation measurements, (ii) comparison of the uptake efficiency of drugs, polymers and carrier systems as well as (iii) utilization of different cell lines for the determination of cell specificity.

In addition to biocompatibility, applications regarding drug or gene delivery require a moderate cellular uptake and an efficient release of the API or the genetic material within the cellular compartment. In general, the cellular uptake of carriers with P(EtOx) was determined to be slower than the pure drugs[14, 16, 66, 77] This finding might be advantageous in terms of blood circulation times and pharmacokinetics. Furthermore, cell specificity of carriers can be increased by the utilization of special targeting units.[14-15]

2.2. *In vivo* biocompatibility and therapeutic efficiency of P(Ox)s

According to standardized *in vitro* assays, P(EtOx) and P(MeOx) are generally cyto- and hemocompatible, *i.e.* they do not induce cytotoxicity, hemolytic activity or cell aggregation up to concentrations of 10 mg mL^{-1}. However, these preliminary experiments can only provide a first impression about the biocompatibility and the therapeutic efficiency. *In vivo*, several attributes of drugs can be altered by using polymers, *e.g.* their solubility. Many drugs are not (well) water soluble. Conjugation to or encapsulation into water-soluble polymeric delivery systems that can be solubilized or suspended in water is a common way to resolve this issue.[21-22] P(EtOx) and P(MeOx) themselves were elucidated to have comparable characteristics like PEG in terms of the prevention of phagocytosis, unwanted protein interaction and renal excretion.[25] The significantly higher hydrodynamic volume of the polymer drug conjugates consequently leads to a reduction of the blood clearance and a following increase of the blood circulation time.[66] Therefore, the encountering of various different tissue and cell types expressing different receptors and markers is possible by equipping polymer carriers with targeting ligands to enhance the cell specificity.[14] Considering these results, P(Ox)s can fulfill all requirements for successful drug and gene delivery systems. For this reason, the current focus of research mainly covers *in vivo* experiments regarding blood circulation times, organ specificity and therapeutic efficiency (Scheme 2.4).

2.2. *In vivo* biocompatibility and therapeutic efficiency of P(Ox)s

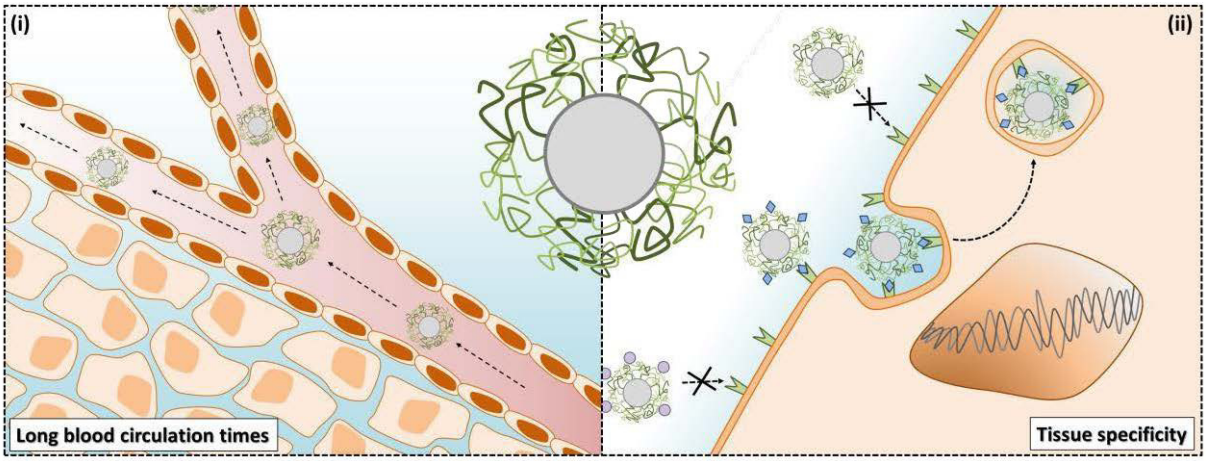

Scheme 2.4. Favorable attributes of polymeric nanocarriers for drug delivery: (i) Long blood circulation times, and (ii) tissue specificity, *i.e.* targeted cellular uptake

The biodistribution and blood clearance of different polymers was already investigated by utilizing radioactive labeling using various tracer elements, such as ^{67}Ga,[24] ^{125}I,[25, 78] ^{89}Zr,[69-70] ^{18}F,[70] or ^{111}In.[79-80] Hereby, measurements of tissue related radioactivity enabled the determination of organ accumulations and blood circulations times. Herein, the blood circulation times were found to be dependent on the molar mass of the polymers, which might be useful in terms of application.[78] Furthermore, it is important to mention that the label itself can also have an influence on the biodistribution of the elucidated polymers.[70] Hence, ^{89}Zr-labeled P(EtOx)$_{50}$ revealed an increased uptake into kidneys, liver and heart after 1 h and 4 h, while ^{18}F labeled P(EtOx) showed an increased uptake into kidneys directly after injection. Consequently, it was shown that even small end groups, such as ^{89}Zr- or ^{19}F-labels, have a tremendous effect on the performance of a polymeric carrier *in vivo* and have to be considered carefully.

Due to the fact that PEG is predominantly used as a stealth polymer, water soluble P(Ox)s are often compared with PEG.[24-25, 70, 80] Hereby, any observed differences between PEG and P(EtOx) decrease with an increasing molar mass of the polymers.[81] Overall, the polymers revealed a similar behavior for comparable molar masses.

Since, P(Ox)s were demonstrated to be biocompatible and the blood clearance rate as well as the biodistribution of P(Ox)s and PEG are similar, they are ideal candidates for the utilization as drug carriers; adjustment of molar mass of the polymers and the choice of monomers can influence the blood circulation time as well as organ accumulations.

Consequently, short blood circulation times and unspecific cellular uptake of drugs might be prevented by covalent conjugation to biocompatible, shielding polymers such as P(EtOx) and P(MeOx).[28, 66, 79] Herein, the conjugation of granulocyte stimulating factor g to P(EtOx) with varying molar mass leads to higher efficiencies when using polymers with a higher degree of polymerization (DP).[79] Furthermore, the conjugation of multiple API units was demostrated using rotigotine.[28] Herein, the drug was attached to the polymer by using biorthogonal copper catalyzed click chemistry (CuAAC). Moreover, a labile ester linker between the drug and the polymer was used to ensure efficient drug release in acidic cellular compartments. *In*

2.2. *In vivo* biocompatibility and therapeutic efficiency of P(Ox)s

vivo investigations revealed steady plasma drug concentrations over several days and, consequently, reduced unwanted side-effects such as dyskinesia.[64]

In particular in terms of cancer therapy, the enhanced blood circulation times might be advantageous to ensure an efficient delivery of the cytostatic agent into the tumor cells, *e.g.* by exploiting the EPR effect. Hereby, conjugation *via* azide cleavable hydrazone linker,[16, 35] the encapsulation into P(Ox) based micelles,[14-16, 19, 76-77, 82] or liposomes[26, 83] leads to an enhanced solubility[67] of the cytostatic agents as well as longer blood circulation times[22, 83] and higher therapeutic efficiencies[14-15, 21, 67, 76] while expressing a high biocompatibility.[22, 77]

3. Synthesis and polymerization of functional 2-oxazolines

Parts of this chapter have been published in: **P1**) M. N. Leiske, M. Hartlieb, F. H. Sobotta, R. M. Paulus, H. Görls, P. Bellstedt, U. S. Schubert, *Polym. Chem.* **2016**, *7*, 4924-4936. **P4)** D. Hoelzer‡, M. N. Leiske‡, M. Hartlieb, T. Bus, D. Pretzel, S. Hoeppener, K. Kempe, R. Thierbach, U. S. Schubert, *Oncotarget* **2018**, in press. **P5**) D. Hertz‡, M. N. Leiske‡, T. Wloka, A. Traeger, M. Hartlieb, M. M. Kessels, S. Schubert, B. Qualmann, U. S. Schubert, *J. Polym. Sci., Part A: Polym. Chem.* **2018**, in press. DOI: 10.1002/pola.29000. **P8**) M. Hartlieb‡, T. Bus‡, J. Kübel, D. Pretzel, S. Hoeppener, M. N. Leiske, K. Kempe, B. Dietzek, U. S. Schubert, *Bioconjugate Chem.* **2017**, *28*, 1229-1235. ‡Equal contribution of both authors.

The synthesis of P(Ox)s *via* CROP facilitates the synthesis of functional homo- and copolymers with a tailored structure. Within this chapter, the synthesis and polymerization route of the Boc protected 2-oxazoline 2-(4-((*tert*-butoxycarbonyl(amino)butyl)-2-oxazoline (BocOx), which is known from literature, will be compared with the newly synthesized *tert*-butyl 2-iminooxazolidine-3-carboxylate (BocOI). Since the polymerization kinetic of a monomer is for instance dependent on the substituent in 2-position, kinetic investigations on the polymerization rate constant (k_p) are indispensable. Furthermore, the copolymerization of different monomers can result in random, gradient or quasi block copolymers, depending on the reactivity ratios of the used monomers. For this reason, detailed kinetic investigations on the homopolymerization of the newly synthesized BocOI as well as on the copolymerization of BocOI and EtOx will be performed. In order to obtain information about the monomer distribution within water soluble cationic P(Ox) copolymers, the copolymerization of BocOx and EtOx as well as BocOx and MeOx will also be investigated. On the basis of the resulting k_p values, a series of functional homo- and copolymers will be synthesized and characterized.

3.1. Monomer synthesis and polymerization mechanism

During the last decade, amino functionalized P(Ox)s have been widely explored. While post-polymerization functionalization represents an effective method to introduce primary,[35, 38, 62, 84-85] secondary,[38] or tertiary amino moieties,[38, 85] suitable protection groups like the acid labile *tert*-butyloxycarbonyl (Boc) protection group enable the possibility of a polymerization of amino functionalized 2-oxazoline monomers.[40-41, 61] M. Hartlieb *et al*. synthesized the Boc protected 2-oxazoline BocOx in a three step synthesis approach (Figure 3.1A).[41] In the first reaction step (a), the amino group of 5-aminovaleric acid is protected using di-*tert*-butyl dicarbonate (DiBoc). Subsequently, the carboxylic acid can be activated by the addition of ethyl chloroformate to facilitate the reaction with 2-chloroethylamine (b). Finally, the ring closure can be conducted under basic conditions (c) to obtain BocOx (**3**), which is suitable for the CROP.

3.1. Monomer synthesis and polymerization mechanism

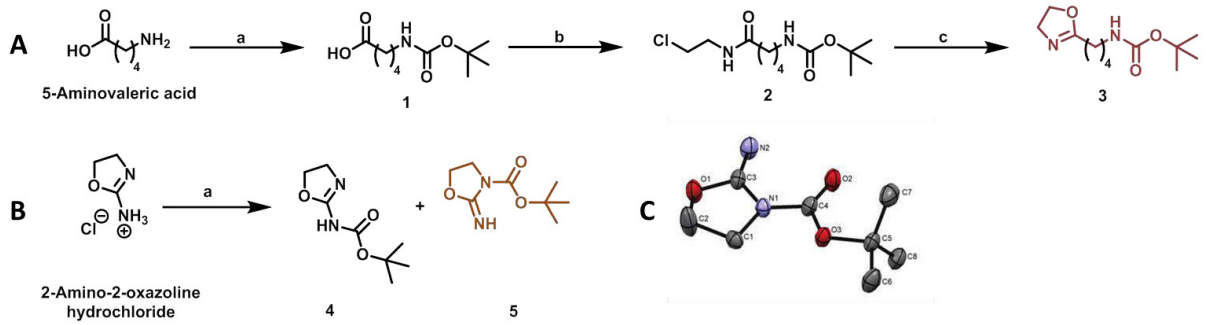

Figure 3.1. Comparison of the synthesis of BocOx (**3**) and BocOI (**5**). A: Three step BocOx (**3**) synthesis. a) DiBoc, dioxane/water, NaOH, RT; b) ethyl chloroformate, 2-chloroethylamine hydrochloride, NEt_3, DMF, RT; c) DMF, K_2CO_3 60 °C. B: Single step BocOI (**5**) synthesis. a) DiBoc, dioxane/water, NaOH, RT. C: Molecular structure of **5** derived by X-ray crystal structure analysis; H-atoms are excluded.

By variation of the spacer length between the oxazoline ring and the substituent in 2-position, it is assumable that the monomer- and, consequently, the polymer characteristics can be altered. A shorter spacer might affect the solubility as well as the biocompatibility or cellular uptake of the resulting polymers. For this reason, it was aimed to compare the properties of 2-amino-oxazoline and 2-(4-aminobutyl)-2-oxazoline) containing polymers.

2-Amino-2-oxazoline hydrochloride can be obtained commercially. As this substance does not have an alkyl spacer between the heterocycle and the functional amino group, this molecule is denoted by its imine-amine tautomerism in solution. Previous investigations already ascertained that in solution mainly the amino form is present.[86] By the utilization of discrete Fourier transform (DFT) calculations, the electronegativity of the nitrogen atoms based on the π-bond lengths could be determined (*endo* N: –0.317; *exo* N: –0.272).[87] Consequently, BocOI (**5**) can be synthesized directly from 2-amino-2-oxazoline (Figure 3.1B). As the tautomeric equilibrium cannot be shifted completely to 2-amino-2-oxazoline, the yield of the accomplished Boc protection reaction was determined to be ~70%. The crude product could be purified by recrystallization from cyclohexanes and the x-ray crystal structure analysis of a single crystal proved the identity of BocOI (**5**, Figure 3.1C). The purity of the final product was proven by ^{1}H-NMR, proving the by-product being less than 10% after purification (Figure 3.2A). HR-ESI MS measurements showed product peaks and verified the lability of the Boc protection group by the appearance of the dominant signal at m/z = 131.0 Da (M – Boc + H^+) (Figure 3.2B).

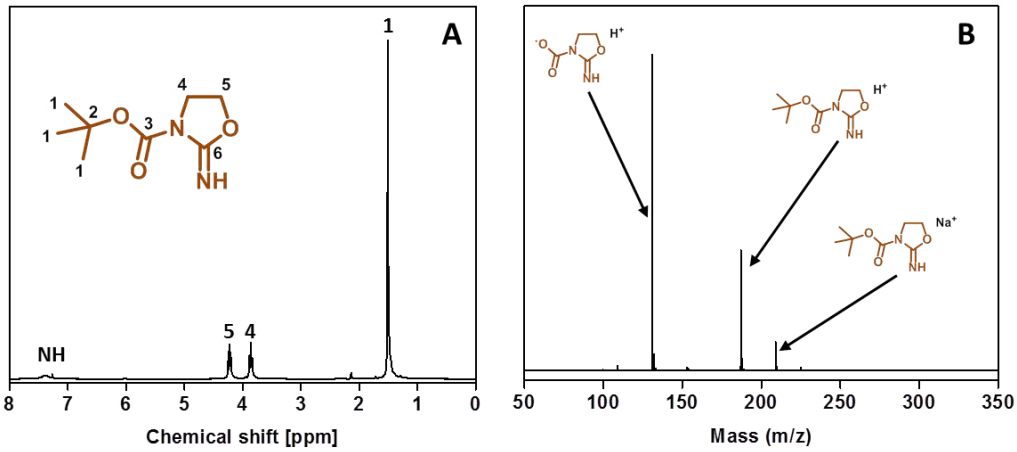

Figure 3.2. Characterization data of BocOI (**5**). A: ^{1}H-NMR (300 MHz, $CDCl_3$) and B: HR-ESI MS.

It was aimed to polymerize BocOI (**5**) by the utilization of a cationic initiator, such as methyl *p*-toluenesulfonate (MeTos), which is commonly used for the CROP of 2-oxazolines. The CROP of 1,3-oxazolidine-2-thione was already described previously, suggesting the possibility to polymerize BocOI (**5**) with the aid of MeTos.[88] Scheme 3.1 shows the postulated mechanism of the controlled polymerization of BocOI (**5**). During the initiation step (a), the free electron of the monomer's *exo* nitrogen attacks the methyl group of the initiator in a nucleophilic way. Subsequently, intramolecular electron shifts lead to a partial positive charge on the carbon atom in 5-position, which can be attacked by another monomer (propagation, b). The chain growth can be terminated by the addition of a nucleophile (c), *e.g.* water. The resulting polymeric structure is a poly(urea) derivative with one Boc protected nitrogen in the polymer backbone. Consequently, the CROP of BocOI (**5**) might facilitate the preparation of poly(urea) in a controlled manner instead of the commonly used polymerization described by O. Bayer in the 1940s.[89]

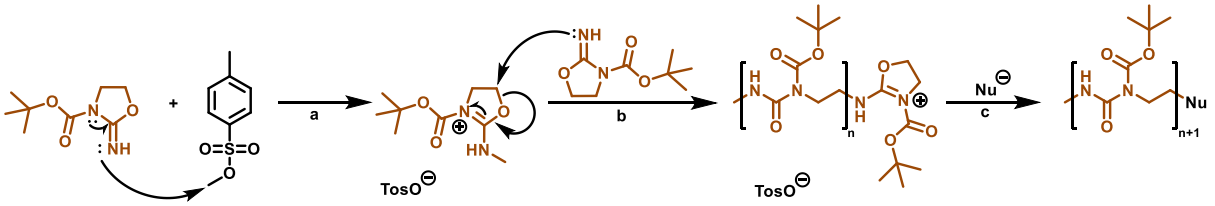

Scheme 3.1. Schematic representation of the postulated mechanism of the CROP of BocOI (**5**) initiated with MeTos. a) Initiation; b) propagation; c) termination.

3.2. Polymerization kinetics

Within this sub-chapter the polymerization kinetics of BocOI (**5**) will be shown. Furthermore, the copolymerization kinetics of BocOI (**5**) and EtOx, BocOx (**3**) and EtOx, as well as BocOx (**3**) and MeOx) will be discussed.

As already described in Chapter 1, P(Ox)s can be synthesized *via* CROP. In general, kinetic investigations are necessary to determine the linearity of the monomer consumption during the polymerization process. By the performance of homopolymerizations kinetics, it is possible to determine the controllability as well as the polymerization speed, respectively the

reaction rate constant (k_p). The k_p of the monomer under the investigated conditions could be calculated by the assumption that $\frac{\ln[M]_0}{\ln[M]_t} = f(t)$ complies with k_{eff}, eventuating equations (3.1) and (3.2).

$$\ln M_0 - \ln M_t = k_{eff} \cdot t \tag{3.1}$$

$$k_{eff} = k_p[I] \tag{3.2}$$

Within copolymerization reactions, monomers with different k_p values can form different copolymers, *i.e.* random,[9, 49] gradient[27, 50-51] or quasi block copolymers,[52-53] as depicted in Chapter 1. In order to obtain a further insight on the monomer distribution within the polymer chain, detailed kinetic investigations on the copolymerization of different monomers are indispensable. Herein, reactivity ratios for copolymerization of the monomer pairs are calculated at four different monomer ratios at 30% conversion of the monomer with the higher reaction constant as determined using least-linear least square fitting (equation (3.3)).[90-91]

$$F_1 = \frac{(r_1-1)f_1^2+f_1}{(r_1+r_2-2)f_1^2+2(1-r_2)f_1+r_2} \tag{3.3}$$

F_1: instantaneous mole fraction, f_1: monomer fraction of monomer 1, f_2: monomer fraction of monomer 2, r_1: reactivity ratio of monomer 1, r_2: reactivity ratio of monomer 2

Homopolymerization kinetics of EtOx,[11] MeOx[48] and BocOx[41] are already known from literature. Consequently, within this sub-chapter, only the homopolymerizations kinetics of BocOI (**5**) will be presented. For the purpose of accomplishing a copolymerization of 2-oxazolines and oxazolidine imines, time-dependent kinetics on the copolymerization of BocOI (**5**) and EtOx were conducted. As BocOx, respectively AmOx, containing cationic polymers were aimed to be used for gene-delivery applications (Chapter 5), the copolymerization with a non-ionic water soluble monomer is indispensable to enhance its biocompatibility. For this reason, copolymerization kinetics of BocOx (**3**) and EtOx as well as the more reactive MeOx and BocOx (**3**) were performed.
Initial kinetics were conducted on the homopolymerization of BocOI (**5**). Due to the fact that a copolymerization with 2-oxazolines, *i.e.* EtOx, was planned, preliminary experiments were conducted at 140 °C, being a well applicable temperature for the polymerization of EtOx considering the reaction speed and the dispersity of the resulting polymers.[11] Unfortunately, k_{eff} in dependence on the polymerization time was not linear under the investigated conditions. It was suggested that the monomer suffers from thermal deprotection at high reaction temperatures as already known from literature for other examples.[92] Furthermore, it is quite likely that a non-protected 2-imino-1,3-oxazolidine monomer can still be polymerized by using a CROP, when referring to A. Nagai *et al.*. Herein, 1,3-oxazolidine-2-thione was polymerized utilizing methyl trifluoromethanesulfonate without any protection groups for the *endo* N.[88] It might be presumed that the 2-imino-1,3-oxazolidine is significantly more reactive than BocOI (**5**), because of a lack in steric hindrance, leading to the lack in linearity

of the conversion in dependence on the time caused by slow initiation speeds compared to the propagation. A. Nagai *et al.* therefore polymerized 1,3-oxazolidine-2-thione at low temperatures of 30 to 40 °C. Unfortunately, by using such low reaction temperatures, the polymerization rate constant of 2-oxazolines is very low, leading to reaction times of several days or weeks.[11] For this reason, the polymerization temperature was lowered to 100 °C, also reducing the side-reactions caused by the high reactivity of BocOI (**5**), however, still being applicable for a copolymerization with 2-oxazolines. Time-dependent polymerization kinetics resulted in a nearly linear dependency of k_{eff} on the polymerization time (Figure 3.3A). With respect to size-exclusion chromatography (SEC) measurements (Figure 3.3B), side-reactions were only present at high molar masses, or monomer conversions above 80%. The positive deviation of the molar mass might be attributed to chain coupling reactions, also known for P(Ox)s.[93]

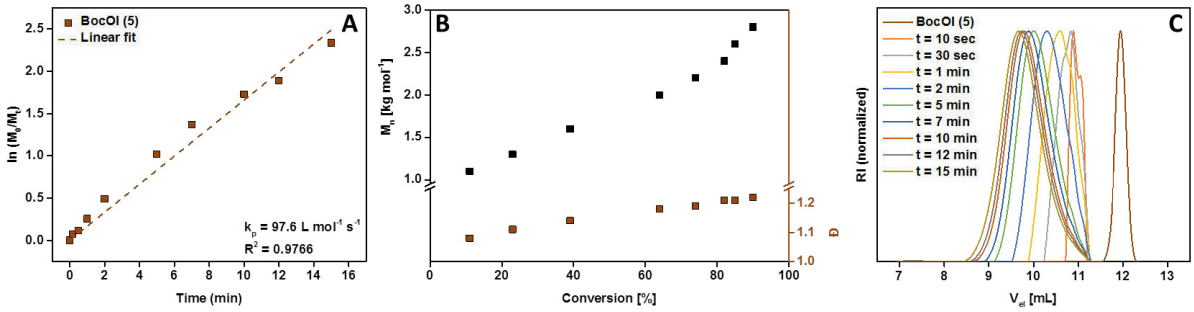

Figure 3.3. Kinetik studies of BocOI (**5**, [M/I] = 60) in CH_2Cl_2 at 100 °C initiated with MeTos. A: Time-dependent polymerization kinetics calculated by the monomer conversion obtained from gas chromatography (GC) analytics. B: Molar mass and dispersity in dependence on the monomer conversion. C: SEC traces ($CHCl_3$-*i*-PrOH-NEt_3, PS-calibrated) of the reaction mixture after distinct polymerization times.

Nevertheless, the polymerization kinetics was determined to follow pseudo first-order under the given conditions and the k_p value of BocOI (**5**) was determined to be 97.6 L mol^{-1} s^{-1}. For comparison, also a kinetic study of EtOx was conducted by using the same conditions as for BocOI (**5**), resulting in a k_p value of 4.6 L mol^{-1} s^{-1}, being 20 times lower than BocOI (**5**). This large difference within the determined reaction constants might lead to the formation of quasi block copolymers by one-pot copolymerization.

In order to obtain a further insight on the monomer distribution within the polymer chain, detailed kinetic investigations on the copolymerization of BocOI (**5**) and EtOx are indispensable. For this reason, copolymerization experiments were conducted using 20, 40, 60 or 80% BocOI (**5**) within the monomer feed. Figure 3.4 shows exemplary logarithmic plots of the copolymerization of 20% BocOI (**5**) with 80% EtOx (Figure 3.4A).

3.2. Polymerization kinetics

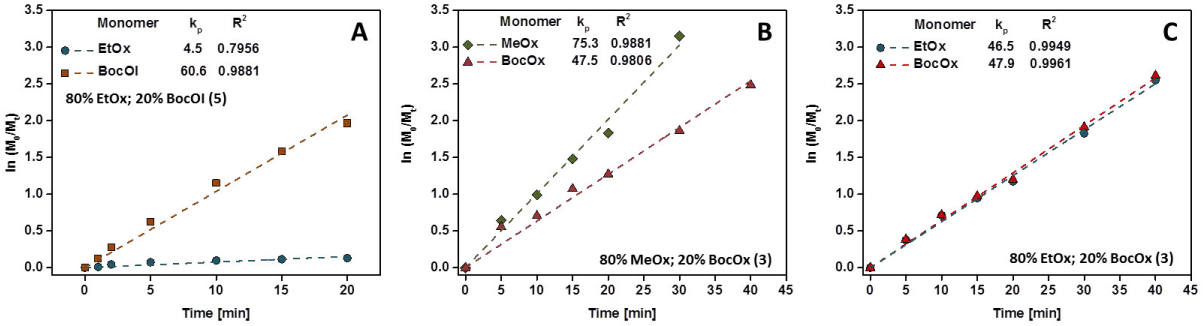

Figure 3.4. Exemplary ln plots of the time-dependent polymerization kinetics of A: EtOx (80%) and BocOI (**5**, 20%) performed in dichloromethane at 100 °C with [M]/[I] = 100 and MeTos as initiator; B: MeOx (80%) and BocOx (**3**, 20%) performed in acetonitrile at 140 °C with [M]/[I] = 150 and methyl tosylate as initiator; C: EtOx (80%) and BocOx (**3**, 20%) performed in acetonitrile at 140 °C with [M]/[I] = 150 and methyl tosylate as initiator.

Herein, the copolymerization of EtOx (k_p = 5.2 ± 1.4 L mol^{-1} s^{-1}, r = 0.000 ± 0.002) and BocOI (**5**, k_p = 58.0 ± 5.6 L mol^{-1} s^{-1}, r = 28.72 ± 10.00) presumably produces quasi block copolymers. To illustrate this fact, the fractions of the monomer with a lower reaction constant were plotted against the total polymer length (Figure 3.5D). During the synthesis of P(BocOI$_n$-*co*-EtOx$_m$) most of the BocOI (**5**) is consumed prior the incorporation of EtOx into the polymer chain, independent on the utilized monomer ratios, verifying a very narrow gradient area within the polymer chain. Consequently, the synthesis of quasi block copolymers can be achieved in a one-pot copolymerization. A similar behavior was already reported for the copolymerization of 2-phenyl-2-oxazoline and MeOx.[52]

In order to obtain information about the monomer distribution within water-soluble cationic copolymers, also the copolymerization kinetics of BocOx (**3**) and EtOx, respectively MeOx were conducted utilizing the same monomer ratios as BocOI (**5**) and EtOx. Figure 3.4 shows exemplary logarithmic plots of the copolymerization of 20% BocOx (**3**) with 80% MeOx (Figure 3.4B), or EtOx (Figure 3.4C). Within the investigated monomer ratios and reaction conditions, the reactivity ratios of EtOx (k_p = 47.2 ± 11.0 L mol^{-1} s^{-1}, r = 0.98 ± 0.06) and BocOx (**3**, k_p = 44.0 ± 13.3 L mol^{-1} s^{-1}, r = 1.02 ± 0.06) are nearly similar, suggesting the formation of random copolymers as already preliminary reported by M. Hartlieb *et al.*.[41]

Moreover, it was previously demonstrated that the k_p value of MeOx is increased compared to EtOx.[27] For this reason, our results on an increased reactivity of MeOx (k_p = 75.4 ± 2.8 L mol^{-1} s^{-1}, r = 1.50 ± 0.16) in relation to BocOx (**3**, k_p = 50.7 ± 4.0 L mol^{-1} s^{-1}, r = 0.67 ± 0.08) comply with the literature and suggest the formation of gradient copolymers.

Copolymers consisting of monomers with similar reactivity ratios such as P(EtOx$_n$-*co*-BocOx$_m$) exhibit a linear increase of the fraction of the monomers (Figure 3.5F), whereas the increase in the instantaneous mole fraction in a gradient copolymer (P(MeOx$_n$-*co*-BocOx$_m$) is more exponential (Figure 3.5E).

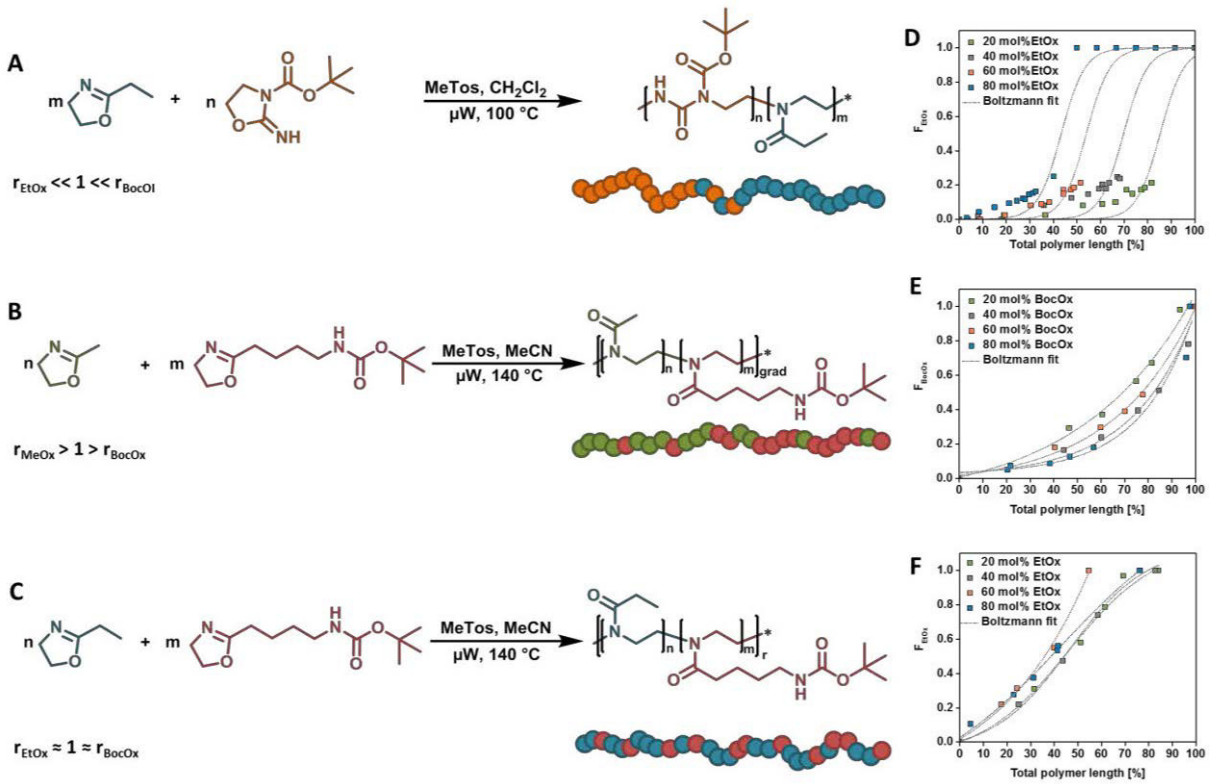

Figure 3.5. A to C: Schematic representation of the polymerization conditions and the proposed polymeric structures of different copolymers synthesized in a one-pot reaction. A: cyan: EtOx, red: BocOx; B: green: MeOx, red. BocOx; C: cyan: EtOx; orange: BocOI. D to F: Monomer distribution calculated from the kinetic plots of the copolymerization. The symbols show the experimental values, the lines show the non-linear Boltzmann fitting of the values. D: Copolymerization of EtOx and BocOx (**3**) performed in acetonitrile at 140 °C with [M]/[I] = 150 and MeTos as initiator. E: Copolymerization of MeOx and BocOx (**3**) performed in acetonitrile at 140 °C with [M]/[I] = 150 and MeTos as initiator. F: Copolymerization of EtOx and BocOI (**5**) performed in dichloromethane at 100 °C with [M]/[I] = 100 and MeTos as initiator.

As shown in Figure 3.5, the results of the kinetic investigations facilitate the synthesis of water-soluble BocOx (**3**), respectively AmOx, containing copolymers with either a random or a gradient monomer distribution by choosing either EtOx or MeOx as a suitable comonomer for polymerization. Furthermore, the copolymerization of BocOI (**5**) and EtOx is achievable by CROP and results in quasi block copolymers. In the following paragraphs, a series of different homo- and copolymers will be synthesized, characterized and compared.

3.3. Synthesis of polymers containing P(Ox) and poly(urea)

This sub-chapter will provide an overview about different homo- and copolymers synthesized using CROP. Firstly, a series of poly(urea) containing homo- and copolymers as well as their characterization will be presented. Then, the preparation of BocOx containing random, gradient and block copolymers will be explained. Finally, Fluorescent labeling of the block copolymers will be shown. Homopolymers that are utilized for nanoparticle stabilization (Chapter 4.1) or drug delivery (Chapter 6) within this thesis were prepared according to literature procedures[17, 48] and are, consequently, not part of the following sub-chapter.

3.3. Synthesis of polymers containing P(Ox) and poly(urea)

After obtaining the polymerization kinetics of BocOI, four Boc protected homopolymers with varying DP from 25 to 100 (**P01** to **P04**) were synthesized and characterized accordingly using ^{1}H-NMR, SEC, differential scanning calorimetry (DSC) and thermogravimetric analysis (TGA) measurements (Table 3.1). Thereby, ^{1}H-, ^{13}C-, ^{1}H correlation spectroscopy (COSY) and ^{1}H-^{13}C heteronuclear single quantum coherence (HSQC) NMR measurements were performed to confirm the predicted polymeric structure (Figure 3.6).

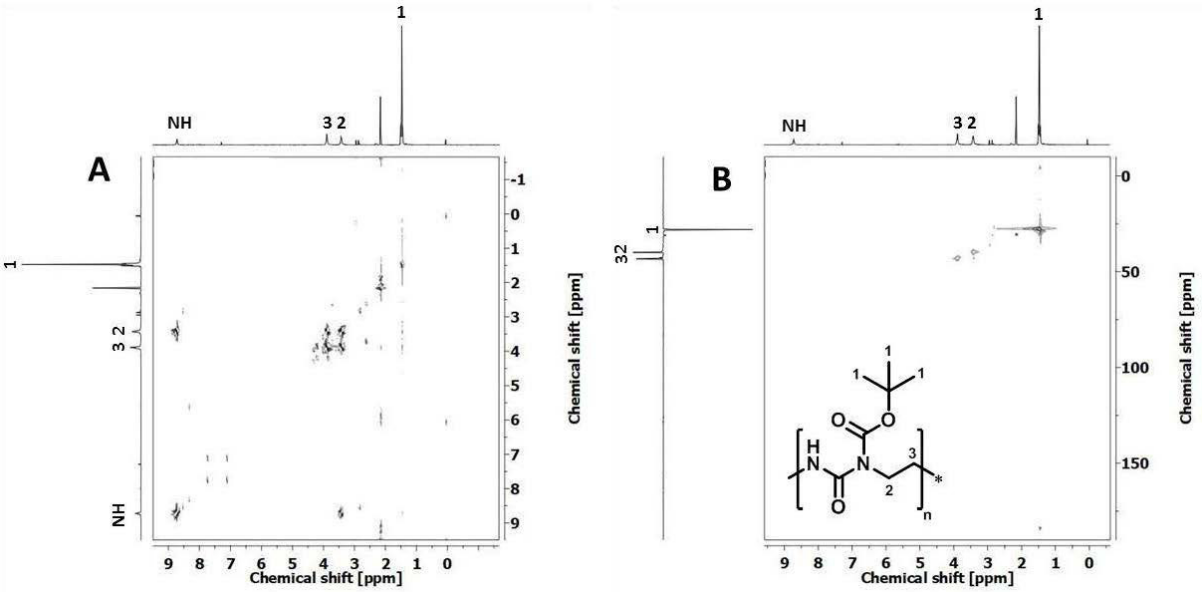

Figure 3.6. Characterization of P(BocOI)$_{54}$ (**P02**). A: ^{1}H-^{1}H-COSY NMR spectrum (300 MHz, $CDCl_3$) and B: HSCQ NMR spectrum (300 MHz, $CDCl_3$).

In the ^{1}H-NMR spectrum, two signals (δ = 3.5 and 3.9 ppm) could be allocated to the backbone of the polymer, indicating different substituents on the nitrogen atoms in the backbone, namely the proton and the Boc protection group. Furthermore, the signal at δ = 8.8 ppm is typical for the proton of an amide group. ^{1}H-COSY NMR measurements were correlated the neighboring of protons. A coupling of the signal at δ = 3.5 ppm with the signals at δ = 3.9 and 8.8 ppm suggests the structure of the proposed poly(urea). Furthermore, the DP of the polymers could be determined by evaluation of ^{1}H-NMR by comparison of the aromatic MeTos protons at δ = 7.15 and 7.67 ppm with the backbone protons at δ = 3.5 ppm. The DP of the homopolymers was determined to be 19, 54, 73 and 112, respectively (Table 3.1).

Table 3.1. Characterization data for P(BocOI)$_n$ (**P01** to **P04**). [a] ^{1}H-NMR (300 MHz) in $CDCl_3$. [b]SEC in $CHCl_3$-*i*-PrOH-NEt_3 (PS-cal.).

ID	Composition	[M]/[I]	NMR[a]			SEC[b]	
			BocOI conversion [%]	*DP*	*Mn [kg mol^{-1}]*	*Mn [kg mol^{-1}]*	*Đ*
P01	P(BocOI)$_{19}$	25	91.9	19	3.5	3.8	1.18
P02	P(BocOI)$_{54}$	50	86.9	54	10.3	4.3	1.22
P03	P(BocOI)$_{73}$	75	85.0	73	13.6	4.4	1.31
P04	P(BocOI)$_{112}$	100	87.2	112	20.9	4.2	1.20

SEC measurements were conducted to gain information about the uniformity of the polymers (Table 3.1). Hereby, polymers with a narrow dispersity (Đ ≤1.3) were obtained. Furthermore,

even though different DPs were calculated using ^{1}H-NMR, die molar masses regarding SEC measurements did not vary significantly. This might be caused by column interactions of the polymers, which were not obtained during kinetic studies. A possible explanation for the different results might be attributed to the differences in the molar mass of the polymers **P01** to **P04** (min. 3.5 kDa) compared to the kinetic studies (max. 2.7 kDa).

Based on the data of the kinetic investigations, copolymers consisting of BocOI and EtOx are found to be block-like. This might be advantageous, *e.g.* in terms of self-assembly properties (Chapter 4.2), and, consequently, also a series of copolymers consisting of BocOI and EtOx was synthesized (Table 3.2). Hereby, the DP of the copolymers was kept constant, while the monomer ratios were varied from 20 to 80% BocOI (Table 3.2). The polymers were characterized using ^{1}H-NMR and SEC measurements (Figure 3.7). ^{1}H-NMR measurements showed that all copolymers revealed a similar DP of around 100 and varying BocOI contents. The dispersity of the polymers was determined to be Đ < 1.4.

Table 3.2. Characterization data for P(BocOI$_n$-*co*-EtOx$_m$) (**P05** to **P08**) and P(EtOx)$_{116}$ (**P09**). [a] ^{1}H-NMR (300 MHz) in $CDCl_3$. [b]SEC in $CHCl_3$-*i*-PrOH-NEt_3 (PS-cal.).

ID	Composition	NMR[a]			SEC[b]	
		DP	*BocOI [mol%]*	*Mn [kg mol^{-1}]*	*Mn [kg mol^{-1}]*	*Đ*
P05	P(BocOI$_{16}$-*co*-EtOx$_{84}$)	95	16	11.3	6.1	1.27
P06	P(BocOI$_{36}$-*co*-EtOx$_{64}$)	96	36	13.0	5.3	1.36
P07	P(BocOI$_{52}$-*co*-EtOx$_{48}$)	100	52	14.4	5.9	1.34
P08	P(BocOI$_{84}$-*co*-EtOx$_{16}$)	100	84	17.2	7.4	1.26
P09	P(EtOx)$_{116}$	116	0	11.5	6.8	1.16

Boc protected urea containing copolymers could be deprotected using trifluoroacetic acid (TFA, Scheme 3.2), resulting in either poly(urea) homopolymers (Scheme 3.2A) or block like copolymers from P(EtOx) and P(OI) (Scheme 3.2B). Due to the fact that the deprotected copolymers were not soluble in any suitable solvent, further analytics, such as mass spectrometry (MS) or SEC were not possible. However, NMR measurements in deuterated TFA could be conducted to verify the successful deprotection of the polymers.

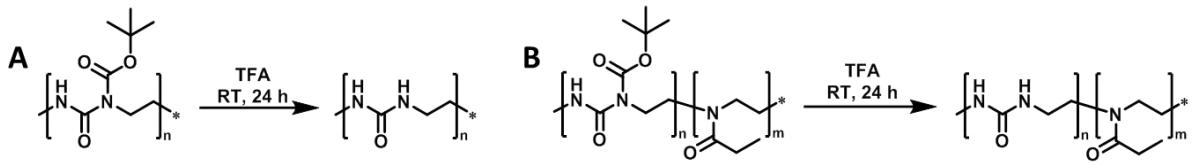

Scheme 3.2. Schematic representation of the performed deprotection reactions of A: P(BocOI)$_n$ to P(OI)$_n$ as well as B: P(BocOI$_n$-*co*-EtOx$_m$) to P(OI$_n$-*co*-EtOx$_m$) utilizing TFA as deprotection agent.

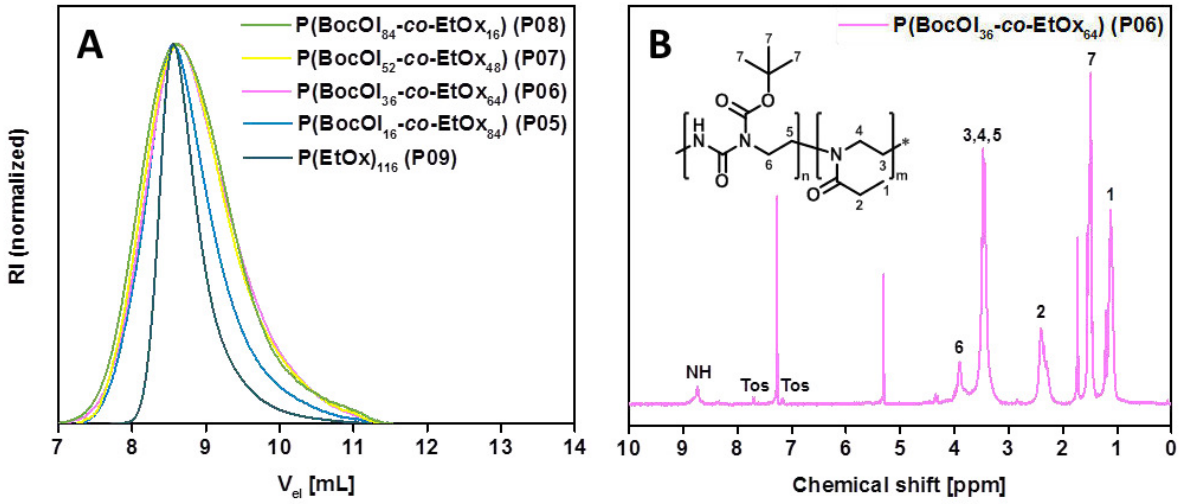

Figure 3.7. A: SEC traces ($CHCl_3$-*i*-PrOH-NEt_3, PS-cal.) of **P05** to **P09**. B: ^{1}H-NMR (300 MHz, $CDCl_3$) of **P06**.

Additionally, DSC and TGA measurements of all deprotected polymers as well as the Boc protected precursors were performed and the results were compared with $P(EtOx)_{166}$ (**P09**) (Table 3.3). Regarding the TGA measurements (Figure 3.8), Boc protected homopolymers (**P01** to **P04**) revealed a slight increase of the T_d from 155 to 170 °C in dependence on the molar mass. Furthermore, a partial decomposition of up to 50% mass loss could be observed, possibly caused by a thermal deprotection of the polymers.[94] A second T_d could be observed around 200 °C, which is also determined to be the T_d of the deprotected homopolymers **P10** to **P13**. Furthermore, after deprotection no significant dependence of the T_d on the molar mass could be observed (Table 3.3). This might be caused by intra- and intermolecular stabilization of the polymers due to hydrogen bond formation during heating process. The increased T_d of the deprotected homopolymers compared to Boc protected homopolymers might also be explained by this phenomenon. In terms of the Boc protected copolymers **P05** to **P08**, no apparent relation between the T_d and the BocOI content within the polymers could be observed (Table 3.3). The sharp decrease in mass above a heating temperature of 200 °C may be related to thermal deprotection (Figure 3.8A).

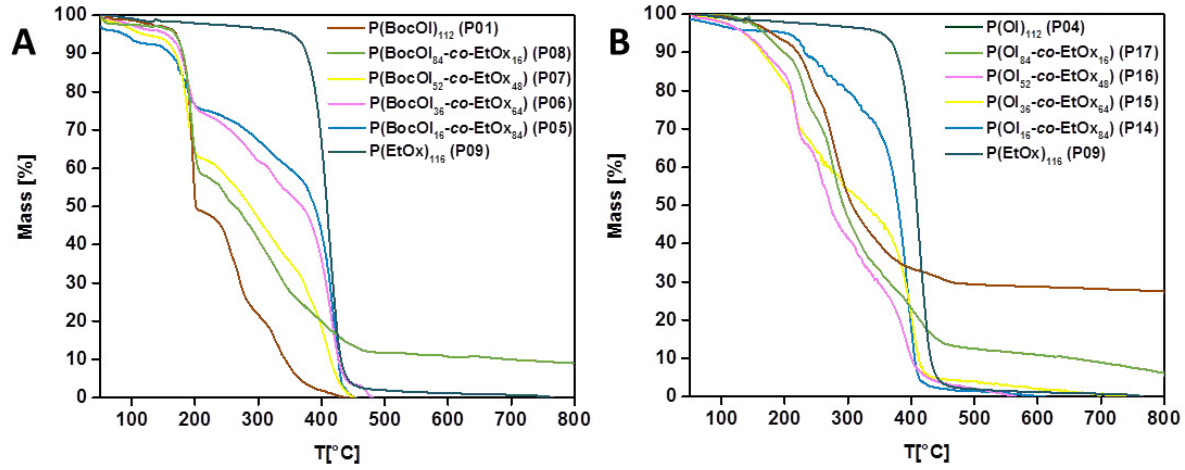

Figure 3.8. TGA of the A: Boc protected polymers **P01** and **P05** to **P09** and B: deprotected polymers **P04** and **P14** to **P17** as well as **P09**.

Further decomposition of copolymers follows the T_d of P(BocOI) and P(EtOx) with respect to the monomer ratios. The degradation temperatures of deprotected copolymers (**P14** to **P17**) are comparable to the homopolymers (**P01** to **P04**) revealing no significant trend at a mass loss of 5%, while further degradation also follows P(OI) or P(EtOx) with respect to the monomer ratios (Table 3.3, Figure 3.8B). DSC measurements were performed to obtain information about a possible glass transition temperature (T_g) of the polymers. The Boc protected homopolymers **P01** to **P03** revealed a T_g of 65 to 70 °C independent on the molar mass of the polymers. However, the reason why the T_g of **P04** (98 °C) was significantly increased compared to the other Boc protected homopolymers is not understood yet. Deprotected homopolymers (**P10** to **P13**) show a distinct lower T_g of 0 to 10 °C. The sharp decrease of the T_g after deprotection of the homopolymers might be caused by inter- and intramolecular interactions of the poly(urea) structure. The T_g of the Boc protected copolymers (**P05** to **P08**) was determined to be 50 to 55 °C independent on the incorporated monomer ratios. In contrast, after deprotection, the influence of the urea amount within the copolymers (**P14** to **P17**) is significant. The T_g of $P(EtOx)_{116}$ (**P09**) was determined to be 62.7 °C, similar to the deprotected copolymer containing 80% EtOx (**P14**, T_g = 65.8 °C). The T_g decreases down to –5 °C for the copolymer containing 20% EtOx (**P17**), which is distinctly lower than $P(EtOx)_{116}$ (**P09**) or the deprotected homopolymers (**P10** to **P13**).

Table 3.3. Characterization data for all synthesized polymers and Boc protected precursors as determined by the utilization of TGA and DSC measurements. The 2nd heating cycle was used for the determination of the T_g.

ID	Pre	Composition	NMR[a]			DSC	TGA
			DP	*BocOI [mol%]*	*Mn [kg mol^{-1}]*	*T_g [°C]*	*T_d [°C]*
P01	-	$P(BocOI)_{19}$	19	100	3.5	69.6	154.3
P02	-	$P(BocOI)_{54}$	54	100	10.3	66.2	164.5
P03	-	$P(BocOI)_{73}$	73	100	13.6	68.9	167.6
P04	-	$P(BocOI)_{112}$	112	100	20.9	97.9	170.2
P05	-	$P(BocOI_{16}$-*co*-$EtOx_{84})$	95	18	11.3	53.2	89.2
P06	-	$P(BocOI_{36}$-*co*-$EtOx_{64})$	96	27	13.0	51.5	155.6
P07	-	$P(BocOI_{52}$-*co*-$EtOx_{48})$	100	47	14.4	56.7	120.0
P08	-	$P(BocOI_{84}$-*co*-$EtOx_{16})$	100	76	17.2	54.2	168.7
P09	-	$P(EtOx)_{116}$	116	0	11.5	62.7	353.1
P10	P01	$P(OI)_{19}$	19	100	1.6	0.8	175.1
P11	P02	$P(OI)_{54}$	54	100	4.7	-	218.2
P12	P03	$P(OI)_{73}$	73	100	6.3	7.6	136.3
P13	P04	$P(OI)_{112}$	112	100	9.6	2.4	179.5
P14	P05	$P(OI_{16}$-*co*-$EtOx_{84})$	95	18	9.7	65.8	203.3
P15	P06	$P(OI_{36}$-*co*-$EtOx_{64})$	96	27	9.4	10.6	136.1
P16	P07	$P(OI_{52}$-*co*-$EtOx_{48})$	100	47	9.2	5.9	137.3
P17	P08	$P(OI_{84}$-*co*-$EtOx_{16})$	100	76	8.8	-4.9	168.1

Possibly, this phenomenon is caused by a homogeneous mixture of both blocks in bulk. Furthermore, a probable explanation could be attributed to the decrease of the T_g of P(EtOx) with decreasing block length.[95]Besides copolymerization of P(Ox)s with BocOI, the synthesis of functionalized P(Ox)s is of significant interest since they can be utilized for post-polymerization functionalization reactions, self-assembly processes as well as drug and gene delivery applications.

3.3. Synthesis of polymers containing P(Ox) and poly(urea)

It was aimed to obtain biocompatible cationic polymers which are suitable for gene transfection (Chapter 5) or drug delivery applications (Chapter 6). For this reason, the amino functionalized monomer BocOx (**3**) was copolymerized with either EtOx, which forms randomly distributed copolymers (Scheme 3.3A) or MeOx in order to obtain gradient copolymers (Scheme 3.3B) as determined by kinetic investigations (Chapter 3.2). By the synthesis *via* CROP, also the synthesis of block copolymers *via* sequential monomer addition is facilitated (Scheme 3.3C). After purification of the Boc protected polymer precursors, acidic deprotection using TFA and subsequent ion exchange leads to AmOx containing copolymers with a different monomer distribution. It is assumed that in aqueous solution, the cationic charges in MeOx containing copolymers are more concentrated due to their gradient monomer distribution, while they are randomly distributed within the whole polymer chain in EtOx containing copolymers.

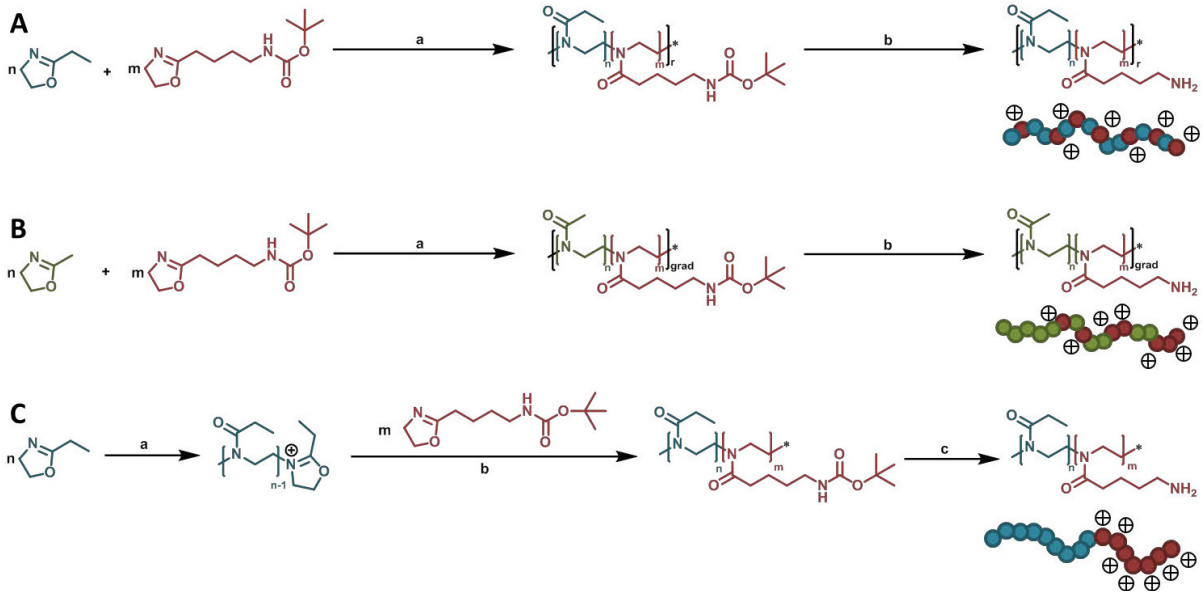

Scheme 3.3. Synthesis route of cationic copolymers. A and B: Copolymers synthesized *via* one-pot polymerization of 2-oxazolines and acidic deprotection. A: P(MeOx$_n$-*grad*-AmOx$_m$). B: P(EtOx$_n$-*r*-AmOx$_m$). a) Polymerization initiated using MeTos performed in acetonitrile at 140 °C. b) i. TFA, RT, overnight; ii. Amberlyst A21, methanol, RT, overnight. C: P(EtOx$_n$-*b*-AmOx$_m$) synthesized *via* sequential monomer addition. a) Polymerization of EtOx block initiated using MeTos performed in acetonitrile at 140 °C. b) Polymerization of BocOx block in acetonitrile at 140 °C. c) i. TFA, RT, overnight; ii. Amberlyst A21, methanol, RT, overnight. Green: MeOx. Cyan: EtOx. Red: BocOx/AmOx.

Herein, the synthesis of the Boc protected precursors and the AmOx containing cationic copolymers is exemplarily described for polymers containing 20% BocOx (**P18** and **P20**), respectively AmOx (**P19** and **P21**). The precursors as well as the final copolymers could be characterized using ^{1}H-NMR (Table 3.4, Figure 3.9) and SEC measurements (Table 3.4).
By means of ^{1}H-NMR measurements of Boc protected precursors (Figure 3.9, bottom spectra), the DP of the polymers and, consequently, the median molar mass could be determined. Hereby, the integrals of the tosylate initiator are compared with the backbone peaks of the polymers (δ = 3.4 ppm). More important, also the amount of BocOx within the polymer could be determined by comparing the integrals of a peak, which is specific for one monomer, *e.g.* the MeOx side chain at δ = 2.1 ppm (Figure 3.9B) and the polymer backbone

peak at δ = 3.4 ppm. Furthermore, the success of the deprotection reaction could be verified by the disappearance of the referring peak at δ = 1.4 ppm (Figure 3.9, top spectra).

Table 3.4. Key properties of the synthesized P(Ox)s determined by either ^{1}H-NMR spectroscopy (300 MHz) in [a]$CDCl_3$, [b]CD_3OD or [c]D_2O; [d]calculated from Boc protected precursor; [e]calculated from deprotected copolymer. [f]SEC in DMAc + 0.21% LiCl, PS-cal.; [g]SEC in 0.3% TFA + 0.1 M NaCl, P2VP-cal.; [h]SEC ($CHCl_3$-*i*-PrOH-NEt_3 (94:2:4), PS-cal.)

ID	Pre	Composition	NMR				SEC	
			DP	*mol% MeOx/ EtOx*	*mol% BocOx/ AmOx*	M_n *[kg mol^{-1}]*	M_n *[kg mol^{-1}]*	*Đ*
P18	-	P($EtOx_{150}$-*r*-$BocOx_{33}$)	183[a]	82[e]	18[e]	22.8	19.1[f]	1.16[f]
P19	P18	P($EtOx_{150}$-*r*-$AmOx_{33}$)	183[b,d]	82	18	19.6	8.0[g]	1.41[g]
P20	-	P($MeOx_{130}$-*grad*-$BocOx_{31}$)	161[a]	81[e]	19[e]	18.6	15.2[f]	1.33[f]
P21	P20	P($MeOx_{130}$-*grad*-$AmOx_{31}$)	161[b,d]	81	19	15.5	7.0[g]	1.48[g]
P22	-	P$(EtOx)_{98}$	98	100	-	10.0	5.7[h]	1.05[h]
P23	P222	P($EtOx_{98}$-*b*-$BocOx_{32}$)	130[a]	75[a]	25[a]	17.5[a]	8.2[h]	1.07[h]
P24	P23	P($EtOx_{98}$-*b*-$AmOx_{32}$)	130[c]	75[c]	25[c]	14.2[c]	13.8[f]	1.11[f]
P25	P24	P($EtOx_{98}$-*b*-[$AmOx_{31}$-*stat*-FOx_1])	130[c]	75[c]	25[c]	15.3[c]	14.1[f]	1.12[f]

SEC measurements were conducted to gain information about the polymer dispersity after preparation (Table 3.4). The Boc protected polymers exhibited a dispersity of Đ ≤ 1.33, being well-suited for further experiments. Furthermore, measurements on an aqueous SEC provided information about the stability of the polymers during acidic deprotection. No degradation of the polymer backbone could be observed.

In addition to random and gradient block copolymers, also the preparation of tailored block copolymers, suitable for self-assembly and core cross-linking (Chapter 4.2) by CROP is enabled using the sequential monomer addition technique (Table 3.4). In order to prepare micelles, a water soluble block copolymer consisting of EtOx and BocOx was synthesized and deprotected (**P24**).

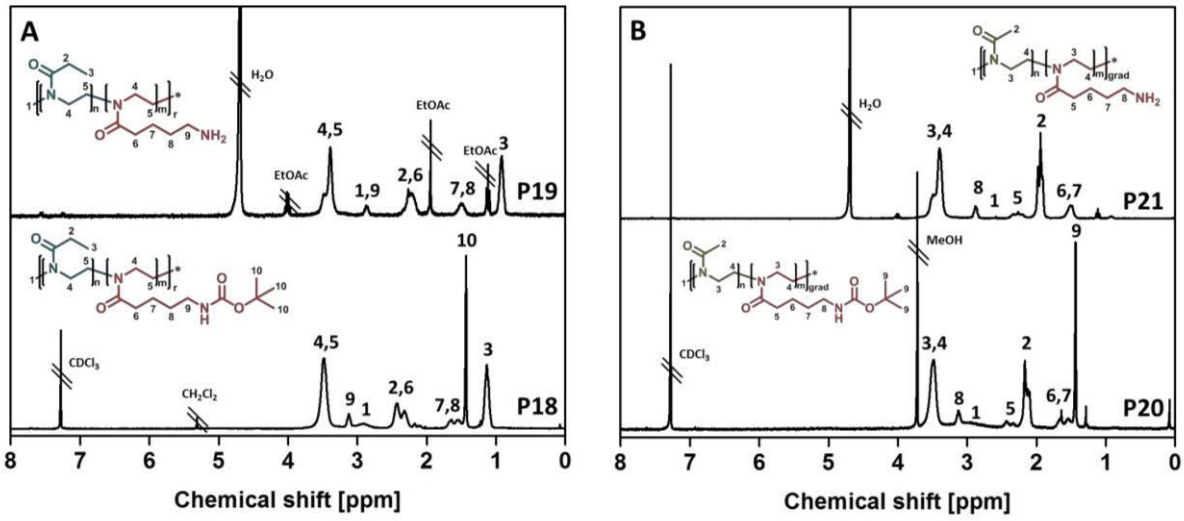

Figure 3.9. ^{1}H NMR (300 MHz) spectra of A: P($EtOx_{150}$-*stat*-$BocOx_{33}$) (**P18**, $CDCl_3$) and P($EtOx_{150}$-*stat*-$AmOx_{33}$) (**P19**, D_2O), as well as B: P($MeOx_{130}$-*grad*-$BocOx_{31}$) (**P20**, $CDCl_3$) and P($MeOx_{130}$-*grad*-$AmOx_{31}$) (**P21**), D_2O.

3.3. Synthesis of polymers containing P(Ox) and poly(urea)

The DP of the polymer blocks could be determined using ^{1}H-NMR (Table 3.4). Furthermore, the block-like chain growth was verified using SEC measurements (Figure 3.10A), revealing a clear shift to lower elution volumes after addition of the second monomer to the reaction mixture.

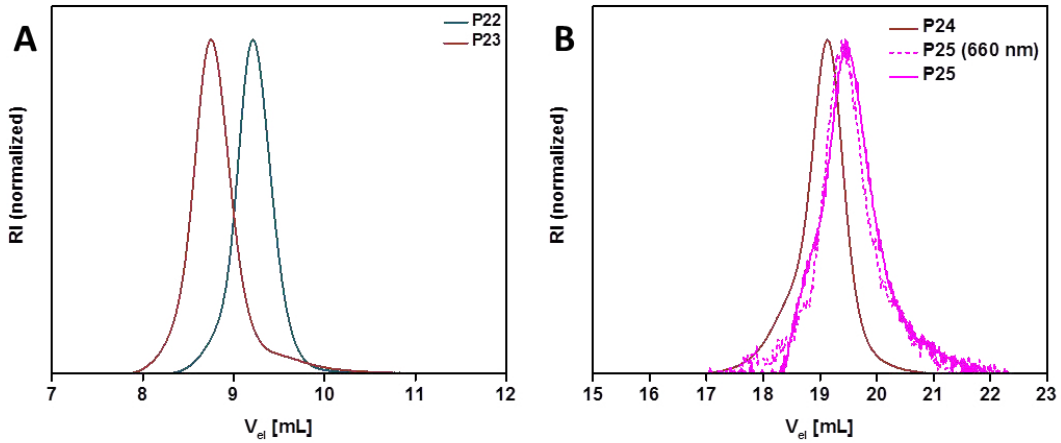

Figure 3.10. A: SEC traces ($CHCl_3$-*i*-PrOH-NEt_3 (94:2:4), PS-cal.) of preparation of P($EtOx_{98}$-*b*-$BocOx_{32}$) (**P23**) *via* the sequential monomer additon. B: SEC traces (DMAc + 0.21% LiCl, PS-cal.) of the Alexafluor 660 labeling P($EtOx_{98}$-*b*-$AmOx_{32}$) (**P24**) yielding P($EtOx_{98}$-*b*-[$AmOx_{31}$-*stat*-FOx_1]) (**P25**).

Additionally, by SEC measurements, the dispersity of the polymers was determined to be narrow (Đ < 1.1) (Table 3.6). After acidic deprotection, P($EtOx_{98}$-*b*-$AmOx_{32}$) (**P24**) was labeled with Alexafluor 660-NHS ester to obtain P($EtOx_{98}$-*b*-[$AmOx_{31}$-*stat*-FOx_1]) (**P25**). The success of the fluorescent labeling as well as the absence of unbound dye or polymer degradation was verified using SEC measurements. Looking at **P24**, after labeling, the RI as well as the UV/Vis trace of the labeled polymer (**P25**) is shifted to higher elution volumes (Figure 3.10B). Since the traces are still narrow and monomodal, a degradation of the polymer is unlikely. The Alexafluor-600 functionality rather altered the column interaction of the polymer.

Within this chapter, the synthesis of BocOx and BocOI was presented (Chapter 3.1). Furthermore, kinetic investigations on the homopolymerizations of BocOI as well as its copolymerization with EtOx, resulting in quasi block copolymers, was demonstrated. In addition to kinetic studies of these two monomers, also the copolymerization of BocOx and EtOx, as well as BocOx and MeOx was evaluated, revealing random and gradient copolymers (Chapter 3.2). Based on the kinetic investigations, a series of poly(urea) and P(Ox) containing homo and copolymers was synthesized and characterized (Chapter 3.3). Within the following chapter, the contribution of water-soluble P(Ox) homopolymers in terms of nanoparticle production will be discussed. Furthermore, the self-assembly of block copolymers will be presented.

4. P(Ox) containing nanostructures

Parts of this chapter have been published in: **P1**) M. N. Leiske, M. Hartlieb, F. H. Sobotta, R. M. Paulus, H. Görls, P. Bellstedt, U. S. Schubert, *Polym. Chem.* **2016**, *7*, 4924-4936. **P2**) M. N. Leiske, A.-K. Trützschler, S. Armoneit, P. Sungur, S. Hoeppener, M. Lehmann, A. Traeger, U. S. Schubert, *J. Mater. Chem. B.* **2017**, *5*, 9102-9113. **P3**) M. N. Leiske, F. H. Sobotta, F. Richter. S. Hoeppener, J. C. Brendel, A. Traeger, U. S. Schubert, *Biomacromolecules* **2018**, *19*, 748-760. **P4**) D. Hoelzer[‡], M. N. Leiske[‡], M. Hartlieb, T. Bus, D. Pretzel, S. Hoeppener, K. Kempe, R. Thierbach, U. S. Schubert, *Oncotarget* **2018**, in press. **P8**) M. Hartlieb[‡], T. Bus[‡], J. Kübel, D. Pretzel, S. Hoeppener, M. N. Leiske, K. Kempe, B. Dietzek, U. S. Schubert, *Bioconjugate Chem.* **2017**, *28*, 1229-1235. [‡]Equal contribution of both authors.

This chapter is dedicated to the utilization of P(Ox) based homopolymers and copolymers in the production of colloidal nanostructures. While the first part of the work focuses on the use of P(Ox) as cryoprotectant and its usage in the stabilization of polymeric nanoparticles, the second sub chapter describes the self-assembly of P(Ox) block copolymers. Here, amphiphilic block copolymers were self- and co-assembled in water in order to form mixed micelles. Furthermore, hydrophilic P(Ox) block copolymers were assembled in chloroform to obtain nanostructures with a cationic core. These nanostructures were cross-linked to obtain nanogels.

4.1. P(Ox) mediated nanoparticle stabilization

Nanomedicine represents one promising approach for the curing of various diseases, which require targeted drug uptake to lower unwanted side-effects.[1] The design and preparation of potent and safe drug carriers play a pivotal role in pharmaceutical, biomedical and chemical research, since nanocarriers offer possibilities of cell and organ specificity, *e.g.* by the introduction of targeting ligands. Furthermore, a minimization of side-effects can be achieved by the encapsulation and protection of the active pharmaceutical ingredient (API). Herein, water-insoluble polyesters, *i.e.* the Food and Drug Administration (FDA) approved poly(lactic-*co*-glycolic acid) (PLGA), are already used in numerous preclinical trials.[96] However, major obstacles regarding the utilization of nanoparticles are caused by their preparation,[97-99] purification or storage, respectively lyophilization.[100] In particular, the encapsulation of hydrophilic drugs is problematic, since it requires the emulsification method for nanoparticle preparation, and, consequently, the utilization of emulsifiers or surfactants.[101-102] Poly(vinyl alcohol) (Mowiol 8-88, PVA) and Pluronic F127 represent two important macromolecules, which are commonly used for nanoparticle stabilization during preparation,[101-102] while lyophilization is usually conducted using glucose, saccharose or trehalose as a cryo-protectant.[100-101, 103] In order to reduce the amount of substances being used for nanoparticle, an all-in-one system being suitable for the stabilization of hydrophobic nanoparticles during preparation, purification and lyophilization is envisioned.

4.1. P(Ox) mediated nanoparticle stabilization

The utilization of P(EtOx) or P(MeOx) could be beneficial, in particular in terms of elongated blood circulation times of nanoparticles, assuming that the surfactant is (partially) incorporated into the polymer shell during emulsification. The possibility to dissolve P(EtOx) and P(MeOx) in water as well as in various organic solvents[27] makes them ideal candidates for investigations on their properties regarding nanoparticle stabilization. For this reason, a small library of water-soluble homopolymers (Table 4.1) consisting of either $P(EtOx)_n$ or $P(MeOx)_n$ was synthesized accordingly to literature procedures.[48] The polymers were characterized utilizing ^{1}H-NMR to obtain information about the DP, which was determined to be 25, 60, 100 or 200 in case of both utilized monomers. Furthermore, SEC measurements were conducted to gain information about the polymer dispersity. With exception of **P35** (Đ = 1.38), all polymers revealed a narrow dispersity (Đ ≤ 1.2).

Table 4.1. Key properties of the synthesized P(Ox)s determined by [a] ^{1}H-NMR (300 MHz, $CDCl_3$) and [b]SEC (DMAc, 0.21% LiCl, PS-cal.). [c]SEC ($CHCl_3$-*i*-PrOH-NEt_3 (94:2:4), PS-cal.).

ID	Pre	Composition	NMR[a]		SEC[b]	
			DP	*Mn* [kg mol^{-1}]	*Mn* [kg mol^{-1}]	*Đ*
P26	-	$P(EtOx)_{25}$	25	2.5	6.3	1.09
P27	-	$P(EtOx)_{61}$	61	6.0	12.2	1.09
					7.0[c]	1.15[c]
P28	-	$P(EtOx)_{107}$	107	10.7	19.1	1.16
P29	-	$P(EtOx)_{184}$	184	18.4	25.3	1.21
P30	P27	$P(EtOx)_{61}$-NH_2	61	6.0	3.5[c]	1.14[c]
P31	P30	$P(EtOx)_{61}$-Rhodamine B	61	6.0	4.2[c]	1.13[c]
P32	-	$P(MeOx)_{25}$	25	2.1	5.3	1.09
P33	-	$P(MeOx)_{57}$	57	4.8	6.3	1.14
P34	-	$P(MeOx)_{98}$	98	8.3	18.0	1.19
P35	-	$P(MeOx)_{211}$	211	17.9	30.1	1.38
P36	-	$P(MeOx)_{57}$-NH_2	57	4.8	12.9	1.07
P37	P36	$P(MeOx)_{57}$-Rhodamine B	57	4.8	13.0	1.09

In order to visualize the P(Ox)s by confocal laser scanning microscopy (CLSM) measurements, homopolymers with a DP of 60 (**P27** and **P33**) were fluorescently labeled with rhodamine B. Two different approaches were used: (i) $P(EtOx)_{61}$ (**P27**) was reacted with ethylene diamine to obtain an ω-terminal amino functionality (**P30**) that can be used for labeling with rhodamine B sulfur chloride (**P31**). (ii) An amino ω-terminated $P(MeOx)_{57}$ was synthesized by quenching of the polymerization with ethylene diamine (**P36**) and, subsequently, reacted with rhodamine B sulfur chloride (**P37**). SEC measurements of all polymers (Figure 4.1) were conducted to prove the attachment of the dye to the polymer as well as the polymer stability and successful purification from excessive dye.

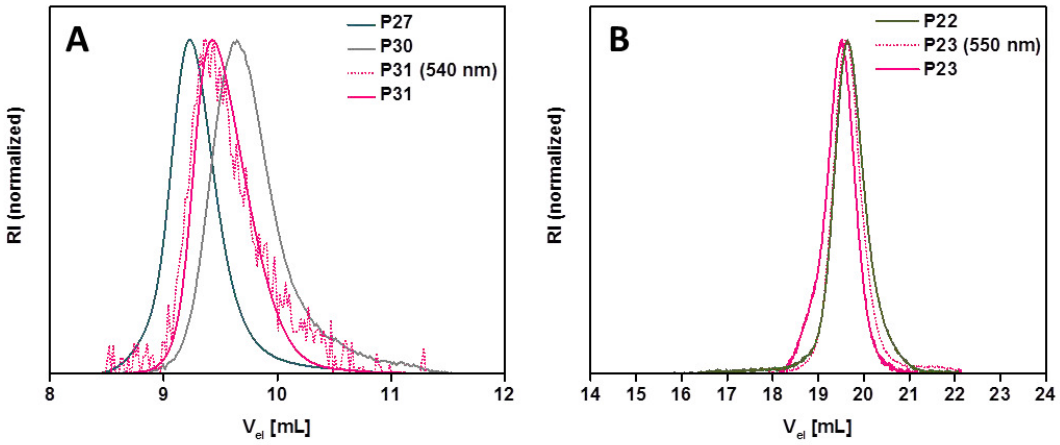

Figure 4.1. A: SEC traces ($CHCl_3$-*i*-PrOH-NEt_3 (94:2:4), PS-cal.) of the rhodamine B labeling of $P(EtOx)_{61}$ (**P27**). B: SEC traces (DMAc + 0.21% LiCl, PS-cal.) of the rhodamine B labeling of $P(MeOx)_{57}$ (**P36**).

For this purpose, the absorption of the labeled polymers at λ = 540 to 550 nm, which is corresponding to the rhodamine B label, was measured in addition to the RI. The traces of **P36** and **P37** perfectly overlap (Figure 4.1B), indicating successful polymer labeling. Looking at $P(EtOx)_{61}$ (**P27**), after labeling, the RI as well as the UV/Vis trace of the labeled polymer (**P30**) is shifted to higher elution volumes (Figure 4.1A). Since the traces are still narrow and monomodal, a degradation of the polymer is improbable. More likely, the rhodamine B ω-functionality altered the column interaction of the polymer on the chloroform based SEC. The labeling efficiencies of the polymers were not determined, as it was not of importance for the planned application as nanoparticle stabilizers. For this reason, both labeling strategies were defined to be of equal success.

After the polymer preparation, P(Ox)s were investigated regarding their ability for nanoparticle stabilization during the preparation of nanoparticles. Hereby, initial experiments were used for the comparison of $P(EtOx)_{61}$ (**P27**) and PVA, respectively Pluronic F127, at different concentrations. More precisely, aqueous solutions of different concentrations, *i.e.* 3, 5 and 10 wt%, of $P(EtOx)_{61}$ (**P27**) were prepared and utilized as stabilizer during emulsification. Nanoparticle characteristics were evaluated using dynamic light scattering (DLS) measurements and compared to nanoparticles produced with PVA or Pluronic F127 (Figure 4.2B). PVA and Pluronic F127 are already stabilizing the emulsion satisfyingly at a concentration of 3wt% resulting in small nanoparticles (d < 150 nm) with a narrow polydispersity index (PDI) lower than 0.2. By using **P27**, much higher surfactant concentrations are required to obtain nanoparticles (d ≈ 200 nm) with a comparable low PDI below 0.2. While Pluronic F127 as an amphiphilic ABA triblock copolymer with a hydrophobic inner block represents a classical emulsifier being able to intrinsically form micelles in aqueous solution,[104] PVA and **P27** do not have this segregation of blocks with different hydrophobicity. One possible explanation for the success of the homopolymers for nanoparticle stabilization might be attributed to their dynamic viscosity (Figure 4.2C). Aqueous PVA solutions of 3 wt% have a dynamic viscosity of 4.5 mPa s, while it is 2.5 mPa s for a 10 wt% solution of **P27**. For this reason, it is assumed that the dynamic viscosity of the polymer solution represents an important factor for the success of a polymer solution in terms

of nanoparticle stabilization. Another important factor might be the increased solubility of **P27** in water and organic solvents. This phenomenon is also known from PVA, which represents a very good emulsifier. With respect to PVA, the stabilization of the interphase between water and the organic droplet is achieved by a different solution behavior of the hydrophobic polymer backbone and the hydrophilic hydroxyl groups within the polymer side-chains.[105] In the case of P(Ox)s similar characteristics are determined, leading to an enhanced stabilization of the interphase and, consequently, a good stabilization of the emulsion (Figure 4.2A).

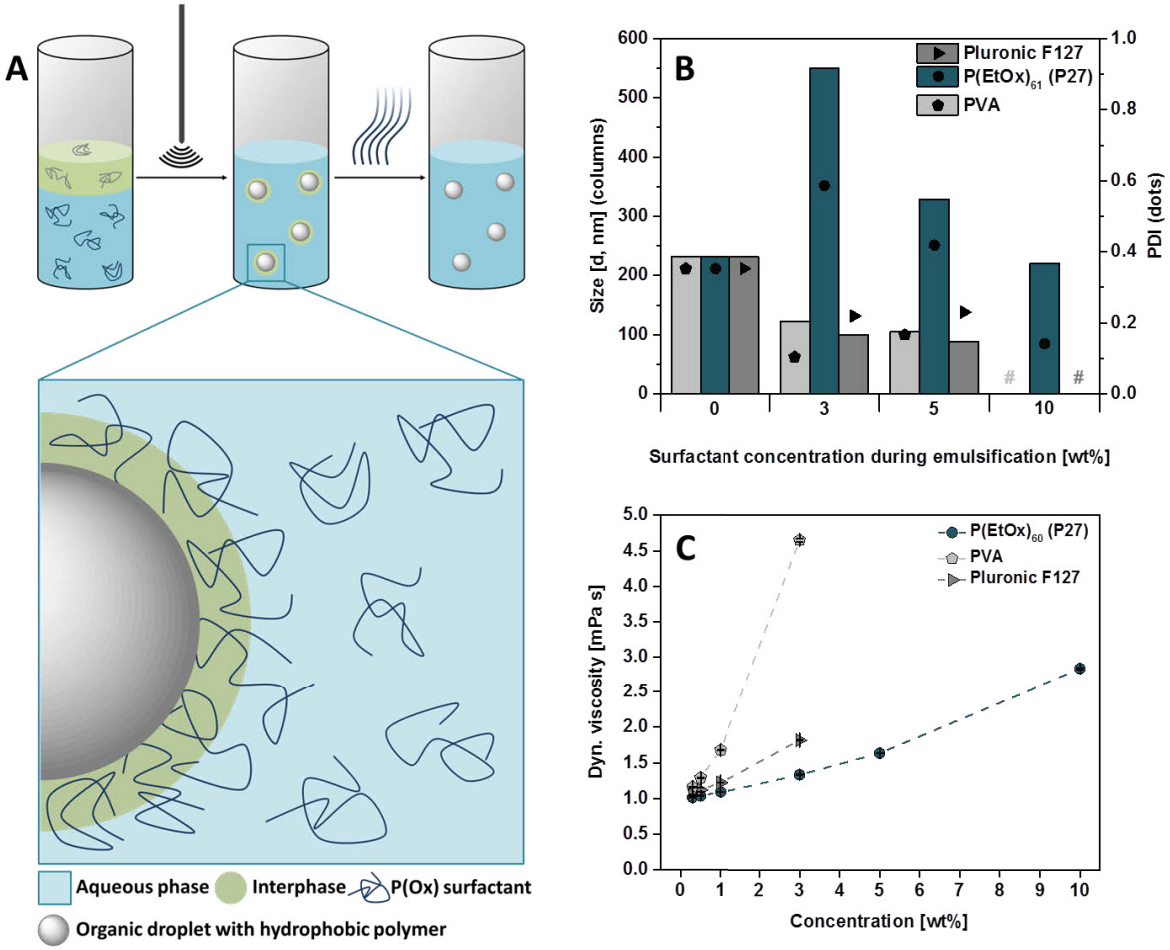

Figure 4.2. A: Schematic representation of the nanoparticle preparation *via* the nanoemulsion technique. A hydrophobic drug and the polymer are dissolved in a not water miscible organic solvent and water is added. Surfactants are added and the solution is emulsified by sonication. After evaporation of the organic solvent, nanoparticles are obtained. Magnification of the nanoparticle-aqueous phase boundary layer is presented, showing the potential behavior of polymer surfactants in the nanoemulsion process. B: Properties of PLGA nanoparticles prepared *via* the nanoemulsion technique (water and ethyl acetate), using different surfactants as determined by DLS measurements (n = 3, 5 measurements each). Hashes represent the position of non-investigated concentrations. C: Dynamic viscosity of aqueous surfactant solutions in dependence in the polymer concentrations.

After these prelimary investigations, further experiments concentrating on differences in the side-chain hydrophobicity and the DP of the utilized polymers were conducted. Hereby, $P(EtOx)_n$ (**P26** to **P29**) and $P(MeOx)_n$ (**P32** to **P35**) were used in a concentration of 10 wt% within the aqueous layer during emulsification. The resulting nanoparticles were characterized

by the mean of DLS measurements in terms of their size and PDI value (Figure 4.3A). P(Ox)s surfactants with a DP of 25 (**P26** and **P32**) did not lead to defined nanoparticles, however, large aggregates. P(Ox) with a DP of 60, 100 or 200 independent on the repeating unit were of equal quality in terms of size and PDI of the resulting nanoparticles. As it was assumed that the dynamic viscosity of the aqueous solution is an important factor for successful nanoparticle stabilization, this parameter was determined for all aqueous P(Ox) solutions (10 wt%) (Figure 4.3B).

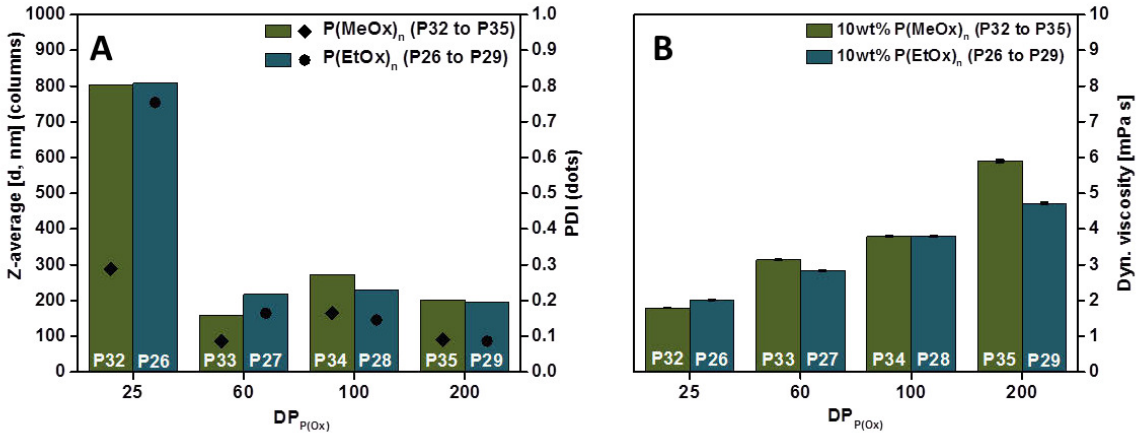

Figure 4.3. A: Characteristics of PLGA nanoparticles produced *via* the nanoemulsion technique (water and ethyl acetate) using different P(Ox)s as surfactants. The P(Ox) concentration during emulsification was 10 wt%. The samples were diluted 1:10 with ultra-pure water after emulsification. Z-average and PDI were determined using DLS measurements. B: Dynamic viscosity of P(Ox) (**P26** to **P29** and **P32** to **P35**) solutions with different DP.

As already known from other water soluble polymers, the dynamic viscosity of the solutions is dependent on the DP of the utilized polymers. P(Ox)s with a DP of 25 (**P26** and **P32**) exhibit a dynamic viscosity of ~2 mPa s, increasing in dependence on the DP of the polymers. Hereby, no significant differences caused by the polymer repeating unit are observable. In addition to the dynamic viscosity of the polymer solution, also the polymer length might influence the stabilization of the emulsion, due to a weaker stabilization of the interphase by shorter polymer chains.

After successful investigations of the particle stabilization during preparation, lyophilization experiments were conducted to test whether hydrophilic P(Ox)s can also be used as suitable cryoprotectants. Since the surfactant experiments revealed no significant advantages of P(Ox)s of a DP of 100 or 200 compared to DP 60, initial lyophilization experiments were performed using $P(EtOx)_{61}$ (**P27**) in comparison to the commonly utilized sugars trehalose, saccharose and glucose.[100-101, 103]

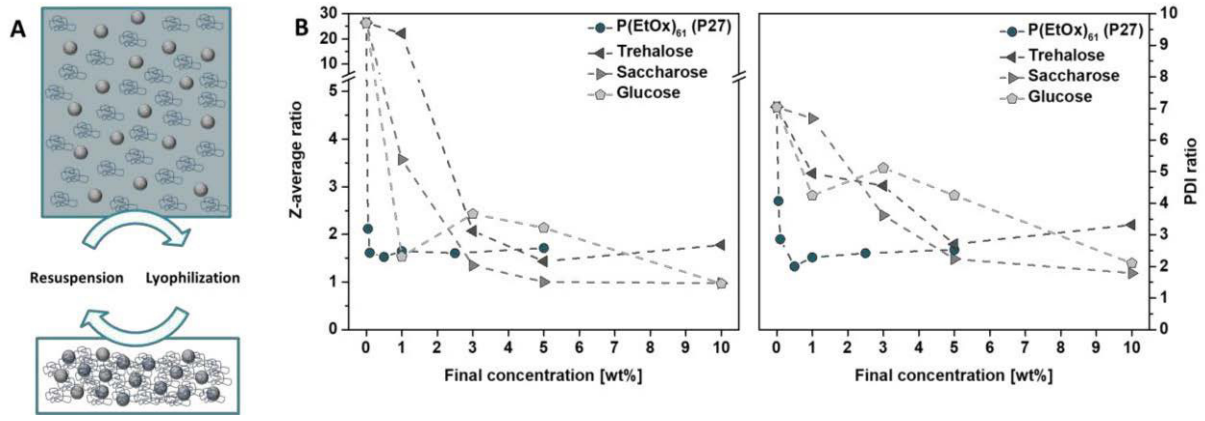

Figure 4.4. A: Schematic representation of the lyophilization and resuspension of polymeric nanoparticles using P(Ox)s as suitable particle stabilizers (cryoprotectants). B: Properties of the lyophilized PLGA nanoparticles using different cryoprotectants at various concentrations. Diameter size ratios of the z-average and PDI ratios were determined by DLS investigations (n = 3, 5 measurements each). Ratios were calculated using equation (4.1) and (4.2).

Here, PLGA nanoparticles were prepared *via* the nanoprecipitation technique without any particle stabilizers. After evaporation of the organic water miscible solvent (acetone), size and PDI of the nanoparticles were determined by DLS measurements. Subsequently, a specific amount of a cryoprotectant was added to the nanoparticle suspension and lyophilization was conducted (Figure 4.4A). Then, the nanoparticles were resuspended in water and characterized by DLS. Z-average ratios (Figure 4.4B) as well as PDI ratios (Figure 4.4C) were calculated using equations (4.1) and (4.2).

$$z-average\ ratio = \frac{z\text{–}average\ after\ lyophilization}{z\text{–}average\ after\ preparation} \tag{4.1}$$

$$PDI\ ratio = \frac{PDI\ after\ lyophilization}{PDI\ after\ preparation} \tag{4.2}$$

Herein, size and PDI ratios of a value of 1 are favorable, indicating no significant changes regarding the nanoparticle characteristics. At very high concentrations of 10 wt% saccharose revealed the best performance (size ratio = 1.0; PDI ratio = 1.8), while Glucose (size ratio = 1.0; PDI ratio = 2.1) and trehalose (size ratio = 1.4, PDI ratio = 2.7) are slightly more unfavorable than saccharose. Possible ranges of **P27** utilized as a cryoprotectant are 0.1 to 5 wt%, *i.e.* 0.5 wt% was determined to be an ideal polymer concentration with regard to the nanoparticle characteristics (size ratio = 1.2; PDI ratio = 2.0). The slight increase in size can be attributed to the polymers that assemble on the nanoparticle surface and, consequently enlarge the hydrodynamic diameter. Hence, at this certain, low cryoprotectant concentration, **P33** is superior to the investigated sugars. Furthermore, sugars are required in 20-fold concentration to achieve comparable results.

After that, the library of water soluble P(EtOx)$_n$ (**P26** to **P29**) and P(MeOx)$_n$ (**P32** to **P35**) was investigated in terms of cryoprotectant applications (Figure 4.5). Herein, the tested polymers revealed similar results as in the surfactant experiments. P(Ox)s with a DP of 25 (**P26** and **P32**) were determined not to be suitable as a cryoprotectant (PDI ratio > 3), while P(Ox)s with a DP of 60 (**P27** and **P33**), 100 (**P28** and **P34**) or 200 (**P29** and **P35**) showed

similar results (size ratio ≈ 1; PDI ratio ≤ 2). For this reason, **P27** and **P33** were used for further investigations.

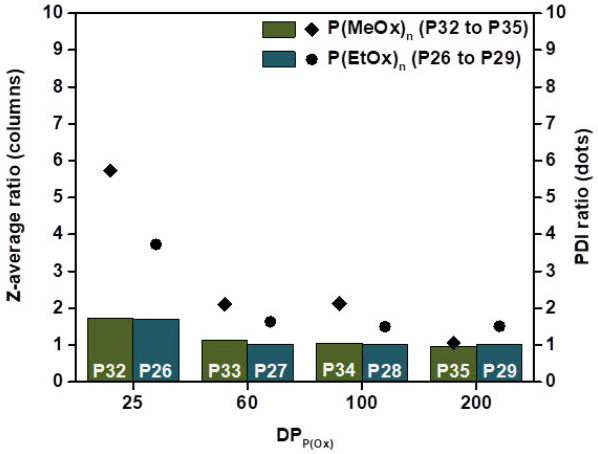

Figure 4.5. Z-average (columns) and PDI (dots) ratios of PLGA nanoparticles prepared by the nanoprecipitation technique (water and acetone) using 0.3 wt% P(Ox). The particles were lyophilized without further purification and the ratios were calculated by using equation (4.1) and (4.2) (n = 3, 5 measurements each).

After successful investigations of P(Ox)s in terms of their suitability to act as surfactants during nanoparticle preparation or cryoprotectants during lyophilization, they were examined regarding their influence on successful nanoparticle purification. For this reason, PLGA nanoparticles were produced *via* nanoprecipitation (water and acetone) by using an 0.3 wt% solution of either **P27** or **P33** as the aqueous phase. After evaporation of the organic solvent, the size (d = 190 nm) and PDI (<0.1) of the resulting nanoparticles was determined using DLS measurements. Subsequently, the nanoparticles were purified by either centrifugation, which is important to separate the nanoparticles from small dissolved molecules, or syringe filtration, which can be used to purify nanoparticles from larger aggregates. Prior to lyophilization nanoparticles were resuspended in either water or a 0.5 wt% P(Ox)s solution. DLS measurements of the lyophilized P(Ox)s provided information about their uniformity, while cryoTEM measurements were utilized to visualize the particle morphology (Figure 4.6).

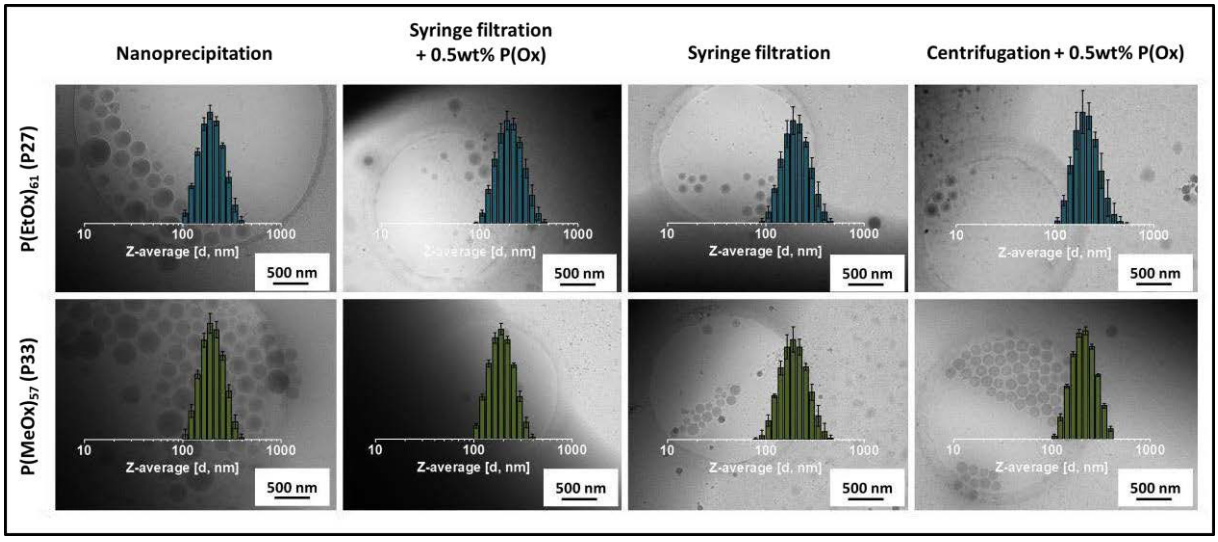

Figure 4.6. Influence of various purification techniques on the size distribution and morphology of PLGA nanoparticles that were prepared by nanoprecipitation, determined by DLS (columns, n = 3, 5 measurements each) and cryoTEM measurements.

With regard to the analytical results, syringe filtration represents a suitable purification method for PLGA nanoparticles prepared using P(Ox)s as particle stabilizers, resulting in small nanoparticles (d ≈ 200 nm; PDI < 0.1). According to cryoTEM measurements, the resulting nanoparticles were well-defined and only few aggregates could be detected.
By using centrifugation as a purification method for polymeric nanoparticles, strong forces are exerted to the particles. Furthermore, it is possible that the water soluble P(Ox)s are separated from the nanoparticles during the centrifugation process. To test this possibility, the supernatant of the centrifuged nanoparticles was discarded and they were resuspended in either water or a 0.5 wt% P(Ox)s solution. DLS measurements of nanoparticles resuspended in water revealed strong aggregation, proving the assumption of a separation of the surfactant and the particle. However, a resuspension in a 0.5 wt% P(Ox)s solution resulted in narrow disperse, well-defined nanoparticles.
To further prove this assumption, the rhodamine B labeled P(Ox)s **P31** and **P37** were used in a similar centrifugation experiment to determine the residual amount of P(Ox) within the nanoparticle suspension. The nanoparticles were characterized by DLS and UV/vis measurements (Figure 4.7A). Hereby, the amount of P(Ox) in solution was determined by the utilization of a Rhodamine B calibration. Nanoparticles that were resuspended in a 0.5 wt% P(Ox) solution contained a 10-fold amount of P(Ox) compared to the nanoparticles, resuspended in water. This low amount of stabilizer led to nanoparticle aggregation, while nanoparticles that were resuspended in a P(Ox) solution are still well-defined. To further illustrate the interaction of the surfactant with the hydrophobic nanoparticles, microparticles were produced using the rhodamine B labeled $P(MeOx)_{57}$ (**P37**) as surfactant. The microparticles were characterized using CLSM measurements (Figure 4.7B), showing a clear fluorescent corona and, hence, verifying the assumption of a strong interaction of the P(Ox) surfactant with the nanoparticle surface.

A

$P(EtOx)_{61}$-Rhodamine B (P31)		
After preparation *via* nanoprecipitation		
Z-average [d, nm]	132.1 ± 0.4	134.0 ± 1.3
PDI	0.096 ± 0.002	0.093 ± 0.017
Lyophilized		
	Centrifugation + ultra-pure water	*Centrifugation + 0.5wt% P(Ox)*
Z-average [d, nm]	n.a.	175.5 ± 4.5
PDI	n.a.	0.273 ± 0.019
P(Ox) [mg][a]	0.7	4.6
$P(MeOx)_{57}$-Rhodamine B (P37)		
After preparation *via* nanoprecipitation		
Z-average [d, nm]	193.8 ± 2.0	190.6 ± 2.3
PDI	0.090 ± 0.038	0.072 ± 0.021
Lyophilized		
	Centrifugation + ultra-pure water	*Centrifugation + 0.5wt% P(Ox)*
Z-average [d, nm]	n.a.	182.7 ± 21.7
PDI	n.a.	0.192 ± 0.062
P(Ox) [mg][a]	0.0	4.0

B

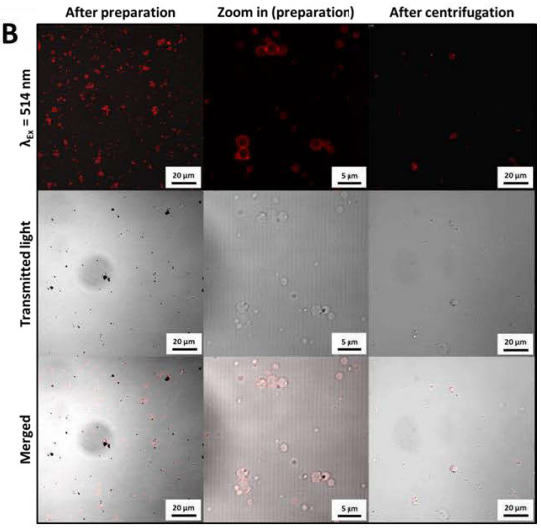

Figure 4.7. Characteristics of the PLGA nanoparticles prepared by nanoprecipitation (water and acetone) using rhodamine B labeled $P(EtOx)_{61}$ as the surfactant. A: Z-average and PDI values were determined *via* DLS measurements. [a]Calculated from UV/Vis absorption measurements at λ_{Ex} = 630 nm. n. a.: not available because of particle aggregation. B: CLSM (λ_{Ex} = 514 nm, λ_{Em} = 531 to 704 nm) of PLGA microparticles prepared by microemulsion (water and dichloromethane) using $P(MeOx)_{57}$-Rhodamine B (**P37**) as surfactant.

Within this study, it could be shown that water soluble P(Ox)s, *i.e.* P(EtOx) and P(MeOx) are utilizable for the stabilization of hydrophobic PLGA nanoparticles. Furthermore, the stabilization of poly(methacrylate) based nanoparticles could be demonstrated (data not shown). Hereby, a minimum DP of 60 was necessary to obtain reproducible and satisfying results during preparation, purification and lyophilization. Hence, an all in one system usable for further applications could be invented.

4.2. Self-assembly of P(Ox) block copolymers

In addition to P(Ox) mediated nanoparticle stabilization, the self-assembly of different block copolymers was investigated. Hence, this subchapter is dedicated to the preparation of polymer colloids consisting of different block copolymers. The resulting nanostructures can be utilized to facilitate the transport of genetic material (Chapter 5) or APIs (Chapter 6).
Firstly, poly(urea) containing quasi block copolymers were assembled in water. Herein, polymers with 28 wt% poly(urea) were found to form very uniform nanostructures accordingly to DLS measurements (d = 297 ±8 nm; PDI = 0.020 ± 0.015; Figure 4.8A). Cryo transmission electron-microscopy (cryoTEM) measurements were conducted to confirm the results obtained by DLS (Figure 4.8A), revealing brush-like spherical structures (Figure 4.8B). It is assumable that the investigated polymers form strong hydrogen bonds in water and, for that reason, self-assemble. However, due to lack of accessible functionalities, the prepared nanostructures could not be used for the complexation of genetic material or the conjugation of an API and were, consequently, not further elucidated within this thesis.

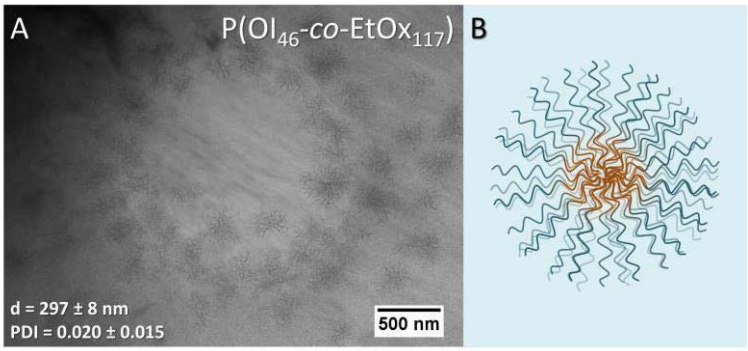

Figure 4.8. Self-assembly of quasi block copolymers consisting of poly(urea) and (PEtOx) ($P(OI_{46}$-*co*-$EtOx_{117})$). A: cryoTEM image. B: Schematic representation of hydrogen bond stabilized nanostructures.

Furthermore, cationic P(Ox) nanostructures were prepared by self- and co-assembly of AmOx and EtOx containing amphiphilic block copolymers. The utilization of these nanostructures as polymeric vectors for the transfection of cells will be further discussed in Chapter 5. For the successful complexation of genetic material and polymers, cationic charges are indispensable. However, they are also known to force membrane disruption.[106] In fact, a shielding of the cationic charges, *e.g.* by EtOx, can reduce membrane disruption by shielding of the cationic charges.[107] For this reason, pH responsive system, in which the cationic charges are shielded at a physiological pH value of 7.4, while they stretch after protonation at lower endolysosomal pH values of 5 to trigger the endosomal release, was aimed. In order to access

functional P(Ox) based nanostructures, two different block copolymers with NonOx representing the hydrophobic block were synthesized. Herein, the hydrophilic block of the macromolecules consisted of either AmOx (**P39**), which allows polyplex formation of the resulting nanostructure, or EtOx (**P38**) to mediate stealth effect and enhanced cytocompatibility. Block copolymers were prepared and deprotected accordingly to copolymer synthesis described in Chapter 3.3. The polymers were characterized using ^{1}H-NMR for determination of the block ratios as well as using SEC to gain insight about the dispersity (Table 4.2). In both polymers, the DP of NonOx was kept similar, leading to different weight ratios of the hydrophobic and the hydrophilic block. P(EtOx$_{155}$-*b*-NonOx$_{76}$ (**P38**) consisted 55 wt% NonOx, leading to a favorable assembly into worm-like structures,[60] while the cationic block copolymer P(NonOx$_{52}$-*b*-AmOx$_{184}$ (**P39**) contained 28 wt% NonOx, favorably leading to spherical micelles during the assembly process.

Table 4.2. Key properties of the synthesized polymers. [a]SEC (eluent: DMAc, 0.21% LiCl; PS-standard); [b] ^{1}H-NMR (300 MHz). [c]Calculated from Boc-protected precursor polymer). [e]SEC (eluent: 0.1 M NaCl$_{(aq)}$ + 0.3% TFA; P2VP-standard).

ID	Composition	NMR			SEC		
		DP	*Wt% (EtOx/AmOx)*	*Wt% (NonOx)*	*Mn [kg mol^{-1}]*	*Mn [kg mol^{-1}]*	*Đ*
P38	P(EtOx$_{155}$-*b*-NonOx$_{76}$)	231	45	55	30.4	38.3	1.14
P39	P(NonOx$_{52}$-*b*-AmOx$_{184}$)	236[c]	72[c]	28[c]	36.4	24.3	1.26

In order to obtain polymeric micelles which express high transfection efficiencies in combination with an enhanced cytocompatibility, mixed micelles were prepared. For the preparation of the nanostructures, the polymers were mixed in different ratios prior to assembly to obtain nanostructures with 0, 20, 40, 60, 80 or 100% of the cationic polymer (**P39**) within the shell. Final nanostructures were prepared in 0.9 wt% NaCl representing physiological salt concentrations.

Preliminary characterization of the nanostructures was conducted by means of DLS measurements to obtain information about the size and uniformity of the micelles (Figure 4.9A). Interestingly, all nanostructures containing at least 20 wt% **P38** are significantly larger (d = 80 to 100 nm) than the nanostructures consisting of 100 wt% **P39** (d = 60 nm). Furthermore, the PDI of the micelles was also shown to be dependent on the ratio of polymers used for preparation, slightly increasing from 0.2 to 0.3 with increasing amount of cationic polymers.

Additionally, cryoTEM measurements were performed to obtain information about the shape of the produced nanostructures (Figure 4.9B). Micelles that did not contain cationic copolymer were determined to be rod- or sheet-like, whereas darker rods are presumably sheets with a parallel orientation with respect to the electron beam. Previously, rod-like structures from ABA triblock copolymers with NonOx representing the hydrophobic inner and MeOx as the hydrophilic outer blocks have been reported.[60]

Nanostructures consisting of the cationic block copolymer (**P39**) were found to be spherical. More interestingly, all mixed micelles showed a rod-like shape regarding the cryoTEM measurements. For this reason, it is quite likely that the prepared nanostructures are mixed micelles instead of two different species present. Furthermore, the shape was determined to by dependent on the polymer ratios within the nanostructures as shown in Figure 4.9C.

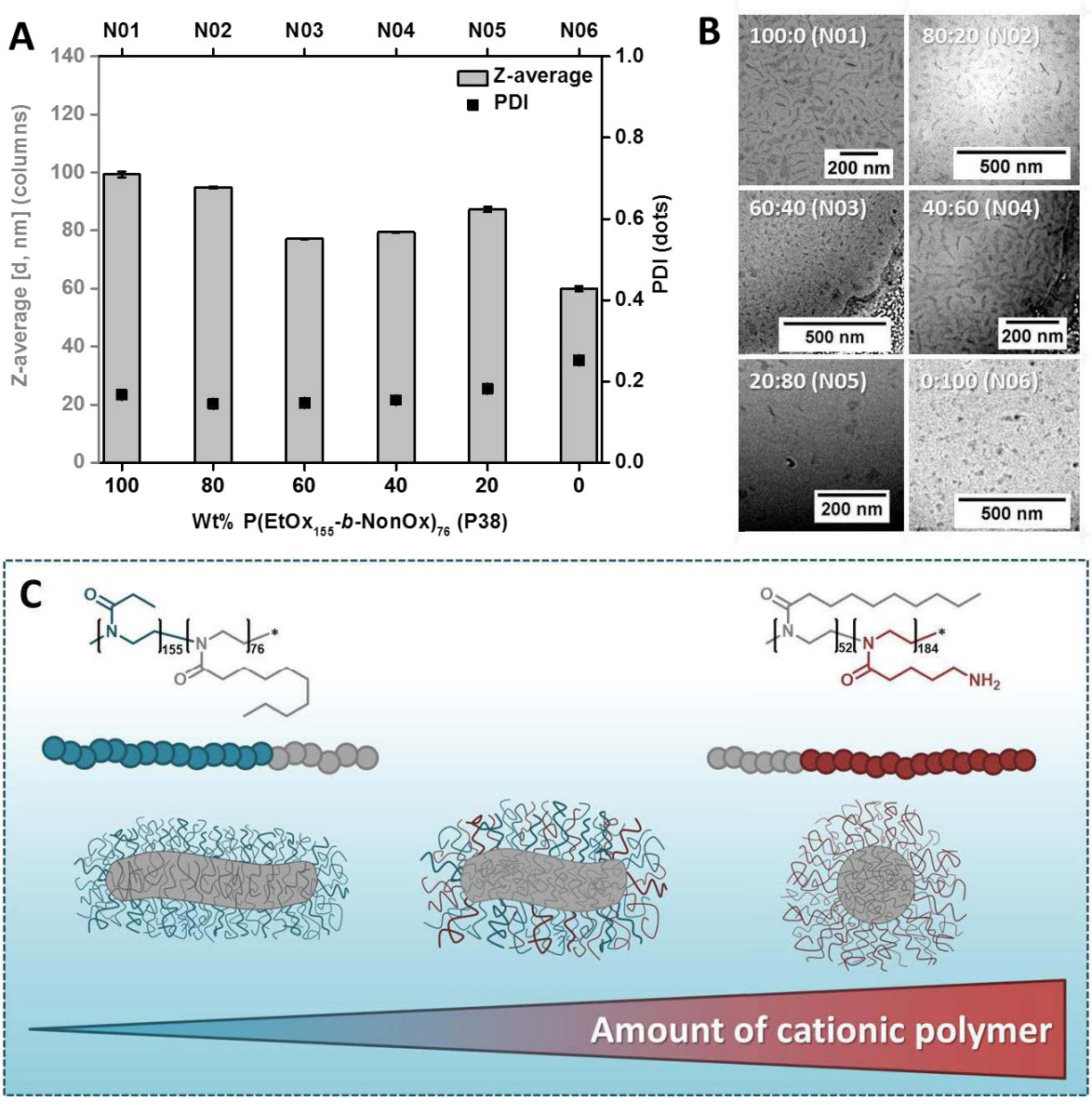

Figure 4.9. A: Z-average and PDI values of the prepared nanostructures (**N01** to **N06**) in 0.9 wt% NaCl determined by DLS. B: Zoom-in cryoTEM images of **N01** to **N06** in 0.9 wt% NaCl. Ratios describe the mass ratios of **P38** and **P39** being used during nanostructure preparation. C: Schematic representation of the obtained shapes of the nanostructures dependent on the used block copolymers **P38** and **P39** in different ratios. Blue: EtOx. Grey: NonOx. Red: AmOx.

Due to the fact that the stability of a polymeric micelle is dependent on its concentration within the aqueous medium, the critical micelle concentration (CMC) was determined using the pyrene method (Table 4.3).[108] Hereby, nanostructures with 60 to 100 wt% P($EtOx_{155}$-*b*-$NonOx_{76}$) (**P38**) (**N01** to **N03**) revealed a CMC of 2×10^{-7} M, while it slightly increased for nanostructures of 0 to 40 wt% **P38** (**N04** to **N06**, 1×10^{-7} M). These values comply with similar systems consisting of block copolymers containing MeOx and NonOx, where CMCs between 10^{-6} M and 10^{-5} M have been reported.[58-59, 109]

Table 4.3. Key properties of nanostructures **N01** to **N06**. CMC of the nanostructures **N01** to **N06** in 0.9 wt% NaCl determined by the pyrene method. For calibration of the CMC, the fluorescence intensity at λ_{Em} = 390.0 nm while exciting at λ_{Ex} = 338.0 nm was divided by the fluorescence intensity at λ_{Em} = 390.0 nm while exciting at λ_{Ex} = 332.5 nm and is plotted against the log of the polymer concentration. [a]The average molar mass of the polymers was calculated from the molar masses of **P38** and **P39**.

Nanostructure	Wt% P(EtOx$_{155}$-*b*-NonOx$_{76}$) (P38)	Wt% P(NonOx$_{52}$-*b*-AmOx$_{184}$) (P39)	M[a] [kg mol^{-1}]	CMC [µg mL^{-1}]	CMC [mol L^{-1}]
N01	100	0	30.3	8.3	2.7×10^{-7}
N02	80	20	31.5	7.3	2.3×10^{-7}
N03	60	40	32.7	6.8	2.2×10^{-7}
N04	40	60	34.0	36.6	1.1×10^{-6}
N05	20	80	35.2	45.2	1.3×10^{-6}
N06	0	100	36.4	35.5	9.8×10^{-7}

In order to obtain information about the pH-responsiveness of the prepared nanostructures **N01** to **N06** DLS measurements at different pH values ranging from 4 to 8 were conducted and the change in the hydrodynamic diameter was calculated by division of the obtained size at a distinct pH value by either the size measured at pH = 4 (Figure 4.10B) or pH = 7 (Figure 4.10C). As already assumed, an increasing pH value led to shrinkage of the hydrodynamic diameter, which is dependent on the amount of cationic **P39** within the shell. Nanostructures consisting only of **P38** were determined to be not pH responsive, as already supposed by the absence of amino groups in the shell (Figure 4.10B). In contrast, nanostructures containing 100 wt% of the cationic **P39** shrink to a hydrodynamic diameter of 80% at a pH value of 7 compared to 4. Less pronounced shrinkages of the mixed micelles with a high amino content are attributed to the participation of the non pH-responsive units within the shell. For this reason, it is assumed that the cationic charges can be shielded by the EtOx units in physiological media, such as the blood stream.

Calculations representing the endolysosomal acidification down to a pH value of 5 showed an increase of the hydrodynamic diameter up to 130%, possibly caused by the increased charge density of the AmOx units within the micellar shell, which further cause a stretching of the polymer chains and might help to force endosomal disruption as well as a release of micelleplexes. Stable PDI values verified the stability of the nanostructures at different pH values and, consequently, changes in die size are attributed to a collapsing, respectively stretching of the cationic blocks of the micellar shell.

Due to the fact that the prepared nanostructures showed favorable characteristics for the complexation, transport and endosomal release of genetic material, they will be further evaluated regarding their biocompatibility, cellular uptake and transfection efficiency in Chapter 5.

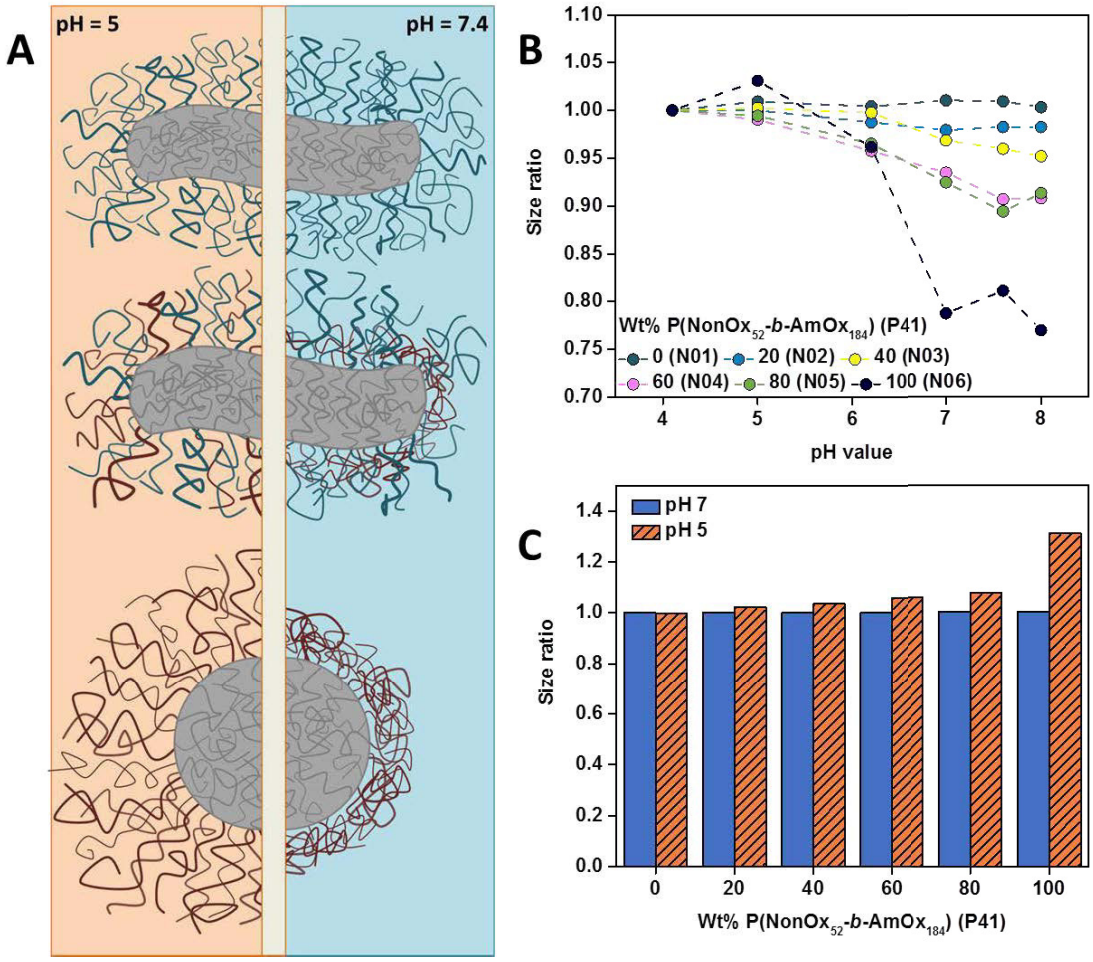

Figure 4.10. A: Schematic representation of the changes in size of the mixed micelles induced by changes in the pH value. Grey represents NonOn, blue represents EtOx, and red represents the cationic AmOx block. B: Size ratios of the nanostructure dependency on the pH value (calculated by the division of the z-average at distinct pH values by the z-average at a pH value of 4). C: Size ratios at pH values of 5 and 7 (calculated by the division of the pH value of 5 by the pH value of 7).

As shown the previous paragraph, self-assembled structures possess a CMC which might be disadvantageous for *in vivo* applications, *i.e.* in terms of drug delivery applications. For this reason, covalent core cross-linkage of assembled structures in combination with the covalent loading of an API might be useful. In order to prepare core-crosslinked nanostructures, water soluble block copolymers consisting of EtOx and AmOx (**P24** and **P25**, Chapter 3.3) were utilized (Table 4.4).

Table 4.4. Composition and analytical data of **P24** and **P25**. [a] ^{1}H-NMR in D_2O.

ID	Pre	Composition	NMR[a]			
			DP	*Wt% (EtOx)*	*Wt% (AmOx)*	*Mn [kg mol^{-1}]*
P24	P23	P(EtOx$_{98}$-*b*-AmOx$_{32}$)	130[b]	68[b]	32[b]	14.2[b]
P25	P24	P(EtOx$_{98}$-*b*-[AmOx$_{31}$-*stat*-FOx$_1$])	130[b]	63[b]	37[b]	15.3[b]

Nanogels of **P24** and **P25** were prepared by dissolving the block copolymers in chloroform, which is an inappropriate solvent for the cationic AmOx block and, consequently, induces self-assembly of the block copolymers caused by a phase segregation of the AmOx block.

Nanogels were subsequently core crosslinked by the addition of glutaraldehyde (GA),[57] leading to the formation of pH-responsive imine bonds.[110] Hereby, excessive aldehyde groups could be quenched by the addition of an amino group containing small molecule, such as 6-amino fluorescein (6AF) or Doxorubicin (DOX) (Scheme 4.1).

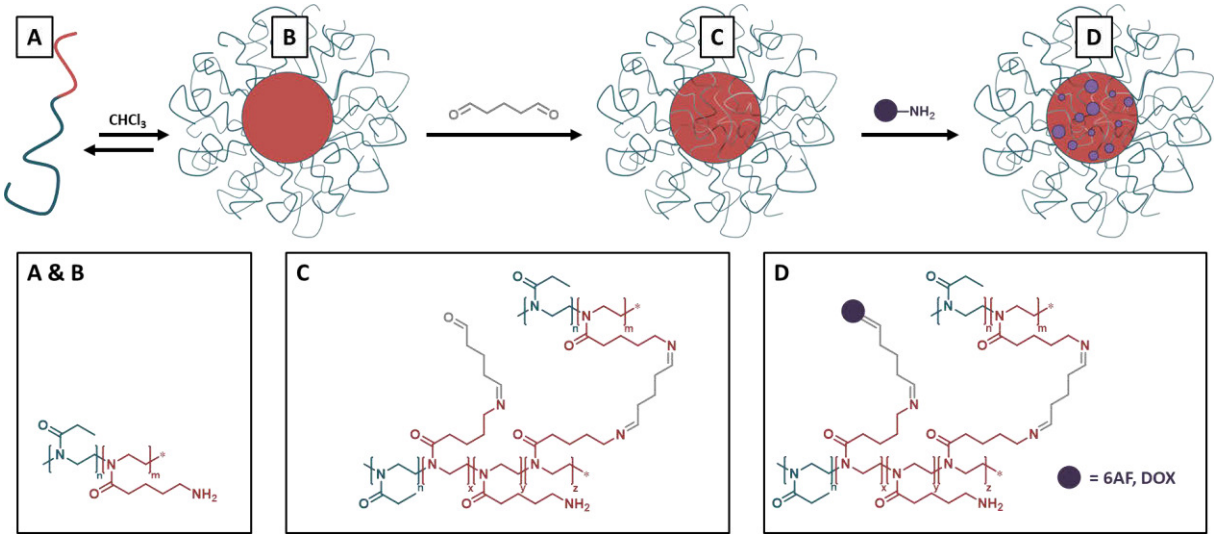

Scheme 4.1. Schematic representation of the preparation of core crosslinked nanogels. A: P($EtOx_n$-*b*-$AmOx_n$). B: Reversible self-assembly in $CHCl_3$. C: Core crosslinking by the utilization of GA. D: Quenching of excessive aldehyde groups using 6AF or DOX.

In this manner, a reversible covalent attachment of the dye, respectively drug to the micelle core could be accomplished. By variation of the GA amount added for crosslinking, the characteristics of the resulting nanostructures could be slightly altered (Table 4.5). Higher amounts of GA lead to nanostructures with an increased size as determined by DLS and cryoTEM as well as a lowered, however, positive zeta potential according to electrophoretic light scattering (ELS) measurements. The positive zeta potential might be beneficial for cellular uptake, caused by an enhanced interaction of the negatively charged cell membrane. Results of the uptake studies will be discussed in Chapter 6. The loading efficiency of the cargo could be determined using UV/via measurements and was found to be 17 to 24 wt% in the case of 6AF and 6 wt% in the case of DOX. Bioassays investigating the nanogels will be part of Chapter 6.

The most important requirement for a drug carrier is the site specific release of the drug. As cargo molecules within the produced nanogels are attached *via* imine bonds, which are known to be reversible at pH values below 7, a release within endosomal or lysosomal cellular compartments is likely as previously shown by M. Hruby and co-workers.[35] In order to investigate the stability of the nanogels at 4 °C (storage temperature) and 37 °C (human body temperature) at a pH value of 7.4, the z-average and the PDI as well as the number mean size value of the DOX-nanogels (**N12**) was evaluated using DLS measurements (Figure 4.11A).

Table 4.5. Characterization of P(Ox) nanogels in an aqueous environment.

ID	Pre		DLS	ELS	UV/vis	cryoTEM
		Equiv. GA (per 2 NH_2)	*Size [d, nm]*	*ζ [mV]*	*6AF[a]/DOX[b] [wt%]*	*Size [d, nm]*
N07	P31	1	26	+28	17[a]	24
N08	P31	1.5	34	+13	27[a]	26
N09	P31	2	40	+10	20[a]	28
N10	P31	2.5	44	+8	24[a]	30
N11	P31	3	48	+8	17[a]	30
N12	P32	3	30	+25	6[b]	30

DOX-nanogels (**N12**) were determined to be stable during the entire measurement time of two weeks, revealing no significant changes in size or PDI. Furthermore, it was necessary to determine the possibility of a drug release at a lysosomal pH value of 5. J. S. Basuki *et al.* previously investigated iron oxide nanoparticles that were loaded with DOX *via* pH sensitive imine bonds *via* DLS measurements, revealing an increase in the particle size at a pH value of 5, caused by drug release.[111] Since glycine was determined to be essential for cancer cell proliferation and, consequently, is present within tumorous compartments,[112] DLS investigations of the DOX-nanogels (**N12**) were conducted in phosphate buffered saline (PBS) and glycine was added representing a competitive amine to the imine bond (Figure 4.11B and C). While DOX-nanogels (**N12**) did not reveal significant changes in size or PDI at a pH value of 7.4, both increase at a pH value of 5.0. Herein, it is noteworthy that after a second addition of glycine, this trend further increases. This might be beneficial for triggering the endosomal burst, similarly to pH responsive P(Ox) micelles (**N02** to **N06**), described previously within this chapter. In order to obtain additional qualitative information about the release of DOX from the DOX-nanogel (**N12**), diffusion order spectroscopy (DOSY) NMR measurements were also conducted (data not shown). Hereby, the diffusion coefficients of labeled DOX-nanogels in NaCl were compared to DOX-nanogels (**N12**) in 150 mM PBS (pH = 5.0), which contained glycine. Pure DOX and glycine were evaluated for comparison. A stacking of the spectra suggests the release of DOX at pH 5.0, while no DOX release could be determined in NaCl. Unfortunately, a quantification of the DOX release from the labeled DOX-nanogels was not possible by the applied methods.

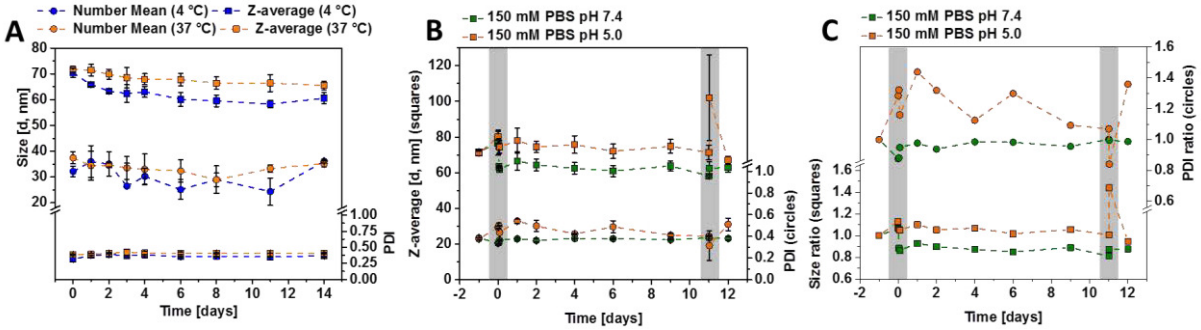

Figure 4.11. Properties of labeled DOX-nanogels determined by DLS measurements. A: Nanogels were incubated in 150 mM PBS (pH = 7.4) at indicated temperatures for a certain time. The measurements were conducted at the indicated temperatures. PDI is derived from the z-average. B and C: Nanogels were incubated at 37 °C in indicated buffers for a certain time. Measurements were conducted at 37 °C. Grey boxes indicate time points of the addition of 100 mmol Glycine. A: Actual values obtained by DLS measurements (n = 3, three measurements each). B: Size and PDI ratios calculated by division of the value obtained on a certain day by the initial value (day -1).

4.2. Self-assembly of P(Ox) block copolymers

Within this chapter, the contribution of different P(Ox)s in terms of nanoparticle formation and self-assembly was presented (Scheme 4.2). Whereas water-soluble P(Ox)s can mediate the stabilization of hydrophobic nanoparticles, such as PLGA or poly(methacrylate)s (Chapter 4.1), amphiphilic block copolymers revealed spherical or worm-like micelle formation in aqueous media (Chapter 4.2). Furthermore, poly(urea) containing polymers formed hydrogen bond-stabilized nanostructures after assembly in water. Water-soluble cationic block copolymers were assembled in chloroform and could be successfully core crosslinked *via* pH-responsive Schiff-base chemistry.

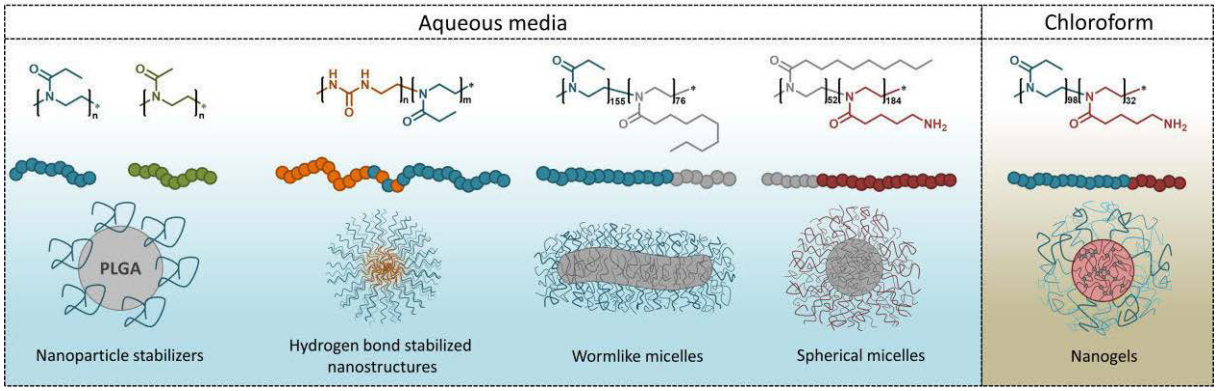

Scheme 4.2. Schematic representation of different P(Ox) containing nanostructures assembled in aqueous media or chloroform. Cyan: EtOx. Green: MeOx. Orange: Urea. Grey: NonOx/PLGA. Red: AmOx.

Whereas this chapter was dedicated to die preparation and characterization of different P(Ox) bases nanostructures, within the following two chapters the application of selected nanoassemblies in terms of gene- and drug-delivery will be presented. Firstly, pH responsive micelles will be compared to water soluble cationic P(Ox) as vectors for gene-delivery applications.

5. Gene delivery systems

Parts of this chapter have been published in: **P3**) M. N. Leiske, F. H. Sobotta, F. Richter. S. Hoeppener, J. C. Brendel, A. Traeger, U. S. Schubert, *Biomacromolecules* **2018**, *19*, 748-760. **P5**) D. Hertz[‡], M. N. Leiske[‡], T. Wloka, A. Traeger, M. Hartlieb, M. M. Kessels, S. Schubert, B. Qualmann, U. S. Schubert, *J. Polym. Sci., Part A: Polym. Chem.* **2018**, in press. DOI: 10.1002/pola.29000. [‡]Equal contribution of both authors.

Besides lipoplexes, also cationic polymers are used for gene delivery, since they are capable of forming polyplexes with the negatively charged phosphate backbone of nucleic acids. Poly(ethylene imine) (PEI) is one of the most commonly used materials for gene delivery applications and for a long time it was claimed to be the gold standard for the transfection of genetic material.[113] Its high charge density leads to the formation of physiological stable PEI-DNA polyplexes. Disadvantages of PEI-based systems are their high *in vitro* and *in vivo* toxicity and their resistance against biodegradation, leading to the accumulation of the polymer in the cells or tissue, which can elicit further toxicity effects.[114] Furthermore, the cytotoxicity has been shown to be dependent on the molar mass of the polymers,[115] but can be improved by the introduction of stealth units, *i.e.* EtOx, into the polymer chain.[74, 116] These drawbacks lead to a necessity to search for alternative polymer systems for gene-delivery applications, which reveal high transfection efficiencies while expressing a low cytotoxicity.

For this reason, cationic copolymers containing non-ionic comonomers with increasing hydrophobicity (MeOx < EtOx < NonOx) were prepared and compared regarding their transfection efficiency. Due to the fact that cytocompatibility as well as transfection efficiency of cationic polymers are dependent on the amount of cationic charges within the macromolecule, water soluble polymers containing 20% (**P25** and **P19**), 40% (**P40** and **P43**), 60% (**P41** and **P44**) or 80% (**P44** and **P45**) AmOx were synthesized accordingly to Chapter 3.3 (Table 5.1). The copolymers consisted of AmOx and either MeOx in order to form gradient copolymers (**P25, P40** to **P42**) or EtOx forming random copolymers (**P19**, **P43** to **P45**) Furthermore, P($EtOx_3$-*b*-$AmOx_{157}$) (**P46**) was synthesized and is from now on denoted as P(AmOx). Cationic polymers were characterized by means of ^{1}H-NMR and SEC (Table 5.1). ^{1}H-NMR measurements provided information about the DP of the polymers, which was determined to be between 130 and 190. SEC measurements confirmed the stability of the macromolecules during acidic deprotection. In addition to the water-soluble cationic copolymers, nanostructures (**N01** to **N06**) consisting of amphiphilic block copolymers were investigated. The preparation and characterization of the pH-responsive nanostructures with varying AmOx content in the shell was already discussed in Chapter 4.2.

Table 5.1. Key properties of the synthesized P(Ox)s determined by either ^{1}H-NMR or SEC measurements. [a]^{1}H-NMR spectroscopy (300 MHz) in CD_3OD; [b]calculated from Boc protected precursor; [c]SEC in 0.3% TFA + 0.1 M NaCl, P2VP-cal.

ID	Composition	NMR[a]				SEC[c]	
		DP[b]	*mol% MeOx/ EtOx*	*mol% BocOx/ AmOx*	M_n *[kg mol^{-1}]*	M_n *[kg mol^{-1}]*	*Đ*
P25	P($MeOx_{130}$-*grad*-$AmOx_{31}$)	161	81	19	15.5	7.0	1.48
P40	P($MeOx_{97}$-*grad*-$AmOx_{55}$)	152	64	36	16.1	8.1	1.33
P41	P($MeOx_{73}$-*grad*-$AmOx_{89}$)	162	45	55	18.9	9.4	1.36
P42	P($MeOx_{29}$-*grad*-$AmOx_{166}$)	195	15	85	24.9	10.7	1.46
P19	P($EtOx_{150}$-*r*-$AmOx_{33}$)	183	82	18	19.6	8.0	1.41
P43	P($EtOx_{77}$-*r*-$AmOx_{55}$)	132	58	42	15.5	8.3	1.32
P44	P($EtOx_{57}$-*r*-$AmOx_{139}$)	196	29	71	25.4	10.7	1.39
P45	P($EtOx_{31}$-*r*-$AmOx_{163}$)	194	16	84	26.3	11.1	1.54
P46	P($EtOx_{3}$-*b*-$AmOx_{157}$)	160	2	98	22.6	13.5	1.56

After polymer synthesis and self-assembly, the polyplex formation and dissociation abilities of the prepared polymers and nanostructures were evaluated. Herein, random (**P19**, **P43** to **P45**) and gradient (**P25, P40** to **P42**) copolymers as well as P(AmOx) (**P46**) were compared to the AmOx containing nanostructures (**N02** to **N06**). Figures 5.1A to C show the decrease of the relative fluorescent units (RFU) of ethidium bromide (EtBr) in the ethidium bromide assay (EBA) after addition of the different cationic polymers. Herein, P(AmOx) (**P46**) exhibits a similar DNA binding ability as linear PEI (*l*-PEI). In the case of water soluble copolymers it was determined to be dependent on the amount of AmOx within the polymer, while the choice of the comonomer (EtOx *vs*. MeOx) and the resulting polymeric structure (random *vs*. gradient) does not have a significant influence on the DNA binding ability (Figure 5.1A and B). Copolymers with 20 mol% AmOx (**P25** and **P19**) were not able to form polyplexes and, consequently, were excluded from further experiments. Interestingly, all other polymers reach a binding plateau at an amino group to phosphate (N*/P) ratio of about 10. However, the RFU values differ significantly in dependence on the AmOx amount within the polymer. Hence, it might be concluded that polymers with less cationic charges interact faster and cannot complex higher amounts of DNA due to lack of cationic charges. In addition to the polyplexes prepared with water soluble cationic copolymers, micelleplexes were prepared using pDNA and the cationic mixed micelles **N02** to **N06**. Regarding EBA (Figure 5.1C), the DNA binding ability with respect to the N*/P ratio was similar for all investigated nanostructures and P(AmOx) (**P46**).

For successful transfection of cells, the possibility of DNA release is also of significant importance. For this reason, DNA dissociation was investigated by the utilization of the heparin release assay (HRA, Figure 5.1D to F). All polyplexes prepared using water-soluble P(Ox)s (**P40** to **P46**) could be dissociated after addition of 10 U mL^{-1} heparin (Figure 5.1D and E), while 20 U mL^{-1} were required for *l*-PEI and nanostructures (**N02** to **N06**, Figure 5.1F) independent on the amount of cationic polymer within the shell.

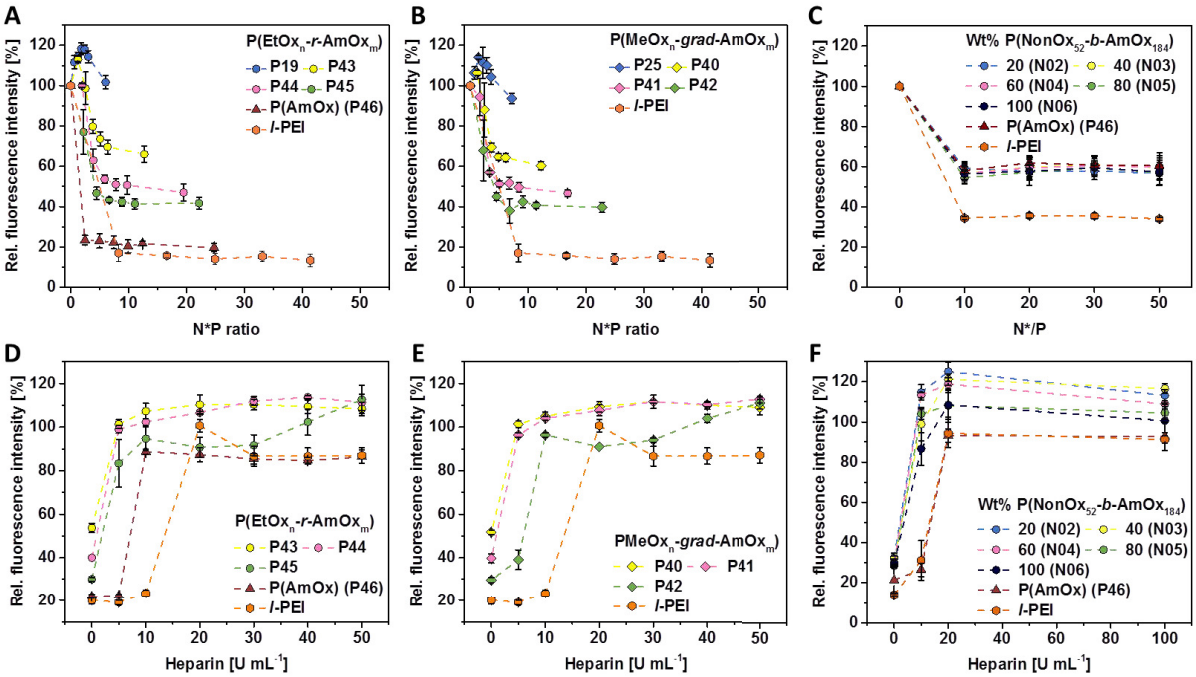

Figure 5.1. Comparison of polyplex formation and stability with pDNA using P(MeOx$_n$-*grad*-AmOx$_m$) (**P25**, **P40** to **P42**) and P(EtOx$_n$-*r*-AmOx$_m$) (**P19**, **P43** to **P45**), AmOx containing micelles (**N02** to **N06**) as well as P(AmOx) (**P46**) and *l*-PEI. A to C: EBA. D to F: HRA of polyplexes formed at distinct N*/P ratios. D: N*/P = 8.8 (**P43**); 12.4 (**P44**); 13.7 (**P45**); 14.9 (**P46**); 30 (*l*-PEI). E: N*/P = 8.0 (**P40**); 10.6 (**P41**); 13.8 (**P42**); 30 (*l*-PEI). F: N*/P = 50.

After preparation of the nanostructures (**N01** to **N06**), their cytocompatibility was evaluated and compared to the water soluble cationic copolymers with either MeOx (**P40** to **P42**) or EtOx (**P43** to **P45**) and P(AmOx) (**P46**). Previous studies already demonstrated the cyto- and hemocompatibility of P(EtOx)[72] and P(MeOx).[73] Furthermore, cationic charges are known to force membrane disruption,[106] however, are indispensable for transfection of cells. Consequently, a reduction of the cell membrane disruption by shielding of the cationic charges was aimed.[107] Cytotoxicity measurements were performed using L929 mouse fibroblasts (Figure 5.2).

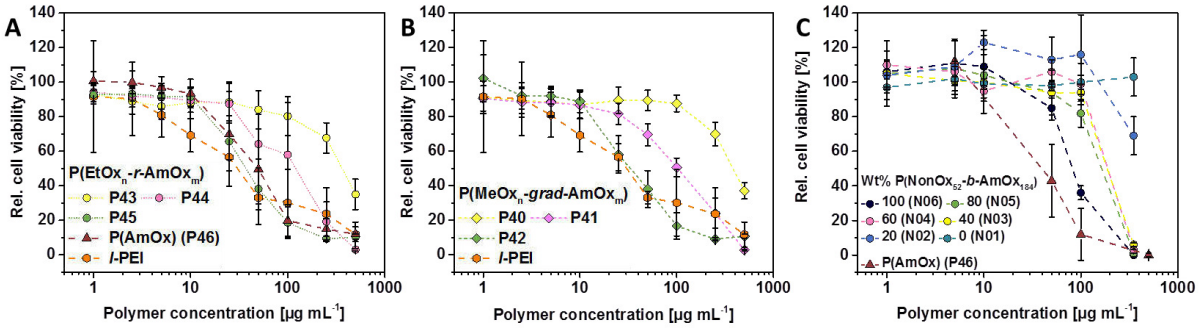

Figure 5.2. Cytotoxicity of indicated polymers against L929 cells after 24 h determined by MTT (A and B) or AlamarBlue (C) assay. Values represent the relative cell viability after treatment with A: P(EtOx$_n$-*r*-AmOx$_m$) (**P43** to **P45**) as well as P(AmOx) (**P46**) and *l*-PEI; B: P(MeOx$_n$-*grad*-AmOx$_m$) (**P40** to **P42**) as well as *l*-PEI or or C: Nanostructures **N01** to **N06** in comparison to **P46**. Non-treated cells served as 100% relative viability. Values represent the mean ± S.D. (n = 3).

The cytotoxicity of the investigated substances was found to be dependent on the amount of cationic charges, however not on the comonomer or macromolecular structure. Furthermore, micelles with 100% AmOx within the shell (**N06**) were slightly less toxic than P(AmOx) (**P46**). Micelles (**N01** to **N06**) and P(AmOx) (**P46**) were further investigated regarding their hemocompatibility (Figure 5.3). Herein, micelles induced less erythrocyte aggregation (Figure 5.3A) than P(AmOx) (**P46**), whereas the hemoglobin release was significantly increased (Figure 5.3B), which can be attributed to higher membrane interactions caused by the increased local charge density of the micelles.

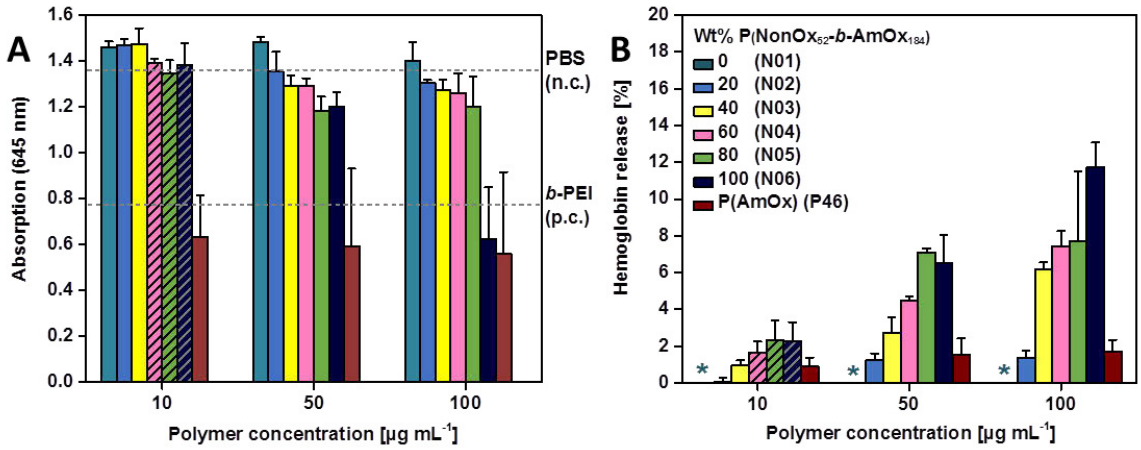

Figure 5.3. Hemocompatibility of indicated nanostructures (**N01** to **N06**) and P(AmOx) (**P47**). A: Concentration dependent erythrocyte aggregation. Branched PEI represents the positive control (p.c.) and PBS the negative control (n.c.). Values represent the mean and S.D. (n = 3). B: Hemoglobin release assay of erythrocytes after incubation at indicated concentrations. A value of less than 2% hemoglobin release is classified as non-hemolytic and more than 5% as hemolytic. Stars depict the position of non-hemolytic samples. Triton-X was used as the p.c. (100%) and PBS served as the n.c. and was subtracted from the values. Values represent the mean and S.D. (n = 3). Striped columns are below the CMC of the nanostructures in A and B.

After successful DNA complexation and dissociation experiments as well as biocompatibility measurements, the polyplex uptake was investigated (Figure 5.4). Uptake experiments of EtOx and MeOx containing polyplexes (Figure 5.4A and B) were conducted in L929 mouse fibroblasts, while micelleplexes were investigated in HEK-293 cells (Figure 5.4C). *l*-PEI and P(AmOx) (**P46**) were elucidated within both cell-lines, leading to a better comparability of the results. According to flow cytometry measurements, the polyplex uptake is very efficient depending on the amount of cationic monomer within the polymers being used. No significant differences between EtOx and MeOx containing copolymers could be observed (Figure 5.4A and B). Copolymers containing 40% AmOx (**P40** and **P43**) revealed the poorest cell internalization (70 to 80% after 4 h of incubation) combined with a very low mean fluorescence intensity (MFI) of 20. All other polymers showed a similar cell uptake (~100%), with an MFI between 60 and 90. Micelleplexes of **N02** to **N06** revealed a similar trend as water soluble polyplexes (Figure 5.4C). Herein, the MFI increased in dependency on the amount of cationic charges. Micelleplexes of **N02** to **N06** showed an increased amount of fluorescent cells (80 to 90%) compared to P(AmOx) (**P46**) and *l*-PEI (60%).

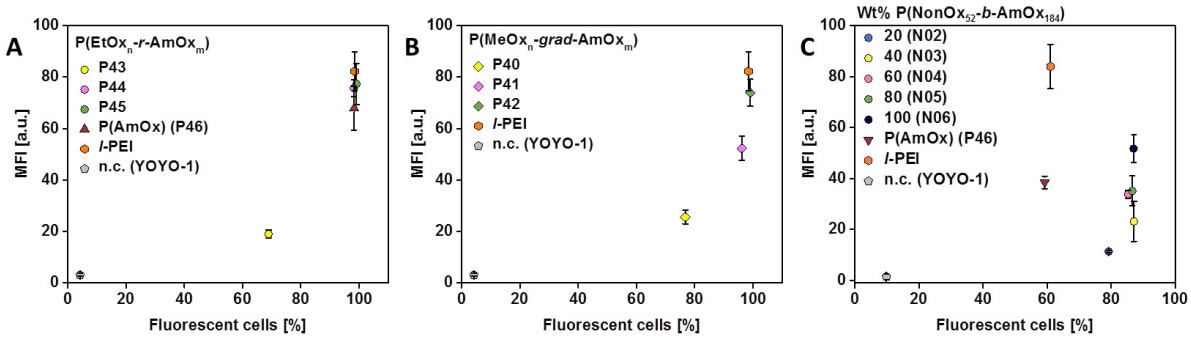

Figure 5.4. Cellular uptake studies of indicated polyplexes YOYO-1 labeled pDNA. L929 (A and B) or HEK-293 (C) cells were treated with polyplexes 4 h in medium with FCS and uptake efficiency as well as MFI were analyzed *via* flow cytometry. The amount of pDNA for cell treatment was kept constant. Graphs show the MFI of the cells in dependence on the amount of fluorescent. MFI values represent the mean ± S.D. (n=3). Values of fluorescent cells represent the mean (n = 3). A: P(EtOx$_n$-*r*-AmOx$_m$) (**P43** to **P45**) and P(AmOx) (**P46**) as well as *l*-PEI. N*/P = 8.8 (**P43**); 12.4 (**P44**); 13.7 (**P45**); 14.9 (**P46**); 30 (*l*-PEI). P(MeOx$_n$-*grad*-AmOx$_m$) (**P40** to **P42**) as well as *l*-PEI. B: N*/P = 8.0 (**P40**); 10.6 (**P41**); 13.8 (**P42**); 30 (*l*-PEI). F: Nanostructures **N02** to **N06** in comparison to **P46** as well as *l*-PEI. N*/P = 50.

Since all investigated polyplexes revealed good uptake efficiencies within the investigated cell lines, the transfection efficiency was analyzed. Hereby, polyplexes of MeOx and EtOx containing polyplexes were investigated within L929 mouse fibroblasts, while NonOx containing micelleplexes were elucidated in HEK-293 cells. With regard to flow cytometry measurements (Figure 5.5), none of the elucidated water soluble P(Ox)s (**P40** to **P46**) caused any transfection in the cells after two days of incubation. In contrast to that, *l*-PEI transfected 40% of the cells.

A possible explanation for the lack in transfection might be attributed to a lack in endosomal release of the polyplexes. For this reason, the micelleplexes beforehand described might represent a suitable alternative to enhance the transfection efficiency of AmOx.

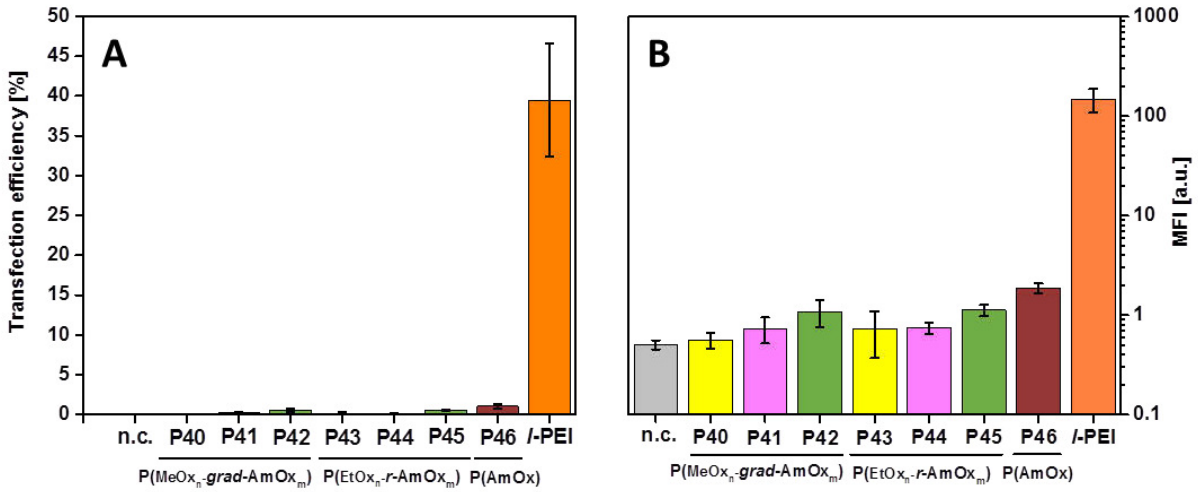

Figure 5.5. Transfection efficiency of different polyplexes for L929 mouse fibroblasts in growth media at N/P = 30 after 2 d analyzed *via* flow cytometry. Values represent the mean (n = 3). A: Relative MFI of all viable cells normalized by the negative control (YOYO-1, n.c.).

HEK-293 cells were incubated with micelleplexes for 4 d and analyzed *via* flow cytometry (Figure 5.6). Hereby, the transfection efficiency as well as the MFI of cells by using

micelleplexes consisting of at least 40% AmOx within the micelle shell (**N03** to **N06**) was enhanced compared to P(AmOx) (**P46**) (Figure 5.6A and B). Furthermore, the cell viability of all micelleplexes (80 to 95%) was superior to *l*-PEI and P(AmOx) (**P46**) (60%). For this reason, the transfection efficiency of all cells was also determined (Figure 5.6C), revealing a superiority of **N05** and **N06** compared to *l*-PEI.

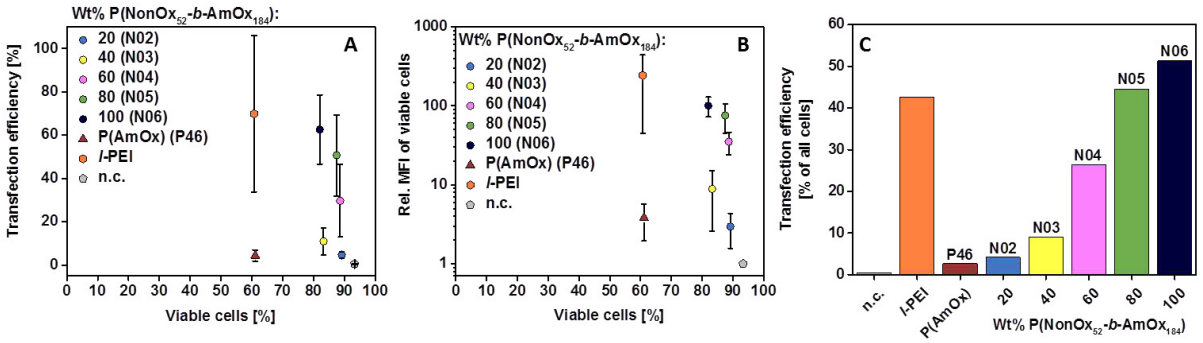

Figure 5.6. Transfection efficiency of different polyplexes for adherent HEK-293 cells in growth media at N*/P = 50 after 4 d analyzed *via* flow cytometry. Values represent the mean (n = 3). A: Relative MFI of all viable cells normalized by the negative control (n.c.). B: Transfection efficiency of all viable cells. C: Transfection efficiency of all cells.

Within this chapter, water soluble cationic copolymers consisting of EtOx and AmOx (random) or MeOx and AmOx (gradient) as well as cationic nanostructures with EtOx and AmOx within the shell were compared to P(AmOx) and *l*-PEI regarding their potential as biocompatible non-viral vectors. Herein, the transfection efficiency of AmOx containing polyplexes could be enhanced by using copolymers with hydrophobic NonOx blocks that were self-assembled into micelles prior to complexation of the genetic material. It might be assumed that the endosomal release can be triggered by stretching of the cationic AmOx blocks during acidification of the endolysosomes (Scheme 5.1). Consequently, amphiphilic copolymers were determined to be more efficient than fully water soluble polymeric carrier systems.

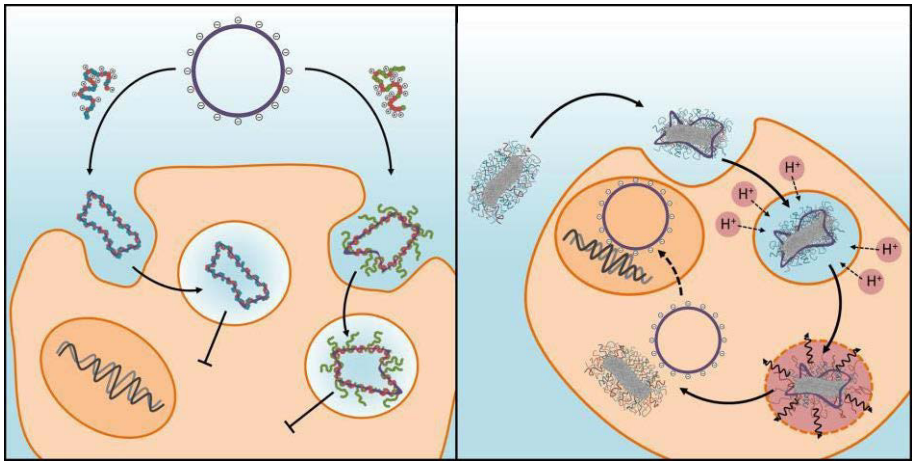

Scheme 5.1. Schematic presentation of the cellular uptake and endosomal release of different polyplexes. Left: water soluble polyplexes of random or gradient hydrophilic copolymers might not be able to be released from the endosomes and, consequently, lack in transfection efficiency. Right: Micelleplexes that were prepared by using amphiphilic polymeric micelles can trigger the endosomal burst by stretching of the cationic polymer blocks during acidification of the endolysosomes and, hence, successfully transfect cells. Cyan: EtOx. Green: MeOx. Red: AmOx. Grey: NonOx. Purple: pDNA.

5. Gene delivery systems

Within the following chapter (Chapter 6), water soluble functional P(Ox)s will be applied in terms of drug-delivery systems by covalent conjugation of drugs to the hydrophilic polymers and their activity, respectively therapeutic efficiency will be elucidated and compared to the pure drugs.

6. Drug delivery systems

Parts of this chapter have been published in: **P4**) D. Hoelzer[‡], M. N. Leiske[‡], M. Hartlieb, T. Bus, D. Pretzel, S. Hoeppener, K. Kempe, R. Thierbach, U. S. Schubert, *Oncotarget* **2018**, in press. **P7**) T. Luehmann, M. Schmidt, M. N. Leiske, V. Spieler, T. C. Majdanski, M. Grube, M. Hartlieb, I. Nischang, S. Schubert, U.S. Schubert, L. Meinel, *ACS Biomater. Sci. Eng.* **2017**, *3*, 304-312. **P8**) M. Hartlieb[‡], T. Bus[‡], J. Kübel, D. Pretzel, S. Hoeppener, M. N. Leiske, K. Kempe, B. Dietzek, U. S. Schubert, *Bioconjugate Chem.* **2017**, *28*, 1229-1235. [‡]Equal contribution of both authors.

In addition to complexation of genetic material, functional groups of polymers can also be utilized for drug conjugation. As already mentioned in Chapter 2, many drugs (*i.e.* small molecules) are poorly water soluble. Conjugation to water soluble polymers can enhance the solubility significantly.[21-22] Furthermore, the blood circulation times can be increased[79] by preventing unspecific cellular uptake, immune response or renal excretion.
Within this work, two different possibilities for the attachment of drugs to polymers were conducted. Firstly, single P(Ox) chains with a defined azide functionalized ω-end group were used for the POxylation of interleukin-4 (IL-4). Hereby, irreversible conjugation of polymers to proteins is mostly known from PEGylation, aiming longer blood circulation times and consequently altering the pharmacokinetics.[117-118] By further evaluating the PEGylation of proteins, some drawbacks are obvious by the nature of the unspecific reaction carried out: (i) Different protein molecules can be attacked at different positions, (ii) the active center of the protein can be blocked, (iii) mono-, di-, or multi-PEGylation occurs, and (iv) 25% of the human population already have PEG antibodies. These unwanted effects can lead to a significant change within the pharmacokinetics of the protein based pharmaceutical, since it cannot be determined precisely how much of the protein is still active or how significantly the blood circulation times are altered. For this reason, CuAAC might be used for the preparation of defined protein P(Ox) conjugates.

6.1. POxylation of proteins

In order to obtain mono-POxylated proteins, an alkyne modified amber codon was synthesized previously.[119] This amino acid can be inserted into the protein structure during protein biosynthesis and, hence, reveals a single, defined position within the protein. Consequently, the synthesis of mono azide functionalized P(Ox)s *via* ω-end functionalization[17-18] was conducted. In order to obtain conjugates of varying size, three different homopolymers of different molar mass were synthesized accordingly to Chapter 3.3 and characterized using NMR as well as SEC (Table 6.1) to gain information about the size and dispersity of the polymers. Polymers **P47** to **P49** revealed a narrow dispersity ($Đ \leq 1.2$) while having a molar mass of 2,600, 4,300 or 9,200 g mol^{-1}. In addition to the P(MeOx) homopolymers, gradient copolymers of MeOx and AmOx (**P50** to **P52**) were synthesized to enhance the cellular uptake mediated by the cationic charges. However, the amount of AmOx units was kept low to minimize cytotoxic effects caused by the cationic charges as reported

within Chapter 5. The polymers were end-functionalized accordingly to the homopolymers and analyzed by SEC and NMR measurements (Table 6.1).

Table 6.1. Properties of azide terminated homo- and copolymers determined by either [a] ^{1}H-NMR (300 MHz, $CDCl_3$) or [b]SEC (DMAc + 0.21% LiCl, PS-cal.). [c] ^{1}H-NMR (300 MHz, CD_3OD). [d]Calculated from Boc protected precursor.

ID	Composition	NMR[a]				SEC[b]	
		DP	*Mol% MeOx*	*Mol% AmOx*	*Mn [kg mol^{-1}]*	*Mn [kg mol^{-1}]*	*Đ*
P47	$P(MeOx)_{30}$-N_3	30	100	0	2.6	5.4	1.10
P48	$P(MeOx)_{50}$-N_3	50	100	0	4.3	8.3	1.11
P49	$P(MeOx)_{108}$-N_3	108	100	0	9.2	14.0	1.20
P50	$P(MeOx_{41}$-*grad*-$AmOx_2)$-N_3[c]	43[d]	95	5	3.8	5.8	1.20
P51	$P(MeOx_{38}$-*grad*-$AmOx_4)$-N_3[c]	42[d]	90	10	3.8	6.3	1.18
P52	$P(MeOx_{32}$-*grad*-$AmOx_8)$-N_3[c]	40[d]	80	12	3.9	6.4	1.19

Utilizing the synthesized polymers, IL-4 was P(Ox)ylated *via* CuAAC to obtain conjugates (Figure 6.1A). The success of the conjugation was verified using SDS-PAGE gel chromatography (Figure 6.1B and C). By using homopolymers with different molar masses, it is obvious that the A-band within the gel shifts to higher molar masses (Figure 6.1B), while it is similar in case of the copolymers, which were prepared with a similar molar mass themselves (Figure 6.1C). Hereby, the successful conjugation of single ω-functional polymer chains to IL-4 by the highly selective CuAAC could be demonstrated. After the demonstration of the successful conjugation of single polymer chains to IL-4 *via* CuAAC, their activity was compared to the wild-type IL-4 in a proliferation as well as an enhanced yellow fluorescent protein (eYFP) reporter gene assay.

Within this sub-chapter the utilization of ω-end functionalized P(Ox) for the mono-POxylation of IL-4 was presented, possibly enabling the preparation of protein pharmaceuticals with defined blood circulation times. Another opportunity for drug conjugation is the reversible drug attachment of small molecules such as doxorubicin (DOX) to polymer carriers, *e.g.* by Schiff base chemistry, which will be discussed in the following paragraph.

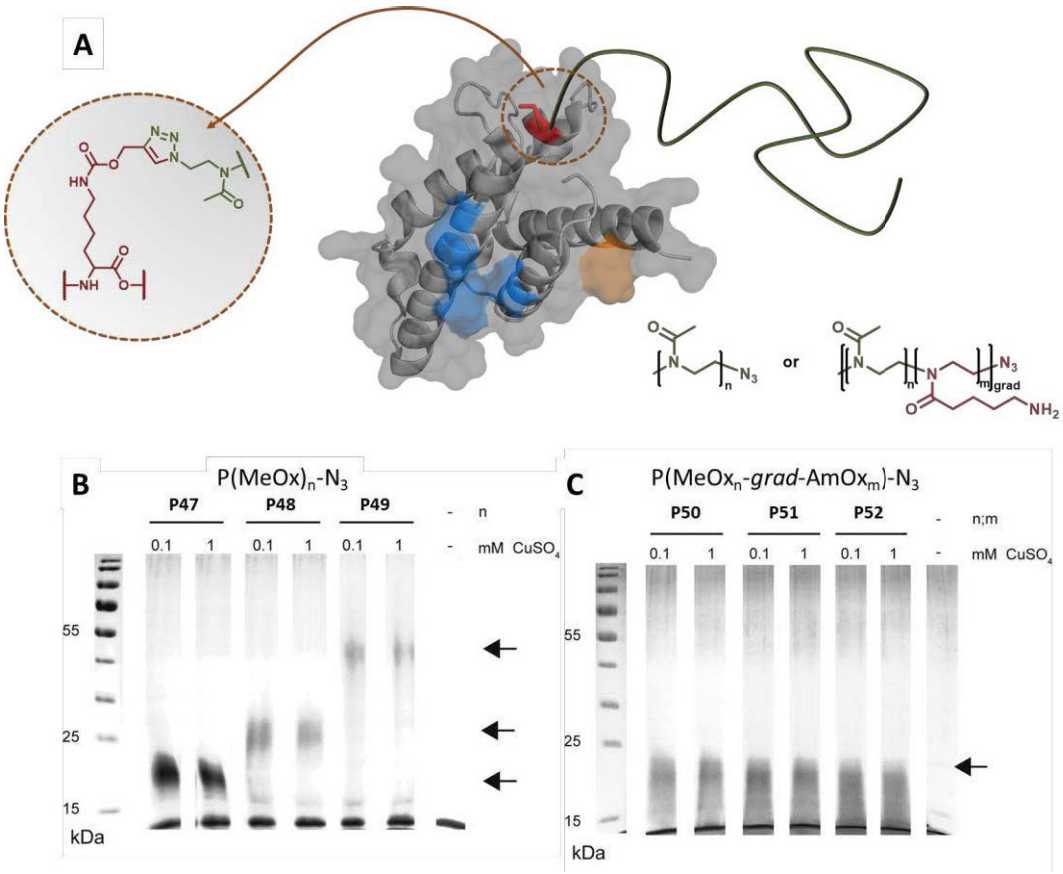

Figure 6.1. P(Ox)ylation of IL-4. A: Schematic representation of the P(Ox)ylation of IL-4. Modified after T. Lühmann *et al.*.[119] B: CuAAC reactions between Plk-IL-4 and $P(MeOx)_n$-N_3 polymers. C: CuAAC reactions between Plk-IL-4 and $P(MeOx_n$-*stat*-$AmOx_m)$-N_3 polymers as analyzed by reduced SDS-PAGE. Plk-IL-4 is shown as control. Arrows indicate polymer conjugated IL-4 species.

6.2. DOX conjugated P(Ox) nanogels

DOX is a cytostatic agent known to cause severe side-effects. Hence, the reversible conjugation of the drug to a polymer might be a good opportunity to resolve this problem by minimization of unspecific uptake and, consequently, enhanced blood circulation times. The preparation and drug loading of the core cross-linked nanogels was described in Chapter 4.2. Furthermore, the stability at physiological pH values as well as the qualitative drug release of the DOX-nanogel (**N12**) was demonstrated (Figure 4.11, Chapter 4.2). Preliminary *in vitro* investigations regarding the cellular internalization of the 6AF loaded nanogels **N07** to **N11** prepared in Chapter 4.2 were conducted, revealing a clear dependency of the cellular uptake of L929 mouse fibroblasts on the amount of GA utilized for cross-linking and, consequently, the zeta potential of the nanogels. Nanogel **N07**, which contains one equivalent GA per two amino groups within **P31**, showed the highest uptake, decreasing in order to a lowering zeta potential. Hence, **N11** revealed the lowest, respectively slowest cellular internalization. Due to the fact that a system was aimed which is exclusively internalized into cancer cells, a low cellular uptake into L929 cells was favored and, consequently, **N11** was used for further experiments and compared to DOX loaded nanogels (**N12**), which were prepared by using similar conditions (Table 4.5, Chapter 4.2). Nanogel stability and pH dependent DOX release were verified by DLS measurements conducted in Chapter 4.2. Firstly, cytotoxicity

experiments comparing the influence of the 6AF (**N11**) and the DOX (**N12**) loaded nanogels as well as pure DOX on the cell viability of L929 mouse fibroblasts, which are known to be sensitive to cytotoxic effects,[120] and HT-29 cells were conducted (Figure 6.2). Hereby **N12** was used at equal DOX concentrations as pure DOX and **N11** was used at the same polymer concentration as **N12**. Independent on the concentration, 6AF loaded nanogels (**N11**) did not show any impairing effects on neither of the investigated cell lines after 72 h. Furthermore, L929 cells were more sensitive to DOX loaded nanogels (**N12**) that HT-29 cells, indicated by a decreased cell viability (25%, Figure 6.2A) at a DOX concentration of 0.1 µg mL^{-1} compared to a cell viability of 80% in HT-29 cells (Figure 6.2B). Furthermore, in L929 cells, the nanogel **N12** is more effective than pure DOX, which is less pronounced in HT-29 cells.

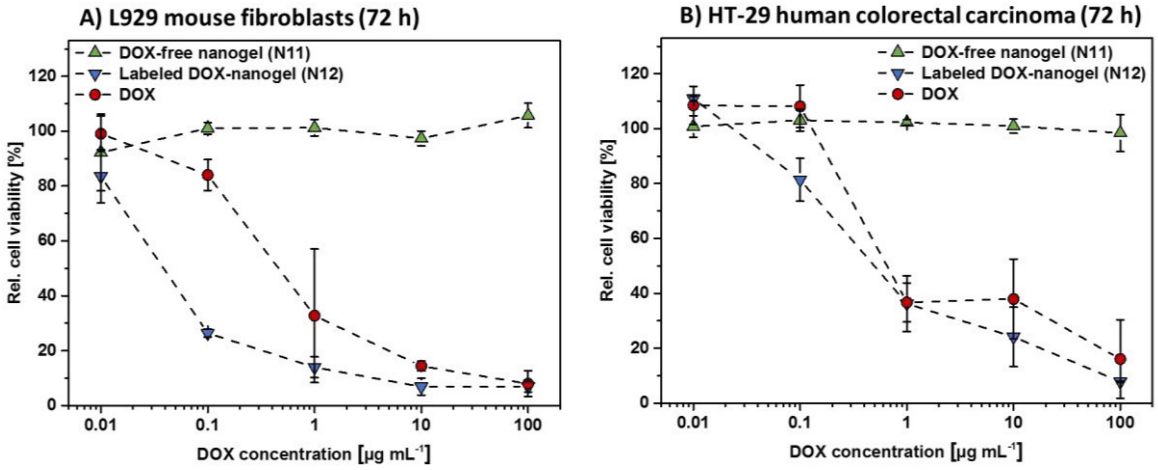

Figure 6.2. Cytotoxicity of DOX-free nanogels (**N11**), labeled DOX-nanogels (**N12**) as well as free DOX were determined by XTT assay. L292 mouse fibroblasts (A) as well as HT-29 human colorectal carcinoma cells (B) were incubated for 72 h. Labeled DOX-nanogels (**N12**) were used at a concentration where the amount of loaded drug resembles the amount of DOX used per data point. DOX-free nanogels (**N11**) were used at the same polymer concentration as labeled DOX-nanogels (**N12**). Data are expressed as mean ± SD of six determinations.

Further elucidation of the cellular uptake and endosomal release was investigated by the means of CLSM imaging (Figure 6.3). Hereby, the DOX loaded nanogel **N12** was compared to pure DOX. Two sets of imaging were taken, *i.e.* after 6 h and after 24 h.
After 6 h of incubation, the free DOX is mostly diffuse localized within the cytosol and nucleus. Previous studies already reported this phenomenon after 3 h.[121-122] **N12**, however, requires more time to enter the nucleus. After 6 h, mostly a colocalization of N12 and lysosomes could be obtained. Furthermore, the signals of DOX and the Alexafluor label are colocalized, indicating that the nanogels were not degraded up to that time point. After 24 h incubation time, the pure DOX was mostly localized in the nucleus. Furthermore, the DOX of **N12** could also be found within the nucleus, whereas the polymer signal was localized outside the nucleus, indicating a successful degradation of the nanogel and, consequently, drug release.

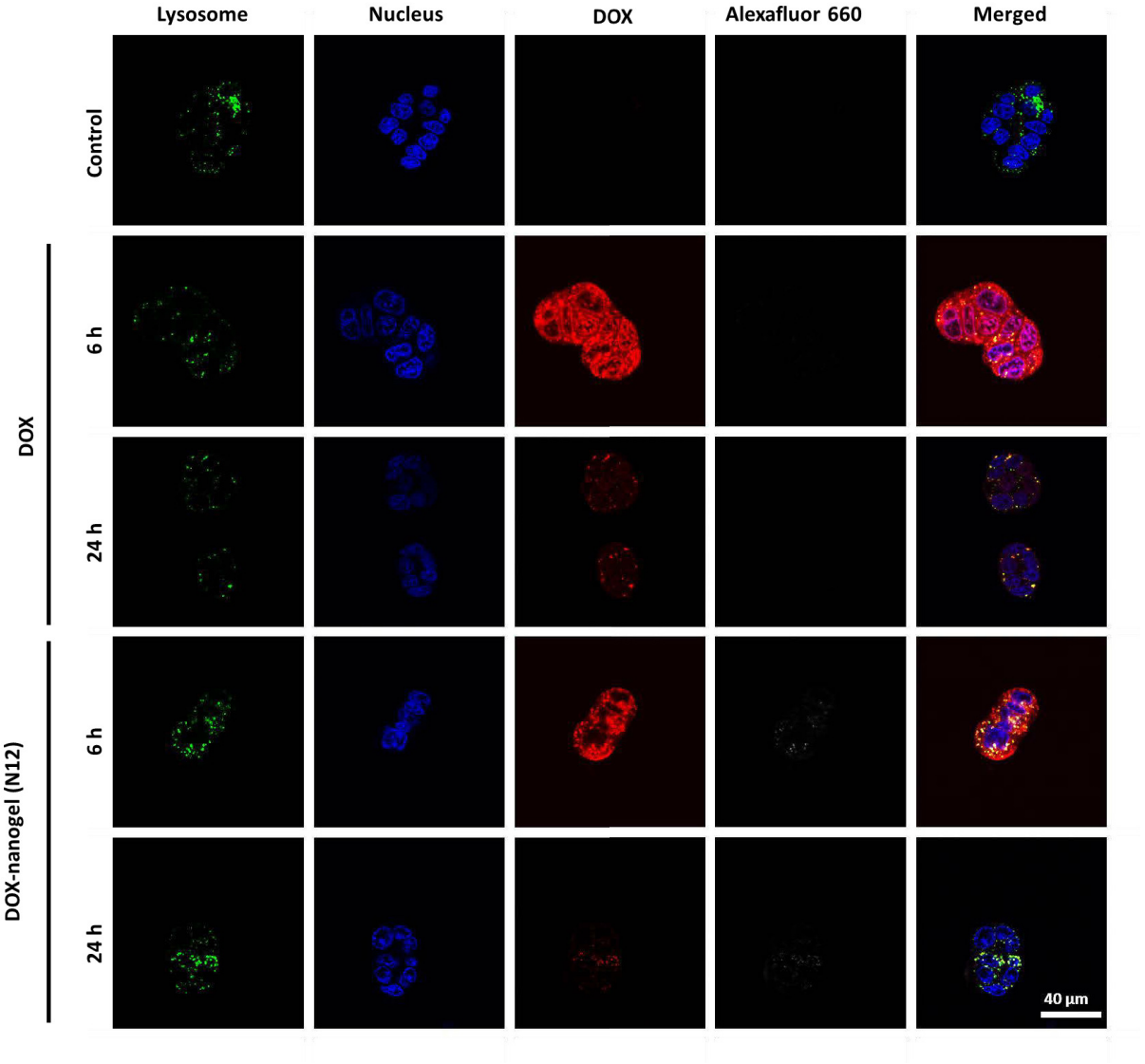

Figure 6.3. CLSM images of free DOX as and labeled DOX-nanogels (**N12**) incubated with HT-29 colorectal carcinoma for 6 h or 24 h. Lysosomal cellular compartments were stained green using LysoTracker Green DND-26 and the nucleus was labeled with Hoechst 33342 (blue). The fluorescence of DOX is depicted in red and the Alexafluor label of the polymer is shown in white.

With regard to the *in vitro* results, an *in vivo* study using the xenograft mouse model was conducted using the DOX-loaded nanogel **N12** in comparison to pure DOX. 6AF loaded nanogels (**N11**) as well as physiological sodium chloride solution represented the control groups. All substances were dissolved in sterile sodium chloride solution and mice were treated *via* tail vein injection. Preliminary experiments on the biocompatibility revealed no toxic effects of the nanogels at a DOX concentration of 1 mg kg^{-1}. For this reason, this amount of DOX was used for the determination of the therapeutic efficiency *in vivo*. HT-29 tumor cells were injected to male nude mice. After the tumor growth reached a certain level, therapy was conducted by the injection of six doses. Mice treated with DOX or **N12** revealed a reduced tumor growth whereas **N11** and NaCl did not have an influence. Interestingly, the DOX loaded nanogel **N12** was slightly more efficient than the pure DOX (Figure 6.4A) and, furthermore, increased the median survival time significantly (**N12**: 73 d; DOX: 39 d; Figure 6.4B).

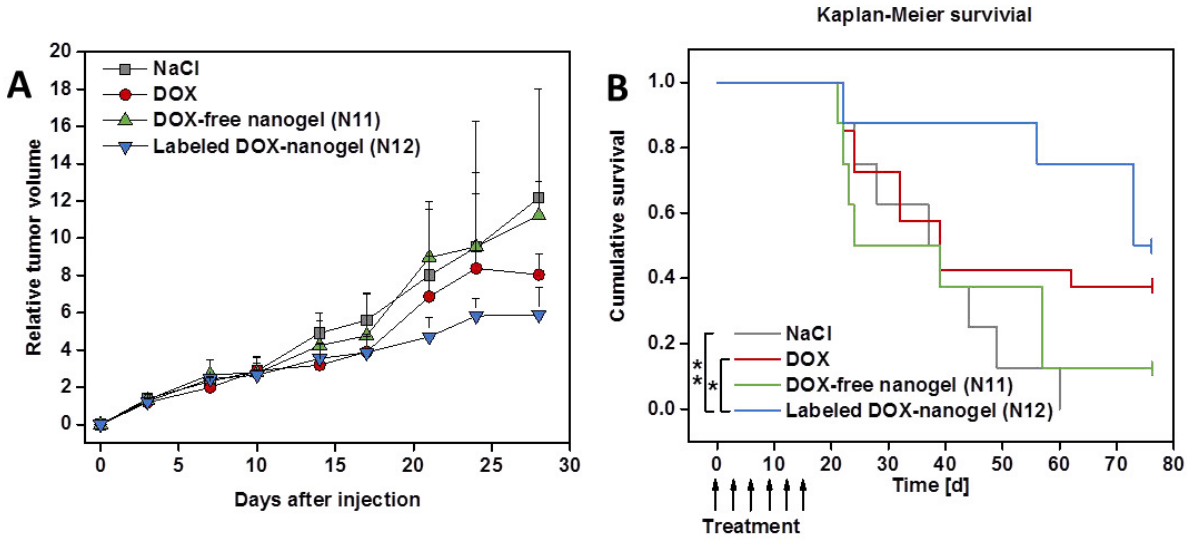

Figure 6.4. A: Development of absolute relative volume for animal groups illustrated over time after treatment (day 0). Male nude mice were subcutaneously injected with HT-29 cells. When tumors reached a volume of 100 to 200 mm^3, mice received six doses of 0.9 wt% NaCl, DOX (1 mg kg^{-1}), DOX-free nanogel (**N11**) or labeled DOX-nanogel (**N12**) (corresponding to 1 mg kg^{-1} Dox) *via* tail vein injection from day 0 to day 15. Data represents the mean and S.D. B: Kaplan-Meier survival curve of mice bearing human HT-29 colorectal adenocarcinoma xenograft. Male nude mice received a subcutaneous injection of HT-29 cells into the flank. When tumors reached 100 to 200 mm^3 mice received six doses of 0.9 wt% NaCl, DOX (1 mg kg^{-1}), DOX-free nanogel (**N11**) or labeled DOX-nanogel (**N12**) (corresponding to 1 mg kg^{-1} DOX) *via* tail vein injection from day 0 to day 15. The individual endpoint was achieved when the tumor volume reached 1500 mm^3. Statistical differences are displayed as *p <0.05 and **p<0.01 according to the log-rank test.

Within this chapter, two different strategies of drug conjugations were presented. Firstly, CuAAC was used for the irreversible conjugation of single P(Ox) chains to alkyne modified proteins. These proteins were afterwards determined to remain actively after P(Ox) conjugation. Furthermore, the reversible conjugation of multiple DOX molecules to the core of cross-linked P(Ox) nanogels was realized *via* Schiff base chemistry. The resulting drug carriers were shown to be more efficient than DOX *in vitro* and *in vivo*.

7. Summary

Since their invention in the 1960s, research on the pseudopeptides poly(2-oxazoline)s (P(Ox)s) has risen significantly. Whereas initial investigations mainly concentrated on the synthesis of defined P(Ox)s with different substituents in 2-position and their chemical characterization, the field of biomedical applications has been focused increasingly during the last decade. Due to this broad scope in academic research on P(Ox)s, the aim of this thesis was to contribute to the understanding of the synthesis and polymerization, self-assembly behavior as well as biomedical applications of P(Ox)s (Figure 7.1).

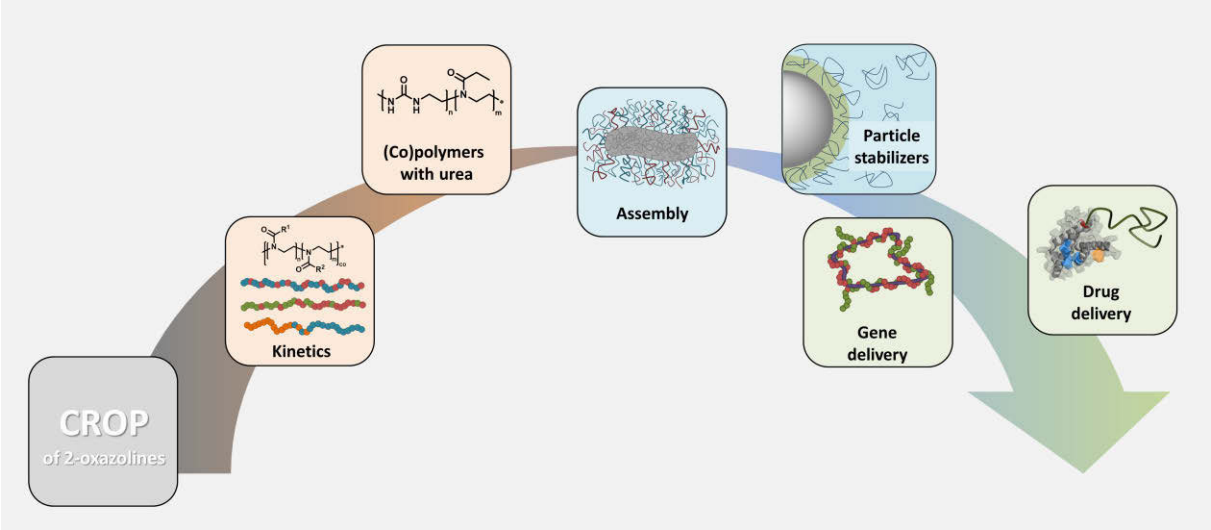

Figure 7.1. With the aid of detailed kinetic investigations, the CROP facilitates the synthesis of tailored polymers consisting of 2-oxazolines and/or urea (orange boxes). P(Ox)s can be utilized for stabilization of hydrophobic polymer particles as well as for direct self- and co-assembly (blue boxes). Functional P(Ox)s are used in a wide range of applications in drug as well as gene delivery (green boxes).

By using distinct synthesis routes, different Boc protected amino-functionalized 2-oxazolines can be obtained. Firstly, the synthesis of 2-(4-((*tert*-butoxycarbonyl)amino)butyl)-2-oxazoline (BocOx), which is already known from literature, is proceeded by using a three step synthesis utilizing 5-aminovaleric acid as starting material. The synthesis resulted in a Boc protected 2-oxazoline, which can be polymerized using the cationic ring-opening polymerization (CROP). On the other hand, *tert*-butyl 2-iminooxazolidine-3-carboxylate (BocOI) can be synthesized from 2-amino-2oxazoline in a single step reaction. Hereby, the *endo*-nitrogen of the molecule was found to be more reactive than the *exo*-nitrogen and, hence, leads to the formation of a Boc protected 2-iminooxazolidine instead of a 2-oxazoline. BocOI was found to be polymerizable by CROP, resulting in Boc protected poly(urea) derivatives, which could be deprotected under acidic conditions to yield poly(urea). Thus, the synthesis of poly(urea) was proceeded in a controlled chain growth polymerization, yielding polymers with a narrow dispersity ($Đ \leq 1.3$) instead of the less controllable step growth polymerization, invented by Otto von Bayer. Furthermore, by using the CROP for the preparation of poly(urea) it was possible to prepare copolymers of P(Ox)s and poly(urea) in a one-pot polymerization. Hereby, the polymerization constant of BocOI was found

to be more than ten times higher than 2-ethyl-2-oxazoline (EtOx), suggesting the formation of quasi block copolymers in a one-pot reaction.
Furthermore, the copolymerization kinetics of the Boc protected 2-oxazoline BocOx and EtOx, respectively 2-methyl-2-oxazoline (MeOx) were evaluated. Here, BocOx was found to be as reactive as EtOx, leading to the formation of random copolymers, while MeOx was more reactive and, consequently, forms gradient copolymers with BocOx. Consequently, BocOI is much more reactive than BocOx, which might be caused by the monomer structure and the differences in the polymerization mechanism. Then, different functional copolymers were synthesized and characterized. The polymers were used for the preparation of colloidal structures and used for gene and drug delivery applications within this thesis.
The second main objective of this thesis concentrated on the application of P(Ox)s for the preparation of nanostructures. Herein, water soluble homopolymers of P(EtOx) or P(MeOx) with different degrees of polymerization (DP; 25, 60, 100 and 200) were synthesized and investigated regarding their properties within the stabilization of hydrophobic nanoparticles during preparation, purification and lyophilization. In general, no significant differences between P(EtOx) and P(MeOx) could be observed. P(Ox)s with a DP of 25 were not suitable for neither of the aimed applications, possible caused by their low dynamic viscosity in aqueous solutions or their short chain length, which cannot stabilize the interphase between the hydrophobic nanoparticle and the aqueous solution in a satisfying manner. Though, P(Ox)s with a DP of 60, 100 or 200 were found to be suitable as stabilizers for nanoparticle preparation, purification and lyophilization at distinct concentrations. Consequently, it could be shown that non-ionic P(Ox)s can be utilized as an all-in-one system to stabilize hydrophobic polymer nanoparticles.
In terms of nano-assembly, the utilization of amphiphilic P(Ox)s for the preparation of pH-responsive nanostructures was investigated. Herein, P(Ox) block copolymers were synthesized consisting of either 2-nonyl-2-oxazoline (NonOx) and EtOx or NonOx and 2-(4-aminobutyl)-2-oxazoline) (AmOx) and self- as well as co-assembled in a simple mixed micelle approach. In both cases, NonOx served as the hydrophobic building block of the block copolymers, forming the micellar core during the assembly process. AmOx was chosen as the cationic core block to facilitate the complexation of genetic material for gene delivery applications. In contrast to that, EtOx served as the non-ionic building block suitable to enhance the biocompatibility of the nanostructures by shielding the cationic charges of AmOx. Nanostructures were prepared with different amino contents by simply mixing the two polymers in different weight ratios prior assembly. By this means, nanostructures with 0, 20, 40, 60, 80, or 100 wt% of the AmOx block copolymer could be prepared and elucidated regarding their size, morphology, critical micelle concentration (CMC), and pH responsiveness. All nanostructures containing the EtOx copolymer were found to be worm- or sheet-like with an average diameter of 100 nm, while the micelles consisting of 100 wt% of the AmOx copolymer where found to be slightly smaller ($d \approx 70$ nm) and spherical. The CMC was very low (10^{-7} to 10^{-6} M) in all cases and the pH responsiveness increased with an increasing AmOx amount within the shell of the micelles.
In addition to assembled micelles, also core cross-linked nanogels were prepared, utilizing AmOx and EtOx containing block copolymers. Hereby, block copolymers consisting of EtOx and AmOx were assembled in chloroform to form nanostructures with a cationic AmOx core. These nanostructures could be successfully prepared and reversible drug (6AF or DOX) conjugation was conducted using Schiff-base chemistry. The nanogels were found to be stable

at 4 °C and 37 °C at physiological pH values, while the DOX was shown to be successfully released at a pH value of 5.0 in the presence of the proteinogenic amino acid glycine.
The transport of genetic material by cationic polymers into cells is one important topic of this thesis. For this reason, all AmOx containing nanostructures as well as a series of water soluble copolymers consisting of EtOx and AmOx (random copolymers), respectively MeOx and AmOx (gradient copolymers) was investigated. The cationic polymers were able to bind and release the genetic material. Complexes of plasmid DNA (pDNA) and AmOx containing micelles (micelleplexes) were evaluated regarding their transfection efficiency *in vitro*. Herein, micelles consisting of 80 or 100 wt% AmOx copolymer could cope with *l*-PEI when comparing the absolute transfection efficiency of the cell population. Hereby, also P(AmOx) was used for comparison, revealing no detectable transfection efficiency. As the transfection efficiency was proven to be enhanced for the amphiphilic micelleplexes in comparison to the AmOx homopolymers, also water-soluble copolymers of AmOx and EtOx (random) or AmOx and MeOx (gradient) were elucidated. Unfortunately, none of the investigated polyplexes were able to successfully transfect cells. For this reason, it was concluded that the hydrophobic NonOx block of the polymers enhances the transfection efficiency of AmOx. Furthermore, the assembled morphology could have an influence on the endosomal burst and the subsequent release of the micelleplexes from the endolysosomes.
In addition to gene delivery systems, also drug delivery represents an important aspect for the application of P(Ox)s. In general, the encapsulation into or the conjugation to polymeric carrier systems aims an enhanced solubility of hydrophobic drugs, longer blood circulation times and reduced side-effects by targeted uptake. Since encapsulation of drugs might lead to unspecific diffusion within an organism, covalent conjugation might be more promising to fulfill these aims. Drugs can be conjugated irreversible or reversible to a polymer based carrier system. Within this thesis, irreversible conjugation was conducted using the copper catalyzed azide alkyne click reaction of the alkyne modified protein IL-4 and azide ω-end group functionalized water soluble P(Ox)s. Hereby, the conjugation of different P(Ox)s could be demonstrated in a very selective manner. SDS-PAGE analysis showed the specific attachment of single polymer chains to the proteins. Furthermore, the remaining activity of the protein was proven by the expression of eYFP. Furthermore, DOX containing nanogels were elucidated in terms of therapeutic efficiency *in vitro* and *in vivo*, revealing enhanced tumor suppression in combination with longer median survival times.
In summary, within this thesis new P(Ox) and poly(urea) containing polymers could be synthesized from amino-functionalized 2-oxazolines and compared to amino-functionalized P(Ox) copolymers regarding their polymerization kinetics and reactivity ratios. The urea containing polymers could be characterized. Furthermore, water soluble P(Ox)s could be used as a suitable all-in-one system for the stabilization of hydrophobic polymer nanoparticles, while amphiphilic P(Ox)s could be self- and co-assembled and successfully applied as gene carriers. They were advantageous to water soluble gene vectors in terms of cell transfection. However, water soluble P(Ox)s could be applied as drug delivery systems by irreversible or reversible drug conjugation.

8. Zusammenfassung

Seit der Entdeckung der Synthese der Poly(2-oxazolin)e (P(Ox)s) hat die Forschung rund um diese Polymerklasse stetig zugenommen. Ursprünglich lag der Forschungsfokus hauptsächlich auf der Synthese hochdefinierter P(Ox)s mit unterschiedlichen Substituenten in 2-Position und deren Charakterisierung bezüglich des Löslichkeitsverhaltens oder der Glasübergangs-temperaturen. Während der letzten Jahre allerdings verschob sich der Fokus zunehmen in Richtung der biomedizinischen Anwendungen (Abbildung 8.1).

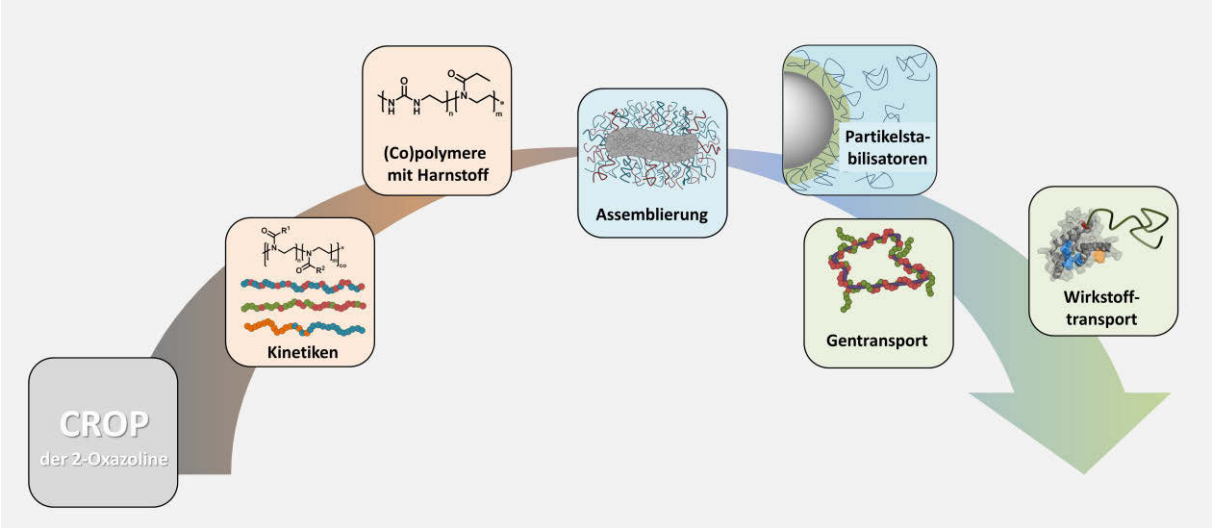

Abbildung 8.1. Mithilfe detaillierter Kinetiken ermöglicht die kationische Rinöffnungspolymerisation (CROP) die Synthese maßgeschneiderter Polymere, welche aus 2-Oxazolinen und/oder Urea bestehen (orange Box). Die P(Ox)s können genutzt werden, um hydrophobe, polymerbasierte Partikel zu stabilisieren oder durch Selbstassemblierung Nanostrukturen aufzubauen (blaue Box). Funktionelle P(Ox)s können in einem breiten Spektrum des Gen- und Wirkstofftransports eingesetzt werden (grüne Box).

Definierte synthetische Routen ermöglichen es, unterschiedliche Boc geschützte Amin-funktionalisierte 2-Oxazoline herzustellen. In dieser Arbeit wurde die Herstellung des literaturbekannten 2-(4-((*tert*-Butoxycarbonyl)amino)butyl)-2-oxazolin (BocOx) in einer Dreistufensynthese, ausgehend von 5-Aminovaleriansäure, durchgeführt. Das Produkt dieser Synthese ist ein Boc geschütztes 2-Oxazolin, welches mithilfe der kationischen Ringöffnungspolymerisation (CROP) polymerisiert werden kann. Zusätzlich zu diesem 2-Oxazolin wurde *tert*-Butyl-2-iminooxazolidin-3-carboxylat (BocOI) in einer Einstufensynthese, ausgehend von 2-Amino-2-oxazolin, synthetisiert. Da der *endo* Stickstoff des Ausgangsstoffes reaktiver ist als der *exo* Stickstoff, entsteht durch die Boc-Schützung das 2-Iminooxazolidin BocOI anstelle eines 2-Oxazolins. BocOI konnte mithilfe der CROP polymerisiert werden. Die resultierenden Polymere sind Poly(harnstoff)derivate mit einer engen Molmassenverteilung ($Đ \leq 1.3$). Des Weiteren ermöglichte die CROP die Synthese von Copolymeren bestehend aus Poly(urea) und Poly(2-ethyl-2-oxazolin) (P(EtOx)). Copolymerisationskinetiken der Monomere zeigten, dass BocOI eine deutlich höhere Reaktionskonstante aufwies als 2-Ethyl-2-oxazolin (EtOx), was folglich die Synthese von blockähnlichen Copolymeren in einer einzigen Polymerisation ermöglicht. Weiterhin wurden Copolymerisationskinetiken des Amin-funktionalisierten BocOx mit EtOx und MeOx durchgeführt. Hierbei zeigte sich eine zufällige

Monomerverteilung bei der Polymerisation von BocOx und EtOx, während Copolymere bestehend aus BocOx und 2-Methyl-2-oxazolin (MeOx) eine graduelle Monomerverteilung aufwiesen. Ausgehend von den durchgeführten Kinetiken konnten verschiedene Copolymere synthetisiert und charakterisiert werden.

Ein zweiter Schwerpunkt dieser Arbeit bestand darin, P(Ox) enthaltende Nanostrukturen herzustellen und zu charakterisieren. Hierbei wurden zunächst wasserlösliche Homopolymere bestehend aus EtOx oder MeOx in Bezug auf ihre Fähigkeiten als Stabilisatoren für hydrophobe Nanopartikel untersucht. Homopolymere mit unterschiedlichem Polymerisationsgrad (DP; 25, 60, 100, 200) wurden synthetisiert und bezüglich ihrer Eignung als Emulgatoren für die Nanoemulsionsmethode mit den kommerziellen Emulgatoren Poly(vinylalkohol) und Pluronic F127 verglichen. Zusätzlich wurden diese Polymere als Kryoprotektoren eingesetzt und mit den standardmäßig genutzten Zuckern Glukose, Trehalose und Saccharose verglichen. Polymere mit einem DP von 60, 100 oder 200 erwiesen sich hierbei als sehr gute Stabilisatoren als „all-in-one“ System während der Präparation, Aufreinigung und Gefriertrocknung der Nanopartikel.

Ein weiterer Schwerpunkt dieses Kapitels beschäftigte sich mit der Selbst- und Co-Assemblierung von P(Ox)-basierten Copolymeren. Es konnte gezeigt werden, dass blockähnliche Copolymere bestehend aus P(EtOx) und Poly(harnstoff) in wässrigem Medium assembliert werden können und die resultierenden Nanostrukturen eine hohe Uniformität aufweisen. Diese Nanostrukturen werden vermutlich durch Wasserstoffbrückenbindungen stabilisiert.

Weiterhin konnten amphiphile Block-Copolymere bestehend aus einem hydrophoben 2-Nonyl-2-oxazolin (NonOx) Block sowie einem hydrophilen EtOx oder 2-(4-Aminobutyl)-2-oxazolin (AmOx) Block selbst- und co-assembliert werden. Nanostrukturen, welche aus ausschließlich mit dem AmOx enthaltenden Copolymere präpariert wurden, waren hierbei sphärisch, während alle Co-Assemblierungen sowie die Selbst-Assemblierungen des EtOx enthaltenden Copolymers stäbchenförmig waren. Es konnte eine kritische Mizellenkonzentration von 10^{-7} bis 10^{-6} M bestimmt werden. Des Weiteren konnte mithilfe von dynamischer Lichtstreuung eine pH-responsive Größenänderung der Nanostrukturen abhängig von Anteil an AmOx bestimmt werden. Diese Nanostrukturen wurden in einem späteren Abschnitt dieser Arbeit für den Transport genetischen Materials genutzt.

Nanostrukturen, genauer gesagt Nanogele, welche für den Transport von Wirkstoffen bestimmt waren, wurden aus wasserlöslichen Block-Copolymeren, bestehend aus AmOx und EtOx, hergestellt. Diese Copolymere wurden in Chloroform assembliert und anschließend über die Aminogruppen mittels einer Imin-Bindung quervernetzt, um definierte Nanogele zu erhalten. Des Weiteren wurde der Quervernetzungsprozess dazu genutzt einen Wirkstoff kovalent in den Kern des Nanogels zu binden. Mittels DLS Messungen konnten die Reversibilität dieser Nanogele nachgewiesen werden. Die Freigabe des Wirkstoffes ist deshalb wahrscheinlich, jedoch nicht quantifizierbar.

Der Transport genetischen Materials in Zellen stellt ein wichtiges Themengebiet dieser Arbeit dar. Aus diesem Grund wurden die zuvor hergestellten pH responsiven Polymernano-strukturen diesbezüglich untersucht. Zusätzlich zu den Nanostrukturen wurden hydrophile Copolymere bestehend aus AmOx und EtOx oder AmOx und MeOx untersucht. Es zeigte sich, dass die kationischen Copolymere das genetische Material reversibel binden konnten.

Zudem wurde eine erwartete Abhängigkeit der Zytotoxizität vom Amin-Gehalt der verwendeten Polymere bestätigt. Obwohl die wasserlöslichen Polymere und die Nanostrukturen ein ähnliches Verhalten bezüglich der zellulären Aufnahme zeigten, konnten nur Mizellen-basierte Systeme erfolgreich transfizieren. Diese Überlegenheit gegenüber den wasserlöslichen System kann sowohl auf dem hydrophoben Anteil der Polymere als auch der Anordnung zur Nanostruktur beruhen.

Im letzten Kapitel dieser Arbeit, welches sich mit dem Transport von kovalent gebundenen Wirkstoffen befasste, wurden ebenfalls hydrophile Polymere genutzt. Hierbei konnte zum einen die gezielte Bindung Azid-endfunktionalisierter Polymere mittels Kupfer katalysierter Click-Chemie demonstriert werden. Zum anderen konnten die wasserlöslichen DOX enthaltenden Nanostrukturen *in vitro* und *in vivo* bezüglich ihrer zellulären Aufnahme und der therapeutischen Effizient untersucht werden. Es konnte festgestellt werden, dass unter *in vitro* Bedingungen eine verlangsamte zelluläre Aufnahme der Nanogele im Vergleich zum reinen Wirkstoff stattfindet. Des Weiteren konnte die Zytotoxizität in HT-29 Zell-Linien gesteigert werden. *In vivo* Experimente zeigten eine erhöhte Lebensdauer der mit DOX Nanogelen behandelten Tiere im Vergleich zu Tieren, welche mit DOX behandelt wurden.

Zusammengefasst konnte in dieser Arbeit die Synthese neuer aus P(Ox) und Poly(urea) bestehenden Polymere gezeigt werden. Diese Polymere wurden ausgehend von Amin-funktionalisierten 2-Oxazolinen hergestellt und bezüglich ihrer Syntheseroute als auch ihrer Polymerisationskinetiken mit Amin-funktionalisierten P(Ox) verglichen. Weiterhin konnten wasserlösliche P(Ox)-basierte Homopolymere als Nanopartikelstabilisatoren während der Herstellung, Aufreinigung und Lyophilisierung verwendet werden. Des Weiteren wurden Blockcopolymere assembliert und die Nanostrukturen charakterisiert. Diese Systeme konnten schließlich erfolgreich zum Transport von Wirkstoffen und genetischem Material verwendet werden.

9. References

[1] R. Duncan, R. Gaspar, *Mol. Pharm.* **2011**, *8*, 2101-2141.
[2] C. Tros de Ilarduya, Y. Sun, N. Düzgüneş, *Eur. J. Pharm. Sci.* **2010**, *40*, 159-170.
[3] N. Adams, U. S. Schubert, *Adv. Drug Deliv. Rev.* **2007**, *59*, 1504-1520.
[4] R. Luxenhofer, Y. Han, A. Schulz, J. Tong, Z. He, A. V. Kabanov, R. Jordan, *Macromol. Rapid Commun.* **2012**, *33*, 1613-1631.
[5] T. Kagiya, S. Narisawa, T. Maeda, K. Fukui, *J. Polym. Sci. C: Polym. Lett.* **1966**, *4*, 441-445.
[6] W. Seeliger, E. Aufderhaar, W. Diepers, R. Feinauer, R. Nehring, W. Thier, H. Hellmann, *Angew. Chem. Int. Ed.* **1966**, *5*, 875-888.
[7] D. Tomalia, D. Sheetz, *J. Polym. Sci. Part A: Polym. Chem.* **1966**, *4*, 2253-2265.
[8] T. Bassiri, A. Levy, M. Litt, *J. Polym. Sci. C: Polym. Lett.* **1967**, *5*, 871-879.
[9] R. Hoogenboom, *Macromol. Chem. Phys.* **2007**, *208*, 18-25.
[10] B. Guillerm, S. Monge, V. Lapinte, J. J. Robin, *Macromol. Rapid Commun.* **2012**, *33*, 1600-1612.
[11] F. Wiesbrock, R. Hoogenboom, C. H. Abeln, U. S. Schubert, *Macromol. Rapid Commun.* **2004**, *25*, 1895-1899.
[12] H. Schlaad, C. Diehl, A. Gress, M. Meyer, A. L. Demirel, Y. Nur, A. Bertin, *Macromol. Rapid Commun.* **2010**, *31*, 511-525.
[13] M. W. Fijten, C. Haensch, B. M. van Lankvelt, R. Hoogenboom, U. S. Schubert, *Macromol. Chem. Phys.* **2008**, *209*, 1887-1895.
[14] L.-Y. Qiu, L. Yan, L. Zhang, Y.-M. Jin, Q.-H. Zhao, *Int. J. Pharm.* **2013**, *456*, 315-324.
[15] Y. Gao, Y. Li, Y. Li, L. Yuan, Y. Zhou, J. Li, L. Zhao, C. Zhang, X. Li, Y. Liu, *Nanoscale* **2015**, *7*, 597-612.
[16] J. Li, Y. Zhou, C. Li, D. Wang, Y. Gao, C. Zhang, L. Zhao, Y. Li, Y. Liu, X. Li, *Bioconjugate Chem.* **2014**, *26*, 110-119.
[17] K. Kempe, R. Hoogenboom, M. Jaeger, U. S. Schubert, *Macromolecules* **2011**, *44*, 6424-6432.
[18] G. Volet, T.-X. Lav, J. Babinot, C. Amiel, *Macromol. Chem. Phys.* **2011**, *212*, 118-124.
[19] Y. Zhao, Y. Zhou, D. Wang, Y. Gao, J. Li, S. Ma, L. Zhao, C. Zhang, Y. Liu, X. Li, *Acta Biomater.* **2015**, *17*, 182-192.
[20] P. H. Kierstead, H. Okochi, V. J. Venditto, T. C. Chuong, S. Kivimae, J. M. Fréchet, F. C. Szoka, *J. Controlled Release* **2015**, *213*, 1-9.
[21] Z. He, A. Schulz, X. Wan, J. Seitz, H. Bludau, D. Y. Alakhova, D. B. Darr, C. M. Perou, R. Jordan, I. Ojima, *J. Controlled Release* **2015**, *208*, 67-75.
[22] Z. He, X. Wan, A. Schulz, H. Bludau, M. A. Dobrovolskaia, S. T. Stern, S. A. Montgomery, H. Yuan, Z. Li, D. Alakhova, *Biomaterials* **2016**, *101*, 296-309.
[23] L. Tauhardt, M. Frant, D. Pretzel, M. Hartlieb, C. Bücher, G. Hildebrand, B. Schröter, C. Weber, K. Kempe, M. Gottschaldt, *J. Mater. Chem. B* **2014**, *2*, 4883-4893.
[24] M. C. Woodle, C. M. Engbers, S. Zalipsky, *Bioconjugate Chem.* **1994**, *5*, 493-496.
[25] S. Zalipsky, C. B. Hansen, J. M. Oaks, T. M. Allen, *J. Pharm. Sci.* **1996**, *85*, 133-137.
[26] H. Xu, W. Zhang, Y. Li, F. Y. Fei, P. P. Yin, X. Yu, M. N. Hu, Y. S. Fu, C. Wang, D. J. Shang, *Pharm. Res.* **2014**, *31*, 3038-3050.
[27] M. Glassner, M. Vergaelen, R. Hoogenboom, *Polym. Int.* **2018**, *67*, 32-45.

[28] K. L. Eskow Jaunarajs, D. G. Standaert, T. X. Viegas, M. D. Bentley, Z. Fang, B. Dizman, K. Yoon, R. Weimer, P. Ravenscroft, T. H. Johnston, *Mov. Disord.* **2013**, *28*, 1675-1682.
[29] R. Luxenhofer, R. Jordan, *Macromolecules* **2006**, *39*, 3509-3516.
[30] K. Kempe, C. Weber, K. Babiuch, M. Gottschaldt, R. Hoogenboom, U. S. Schubert, *Biomacromolecules* **2011**, *12*, 2591-2600.
[31] G. Le Fer, C. Le Cœur, J.-M. Guigner, C. Amiel, G. Volet, *Langmuir* **2017**, *33*, 2849-2860.
[32] G. Le Fer, C. Amiel, G. Volet, *Eur. Polym. J.* **2015**, *71*, 523-533.
[33] T.-X. Lav, P. Lemechko, E. Renard, C. Amiel, V. Langlois, G. Volet, *React. Funct. Polym.* **2013**, *73*, 1001-1008.
[34] S. Cesana, A. Kurek, M. A. Baur, J. Auernheimer, O. Nuyken, *Macromol. Rapid Commun.* **2007**, *28*, 608-615.
[35] O. Sedlacek, B. D. Monnery, J. Mattova, J. Kucka, J. Panek, O. Janouskova, A. Hocherl, B. Verbraeken, M. Vergaelen, M. Zadinova, R. Hoogenboom, M. Hruby, *Biomaterials* **2017**, *146*, 1-12.
[36] G. Vancoillie, W. L. A. Brooks, M. A. Mees, B. S. Sumerlin, R. Hoogenboom, *Polym. Chem.* **2016**, *7*, 6725-6734.
[37] A. Gress, A. Völkel, H. Schlaad, *Macromolecules* **2007**, *40*, 7928-7933.
[38] A. C. Rinkenauer, L. Tauhardt, F. Wendler, K. Kempe, M. Gottschaldt, A. Traeger, U. S. Schubert, *Macromol. Biosci.* **2015**, *15*, 414-425.
[39] C. Taubmann, R. Luxenhofer, S. Cesana, R. Jordan, *Macromol. Biosci.* **2005**, *5*, 603-612.
[40] S. Cesana, J. Auernheimer, R. Jordan, H. Kessler, O. Nuyken, *Macromol. Chem. Phys.* **2006**, *207*, 183-192.
[41] M. Hartlieb, D. Pretzel, K. Kempe, C. Fritzsche, R. M. Paulus, M. Gottschaldt, U. S. Schubert, *Soft Matter* **2013**, *9*, 4693-4704.
[42] R. Hoogenboom, M. W. M. Fijten, U. S. Schubert, *J. Polym. Sci. Part A: Polym. Chem.* **2004**, *42*, 1830-1840.
[43] M. Glassner, D. R. D'hooge, J. Young Park, P. H. M. Van Steenberge, B. D. Monnery, M.-F. Reyniers, R. Hoogenboom, *Eur. Polym. J.* **2015**, *65*, 298-304.
[44] T. Saegusa, S. Kobayashi, A. Yamada, *Macro. Chem. Phys.* **1976**, *177*, 2271-2283.
[45] M. W. M. Fijten, R. Hoogenboom, U. S. Schubert, *J. Polym. Sci. Part A: Polym. Chem.* **2008**, *46*, 4804-4816.
[46] R. Hoogenboom, M. W. M. Fijten, H. M. L. Thijs, B. M. van Lankvelt, U. S. Schubert, *Des. Monomers Polym.* **2005**, *8*, 659-671.
[47] H. Goossens, S. Catak, M. Glassner, V. R. de la Rosa, B. D. Monnery, F. De Proft, V. Van Speybroeck, R. Hoogenboom, *ACS Macro Lett.* **2013**, *2*, 651-654.
[48] F. Wiesbrock, R. Hoogenboom, M. A. M. Leenen, M. A. R. Meier, U. S. Schubert, *Macromolecules* **2005**, *38*, 5025-5034.
[49] R. Hoogenboom, M. W. Fijten, S. Wijnans, A. M. van den Berg, H. M. Thijs, U. S. Schubert, *J. Comb. Chem.* **2006**, *8*, 145-148.
[50] P. Wilson, P. C. Ke, T. P. Davis, K. Kempe, *Eur. Polym. J.* **2017**, *88*, 486-515.
[51] M. Hartlieb, K. Kempe, U. S. Schubert, *J. Mater. Chem. B* **2015**, *3*, 526-538.
[52] R. Hoogenboom, H. M. L. Thijs, M. W. M. Fijten, B. M. van Lankvelt, U. S. Schubert, *J. Polym. Sci. Part A: Polym. Chem.* **2007**, *45*, 416-422.
[53] C.-A. Fustin, N. Lefèvre, R. Hoogenboom, U. S. Schubert, J.-F. Gohy, *Macromol. Chem. Phys.* **2007**, *208*, 2026-2031.
[54] M. N. Leiske, M. Hartlieb, F. H. Sobotta, R. M. Paulus, H. Gorls, P. Bellstedt, U. S. Schubert, *Polym. Chem.* **2016**, *7*, 4924-4936.

[55] K. Kempe, S. L. Ng, K. F. Noi, M. Müllner, S. T. Gunawan, F. Caruso, *ACS Macro Lett.* **2013**, *2*, 1069-1072.
[56] M. N. Leiske, M. Hartlieb, C. Paulenz, D. Pretzel, M. Hentschel, C. Englert, M. Gottschaldt, U. S. Schubert, *Adv. Funct. Mater.* **2015**, *25*, 2458-2466.
[57] M. Hartlieb, D. Pretzel, M. Wagner, S. Hoeppener, P. Bellstedt, M. Görlach, C. Englert, K. Kempe, U. S. Schubert, *J. Mater. Chem. B* **2015**, *3*, 1748-1759.
[58] T. B. Bonné, K. Lüdtke, R. Jordan, P. Štěpánek, C. M. Papadakis, *Colloid Polym. Sci.* **2004**, *282*, 833-843.
[59] R. Ivanova, T. Komenda, T. B. Bonné, K. Lüdtke, K. Mortensen, P. K. Pranzas, R. Jordan, C. M. Papadakis, *Macromol. Chem. Phys.* **2008**, *209*, 2248-2258.
[60] S. Jaksch, A. Schulz, Z. Di, R. Luxenhofer, R. Jordan, C. M. Papadakis, *Macromol. Chem. Phys.* **2016**, *217*, 1448-1456.
[61] Z. He, L. Miao, R. Jordan, D. S-Manickam, R. Luxenhofer, A. V. Kabanov, *Macromol. Biosci.* **2015**, *15*, 1004-1020.
[62] T. Bus, C. Englert, M. Reifarth, P. Borchers, M. Hartlieb, A. Vollrath, S. Hoeppener, A. Traeger, U. S. Schubert, *J. Mater. Chem. B* **2017**, *5*, 1258-1274.
[63] M. N. Leiske, F. H. Sobotta, S. Hoeppener, J. C. Brendel, A. Traeger, U. S. Schubert, *Biomacromolecules* **2018**, *19*, 748-760.
[64] R. W. Moreadith, T. X. Viegas, M. D. Bentley, J. M. Harris, Z. Fang, K. Yoon, B. Dizman, R. Weimer, B. P. Rae, X. Li, *Eur. Polym. J.* **2017**, *88*, 524-552.
[65] Y. Seo, A. Schulz, Y. Han, Z. He, H. Bludau, X. Wan, J. Tong, T. K. Bronich, M. Sokolsky, R. Luxenhofer, *Polym. Adv. Technol.* **2015**, *26*, 837-850.
[66] J. Tong, X. Yi, R. Luxenhofer, W. A. Banks, R. Jordan, M. C. Zimmerman, A. V. Kabanov, *Mol. Pharm.* **2012**, *10*, 360-377.
[67] R. Luxenhofer, A. Schulz, C. Roques, S. Li, T. K. Bronich, E. V. Batrakova, R. Jordan, A. V. Kabanov, *Biomaterials* **2010**, *31*, 4972-4979.
[68] L. Tauhardt, K. Kempe, M. Gottschaldt, U. S. Schubert, *Chem. Soc. Rev.* **2013**, *42*, 7998-8011.
[69] T. Verbrugghen, B. D. Monnery, M. Glassner, S. Stroobants, R. Hoogenboom, S. Staelens, *J. Controlled Release* **2016**, *235*, 63-71.
[70] M. Glassner, L. Palmieri, B. D. Monnery, T. Verbrugghen, S. Deleye, S. Stroobants, S. Staelens, L. Wyffels, R. Hoogenboom, *Biomacromolecules* **2016**, *18*, 96-102.
[71] Y. Liu, Y. Wang, Y. Wang, J. Lu, V. Piñón III, M. Weck, *J. Am. Chem. Soc.* **2011**, *133*, 14260-14263.
[72] M. Bauer, C. Lautenschlaeger, K. Kempe, L. Tauhardt, U. S. Schubert, D. Fischer, *Macromolecular Bioscience* **2012**, *12*, 986-998.
[73] M. Bauer, S. Schroeder, L. Tauhardt, K. Kempe, U. S. Schubert, D. Fischer, *J. Polym. Sci. Part A: Polym. Chem.* **2013**, *51*, 1816-1821.
[74] R. Shah, Z. Kroneková, A. Zahoranová, L. Roller, N. Saha, P. Sáha, J. Kronek, *J. Mater. Sci. Mater. Med.* **2015**, *26*, 157.
[75] H. P. C. Van Kuringen, J. Lenoir, E. Adriaens, J. Bender, B. G. De Geest, R. Hoogenboom, *Macromol. Biosci.* **2012**, *12*, 1114-1123.
[76] Y. Gao, Y. Zhou, L. Zhao, C. Zhang, Y. Li, J. Li, X. Li, Y. Liu, *Acta Biomater.* **2015**, *23*, 127-135.
[77] M.-J. Shieh, C.-L. Peng, W.-L. Chiang, C.-H. Wang, C.-Y. Hsu, S.-J. J. Wang, P.-S. Lai, *Mol. Pharm.* **2010**, *7*, 1244-1253.
[78] P. Goddard, L. E. Hutchinson, J. Brown, L. J. Brookman, *J. Controlled Release* **1989**, *10*, 5-16.
[79] A. Mero, Z. Fang, G. Pasut, F. M. Veronese, T. X. Viegas, *J. Controlled Release* **2012**, *159*, 353-361.

[80] F. C. Gaertner, R. Luxenhofer, B. Blechert, R. Jordan, M. Essler, *J. Controlled Release* **2007**, *119*, 291-300.
[81] L. wyffels, T. Verbrugghen, B. D. Monnery, M. Glassner, S. Stroobants, R. Hoogenboom, S. Staelens, *J. Controlled Release* **2016**, *235*, 63-71.
[82] R. Gaspar, R. Duncan, *Adv. Drug Deliv. Rev.* **2009**, *61*, 1220-1231.
[83] H. Xu, M. Hu, X. Yu, Y. Li, Y. Fu, X. Zhou, D. Zhang, J. Li, *Eur. J. Pharm. Biopharm.* **2015**, *91*, 66-74.
[84] C. Englert, A.-K. Trützschler, M. Raasch, T. Bus, P. Borchers, A. S. Mosig, A. Traeger, U. S. Schubert, *J. Controlled Release* **2016**, *241*, 1-14.
[85] M. A. Mees, R. Hoogenboom, *Macromolecules* **2015**, *48*, 3531-3538.
[86] I. Forfar, C. Jarry, J.-P. Fayet, A. Carpy, *Arch. Pharm.* **1992**, *325*, 541-543.
[87] J.-J. Bosc, I. Forfar, C. Jarry, J. Ouhabi, J.-M. Leger, A. Carpy, *Arch. Pharm.* **1990**, *323*, 561-566.
[88] A. Nagai, T. Miyagawa, H. Kudo, T. Endo, *Macromolecules* **2003**, *36*, 9335-9339.
[89] O. Bayer, *Angew. Chem.* **1947**, *59*, 257-272.
[90] V. E. Meyer, G. G. Lowry, *J. Polym. Sci. A: Gen. Pap.* **1965**, *3*, 2843-2851.
[91] S. M. Shawki, A. E. Hamielec, *J. Appl. Polym. Sci.* **1979**, *23*, 3155-3166.
[92] T. Yamamoto, M. Yoshizawa, A. Mahmut, M. Abe, S.-i. Kuroda, T. Imase, S. Sasaki, *J. Polym. Sci. A: Polym. Chem.* **2005**, *43*, 6223-6232.
[93] F. Wiesbrock, R. Hoogenboom, M. Leenen, S. F. G. M. van Nispen, M. van der Loop, C. H. Abeln, A. M. J. van den Berg, U. S. Schubert, *Macromolecules* **2005**, *38*, 7957-7966.
[94] T.-H. Liu, W.-T. Cheng, K.-T. Hunang, *J. Photopolym. Sci. Technol.* **2010**, *23*, 529-533.
[95] K. Kempe, E. F.-J. Rettler, R. M. Paulus, A. Kuse, R. Hoogenboom, U. S. Schubert, *Polymer* **2013**, *54*, 2036-2042.
[96] F. Danhier, E. Ansorena, J. M. Silva, R. Coco, A. Le Breton, V. Préat, *J. Controlled Release* **2012**, *161*, 505-522.
[97] J. M. Barichello, M. Morishita, K. Takayama, T. Nagai, *Drug Dev. Ind. Pharm.* **1999**, *25*, 471-476.
[98] H. Fessi, F. Puisieux, J. P. Devissaguet, N. Ammoury, S. Benita, *Int. J. Pharm.* **1989**, *55*, R1-R4.
[99] C. Song, V. Labhasetwar, H. Murphy, X. Qu, W. Humphrey, R. Shebuski, R. Levy, *J. Controlled Release* **1997**, *43*, 197-212.
[100] P. Fonte, S. Soares, F. v. Sousa, A. Costa, V. Seabra, S. Reis, B. Sarmento, *Biomacromolecules* **2014**, *15*, 3753-3765.
[101] P. Fonte, S. Reis, B. Sarmento, *J. Controlled Release* **2016**, *225*, 75-86.
[102] H. K. Makadia, S. J. Siegel, *Polymers* **2011**, *3*, 1377-1397.
[103] S. Bozdag, K. Dillen, J. Vandervoort, A. Ludwig, *J. Pharm. Pharmacol.* **2005**, *57*, 699-707.
[104] R. Basak, R. Bandyopadhyay, *Langmuir* **2013**, *29*, 4350-4356.
[105] S. Galindo-Rodriguez, E. Allémann, H. Fessi, E. Doelker, *Pharm. Res.* **2004**, *21*, 1428-1439.
[106] K. Jain, P. Kesharwani, U. Gupta, N. K. Jain, *Int. J. Pharm.* **2010**, *394*, 122-142.
[107] E. Betthausen, M. Drechsler, M. Fortsch, F. H. Schacher, A. H. E. Muller, *Soft Matter* **2011**, *7*, 8880-8891.
[108] M. Wilhelm, C. L. Zhao, Y. Wang, R. Xu, M. A. Winnik, J. L. Mura, G. Riess, M. D. Croucher, *Macromolecules* **1991**, *24*, 1033-1040.
[109] T. B. Bonné, C. M. Papadakis, K. Lüdtke, R. Jordan, *Colloid Polym. Sci.* **2007**, *285*, 491-497.

[110] A. W. Jackson, D. A. Fulton, *Macromolecules* **2012**, *45*, 2699-2708.
[111] J. S. Basuki, H. T. Duong, A. Macmillan, R. B. Erlich, L. Esser, M. C. Akerfeldt, R. M. Whan, M. Kavallaris, C. Boyer, T. P. Davis, *ACS Nano* **2013**, *7*, 10175-10189.
[112] I. Amelio, F. Cutruzzolá, A. Antonov, M. Agostini, G. Melino, *Trends Biochem. Sci.* **2014**, *39*, 191-198.
[113] W. Godbey, M. A. Barry, P. Saggau, K. K. Wu, A. G. Mikos, *J. Biomed. Mater. Res.* **2000**, *51*, 321-328.
[114] C.-H. Ahn, S. Y. Chae, Y. H. Bae, S. W. Kim, *J. Controlled Release* **2002**, *80*, 273-282.
[115] B. D. Monnery, M. Wright, R. Cavill, R. Hoogenboom, S. Shaunak, J. H. Steinke, M. Thanou, *Int. J. Pharm.* **2017**, *521*, 249-258.
[116] G.-H. Hsiue, H.-Z. Chiang, C.-H. Wang, T.-M. Juang, *Bioconjugate Chem.* **2006**, *17*, 781-786.
[117] J. M. Harris, N. E. Martin, M. Modi, *Clin. Pharmacokinet.* **2001**, *40*, 539-551.
[118] M. Hamidi, A. Azadi, P. Rafiei, *Drug Delivery* **2006**, *13*, 399-409.
[119] T. Lühmann, V. Spieler, V. Werner, M.-G. Ludwig, J. Fiebig, T. D. Mueller, L. Meinel, *ChemBioChem* **2016**, *17*, 2123-2128.
[120] B. Thonemann, G. Schmalz, K.-A. Hiller, H. Schweikl, *Dent. Mater.* **2002**, *18*, 318-323.
[121] T. Yildirim, A. Traeger, P. Sungur, S. Hoeppener, C. Kellner, I. Yildirim, D. Pretzel, S. Schubert, U. S. Schubert, *Biomacromolecules* **2017**, *18*, 3280-3290.
[122] K. K. Upadhyay, A. N. Bhatt, A. K. Mishra, B. S. Dwarakanath, S. Jain, C. Schatz, J.-F. Le Meins, A. Farooque, G. Chandraiah, A. K. Jain, *Biomaterials* **2010**, *31*, 2882-2892.

List of abbreviations

^{1}H-NMR	-	Proton nuclear magnetic resonance spectroscopy
6AF	-	6-Amino fluorescein
AmOx	-	2-(4-Aminobutyl)-2-oxazoline)
API	-	Active pharmaceutical ingredient
Boc	-	*tert*-Butyloxycarbonyl
BocOI	-	*tert*-Butyl 2-iminooxazolidine-3-carboxylatePoly
BocOx	-	2-(4-((*tert*-Butoxycarbonyl)amino)butyl)-2-oxazoline
CLSM	-	Confocal laser scanning microscopy
CMC	-	Critical micelle concentration
COSY -	-	Correlation spectroscopy
CROP	-	Cationic ring-opening polymerization
cryoTEM	-	Cryo transmission electron microscopy
CuAAC	-	Copper catalyzed alkyne azide click chemistry
Đ	-	Dispersity
d	-	Diameter
Da	-	Dalton
DFT	-	Discrete Fourier transform
DiBoc	-	Di-*tert*-butyl dicarbonate
DLS	-	Dynamic light scattering
DOSY	-	Diffusion ordered spectroscopy
DOX	-	Doxorubicin
DMAc	-	*N*,*N*-Dimethylacetamide
DMF	-	Dimethyl formamide
DNA	-	Deoxyribonucleic acid
DSC	-	Differential scanning calorimetry
DP	-	Degree of polymerization
EBA	-	Ethidium bromide assay
ELS	-	Electrophoretic light scattering
Em	-	Emission
EtBr	-	Ethidium bromide
EtOx	-	2-Ethyl-2-oxazoline
Ex	-	Excitation
eYFP	-	Enhanced yellow fluorescent protein
GA	-	Glutaraldehyde
GC	-	Gas chromatography
HEK-293	-	Human embryonic kidney cells 293
HR-ESI MS	-	High resolution electrospray ionization mass spectrometry
HRA	-	Heparin release assay
HSQC	-	Heteronuclear single quantum coherence
HT-29	-	Human colorectal adenocarcinoma cell line
i-PrOH	-	*iso*-Propanol

I	-	Initiator
IL-4	-	Interleukin-4
k_p	-	Reaction rate constant
L929	-	L929 mouse fibroblasts
*l*PEI	-	linear poly(ethylene imine)
µW	-	Microwave
M	-	Monomer
m/z	-	Mass to charge ratio
MeOx	-	2-Methyl-2-oxazoline
MeTos	-	Methyl *p*-toluenesulfonate
MFI	-	Mean fluorescence intensity
M_n	-	Number average molar mass
N	-	Nanostructure
N/P	-	Nitrogen to phosphate ratio
N*/P	-	Amino group to phosphate ratio
n.a.	-	Not available
NEt_3	-	Triethylamine
NHS	-	*N*-Hydroxysuccinimide
NMR-	-	Nuclear magnetic resonance spectroscopy
NonOx	-	2-Nonyl-2-oxazoline
p	-	para
P	-	Polymer
P2VP	-	Poly(2-vinylpyridine)
P(AmOx)	-	Poly(2-(4-aminobutyl)-2-oxazoline)
P(BocOI)	-	Poly(*tert*-butyl 2-iminooxazolidine-3-carboxylate)
P(EtOx)	-	Poly(2-ethyl-2-oxazoline)
P(MeOx)	-	Poly(2-methyl-2-oxazoline)
P(OI)	-	Poly(2-iminooxazolidine-3-carboxylate)
P(Ox)	-	Poly(2-oxazoline)
PBS	-	Phosphate buffered saline
PDI	-	Polydispersity index
pDNA	-	Plasmid deoxyribonucleic acid
PEG	-	Poly(ethylene glycol)
PEI	-	Poly(ethylene imine)
PLA	-	Poly(lactic acid)
PLGA	-	Poly(lactic-*co*-glycolic acid)
ppm	-	parts per million
Pre	-	Precursor
PS	-	Poly(styrene)
PVA	-	Poly(vinyl alcohol)
r	-	Reactivity ratio
RFU	-	Relative fluorescent unit
RI	-	Refractive index
RNA	-	Ribonucleic acid

RT	-	Room temperature
SD	-	Standard deviation
SEC	-	Size-exclusion chromatography
T_d	-	Decomposition temperature
TFA	-	Trifluoroacetic acid
T_g	-	Glass transition temperature
TGA	-	Thermogravimetrical analysis
Wt	-	Weight

Curriculum vitae

09/10/1989	Born in Delmenhorst, Germany
1996 – 2000	Grundschule am Grünen Kamp, Delmenhorst
2000 – 2002	Hermann-Allmers Schule, Delmenhorst
2002 – 2009	Gymnasium an der Willmsstraβe, Delmenhorst General qualification for university entrance
2009 – 2012	Academic studies in Biology and Chemistry (B.Sc.) Car von Ossietzky University, Oldenburg
2011/2012	Student assistant in General and Inorganic Chemistry
2012	Bachelor thesis in the group of Prof. Dr. Ralf. A. Rabus Carl von Ossietzky University, Oldenburg Title: Enzymatic studies on the degradation of branched chain amino acids in *Phaeobacter gallaeciensis*
2012 – 2014	Academic studies in Chemical Biology (M.Sc.) Friedrich Schiller University Jena, Jena
2013 - 2014	Student assistant in the group of Prof. Dr. Ulrich S. Schubert
2014	Master thesis in the group of Prof. Ulrich S. Schubert Friedrich Schiller University Jena, Jena Title: Poly(2-oxazoline)s for DNA applications
2013	Internship in the group of Prof. Dr. Michael Haley University of Oregon, Eugene (USA)
Since 2015	PhD student at the Laboratory of Organic and Macromolecular Chemistry (IOMC) at the Friedrich Schiller University Jena in the group of Prof. Dr. Ulrich S. Schubert Thesis: Poly(2-oxazoline)s: Synthesis, self-assembly and biomedical applications

Meike Nicole Leiske **22.03.2018** **Jena** _____

Publication list

Peer reviewed publications

D. Hoelzer‡, M. N. Leiske‡, M. Hartlieb, T. Bus, D. Pretzel, S. Hoeppener, K. Kempe, R. Thierbach, U. S. Schubert, "Tumor targeting with pH-responsive poly(2-oxazoline)-based nanogels for metronomic doxorubicin treatment", *Oncotarget* **2018**, in press.

D. Hertz‡, M. N. Leiske‡, T. Wloka, A. Traeger, M. Hartlieb, M. M. Kessels, S. Schubert, B. Qualmann, U. S. Schubert, "Comparison of statistical and gradient amino functionalized poly(2-oxazoline)s: Can the transfection efficiency be tuned by the macromolecular structure?", *J. Polym. Sci. Part A: Polym. Chem.* **2018**, in press.
DOI: 10.1002/pola.29000.

M. Grube, M. N. Leiske, U. S. Schubert, I. Nischang, "POx as an alternative to PEG? A hydrodynamic and light scattering study", *Macromolecules* **2018**, *51*, 1905-1916.
DOI: 10.1021/acs.macromol.7b02665.

M. N. Leiske, F. H. Sobotta, F. Richter, S. Hoeppener, J. C. Brendel, A. Traeger, U. S. Schubert, "How to tune the gene delivery and biocompatibility of poly(2-(4-aminobutyl)-2-oxazoline) by self- and co-assembly", *Biomacromolecules* **2018**, *19*, 748-760.
DOI: 10.1021/acs.biomac.7b01535.

M. N. Leiske, A.-K. Trützschler, S. Armoneit, P. Sungur, S. Hoeppener, M. Lehmann, A. Traeger, U. S. Schubert, "Mission imPOxable - Or the unknown utilization of non-toxic poly(2-oxazoline)s as cryoprotectant and surfactant at the same time", *J. Mater. Chem. B* **2017**, *5*, 9102-9113.
DOI: 10.1039/C7TB02443F.

M. Hartlieb‡, T. Bus‡, J. Kübel, D. Pretzel, S. Hoeppener, M. N. Leiske, K. Kempe, B. Dietzek, U.S. Schubert, "Tailoring cellular uptake and fluorescence of poly(2-oxazoline)-based nanogels", *Bioconjugate Chem.* **2017**, *28*, 1229-1235.
DOI: 10.1021/acs.bioconjchem.7b00067.

T. Lühmann, M. Schmidt, M. N. Leiske, V. Spieler, T. C. Majdanski, M. Grube, M. Hartlieb, I. Nischang, S. Schubert, U. S. Schubert, L. Meinel, „Site-specific POxylation of interleukin-4", *ACS Biomater. Sci. Eng.* **2017**, *3*, 304-312.
DOI: 10.1021/acsbiomaterials.6b00578.

M. N. Leiske, M. Hartlieb, F. H. Sobotta, R. M. Paulus, H. Gorls, P. Bellstedt, U. S. Schubert, "Cationic ring-opening polymerization of protected oxazolidine imines resulting in gradient copolymers of poly(2-oxazoline) and poly(urea)", *Polym. Chem.* **2016**, *7*, 4924-4936.
DOI: 10.1039/C6PY00785F.

M. N. Leiske, M. Hartlieb, C. Paulenz, D. Pretzel, M. Hentschel, C. Englert, M. Gottschaldt, U. S. Schubert, „Lab in a tube: Purification, amplification and detection of DNA using poly(2-oxazoline) multilayers.“ *Adv. Func. Mat.* **2015**, *25*, 2458-2466.
DOI: 10.1002/adfm.201404510.

Submitted manuscripts

M. N. Leiske, M. Hartlieb, A. Traeger, U. S. Schubert, “Evolution of poly(2-oxazoline)s from *in vitro* and *in vivo* studies to clinical trials.” *Submitted*.

[‡]Equal contribution of both authors.

Declared patents

Friedrich-Schiller-Universität Jena. Organische Polymerpartikel enthaltend Poly(oxazolin)-Stabilisatoren und Verwendung von Poly(oxazolinen) zur Stabilisierung von organischen Polymerpartikeln. Erfinder: Meike N. Leiske, Anja Traeger und Ulrich S. Schubert. 14.03.2017. DE 10 2017 002 454.5.

Friedrich-Schiller-Universität Jena. Stabilisierung von Zellkulturen durch Polyoxazoline. Erfinder: Meike N. Leiske, Anja Traeger und Ulrich S. Schubert. 26.05.2017. DE 10 2017 005 048.1.

Non-peer reviewed conference proceedings

252nd ACS national meeting (Philadelphia, PA, USA):
M. N. Leiske[§], M. Hartlieb, F. H. Sobotta, R. M. Paulus, H. Gorls, P. Bellstedt, U. S. Schubert (2016): Co-polymers of poly(2-oxazoline) and substituted poly(urea) as an easy access to hydrogen-bond stabilized nanostructures (final paper number: POLY 60).

252nd ACS National meeting (Philadelphia, PA, USA):
M. N. Leiske[§], M. Hartlieb, C. Paulenz, D. Pretzel, M. Hentschel, C. Englert, M. Gottschaldt, U. S. Schubert (2016): Lab in a tube: Purification, amplification, and detection of DNA using poly(2-oxazoline) multilayers (final paper number: POLY 276).

Printing Future Days 2015 (Chemnitz, Germany):
M. Herzig, M. N. Leiske, E. Preußger, T. Luehmann, M. Hartlieb, S. Hoeppener, S. Hoelzer, L. Meinel, U. S. Schubert (2015): Reactive inkjet printing of functional poly(oxazoline)s for biomedical applications.

Oral presentations

FSU Jena – U. Tokyo workshop 2017 (Jena, Germany):
M. N. Leiske[§], A.-K. Trützschler, S. Armoneit, P. Sungur, S. Hoeppener, M. Lehmann, A. Traeger, U. S. Schubert (2017): Mission imPOxable – Or the unknown utilization of non-toxic poly(2-oxazoline)s as cryoprotectant and surfactant at the same time.

4th Euro BioMAT 2017 (Weimar, Germany):
M. N. Leiske[§], M. Hartlieb, C. Paulenz, D. Pretzel, M. Hentschel, C. Englert, M. Gottschaldt, U. S. Schubert (2017): Lab in a tube: Or the combination of DNA purification and amplification by using a poly(2-oxazoline) based all-in one system.

252nd ACS national meeting (Philadelphia, PA, USA):
M. N. Leiske[§], M. Hartlieb, F. H. Sobotta, R. M. Paulus, H. Gorls, P. Bellstedt, U. S. Schubert (2016): Co-polymers of poly(2-oxazoline) and substituted poly(urea) as an easy access to hydrogen-bond stabilized nanostructures (final paper number: POLY 60).

252nd ACS National meeting (Philadelphia, PA, USA):
M. N. Leiske[§], M. Hartlieb, C. Paulenz, D. Pretzel, M. Hentschel, C. Englert, M. Gottschaldt, U. S. Schubert (2016): Lab in a tube: Purification, amplification, and detection of DNA using poly(2-oxazoline) multilayers (final paper number: POLY 276).

IRTG workshop, Polymers: Random coils and beyond (Wittenberg, Germany, November 2015):
M. N. Leiske[§] (2015): Interaction between DNA and polyamines in solution.

[§]Presenter

Poster presentations

Macromolecular Colloquium Freiburg (Freiburg, Germany):
M. N. Leiske[§], F. H. Sobotta, S. Hoeppener, J. C. Brendel, A. Traeger, U. S. Schubert (2018): How to tune the cellular uptake of amino functionalized poly(2-oxazoline)s by appropriate self-assembly.

The 12th International Conference on Advanced Polymers *via* Macromolecular Engineering (Ghent, Belgium):
M. N. Leiske[§], M. Hartlieb, D. Poburski, T. Bus, D. Pretzel, S. Hoeppener, K. Kempe, R. Thierbach, U. S. Schubert (2017): Core-crosslinked poly(2-oxazoline) nanogels as doxorubicin carriers for cancer therapy.

[§]Presenter

Acknowledgement / Danksagung

Last but not least I want to thank all the people who supported me over all the years and worked hard to make all this possible. At first, I want to express my deep grant to my scientific supervisor Prof. Dr. Ulrich S. Schubert. Thank you, Uli, for all the support and the trust in my work over the years. I really enjoyed working in such an interdisciplinary, international and incredibly well equipped group. It is very impressive what you developed in Jena and I am keen to see what the future will bring.
Furthermore, I want to thank Dr. Matthias Hartlieb for his continuous support and supervision over the years. Matthias, thank you for bringing me to the subject of polymer synthesis, for your patience and your never-ending help and discussions. During the last years, your tutoring helped me improving my skills and made my thesis joyful, even on a rocky road. I am happy to see how your carrier develops in the future and who else you are going to rise during the next years.
I also want to thank Dr. Anja Träger for daily supervision. Anja, you always trusted in my knowledge and helped me to realize my ideas and to fill them with life. I am also very thankful that I could find a sympathetic ear in you whenever it was needed. Thank you for challenging all the small problems at work with me. I wish you all the best for your future research group.
I would also like to thank the Bundesministerium für Bildung und Forschung for funding (project: smart-dye-livery, #13N13416).
In the following I want to acknowledge all the coworkers within or outside the Schubert group who supported me and cooperated with me over the years. Firstly, I want to thank Fabian Sobotta who was so kind to act as my first guinea pig as a master student. Fabi, thank you for all the help and support in the lab. You did a great job and I wish you all the best for your future carrier. I would also like to thank Dr. Johannes C. Brendel, Dr. Christine Weber and Dr. Marc Lehmann for all the discussions and the support.
Additionally, I want to thank the people who helped me working out my projects with their great contributions. Thanks to Anne-Kristin Trützschler, David Hertz, Fabian Sobotta, Friederike Richter, Mandy Grube, Marcel Schmidt, Pelin Sungur, Renzo Paulus, Sabine Armoneit, Tanja Bus, Thomas Wloka, Valerie Spieler, Dr. Anja Träger, Dr. David Pretzel, Dr. Dörte Hölzer, Dr. Helmar Görls, Dr. Ivo Nischang, Dr. Joachim Kübel, Dr. Johannes C. Brendel, Dr. Kristian Kempe, Dr. Dr. Marc Lehmann, Matthias Hartlieb, Dr. Michael Kessels, Dr. Peter Bellstedt, Dr. Rene Thierbach, Dr. Stephanie Schubert, Dr. Stephanie Höppener, Dr. Tessa Lühmann, Prof. Dr. Benjamin Dietzek, Prof. Dr. Britta Qualmann and Prof. Dr. Dr. Lorenz Meinel.
Further thanks go to all the students who did practical courses and contributed to my work. Thank you, Nora Engel, Linda Lattermann, Andre Schumann and Stefanie Raps. And thank you, Thomas Wloka. I am sorry I have to mention you with the interns, but this was too funny for me. I know you can deal with it, you workaholic kinetics beast!
Furthermore, I want to thank the people, who keep the whole system running. I want to thank Sandra Köhn, Kristin Schreyer, Nicole Fritz, Carolin Kellner, Annett Urbanek, Dr. Grit

Festag, Dr. Jürgen Vitz, Renzo Paulus, Alexander Meyer, Maximilian Kleinsteuber, Jens Ulbrich, Friederike Pielenz, Steffi Stumpf and Gabi Sentis for instrument introductions, maintenance and service measurements. Furthermore, I would like to thank Dr. Uwe Köhn and Silvia Pfeifer for ordering management.
I further would like to thank Franca Frister, Sylvia Braunsdorf, Simone Burchardt and Doreen Küchler for managing the bureaucracy. Without you, we all would have been stranded.
I would also like to thank the people who helped me to survive the nerve-racking times by supporting my work with jokes, coffee breaks and senseless discussions. Thank you, Franca Frister, Anne-Kristin Trützschler, Renzo Paulus, Dr. Christian Friebi, Tina Mede, Thomas "Das Tier" Wloka, Michi Dirauf, Susi Seupel and Michael "The Lat" Pröhl.
In this regard, I would also like to thank the people in my old and new home for cheering me up, whenever necessary. Thank you Hannah Eilers, Tini Witte, Stella Kaiser and Thesi Wilke. You are the best friends I could have found. Thank you so much for accepting (or at least ignoring) all my quirks for several years.
I also want to thank my parents Heidrun and Jürgen Leiske, my grandparents Margarete and Heinz Leiske as well as my brother Heiko Leiske and my sister-in-law Stephanie Leiske for their continuous support in all situations in life.
Finally, I want to thank my boyfriend and soulmate Thomas, who is already waiting in Melbourne to experience the great adventure of living at the end of the world with me. Contigo al fin del mundo.

Declaration of authorship / Selbstständigkeitserklärung

Hiermit erkläre ich, dass ich die vorliegende Arbeit selbständig angefertigt, nicht anderweitig zu Prüfungszwecken vorgelegt und keine anderen als die angegebenen Hilfsmittel verwendet habe. Sämtliche wissentlich verwendete Textausschnitte, Zitate oder Inhalte anderer Verfasser wurden ausdrücklich als solche gekennzeichnet.

I hereby certify that the work disclosed here is, to the best of my knowledge, original and the result of my own investigations, except as acknowledged, and has not been submitted, either in part or whole, for a degree at this or any other university.

Jena, den 22.03.2018

_____

Meike Nicole Leiske

Publications P1 to P8

Publication P1

Cationic ring-opening polymerization of protected oxazolidine imines resulting in gradient copolymers of poly(2-oxazoline) and poly(urea)

M. N. Leiske, M. Hartlieb, F. H. Sobotta, R. M. Paulus, H. Görls, P. Bellstedt, U. S. Schubert,
Polym. Chem. **2016**, *7*, 4924-4936.

The paper as well as the supporting information (free of charge) is available online: doi.org/10.1039/C6PY00785F.

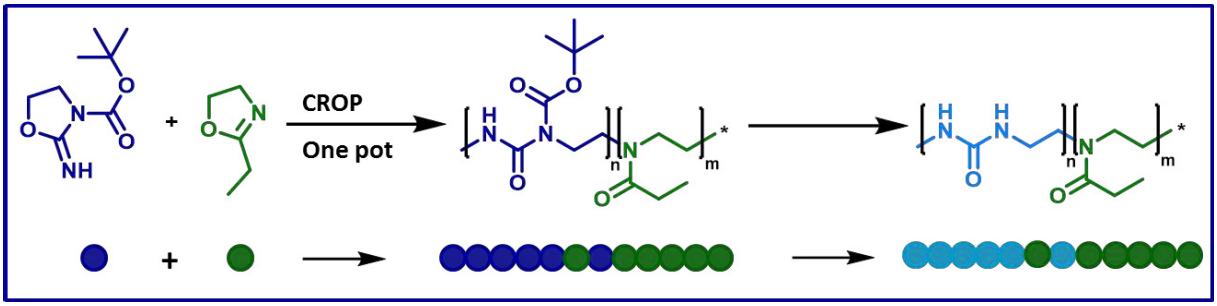

Polymer Chemistry

PAPER

View Article Online
View Journal | View Issue

Cite this: *Polym. Chem.*, 2016, **7**, 4924

Cationic ring-opening polymerization of protected oxazolidine imines resulting in gradient copolymers of poly(2-oxazoline) and poly(urea)†

Meike N. Leiske,[a,b] Matthias Hartlieb,‡[a,b] Fabian H. Sobotta,[a,b] Renzo M. Paulus,[a,b] Helmar Görls,[c] Peter Bellstedt[a] and Ulrich S. Schubert*[a,b]

Received 4th May 2016,
Accepted 24th June 2016

DOI: 10.1039/c6py00785f

www.rsc.org/polymers

Poly(urea)s are a polymer class widely used in industry. Their utilization in biomedical applications is already described, however, the use of controlled polymerization methods instead of polycondensation approaches would allow a better control over the degree of polymerization and the dispersity of the resulting polymers, improving their suitability for this particular field of application. Cationic ring-opening polymerization (CROP) as a chain growth polymerization enables those requirements and, additionally, allows the copolymerization with 2-oxazolines, which are generally known for their biocompatibility. In this report, a Boc protected oxazolidine imine monomer is synthesized and polymerized in a homopolymerization, as well as in a copolymerization with 2-ethyl-2-oxazoline (EtOx) *via* CROP. The synthesized polymers were analyzed regarding their chemical and physical properties, using NMR, GC, MALDI-MS, SEC, TGA and DSC. Copolymerization kinetics revealed the formation of quasi-block copolymers, able to self-assemble in aqueous solution as indicated by DLS.

Introduction

Poly(urea)s are commonly synthesized by polyaddition of diisocyanates and diamines, a method, which was first described by Otto Bayer in 1947.[1] Their major applications are *in situ* formed foams,[1] anti-fouling coatings,[2] grease[3] and anticorrosives.[4] However, also biomedical applications such as siRNA delivery are described.[5–9]

Modifications of the polymerization technique allow the formation of nanocapsules by interfacial polyaddition in inverse mini emulsion reactions[9] or ring-opening polyaddition-condensations.[10] One major advantage of these methods is their insensitivity to moisture,[1] however, the described reaction times extend to several hours depending on their functionalization,[6,11,12] which can be significantly reduced to a few minutes by using the microwave technique.[13]

Nevertheless, the step-growth polyaddition is not suited for the synthesis of well-defined poly(urea)s with controlled macromolecular architectures, molar mass as well as a head-to-tail structure.

Living and controlled polymerization techniques like the living anionic and cationic as well as controlled radical polymerizations facilitate an improved control over the molar masses and the use of functionalized monomers.[14] The group of Hedrick already described a method to synthesize well-defined poly(carbonate)s *via* controlled ring-opening polymerization instead of using polycondensation methods,[15–17] leading to materials which can be applied for biomedical applications.[18] Moreover, the controlled cationic ring-opening polymerization (CROP) of 1,3-oxazolidine-2-thione with methyl triflate was already performed,[19] yielding a sulfur analogue to poly(urea)s. The focus of this report is the CROP of an oxazolidine-2-imine and a possible copolymerization with 2-oxazolines to produce poly(urea)s or copolymeric systems with poly(oxazoline)s (POx).

The polymerization of 2-oxazolines *via* CROP[20] was first described in the 1960s by four independent research groups.[21–24] The use of microwave technology allows a signifi-

[a]*Laboratory of Organic and Macromolecular Chemistry (IOMC), Friedrich Schiller University Jena, Humboldtstraße 10, 07743 Jena, Germany.*
E-mail: ulrich.schubert@uni-jena.de
[b]*Jena Center for Soft Matter (JCSM), Friedrich Schiller University Jena, Philosophenweg 7, 07743 Jena, Germany*
[c]*Institute of Inorganic and Analytical Chemistry, Friedrich Schiller University Jena, Humboldtstraße 8, 07743 Jena, Germany*

†Electronic supplementary information (ESI) available: NMR, SEC, TGA, DSC, HR-ESI-MS, ESI-MS, DLS and X-ray data, a detailed overview about all kinetic studies. Crystallographic data (excluding structure factors) has been deposited with the Cambridge Crystallographic Data Centre as supplementary publication. CCDC 1477579 for **1b**. For ESI and crystallographic data in CIF or other electronic format see DOI: 10.1039/c6py00785f

‡Current address: Department of Chemistry, University of Warwick, Gibbet Hill Road, Coventry, CV4 7AL, UK.

cant reduction of the polymerization time by increasing the reaction temperatures.[25]

By varying the initiator, moieties like alkyl chains[26–29] or unsaturated double and triple bonds[30–32] can be introduced to tune the solubility or to enable post-modification strategies of the polymers. Furthermore, termination of the living chain end using nucleophiles results in end-functionalized polymers.[33,34] The substituent in 2-position of the monomer can be varied in order to alter the polymeric side group[20] and different monomers can be combined to yield copolymeric systems of various architectures.[35]

A further advantage of POx is their suitability as biomaterial, as derivatives with small substituents like 2-ethyl-2-oxazoline (EtOx) and 2-methyl-2-oxazoline (MeOx) are known to be biocompatible and possess a stealth effect similar to polyethylene glycol (PEG).[36–39] In particular, EtOx is polymerizable with a high degree of control[40] and shows PEG-like characteristics concerning biodistribution and excretion.[41–43] During the last years, polymers based on EtOx have been widely characterized regarding toxicity and cellular uptake.[37,39,44] Currently, the *in vivo* behavior of POx is receiving an increasing attention[45,46] due to their numerous previously described benefits *in vitro*.[47,48] The usage of POx in drug delivery systems by conjugation of low molar mass therapeutics[49] and proteins[50] are promising for clinical studies. Additionally, the formation of micelles as drug carriers,[51] nanogels[44] and surface coatings for bio-analytics[52] supports the increasing importance of POx.

The aim of this study is to combine the advantages of POx and poly(urea)s by an easy CROP based copolymerization process. The mechanism and kinetic behavior of the homopolymerization of a substituted oxazolidine imine, as well as the copolymerization with EtOx are described. Homopolymers and copolymers are characterized in detail regarding structure and physical properties. Finally, the copolymer systems were investigated in terms of reactivity ratios and their potential to form nanostructures by hydrogen bond mediated self-assembly.

Results and discussion

Monomer synthesis

In order to synthesize a monomer, which can be polymerized by CROP to yield a poly(urea) structure, the commercially available 2-amino-2-oxazoline hydrochloride was reacted with di-*tert*-butyl dicarbonate (DiBoc) since the Boc protection group is stable during CROP and can be removed under acidic conditions.[53] As the starting material is in a tautomeric equilibrium, the molecule can react on two positions, at the *endo*- and the *exo*-nitrogen (Fig. 1A).

It was already described in literature that the *endo*-nitrogen of 2-amino-2-oxazoline, which is mainly present in solution,[54] is more reactive as compared to the *exo*-nitrogen.[55] The reactivity was predicted by density functional theory (DFT) from the molecule's geometry derived by X-ray crystal analysis. Based on the π-bond lengths, the electronegativity of the atoms could be calculated (*endo*-nitrogen: −0.317, *exo*-nitrogen: −0.272), explaining the differences in reactivity.

As a result, the monomer *tert*-butyl 2-iminooxazolidine-3-carboxylate (**1b**, BocOI) can be synthesized from 2-amino-2-oxazoline hydrochloride by reaction with DiBoc in the presence of triethyl amine (TEA). Since the tautomeric equilibrium cannot be shifted completely to the 2-amino-2-oxazoline, the crude product is a mixture of the two possible products *tert*-butyl (4,5-dihydrooxazol-2-yl)carbamate (~30%, **1a**) and BocOI (~70%, **1b**) (Fig. 1A) according to proton NMR experiments (data not shown). The monomer was purified by recrystallization and the structure was analyzed by ^{1}H-NMR (Fig. S1A†), ^{13}C-NMR (Fig. S1B†), Fourier transform infrared spectroscopy (FTIR, Fig. S3†) and high-resolution electrospray ionization mass spectrometry (HR-ESI-MS, Fig. S2†). HR-ESI-MS shows the lability of the Boc protection group, as indicated by the appearance of the dominant signal at m/z = 131.0 [M − Boc + H^{+}]. Information about the exact structure of the synthesized monomer was obtained by X-ray structure analysis of a single crystal (Fig. 1B, crystallographic data in Table S1†), proving the identity of BocOI (**1b**).

Homopolymerization of BocOI (1b)

A kinetic study of the homopolymerization of BocOI (**1b**) was performed by preparing a stock solution of BocOI (**1b**) and methyl tosylate (MeTos) ([M]/[I] = 60) in dry dichloromethane under a stream of argon and aliquoting the solution over several microwave vials, which were heated in a microwave synthesizer for various times. The conversion was determined *via* gas chromatography (GC) by comparing the monomer concentration with the initial concentration in the stock solution.

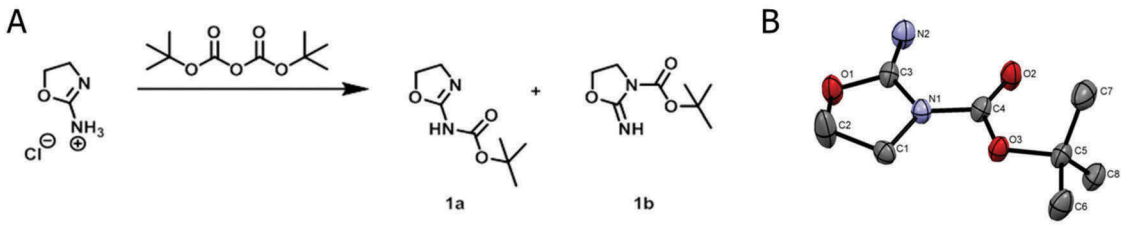

Fig. 1 A: Schematic representation of the Boc protection of 2-amino-2-oxazoline hydrochloride using DiBoc resulting in two possible tautomeric products (*tert*-butyl (4,5-dihydrooxazol-2-yl)carbamate (**1a**) and *tert*-butyl 2-iminooxazolidine-3-carboxylate (**1b**)), and B: Molecular structure of **1b** derived by X-ray crystal structure analysis; H-atoms are excluded.

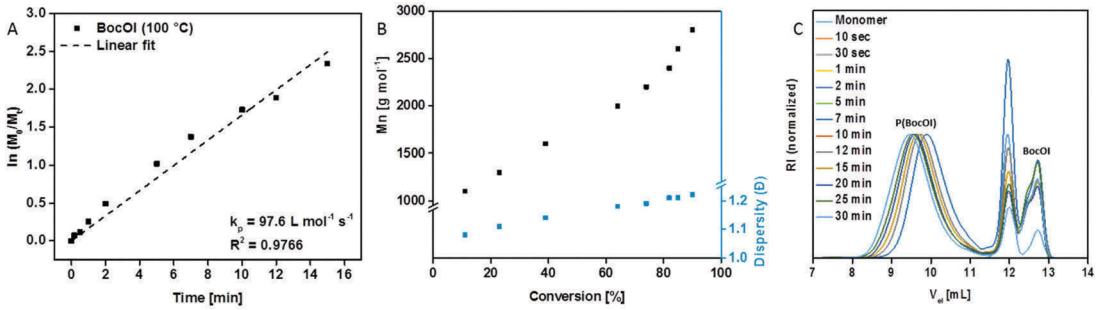

Fig. 2 Kinetic studies of BocOI ([M]/[I] = 60) in CH_2Cl_2 at 100 °C. A: Time-dependent polymerization kinetics calculated by the monomer conversion obtained from GC-analytics. B: Molar mass and dispersity in dependence on the monomer conversion. C: SEC-traces ($CHCl_3$-i-PrOH-TEA, PS-cal.; 1st system peak after 12 min) of the reaction mixture after several polymerization times.

As the concentrations of BocOI (**1b**) and MeTos were equal in all reaction vessels, dichloromethane could be used as an internal standard. By plotting the natural logarithm of the quotient of these amounts, the reaction constant (k_p) could be determined from the slope of the linear fit and the initial initiator concentration (Fig. 2A).

Since the monomer should be copolymerized with EtOx, 140 °C was chosen as the reaction temperature being the optimum for the synthesis of P(EtOx)s using the microwave approach.[25] However, at 140 °C the time dependence of k_p is not linear (Fig. S4A†). Possible explanations for this phenomenon might include the thermal deprotection of BocOI (**1b**), as well as an increased reactivity of BocOI (**1b**), as compared to EtOx. Hence, a reaction temperature of 100 °C was applied.

The time-dependent polymerization kinetics calculated by the monomer conversion obtained from GC-analytics of BocOI (**1b**) at 100 °C shows a nearly linear dependence of conversion with time, however, side-reactions at higher molar masses are still present as can be seen in the conversion dependent M_n values and dispersities (Fig. 2B). The positive deviation of the molar mass from linearity might be attributed to side reactions, such as chain coupling at high conversions. Nevertheless, a pseudo-1st-order kinetics can be postulated for the CROP of BocOI (**1b**, Fig. 2A), having a k_p of 97.6 L mol^{-1} s^{-1}, which is about 20 times higher than the k_p of EtOx at this temperature (k_{pEtOx} = 4.6 L mol^{-1} s^{-1}, Fig. S6B†).

SEC measurements were performed to obtain information about the increase in molar mass as well as the dispersity of the resulting polymers (Fig. 2B and C), showing a linear increase in molar mass and narrow dispersities below 1.3 and mono-modal elution curves, indicating a living polymerization at the given conditions. The increase in dispersity over time could be explained on the same basis as the non-linearity of the polymerization at 140 °C. The decrease in temperature, however, lowers those unintended side-reactions.

NMR spectra of the purified polymer were collected to obtain information about the polymeric structure (Fig. 3). In the ^{1}H-NMR spectrum, two signals for the backbone protons are present at δ = 3.5 and 3.9 ppm, indicating different substituted nitrogens in the polymer backbone as expected for P(BocOI) (Scheme 1). Additionally, the peak at δ = 8.8 ppm is

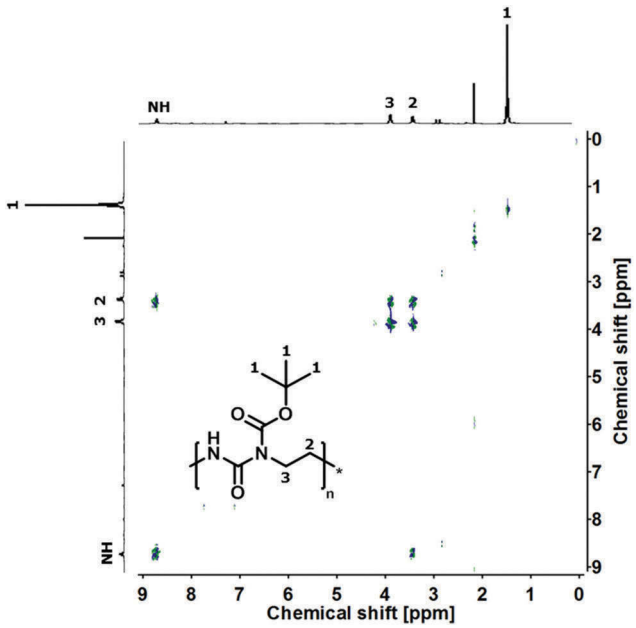

Fig. 3 ^{1}H–^{1}H-COSY NMR spectrum (300 MHz, $CDCl_3$) of P(BocOI)$_n$.

typical for an amide group. Further information was obtained from the ^{1}H–^{1}H-COSY-NMR spectrum, correlating protons on neighboring carbon-atoms in the polymer. It is clearly visible that the protons at δ = 3.5 and 3.9 ppm are coupling with each other. Furthermore, the proton of the downfield shifted backbone signal couples with the amide group at δ = 8.8 ppm indicating a poly(urea) like polymeric structure.

Since BocOI (**1b**) shows comparable structural characteristics as 1,3-oxazolidine-2-thione,[19] a plausible mechanism for the CROP of this monomer can be postulated (Scheme 1). The electrophilic methyl group of the initiator can be attacked by the electron pair of the monomer's imine functionality. This results in a positively charged oxazolidinium ion as an intermediate and a finally partial positively charged carbon atom in 5-position, that can be attacked by another imine group. This leads to a ring-opening and the final poly(urea) like Boc protected backbone structure.

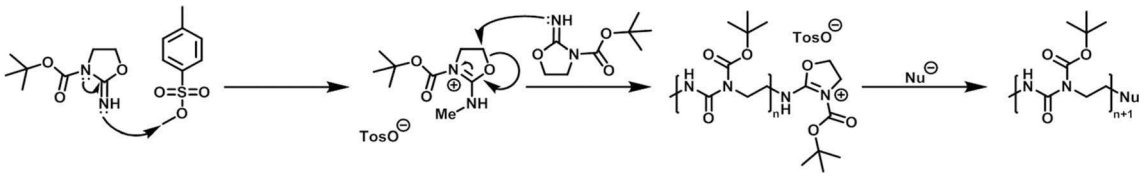

Scheme 1 Schematic representation of the postulated mechanism of the CROP of BocOI (**1b**) initiated with MeTos.

The postulated mechanism of polymerization was further analyzed by a polymerization of BocOI (**1b**) inside an NMR tube. For practical reasons, deuterated chloroform was chosen as solvent instead of dichloromethane. The reaction temperature had to be lowered to 55 °C and was, therefore, slower than the polymerization at 100 °C using the microwave. By comparing the chemical shifts of the pure monomer with the reaction mixture and the purified polymer (Fig. S7†), an assumption about the active species can be made. The spectrum of the monomer has two main triplets at δ = 3.86 and 4.22 ppm belonging to BocOI (**1b**). In the reaction mixture, several new signals appear. An individual integration was not possible due to overlap of these signals, which are vanished after purification of the polymer. However, the signals in this region match with the chemical shift of protons of the active species during the CROP of BocOI (**1b**) as predicted by increment analysis. The protonation of the *exo*-nitrogen leads to a shift of the protons next to the *endo*-nitrogen (4-position). After methylation (B), a slight high field shift (δ = 3.1 ppm) is also indicated by increment analysis. Furthermore, the electron rearrangement that leads to a positively charged *endo*-nitrogen (C) and, therefore, to a stronger shift to high fields (δ = 1.39 ppm) is observed. Additionally, there are further signals between δ = 3.0 and 5.0 ppm matching with the predicted intermediates. However, these signals cannot be assigned certainly.

On the basis of the kinetic data, homopolymers of four different lengths (**2a–d**) were synthesized (**2a–d**). In order to yield poly(urea)s, all purified homopolymers were deprotected using TFA (**3a–d**, Scheme 2). The resulting poly(urea)s and the Boc protected precursors were analyzed using ^{1}H-NMR, SEC, TGA and DSC (Table 1).

By ^{1}H-NMR of the Boc protected homopolymers (Fig. S8†) the degree of polymerization (DP) was determined directly from the reaction mixture (data not shown) by comparing inte-

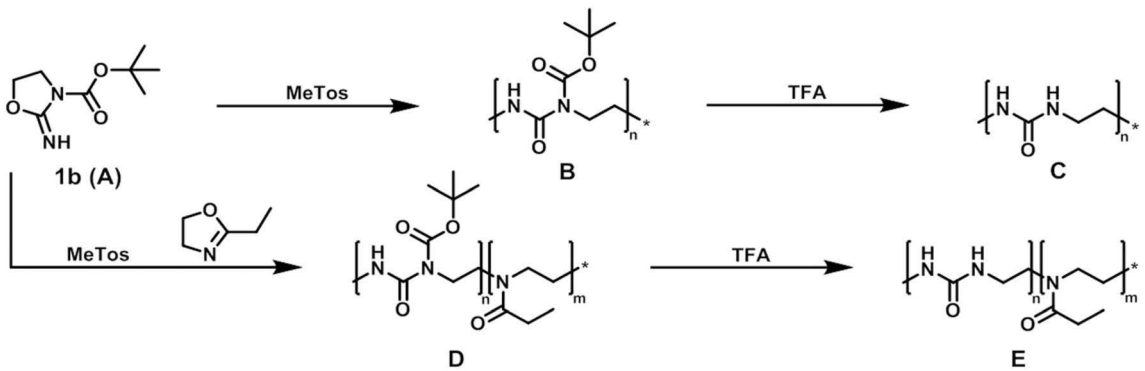

Scheme 2 Overview of the performed polymerization and deprotection reactions, showing the homopolymers P(BocOI)$_n$ (B)and P(OI)$_n$ (C) as well as the copolymers P(BocOI$_n$-*co*-EtOx$_m$) (D) and P(OI$_n$-*co*-EtOx$_m$) (E) obtained by CROP of BocOI (**1b**, A) initiated with MeTos.

Table 1 Characterization data for P(BocOI)$_n$

Polymer	Composition	[M]/[I]	BocOI conversion [%]	DP	M_n [a] [g mol^{-1}]	M_n [b] [g mol^{-1}]	$Đ$ [b]	T_g [c] [°C]	T_d [d] [°C]
2a	P(BocOI)$_{19}$	25	91.9	19[a]	3500	3800	1.18	69.6	154.3
2b	P(BocOI)$_{54}$	50	86.9	55[a]	10 300	4300	1.22	66.2	164.5
2c	P(BocOI)$_{73}$	75	85.0	73[a]	13 600	4400	1.31	68.9	167.6
2d	P(BocOI)$_{112}$	100	87.2	112[a]	20 900	4200	1.20	97.9	170.2
3a	P(OI)$_{19}$	n.a.	n.a.	19	1600	n.d.	n.d.	0.8	175.1
3b	P(OI)$_{54}$	n.a.	n.a.	55	4700	n.d.	n.d.	—	218.2
3c	P(OI)$_{73}$	n.a.	n.a.	73	6300	n.d.	n.d.	7.6	136.3
3d	P(OI)$_{112}$	n.a.	n.a.	112	9600	n.d.	n.d.	2.4	179.5

[a] ^{1}H-NMR (300 MHz) in $CDCl_3$. [b] SEC (PS-calibration) in $CHCl_3$-i-PrOH-TEA. [c] DSC. [d] TGA; n.d.: not determinable due to insolubility; n.a. not applicable. DP and M_n of **3a–d** were calculated from ^{1}H-NMR results of **2a–d**.

grals of the aromatic protons of the MeTos initiator (δ = 7.15 and 7.67 ppm) with one of the polymer backbone peaks (δ = 3.5 ppm). As a consequence, DP values of 19, 54, 73 and 112 could be obtained, respectively. A polymerization at [M]/[I] = 300 was attempted, however resulted in increased dipseristies, which is a result of the longer reaction times required leading to more side reactions (ESI Fig. S31†) According to the ^{1}H-NMR investigations, the monomer consumption was between 85 and 90% (Table 1). Therefore, the positive deviation of the obtained DP from the aimed [M]/[I] can most probably be explained by inaccuracies while weighting the solid monomer. Additionally, ^{13}C-NMR spectra of all Boc protected homopolymers were recorded (Fig. S10†). These spectra provide qualitative information about the polymeric structure. At δ = 28.0 ppm, the peak of the Boc protection group is visible. Moreover, the methyl group of the initiator results in a peak at δ = 30.9 ppm. The two different methylene carbons of the polymeric backbone split into two peaks at δ = 39.9 and 43.3 ppm. At δ = 126.0 and 128.6 ppm, the carbonyl carbons can be identified. Furthermore, SEC measurements of the Boc protected polymers (Fig. S13†) were performed to gain information about their dispersity, revealing narrow values (Table 1). The molar mass does not vary markedly with respect to the DP, which might be due to column interactions. Although it is not obvious from the kinetic studies (Fig. 2), the maximum molar mass for kinetic samples was M_n = 2700 g mol^{-1} and, therefore, is significantly lower than the length of the herein synthesized homopolymers. Additionally, an ESI-MS spectrum (Fig. S14†) of P(BocOI)$_{19}$ (**2a**) was recorded to verify the mass of the repeating unit. The spectrum shows specific peaks for P(BocOI) as well as partially and fully deprotected poly(urea).

FTIR measurements provided further information about the Boc protected (Fig. S11†) and deprotected (Fig. S12†) homopolymers. The spectra of the protected polymers show specific bands at λ = 1533 and 3336 cm^{-1}, representing the NH oscillations of the polymers. At λ = 2937 to 3009 cm^{-1}, the CH_2 vibrations of the polymeric backbone are visible as three different peaks. Furthermore, the Boc protection group shows oscillations at λ = 754, 852 and 1371 cm^{-1}, respectively. Carbonyl vibrations in the FTIR spectrum are visible at λ = 1157, 1231, 1681 and 1719 cm^{-1}, respectively.

The spectra of the deprotected polymers lack specific bands at λ = 1371 and 852 cm^{-1} verifying the deprotection. Furthermore, the carbonyl band at λ = 1719 cm^{-1} shift to a lower value around λ = 1681 cm^{-1}, overlapping with the previous amide band, after deprotection.

^{1}H-NMR measurements of the deprotected homopolymers were performed in deuterated hydrochloric acid and verified the success of the deprotection by disappearance of the Boc peak in the spectrum (Fig. S9†) while keeping the backbone signals at δ = 3.4 to 3.8 ppm. The peaks at high ppm values (δ = 7.15 and 7.67 ppm) could be attributed to a degradation of the polymer in the presence of high DCl concentrations. SEC and MS measurements of deprotected polymers could not be performed due to the insolubility in the available solvents.

To elucidate the thermal properties of the polymers, TGA and DSC measurements were performed. The TGA results revealed a T_d of 150 to 170 °C for the protected homopolymers (**2a–d**) that increases slightly with the polymer length (Table 1). Since this temperature does not change significantly with the polymer length and the graph (Fig. S26A†) only shows a partial decomposition (~50%), a thermal deprotection of the polymers can be assumed. Issues regarding this phenomenon have already been reported[56] and might also be the trigger of the lack in controllability while polymerizing BocOI at 140 °C. After this first mass loss, all polymers show a comparable decomposition behavior with a second T_d around 200 °C. Likewise, this is roughly the T_d of the deprotected polymers (**3a–d**) (Fig. S27A†), verifying the hypothesis of a thermal deprotection. The lack of a clear trend of the T_d of **3a–d** might be caused by intra- and intermolecular stabilization of the polymers due to hydrogen-bond formation during the heating process, which is also explaining the higher degradation temperatures of the polymers.

According to the DSC measurements (Fig. S28A†), the Boc protected homopolymers (**2a–d**) show a T_g between 65 and 70 °C, except polymer **2d** which shows a significantly increased T_g of 98 °C (Table 1). The reason for this sudden increase in T_g is not understood jet. The deprotected homopolymers (**3a–d**) have a glass-transition temperature between 0 and 10 °C (Fig. S29A†), again showing no dependency of the chain length of the polymers. This sharp decrease in the T_g is caused by intra- and intermolecular interactions of the urea structure.

Copolymerization of BocOI and EtOx

After the successful homopolymerization of BocOI (**1b**) *via* CROP, the copolymerization with EtOx was investigated. The formation of gradient or quasi-block structured polymers was assumed to be likely due to the high difference in the reaction constants between the two monomers based on the homopolymerization kinetics. To confirm this assumption, the reactivity ratios were assessed by determination of velocity constants of both monomers while copolymerizing at different monomer ratios. The general reaction conditions were kept equal to the homopolymerization. Four stock solutions bearing different monomer ratios were prepared under a stream of argon, divided over several reaction vessels and heated to 100 °C in a microwave synthesizer for predetermined times. After the reaction times, the k_p values for both monomers were calculated from the linear fit of the monomer conversion determined by GC measurements (Fig. 4). BocOI shows slight deviation from ideal linear behavior, which could be assigned to interactions with EtOx, as linearity increases at higher BocOI contents. The resulting averaged constant for BocOI (k_p = 58.0 ± 5.6 L mol^{-1} s^{-1}) is about ten times higher than for EtOx (k_p = 5.2 ± 1.4 L mol^{-1} s^{-1}).

The formation of gradient copolymers from 2-oxazoline monomers having different k_p values is described in literature for several monomer pairs like 2-nonyl-2-oxazoline and 2-phenyl-2-oxazoline (PhOx),[51] as well as MeOx and 2-(3-butenyl)-2-oxazoline.[57,58] However, it should be pointed out that the difference between EtOx and BocOI is significantly

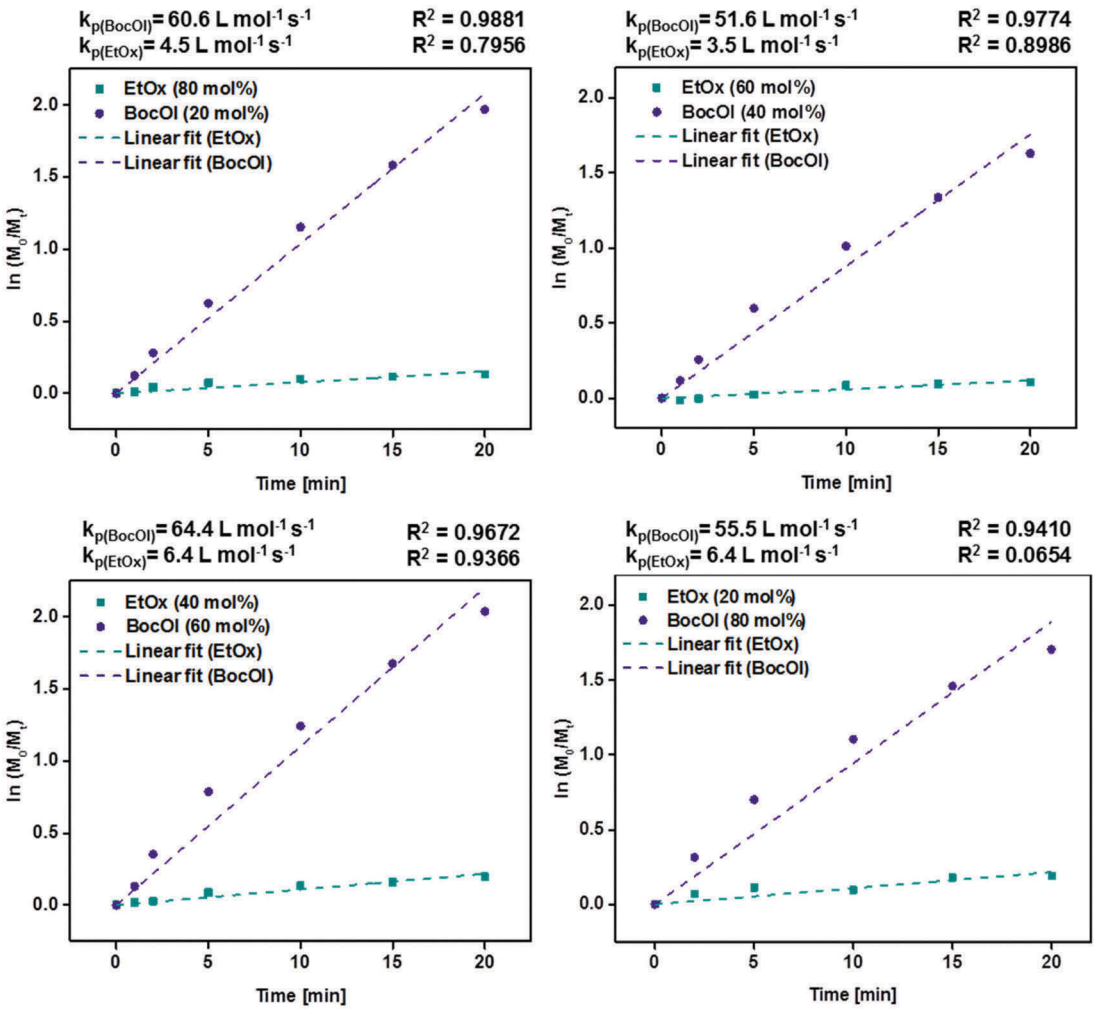

Fig. 4 Time-dependent polymerization kinetics calculated by the monomer conversion obtained from GC-analytics for BocOI (**1b**) and EtOx at four monomer compositions, namely 20, 40, 60 and 80 mol% BocOI (**1b**), performed in dichloromethane at 100 °C with [M]/[I] = 100 and methyl tosylate as initiator.

larger, leading to the assumption of a quasi-block polymeric structure. Using the data from the kinetic studies, the reactivity ratios (r) were calculated by non-linear least square fitting (Fig. 5A).[59] For these calculations, the kinetic plots were used to determine the ratio of consumed monomers at 30% of conversion of the faster monomer (BocOI, **1b**) to ensure that monomer feed ratios are unaffected by the polymerization, excluding a falsification of the calculation by changing monomer ratios at high conversions. Subsequently, the conversion of EtOx as the less reactive monomer is calculated at this time. By plotting the incorporated EtOx fraction (F_1) against the theoretical EtOx fraction in the monomer feed (f_1), a non-linear dependence is obtained. The reactivity ratios were calculated using eqn (3) as adapted from literature,[60] excluding negative values. A similar behavior was already reported by Hoogenboom *et al.*[61] and Kagiya *et al.*[62] for MeOx and PhOx, respectively.

The calculations resulted in $r_{\mathrm{BocOI}} = 28.72 \pm 10.07 \gg 1 \gg r_{\mathrm{EtOx}} = 0.000 \pm 0.002$. The very large difference between the two monomers as well as the fact that the reactivity ratio of EtOx is close to zero, while BocOI monomers are present in the reaction mixture, leads to the conclusion of a very narrow gradient area in the polymer chain. To illustrate this fact, the monomer distribution over the polymer chain (Fig. 5B) was calculated based on the kinetic plots (Fig. 4). Symbols represent the actual values of the EtOx fraction in the polymer chain. These values were fitted by a non-linear Boltzmann fitting (lines) to obtain information about the monomer distribution in the polymer from initiation to termination, showing that most BocOI (**1b**) is polymerized prior to the EtOx incorporation.

Based on the information obtained by the kinetic data, a series of copolymers with different monomer ratios was synthesized and deprotected with TFA. Polymerizations were carried out under microwave irradiation at 100 °C under argon atmosphere. Aiming for a DP of 100, polymers with 20%, 40%, 60% and 80% BocOI (**1b**) content were synthesized. The analytical details for all copolymers can be found in Table 2. The DP was determined by ^{1}H-NMR directly from the reaction

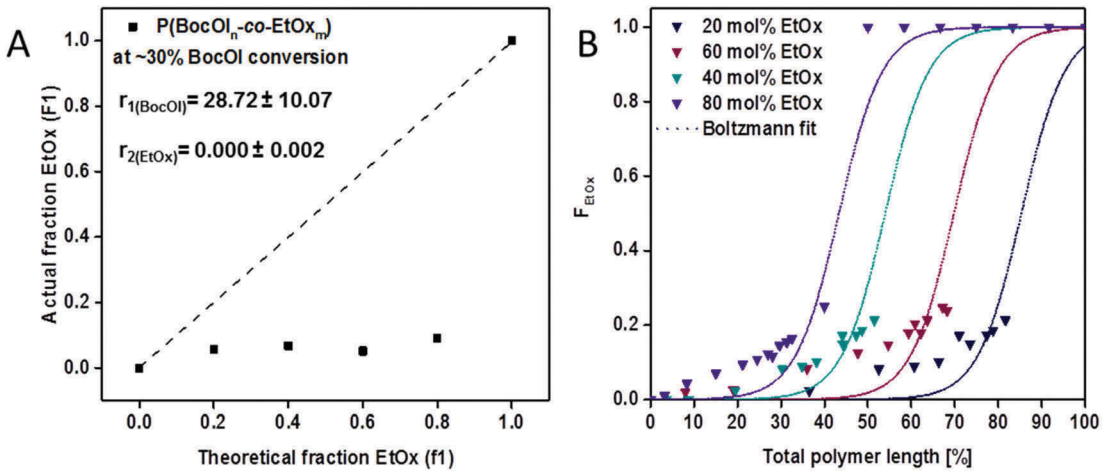

Fig. 5 A: Relation between the fraction of EtOx in the monomer feed (f_1) and the incorporated fraction of EtOx in the copolymerization (F_1) determined *via* GC-measurements at ~30% BocOI (**1b**) conversion ($\ln(M_0/M_t)$ = 0.36). B: Monomer distribution calculated from the kinetic plot of the copolymerization (Fig. 4). Symbols show the experimental values, the lines show the non-linear Boltzmann fitting of the values.

mixture (data not shown), comparing the aromatic protons of the MeTos initiator (δ = 7.15 and 7.67 ppm) with the backbone protons of BocOI (δ = 3.5 and 3.9 ppm) and EtOx (δ = 3.44 ppm). It should be noted that the polymer peaks overlap with the oxazolidine monomer peaks of BocOI (δ = 3.88 and 4.31 ppm) and, therefore, the isolated monomer integral at δ = 4.31 ppm needs to be subtracted from the calculated backbone integral to obtain the value of the averaged DP. The monomer composition was calculated from ^{1}H-NMR of the purified protected polymers (Fig. S20†) by determination of the BocOI (**1b**) content using the Boc-peak at δ = 1.48 ppm. Moreover, ^{13}C NMR spectra of all Boc protected copolymers (Fig. S21†) were recorded to gain information about the polymeric structure. These spectra showed additional signals compared to the ^{13}C NMR spectra of the homopolymers. The peaks at δ = 9.3 and 26.0 ppm can be allocated to EtOx. Additionally, the backbone signals at δ = 39.9 to 47.1 ppm further split, reflecting the two different backbone types of the urea and the 2-oxazoline part of the polymer.

In addition, FTIR spectra of all Boc protected (Fig. S24†) and deprotected (Fig. S25†) copolymers were recorded. The main difference to the spectra of the homopolymers is shown in a band at λ = 3422 cm^{-1}, which is, compared to the homopolymers, much broader. This is caused by the presence of EtOx in the copolymers. Furthermore, the carbonyl peak at λ = 1620 cm^{-1}, specific for EtOx, varies within the polymer composition. With an increasing BocOI amount, a slight shift to λ = 1650 cm^{-1}, characteristic for the urea, can be observed. Moreover, the amide band at λ = 1480 cm^{-1} specific for EtOx, while a band at λ = 1460 cm^{-1} is characteristic for the urea derivative.

Furthermore, ^{1}H-NMR spectra of all deprotected copolymers and P(EtOx)$_{116}$ (Fig. S22†) were recorded to gain further information about the success of the deprotection. The spectra do not show a signal of the Boc protection group, verifying the deprotection of the polymers. Additionally, the spectra provide information about the stability of the polymer backbone against acidic degradation. After deprotection, two different backbone signals are visible in the ^{1}H-NMR spectrum. Between δ = 3.09 and 4.32 ppm, different overlapping peaks represent the polymer backbone protons of the EtOx and the OI part.

Table 2 Characterization data for P(BocOI$_n$-*co*-EtOx$_m$)

Polymer	Composition	[M]/[I]	DP	M_n [g mol^{-1}]	M_n [g mol^{-1}]	$Đ$	BocOI [%]	T_g [°C]	T_d [°C]
4a	P(BocOI$_{16}$-*co*-EtOx$_{84}$)	100	95[a]	11300	6100	1.27	16[a]	53.2	89.2
4b	P(BocOI$_{36}$-*co*-EtOx$_{64}$)	100	96[a]	13 000	5300	1.36	36[a]	51.5	155.6
4c	P(BocOI$_{52}$-*co*-EtOx$_{48}$)	100	100[a]	14 400	5900	1.34	52[a]	56.7	120.0
4d	P(BocOI$_{84}$-*co*-EtOx$_{16}$)	100	100[a]	17 200	7400	1.26	84[a]	54.2	168.7
5a	P(OI$_{16}$-*co*-EtOx$_{84}$)	n.a.	95	9700	n.d.	n.d.	18[c]	65.8	203.3
5b	P(OI$_{36}$-*co*-EtOx$_{64}$)	n.a.	96	9400	n.d.	n.d.	27[c]	10.6	136.1
5c	P(OI$_{52}$-*co*-EtOx$_{48}$)	n.a.	100	9200	n.d.	n.d.	47[c]	5.9	137.3
5d	P(OI$_{84}$-*co*-EtOx$_{16}$)	n.a.	100	8800	n.d.	n.d.	76[c]	−4.9	168.1
6	P(EtOx)$_{116}$	100	116[a]	11 500[a]	6800[b]	1.16[b]	0[a]	62.7	353.8

[a] ^{1}H-NMR (300 MHz) in $CDCl_3$. [b] SEC (PS-calibration) in $CHCl_3$-i-PrOH-TEA. [c] ^{1}H-NMR (300 MHz) in 35% DCl in D_2O, $CDCl_3$-standard. [d] DSC. [e] TGA. n.d.: not determinable due to insolubility. n.a.: not applicable. DP and M_n of **5a–d** were calculated from ^{1}H-NMR results of **4a–d**.

The molar masses, as determined by SEC (Fig. S23†) are almost constant for all protected polymers, whereas the differences might originate from changes in monomer compositions and the associated differences in molar mass as well as interactions of the column material with P(BocOI). SEC investigations of the deprotected P(OI) copolymers were not possible since the polymers assembled in the SEC eluent.

TGA and DSC measurements of all copolymers and $P(EtOx)_{116}$ (**6**) were performed to obtain information about the thermal properties. TGA analysis of the protected copolymers (**4a–d**) shows varying T_d values, however, no apparent relation between the BocOI (**1b**) amount and the temperature can be observed. Nevertheless, all Boc protected copolymers reveal the same sharp decrease in mass as the homopolymers below 200 °C, caused by thermal deprotection. Further decomposition follows the behavior of P(BocOI) and P(EtOx) (Fig. S26B†). The deprotected copolymers (**5a–d**) show a similar degradation behavior as the homopolymers (Fig. S27B†). The low T_d observed for protected polymers is attributed to thermal deprotection, which is not possible for deprotected polymers. It should be noted that T_d is defined as the temperature at which 5% of mass loss is observed and does not necessarily mean a full decomposition. According to the OI amount in the polymers, no obvious trend is observed. However, the T_d of copolymers (100 to 200 °C) is in the same range as observed for the homopolymers.

The Boc protected copolymers (**4a–d**) reveal a T_g around 50 to 55 °C (Fig. S28B†), independent on the monomer ratio, as determined by DSC measurements.

After deprotection, a significant influence of the polymer composition on the T_g values is visible, caused most probably by intermolecular interactions of the macromolecules. P(BocOI) precursors (**2a–d**) as well as $P(EtOx)_{116}$ (**6**) possess T_g values around 60 °C, resulting in an overall T_g between 50 and 55 °C. Until now, we do not have an explanation for this decrease in T_g of the copolymers compared to the homopolymers. The deprotected macromolecules (**5a–d**), however, show a distinct decrease in the T_g with increasing OI amount (Fig. S29B†). As the T_g of the P(OI) homopolymers is significantly lower than the T_g of $P(EtOx)_{116}$, this could as well be the result of a homogenious mixture of both blocks in bulk. Previous investigations on POx also described a decrease in T_g associated with the decreasing length of the EtOx block.[63]

Self-assembly

The results of the copolymerization studies from BocOI and EtOx show the formation of quasi-block copolymers with narrow dispersity. As the P(OI) homopolymers are not water soluble, block-like copolymers of P(OI) and P(EtOx) are expected to self-assemble or aggregate in aqueous solution. To evaluate the formation of such hydrogen bond stabilized[64,65] nano-assemblies, the polymers were dissolved in TFA, which is known to break hydrogen bonds, and MilliQ water was added slowly under stirring to induce phase segregation. The resulting solution was dialyzed to remove the acid and to obtain nanostructures in solution. Larger aggregates were removed by syringe filtration (0.45 μm) and the size distribution was determined by DLS measurements (Table 3, Fig. S30†).

$P(EtOx)_{116}$ (**6**) and copolymers with a low OI content (~20 to 30%, **5a,b**) have a *z*-average around 4 nm in diameter, indicating unimers or small aggregates. In contrast, copolymers with a high OI amount (**5c,d**) form nanostructures in aqueous solution, having diameters of 55.3 ± 13.4 and 107.7 ± 53.4 with increasing co-monomer content. Furthermore, the zeta potential of the aggregates was investigated. As shown in Table 3, $P(EtOx)_{116}$ (**6**) shows a slightly negative zeta potential. The copolymers, on the other hand, show a positive zeta potential, which could be attributed to a partial degradation of PEtOx resulting in a minor amount of poly(ethylene imine) units in the PEtOx segment, caused by the acidic conditions of de-

Table 3 Characterization of the formed nanostructures after precipitation of the copolymers in MilliQ water by DLS

Polymer	Composition	Concentration[a] [mg mL^{-1}]	Size[b] [*d*, nm]	ζ [mV]
5a	$P(OI_{16}$-*co*-$EtOx_{84})$	1	4.7 ± 0.1	18.6 ± 15.7
5b	$P(OI_{36}$-*co*-$EtOx_{64})$	1	5.1 ± 0.6	8.2 ± 0.5
5c	$P(OI_{52}$-*co*-$EtOx_{48})$	1	55.3 ± 13.4	9.1 ± 3.3
5d	$P(OI_{84}$-*co*-$EtOx_{16})$	0.1	107.7 ± 53.4	1.3 ± 1.8
6	$P(EtOx)_{116}$	10	4.3 ± 0.7	−5.0 ± 0.4

[a] Determined after freeze-drying of the dialyzed solutions. [b] Number PSD.

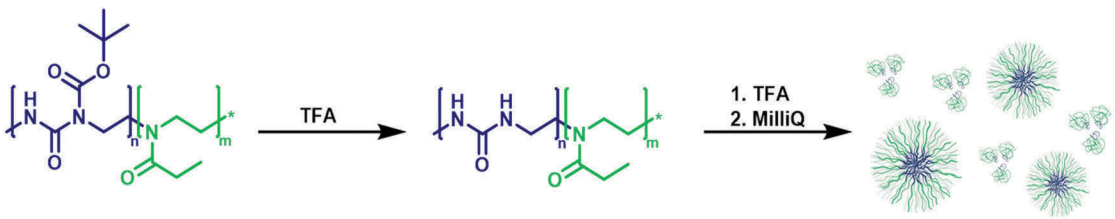

Scheme 3 Schematic representation of the possible macrostructures derived from $P(OI_n$-*co*-$EtOx_m)$ bearing different co-monomer ratios in water.

protection and a self assembly process (the P(EtOx) homopolymer was not treated with TFA prior to DLS measurements). Due to the low solubility of the polymers and the resulting low resolution of the ^{1}H NMR spectra it was not possible to prove this hypothesis.

It should be noted that the results on the self-assembly behavior are preliminary and the optimization of copolymer composition regarding aggregation and possibly micelle formation, as well as the investigation on the self-assembling process and the resulting nanostructures will be the subject of subsequent studies (Scheme 3).

Conclusion

A Boc protected oxazolidine imine was synthesized, polymerized *via* CROP and deprotected to form poly(urea)s with a low dispersity. Homopolymers of different lengths were synthesized and characterized *via* NMR, SEC, MALDI-MS, TGA and DSC. A copolymerization kinetic with EtOx was performed and the resulting reactivity ratios of the two monomers suggest the formation of quasi-block copolymers. Copolymers with different monomer ratios were synthesized and characterized regarding their composition and thermal properties. Self-assembly of those polymers in aqueous solution resulted in nano-assemblies as detected by DLS measurements. These structures are believed to be a result of hydrogen bond formation between the P(OI) segments. The presented copolymer system offers an easy access to quasi-block systems with the potential to self-assemble in solution.

Further research will focus on the self-assembly process and the nature of the resulting nano-structures, as well as the assessment of their suitability for biomedical applications.

Experimental part

Material and instrumentation

All chemicals were purchased from Sigma-Aldrich, Merck, TCI and Synthon-Chemicals. Triethylamine (TEA), 2-ethyl-2-oxazoline (EtOx) and methyl tosylate (MeTos) were distilled to dryness under argon atmosphere prior to usage. Dichloromethane was obtained from a solvent purification system (MB-SPS-800 by MBraun) and stored under argon.

Polymerization reactions were performed under microwave irradiation, using an Initiator Sixty single-mode microwave synthesizer from Biotage, equipped with a noninvasive IR sensor (accuracy: 2%). Microwave vials were heated overnight at 100 °C under vacuum and allowed to cool to RT under argon before usage. Polymerizations were performed using temperature control.

Size-exclusion chromatography (SEC) of the protected homo- and copolymers was performed on a Shimadzu system equipped with a SCL-10A system controller, a LC-10AD pump, a RID-10A refractive index detector and a PSS SDV column with chloroform-TEA-2-propanol (94 : 4 : 2) as eluent. The column oven was set to 50 °C and a polystyrene (PS) standard was used for calibration.

Proton NMR spectroscopy (^{1}H-NMR) was performed at RT using a Bruker Avance I 300 MHz spectrometer, utilizing either $CDCl_3$ or 35% DCl in D_2O as solvent. The chemical shifts are given in ppm relative to the signal from the residual non-deuterated chloroform. Measurements in DCl were performed with an additional $CDCl_3$ standard.

^{1}H–^{1}H-COSY NMR and ^{1}H-NMR experiments of the polymerization inside the NMR tube were performed at RT or 55 °C on a Bruker Avance II 400 MHz, using $CDCl_3$ as solvent.

IR spectra were recorded using an Affinity-1 FT-IR from Shimadzu, utilizing the reflection technique.

High resolution electrospray ionization (HR-ESI) mass spectrometry (MS) was performed on a micrOTOF Q-II (Bruker Daltonics) mass spectrometer equipped with an automatic syringe pump from KD Scientific for sample injection at 4.5 kV at a desolvation temperature of 180 C. The mass spectrometer was operating in the positive ion mode.

Batch dynamic light scattering (DLS) was performed on a Zetasizer Nano ZS (Malvern Instruments, Herrenberg, Germany). All measurements were performed in folded capillary cells (DTS1071, Malvern Instruments, Herrenberg, Germany). After an equilibration time of 180 s, 3 × 30 s runs were carried out at 25 °C (λ = 633 nm). Scattered light was detected at an angle of 173°. Each measurement was performed in triplicates. Apparent hydrodynamic radii, R_h, were calculated according to the Stokes–Einstein equation.

Differential scanning calorimetry (DSC) experiments were performed on a Netzsch DSC 204 F1 Phoenix under a nitrogen atmosphere with a heating rate of 20 K min^{-1} from −20 to 140 °C, if not indicated differently. Three cycles were recorded for each sample. The glass transition temperature (T_g) values are reported for the second heating run. Thermo-gravimetric analysis (TGA) was performed under a nitrogen atmosphere on a Netzsch TG 209 F1 Iris in the range from room temperature to 800 °C with a heating rate of 10 K min^{-1}.

For crystal structure determination, the intensity data were collected on a Nonius KappaCCD diffractometer, using graphite-monochromated Mo-K_α radiation. Data were corrected for Lorentz and polarization effects; absorption was taken into account on a semi-empirical basis using multiple-scans.[66–68]

The structure was solved by direct methods (SHELXS[69]) and refined by full-matrix least squares techniques against F_o^2 (SHELXL-97 [69]). All hydrogen atoms were located by difference Fourier synthesis and refined isotropically. All non-hydrogen atoms were refined anisotropically. MERCURY[70] was used for structure representations.

tert-Butyl 2-iminooxazolidine-3-carboxylate (BocOI) (1b)

2-Amino-2-oxazoline hydrochloride (20 g, 163 mmol) was dissolved in a mixture of 1,4-dioxane (300 mL) and aqueous sodium hydroxide (3 wt%, 300 mL). Dry TEA (16.5 g, 163 mmol) was added to this mixture to remove hydrochloric acid. DiBoc, (35 g, 163 mmol) was dissolved in 1,4-dioxane (150 mL) and added dropwise to the solution of 2-amino-2-oxa-

zoline The reaction mixture was stirred at RT for 24 h and, subsequently, extracted with dichloromethane (3 × 200 mL). The organic phase was dried over sodium sulfate before evaporation of the solvent under reduced pressure. The crude product was further purified *via* recrystallization from cyclohexanes to give the final product as a white crystalline solid (24.0 g, 87.2%).

^{1}H-NMR ($CDCl_3$, 300 MHz): δ = 7.38 (1H, s, NH), 4.23 (2H, t, CH_2-oxazolidine), 3.86 (2H, t, CH_2-oxazolidine), 1.51 (9H, s, CH_3) ppm.

^{13}C-NMR ($CDCl_3$, 300 MHz): δ = 154.89 (O–CNH–N), 151.37 (N–CO–O), 83.57 (O–C–$(CH_3)_3$), 62.21 (CH_2-oxazolidine), 44.39 (CH_2-oxazolidine), 28.06 (CH_3) ppm.

HR-ESI: *m*/*z* calc. for $C_8H_{14}N_2O_3H$ [M + H]: 187.1007, found: 187.1081 (error: 1.9 ppm).

FTIR: λ [cm^{-1}] = 3422 (w, carbonyl), 3336 (m, NH), 2939 (s, CH_2 CH_3), 1620, 1570 (s, amide), 1165 (m, CH_3).

Crystal data for 1b. $C_8H_{14}N_2O_3$, M_r = 186.21 g mol^{-1}, colourless prism, size 0.098 × 0.088 × 0.068 mm^3, monoclinic, space group $P2_1/n$, a = 9.7713(7), b = 9.5154(7), c = 11.5372(9) Å, β = 113.738(4)°, V = 981.95(13) Å^3, T = −140 °C, Z = 4, ρ_{calcd} = 1.260 g cm^{-3}, μ (Mo-K_α) = 0.97 cm^{-1}, multi-scan, transmin: 0.6395, transmax: 0.7456, F(000) = 400, 6408 reflections in h(−12/12), k(−11/11), l(−14/14), measured in the range 2.32° ≤ Θ ≤ 26.37°, completeness Θ_{max} = 99.9%, 2004 independent reflections, R_{int} = 0.0448, 1736 reflections with $F_o > 4\sigma(F_o)$, 174 parameters, 0 restraints, R_{1obs} = 0.0682, wR^2_{obs} = 0.1284, R_{1all} = 0.0802, wR^2_{all} = 0.1320, GOOF = 1.307, largest difference peak and hole: 0.237/−0.213 e Å^{-3}.

Kinetic studies

For kinetic investigations a stock solution of BocOI, (and EtOx for copolymerizations), MeTos and CH_2Cl_2 ([M] = 1 mol^{-1}, [M]/[I] = 60) was prepared, aliquoted into microwave vials (1 mL per vial) and heated in a microwave synthesizer (100 °C, varying reaction times). After polymerization, the conversions of the monomers were determined using GC using the solvent as an internal standard. The reaction rate constants k_p of the monomers were determined using eqn (1) and (2) assuming that the slope of the linear fit of $\ln([M]_0/[M]_t) = f(t)$ complies with k_{eff}.

$$\ln M_0 - \ln M_t = k_{eff} t \quad (1)$$

$$k_{eff} = k_p[I] \quad (2)$$

Reactivity ratios of both monomers were calculated for four different monomer ratios at 30% BocOI conversion (determined by GC) using non-linear least square fitting[60] (eqn (3)):

$$F_1 = \frac{(r_1 - 1)f_1^2 + f_1}{(r_1 + r_2 - 2)f_1^2 + 2(1 - r_2)f_{1+}r_2}, \quad r_1 \geq 0 \quad (3)$$

F_1 = instantaneous mole fraction; f_1 = mole fraction of monomer EtOx; f_2 = mole fraction of monomer BocOI; r_1 = reactivity ratio of EtOx; r_2 = reactivity ratio of BocOI.

Homopolymerization inside an NMR tube

In an NMR tube BocOI (112 mg, 0.6 mmol), MeTos (0.8 μL, 0.024 mmol) and $CDCl_3$ (550 μL) were mixed under inert conditions and the reaction mixture was heated to 55 °C for a predetermined time. ^{1}H-NMR spectra at RT were recorded at specific points of time to determine the reactive species during polymerization.

Homopolymerization of BocOI (2a–d)

The experimental procedure for homopolymerizations is exemplarily described on polymers with [M]/[I] = 25 (**2a**).

In a microwave vial BocOI (2793 mg, 15.0 mmol), MeTos (19.8 μL, 0.6 mmol) and dichloromethane (14.9 mL) were mixed under inert conditions and the reaction mixture was heated to 100 °C for a predetermined time. The resulting solution was purified *via* BioBeads SX-1 column using CH_2Cl_2 as eluent. After combining the polymer fractions, the solvent was evaporated under reduced pressure to obtain the product as a white crystalline solid.

^{1}H-NMR ($CDCl_3$, 300 MHz): δ = 8.70 (0.8H, s, NH-backbone), 3.87 (2H, m, backbone), 3.41 (2H, m, backbone), 2.80 (0.06H, d, CH_3), 1.46 (9H, m, CH_3) ppm.

SEC (eluent: $CHCl_3$-i-propanol-TEA, PS-standard): M_n = 3700 g mol^{-1}, M_w = 4700 g mol^{-1}, $Đ$ = 1.18.

FTIR: λ [cm^{-1}] = 3336 (m, NH (backbone)), 3009, 2978, 2937 (s, CH_2 (backbone), CH_3 (Boc)). 1719, 1681 (s, carbonyl), 1533 (s, NH (backbone)), 1371 (s, CH_3 (Boc)), 1231 (s, carbonyl), 1157 (s, carbonyl), 852 (m, CH_3 (Boc)), 754 (m, CH_2 (backbone)).

Deprotection of P(BocOI) (3a–d)

The experimental procedure for deprotection is exemplarily described for the polymers with a [M]/[I] = 25 (**3a**).

10 mL of TFA were added to the polymer and the solution was stirred at RT overnight. Subsequently, the reaction mixture was diluted with methanol and precipitated from ice-cold diethyl ether (300 mL). The polymer was filtered off and dried in a high vacuum to obtain the product as a white crystalline solid.

FTIR: λ [cm^{-1}] = 3333 (s, NH (backbone)), 2939 (s, CH_2 (backbone)), 1620, 1570 (s, amide (backbone)), 1446 (CH_2 (backbone)), 1141 (s, carbonyl).

Copolymerization of BocOI and EtOx (4a–d)

The experimental procedure for copolymerizations is exemplarily described for the polymers with a [M]/[I] = 100 aiming a BocOI amount of 20% (**4a**).

In a microwave vial BocOI (745 mg, 4.0 mmol), EtOx (1586 μL, 16.0 mmol), MeTos (30.3 μL, 0.2 mmol) and dichloromethane (8.35 mL) were mixed under inert conditions and the reaction mixture was heated to 100 °C for 15 h. The resulting solution was purified by precipitation into ice cold diethyl ether. The white solid was filtered off and re-dissolved in CH_2Cl_2 and the solvent was evaporated under reduced pressure to obtain the product as a white crystalline solid.

^{1}H-NMR ($CDCl_3$, 300 MHz): δ = 8.73 (0.1H, s, NH-backbone), 3.90 (0.3H, m, backbone), 3.45 (3.6H, s, backbone), 2.40 (1.7H, s, CH_2 (EtOx)), 1.51 (1.3H, d, CH_3 (BocOI)), 1.12 (2.5H, s, CH_3 (EtOx)) ppm.

SEC (eluent: $CHCl_3$-i-propanol-TEA, PS-standard): M_n = 6100 g mol^{-1}, M_w = 7700 g mol^{-1}, $Đ$ = 1.27.

FTIR: λ [cm^{-1}] = 3422 (w, carbonyl), 3336 (m, NH (backbone)), 2939 (s, CH_2 (backbone), CH_3 (Boc)), 1720 (s, carbonyl), 1632 (m, amide), 1431 (m, CH_3 (Boc), CH_2 (backbone)), 1373 (m, CH_3 (Boc)), 1141 (s, carbonyl), 754 (m, CH_2 (backbone)).

Deprotection of P(BocOI-*co*-EtOx) (5a–d)

The experimental procedure for deprotection is exemplarily described for the polymers with a [M]/[I] = 100 aiming a BocOI amount of 20% (**5a**).

10 mL of TFA were added to P(BocOI-*co*-EtOx) and stirred at RT overnight. Subsequently, the solution was diluted with methanol and purified by precipitation into ice cold diethyl ether (300 mL). The white solid was filtered off and dried in a high vacuum to obtain the product as a white crystalline solid.

^{1}H-NMR (35% DCl in D_2O, $CDCl_3$-standard, 300 MHz): 3.09–4.32 (4H, m, backbone), 2.63 (1.7H, s, CH_2 (EtOx)), 1.11 (2.4H, s, CH_3 (EtOx)) ppm.

FTIR: λ [cm^{-1}] = 3422 (w, carbonyl), 3336 (m, NH (backbone)), 2939 (s, CH_2 (backbone), CH_3 (Boc)), 1616 (s, amide (BocOI)), 1580, 1562 (s, amide (EtOx)), 1138 (m, CH_2, CH_3 (EtOx)). 813 (m, CH_2, CH_3 (EtOx), CH_3 (EtOx)).

Homopolymerization of EtOx (6)

In a microwave vial, EtOx (8076 μL, 80.0 mmol), MeTos (121.1 μL, 0.8 mmol) and acetonitrile (11.8 mL) were mixed under inert condition and the reaction mixture was heated to 140 °C for a predetermined time and subsequently quenched by the addition of 500 μL of deionized H_2O. The resulting solution was purified *via* precipitation into ice cold diethyl ether. The polymer was filtered off and re-dissolved in CH_2Cl_2 and the solvent was evaporated under reduced pressure to obtain the product as a white crystalline solid.

^{1}H-NMR ($CDCl_3$, 300 MHz): δ = 4.34 (0.1H, s, backbone-OH), 3.44 (4.0H, s, backbone), 3.02 (0.3H, s, CH_3-backbone), 2.4 (1.7H, m, CH_2 (EtOx)), 1.11 (2.5H, s, CH_3 (EtOx)) ppm.

^{1}H-NMR (35% DCl in D_2O, $CDCl_3$-standard, 400 MHz): 4.08 (4H, s, backbone), 2.55 (2.4H, d, CH_2 (EtOx)),1.10 (2.8H, s, CH_3 (EtOx)) ppm.

SEC (eluent: $CHCl_3$-i-propanol-TEA, PS-standard): M_n = 6800 g mol^{-1}, M_w = 7900 g mol^{-1}, $Đ$ = 1.16.

FTIR: λ [cm^{-1}] = 3422 (w, carbonyl), 2939 (s, CH_2, CH_3), 1620, 1570 (s, amide (backbone)), 1427 (s, CH_2, CH_3), 1160 (m, CH_2, CH_3).

Self-assembly of P(OI-*co*-EtOx)

30 mg of deprotected copolymer (**5a–d**) were dissolved in TFA (600 μL). 3.0 mL of MilliQ water were added *via* syringe pump (10 mL h^{-1}) while stirring (1400 rpm). Directly after the addition, the solution was dialyzed against deionized H_2O (MWCO 3500 g mol^{-1}) for 72 h. The final concentration of the solution was provided by lyophilization and determined as 1 mg mL^{-1} for **5a–c**, 0.1 mg mL for **5d** and 10 mg mL^{-1}.

Acknowledgements

The authors gratefully acknowledge the Bundesministerium für Bildung und Forschung (Germany) (project: smart-dye-livery, 081220/127) for funding. The authors thank Tina Schlotthauer for ESI-MS measurements. M. H. gratefully acknowledges the German Research Foundation (DFG, GZ: HA 7725/1-1) for funding.

References

1 O. Bayer, *Angew. Chem.*, 1947, **59**, 257–272.
2 S. Holberg and C. Bischoff, *Prog. Org. Coat.*, 2014, **77**, 1591–1595.
3 S. L. Kwolek, *J. Polym. Sci., Part A: Polym. Chem.*, 1964, **2**, 5149–5160.
4 L. Feng and J. O. Iroh, *Prog. Org. Coat.*, 2014, **77**, 590–599.
5 P. Cass, W. Knower, T. Hinton, S. Shi, F. Grusche, M. Tizard and P. Gunatillake, *Acta Biomater.*, 2013, **9**, 8299–8307.
6 R. Kumar, R. Narayan, T. Aminabhavi and K. V. S. N. Raju, *J. Polym. Res.*, 2014, **21**, 1–16.
7 G. Morral-Ruíz, P. Melgar-Lesmes, M. L. García, C. Solans and M. J. García-Celma, *Polymer*, 2012, **53**, 6072–6080.
8 G. Morral-Ruíz, C. Solans, M. L. García and M. J. García-Celma, *Langmuir*, 2012, **28**, 6256–6264.
9 E.-M. Rosenbauer, K. Landfester and A. Musyanovych, *Langmuir*, 2009, **25**, 12084–12091.
10 Y. Saegusa and S. Nakamura, *Macromol. Rapid Commun.*, 1998, **19**, 177–180.
11 S. Li, J. Zhao, Z. Zhang, J. Zhang and W. Yang, *RSC Adv.*, 2015, **5**, 6843–6852.
12 H. Mighani, *Carbon*, 2012, **10**, 235oC.
13 S. Mallakpour and Z. Rafiee, *J. Appl. Polym. Sci.*, 2004, **91**, 2103–2113.
14 K. Stridsberg, M. Ryner and A.-C. Albertsson, in *Degradable Aliphatic Polyesters*, Springer, Berlin, Heidelberg, 2002, vol. 157, pp. 41–65.
15 K. R. Carter, R. Richter, H. R. Kricheldorf and J. L. Hedrick, *Macromolecules*, 1997, **30**, 6074–6076.
16 X. Ding, C. Yang, T. P. Lim, L. Y. Hsu, A. C. Engler, J. L. Hedrick and Y.-Y. Yang, *Biomaterials*, 2012, **33**, 6593–6603.
17 D. P. Sanders, K. Fukushima, D. J. Coady, A. Nelson, M. Fujiwara, M. Yasumoto and J. L. Hedrick, *J. Am. Chem. Soc.*, 2010, **132**, 14724–14726.
18 F. Nederberg, Y. Zhang, J. P. K. Tan, K. Xu, H. Wang, C. Yang, S. Gao, X. D. Guo, K. Fukushima, L. Li, J. L. Hedrick and Y.-Y. Yang, *Nat. Chem.*, 2011, **3**, 409–414.
19 A. Nagai, T. Miyagawa, H. Kudo and T. Endo, *Macromolecules*, 2003, **36**, 9335–9339.

20 K. Kempe, M. Lobert, R. Hoogenboom and U. S. Schubert, *J. Polym. Sci., Part A: Polym. Chem.*, 2009, **47**, 3829–3838.
21 T. G. Bassiri, A. Levy and M. Litt, *J. Polym. Sci., Part B: Polym. Lett.*, 1967, **5**, 871–879.
22 T. Kagiya, S. Narisawa, T. Maeda and K. Fukui, *J. Polym. Sci., Part B: Polym. Lett.*, 1966, **4**, 441–445.
23 W. Seeliger, E. Aufderhaar, W. Diepers, R. Feinauer, R. Nehring, W. Thier and H. Hellmann, *Angew. Chem., Int. Ed. Engl.*, 1966, **5**, 875–888.
24 D. A. Tomalia and D. P. Sheetz, *J. Polym. Sci., Part A: Polym. Chem.*, 1966, **4**, 2253–2265.
25 F. Wiesbrock, R. Hoogenboom, C. H. Abeln and U. S. Schubert, *Macromol. Rapid Commun.*, 2004, **25**, 1895–1899.
26 R. Jordan, K. Martin, H. J. Räder and K. K. Unger, *Macromolecules*, 2001, **34**, 8858–8865.
27 T. Saegusa and H. Ikeda, *Macromolecules*, 1973, **6**, 808–811.
28 G. Volet, V. Chanthavong, V. Wintgens and C. Amiel, *Macromolecules*, 2005, **38**, 5190–5197.
29 C. J. Waschinski, V. Herdes, F. Schueler and J. C. Tiller, *Macromol. Biosci.*, 2005, **5**, 149–156.
30 Y. Chujo, E. Ihara, H. Ihara and T. Saegusa, *Macromolecules*, 1989, **22**, 2040–2043.
31 M. W. M. Fijten, C. Haensch, B. M. van Lankvelt, R. Hoogenboom and U. S. Schubert, *Macromol. Chem. Phys.*, 2008, **209**, 1887–1895.
32 B. Guillerm, V. Darcos, V. Lapinte, S. Monge, J. Coudane and J.-J. Robin, *Chem. Commun.*, 2012, **48**, 2879–2881.
33 K. Kempe, R. Hoogenboom, M. Jaeger and U. S. Schubert, *Macromolecules*, 2011, **44**, 6424–6432.
34 S. Kobayashi, H. Uyama and H. Shirasaka, *Die Makromol. Chem., Rapid Commun.*, 1990, **11**, 11–14.
35 M. M. Bloksma, S. Rogers, U. S. Schubert and R. Hoogenboom, *J. Polym. Sci., Part A: Polym. Chem.*, 2011, **49**, 2790–2801.
36 Z. K. Juraj Kronek, J. Lustoň, E. Paulovičová, L. Paulovičová and B. Mendrek, *J. Mater. Sci. Mater. Med.*, 2011, **22**, 1725–1734.
37 R. Luxenhofer, G. Sahay, A. Schulz, D. Alakhova, T. K. Bronich, R. Jordan and A. V. Kabanov, *J. Controlled Release*, 2011, **153**, 73–82.
38 M. Barz, R. Luxenhofer, R. Zentel and M. J. Vicent, *Polym. Chem.*, 2011, **2**, 1900–1918.
39 K. Knop, R. Hoogenboom, D. Fischer and U. S. Schubert, *Angew. Chem., Int. Ed.*, 2010, **49**, 6288–6308.
40 F. Wiesbrock, R. Hoogenboom, M. Leenen, S. F. G. M. van Nispen, M. van der Loop, C. H. Abeln, A. M. J. van den Berg and U. S. Schubert, *Macromolecules*, 2005, **38**, 7957–7966.
41 F. C. Gaertner, R. Luxenhofer, B. Blechert, R. Jordan and M. Essler, *J. Controlled Release*, 2007, **119**, 291–300.
42 S. Zalipsky, C. B. Hansen, J. M. Oaks and T. M. Allen, *J. Pharm. Sci.*, 1996, **85**, 133–137.
43 A. Mero, G. Pasut, L. D. Via, M. W. M. Fijten, U. S. Schubert, R. Hoogenboom and F. M. Veronese, *J. Controlled Release*, 2008, **125**, 87–95.
44 M. Hartlieb, D. Pretzel, M. Wagner, S. Hoeppener, P. Bellstedt, M. Gorlach, C. Englert, K. Kempe and U. S. Schubert, *J. Mater. Chem. B*, 2015, **3**, 1748–1759.
45 Z. He, A. Schulz, X. Wan, J. Seitz, H. Bludau, D. Y. Alakhova, D. B. Darr, C. M. Perou, R. Jordan, I. Ojima, A. V. Kabanov and R. Luxenhofer, *J. Controlled Release*, 2015, **208**, 67–75.
46 A. Mero, Z. Fang, G. Pasut, F. M. Veronese and T. X. Viegas, *J. Controlled Release*, 2012, **159**, 353–361.
47 J. Kronek, Z. Kroneková, J. Lustoň, E. Paulovičová, L. Paulovičová and B. Mendrek, *J. Mater. Sci. Mater. Med.*, 2011, **22**, 1725–1734.
48 J. Kronek, E. Paulovičová, L. Paulovičová, Z. Kroneková and J. Lustoň, *J. Mater. Sci. Mater. Med.*, 2012, **23**, 1457–1464.
49 K. L. Eskow Jaunarajs, D. G. Standaert, T. X. Viegas, M. D. Bentley, Z. Fang, B. Dizman, K. Yoon, R. Weimer, P. Ravenscroft, T. H. Johnston, M. P. Hill, J. M. Brotchie and R. W. Moreadith, *Mov. Disord.*, 2013, **28**, 1675–1682.
50 J. Tong, X. Yi, R. Luxenhofer, W. A. Banks, R. Jordan, M. C. Zimmerman and A. V. Kabanov, *Mol. Pharm.*, 2013, **10**, 360–377.
51 A. C. Rinkenauer, L. Tauhardt, F. Wendler, K. Kempe, M. Gottschaldt, A. Traeger and U. S. Schubert, *Macromol. Biosci.*, 2015, **15**, 414–425.
52 M. N. Leiske, M. Hartlieb, C. Paulenz, D. Pretzel, M. Hentschel, C. Englert, M. Gottschaldt and U. S. Schubert, *Adv. Funct. Mater.*, 2015, **25**, 2458–2466.
53 M. Hartlieb, D. Pretzel, K. Kempe, C. Fritzsche, R. M. Paulus, M. Gottschaldt and U. S. Schubert, *Soft Matter*, 2013, **9**, 4693–4704.
54 I. Forfar, C. Jarry, J.-P. Fayet and A. Carpy, *Arch. Pharm.*, 1992, **325**, 541–543.
55 J.-J. Bosc, I. Forfar, C. Jarry, J. Ouhabi, J.-M. Leger and A. Carpy, *Arch. Pharm.*, 1990, **323**, 561–566.
56 T.-H. Liu, W.-T. Cheng and K.-T. Hunang, *J. Photopolym. Sci. Technol.*, 2010, **23**, 529–533.
57 H. M. L. Lambermont-Thijs, M. J. H. C. Jochems, R. Hoogenboom and U. S. Schubert, *J. Polym. Sci., Part A: Polym. Chem.*, 2009, **47**, 6433–6440.
58 K. Kempe, S. Jacobs, H. M. L. Lambermont-Thijs, M. M. W. M. Fijten, R. Hoogenboom and U. S. Schubert, *Macromolecules*, 2010, **43**, 4098–4104.
59 S. M. Shawki and A. E. Hamielec, *J. Appl. Polym. Sci.*, 1979, **23**, 3155–3166.
60 V. E. Meyer and G. G. Lowry, *J. Polym. Sci., Part A: Polym. Chem.*, 1965, **3**, 2843–2851.
61 R. Hoogenboom, H. M. L. Thijs, M. W. M. Fijten, B. M. van Lankvelt and U. S. Schubert, *J. Polym. Sci., Part A: Polym. Chem.*, 2007, **45**, 416–422.
62 T. Kagiya, T. Matsuda, M. Nakato and R. Hirata, *J. Macromol. Sci., Part A: Pure Appl.Chem.*, 1972, **6**, 1631–1652.
63 K. Kempe, E. F. J. Rettler, R. M. Paulus, A. Kuse, R. Hoogenboom and U. S. Schubert, *Polymer*, 2013, **54**, 2036–2042.
64 M. M. Coleman, M. Sobkowiak, G. J. Pehlert, P. C. Painter and T. Iqbal, *Macromol. Chem. Phys.*, 1997, **198**, 117–136.

65 J. Mattia and P. Painter, *Macromolecules*, 2007, **40**, 1546–1554.
66 R. Hooft, *Collect, Data Collection Software*, Nonius BV, Delft, 1998.
67 Z. Otwinowski and W. Minor, in *Methods Enzymol*, Academic Press, 1997, vol. 276, pp. 307–326.
68 B.-A. Inc., Madison, WI, USA, 2002.
69 G. Sheldrick, *Acta Crystallogr., Sect. A: Fundam. Crystallogr.*, 2008, **64**, 112–122.
70 C. F. Macrae, P. R. Edgington, P. McCabe, E. Pidcock, G. P. Shields, R. Taylor, M. Towler and J. van de Streek, *J. Appl. Crystallogr.*, 2006, **39**, 453–457.

Publication P2

Mission ImPOxable - Or the unknown utilization of non-toxic poly(2-oxazoline)s as cryoprotectant and surfactant at the same time

M. N. Leiske, A.-K. Trützschler, S. Armoneit, P. Sungur, S. Hoeppener, M. Lehmann, A. Traeger, U. S. Schubert, *J. Mater. Chem. B.* **2017**, *5*, 9102 - 9113.

The paper as well as the supporting information (free of charge) is available online: doi.org/10.1039/C7TB02443F.

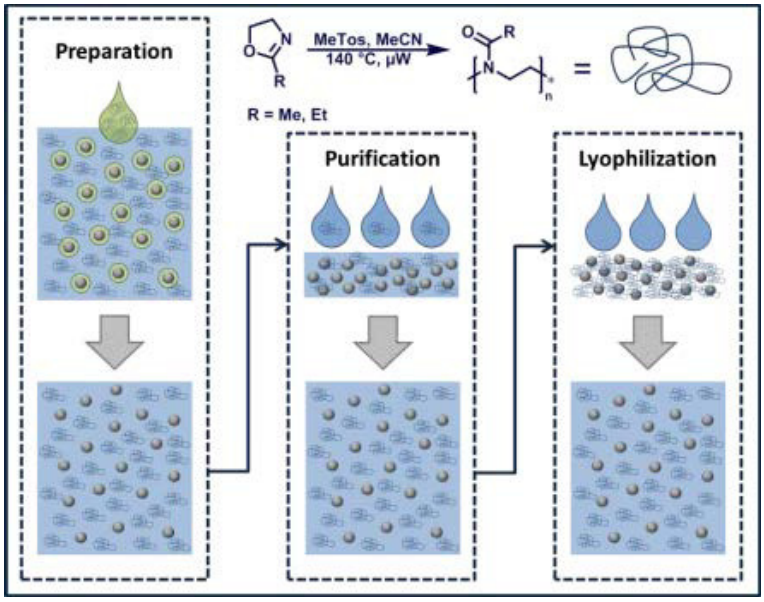

Volume 5 | Number 46 | 14 December 2017 | Pages 9047–9240

Journal of Materials Chemistry B

Materials for biology and medicine

rsc.li/materials-b

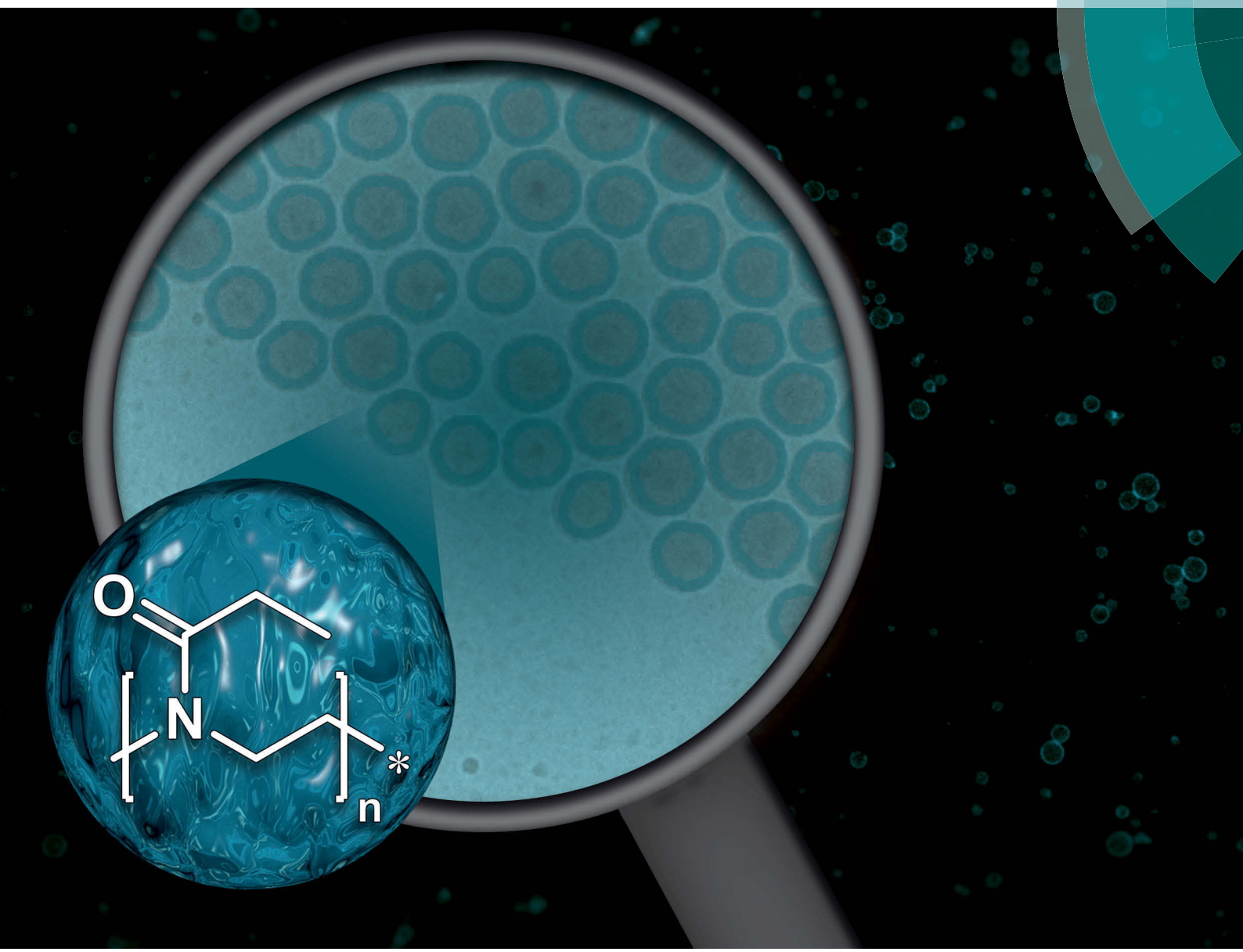

ISSN 2050-750X

ROYAL SOCIETY OF CHEMISTRY

PAPER

Anja Traeger, Ulrich S. Schubert *et al.*

Mission ImPOxable – or the unknown utilization of non-toxic poly(2-oxazoline)s as cryoprotectants and surfactants at the same time

Journal of
Materials Chemistry B

PAPER

View Article Online
View Journal | View Issue

Cite this: J. Mater. Chem. B, 2017, 5, 9102

Mission ImPOxable – or the unknown utilization of non-toxic poly(2-oxazoline)s as cryoprotectants and surfactants at the same time†

Meike N. Leiske,[ab] Anne-Kristin Trützschler,[ab] Sabine Armoneit,[c] Pelin Sungur,[ab] Stephanie Hoeppener,[ab] Marc Lehmann,[c] Anja Traeger*[abc] and Ulrich S. Schubert *[abd]

Received 11th September 2017,
Accepted 16th October 2017

DOI: 10.1039/c7tb02443f

rsc.li/materials-b

Polymer based nanoparticles offer great opportunities for diverse applications, *i.e.* their drug delivery potential is promising. However, their major drawback is identified in preparation *via* the nanoemulsion technique, which is needed for the encapsulation of hydrophilic drugs and whereby the utilization of surfactants, *e.g.* poly(vinyl alcohol) (PVA), is mandatory. Furthermore, the preparation of nanoparticles is critical due to the need of lyophilization for storage. For this reason it is common to use cryoprotectants, which are usually sugar based. In the current study, we present the use of non-toxic, water-soluble poly-(2-oxazoline)s (P(Ox)s) in terms of polymeric nanoparticle stabilizers for preparation, purification, and lyophilization. The nanoparticles were characterized *via* dynamic light scattering (DLS) and cryo-transmission electron microscopy (cryoTEM). The use of hydrophilic P(Ox)s with a degree of polymerization of about 60 yielded stable nanoparticles. For the preparation *via* nanoemulsion a PDI below 0.2 could be obtained after adjustment of the surfactant concentration. All nanoparticles were in the size range of 100 to 200 nm according to DLS. Furthermore, the addition of P(Ox) was beneficial during particle purification *via* centrifugation and filtration as well as lyophilization, yielding nanoparticles with a PDI below 0.3 as determined *via* DLS and confirmed *via* cryoTEM measurements. Cytotoxicity, hemolysis and erythrocyte aggregation measurements of these P(Ox)s did not show any harmful effect on the treated cells.

1. Introduction

The design and preparation of potent drug carriers play a pivotal role in pharmaceutical, biomedical, and chemical research, since carriers offer possibilities for targeted drug release by the introduction of targeting moieties, reduction of side effects, or protection of active pharmaceutical ingredients (APIs). Nanoparticles based on polymers can be tuned in a tailor-made fashion regarding their size, charge, loading, release, and functionality.[1] Water-insoluble polyesters, such as Food and Drug Administration (FDA) approved poly(lactic-*co*-glycolic acid) (PLGA), are commonly used in a number of preclinical trials at the moment.[2] PLGA is a biodegradable polymer that can be degraded by esterases, which can be found inside the endosomal compartments of cells, under acidic conditions within minutes into its natural degradation products.[3]

Lipid-based carriers, *i.e.*, liposomes, which are already used in therapeutics, also show high efficiencies, a high cargo capacity and a wide range of design opportunities. Nevertheless, liposomes also feature potential immune response activation, expensive fabrication, and complex pharmacodynamics.[4] Polymer systems, on the other hand, are affordable, easily storable as powder and highly designable. In comparison to viral vectors or lipid based systems, concerns about immunogenicity or expensive and difficult up-scaling are limited. The benefits of polymeric nanoparticles seem to make them ideal drug carriers; however, there are limitations regarding their efficiency. One possible obstacle is originated in the particle preparation. Particles are commonly prepared *via* solvent-evaporation methods using nanoprecipitation with water-miscible organic solvents or emulsions with water-immiscible solvents.[5–7] The resulting suspension might not be stable for an unlimited time as the precipitants tend to aggregate during preparation, purification or evaporation and subsequent storage. Furthermore, the possible diffusion of

[a] Laboratory of Organic and Macromolecular Chemistry (IOMC), Friedrich Schiller University Jena, Humboldtstrasse 10, 07743 Jena, Germany. E-mail: anja.traeger@uni-jena.de, ulrich.schubert@uni-jena.de
[b] Jena Center for Soft Matter (JCSM), Friedrich Schiller University Jena, Philosophenweg 7, 07743 Jena, Germany
[c] SmartDyeLivery GmbH, Botzstrasse 5, 07743 Jena, Germany
[d] Center for Sepsis Control & Care (CSCC), Jena University Hospital, Erlanger Allee 101, 07747 Jena, Germany

† Electronic supplementary information (ESI) available: Experimental section, raw data, sepctra. See DOI: 10.1039/c7tb02443f

hydrophilic drugs in water-based particle suspension might reduce the drug loading in a time dependent manner. To avoid these limitations, the particles can be lyophilized using cryoprotectants, which are necessary due to the difficult resuspension of pure particles. Saccharides, such as trehalose, sucrose, and glucose, are the most commonly used cryoprotectants.[8] In the literature, the common amount of sugar used is 5.0 wt% or even higher.[9,10] Unfortunately sugars are hygroscopic, which can be a disadvantage for long-term storage. Furthermore, many saccharides themselves already owe biochemical activity by specific uptake mechanisms *via* GLUT transporters.[11] For this reason, research on finding alternatives for these cryoprotectants was already started by some groups.[12,13]

The second issue regarding nanoparticles is related to their preparation for encapsulation of hydrophilic drugs, *e.g.* siRNA. These drugs cannot be easily incorporated by nanoprecipitation methods, but require double emulsion techniques instead.[7] As this preparation method uses a solvent, which is not miscible with water, the emulsion has to be further stabilized by using a surfactant. The most common surfactant in this context is the water-soluble poly(vinyl alcohol) (PVA).[8,14] In nanoscience it is well-known that the utilization of amphiphilic particle stabilizers, such as PVA, is beneficial and can reduce the surface tension of the nanoparticles. The resulting nanoparticles are uniform with a narrow size distribution but, however, PVA influences the physical properties and the cellular uptake of nanoparticles.[15] Furthermore, it is declared to be possibly carcinogenic and might influence the cellular uptake of the nanoparticles.[15–17] As a consequence, the use of PVA leads to the necessity of excessive purification of the nanoparticle formulations before administration.

Usually in terms of purification, crude particles are centrifuged, filtered, or dialyzed.[3] In particular during centrifugation, immense forces operate on the particles and potentially influence the particle characteristics.

Taking all these facts into account, the research for new, biocompatible surfactants and cryoprotectants is indispensable.

Biocompatible poly(2-oxazoline) (P(Ox)) polymers might be interesting candidates to address this issue. Since their invention in the 1960s by four different research groups,[18–21] the interest in this polymer class has risen exponentially. Fundamental studies mainly included monomer synthesis and polymerization parameter optimization as well as the characterization of the resulting polymers.[22–26] As the polymerization process of the cationic ring-opening polymerization (CROP) of 2-oxazolines is slow, it requires high temperatures in order to reach useful reaction times. The usage of the microwave technique (polymerization under pressure) since 2004 has decreased the synthesis time from several days to only a few minutes.[27] Since this circumstance makes P(Ox)s affordable, biocompatibility and pharmaceutical studies have come to the fore.[28] FDA approved polymers consisting of the water-soluble monomer 2-ethyl-2-oxazoline (EtOx)[29] as well as 2-methyl-2-oxazoline (MeOx) are of major interest in this context. Their biocompatibility and biodistribution mechanisms have already been tested *in vitro*[30] and *in vivo*,[31] and at the moment the first clinical trial is running.[32]

P(Ox)s have already been studied in terms of surfactant abilities, *e.g.*, by investigations on the surface activity of different block copolymer compositions.[33–35] Kobayashi *et al.* additionally studied hydrophilic P(Ox) homopolymers providing a hydrophobic end-group.[36] Furthermore, P(Ox)s were investigated as stabilizers for hydroxyapatite[37] and metal-based nanoparticles.[38]

The aim of this study is to use purely hydrophilic P(Ox) homopolymers as an all-in-one-system for polymeric nanoparticles to replace both the surfactant necessary for particle preparation and the cryoprotectant required for particle storage. A series of poly(2-ethyl-2-oxazoline)s (P(EtOx)) and poly(2-methyl-2-oxazoline)s (P(MeOx)) with varying degree of polymerization (DP) were synthesized. In detail, $P(EtOx)_{61}$ was used as a surfactant for PLGA nanoparticle preparation in comparison with commercial PVA and Pluronic® F127. Furthermore, $P(EtOx)_{61}$ was compared with $P(EO)_{57}$ and saccharides regarding its cryoprotectant properties for PLGA nanoparticles. After optimizing the conditions regarding stabilizer concentration, P(Ox)s of varying DPs were compared in terms of surfactant and cryoprotectant abilities. Additionally, the purification techniques (centrifugation and filtration) were evaluated. Their potential as additives in the encapsulation of hydrophilic drugs was exemplarily shown for Nile red and PKC 412, a kinase inhibitor, *e.g.* for protein kinase C. The nanoparticles were analyzed using DLS and cryoTEM.

2. Results and discussion

2.1. Surfactant abilities

2.1.1. Comparison of P(Ox)s and commercial surfactants. Since nanoparticles for drug delivery are often prepared *via* nanoemulsion, which requires the use of surfactants, whose absolute removal is nearly impossible, investigations regarding *in vitro* cytotoxicity (AlamarBlue®) and hemolysis behavior (hemoglobin release) of potential candidates were conducted (Fig. 1). Therefore the potential surfactants were tested in a range of 0.0003 to 5.0 wt%. Due to difficulties with their solubility, PVA and Pluronic® F127 could not be tested at 5.0 wt%. Even at a high polymer concentration of 5.0 wt% none of the tested surfactants is cytotoxic as revealed by the AlamarBlue® assay (Fig. 1A); however, hemolysis experiments showed an enhanced hemolytic activity of PVA and Pluronic® F127 at concentrations of 1.0 wt% and higher, while the investigated P(Ox)s are not hemolytic even at a concentration of 5.0 wt%, proving their good biocompatibility (Fig. 1B). Biotests regarding the erythrocyte aggregation (Fig. S1, ESI†) and an LDH-assay (Fig. S2, ESI†) showed no significant differences between the tested surfactants PVA, Pluronic® F127, $P(EtOx)_{61}$ and $P(MeOx)_{57}$.

Initial particle preparation experiments were performed using the nanoprecipitation method (Fig. S3A, ESI†) for PVA, Pluronic® F127 and $P(EtOx)_{61}$ as nanoparticle stabilizers using concentrations of 0.3, 0.5 and 1.0 wt%. In fact, the precipitation method results in good PLGA nanoparticles without using surfactants. However, PLGA nanoparticles, which are used for therapeutical purposes, often carry drugs and therefore need to

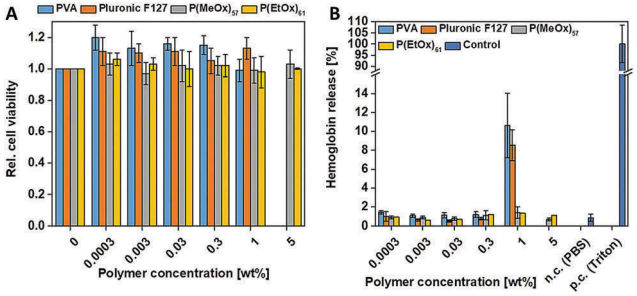

Fig. 1 Concentration dependent biocompatibility of different surfactants. (A) Cytotoxicity of indicated polymers using AlamarBlue® assay. Non-treated cells were set to 1 for relative viability. L929 cells were treated for 24 h with the indicated concentrations of the polymers. Values represent the mean ± S.D. (n = 3). (B) Hemoglobin release of erythrocytes after incubation for 60 min at 37 °C with polymers at indicated concentrations. A value of less than 2% hemoglobin release is classified as non-hemolytic and >5% as hemolytic. Values represent the mean ± S.D. (n = 3).

be prepared using surfactants. For this reason, first particle preparation experiments were performed *via* nanoprecipitation of solely PLGA to provide information about a possible disturbance introduced by non-suitable additives. The resulting nanoparticles were compared regarding z-average and PDI values (Fig. S3B and Table S3, ESI†). Nanoparticles prepared using Pluronic® F127 and $P(EtOx)_{61}$ were rather small ($d_{Pluronic® F127} \approx 120$ nm; $d_{P(EtOx)} \approx$ 115–135 nm), while the usage of the more hydrophilic PVA and $P(MeOx)_{57}$ produces larger nanoparticles ($d_{PVA} \approx 150$ nm; $d_{P(EtOx)} \approx 195$ nm).

We assume that these differences are caused by hydrophilicity of the surfactants. The PDI of the nanoparticles was below 0.160 in all cases, indicating the formation of well-shaped particles.

Furthermore, the more sophisticated emulsion technique was investigated (Scheme 1) concerning a comparison of common and new potential surfactants.[39]

Since this method uses an organic solvent, which is not water-miscible, representing the hydrophobic phase, a surfactant is generally necessary to avoid subsequent phase separation and particle aggregation.

PVA, as a commonly used surfactant, $P(EtOx)_{61}$, as representative of the P(Ox)s, and Pluronic® F127, a surfactant and shearforce protecting agent, were evaluated for this method by comparing the z-average and PDI value of the resulting nanoparticles (Fig. 2 and Table S4, ESI†).

In the range of 0 to 1.0 wt% polymer the optimum surfactant concentration was evaluated for each surfactant tested. Particles prepared using PVA or Pluronic® F127 tend to be very small ($d \approx 100$ nm) and show PDI values < 0.2 at low concentrations (0.3 to 0.5 wt%). $P(EtOx)_{61}$ leads to small particles ($d \approx 110$ nm) with low PDI values (PDI < 0.2) at concentrations of about 1.0 wt%. The preparation of nanoparticles utilizing lower $P(EtOx)_{61}$ concentrations was not possible. Nevertheless, by using 1.0 wt% of $P(EtOx)_{61}$ particles of equal quality as PVA stabilized particles could be produced. Furthermore, it is obvious that particle preparation without a surfactant leads to poor PDI values of about 0.4 and is, therefore, not appropriate. After pre-evaluation of $P(EtOx)_{61}$ the more hydrophilic $P(MeOx)_{57}$ was examined only at the most convenient concentration of $P(EtOx)_{61}$ and led to similar PDI values. For this reason, the preparation of block-copolymers, which consist for example of the monomers MeOx and 2-butyl-2-oxazoline (BuOx), leads to amphiphilicity and, consequently, good stabilization abilities in aqueous solution.[40]

It can be assumed that the ability of the homopolymers to stabilize the emulsion is caused by their solubility in water as well as in the organic solvents used for preparation (Scheme 1).[41] This phenomenon was already evaluated for PVA by S. Galindo-Rodriguez *et al.*,[42] who declared that the polymer chains can be solubilized by the aqueous phase as well as the interphase and

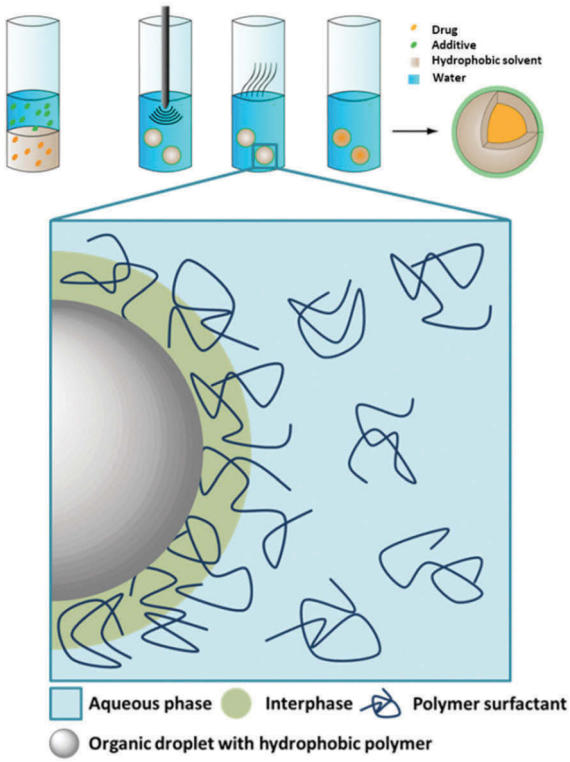

Scheme 1 Schematic representation of the nanoparticle preparation *via* the nanoemulsion technique. A hydrophobic drug and the polymer are dissolved in a not miscible organic solvent and water. Surfactants are added and the solution is emulsified by sonication. After evaporation of the organic solvent, nanoparticles are obtained. Magnification of the nanoparticle–aqueous phase boundary layer is presented, showing the potential behavior of polymer surfactants in the nanoemulsion process.

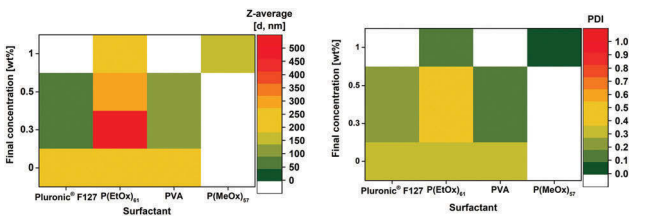

Fig. 2 Properties of PLGA nanoparticles prepared *via* the nanoemulsion technique (water and ethyl acetate), using different surfactants as determined by DLS measurements (n = 3, 5 measurements each). Values colored in white were not investigated. See values in Table S4 (ESI†).

the organic phase. Inter- and intrachain interactions of the surfactant polymer lead to repulsion and steric effects that might stabilize the droplet. Furthermore, a reduction of the interfacial tension is beneficial for the stabilization of an emulsion as known from the literature. This explanation could also fit to the 2-oxazoline homopolymers used in this study. For this reason, the surface tension of surfactant containing water droplets was measured for all the surfactants used (Fig. S4, ESI†). From the comparison of results, all surfactants were found to reduce the surface tension of water at least slightly. However, the comparison of the different P(Ox) solutions does not show any dependence of the surface tension on the concentration or the molar mass of the polymer ($\gamma_{P(EtOx)n} \approx 60$ N m^{-1}, $\gamma_{P(MeOx)n} \approx 70$ N m^{-1}), while PVA and Pluronic® F127 do ($\gamma_{PVAn} \approx 55$ to 45 N m^{-1}, $\gamma_{Pluronic® F127} \approx 45$ to 40 N m^{-1}). Therefore, the concentration dependent surfactant ability might be mainly caused by the viscosity of the solutions (Fig. 4A). It is already known from the literature that the viscosity of the aqueous P(Ox) solution can be influenced by the molar mass as well as the polymer concentration.[43] As shown in Fig. 4A, the dynamic viscosity of the used PVA solution (3 wt%) is between 4.5 and 5.0 mPA s, whereas the utilized $P(EtOx)_{60}$ and $P(MeOx)_{60}$ solutions have much lower viscosities. At a concentration of 10 wt% the P(Ox) solutions have a dynamic viscosity of ~3.0 mPA s, which seems to be an applicable value for the stabilization of the emulsion. Even though PVA has great surfactant abilities at the determined values of surface tension and viscosity, P(Ox)s also work at significantly lower viscosities and reduced surface tension. Since Pluronic® F127 has very good potential to reduce the surface tension of water, the lower viscosity of the solution might not be disadvantageous. These findings support the hypothesis that the stabilization of the particles is influenced by the surface tension and the viscosity of the used surfactant.

2.1.2. Influence of the molar mass of the surfactant. To prove whether the success of surfactant ability of the different polymers depends on the polymer size, hydrophilic P(Ox)s with a varying DP (~25, ~60, ~100, ~200) were tested and characterized regarding the *z*-average and PDI values of the resulting particles using DLS (Fig. 3 and Fig. S5, ESI†).

While using the nanoprecipitation technique, the resulting nanoparticles are of comparable *z*-average ($d \approx 160$ nm) and have a narrow dispersity (PDI < 0.1) (Fig. S5 and Table S5, ESI†). By using the more sophisticated nanoemulsion technique (Fig. 3 and Table S5, ESI†), P(Ox)s with a DP of 60, 100 and 200 produce larger nanoparticles ($d \approx 200$ nm) with a moderate dispersity (PDI < 0.2), while the P(Ox)s with a DP of 25 cannot be used for the production of stable, narrow disperse nanoparticles ($d \approx 800$ nm, PDI ≥ 0.3). These results indicate the dependence of the surfactant ability on the DP of the used polymers for the nanoemulsion technique. A possible explanation for this phenomenon might be given by the viscosity of the polymer solutions. Fig. 4B shows the strong dependence of the viscosity on the DP of the used P(Ox)s. T. X. Viegas *et al.* have already investigated this using a different molar mass range of $P(EtOx)_n$.[43] If we consider these results, a DP of 60 is the minimum possible for successful particle stabilization within the tested range. Low molar mass polymers with a DP below 60 are not capable of stabilizing the PLGA nanoparticles. However, after crossing a certain point, which was a DP of 60 in the current study, an increase of the molar mass seems to be neither beneficial nor disadvantageous for the stabilization of the nanoparticles.

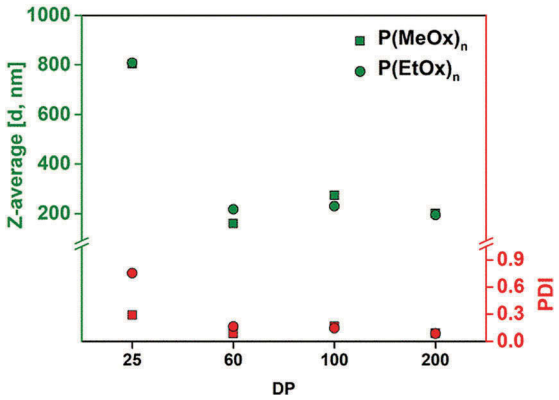

Fig. 3 Properties of PLGA nanoparticles prepared by nanoemulsion (water and ethyl acetate), using hydrophilic P(Ox)s with varying DP as surfactants (1.0 wt%). *z*-Average and PDI values were determined *via* DLS investigations (n = 3, 5 measurements each). See values in Table S5 (ESI†).

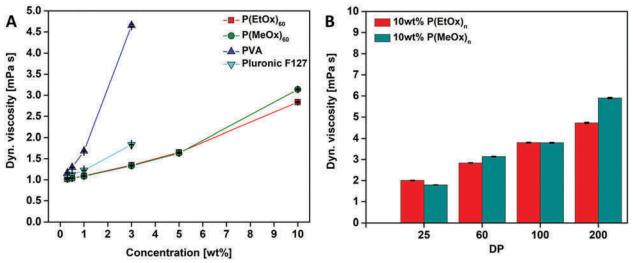

Fig. 4 Dynamic viscosity of different polymer solutions. (A) Dynamic viscosity dependent on the polymer concentration. (B) Dynamic viscosity of P(Ox) solutions with different DP.

2.2. Lyophilization experiments

2.2.1. Comparison of P(Ox)s and commercial cryoprotectants. Successful nanoparticle lyophilization and resuspension are crucial elements for particle preparation and storage (Fig. 5A). Usually, polymeric nanoparticles show difficulties in resuspension after lyophilization and lack in quality. Therefore, first experiments concentrated on the possible capability of P(Ox)s to act as a stabilizing agent during lyophilization of nanoparticles after successful preparation.

$P(EtOx)_{61}$ was used for initial lyophilization experiments to determine the polymer amount necessary for particle stabilization. PLGA nanoparticles were prepared *via* the nanoprecipitation technique without using any stabilizers. Their *z*-average and PDI values were determined by DLS measurements. Subsequently, different amounts of the cryoprotectants ranging from 0.05 to 10 wt% were added to the crude nanoparticle suspension, which was lyophilized afterwards and tested regarding the *z*-average and PDI values of the particles and

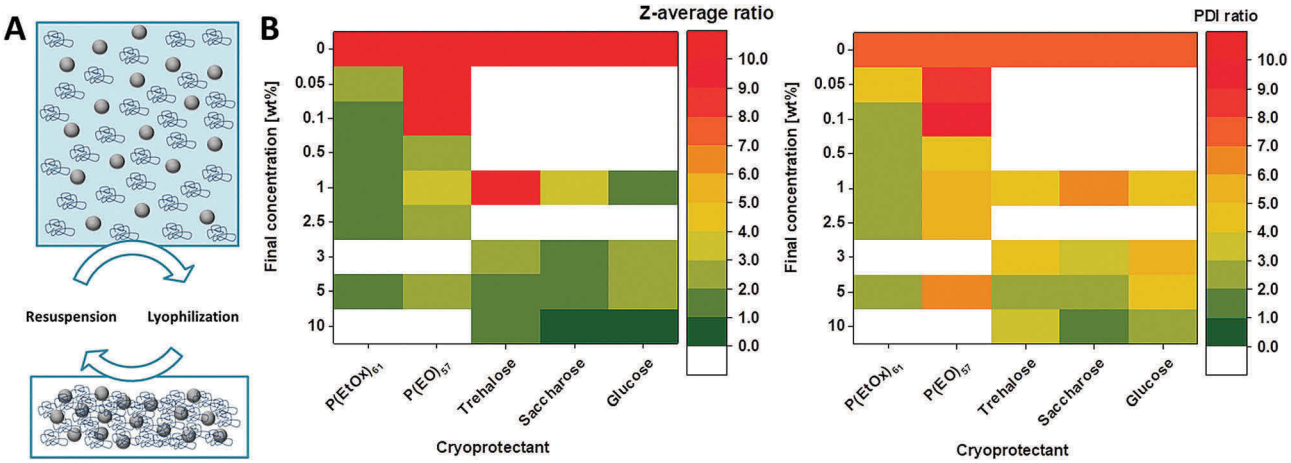

Fig. 5 (A) Schematic representation of the lyophilization and resuspension of polymeric nanoparticles using P(Ox)s as suitable particle stabilizers (cryoprotectants). (B) Properties of the lyophilized PLGA nanoparticles using different cryoprotectants at various concentrations. Diameter size ratios of the *z*-average and PDI ratios of the nanoparticles were determined by DLS investigations (n = 3, 5 measurements each). Ratios were calculated using eqn (1) and (2). Values colored in white were not investigated. See values in Table S3 (ESI†).

compared to the previous results (Fig. 5B and Table S3, ESI†). *z*-Average and PDI ratios of 1.0 are favorable in this context. In Fig. 5B the results of the dynamic light scattering of the particles after lyophilization are summarized compared to the particle properties before. Thereby the ratios of the *z*-average and the PDI were calculated as shown in eqn (1) and (2).

$$z\text{-average ratio} = \frac{z\text{-average after lyophilization}}{z\text{-average after preparation}} \quad (1)$$

$$\text{PDI ratio} = \frac{\text{PDI after lyophilization}}{\text{PDI after preparation}} \quad (2)$$

In this experimental setup, saccharose showed the best performance (*z*-average ratio = 1.0; PDI ratio = 1.8) at a used sugar concentration of 10 wt%. Glucose (*z*-average ratio = 1.0; PDI ratio = 2.1) and trehalose (*z*-average ratio = 1.4; PDI ratio = 2.7) were slightly more unfavorable at concentrations of 10 and 5 wt%, respectively. In contrast, at a low cryoprotectant concentration of about 0.5 wt% $P(EtOx)_{61}$, the *z*-average (ratio = 1.5) and PDI (ratio = 2.0) mostly remain constant, while increasing significantly by the utilization of other cryoprotectants. Even though saccharose shows a better performance at a high concentration of 5.0 wt%, P(Ox)s at low concentrations offer better stabilization. Using P(Ox)s, the increase in the size can be explained by the cryoprotectant addition. $P(EtOx)_{61}$ chains themselves seem to assemble on the PLGA particle surface, whereby the size of the particle increases. It should be noted that a PDI ratio of two, which means a doubling in the actual values, results in PDI values of around 0.2, which still represents a very good value. For comparison, also poly(ethylene oxide) (P(EO)), *i.e.* $P(EO)_{57}$, was tested regarding its cryoprotectant abilities, since P(Ox) and P(EO) are often claimed to show comparable characteristics.

Nanoparticles that were stabilized using $P(EO)_{57}$ showed a huge increase in *z*-average (ratio > 2.5) and PDI (ratio > 4.5) in all tested concentrations ranging from 0.05 to 5 wt%. For this reason, $P(EO)_{57}$ does not seem to be suitable for PLGA nanoparticle stabilization, while $P(EtOx)_{61}$ is superior to commonly used cryoprotectants when used at low concentrations. The tested sugars show their best cryoprotective ability at a concentration of 10.0 wt%, which is twenty times higher than the investigated $P(EtOx)_{61}$. Since sugars are known to be hygroscopic, the use of P(Ox)s, which can be used at much lower amounts, represents a possible alternative for the common cryoprotectants.

2.2.2. Influence of the molar mass of the cryoprotectant. After initial experiments using $P(EtOx)_{61}$, P(Ox)s with varying molar masses were investigated. Herein, $P(EtOx)_n$ and the more hydrophilic $P(MeOx)_n$ were used for the surfactant experiments (DP ≈ 25, 60, 100, 200). As an all-in-one system was targeted, nanoparticle samples prepared with those polymers acting as surfactants were directly lyophilized and re-suspended in double deionized water. The resulting size and PDI values were compared to the values that were determined directly after preparation and are plotted in Fig. 6.

By using the P(Ox)s with a DP of 60, 100 and 200 the characteristics of the PLGA nanoparticles can be maintained during lyophilization (size ratio ≈ 1, PDI ratio: 1 to 2), while the

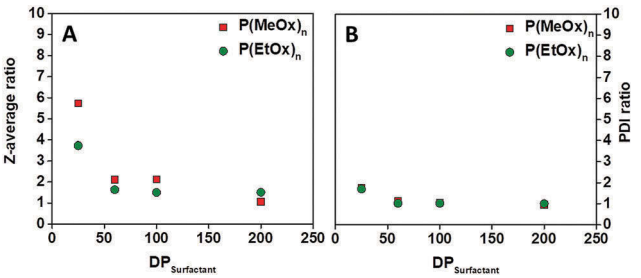

Fig. 6 *z*-Average and PDI ratios of PLGA nanoparticles prepared by the nanoprecipitation technique using 0.3 wt% P(Ox). The particles were lyophilized without further purification and the ratios were calculated using eqn (1) and (2) (n = 3, 5 measurements each). See values in Table S6 (ESI†).

usage of P(Ox)s with a DP of 25 does not seem to be beneficial (size ratio ≈ 2, PDI ratio: 4 to 6).

According to the determined ratios, a P(Ox) based all-in-one system is possible. Direct lyophilization of the PLGA nanoparticles after preparation leads to nanoparticles of defined size and PDI values which seem to be improved by using P(Ox)s with higher molar masses. However, drug encapsulation usually leads to the necessity of particle purification to eliminate free drug from the particle suspension. Furthermore, P(Ox)s with lower molar masses are known to undergo faster renal excretion[44] and are, therefore, further examined in the current study.

2.3. Particle purification

After successful investigation of P(Ox)s as surfactants, the influence of particle purification (centrifugation or filtration) on their size and PDI values was elucidated. For this reason PLGA nanoparticles were produced by nanoprecipitation using 0.3 wt% P(Ox) as the surfactant. The resulting nanoparticles were either centrifuged for 45 min at 11 000 rpm and 4 °C or filtered using a 0.45 μm nylon filter before lyophilization. To see whether it is necessary to use an additional amount of P(Ox) solution for good resuspension, the same amounts of P(Ox) solutions were added before lyophilization to either centrifuged or filtered nanoparticles. For comparison, nanoparticle suspensions which have not been purified before were lyophilized as well (Fig. 7A and Table S7, ESI†). The *z*-average distribution values of the particles before and after purification were investigated *via* DLS and cryoTEM measurements and are summarized in Fig. 7B.

After preparation, the nanoparticles are of comparable size ($d \approx 190$ nm) and dispersity (PDI < 0.1) and, furthermore, suitable for syringe filtration as well as centrifugation. The particles moreover feature a perfect spherical shape. Syringe filtration was conducted using a 0.45 μm nylon syringe filter. Standard sterile filtration would be usually performed using a 0.2 μm syringe filter but to be sure not to filter out possible aggregation of particles a larger filter was used.

DLS measurements provided initial information about the stability of the nanoparticles. Nanoparticles prepared with $P(MeOx)_{57}$ resulted in a diameter of about 200 nm and the PDI was ≈ 0.1, while for nanoparticles prepared by using $P(EtOx)_{61}$ the addition of a P(Ox) solution was necessary ($d = 165.1 \pm 1.0$ nm; PDI = 0.172 ± 0.044) after purification to avoid particle aggregation ($d = 1075 \pm 112$ nm; PDI = 0.948 ± 1). However, by having a close look at the particle morphology *via* cryoTEM, it is also visible that most of the nanoparticles are still well defined and only a few aggregates are present. Nanoparticle sizes obtained by DLS measurements could mostly be confirmed by cryoTEM measurements. Regarding the DLS and cryoTEM results, this purification has no influence on the particle morphology and is, therefore, a suitable purification method that can be used, *e.g.*, to separate the particles from larger aggregates.

Centrifugation of nanoparticles is a common purification method for their separation from small and dissolved molecules. This technique potentially has stronger forces which are exerted onto the nanoparticles; hence, the stability of the

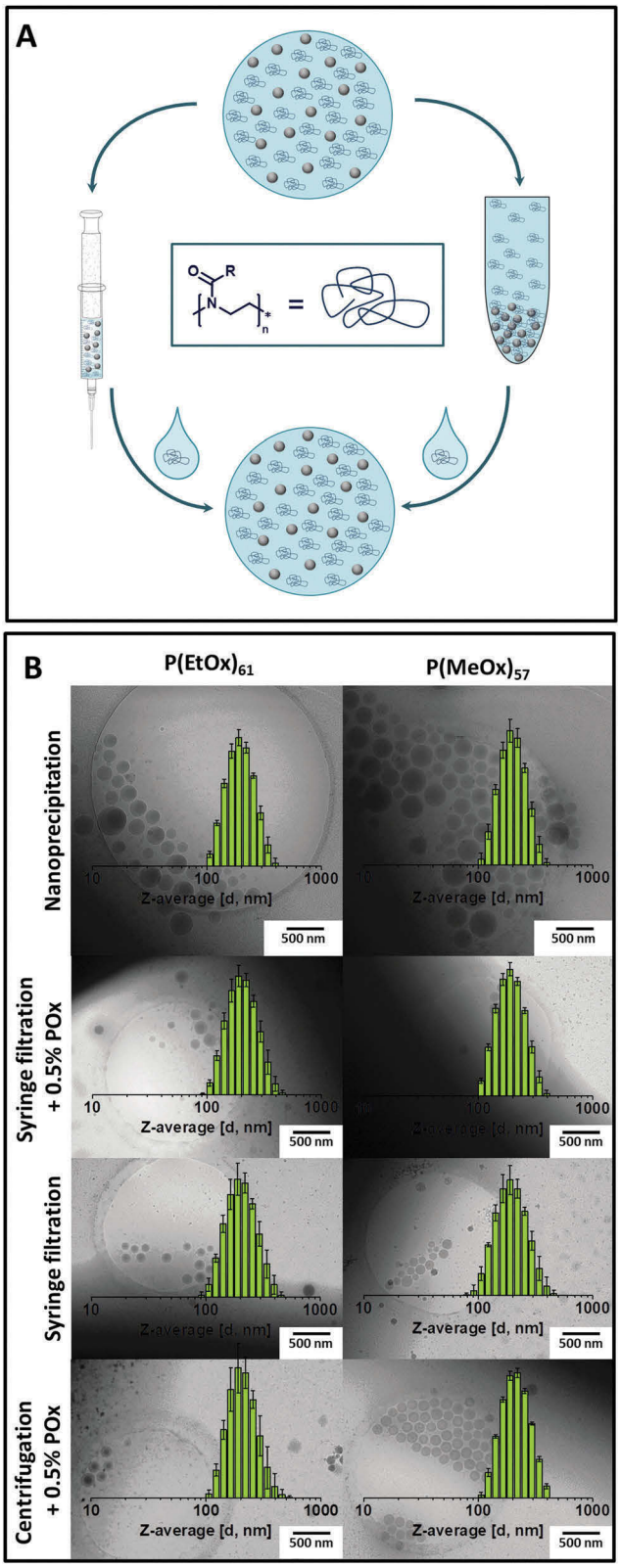

Fig. 7 (A) Schematic representation of nanoparticle purification by either syringe filtration or centrifugation using P(Ox) as the particle stabilizer. (B) Influence of various purification techniques on the size distribution and morphology of PLGA nanoparticles that were prepared by nanoprecipitation, determined by DLS (green columns, $n = 3$, 5 measurements each) and cryoTEM measurements. See values in Table S7 (ESI†). See raw cryoTEM images in Fig. S6 (ESI†).

Table 1 Characteristics of PLGA nanoparticles prepared by nanoprecipitation (water and acetone) using rhodamine B labeled $P(EtOx)_{61}$ as the surfactant. *z*-Average and PDI values were determined *via* DLS measurements

$P(EtOx)_{61}$-rhodamine		
After preparation *via* nanoprecipitation		
z-Average [*d*, nm]	132.1 ± 0.4	134.0 ± 1.3
PDI	0.096 ± 0.002	0.093 ± 0.017
Lyophilized		
	Centrifugation + ultra-pure water	Centrifugation + 0.5 wt% P(Ox)
z-Average [*d*, nm]	n.a.	175.5 ± 4.5
PDI	n.a.	0.273 ± 0.019
P(Ox)[a] [mg]	0.7	4.6
$P(MeOx)_{57}$-rhodamine		
After preparation *via* nanoprecipitation		
z-Average [*d*, nm]	193.8 ± 2.0	190.6 ± 2.3
PDI	0.090 ± 0.038	0.072 ± 0.021
Lyophilized		
	Centrifugation + ultra-pure water	Centrifugation + 0.5 wt% P(Ox)
z-Average [*d*, nm]	Particle aggregation	182.7 ± 21.7
PDI	Particle aggregation	0.192 ± 0.062
P(Ox)[a] [mg]	0.0	4.0

[a] Calculated from UV/Vis absorption measurements at λ_{Ex} = 630 nm. n.a.: not available because of particle aggregation. For absorbance and emission spectra of the labelled P(Ox)s, see Fig. S7 (ESI).

particle solutions was also tested under these conditions. Therefore, the raw particle suspensions were centrifuged for a predetermined time, decanted and afterwards resuspended in either ultra-pure water or a 0.5 wt% P(Ox) solution. Unfortunately, the nanoparticles, which were resuspended in ultra-pure water, formed large aggregates and were, therefore, excluded from further studies. On the other hand, the resuspension in a 0.5 wt% P(Ox) solution resulted in well-defined nanoparticles. For this reason, we conclude that a certain amount of the surfactant is washed out by centrifugation and has to be added afterwards to reach the amount necessary for particle stabilization.

With the aid of rhodamine B labeled P(Ox)s, which were used for nanoparticle preparation *via* nanoprecipitation (water and acetone), we could obtain further information regarding the interaction of P(Ox)s and particles. The raw nanoparticles were subsequently centrifuged and the particle pellet was resuspended in either ultra-pure water or in a 0.5 wt% solution of rhodamine B labeled P(Ox)s. The resulting nanoparticles were then lyophilized and resuspended in ultra-pure water. A control batch, which was lyophilized without further purification, was also prepared. The final particles were characterized using DLS and UV/Vis measurements (Table 1) to determine the P(Ox) amount within the polymer particle by using rhodamine B calibration. Nanoparticles that were centrifuged and resuspended in ultra-pure water aggregate after lyophilization as revealed by the DLS results ($d_{P(MeOx)}$: particle aggregation; $d_{P(EtOx)}$ not available because of particle aggregation). UV/Vis measurements resulted in less than 1 mg P(Ox)s per mg PLGA within the purified nanoparticles. For comparison, nanoparticles which were resuspended in a 0.5 wt% P(Ox) solution possessed a P(Ox) amount of more than 4 mg P(Ox)s per mg PLGA.

The nanoparticles are of smaller size ($d_{P(MeOx)}$ = 182.7 ± 21.7 nm; $d_{P(EtOx)}$ = 175.4 ± 4.5 nm) and with lower PDI ($PDI_{P(MeOx)}$ = 0.192 ± 0.062 nm; $PDI_{P(EtOx)(MeOx)}$ = 0.273 ± 0.019 nm) than the nanoparticles which were purified without a surfactant.

By comparing the DLS and the UV/Vis results of the nanoparticles, it is clearly visible that the *z*-average as well as the PDI value depends on the P(Ox) amount of the particles. Therefore, a resuspension in 0.5 wt% P(Ox) solutions is defined to be beneficial for the nanoparticle uniformity.

These findings could also be confirmed *via* CLSM measurements. For this purpose, microparticles were produced using the microemulsion technique (water and dichloromethane) and rhodamine B labeled $P(MeOx)_{57}$ as the surfactant. After evaporation of the solvent, the PLGA microparticles were characterized. The particles have a clear pink corona (Fig. 8), indicating a surfactant layer, which is visible even after centrifugation.

2.4. Variation of hydrophobic particle forming polymers

It is of fundamental interest to verify that the introduced method is also applicable to other polymer systems. Therefore, the effect of P(Ox) surfactants on PCL and methacrylate based particles was also evaluated. Regarding the previous experiments, the hydrophilic P(Ox)s $P(EtOx)_{61}$ and $P(MeOx)_{57}$ are suitable cryoprotectants and surfactants for PLGA nanoparticles. In addition to PLGA, also the nanoparticle formation of the polymers poly(caprolactone) (P(CL)), Eudragit RS100, and $P(MMA_{97}$-*co*-$MAEMA_{32})$ *via* nanoemulsion was tested (Table S8, ESI†).

Unfortunately, preparation of nanoparticles consisting of PCL was not possible using P(Ox)s as a surfactant, since the particles were not stable in aqueous solution. Nevertheless, excellent particles could be prepared from Eudragit RS100 and $P(MMA_{97}$-*co*-$MAEMA_{32})$ methacrylate based copolymers (Fig. 9). Eudragit RS100 forms large particles ($d_{P(EtOx)}$ = 214.0 ± 0.7 nm; $d_{P(MeOx)}$ = 244.3 ± 2.5 nm; $d_{ultra\text{-}pure\ water}$ = 101.6 ± 0.5 nm), when using P(Ox)s as a surfactant. Furthermore, well-defined

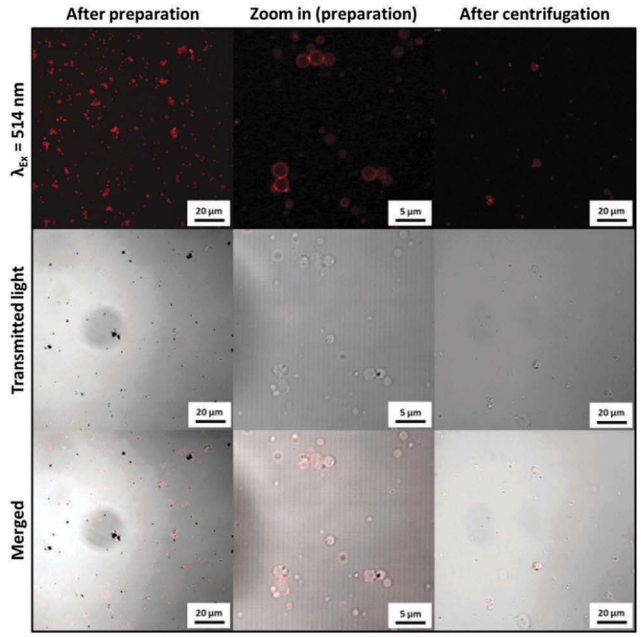

Fig. 8 CLSM (λ_{Ex} = 514 nm, λ_{Em} = 531 to 704 nm) of PLGA microparticles prepared by microemulsion (water and dichloromethane) using P(MeOx)$_{57}$-rhodamine as a surfactant. For absorbance and emission spectra of the labelled P(Ox)s, see Fig. S7 (ESI†).

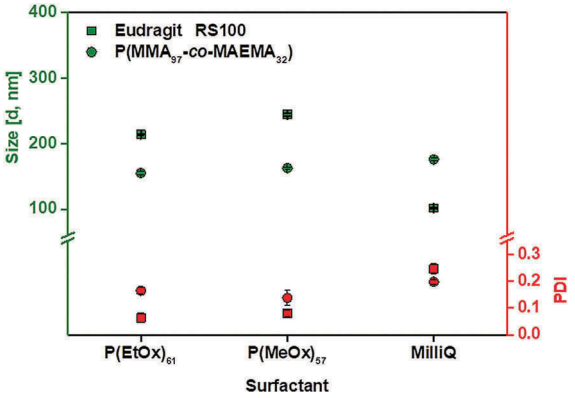

Fig. 9 Properties of the nanoparticles prepared by nanoemulsion (water and ethyl acetate), using P(Ox)s as surfactants. *z*-Average and PDI values were determined *via* DLS (n = 3, 5 measurements each). See values in Table S8 (ESI†).

nanoparticles can only be achieved by utilization of P(Ox) surfactants ($PDI_{P(EtOx)}$ = 0.063 ± 0.018; $PDI_{P(MeOx)}$ = 0.081 ± 0.012; $PDI_{ultra\text{-}pure\ water}$ = 0.246 ± 0.020).

When using P(MMA$_{97}$-*co*-MAEMA$_{32}$), the more hydrophilic surfactant P(MeOx)$_{57}$ leads to less disperse ($PDI_{P(MeOx)}$ = 0.087 ± 0.023; $PDI_{P(EtOx)}$ = 0.147 ± 0.030) nanoparticles. However, at this point, it should also be pointed out that the PDI values of the nanoparticles prepared using P(EtOx)$_{61}$ are still very good. However, the prepared particles are only slightly less disperse than particles prepared without using a surfactant ($PDI_{ultra\text{-}pure\ water}$ = 0.191 ± 0.012). Therefore, at first glance, the particles do not seem to benefit the usage of P(Ox)s as a surfactant. Since the non-ionic P(Ox)s have a neutral zeta potential, the zeta potential of the nanoparticles ($\zeta_{P(MeOx)} > 30$ mV; $\zeta_{P(EtOx)} > 30$ mV; $\zeta_{MilliQ} > 40$ mV) is more or less unaffected by the surfactant as it remains being strongly positive.

More interestingly, for P(MMA$_{97}$-*co*-MAEMA$_{32}$) both P(Ox)s seem to have a comparable ability of being a surfactant agent; however, the prepared particles are only slightly less disperse than particles prepared without using a surfactant ($PDI_{ultra\text{-}pure\ water}$ = 0.191 ± 0.012). Therefore, at first glance, the particles do not seem to benefit the usage of P(Ox)s as a surfactant. In both cases the particle size is dependent on the surfactant as well as on the type of hydrophibic polymer being used. As this study mainly concentrates on the investigation of P(Ox)s as suitable surfactants for all tested polymers, the particles consisting of different types of polymers are not compared with each other directly. However, the influence of P(Ox) based surfactants on the nanoparticle size and PDI value was examined. Purification *via* centrifugation and filtration as well as lyophilization experiments with these nanoparticles were also investigated (Fig. 10 and Tables S9, S10, ESI†).

The purification of Eudragit RS100 yielded stable nanoparticles when prepared using P(Ox) based surfactants (size ratio < 1.3; PDI ratio: < 1.7 (except centrifugation and resuspension in ultra-pure water)), while nanoparticles without surfactants aggregated after lyophilization (Fig. 10A). While purifying P(MMA$_{97}$-*co*-MAEMA$_{32}$) filtration did not work in any case. However, the addition of a P(Ox) solution after filtration was beneficial even for P(MMA$_{97}$-*co*-MAEMA$_{32}$) nanoparticles prepared without a surfactant. Centrifugation and resuspension in ultra-pure water before lyophilization also yielded stable nanoparticles with respect to their size and PDI ratios, which are below a value of two.

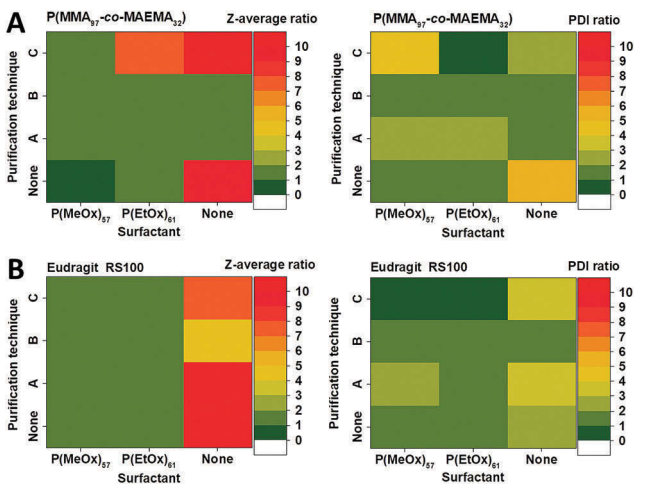

Fig. 10 Dependence of *z*-average and PDI ratios of (A) Eudragit RS100 and (B) P(MMA$_{97}$-*co*-MAEMA$_{32}$) nanoparticles on the purification method by either direct lyophilization of the particle suspension (None), centrifugation at 11 000 rpm for 45 min and resuspension in ultra-pure water (A), centrifugation at 11 000 rpm for 45 min and resuspension in a 0.5% P(Ox) solution (B) or syringe filtration using a 0.45 µm nylon filter (C). Nanoparticles were prepared *via* nanoprecipitation (water and acetone). See values in Tables S9 and S10 (ESI†).

2.5. Drug encapsulation

2.5.1. Encapsulation of Nile red. After the successful investigation of P(Ox)s for combined cryoprotection and stabilization, the influence of drug encapsulation was examined. For this purpose, the model drug Nile red was tested. Nile red containing PLGA nanoparticles were prepared with both nanoprecipitation (water and acetone) and nanoemulsion (water and ethyl acetate) technique with either $P(EtOx)_{61}$ or $P(MeOx)_{57}$ as the surfactant under previously determined optimum conditions. Nile red could be dissolved in the same organic solvent as the PLGA in both cases. 10 μg Nile red per 1 mg PLGA was used. For comparison particles without a surfactant were prepared. All the resulting particles were compared with regard to the *z*-average and PDI values (Fig. 11 and Table S11, ESI†).

The particle preparation using Nile red as a model drug resulted in well-defined nanoparticles in all cases. Similar to the preparation of nanoparticles without drug, the preparation of nanoparticles with Nile red using the nanoprecipitation method is possible without using surfactants (d = 145.2 ± 2.5 nm; PDI = 0.075 ± 0.018); however, the utilization of P(Ox)s leads to slightly larger particles ($d_{P(EtOx)}$ = 160.8 ± 1.5 nm; $d_{P(MeOx)}$ = 151.2 ± 0.8 nm), which are still well-defined ($PDI_{P(EtOx)}$ = 0.053 ± 0.028; $PDI_{P(MeOx)}$ = 0.065 ± 0.021).

More interestingly, the particle preparation *via* nanoemulsion techniques also results in nanoparticles with low PDI values ($PDI_{P(EtOx)}$ = 0.124 ± 0.013; $PDI_{P(MeOx)}$ = 0.099 ± 0.014), while a stable particle formation without an additional surfactant is impossible (Table S11, ESI†). The nanoparticles prepared using $P(EtOx)_{61}$ as a surfactant are about 10 nm larger than the particles prepared with $P(MeOx)_{57}$. This phenomenon correlates well with the steric properties resulting from the longer side-chains of the polymers. Again, different purification techniques were examined on the nanoparticles prepared *via* nanoprecipitation (Fig. 11 and Tables S12, S13, ESI†) to complete the investigation on encapsulated particles as done before for particles without the model drug. Nile red could be dissolved in the same organic solvent as the PLGA in both cases. 10 μg Nile red and 3 mg P(Ox)s per 1 mg PLGA were used. Consequently, encapsulation efficiency (EE) of approximately 2.5 μg Nile red per 1 mg nanoparticle corresponds to 100% EE. P. Pietzonka *et al.* have already encapsulated 0.1 μg per 1 mg PLGA nanoparticle (0.1 wt%) by using PVA as a suitable surfactant.[45]

Interestingly, direct lyophilization of the raw nanoparticles resulted in aggregation only when prepared with $P(MeOx)_{57}$; however, nanoparticles prepared with $P(EtOx)_{61}$ remained stable (d = 168.0 ± 1.6; PDI = 0.087 ± 0.031). The same observations were made for nanoparticles that were purified *via* syringe filtration. While nanoparticles that were prepared using $P(MeOx)_{57}$ aggregated after purification, $P(EtOx)_{61}$ is beneficial (d = 161.7 ± 3.4; PDI = 0.157 ± 0.011). This disadvantage of $P(MeOx)_{57}$ compared to $P(EtOx)_{61}$ can be explained by its enhanced hydrophilicity, caused by the shorter side chains. Since it is uncertain whether the particle shell of PLGA is probably permeated by the surfactant, we guess that the more hydrophobic $P(EtOx)_{61}$ interacts with the hydrophobic drug in a more stabilizing manner than $P(MeOx)_{57}$ leading to more stable nanoparticles.

At this point it should also be noted that nanoparticles that were purified using centrifugation and resuspended in a 0.5 wt% solution of the corresponding P(Ox), as shown before for particles without the model drug, are stable and well-defined in both cases ($d_{P(EtOx)}$ = 184.3 ± 1.6 nm; $d_{P(MeOx)}$ = 187.4 ± 3.2 nm; $PDI_{P(EtOx)}$ = 0.145 ± 0.028; $PDI_{P(MeOx)}$ = 0.123 ± 0.052), whereas the nanoparticles that were prepared without a surfactant were not resuspendable. Particles prepared with a surfactant and resuspended in ultra-pure water have not been under investigation due to the unpleasant results without the model drug. The encapsulation efficiency was moderate in all cases, ranging from 0.21 to 0.52 μg Nile red per mg nanoparticle, which corresponds to 10 to 20%. We could not define any dependency on the surfactant or purification technique.

In order to obtain information about the influence of the P(Ox) surfactants on cellular uptake of drug loaded nanoparticles, CLSM measurements were performed (Fig. 12).

CLSM images show an uptake of all nanoparticles. Even though the fluorescence intensity of Nile red was slightly weaker when using $P(MeOx)_{57}$, quantification *via* CLSM is difficult. However, intense cellular uptake studies, *e.g. via* flow cytometry, were not part of the current study and have to be investigated in an additional project.

Cells that were treated with Nile red solutions, which do not contain PLGA, were not fluorescent. This finding supports the

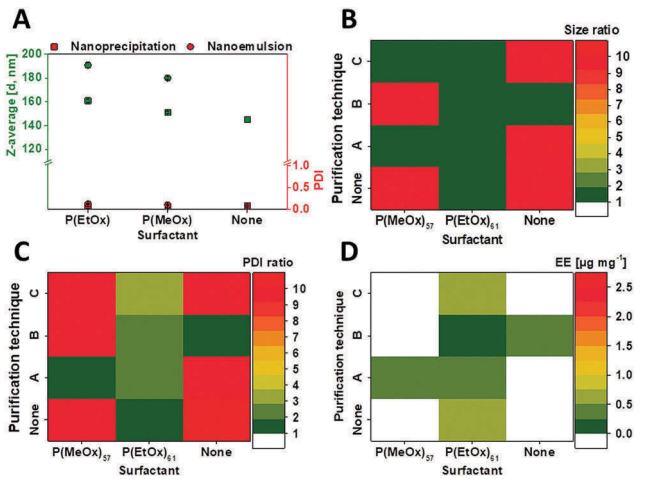

Fig. 11 (A) *z*-Average and PDI of PLGA nanoparticles encapsulating the model drug Nile red, prepared by either nanoprecipitation (water and acetone) or nanoemulsion (water and ethyl acetate) determined using DLS measurements (n = 3, 5 measurements each). See values in Table S11 (ESI†). (B–D) *z*-Average and PDI ratios as well as encapsulation efficiency (EE) of PLGA nanoparticles using Nile red as a model drug depending on the purification method by either direct lyophilization of the particle suspension (none), centrifugation at 11 000 rpm for 45 min and resuspension in 0.5 wt% P(Ox) solution ("A"), syringe filtration using a 0.45 μm nylon filter and addition of 1 mL of 0.5 wt% P(Ox) solution ("B") or syringe filtration using a 0.45 μm nylon filter ("C"). EE (μg Nile red per mg nanoparticle, 2.5 μg mg^{-1} corresponds to 100%) is calculated from UV/vis absorption measurements at λ_{Ex} = 630 nm, mean value of n = 3. Values colored in white were not investigated. Nanoparticles were prepared by nanoprecipitation (water and acetone). See values in Tables S12 and S13 (ESI†).

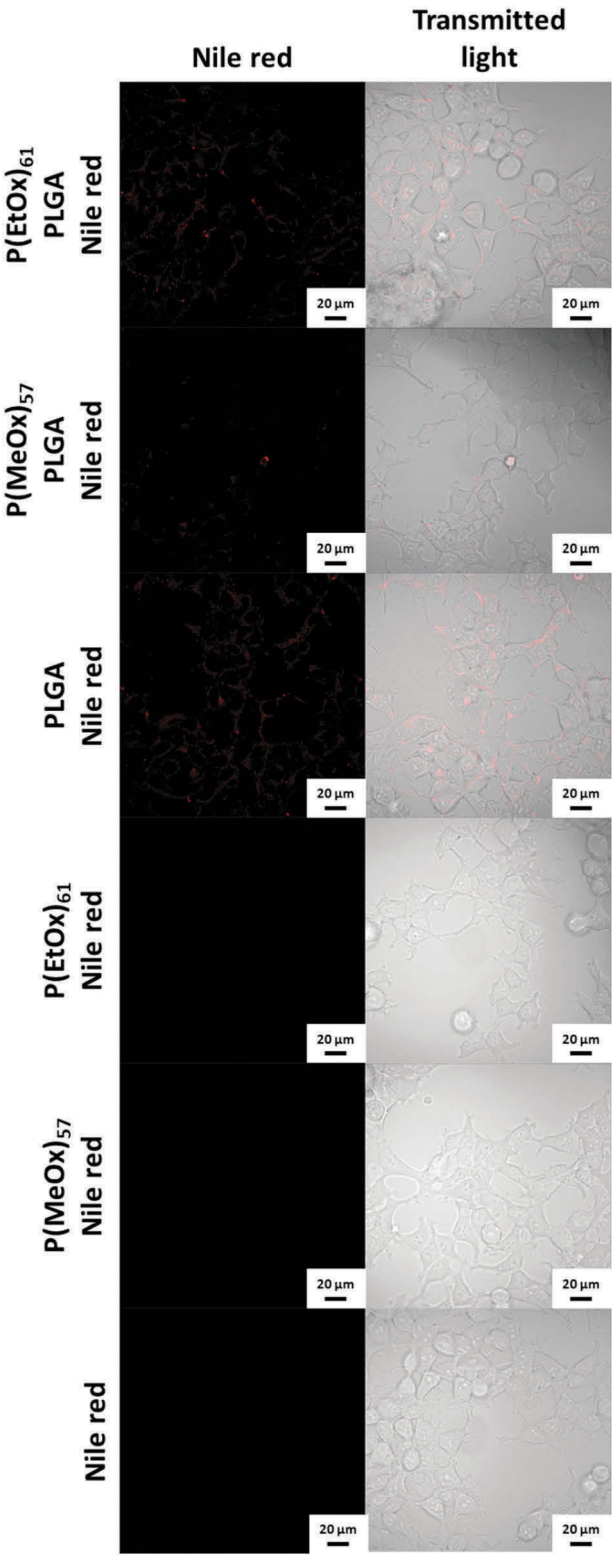

Fig. 12 Cellular uptake study of different Nile red formulations. HEK-293 cells were treated with formulations for 30 min in growth media and analyzed *via* CLSM (red: Nile red). See Fig. S8 (ESI†) for zoom-in images and control.

fact that the P(Ox) surfactants do not encapsulate Nile red, which is beneficial for the removal of not encapsulated drug after preparation. An *in vitro* or *in vivo* influence of not encapsulated drug can consequently be reduced.

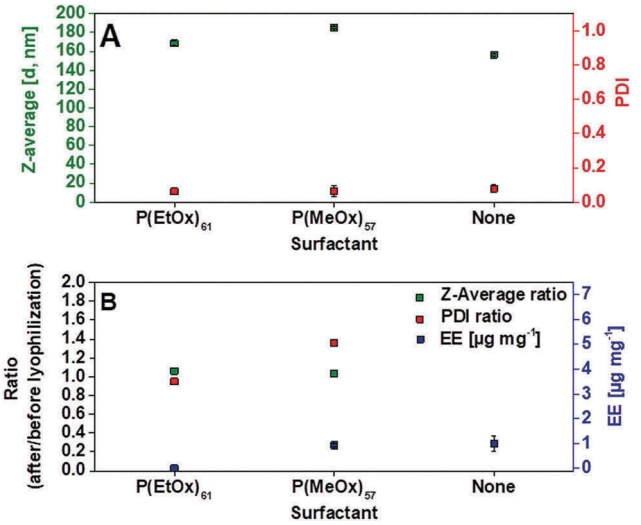

Fig. 13 Characteristics of PLGA nanoparticles using PKC 412 as drug. (A) *z*-Average and PDI value after preparation determined by DLS investigations. Data represent the mean of 3 samples and 5 measurements each. (B) *z*-Average and PDI ratios after lyophilization of the nanoparticles calculated using eqn (1) and (2). Data represent the mean of three samples and five measurements each. EE (µg PKC 412 per mg PLGA; 7.5 µg PKC 412 per 1 mg nanoparticle corresponds to 100% EE) determined by UV/Vis (λ_{Ex} = 293 nm). Nanoparticles were prepared by nanoprecipitation (water and acetone/dimethyl sulfoxide). Ratios larger than two (no surfactant) are excluded. See values in Tables S14 and S15 (ESI†).

2.5.2. Encapsulation of PKC 412. Since Nile red is only a model drug for the encapsulation of a drug into nanoparticles, additional studies on the encapsulation of the application-related drug PKC 412 into PLGA nanoparticles were conducted (Fig. 13 and Table S14, ESI†) using $P(EtOx)_{61}$ or $P(MeOx)_{57}$ as a surfactant. In general, the preparation of nanoparticles *via* nanoprecipitation is possible by using either no surfactant (none), $P(EtOx)_{61}$ or $P(MeOx)_{57}$ as a surfactant. However, PKC 412 is only soluble in dimethyl sulfoxide, which was mixed with the polymer–acetone solution, leading to the necessity of further purification after preparation. For this reason, the usage of P(Ox) based surfactants was investigated. 30 µg PKC 412 and 3 mg P(Ox)s per 1 mg PLGA were used. Consequently, encapsulation efficiency (EE) of approximately 7.5 µg PKC 412 per 1 mg nanoparticle corresponds to 100% EE.

After preparation, all the resulting nanoparticles revealed good properties regarding size (d_{PEtOx} = 168.6 ± 2.4 nm; d_{PMeOx} = 184.6 ± 1.1 nm; $d_{ultra\text{-}pure\ water}$ = 156.1 ± 0.9 nm) and PDI characteristics (PDI_{PEtOx} = 0.061 ± 0.019; PDI_{PMeOx} = 0.063 ± 0.034; $PDI_{ultra\text{-}pure\ water}$ = 0.077 ± 0.024).

In preliminary experiments, the preparation of PKC 412 loaded nanoparticles using PVA resulted in much larger particles (d = 276 nm, data not shown). As the drug has enhanced solubility in DMSO, the nanoparticles were purified using centrifugation to remove the solvent and avoid the drug diffusing out. The nanoparticles were resuspended in either ultra-pure water or a 0.5 wt% P(Ox) solution of the polymer that was used for preparation.

As expected, nanoparticles prepared without any additives aggregate when resuspended after lyophilization. In contrast, the nanoparticles prepared using P(Ox)s are well resuspendable and maintain their size ($d_{P(EtOx)}$ = 178.9 ± 2.0 nm; $d_{P(MeOx)}$ = 190.4 ± 2.4 nm) and PDI characteristics ($PDI_{P(EtOx)}$ = 0.058 ± 0.025; $PDI_{P(MeOx)}$ = 0.086 ± 0.022). Surprisingly, nanoparticles prepared by using $P(EtOx)_{61}$ do not show any drug encapsulation, while the encapsulation efficiency for nanoparticles prepared with $P(MeOx)_{57}$ is around 0.92 ± 0.08 μg mg^{-1} nanoparticle, corresponding to 12% EE. Regarding these characteristics, the encapsulation of PKC 412 is possible by using $P(MeOx)_{57}$. Preliminary experiments using PVA as a stabilizer showed much lower encapsulation efficiencies (~1%, data not shown).

3. Conclusion

In the presented study, we demonstrated the ability of water soluble and biocompatible P(Ox)s to act as stabilizing agents for polymer based nanoparticles. First, we showed their ability to replace the commonly used sugar based cryoprotectants and result in resuspendable particles with constant properties. After successful lyophilization experiments, we also used the polymers as biocompatible surfactants. By adjusting the optimum P(Ox) concentration, PLGA nanoparticles could be prepared *via* nanoprecipitation and nanoemulsion techniques omitting the use of PVA, which allows the preparation of well-defined nanoparticles at the expense of cytotoxicity and additionally required purification steps. Furthermore, we demonstrated the possibility to use P(Ox)s as an all-in-one system for the stabilization of polymeric nanoparticles during preparation, purification and lyophilization. After a proof of concept using PLGA serving as the shell-polymer for the nanoparticles, some other polymers were investigated including PCL and methacrylate based copolymers, *i.e.* Eudragit RS100. Finally, the P(Ox) based nanoparticle surfactants were used to stabilize nanoparticles while encapsulating the model drug Nile red or the application-relevant drug PKC 412. Thereby, the properties, especially the stability in purification processes, of the nanoparticles could be improved as well. Since these non-toxic polymers are not known to mediate cellular responses like P(EO) or specific uptake mechanisms like sugars, they could be used as promising stabilizing agents for nanoparticles that are supposed to be used in biomedical applications. Further experiments will concentrate on the preparation of micro- and nanoparticles, using labeled polymers as suitable surfactants for cell-specific targeting.

We are confident that it will be possible to improve the performance of P(Ox)s for use in drug encapsulation and with this their application in biomedical treatment will be of high interest to the pharmaceutical community.

Conflicts of interest

There are no conflicts to declare. A. Traeger and M. Lehmann are shareholders of the SmartDyeLivery GmbH, a university spin-off company engaged in the development of a platform for nanoformulated drugs to restore critical cellular signalling functions.

Acknowledgements

The authors gratefully acknowledge the Bundesministerium für Bildung und Forschung (BMBF, Germany, #13N13416 smart-dye-livery, #031A518B Vectura, and #01EO1502 TarOrgSterol CSCC 2.0) and the Thüringer Ministerium für Wirtschaft, Wissenschaft, und Digitale Gesellschaft (TMWWDG, ProExzellenzII, NanoPolar) for funding. A. Traeger acknowledges the Carl Zeiss Foundation for funding. The authors thankfully acknowledge Carolin Kellner and Claudia Meier for the conduction of AlamarBlue, hemolysis, and aggregation assays, Steffi Stumpf for surface tension measurements and Dr. Jürgen Vitz for providing the $P(EO)_{57}$. Cryo-TEM investigations were performed at the Electron Microsocpy Facilities of the Jena Center for Soft Matter (JCSM), which was established with grants from the Deutsche Forschungsgemeinschaft (DFG) and the European Fund for Regional Development (EFRE). The LSM880 ELYRA PS.1 was further funded with a grant from the DFG.

Notes and references

1 G. De Crozals, R. Bonnet, C. Farre and C. Chaix, *Nano Today*, 2016, **11**, 435–463.
2 F. Danhier, E. Ansorena, J. M. Silva, R. Coco, A. Le Breton and V. Préat, *J. Controlled Release*, 2012, **161**, 505–522.
3 A. T. Press, A. Traeger, C. Pietsch, A. Mosig, M. Wagner, M. G. Clemens, N. Jbeily, N. Koch, M. Gottschaldt, N. Bézière, V. Ermolayev, V. Ntziachristos, J. Popp, M. M. Kessels, B. Qualmann, U. S. Schubert and M. Bauer, *Nat. Commun.*, 2014, **5**, 5565.
4 M. C. Pedroso de Lima, S. Simões, P. Pires, H. Faneca and N. Düzgüneş, *Adv. Drug Delivery Rev.*, 2001, **47**, 277–294.
5 J. M. Barichello, M. Morishita, K. Takayama and T. Nagai, *Drug Dev. Ind. Pharm.*, 1999, **25**, 471–476.
6 H. Fessi, F. Puisieux, J. P. Devissaguet, N. Ammoury and S. Benita, *Int. J. Pharm.*, 1989, **55**, R1–R4.
7 C. X. Song, V. Labhasetwar, H. Murphy, X. Qu, W. R. Humphrey, R. J. Shebuski and R. J. Levy, *J. Controlled Release*, 1997, **43**, 197–212.
8 P. Fonte, S. Reis and B. Sarmento, *J. Controlled Release*, 2016, **225**, 75–86.
9 S. Bozdag, K. Dillen, J. Vandervoort and A. Ludwig, *J. Pharm. Pharmacol.*, 2005, **57**, 699–707.
10 P. Fonte, S. Soares, F. Sousa, A. Costa, V. Seabra, S. Reis and B. Sarmento, *Biomacromolecules*, 2014, **15**, 3753–3765.
11 L.-Q. Chen, L. S. Cheung, L. Feng, W. Tanner and W. B. Frommer, *Annu. Rev. Biochem.*, 2015, **84**, 865–894.
12 Y. Takashima, R. Saito, A. Nakajima, M. Oda, A. Kimura, T. Kanazawa and H. Okada, *Int. J. Pharm.*, 2007, **343**, 262–269.

13 P. Fonte, P. R. Lino, V. Seabra, A. J. Almeida, S. Reis and B. Sarmento, *Int. J. Pharm.*, 2016, **503**, 163–173.
14 H. K. Makadia and S. J. Siegel, *Polymers*, 2011, **3**, 1377–1397.
15 S. K. Sahoo, J. Panyam, S. Prabha and V. Labhasetwar, *J. Controlled Release*, 2002, **82**, 105–114.
16 M. F. Zambaux, F. Bonneaux, R. Gref, P. Maincent, E. Dellacherie, M. J. Alonso, P. Labrude and C. Vigneron, *J. Controlled Release*, 1998, **50**, 31–40.
17 G. Wang, Y. Fang, P. Kim, A. Hayek, M. R. Weatherspoon, J. W. Perry, K. H. Sandhage, S. R. Marder and S. C. Jones, *Adv. Funct. Mater.*, 2009, **19**, 2768.
18 T. Kagiya, S. Narisawa, T. Maeda and K. Fukui, *J. Polym. Sci., Part B: Polym. Phys.*, 1966, **4**, 441–445.
19 W. Seeliger, E. Aufderhaar, W. Diepers, R. Feinauer, R. Nehring, W. Thier and H. Hellmann, *Angew. Chem., Int. Ed.*, 1966, **5**, 875–888.
20 T. G. Bassiri, A. Levy and M. Litt, *J. Polym. Sci., Part B: Polym. Phys.*, 1967, **5**, 871–879.
21 D. A. Tomalia and D. P. Sheetz, *J. Polym. Sci., Part A: Polym. Chem.*, 1966, **4**, 2253–2265.
22 K. Kempe, E. F. J. Rettler, R. M. Paulus, A. Kuse, R. Hoogenboom and U. S. Schubert, *Polymer*, 2013, **54**, 2036–2042.
23 H. M. L. Lambermont-Thijs, M. W. M. Fijten, A. J. van der Linden, B. M. van Lankvelt, M. M. Bloksma, U. S. Schubert and R. Hoogenboom, *Macromolecules*, 2011, **44**, 4320–4325.
24 H. M. L. Lambermont-Thijs, M. J. H. C. Jochems, R. Hoogenboom and U. S. Schubert, *J. Polym. Sci., Part A: Polym. Chem.*, 2009, **47**, 6433–6440.
25 K. Kempe, S. Jacobs, H. M. L. Lambermont-Thijs, M. M. W. M. Fijten, R. Hoogenboom and U. S. Schubert, *Macromolecules*, 2010, **43**, 4098–4104.
26 K. Kempe, M. Lobert, R. Hoogenboom and U. S. Schubert, *J. Polym. Sci., Part A: Polym. Chem.*, 2009, **47**, 3829–3838.
27 F. Wiesbrock, R. Hoogenboom, C. H. Abeln and U. S. Schubert, *Macromol. Rapid Commun.*, 2004, **25**, 1895–1899.
28 R. Luxenhofer, Y. Han, A. Schulz, J. Tong, Z. He, A. V. Kabanov and R. Jordan, *Macromol. Rapid Commun.*, 2012, **33**, 1613–1631.
29 F. a. D. Administration, in 21, Vol. 21CFR175, 105, ed. D. o. H. a. H. Services, 2016.
30 Z. K. J. Kronek, J. Lustoň, E. Paulovičová, L. Paulovičová and B. Mendrek, *J. Mater. Sci.: Mater. Med.*, 2011, **22**, 1725–1734.
31 L. Wyffels, T. Verbrugghen, B. D. Monnery, M. Glassner, S. Stroobants, R. Hoogenboom and S. Staelens, *J. Controlled Release*, 2016, **235**, 63–71.
32 K. L. Eskow Jaunarajs, D. G. Standaert, T. X. Viegas, M. D. Bentley, Z. Fang, B. Dizman, K. Yoon, R. Weimer, P. Ravenscroft, T. H. Johnston, M. P. Hill, J. M. Brotchie and R. W. Moreadith, *Mov. Disord.*, 2013, **28**, 1675–1682.
33 M. Miyamoto, K. Aoi, H. Yamanaka and T. Saegusa, *Polym. J.*, 1992, **24**, 405–409.
34 S. Kobayashi, *Macromolecules*, 1991, **24**, 5473–5475.
35 C. Giardi, V. Lapinte, C. Charnay and J. J. Robin, *React. Funct. Polym.*, 2009, **69**, 643–649.
36 S. Kobayashi, *Macromolecules*, 1987, **20**, 1729–1734.
37 Z. Amjad and D. Morgan, *Phosphorus Res. Bull.*, 2011, **25**, 33–38.
38 O. Poncelet, R. Borlet and D. Getto, Google Patents, 2014.
39 T. Trimaille, C. Pichot, A. Elaïssari, H. Fessi, S. Briançon and T. Delair, *Colloid Polym. Sci.*, 2003, **281**, 1184–1190.
40 R. Luxenhofer, A. Schulz, C. Roques, S. Li, T. K. Bronich, E. V. Batrakova, R. Jordan and A. V. Kabanov, *Biomaterials*, 2010, **31**, 4972–4979.
41 T. T. Chiu, B. P. Thill and W. J. Fairchok, in *Water-Soluble Polymers*, American Chemical Society, 1986, vol. 213, pp. 425–433.
42 S. Galindo-Rodriguez, E. Allémann, H. Fessi and E. Doelker, *Pharm. Res.*, 2004, **21**, 1428–1439.
43 T. X. Viegas, M. D. Bentley, J. M. Harris, Z. Fang, K. Yoon, B. Dizman, R. Weimer, A. Mero, G. Pasut and F. M. Veronese, *Bioconjugate Chem.*, 2011, **22**, 976–986.
44 L. E. H. P. Goddard, J. Brown and L. J. Brookman, *J. Controlled Release*, 1989, **10**, 5–16.
45 P. Pietzonka, B. Rothen-Rutishauser, P. Langguth, H. Wunderli-Allenspach, E. Walter and H. P. Merkle, *Pharm. Res.*, 2002, **19**, 595–601.

Publication P3

How to tune the gene delivery and biocompatibility of poly(2-(4-aminobutyl)-2-oxazoline) by self and co assembly

M. N. Leiske, F. H. Sobotta, F. Richter, S. Hoeppener, J. C. Brendel, A. Traeger, U. S. Schubert, *Biomacromolecules* **2018**, *19*, 748 - 760.

The paper as well as the supporting information (free of charge) is available online: doi.org/10.1021/acs.biomac.7b01535.

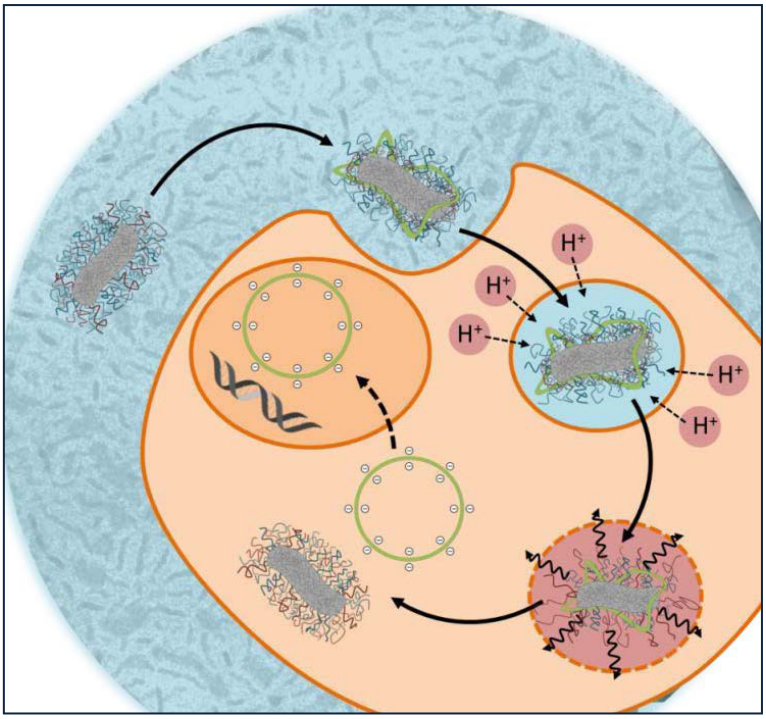

Article

Cite This: Biomacromolecules 2018, 19, 748−760

pubs.acs.org/Biomac

How To Tune the Gene Delivery and Biocompatibility of Poly(2-(4-aminobutyl)-2-oxazoline) by Self- and Coassembly

Meike N. Leiske,[†,‡] Fabian H. Sobotta,[†,‡] Friederike Richter,[†,‡] Stephanie Hoeppener,[†,‡] Johannes C. Brendel,[†,‡] Anja Traeger,*[,†,‡] and Ulrich S. Schubert*[,†,‡]

[†]Laboratory of Organic and Macromolecular Chemistry (IOMC) and [‡]Jena Center for Soft Matter (JCSM), Friedrich Schiller University Jena, Humboldtstrasse 10, 07743 Jena, Germany

Supporting Information

ABSTRACT: Despite their promising potential in gene transfection, the toxicity and limited efficiency of cationic polymers as nonviral vectors are major obstacles for their broader application. The large amount of cationic charges, for example, in poly(ethylene imine) (PEI) is known to be advantageous in terms of their transfection efficiency but goes hand-in-hand with a high toxicity. Consequently, an efficient shielding of the charges is required to minimize toxic effects. In this study, we use a simple mixed-micelle approach to optimize the required charge density for efficient DNA complex formation and to minimize toxicity by using a biocompatible polymer. In detail, we coassembled mixed poly(2-oxazoline) nanostructures ($d \approx 100$ nm) consisting of a hydrophobic-cationic block copolymer (P($NonOx_{52}$-*b*-$AmOx_{184}$)) and a hydrophobic−hydrophilic stealth block copolymer (P($EtOx_{155}$-*b*-$NonOx_{76}$) in ratios of 0, 20, 40, 60, 80, and 100 wt % P($NonOx_{52}$-*b*-$AmOx_{184}$). All micelles with cationic polymers exhibited a very good DNA binding efficiency and dissociation ability, while the bio- and hemocompatibility improved with increasing EtOx content. Analytics via confocal laser scanning microscopy and flow cytometry showed an enhanced cellular uptake, transfection ability, and biocompatibility of all prepared micelleplexes compared to AmOx homopolymers. Micelleplexes with 80 or 100 wt % revealed a similar transfection efficiency as PEI, while the cell viability was significantly higher (80 to 90% compared to 60% for PEI).

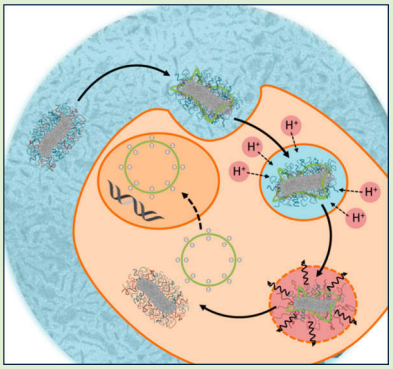

INTRODUCTION

Modern gene therapy uses two different types of gene carriers, namely viral and nonviral systems. Because of their high transfection efficiency and approval in clinical trials, virus-based systems are more common in recent gene therapy approaches.[1] Although viruses are predestinated for gene delivery, caused by their evolutionary optimization, there are some disadvantages, which hamper the use of viruses in gene therapy. One major drawback of viral vectors is the occurring immunogenicity, which may cause an activation of inflammatory cells leading to the degeneration of treated tissue. Moreover, toxin production and insertional mutagenesis were observed in some cases. Because of their size, viral vectors are limited by the transgenic capacity; furthermore, the upscaling of these systems is challenging.[2]

Thus, even if the efficiency of nonviral systems is lower compared to viral systems, there are significant advantages, which constitute nonviral systems as relevant alternatives in the area of gene delivery. In general, nonviral vectors show relatively low host immunogenicity; moreover, they allow an almost unlimited transgene size and provide the ability of repeated application.[3] Additionally, compared to viruses, nonviral systems benefit from low-cost production and their ability for an easy upscaling. Most commonly, cationic polymers are used for gene delivery since they are capable of forming polyplexes with the negatively charged phosphate backbone of nucleic acids. Because of the positive charges of the polymer, the polyplex can interact with the negatively charged cell membrane and is consequently internalized via endocytosis. Subsequently, the complexes need to undergo endosomal escape into the cytoplasm, resulting in the release of the polyplexes.[4] P. Stayton et al. demonstrated that pH-dependent amphiphilic nanocarriers are capable to trigger an enhanced endosomal release by interaction with the endosomal membrane.[5] Thus, changes in the pH value and protein interactions trigger the dissociation of the polyplex, and thus, the genetic material can enter the nucleus to transfect the cells. Poly(ethylene imine) (PEI) is one of the most commonly used materials for gene delivery applications and for a long time it was claimed to be the gold standard for the transfection of genetic material.[6] Its high charge density leads to the formation of physiological stable PEI−DNA polyplexes. In general, the high efficiency of PEI is based on the ability of the amine groups to buffer the pH value over a wide range, causing an efficient endosomal escape (proton sponge effect).[7] Disadvantages of PEI-based systems are their high *in vitro* and *in vivo* toxicity and their resistance against biodegradation, leading to the accumulation of the polymer in the cells or tissue, which

Received: October 26, 2017
Revised: December 11, 2017
Published: December 20, 2017

DOI: 10.1021/acs.biomac.7b01535
Biomacromolecules 2018, 19, 748−760

can elicit further toxicity effects.[8] Furthermore, the cytotoxicity has been shown to be dependent on the molar mass of the polymers[9] but can be improved by the introduction of stealth units, that is, EtOx, into the polymer chain.[10,11] These drawbacks lead to a necessity to search for alternative polymer systems for gene delivery applications, which reveal high transfection efficiencies while expressing a low cytotoxicity. K. Miyata et al. introduced primary and secondary amines into the side chains of poly(aspartamide) to induce pH-sensitive membrane destabilization at an endosomal pH value of 5, resulting in enhanced cytocompatibility at physiological pH values of 7.[12] Another possibility to fulfill this aim was shown to be the introduction of hydrophobic units, such as cholesterol[13] or stearic acid,[14] to the cationic polymer chains. The hydrophobic units could be shown to increase the cellular uptake as well as the transfection efficiency, however, not the cytotoxicity.

The aim of this study was the development of a micellar polymeric gene delivery system with low cytotoxicity combined with enhanced cellular uptake and transfection efficiency by adjusting the ratio of stealth and cationic units. Poly(2-oxazoline)s (P(Ox)s) are a class of polymers that were intensively studied during the past years in the context of several potential applications.[15−17] In the field of nanomedicine, the combination of enhanced biocompatibility and structure variability has been shown to be an essential benefit of this polymer class.[17−19] The synthesis of P(Ox)s by the living cationic ring-opening polymerization (CROP) provides even access to sophisticated polymer architectures such as block copolymers[20] and star-shaped,[21,22] hyperbranched,[23] and cross-linked networks.[24,25] The combination of monomer units bearing side-chains with different hydrophilicities leads to amphiphilic copolymers, which can self-assemble into different nanostructures.[25] Block copolymers of two or more chemically different polymer chains,[26] which potentially phase separate in bulk or selective solvents, provide access to several defined self-assembled structures. Furthermore, cationic P(Ox)s have already shown their potential in gene delivery applications.[27,28]

For these reasons, we synthesized two different amphiphilic block copolymers. The first copolymer consisted of NonOx for the formation of a hydrophobic core and the amino-functionalized AmOx to facilitate polyplex formation with the genetic material. The second copolymer consisted of the same hydrophobic unit; however, EtOx served as the hydrophilic block since it is known for its stealth properties.[29] Finally, mixed nanostructures with different weight ratios of these two block copolymers were prepared and characterized regarding the micelle size, PDI value, pH-responsiveness, CMC, toxicity, polyplex formation, and dissociation as well as their cellular uptake and transfection efficiency.

MATERIALS AND METHODS

Materials and Instrumentation. Triethylamine (TEA, Sigma-Aldrich), butyronitrile (VWR), 2-ethyl-2-oxazoline (EtOx, Sigma-Aldrich), 2-nonyl-2-oxazoline (NonOx, Henkel), and methyl tosylate (MeTos, Sigma-Aldrich) were distilled to dryness over calcium hydride (VWR) under argon atmosphere prior to usage. Ethyl acetate (EtOAc) and acetone, hydrochloric acid, *N*,*N*-dimethylformamide (DMF), and tetrahydrofuran (THF) were purchased from VWR Chemicals. Acetonitrile was obtained from a solvent purification system (MB-SPS-800 by MBraun) and stored under argon. All other solvents used were obtained from standard suppliers. Ethidium bromide solution (1%, 10 mg mL^{-1}) was purchased from Carl Roth (Karlsruhe, Germany). AlamarBlue YOYO-1 iodide and Hoechst 33342 trihydrochloride as well as all other indicated CLSM dyes were obtained from Life Technologies (Thermo Fisher Scientific, Germany). If not stated otherwise, cell culture media and solutions (L-glutamine, antibiotics) were obtained from Biochrom (Berlin, Germany). Plasmid eGFP (pEGFP-N1, 4.7 kb, Clontech, USA) enhanced green fluorescent protein (eGFP) was isolated with the Giga Plasmid Kit provided by Qiagen (Hilden, Germany). Plasmid pCMV-GFP was obtained from PlasmidFactory (Bielefeld, Germany).

The synthesis of 2-(4-((*tert*-butoxycarbonyl)amino)butyl)-2-oxazoline (BocOx) was described previously in our research group.[24]

Cryo transmission electron microscopy (cryoTEM) investigations were conducted with a FEI Tecnai G^2 20 at 200 kV acceleration voltage. Specimens were vitrified by a Vitrobot Mark V system on Quantifoil grids (R2/2). The blotting time was 1 s with an amount of solution of 8.5 μL. Samples were plunge frozen in liquid ethane and stored under liquid nitrogen until transfer to the Gatan cryo-holder and brought into the microscope. Images were acquired with an Olympus Mega View camera (Olympus Soft Imaging Solutions; 1376 × 1032 pixels) or an Eagle 4 × 4 k CCD camera system.

Proton NMR spectroscopy (^{1}H NMR) was performed at room temperature using a Bruker Avance I 300 MHz spectrometer, utilizing either $CDCl_3$, CD_3OD, or D_2O as solvent. The chemical shifts were given in ppm relative to the signal from the residual nondeuterated solvent.

Size exclusion chromatography (SEC) of the copolymers was performed on an Agilent 1200 series system, equipped with a PSS degasser, G1329A pump, a PSS GRAM guard/30/1000 Å with 10 μm particle size, and a G1362 refractive index (RI) detector. DMAc containing 0.21% LiCl served as eluent. The column oven was set to 40 °C at a flow rate of 1 mL min^{-1} and polystyrene (PS, 400−1 000 000 g mol^{-1}) served as the calibration.

SEC of the Boc-protected P($EtOx_3$-*b*-$BocOx_{157}$) was performed on a Shimadzu system equipped with a CBM-20A controller, GDU-14A degasser and a LC-10AD VP pump, a PSS SDV guard/linear S column with 5 μm particle size, and a RID-10A RI detector. $CHCl_3$-*iso*-propanol (*i*-PrOH)-NEt_3 (94:2:4) served as eluent. The column oven was set to 40 °C using a flow rate of 1 mL min^{-1}. PS (400−100 000 g mol^{-1}) served as the calibration.

SEC of the P($EtOx_3$-*b*-$AmOx_{157}$) was conducted using a Jasco system equipped with a DG-980−50 degasser and a PU-980 pump, PSS SUPREMA-MAX guard/300 Å column with 10 μm particle size, and a RI-930 RI detector. 0.3% (v/v) TFA containing 0.1 M NaCl served as aqueous eluent. The column oven was set to 30 °C utlizining a flow rate of 1 mL min^{-1}. Poly(2-vinylpyridine) (P2VP, 1 300−81 000 g mol^{-1}) served as the calibration.

Lyophilization of the nanostructure suspensions was conducted using an Alpha 1−2 LDplus freeze-dryer from Martin Christ Gefriertrocknungsanlagen GmbH (Germany). Absorbance and fluorescence measurements of the bioassays were performed at RT using a TECAN Infinite M200 PRO.

Confocal laser scanning microscopy (CLSM) was performed with an LSM880 ELYRA PS.1 system (Zeiss, Oberkochen, Germany) applying a 63 × 1.4 NA plan apochromat oil objective.

Batch dynamic light scattering (DLS) was performed on a Zetasizer Nano ZS (Malvern Instruments, Herrenberg, Germany). All measurements were performed in standard polypropylene semi micro cuvettes, Malvern Instruments, Herrenberg, Germany). After an equilibration time of 180 s, 3 × 300 s runs were carried out at 25 °C (λ = 633 nm). Scattered light was detected at an angle of 173°. Each measurement was performed in triplicates (three measurements consisting of three runs each per sample). Apparent hydrodynamic radii, R_h, were calculated according to the Stokes−Einstein eq 1:

$$R_h = \frac{kT}{6\pi\eta D} \quad (1)$$

Synthesis of P(Ox)s. All polymerization solutions were prepared within a glovebox under nitrogen atmosphere.

Polymerization reactions of 2-oxazolines were performed under microwave irradiation using an Initiator Sixty single-mode microwave

DOI: 10.1021/acs.biomac.7b01535
Biomacromolecules 2018, 19, 748−760

synthesizer from Biotage, equipped with a noninvasive IR sensor (accuracy: 2%). Microwave vials were heated overnight at 100 °C under vacuum and allowed to cool to room temperature under argon before usage. Polymerizations were performed under temperature control. According to the polymer characteristics, SEC of the polymers was performed on different systems and noted in the respective part. The synthesis of P(Ox)s was described previously.[30]

P(EtOx$_3$-*b*-BocOx$_{157}$). In a microwave vial, MeTos (1.9 mg, 0.01 mmol), EtOx (3.0 mg, 0.03 mmol), and acetonitrile (392.6 mg) were mixed under inert conditions and heated in the microwave to 140 °C for 63.5 min. Subsequently the vial was opened under an inert atmosphere, and BocOx (477.4 mg, 1.97 mmol) was added. The reaction mixture was heated in the microwave at 140 °C for additional 18.0 min. The resulting polymer diluted with chloroform and precipitated in ice-cold diethyl ether. The precipitate was filtered off and redissolved in chloroform. The solvent was evaporated under reduced pressure to obtain the product as a white solid (391 mg, 82%).

Deprotection of P(EtOx$_3$-*b*-BocOx$_{157}$) Yielding P(EtOx$_3$-*b*-AmOx$_{157}$). P(EtOx$_3$-*b*-BocOx$_{157}$) (390 mg, 10.2 mmol) was dissolved in 10 mL of MeOH, and 2 mL of concentrated hydrochloric acid was added. The reaction mixture was stirred at room temperature for 24 h. Subsequently, the solvent was evaporated under reduced pressure, and the crude product was redissolved in 10 mL of MeOH and precipitated in ice cold diethyl ether. Then the precipitate was filtered off and redissolved in 100 mL of MeOH. Amberlyst A21 was added and the mixture was stirred slowly (100 rpm) overnight at room temperature. Then the Amberlyst A21 was filtered off and the organic solvent was evaporated under reduced pressure. The polymer was redissolved in 10 mL of deionized water and lyophilized to obtain the product as a white powder (186 mg, 81%).

P(EtOx$_{155}$-*b*-NonOx$_{76}$). In a microwave vial, MeTos (24.8 mg, 0.13 mmol), EtOx (1.98 g, 20.0 mmol), and butyronitrile (13.0 g) were mixed under inert conditions and heated in the microwave to 140 °C for 130 min. Subsequently, the vial was opened under an inert atmosphere, a sample of 100 μL was taken, and NonOx (1.58 g, 8.0 mmol) was added. The reaction mixture was heated in the microwave at 140 °C for another 120 min. The resulting polymer was precipitated in ice-cold diethyl ether and centrifuged at 11 000 rpm for 5 min. The supernatant was discarded, and the solid was redissolved in CH_2Cl_2. The solvent was evaporated under reduced pressure to obtain the product as a white solid (1.7 g, 86%).

P(NonOx$_{52}$-*b*-BocOx$_{184}$). In a microwave vial, MeTos (7.8 mg, 0.04 mmol), NonOx (493 mg, 2.5 mmol), and butyronitrile (6.1 g) were mixed under inert conditions and heated in the microwave to 140 °C for 120 min. Subsequently, the vial was opened under an inert atmosphere, a sample of 100 μL was taken, and BocOx (1.75 g, 7.2 mmol) was added. The reaction mixture was heated in the microwave at 140 °C for another 90 min. The resulting polymer was precipitated in ice-cold diethyl ether, and the solid was resuspended in deionized water and centrifuged at 11 000 rpm for 5 min. The supernatant was discarded, and the solid was suspended in deionized water. The solvent was lyophilized under reduced pressure to obtain the product as a white powder (740 mg, 33%).

Deprotection of P(NonOx$_{52}$-*b*-BocOx$_{184}$) Yielding P-(NonOx$_{52}$-*b*-AmOx$_{184}$). P(NonOx$_{52}$-*b*-BocOx$_{184}$) (700 mg, 12.8 mmol) was dissolved in 5 mL of TFA and stirred at room temperature overnight. Subsequently, 5 mL of MeOH was added, and the polymer was precipitated in ice-cold diethyl ether. The precipitate was redissolved in MeOH, Amberlyst A21 was added, and the solution was stirred slowly at room temperature for 72 h. Afterward, Amberlyst A21 was filtered off, and the solvent was evaporated under reduced pressure. The polymer was resuspended in deionized water, and the solvent was lyophilized under reduced pressure to obtain the product as a white powder (457 mg, 98%).

Self-Assembly. Fifty milligrams of polymer was dissolved in 10 mL of DMAc by vortexing and ultrasonification. Subsequently, 10 mL of ultrapure water was added slowly using a syringe pump (5 mL h^{-1}) under continuous stirring (1000 rpm). After that, the resulting solution was transferred to a dialysis tube (cellulose, MWCO 3.5 kDa) and dialyzed against distilled water for 4 days by daily water exchange. Subsequently, it was diluted using a 1.8 wt % aqueous NaCl solution to adjust the salt concentration to 0.9 wt % (pH = 6). The resulting nanostructures were filtered using a 0.2 μm syringe filter and characterized by DLS measurements.

The concentration of the polymer in the resulting solution was determined gravimetrically (n = 3) after lyophilization of the samples. For this reason, also a 0.9 wt % aq. NaCl solution was lyophilized (n = 3). The mean of the mass of the NaCl samples was subtracted from each polymer containing sample to obtain the absolute polymer mass.

The average molar mass of the micelles was calculated by using eq 2:

$$M = \frac{M_n \times Wt\ \%(\mathrm{P(NonOx_{52}\text{-}b\text{-}AmOx_{184})}) + M_n \times Wt\ \%(\mathrm{P(EtOx_{155}\text{-}b\text{-}NonOx_{76})}}{100} \quad (2)$$

pH Responsive Behavior. The pH-responsiveness of the nanostructures was determined by mixing 1 mL of a 1.0 mg mL^{-1} solution with 1 mL of the following buffers (Table S1).

The solutions were incubated at room temperature overnight at 200 rpm (BioShake iQ, Qantifoil Intruments GmbH, Jena, Germany). Afterward the pH value was checked and the Z-average and PDI were determined by DLS measurements.

Determination of Critical Micelle Concentration (CMC). The determination of the CMC via pyrene method was described previously.[31] Fluorescence was recorded with a Jasco FP 6500. A serial dilution of the nanostructure suspension in 0.9 wt % aq. NaCl was prepared.

A saturated pyrene solution in 0.9 wt % aq. NaCl was prepared as follows. Pyrene was dissolved in acetone (1 mg mL^{-1}) and added dropwise to a solution of 0.9 wt % in ultrapure water until a slight precipitation (visible turbidity) occurred. The solution was stirred for 48 h at room temperature (1000 rpm) to evaporate the acetone. Then the solution was filtered using a pleated filtered to remove any precipitate. Subsequently, the same volume of the saturated solution of pyrene in 0.9 wt % aq. NaCl was added to each dilution of the micelles to obtain a total volume of 2 mL. The mixtures were incubated overnight at room temperature at 200 rpm (BioShake iQ, Qantifoil Intruments GmbH, Jena, Germany). Excitation spectra were collected at λ_{Em} = 390 nm and λ_{Ex} = 300−380 nm. The pyrene stock solution served as the calibration sample and was subtracted from all spectra prior to calculations to remove any fluorescence artifacts. For calculation of the CMC, the resulting spectra were used. The fluorescence intensity at λ_{Em} = 390.0 nm while exciting at λ_{Ex2} = 338.0 nm was divided by the fluorescence intensity at λ_{Em} = 390.0 nm while exciting at λ_{Ex2} = 332.5 nm and plotted against the log of the polymer concentration. A nonlinear Boltzmann fitting and a subsequent linear fitting were conducted using OriginPro 2015G. Hereby, the Boltzmann fitting was used to visualize visible areas, while the linear fit was utilized to obtain the cross-point of two different linear areas, which corresponds to the CMC of the nanostructures.

Cell Culture. HEK-293 cells (CRL-1573) were cultured in DMEM medium with L-glutamine (Biochrom, Berlin, Germany) supplemented with 1 g L^{-1} glucose, 10% fetal calf serum (FCS, v/v), 100 μg mL^{-1} streptomycin and 100 IU mL^{-1} penicillin at 37 °C in a humidified 5% CO_2 atmosphere.

Cytotoxicity. The cytotoxicity was tested with L929 cells, as this cell line is recommended by ISO10993−5. In detail, cells were seeded at 10^4 cells per well in a 96-well plate and incubated for 24 h. No cells were seeded in the outer wells. After exchanging the media with fresh one and 30 min incubation, polymers at the indicated end concentrations were added, and the cells were incubated at 37 °C

DOI: 10.1021/acs.biomac.7b01535
Biomacromolecules 2018, 19, 748−760

Scheme 1. Schematic Representation of Block Copolymerization of 2-Oxazolines via CROP[a]

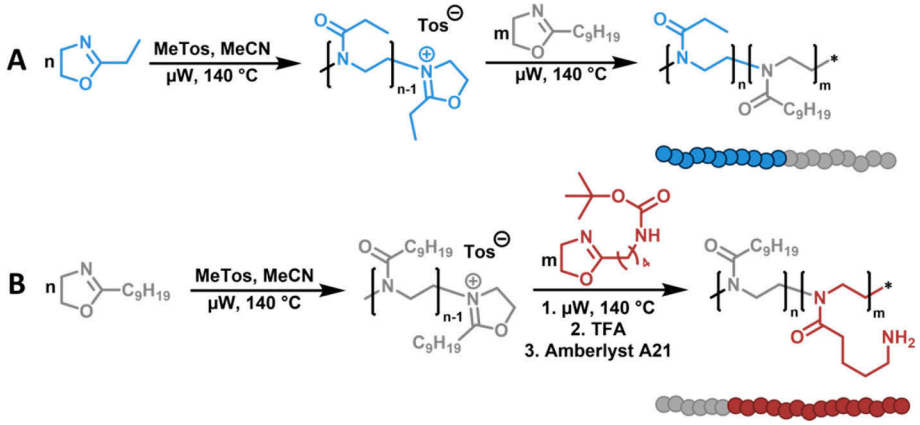

[a](A) P(EtOx$_{155}$-*b*-NonOx$_{72}$) was synthesized using the sequential monomer addition of EtOx and NonOx. (B) P(NonOx$_{52}$-*b*-AmOx$_{184}$) was synthesized via the sequential monomer addition of NonOx and BocOx. The resulting block copolymers were deprotected using TFA and neutralized with Amberlyst A21. Blue: EtOx. Grey: NonOx. Red: BocOx/AmOx.

for additional 24 h. Subsequently, the medium was replaced by fresh media and AlamarBlue (Life Technologies, Darmstadt, Germany) as recommended by the supplier. After incubation for 4 h, the fluorescence was measured at λ_{Ex} = 570 nm, λ_{Em} = 610 nm, with untreated cells on the same well plate serving as controls. The experiments were performed independently three times on three different well-plates.

Hemolysis Assay and Erythrocyte Aggregation. All animal husbandry is performed in compliance with the relevant European and German laws, institutional guidelines, and to state the institutional animal committee. The sheep blood was taken for general veterinary management of the animal health.

To assess the hemolytic activity of the polymer solutions, blood from sheep, collected in heparinized-tubes (Institut für Versuchstierkunde and Tierschutz/Laboratory of Animal Science and Animal Welfare, Friedrich Schiller University Jena), was centrifuged at 4500 × *g* for 5 min, and the pellet was washed three times with cold 1.5 mmol L^{-1} phosphate buffered saline (PBS, pH = 7.4). After dilution with PBS in a ratio of 1:7, aliquots of erythrocyte suspension were mixed 1:1 with the polymer solution and incubated in a water bath at 37 °C for 60 min. After centrifugation at 2400 × *g* for 5 min, the hemoglobin release into the supernatant was determined spectrophotometrically using a microplate reader at λ_{Ex} = 544 nm wavelength. Complete hemolysis (100%) was achieved using 1% Triton X-100 serving as positive control. Thereby, PBS served as negative control (0%). A value less than 2% hemolysis rate was taken as nonhemolytic. Experiments were run in triplicates and were performed with three different blood donors. The hemolytic activity of the polycations was calculated by eq 3:

$$\%\ \text{Hemolysis} = 100 \times \frac{(A_{\text{sample}} - A_{\text{negative control}})}{A_{\text{positive control}}} \quad (3)$$

For the examination of the erythrocyte aggregation, erythrocytes were isolated as described above. An erythrocytes suspension was mixed with the same volume of polymeric micelle solution in a clear flat bottomed 96-well plate. The cells were incubated at 37 °C for 2 h, and the absorbance was measured at λ_{Ex} = 645 nm in a microplate reader. *b*-PEI (25 kDa, 50 μg mL^{-1}) was used as positive control and PBS-treated cells served as the negative control. Absorbance values of the test solutions lower than the negative control were regarded as aggregation. Experiments are the result of triplicates and were performed with three different donor blood batches.

Polyplex Formation. Polyplexes of pDNA and polymeric micelles were prepared by mixing stock solutions of 1.5 μL pDNA (1 mg mL^{-1}) and different amounts of polymeric micelle solutions (1 mg mL^{-1}) to obtain various N*/P ratios (amines of polymer to phosphate of pDNA) 150 mM aq. NaCl solution. 150 mM aq. NaCl was used to equalize the volumina of the different solutions. The solutions were vortexed for 10 s at maximal speed (2700 min^{-1}) and incubated at room temperature for 20 min to ensure complex formation.

Ethidium Bromide Quenching Assay (EBA). Briefly, a master mix containing 69 μg mL^{-1} pDNA and 4.6 μg mL^{-1} ethidium bromide was prepared in 150 mM NaCl and incubated in the dark for 10 min at room temperature. Subsequently, polyplexes were prepared in black 96-well plates (Nunc Thermo Fisher) by adding different amounts of polymeric micelles (various N*/P ratios) to 20 μL of master mix per well. The differences in the final volume of polymer were equalized by filling up with 150 mM NaCl to 230 μL per well (for exact amounts, see also Table S2; for final polymer concentrations, see Table S3).

The samples were incubated in the dark at room temperature for 5 min. The fluorescence of the samples was measured at λ_{Ex} = 525 nm and λ_{Em} = 605 nm using a microplate reader. A sample containing the same amount of pDNA and ethidium bromide diluted using 150 mM NaCl was used as a reference for 100% fluorescence to calculate the percentage of dye displaced upon polyplex formation (eq 4):

$$\text{RFU}\ [\%] = \frac{F_{\text{sample}}}{F_{\text{pDNA}}} \times 100 \quad (4)$$

Here, RFU is the relative fluorescence, and F_{sample} and F_{pDNA} are the fluorescence intensities of a given sample and the ethidium bromide intercalated into pDNA alone.

Heparin Dissociation Assay. To investigate the release of pDNA from polyplexes, the heparin dissociation assay was performed. Polyplexes with an N*/P ratio of 50 were prepared as described above in a total volume of 115 μL of 150 mM NaCl containing ethidium bromide (0.4 μg mL^{-1}) (for exact amounts, see also Table S2). After incubation in the dark at room temperature for 10 min, the master mix was transferred into 1.5 mL reaction tubes (one per polymer) and polymers were added. Subsequently, the polyplexes were transferred into a black 96-well plate, and heparin of indicated concentrations was added. The solution was mixed and incubated for further 15 min at 37 °C in the dark.

Flow Cytometry. For transfection and uptake studies, HEK-293 cells were used. In detail, 5 × 10^4 cells were seeded in each well of a 24-well plate and cultured for 24 h. One hour prior to the addition of the polyplexes, the medium was changed to 0.5 mL of fresh culture media. For kinetic studies, pDNA was labeled with YOYO-1 iodide (YOYO-1) prior to the polyplex preparation. For labeling of 1 μg of pDNA, 0.026 μL of 1 M YOYO-1 solution was mixed with pDNA and incubated for 20 min at 4 °C protected from light. The polyplexes were prepared as described above, and at least 50 μL was added to the cells (dependent on the N*/P ratio of the polymers, for the exact

DOI: 10.1021/acs.biomac.7b01535
Biomacromolecules 2018, 19, 748−760

Table 1. Key Properties of Synthesized Polymers

ID	SEC[a]			^{1}H NMR[b]					
	M_n [kDa]	M_w [kDa]	$Đ$	DP hydrophilic block	DP NonOx block	mol % hydrophilic block	mol % NonOx block	wt % hydrophilic block	wt % NonOx block
P(EtOx)$_{155}$	22.6	25.0	1.11	155	n.a.[f]	100	n.a.	100	n.a.
	7.6[d]	9.4[d]	1.24[d]						
P(EtOx$_{155}$-*b*-NonOx$_{76}$)	38.3	43.6	1.14	155	76	67	33	45	55
	17.2[d]	18.4[d]	1.07[d]						
P(NonOx)$_{52}$	12.4	13.0	1.04	n.a.	52	n.a.	100	n.a.	100
	9.0[d]	9.7[d]	1.08[d]						
P(NonOx$_{52}$-*b*-BocOx$_{184}$)	32.2	38.3	1.19	184	52	78	22	81	19
	22.1[d]	22.9[d]	1.29[d]						
P(NonOx$_{52}$-*b*-AmOx$_{184}$)	24.3	30.5	1.26	184[c]	52[c]	78[c]	22[c]	72[c]	28[c]
P(EtOx$_3$-*b*-BocOx$_{157}$)	15.3[d]	16.8[d]	1.10[d]	160	0	100	0	100	0
P(EtOx$_3$-*b*-AmOx$_{157}$)	13.5[e]	21.0[e]	1.56[e]	160[c]	0[c]	100[c]	0[c]	100[c]	0[c]

[a]SEC (eluent: DMAc, 0.21% LiCl; PS-standard). [b]^{1}H NMR (300 MHz). [c]Calculated from Boc-protected precursor polymer. [d]SEC (eluent: $CHCl_3$-*i*-PrOH-NEt_3 94:2:4; PS-standard). [e]SEC (eluent: 0.1 M $NaCl_{(aq)}$ + 0.3% TFA; P2VP-standard). [f]n.a., not available.

amounts see also Table S4). The amount of pDNA added to the cells was kept constant (0.75 μg pDNA). The plates were incubated for the indicated time point at 37 °C, 5% CO_2. Afterward, the cells were harvested by trypsinization and were resuspended in PBS supplemented with 1% FCS. To determine the transfection efficiency or polyplex uptake of the polyplexes, 10 000 cells were measured by flow cytometry using a Cytomics FC 500 (Beckman Coulter). The amount of viable cells showing YOYO-1 or eGFP signals were gated and the mean fluorescence intensity (MFI) of all viable cells were compared. To quench the outer fluorescence of YOYO-1 labeled polyplexes, 10% trypan blue was added prior to the measurement. Dead cells were identified via shift in the side and forward scatter of cells.[32] The experiments were performed at least three times.

Confocal Microscopy. For CLSM studies, 5 × 10^4 cells were seeded on glass-bottomed dishes (CellView cell culture dishes with four compartments, Greiner bio-one) and cultivated for 24 h. One hour prior to the polymer addition, the medium was changed to 0.5 mL of fresh growth media. The polyplexes were formed using YOYO-labeled pDNA as described above, added to the cells, and incubated for additional 4 h. Subsequently, medium was replaced by fresh culture medium supplemented with Hoechst 33342 for nucleus staining, LysoTracker Red DND-99 (all from Thermo Fisher Scientific) for lysosome staining respecting the instructions given by the Supplier. Prior to imaging, 10% trypan blue was added to quench the outer fluorescence of YOYO-1 labeled pDNA.

Live-cell imaging was performed on an LSM880, Elyra PS.1 system (Zeiss, Oberkochen, Germany). Three color channels were recorded: blue (nucleus, Hoechst 33342, λ_{Ex} = 405 nm,), green (pDNA, YOYO-1 Iodide, λ_{Ex} = 488 nm), and red (lysosome, LysoTracker Red DND-99, λ_{Ex} = 561 nm). To avoid possible cellular motions in the time frame of the experiment, a quick measurement was warranted by the simultaneous acquisition of all three color channels.

RESULTS AND DISCUSSION

Polymer Synthesis. The aim of this study was to obtain mixed polymeric micelles, with a cationic and a stealth polymer within the shell for efficient cellular uptake, transfection, and reduced cyto- and hemotoxicity. For this purpose, two different block copolymers were synthesized via the sequential monomer addition method (Scheme 1). By using this preparation method, the order of the block sequence is of significance importance for the dispersity of the resulting block copolymers. Utilizing the less reactive monomer first might lead to slower initiation speeds during the polymerization of the second block, and, consequently a loss of the living/controlled character of the polymerization. For this reason, the nonionic copolymer was polymerized with EtOx representing the first and NonOx as the second block (Scheme 1A). For a successful preparation of the cationic block copolymer, on the other hand, it was necessary to use NonOx as the first block since the polymerization of Boc-protected primary amine functionalized 2-oxazolines with common initiators leads to side-reactions during polymerization.[33]

NonOx served as the hydrophobic block in both copolymers, while the hydrophilic block either contained AmOx, to obtain good DNA binding capabilities, or EtOx to enhance the biocompatibility of the micelles due to its stealth properties. The polymers were analyzed using ^{1}H NMR and SEC measurements (Table 1, Figures S1−S5). In both polymers, the degree of polymerization (DP) of the NonOx block was kept similar, resulting in different weight ratios of the hydrophobic and the hydrophilic blocks, namely 55% to 45% in case of P(EtOx$_{155}$-*b*-NonOx$_{76}$) and 28% to 72% in case of P(NonOx$_{52}$-*b*-AmOx$_{184}$), respectively. The DP of the AmOx block was adjusted higher than the EtOx block to facilitate the endosomal release of the micelle−DNA complexes (micelleplexes) and, consequently, of the genetic material by stretching of the cationic blocks within the endolysosome (fusion of and endosome and a lysosome) caused by a decrease of the pH value from 7.4 to 5. Prelimary polymerizations in acetonitrile (data not shown) lead to the precipitation of NonOx containing polymers. For this reason, butyronitrile was chosen as a suitable solvent for block copolymerization, even though the obtained dispersity of polymers is in general increased compared to polymers synthesized in acetonitrile. Nevertheless, both block copolymers also showed a comparable total DP as well as a narrow dispersity ($Đ$ < 1.2) regarding SEC measurements in DMAc (Figure S4). In addition to that, an entirely hydrophilic polymer, mainly consisting of AmOx (P(EtOx$_3$-*b*-AmOx$_{157}$)), was synthesized using an oligo(EtOx) initiator and characterized for comparison. Since the controllability of the polymer dispersity was determined to be enhanced by using acetonitrile as the solvent for polymerization compared to butyronitrile, this polymer was prepared in acetonitrile. Because of its high AmOx content, it is entitled as AmOx homopolymer in the following discussion.

DOI: 10.1021/acs.biomac.7b01535
Biomacromolecules 2018, 19, 748−760

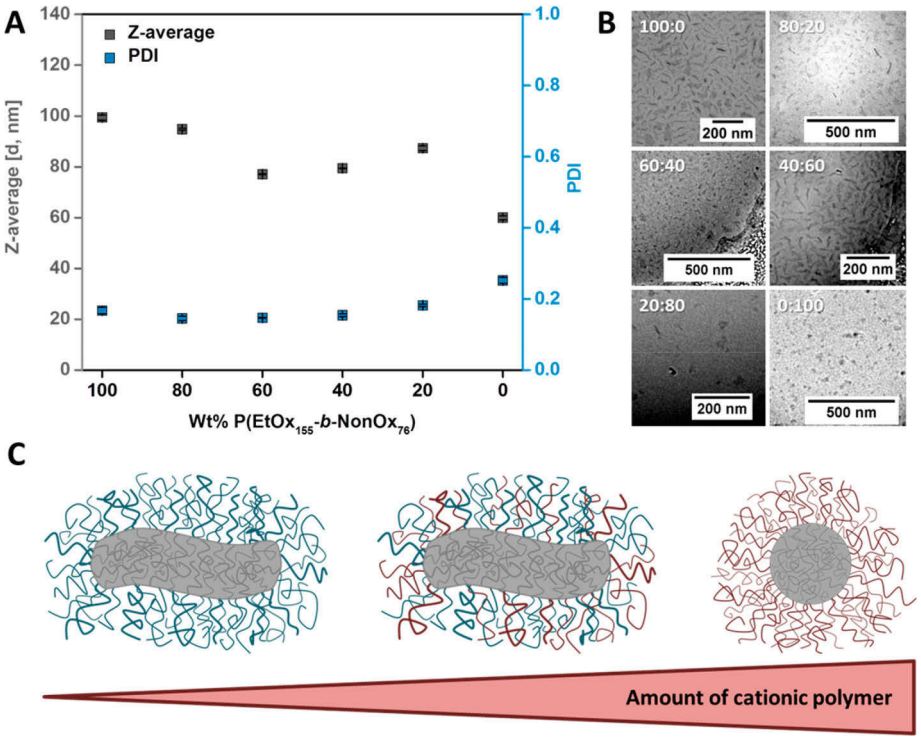

Figure 1. (A) *Z*-average and PDI values of the prepared nanostructures in 0.9 wt % aq. NaCl determined by DLS. (B) Zoom-in cryoTEM images of the prepared nanostructures in 0.9 wt % aq. NaCl. Ratios describe the mass ratios of P($EtOx_{155}$-*b*-$NonOx_{76}$) to P($NonOx_{52}$-*b*-$AmOx_{184}$) being used during nanostructure preparation. Full pictures can be found in the Supporting Information. (C) Schematic representation of the obtained shapes of the nanostructures dependent on the used block copolymers in different ratios. Blue represents EtOx, gray represents NonOx, and red represents the cationic AmOx block.

Self-Assembly. For self-assembly, the polymers were mixed in different weight ratios and dissolved in DMAc serving as the nonselective solvent. Subsequently, an equal amount of ultrapure water serving as the selective solvent was added very slowly (1 mL h^{-1}) to induce micelle formation. Subsequently, the solution was dialyzed against deionized water to allow a slow increase of the total water content while the organic solvent diffuses out. The stability of the nanostructures in physiological medial, for example, NaCl solution, represents an important criterion for further *in vivo* applications. For this reason, the nanostructures were mixed with aq. NaCl to obtain a total NaCl amount of 0.9 wt % in solution. All micelles were characterized regarding their size and PDI value by DLS measurements (Figure 1A and S6, Tables S5 and S6). All nanostructures containing P($EtOx_{155}$-*b*-$NonOx_{76}$) formed nanostructures with an average diameter of about 80 to 100 nm, while the self-assembly of P($NonOx_{52}$-*b*-$AmOx_{184}$) resulted in significantly smaller structures with a diameter of 60 nm. Furthermore, all micelles with P($EtOx_{155}$-*b*-$NonOx_{76}$) exhibited a PDI below 0.2 while micelles, which consist only of P($NonOx_{52}$-*b*-$AmOx_{184}$), showed a PDI of 0.25.

The size differences of the self-assembled micelles of either P($EtOx_{155}$-*b*-$NonOx_{76}$) or P($NonOx_{52}$-*b*-$AmOx_{184}$) are distinct and all measured DLS curves were monomodal in terms of intensity, volume, and number PSD (Figures 1A and S6, Table S2).

After size determination via DLS, cryoTEM measurements were used to obtain further information about the shape and uniformity of the nanostructures (Figure 1B, Figure S8). Micelles consisting of only of P($EtOx_{155}$-*b*-$NonOx_{76}$) formed rod-like structures, while those prepared from pure P($NonOx_{52}$-*b*-$AmOx_{184}$) were predominantly spherical. Next to the rod-like structures formed exclusively by P($EtOx_{155}$-*b*-$NonOx_{76}$) also sheet-like structures were observable. Darker rods are presumably sheets with a parallel orientation with respect to the electron beam. More interestingly, by mixing the two polymers P($EtOx_{155}$-*b*-$NonOx_{76}$) and P($NonOx_{52}$-*b*-$AmOx_{184}$) using ratios of 20, 40, 60, or even 80% of P($NonOx_{52}$-*b*-$AmOx_{184}$), the micelles were still rod-like with respect to the cryoTEM measurements. Furthermore, in cryoTEM, all samples feature the same mixture of similar structures that indicates the formation of mixed micelles rather than the formation of two species consisting of the two polymer components. Moreover, already the 100:0 sample featured the coexistance of rod-like structures and sheet-like aggregates. Recently, S. Jaksch et al. reported on the formation of worm-like micelles using triblock (ABA) copolymers with NonOx as the hydrophobic block (B) and MeOx as the hydrophilic blocks (A).[34] Hereby, it was also possible to observe changes in the nanostructure by the encapsulation of hydrophobic drugs such as paclitaxel.

After characterization of the micelles via DLS and cryoTEM, the critical micelle concentration (CMC) in physiological sodium chloride solution was determined by the pyrene method. After incubation overnight, excitation measurements at λ_{Em} = 390.0 nm were conducted. The peak intensities at λ_{Ex1} = 332.5 nm and λ_{Ex2} = 338.0 nm were compared to calculate the CMC (Table 2, Figure S9). The nanostructures consisting of 100, 80, and 60 wt % P($EtOx_{155}$-*b*-$NonOx_{76}$)) exhibited a CMC of around 2 × 10^{-7} M, those with 40, 20, and 0 wt % P($EtOx_{155}$-*b*-$NonOx_{76}$)) showed a CMC of about 1 × 10^{-6} M. These values are expected since nanostructures from P($MeOx_n$-

DOI: 10.1021/acs.biomac.7b01535
Biomacromolecules 2018, 19, 748−760

Table 2. CMC of Nanostructures in 0.9 wt % aq. NaCl by the Pyrene Method[a]

wt % P($EtOx_{155}$-*b*-$NonOx_{76}$)	wt % P($NonOx_{52}$-*b*-$AmOx_{184}$)	M^b [kg mol^{-1}]	CMC [μg mL^{-1}]	CMC [mol L^{-1}]
100	0	30.3	8.3	2.7×10^{-7}
80	20	31.5	7.3	2.3×10^{-7}
60	40	32.7	6.8	2.2×10^{-7}
40	60	34.0	36.6	1.1×10^{-6}
20	80	35.2	45.2	1.3×10^{-6}
0	100	36.4	35.5	9.8×10^{-7}

[a]For calculation of the CMC, the fluorescence intensity at λ_{Em} = 390.0 nm while exciting at λ_{Ex2} = 338.0 nm was divided by the fluorescence intensity at λ_{Em} = 390.0 nm while exciting at λ_{Ex2} = 332.5 nm and is plotted against the log of the polymer concentration. [b]Molar mass was calculated by using eq 2 (see Figure S8 for original plots).

b-$NonOx_m$) are reported to have a CMC between 10^{-6} and 10^{-5} M.[35−37]

pH Responsiveness. The transport of the genetic material is presumably realized by endosomal pathways. Hereby, the decrease in the pH values inside the endolysosomes leads to an endosomal burst and the subsequent release of the polyplex. Cationic charges are known to force this membrane disruption.[38] This side effect should be reduced outside the cell but be active inside the endolysosomes. Consequently, a pH-dependent shielding of the cationic charges is a favorable polymer design strategy.[39] By the preparation of mixed micelles, we aim to obtain a system that is composed of the pH dependent AmOx shell that expands upon reduction of the surrounding pH value, mixed with EtOx units, which should provide stealth properties and do not show pH-responsiveness (Figure 2A).

To prove our assumption, we diluted the nanostructures in aqueous buffers of different pH values (pH = 4.10, 5.04, 6.17, 7.04, 7.58, 8.00, Table S1) and determined the changes in *Z*-average and PDI value by DLS measurements (Figure S9). Control measurements, diluting the nanostructures with an equal volume of 0.9 wt % NaCl did not reveal any significant changes regarding size or PDI (Table S7). Furthermore, the PDI values of the nanostructures at different pH values remained constant, verifying the stability of the nanostructures. Furthermore, with regard cryoTEM measurements, no morphological changes could be observed by increasing the pH value to 8 (Figure S11). Figure 2B and C show a dependence of the pH responsiveness on the amount of P($NonOx_{52}$-*b*-$AmOx_{184}$). While nanostructures with 100 wt % P($EtOx_{155}$-*b*-$NonOx_{76}$) maintained a similar size at any tested pH value, nanostructures of 100 wt % P($NonOx_{52}$-*b*-$AmOx_{184}$) increased in size up to 130% when changing the pH value from 7 to 5. This increased size at acidic conditions is related to an increased charge density on the AmOx block, which causes the stretching of the polymer chains in the shell. The increased charge density might help to force an enhanced endosomal

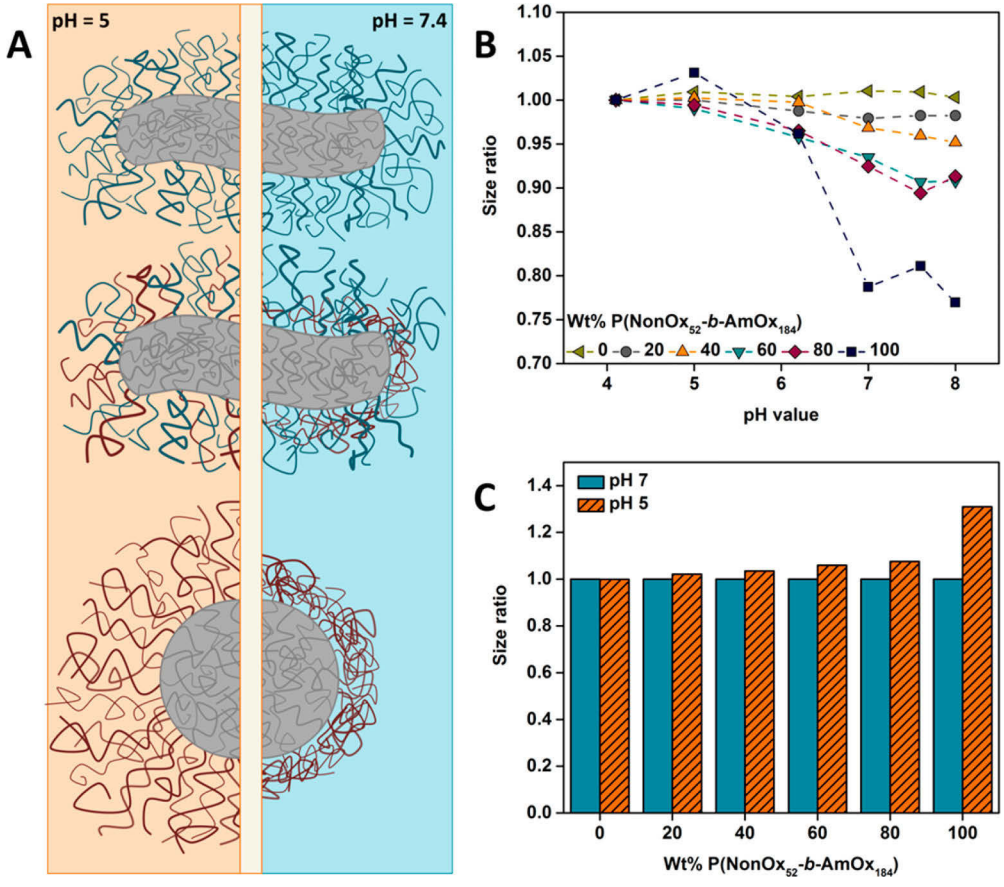

Figure 2. (A) Schematic representation of the changes in size of the mixed micelles induced by changes in the pH value. Gray represents NonOx, blue represents EtOx, and red represents the cationic AmOx block. (B) Size ratios of the nanostructure dependency on the pH value (calculated by division of the *Z*-average at distinct pH values by the *Z*-average at a pH value of 4). (C) Size ratios of the nanostructures at pH values of 5 and 7 (calculated by division of the *Z*-average at distinct pH values by the *Z*-average at a pH value of 7). For values, see Figure S10.

DOI: 10.1021/acs.biomac.7b01535
Biomacromolecules 2018, 19, 748−760

release, one major bottleneck during the transfection process. By reducing the content of the AmOx polymer, the change in size with decreasing pH value becomes less pronounced, which correlates well with the assumption of mixed micelles, as only the responsive AmOx in the shell will react on the change in pH value and become more stretched at low pH values, but not the EtOx polymer. For this reason, the measurability of the changes in size of the mixed nanostructures might be difficult since the hydrodynamic radius is influenced by both blocks in the shell, EtOx or AmOx. This might explain the rather low changes of nanostructures containing 60 or 80% AmOx. Additionally, all intensity weighted size distributions revealed a monomodal distribution, further proving the assumption of mixed micelles instead of two species.

Cytotoxicity, Hemolysis, and Erythrocyte Aggregation. Enhanced cyto- and hemocompatibility of polymeric gene carriers represents an important criterion for *in vivo* investigations. Unfortunately, PEI, the gold standard in terms of transfection abilities, is very cytotoxic and leads to high hemoglobin release and erythrocyte aggregation,[40,41] which might cause severe side-effects.

For this reason, subsequently to the characterization of the physical properties of the prepared micelles, they were also investigated regarding their cytotoxicity, hemolysis, and erythrocyte aggregation (Figure 3). The cytotoxicity measurements (AlamarBlue assay) demonstrated that the micelles are not toxic up to a concentration of 50 μg mL^{-1} (rel. cell viability ≥80%). As expected, an increase of the cytotoxicity with the AmOx content in the micelle shell was observed (Figure 3A), that is, all micelles with EtOx in the shell, are nontoxic at 100 μg mL^{-1}. These data support our assumption that the toxicity can be reduced by introduction of a neutral, biocompatible polymer such as EtOx into the micellar shell. These results comply with previous studies conducted on copolymers of P(EtOx) and PEI.[10,11] By preparing statistically distributed copolymers, the cytotoxicity could be decreased significantly at concentrations of 5 mg mL^{-1} when reducing the PEI content from 100 to 59% (24 h incubation).[11] Block copolymers of P(EtOx) and PEI also reduced the cytotoxicity;[10] however, the cell viability was lower (40 to 60% in HeLa cells) compared to the statistic copolymers (80% in 3T3 fibroblasts) with a similar PEI amount (~60%). These differences might be caused by the charge density within the polymers. Presumably, the shielding of the cytotoxic cationic charges is enhanced by a random distribution of the stealth units compared to the block structures, when assuming the polymers to coil in aqueous solution. Within the current study, the cationic blocks consisted of more repeating units than the stealth block to enhance the endosomal release of the polyplexes caused by a possible stretching of the cationic arms. This circumstance might also explain the lack in terms of cytocompatibility and could be further evaluated by preparing nanostructures with longer stealth blocks. However, this was not part of the current study. Interestingly, the P(AmOx) homopolymers revealed a reduced viability to approximately 50% even at concentrations of 50 μg mL^{-1}, whereas our group previously showed that *l*-PEI$_{575}$ reveals a similar effect on different cell lines after treatment with a 3.5 μg mL^{-1} solution.[41] B. D. Monnery et al. recently published results on the dependency of the cytotoxicity of polycations on their molar mass.[9] Even though both polymers have a similar molar mass (M_n ≈ 24 kDa), their cytotoxicity differs significantly. Consequently, we attribute these differences to the amount of cationic charges, respectively the charge

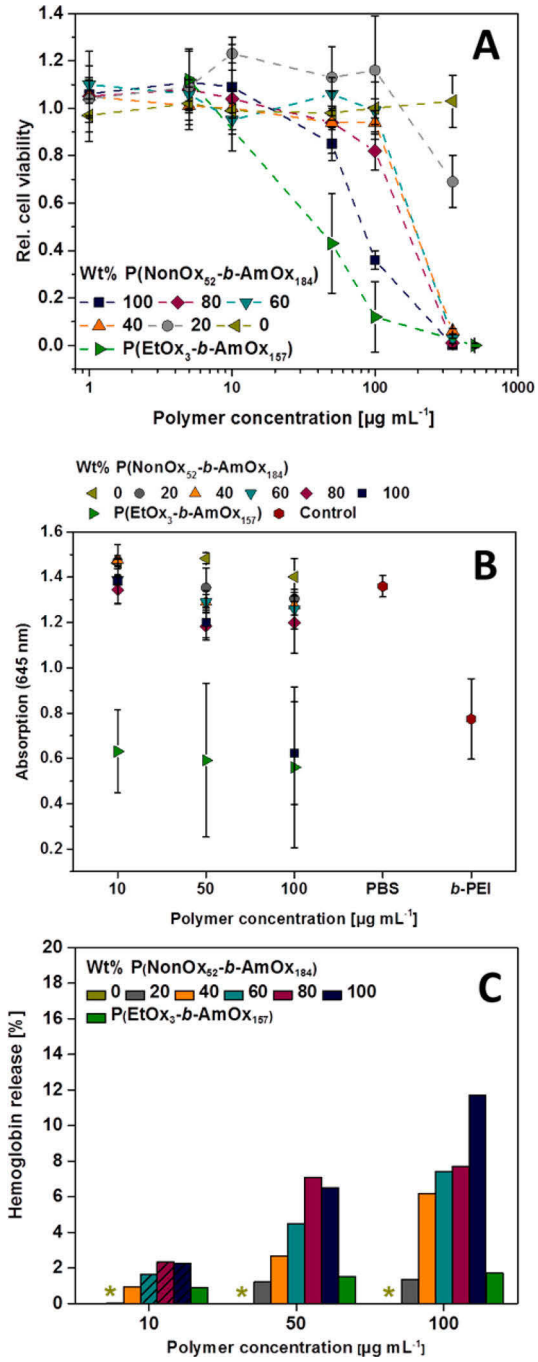

Figure 3. Concentration dependent cyto- and hemocompatibility of nanostructures. (A) Cytotoxicity assay of indicated polymers using AlamarBlue. Nontreated cells served as 100% relative viability. L929 cells were treated 24 h with the indicated concentrations of the polymer micelle solutions. Values represent the mean ± SD (n = 3). (B) Concentration dependent erythrocyte aggregation of nanostructures. *b*-PEI represents the positive control (p.c.) and PBS the negative control (n.c.). Values represent the mean ± SD (n = 3). For microscopy images, see Figure S12. (C) Hemolysis assay of erythrocytes after incubation with nanostructures at indicated concentrations. A value of less than 2% hemoglobin release is classified as nonhemolytic and more than 5% as hemolytic. Stars depict the position of nonhemolytic samples. Triton X was used as the p.c. (100%) and PBS served as the n.c. and was subtracted from the values. Values represent the mean (n = 3). Striped columns are below the CMC of the nanostructures.

DOI: 10.1021/acs.biomac.7b01535
Biomacromolecules 2018, 19, 748−760

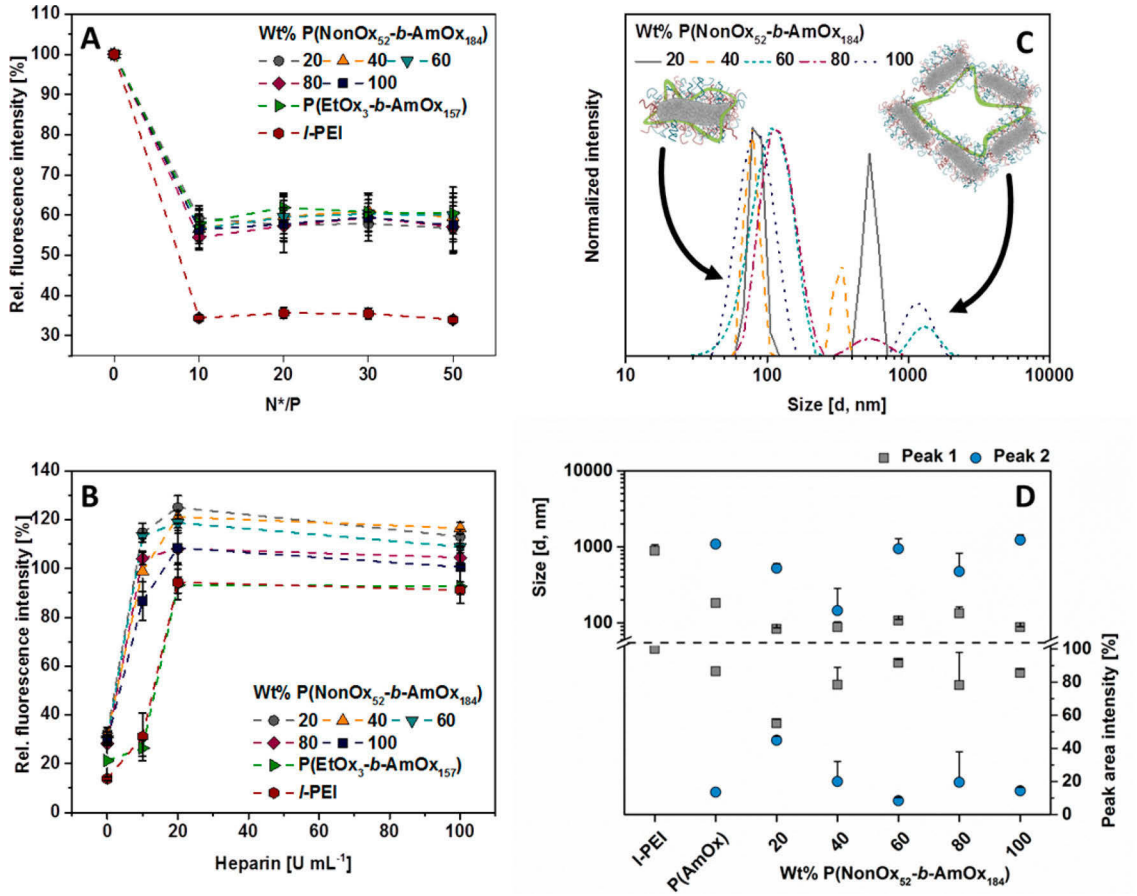

Figure 4. Micelleplex formation with pDNA and stability test using the polymer P($EtOx_3$-*b*-$AmOx_{157}$) and micelles with 20 to 100 wt % P($NonOx_{52}$-*b*-$AmOx_{184}$). (A) EBA of all polymers at the indicated N*/P (amino groups in the polymers per phosphate groups in the DNA) ratios utilizing a pCMV-GFP plasmid for polyplex formation in HBG buffer. Values represent the mean ± SD (n = 3). (B) Heparin dissociation assay of polyplexes formed at N*/P 50 using heparin as polyanion. Values represent the mean ± SD (n = 3). (C, D) DLS determination of size (diameter) and size distribution of polyplexes (N*/P = 50) formed with pCMV-GFP plasmid and homopolymers as well as polyplex forming micelles. Values represent the mean and SD (n = 3). (C) One representative DLS curve and possible micelleplexe structures are shown. (D) As two populations were found, the intensity as well as the size of the two populations was plotted.

density within the different polymers, which is 3.5-times higher in the utilized *l*-PEI.

In addition to the AlamarBlue cytotoxicity assay, the hemolysis of the nanostructures at varying polymer concentrations was measured (Figure 3C). Using these measurements, a hemoglobin release below 2% is considered to be not hemolytic, while 2 to 5% is slightly hemolytic and a rate above 5% is hemolytic. At low polymer concentration of 10 μg mL^{-1}, none of the tested nanostructures was hemolytic; however, it should be mentioned that this concentration was already below the CMC of nanostructures with 60, 80, and 100 wt % P($NonOx_{52}$-*b*-$AmOx_{184}$), which were hemolytic at concentrations of 50 μg mL^{-1}. In contrast to that, micelles with 0 or 20 wt % P($NonOx_{52}$-*b*-$AmOx_{184}$) as well as the homopolymers were not hemolytic even at polymer concentrations of 100 μg mL^{-1}, while those with 40 wt % P($NonOx_{52}$-*b*-$AmOx_{184}$) were not hemolytic up to 50 μg mL^{-1}. *l*-PEI was only slightly hemolytic at concentrations of 100 μg mL^{-1}.[40] By comparing these results, it is obvious that the hemolytic activity of the polymeric micelles depends on the amount of AmOx within the shell and that the micellar structure enhances the membrane disruption. It should be mentioned that the hemolytic activity was tested in PBS as buffer system without any proteins to further protect the cells, meaning that the critical concentrations might be different in *in vivo* or even *in vitro* situations. However, the erythrocyte aggregation represents also a method to measure the membrane interactions of polymers (Figure 3B).[42,43] Again, the aggregation rate of cells was clearly dependent on the ratio of cationic to stealth units within the micellar shell. In particular, the homopolymers of AmOx showed membrane aggregation comparable to the ISO-standard *b*-PEI even at the lowest concentration, whereas the micelles revealed no erythrocyte aggregation except the 100 wt % P($NonOx_{52}$-*b*-$AmOx_{184}$) at 100 μg mL^{-1}. Interestingly, P($EtOx_3$-*b*-$AmOx_{157}$) did not show hemolytic activity but a high membrane aggregation potential. Micelles, on the other hand, were more hemolytic, however, had a lower membrane aggregation potential. This indicates that the micelles forces a membrane hole formation in contrast to the homopolymers, which is beneficial for the endosomal release of these nanostructures.

DNA Binding and Dissociation Capabilities. As the prepared nanostructures are supposed to act as transfection vectors, investigations on the DNA binding and dissociation capabilities of nanostructures with 20 to 100 wt % P($NonOx_{52}$-*b*-$AmOx_{184}$) were conducted. The DNA binding ability was determined by the ethidium bromide assay (EBA) and was evaluated with respect to the nitrogen atoms bearing the

DOI: 10.1021/acs.biomac.7b01535
Biomacromolecules 2018, 19, 748−760

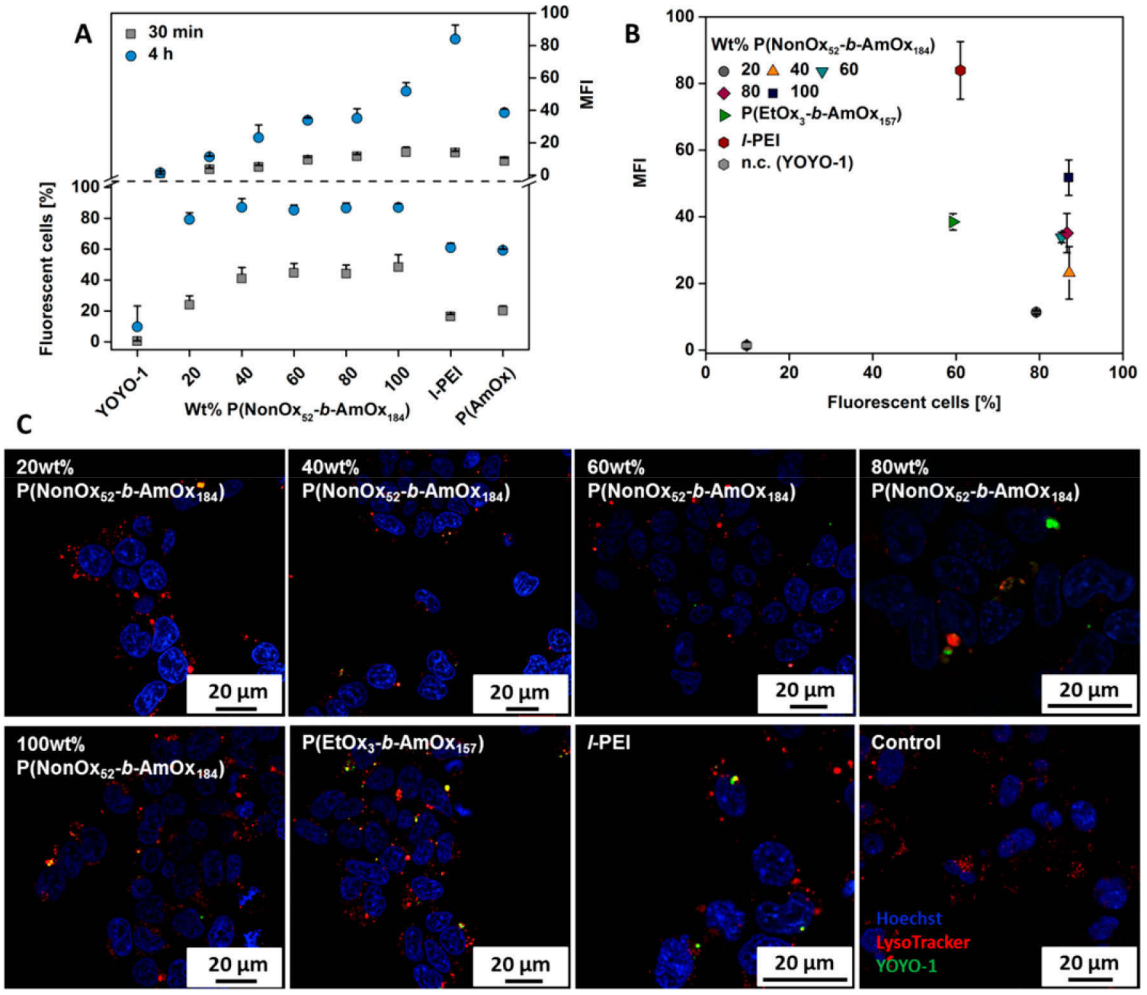

Figure 5. Cellular uptake study of different polyplexes (N*/P 50) using YOYO-1 labeled pDNA. (A) HEK-293 cells were treated with micelleplexes for 30 min and 4 h in growth media and uptake was analyzed via flow cytometry (MFI, mean fluorescence intensity). Values represent the mean and SD ($n = 3$). (B) MFI of the cells in dependence on the amount of fluorescent cells after 4 h of incubation. (C) CLSM images of micelleplexes (N*/P 50) after 4 h of incubation. The cell nucleus is stained with Hoechst (blue), endosomes are stained with LysoTracker (red), and pDNA with YOYO-1 (green). Yellow dots indicate a colocalization of green and red fluorescence. Dead cells and outer fluorescence of noninternalized micelleplexes were quenched by the addition of trypan blue.

potential for DNA binding (amino group in the polymer side chain) (N*/P, Figure 4A).

By comparing the nanostructures of different AmOx content in the micelle shell with respect to the DNA complexation, the N*/P ratios are similar for all nanostructures. Interestingly, the same plateau at approximately 60% fluorescence intensity was reached, even if only 20% of the shell contains DNA binding amines. It leads to the conclusion that all nanostructures are of the same quality for polyplex formation and the EtOx units do not interfere with the DNA interaction, demonstrating the potential of the block copolymers. Subsequently, the DNA dissociation of the polyplexes was investigated by the heparin assay (Figure 4B). A release of the DNA from micelles and homopolymers was possible using 20 U mg^{-1} heparin, a representative polyanion commonly used for DNA release.[44,45] In the case of the micelles, a release was even observed at 10 U mL^{-1} heparin. This result supported the assumption that the self-assembly has an influence on the critical gene carrier parameters, for example, caused by sterically phenomena of the charging density. A release of the genetic material is desired to enable transfer to the nucleus or transcription. Polyplexes were further evaluated via DLS measurements, showing a main peak distribution with a diameter of 100 nm and some larger aggregates (Figure 4C,D). Even though a quantification and discussion of the DLS results are difficult, the micelleplexes containing 60 to 100 wt % of P($NonOx_{52}$-*b*-$AmOx_{184}$) seem to form less aggregates than micelleplexes with 20 or 40 wt % P($NonOx_{52}$-*b*-$AmOx_{184}$), possibly due to higher local charge densities. For this reason, it is likely that micelles with more cationic charges tend to bind one molecule of pDNA per micelle, while micelles with less density of cationic charges might be bound to the pDNA in groups (Figure 4C). Since the polyplexes are prepared by aiming an N*/P ratio of 50, we observe an excess of polymeric micelles in all cases; however, the amount of polymers increases with a decreasing amount of P($NonOx_{52}$-*b*-$AmOx_{184}$), which makes the formation of such larger micelleplexes quite likely.

Cellular Uptake. To prove whether the micelles are able to transport the genetic material into cells, the pDNA was stained with the intercalating dye YOYO-1 that is also not released by the cationic polymers. Different amounts of micelleplex solution were added to the cells according to their N*/P ratio. The amount of pDNA added was kept constant. After 30 min and 4 h of incubation, the cells were analyzed via flow

DOI: 10.1021/acs.biomac.7b01535
Biomacromolecules 2018, 19, 748−760

cytometry using trypan blue to quench fluorescent polyplexes outside the cells. All polymers revealed a time-dependent uptake in the mean fluorescence intensity (MFI) as well as the amount of cells, which internalized the micelleplexes (Figure 5A).

The transport of the genetic material of the micelles was enhanced with increasing AmOx amount in the shell and the micelle with 100% AmOx in the shell showed an enhanced transfer capacity compared to the AmOx homopolymer. If these structures are compared with the gold standard PEI it is obvious that more cells take up polyplexes; in particular the amount of cells is increased for all tested micelles. However, the MFI of PEI exceeded the micelles after 4 h of incubation, showing the better transport potential of PEI, although less cells take up the polyplexes. This can be also observed by CLSM investigations, where the green signal (YOYO-1) was more intensive for the homopolymers compared to the micelles (Figure 5C). For a better comparison of the polymers and to obtain insight into a structure−property-relationship, the MFI was plotted against the amount of cells (Figure 5B). Here, two trends are visible. (i) The MFI increased with increasing amount of AmOx in the micellar shell. The amount of cells was constant throughout the different compositions except for the micelles with the lowest AmOx content (20 wt % P($NonOx_{52}$-*b*-$AmOx_{184}$)), which showed a slightly reduced percentage. These facts indicate an uptake independent of the cationic charge density in the micellar shell. In particular, the micelles with lower AmOx content can therefore be considered as a potential gene carrier with high bio- and hemocompatibility, which still can transfect a high percentage of the desired cells. (ii) The micellar structure enhances the performance of AmOx in terms of MFI and the amount of cells taking up the genetic material. These results underline the favorable uptake and transport capabilities of micellar structures compared to homopolymers.

Transfection Efficiency. Finally, the transfection efficiencies of the polymers were investigated using an eGFP expressing plasmid and the analysis via flow cytometry. Again, the amount of cells expressing eGFP as well the MFI of all viable cells was detected. Moreover, the viability of each measurement was analyzed and plotted against the transfection efficiency (Figure 6). The polymers can be categorized into two classes, where the first showed only marginal transfection efficiency, namely P($EtOx_3$-*b*-$AmOx_{157}$), and the nanostructures that are composed of 20 or 40 wt % P($NonOx_{52}$-*b*-$AmOx_{184}$), respectively. The second class revealed acceptable to high transfection efficiencies in the following order: 60 wt % P($NonOx_{52}$-*b*-$AmOx_{184}$) < 80 wt % P($NonOx_{52}$-*b*-$AmOx_{184}$) < 100 wt % P($NonOx_{52}$-*b*-$AmOx_{184}$) < *l*-PEI. In parallel to the uptake efficiency of the polymers, the performance of the micelles increased with increasing P($NonOx_{52}$-*b*-$AmOx_{184}$) content from 40 to 100 wt %. Micelles with 100 and 80 wt % P($NonOx_{52}$-*b*-$AmOx_{184}$) showed transfection efficiencies similar to PEI with a distinct reduction in cytotoxicity (micelles >80% viability, PEI 60% viability). It is noteworthy that architecture or the assembly of the materials, respectively, has a tremendous influence on the transfection efficiency. Although P($EtOx_3$-*b*-$AmOx_{157}$) revealed the smallest transfection efficiency, the micelle of 100 wt % P($NonOx_{52}$-*b*-$AmOx_{184}$) showed a performance similar to PEI, although applying the same N*/P ratio (same amount of protonable nitrogen atoms). This result demonstrates the potential of the micellar structure for the development of more efficient polymeric materials for transfection.

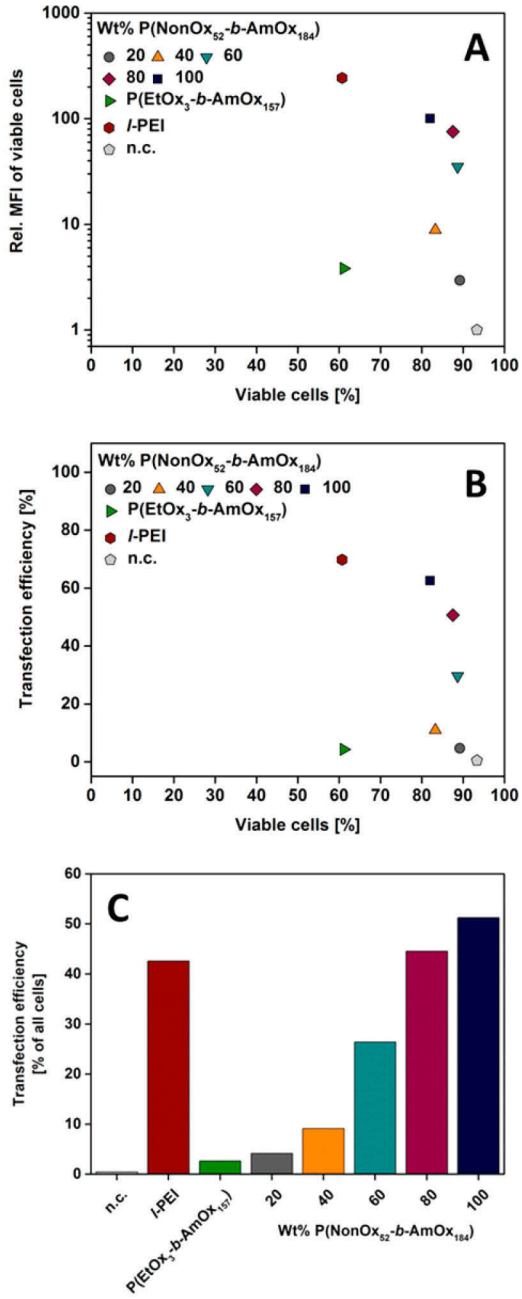

Figure 6. Transfection efficiency of different polyplexes for adherent HEK-293 cells in growth media at N*/P = 50 after 4 d analyzed via flow cytometry. Values represent the mean. (n = 3). (A) Relative MFI of all viable cells normalized by the negative control (n.c.). (B) Transfection efficiency of all viable cells. (C) Transfection efficiency of all cells. For values, see Table S8.

CONCLUSIONS

In the current study, we synthesized two different amphiphilic block copolymers, namely P($NonOx_{52}$-*b*-$AmOx_{184}$), to induce cationic charges and P($EtOx_{155}$-*b*-$NonOx_{75}$) for the introduction of stealth units. The two P(Ox)s were coassembled in aqueous physiological NaCl solution and subsequently characterized via DLS and cryoTEM. All nanostructures that contained at least a maximum P($NonOx_{52}$-*b*-$AmOx_{184}$) content

DOI: 10.1021/acs.biomac.7b01535
Biomacromolecules 2018, 19, 748−760

of 80 wt % resulted in rod-like micelles with an apparent average diameter of 100 nm (assuming spheres by DLS measurements), whereas pure P($NonOx_{52}$-*b*-$AmOx_{184}$) micelles were spherical. DLS measurements of the nanostructures in buffers of distinct pH values resulted in a pH-dependent alteration of the size with respect to the pH value and the amount of P($NonOx_{52}$-*b*-$AmOx_{184}$). A reversible polyplex formation was possible with all amino group containing nanostructures. We observed that the cytotoxicity, erythrocyte aggregation, and hemolytic activity were dependent on the polymer composition within the nanostructures. The high charge density of the micelles led to an enhanced hemoglobin release compared to the P(AmOx) homopolymer. Examinations on the cellular uptake showed that the number of fluorescent cells is similar for all nanostructures (~80%), while the MFI increases applying micelles with more cationic charges. In comparison, we observed 60% fluorescent cells using *l*-PEI or AmOx homopolymers and the MFI of P(AmOx) was considerably lower than for *l*-PEI. Flow cytometry analysis of the transfection efficiency revealed an enhanced viability of the cells when treated with micelleplexes (80−90%) compared to polyplexes of P(AmOx) or *l*-PEI (60%). The transfection efficiency was strongly dependent on the amount of cationic polymer within the micelles and ranged from less than 5% (20 wt % P($NonOx_{52}$-*b*-$AmOx_{184}$)) to more than 60% (100 wt % P($NonOx_{52}$-*b*-$AmOx_{184}$)). Micelleplexes with 80 or 100 wt % P($NonOx_{52}$-*b*-$AmOx_{184}$) showed a better allover performance in terms of transfection efficiency than *l*-PEI, while P(AmOx) was worse than the micelleplexes with 20 wt % P($NonOx_{52}$-*b*-$AmOx_{184}$). We attribute these advantages to the architecture of the micelles and the following accumulation of cationic charges on their surface due to the cationic blocks. On the basis of these findings, we were able to improve the performance of a toxic, poorly transfecting polymer by appropriate self- and coassembly process to obtain nanostructures with a decreased cytotoxicity and improved transfection efficiency compared to *l*-PEI and the AmOx homopolymer.

Further studies might concentrate on the utilization of cationic block copolymers with different lengths to obtain nanostructures, which have an optimum balance between shielding by the EtOx blocks and efficient endosomal release by the stretching of the cationic blocks within the endolysosomes. These experiments might help to find biocompatible and efficient gene carrier systems.

■ ASSOCIATED CONTENT

Supporting Information

The Supporting Information is available free of charge on the ACS Publications website at DOI: 10.1021/acs.biomac.7b01535.

NMR spectra, SEC traces, DLS curves, magnified cryoTEM images, CMC determination graphs, erythrocyte aggregation microscopy images, raw values of DLS measurements (PDF)

■ AUTHOR INFORMATION

Corresponding Authors

*E-mail: anja.traeger@uni-jena.de.
*E-mail: ulrich.schubert@uni-jena.de.

ORCID

Ulrich S. Schubert: 0000-0003-4978-4670

Author Contributions

The manuscript was written through contributions of all authors. All authors have given approval to the final version of the manuscript.

Notes

The authors declare no competing financial interest.

■ ACKNOWLEDGMENTS

The authors gratefully acknowledge the Bundesministerium für Bildung und Forschung (BMBF, Germany, No. 13N13416 smart-dye-livery) and the Thüringer Ministerium für Wirtschaft, Wissenschaft und Digitale Gesellschaft (ProExzellenzII, NanoPolar). Furthermore, funding of the collaborative research center PolyTarget (SFB 1278) by the Deutsche Forschungsgemeinschaft (DFG) is highly acknowledged. A.T. acknowledges the Carl Zeiss Foundation and the BMBF (No. 13XP5034A PolyBioMik) for funding. J.C.B. further thanks the DFG for support (Emmy-Noether Program, BR 4905/3-1). The authors thankfully acknowledge Carolin Kellner and Elisabeth Moek for the conduction of AlamarBlue, hemolysis, and aggregation assays as well as Dr. Grit Festag for SEC measurements on an aqueous system. CryoTEM investigations were performed at the Electron Microsocpy facilities of the Jena Center for Soft Matter (JCSM), which was established with grants from the Deutsche Forschungsgemeinschaft (DFG) and the European Fund for Regional Development (EFRE). The LSM880 ELYRA PS.1 was further funded with a grant from the DFG.

■ REFERENCES

(1) Huang, Y.; Liu, X.; Dong, L.; Liu, Z.; He, X.; Liu, W. Development of viral vectors for gene therapy for chronic pain. *Pain Res. Treat.* **2011**, *2011*, 968218.

(2) Schatzlein, A. G. Non-viral vectors in cancer gene therapy: Principles and progress. *Anti-Cancer Drugs* **2001**, *12* (4), 275−304.

(3) Gardlik, R.; Palffy, R.; Hodosy, J.; Lukacs, J.; Turna, J.; Celec, P. Vectors and delivery systems in gene therapy. *Med. Sci. Monit.* **2005**, *11* (4), Ra110−21.

(4) Zhang, S.; Zhao, B.; Jiang, H.; Wang, B.; Ma, B. Cationic lipids and polymers mediated vectors for delivery of sirna. *J. Controlled Release* **2007**, *123* (1), 1−10.

(5) Bulmus, V.; Woodward, M.; Lin, L.; Murthy, N.; Stayton, P.; Hoffman, A. A new ph-responsive and glutathione-reactive, endosomal membrane-disruptive polymeric carrier for intracellular delivery of biomolecular drugs. *J. Controlled Release* **2003**, *93* (2), 105−120.

(6) Godbey, W. T.; Barry, M. A.; Saggau, P.; Wu, K. K.; Mikos, A. G. Poly(ethylenimine)-mediated transfection: A new paradigm for gene delivery. *J. Biomed. Mater. Res.* **2000**, *51* (3), 321−8.

(7) Behr, J.-P. The proton sponge: A trick to enter cells the viruses did not exploit. *Chimia* **1997**, *51* (1−2), 34−36.

(8) Ahn, C. H.; Chae, S. Y.; Bae, Y. H.; Kim, S. W. Biodegradable poly(ethylenimine) for plasmid DNA delivery. *J. Controlled Release* **2002**, *80* (1−3), 273−82.

(9) Monnery, B. D.; Wright, M.; Cavill, R.; Hoogenboom, R.; Shaunak, S.; Steinke, J. H. G.; Thanou, M. Cytotoxicity of polycations: Relationship of molecular weight and the hydrolytic theory of the mechanism of toxicity. *Int. J. Pharm.* **2017**, *521* (1), 249−258.

(10) Hsiue, G. H.; Chiang, H. Z.; Wang, C. H.; Juang, T. M. Nonviral gene carriers based on diblock copolymers of poly(2-ethyl-2-oxazoline) and linear polyethylenimine. *Bioconjugate Chem.* **2006**, *17* (3), 781−6.

(11) Shah, R.; Kronekova, Z.; Zahoranová, A.; Roller, L.; Saha, N.; Saha, P.; Kronek, J. vitro study of partially hydrolyzed poly(2-ethyl-2-oxazolines) as materials for biomedical applications. *J. Mater. Sci.: Mater. Med.* **2015**, *26* (4), 157.

(12) Miyata, K.; Oba, M.; Nakanishi, M.; Fukushima, S.; Yamasaki, Y.; Koyama, H.; Nishiyama, N.; Kataoka, K. Polyplexes from

DOI: 10.1021/acs.biomac.7b01535
Biomacromolecules 2018, 19, 748−760

poly(aspartamide) bearing 1,2-diaminoethane side chains induce ph-selective, endosomal membrane destabilization with amplified transfection and negligible cytotoxicity. *J. Am. Chem. Soc.* **2008**, *130* (48), 16287−16294.
(13) Oba, M.; Miyata, K.; Osada, K.; Christie, R. J.; Sanjoh, M.; Li, W.; Fukushima, S.; Ishii, T.; Kano, M. R.; Nishiyama, N.; Koyama, H.; Kataoka, K. Polyplex micelles prepared from ω-cholesteryl peg-polycation block copolymers for systemic gene delivery. *Biomaterials* **2011**, *32* (2), 652−663.
(14) Kim, H. J.; Ishii, A.; Miyata, K.; Lee, Y.; Wu, S.; Oba, M.; Nishiyama, N.; Kataoka, K. Introduction of stearoyl moieties into a biocompatible cationic polyaspartamide derivative, pasp(det), with endosomal escaping function for enhanced sirna-mediated gene knockdown. *J. Controlled Release* **2010**, *145* (2), 141−148.
(15) Barz, M.; Luxenhofer, R.; Zentel, R.; Vicent, M. J. Overcoming the peg-addiction: Well-defined alternatives to peg, from structure-property relationships to better defined therapeutics. *Polym. Chem.* **2011**, *2* (9), 1900−1918.
(16) Hoogenboom, R. Poly(2-oxazoline)s: A polymer class with numerous potential applications. *Angew. Chem., Int. Ed.* **2009**, *48* (43), 7978−94.
(17) Luxenhofer, R.; Han, Y.; Schulz, A.; Tong, J.; He, Z.; Kabanov, A. V.; Jordan, R. Poly(2-oxazoline)s as polymer therapeutics. *Macromol. Rapid Commun.* **2012**, *33* (19), 1613−1631.
(18) Gaertner, F. C.; Luxenhofer, R.; Blechert, B.; Jordan, R.; Essler, M. Synthesis, biodistribution and excretion of radiolabeled poly(2-alkyl-2-oxazoline)s. *J. Controlled Release* **2007**, *119* (3), 291−300.
(19) Salzinger, S.; Huber, S.; Jaksch, S.; Busch, P.; Jordan, R.; Papadakis, C. M. Aggregation behavior of thermo-responsive poly(2-oxazoline)s at the cloud point investigated by fcs and sans. *Colloid Polym. Sci.* **2012**, *290* (5), 385−400.
(20) Cai, G.; Litt, M. H. Preparation and characterization of phenyl and undecyl oxazoline block copolymers. *J. Polym. Sci., Part A: Polym. Chem.* **1989**, *27* (11), 3603−3618.
(21) McAlvin, J. E.; Fraser, C. L. Metal-centered star block copolymers: Amphiphilic iron tris(bipyridine)-centered polyoxazolines and their chemical fragmentation to bipyridine-centered bab triblock copolymers. *Macromolecules* **1999**, *32* (5), 1341−1347.
(22) Jin, R.-H. Water soluble star block poly(oxazoline) with porphyrin label: A unique emulsion and its shape direction. *J. Mater. Chem.* **2004**, *14* (3), 320−327.
(23) Lach, C.; Hanselmann, R.; Frey, H.; Mülhaupt, R. Hyperbranched carbosilane oxazoline-macromonomers: Polymerization and coupling to a trimesic acid core. *Macromol. Rapid Commun.* **1998**, *19* (9), 461−465.
(24) Hartlieb, M.; Pretzel, D.; Kempe, K.; Fritzsche, C.; Paulus, R. M.; Gottschaldt, M.; Schubert, U. S. Cationic poly(2-oxazoline) hydrogels for reversible DNA binding. *Soft Matter* **2013**, *9* (18), 4693−4704.
(25) Christova, D.; Velichkova, R.; Goethals, E. J.; Du Prez, F. E. Amphiphilic segmented polymer networks based on poly(2-alkyl-2-oxazoline) and poly(methyl methacrylate). *Polymer* **2002**, *43* (17), 4585−4590.
(26) Hadjichristidis, N., Pispas, S., Floudas, G. A. *Block Copolymers: Synthetic Strategies, Physical Properties, and Applications*; Wiley: Weinheim, 2003.
(27) He, Z.; Miao, L.; Jordan, R.; S-Manickam, D.; Luxenhofer, R.; Kabanov, A. V. A low protein binding cationic poly(2-oxazoline) as non-viral vector. *Macromol. Biosci.* **2015**, *15* (7), 1004−1020.
(28) Rinkenauer, A. C.; Tauhardt, L.; Wendler, F.; Kempe, K.; Gottschaldt, M.; Traeger, A.; Schubert, U. S. A cationic poly(2-oxazoline) with high in vitro transfection efficiency identified by a library approach. *Macromol. Biosci.* **2015**, *15* (3), 414−425.
(29) Bauer, M.; Lautenschlaeger, C.; Kempe, K.; Tauhardt, L.; Schubert, U. S.; Fischer, D. Poly(2-ethyl-2-oxazoline) as alternative for the stealth polymer poly(ethylene glycol): Comparison of in vitro cytotoxicity and hemocompatibility. *Macromol. Biosci.* **2012**, *12* (7), 986−998.
(30) Wiesbrock, F.; Hoogenboom, R.; Abeln, C. H.; Schubert, U. S. Single-mode microwave ovens as new reaction devices: Accelerating the living polymerization of 2-ethyl-2-oxazoline. *Macromol. Rapid Commun.* **2004**, *25* (22), 1895−1899.
(31) Wilhelm, M.; Zhao, C. L.; Wang, Y.; Xu, R.; Winnik, M. A.; Mura, J. L.; Riess, G.; Croucher, M. D. Poly(styrene-ethylene oxide) block copolymer micelle formation in water: A fluorescence probe study. *Macromolecules* **1991**, *24* (5), 1033−1040.
(32) Vollrath, A.; Schallon, A.; Pietsch, C.; Schubert, S.; Nomoto, T.; Matsumoto, Y.; Kataoka, K.; Schubert, U. S. A toolbox of differently sized and labeled pmma nanoparticles for cellular uptake investigations. *Soft Matter* **2013**, *9* (1), 99−108.
(33) Cesana, S.; Auernheimer, J.; Jordan, R.; Kessler, H.; Nuyken, O. First poly(2-oxazoline)s with pendant amino groups. *Macromol. Chem. Phys.* **2006**, *207* (2), 183−192.
(34) Jaksch, S.; Schulz, A.; Di, Z.; Luxenhofer, R.; Jordan, R.; Papadakis, C. M. Amphiphilic triblock copolymers from poly(2-oxazoline) with different hydrophobic blocks: Changes of the micellar structures upon addition of a strongly hydrophobic cancer drug. *Macromol. Chem. Phys.* **2016**, *217* (13), 1448−1456.
(35) Bonné, T. B.; Papadakis, C. M.; Lüdtke, K.; Jordan, R. Role of the tracer in characterizing the aggregation behavior of aqueous block copolymer solutions using fluorescence correlation spectroscopy. *Colloid Polym. Sci.* **2007**, *285* (5), 491−497.
(36) Bonné, T. B.; Lüdtke, K.; Jordan, R.; Štěpánek, P.; Papadakis, C. M. Aggregation behavior of amphiphilic poly(2-alkyl-2-oxazoline) diblock copolymers in aqueous solution studied by fluorescence correlation spectroscopy. *Colloid Polym. Sci.* **2004**, *282* (8), 833−843.
(37) Ivanova, R.; Komenda, T.; Bonné, T. B.; Lüdtke, K.; Mortensen, K.; Pranzas, P. K.; Jordan, R.; Papadakis, C. M. Micellar structures of hydrophilic/lipophilic and hydrophilic/fluorophilic poly(2-oxazoline) diblock copolymers in water. *Macromol. Chem. Phys.* **2008**, *209* (21), 2248−2258.
(38) Jain, K.; Kesharwani, P.; Gupta, U.; Jain, N. K. Dendrimer toxicity: Let's meet the challenge. *Int. J. Pharm.* **2010**, *394* (1), 122−142.
(39) Betthausen, E.; Drechsler, M.; Fortsch, M.; Schacher, F. H.; Muller, A. H. E. Dual stimuli-responsive multicompartment micelles from triblock terpolymers with tunable hydrophilicity. *Soft Matter* **2011**, *7* (19), 8880−8891.
(40) Bus, T.; Englert, C.; Reifarth, M.; Borchers, P.; Hartlieb, M.; Vollrath, A.; Hoeppener, S.; Traeger, A.; Schubert, U. S., 3rd generation poly(ethylene imine)s for gene delivery. *J. Mater. Chem. B* **2017**, *5* (6), 1258−1274.
(41) Englert, C.; Pröhl, M.; Czaplewska, J. A.; Fritzsche, C.; Preußger, E.; Schubert, U. S.; Traeger, A.; Gottschaldt, M. D-fructose-decorated poly(ethylene imine) for human breast cancer cell targeting. *Macromol. Biosci.* **2017**, *17* (8), 1600502.
(42) Lee, Y.; Miyata, K.; Oba, M.; Ishii, T.; Fukushima, S.; Han, M.; Koyama, H.; Nishiyama, N.; Kataoka, K. Charge-conversion ternary polyplex with endosome disruption moiety: A technique for efficient and safe gene delivery. *Angew. Chem.* **2008**, *120* (28), 5241−5244.
(43) Rinkenauer, A. C.; Schallon, A.; Günther, U.; Wagner, M.; Betthausen, E.; Schubert, U. S.; Schacher, F. H. A paradigm change: Efficient transfection of human leukemia cells by stimuli-responsive multicompartment micelles. *ACS Nano* **2013**, *7* (11), 9621−9631.
(44) Mislick, K. A.; Baldeschwieler, J. D. Evidence for the role of proteoglycans in cation-mediated gene transfer. *Proc. Natl. Acad. Sci. U. S. A.* **1996**, *93* (22), 12349−12354.
(45) Xu, Y.; Szoka, F. C. Mechanism of DNA release from cationic liposome/DNA complexes used in cell transfection. *Biochemistry* **1996**, *35* (18), 5616−5623.

DOI: 10.1021/acs.biomac.7b01535
Biomacromolecules 2018, 19, 748−760

Publication P4

Tumor targeting with pH-responsive poly(2-oxazoline)-based nanogels for metronomic doxorubicin treatment

D. Hoelzer[‡], M. N. Leiske[‡], M. Hartlieb, T. Bus, D. Pretzel, S. Hoeppener, K. Kempe, R. Thierbach, U. S. Schubert, *Oncotarget* **2018**, in press.

The paper as well as the supporting information (free of charge) is available online.

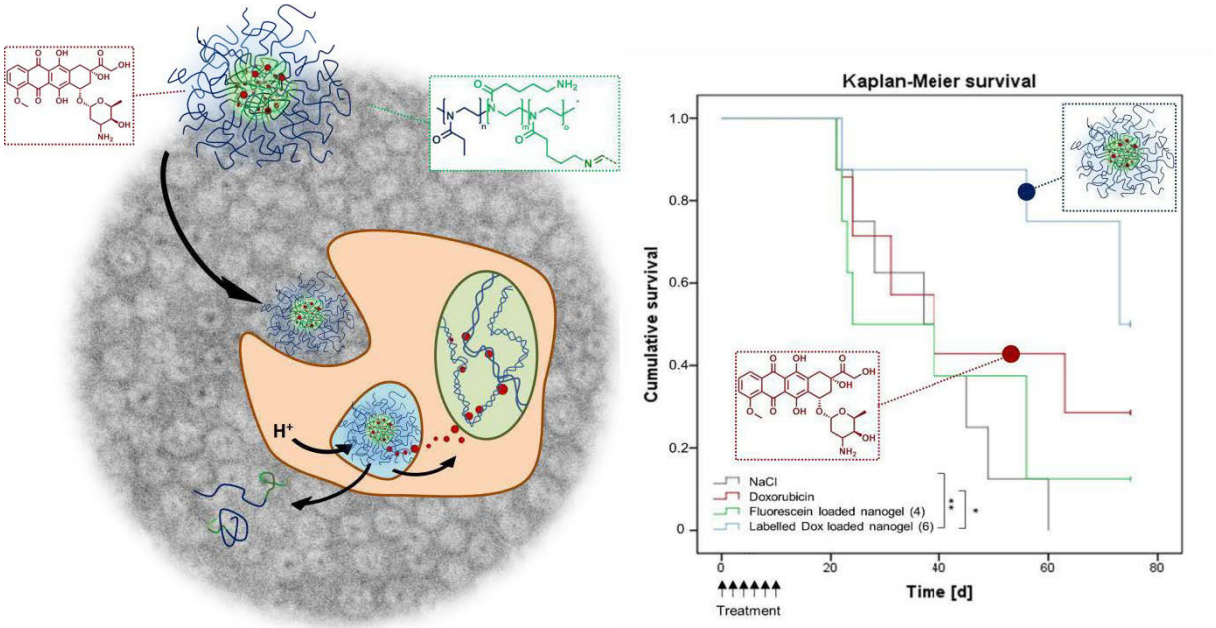

[‡]Equal contribution.

Tumor targeting with pH-responsive poly(2-oxazoline)-based nanogels for metronomic doxorubicin treatment

Doerte Hoelzer[1,*], Meike N. Leiske[2,3,*], Matthias Hartlieb[2,3,4], Tanja Bus[2,3], David Pretzel[2,3], Stephanie Hoeppener[2,3], Kristian Kempe[2,3,5], René Thierbach[1] and Ulrich S. Schubert[2,3]

[1]Institute of Nutrition, Friedrich Schiller University Jena, 07743 Jena, Germany

[2]Laboratory of Organic and Macromolecular Chemistry (IOMC), Friedrich Schiller University Jena, 07743 Jena, Germany

[3]Jena Center for Soft Matter (JCSM), Friedrich Schiller University Jena, 07743 Jena, Germany

[4]Current address: Institute of Biomaterial Science, Helmholtz-Zentrum Geesthacht, 14513 Teltow, Germany

[5]Current address: Monash Institute of Pharmaceutical Sciences, Monash University, Parkville, VIC 3052, Australia

[*]These authors contributed equally to the work

Correspondence to: *Ulrich S. Schubert,* ***email:*** *ulrich.schubert@uni-jena.der*

Keywords: *poly(2-oxazoline); doxorubicin; drug delivery; nanogel; metronomic*

Received: *October 18, 2017* ***Accepted:*** *February 24, 2018* ***Published:***

ABSTRACT

The synthesis of a new nanogel drug carrier system loaded with the anti-cancer drug doxorubicin (DOX) is presented. Poly(2oxazoline) (POx) based nanogels from block copolymer micelles were cross-linked and covalently loaded with DOX using pH-sensitive Schiff' base chemistry. DOX loaded POx based nanogels showed a toxicity profile comparable to the free drug, while unloaded drug carriers showed no toxicity. Hemolytic activity and erythrocyte aggregation of the drug delivery system was found to be low and cellular uptake was investigated by flow cytometry and fluorescence microscopy. While the amount of internalized drug was enhanced when incorporated into a nanogel, the release of the drug into the nucleus was delayed. For *in vivo* investigations the nanogel drug delivery system was combined with a metronomic treatment of DOX. Low doses of free DOX were compared to equivalent DOX loaded nanogels in a xenograft mouse model. Treatment with POx based nanogels revealed a significant tumor growth inhibition and increase in survival time, while pure DOX alone had no effect on tumor progression. The biodistribution was investigated by microscopy of organs of mice and revealed a predominant localization of DOX within tumorous tissue. Thus, the POx based nanogel system revealed a therapeutic efficiency despite the low DOX concentrations and could be a promising strategy to control tumor growth with fewer side effects.

INTRODUCTION

In modern oncology it is a major challenge to deliver therapeutic agents more safely and directly to the tumor. Doxorubicin (DOX) is an anthracycline antibiotic and is one of the most effective as well as commonly used chemotherapeutic drugs. It is used as a first-line treatment of various types of cancer, including hematologic malignancies, breast and ovarian carcinoma, neuroblastoma as well as soft tissue and bone sarcoma. The antitumor activity of DOX can be triggered by different mechanisms: (i) By intercalating into DNA strands and (ii) prevention of replication and transcription of DNA by inhibiting the enzyme topoisomerase II or, (iii) formation of free radicals leading to membrane and DNA damage as well as apoptosis [1, 2] However, the clinical benefit of DOX is limited by different side effects, *i.e.* cardiotoxicity [3, 4].

The use of nanosized drug carriers is rapidly emerging and can help to reduce these side effects as well as improve the drugs solubility [5], blood circulation time [6] and tissue distribution [7]. In particular nanogels, hydrogel nanoparticles with crosslinked hydrophilic polymers, offer several advantages for their use as a drug delivery system [8]. For this reason, the utilization of nanocarriers (*e.g.* nanoparticles) in terms of delivery of anti-cancer drugs has increased significantly during the last years [9–11]. Nanogels enable a high drug loading capacity, can protect and shield drugs until they reach their desired target and are highly biocompatible and biodegradable [12]. Due to the leaky structure of cancerous tissue together with the lack of effective lymphatic drainage, nanogels tend to accumulate in the tumor tissue known as enhanced permeability and retention (EPR) effect [13]. To achieve an effective delivery of the drug to the tumor it is also very important to prevent a premature disassembly or drug release from the carrier. A common strategy is the use of covalently cross-linked drug delivery systems (*i.e.* core cross-linked micelles or other nanogels) and a likewise covalently but reversibly attached drug [14–16].

The majority of drug delivery systems utilize a poly(ethylene glycol) (PEG) shell to shield themselves from unspecific interactions with healthy tissue or the components of the blood stream. However, reports about complement activation by PEG [17–19] and vacuolation [20–22] in the body have raised concerns about safety and reliability of the polymer. Poly(2-oxazoline)s (POx) represent a promising alternative as they are biocompatible, [13, 23, 24] and show a stealth behavior similar to PEG when the side chain substitution is chosen correctly [25, 26]. Recent studies elucidate the pharmacokinetic behavior of the polymer dependent on its molar mass, demonstrating superior behavior when compared to PEG [27, 28]. The first clinical study using a POx derivative is currently ongoing (SER-214, phase I) [14] and the polymer was approved by the federal food administration (FDA) as an indirect additive used in food contact substances (21CFR175.105) in 2016. In addition, POx based formulations of the cancer drug paclitaxel show great promise *in vivo* [5]. One major advantage of the polymer over PEG is its versatile functionalization chemistry [29] enabling easy access to a multitude of functional polymers and materials [15]. POx based nanogels have been reported, [30] but far have not been exploited for the use as a cancer drug delivery system.

Recently, we reported the synthesis of nanogels based on double hydrophilic POx block copolymers. They were based on micellar architecture with a cationic block forming the core and a poly(2-ethyl-2-oxazoline) (P(EtOx)) shell. The material was cross-linked and dye loaded by imine bonds [31]. The materials showed excellent biocompatibility and their charge and cellular uptake could be tailored by varying the cross-linking density [32]. Within this contribution, DOX is to be used as a payload in order to increase the efficiency and specificity of the drug towards cancer cells *in vitro* and *in vivo*. Drug attachment as well as cross-linking is accomplished using pH sensitive Schiff's base chemistry, to enable intracellular drug release [31, 33].

In addition to the drug delivery system itself, the regime of drug administration is of particular interest. Conventional chemotherapy relies on the administration of the maximum tolerated dose (MTD) to achieve the desired effect without unacceptable side effects. Because of the high toxicity and potential development of chemoresistance other concepts of drug administration are evolving. Metronomic chemotherapy is defined as a chronic administration of low doses of cytotoxic agents and can help to improve the efficiency of cancer treatment [34, 35]. Herein we report the straightforward synthesis of a POx based nanogel in a one pot approach, reversibly linked to (or loaded with) the anti-cancer drug DOX. The drug delivery system is biocompatible and able to release its payload as shown by *in vitro* investigations. In addition, *in vivo* experiments in mice show a promising increase in survival rate as compared to pure DOX at relatively low concentrations.

RESULTS AND DISCUSSION

Synthesis and loading of the poly(2-oxazoline)-based nanogels

Polymers were synthesized by sequential monomer addition using microwave technology employing 2-ethyl-2-oxazoline (EtOx) for the first and 2-(4-((*tert*-butoxycarbonyl)amino)butyl)-2-oxazoline (BocOx) for the second block. The second monomer was introduced within a glove box under nitrogen atmosphere to reduce termination prior to block extension. P($EtOx_{98}$-*b*-$BocOx_{32}$) (1) was synthesized with a narrow dispersity of Đ = 1.07, which did not increase drastically after deprotection of the amine groups to yield poly(2-ethyl-2-oxazoline)-*block*-(poly(2-(4-amino)butyl)-2-oxazoline)) (P(EtOx-*b*-AmOx)) (Supplementary Table 1, Supplementary Scheme 1, Supplementary Figures 1–2). While size exclusion chromatography (SEC) measurements of initial polymers could be performed in chloroform, deprotected P($EtOx_{98}$-*b*-$AmOx_{32}$) (2) had to be measured in *N*,*N*-dimethylacetamide (DMAc), explaining the difference in molar mass compared to the precursor polymer.

While DOX is fluorescent and can, therefore, be tracked directly within cells, its emission is highly dependent on the environment [36, 37]. To circumvent this issue and create nanogels, which can be tracked independent of their DOX release, polymer 2 was labeled with a fluorescent dye prior to the nanogel preparation. To this end, a dye with a near-infra red fluorescence (Alexafluor 660) was chosen to not interfere with the fluorescence of the drug. The dye possesses a *N*-hydroxy succinimide

(NHS) ester function, able to react with the amine groups of the P(AmOx) block of polymer 2. One equivalent of dye per polymer chain was applied to retain a sufficient amount of free amine groups for further self-assembly processes, and cross-linking reactions. To separate the labeled polymer 3 from unreacted dye molecules, precipitation in diethyl ether, as well as dialysis in deionized water was performed. The success of the attachment was confirmed by SEC measurements (Supplementary Figure 2) comparing the refractive index (RI). and UV traces of the polymer. The lack of an UV signal at high elution volumes indicates the absence of unbound dye. The fluorescence maximum of the dye coupled to the polymer was found to be similar to the free chromophore (Supplementary Figure 3). The coupling efficiency as determined by the emission of the polymer was determined *via* UV/Vis measurements and found to be 30%.

The self-assembly of these systems to form polymeric micelles was conducted as reported previously [38]. Briefly, the polymers were dissolved in chloroform, which leads to the formation of micellar structures comprising a P(AmOx) core and a P(EtOx) shell. Cross-linking was performed using glutaraldehyde (GA) resulting in the formation of nanogels. As previous investigations [32] showed a reduced cellular uptake of systems with a higher cross linking density, three equivalents of cross-linker (in respect to amine groups) were used. A reduced positive charge density is supposed to lead to prolonged circulation times *in vivo*. Drug loading was performed by reacting excessive aldehyde functionalities with DOX. The free amine groups of the molecule reacts with free aldehyde groups of the cross-linker resulting in a covalent attachment to the nanogel (Figure 1). As the imine function, which stabilizes the nanogel core and the drug, is labile at low pH values, created systems are expected to be disintegrating. Alexafluor-labeled (referred to as "labeled DOX-nanogel"), as well as unlabeled DOX-containing (referred to as "unlabeled DOX-nanogel") nanogels were produced. As a non-toxic equivalent DOX-free 6-aminofluorescein (6AF) loaded nanogels (referred to as "DOX-free nanogel") were synthesized using the same method.

Characterization of the nanogels

Due to the fact that the drug is not encapsulated into, but covalently bound to the nanogel, the term loading efficiency is used instead of the commonly utilized encapsulation efficiency. To determine the loading efficiency of produced nanogels the absorbance of the system was measured and compared to a calibration of the small molecule (Supplementary Figure 4). In the case of DOX-free nanogels, absorbance was measured at λ_{ex} = 490 nm whereas for labeled and unlabeled DOX-nanogels the absorbance was detected at λ_{ex} = 480 nm. A three-fold difference in mass loading was observed between fluorescein (17 wt%) and DOX (5 to 6 wt%) immobilization, (Table 1), while loading was relatively independent on the presence of Alexafluor 660 labels on the polymer chain. The difference can be explained by the nature of the cargo molecules. While both possess an amine functionality, which can be coupled covalently to aldehyde functionalities, 6AF also possesses a carboxylic acid function, which can interact in an electrostatic way with the positively charged core of the nanogel, leading to an increase in loading efficiency by electrostatic interaction.

As shown in Supplementary Figure 4, the fluorescence spectrum of DOX broadens significantly when incorporated into nanogels. The emission properties of the chromophore are known to be highly dependent on

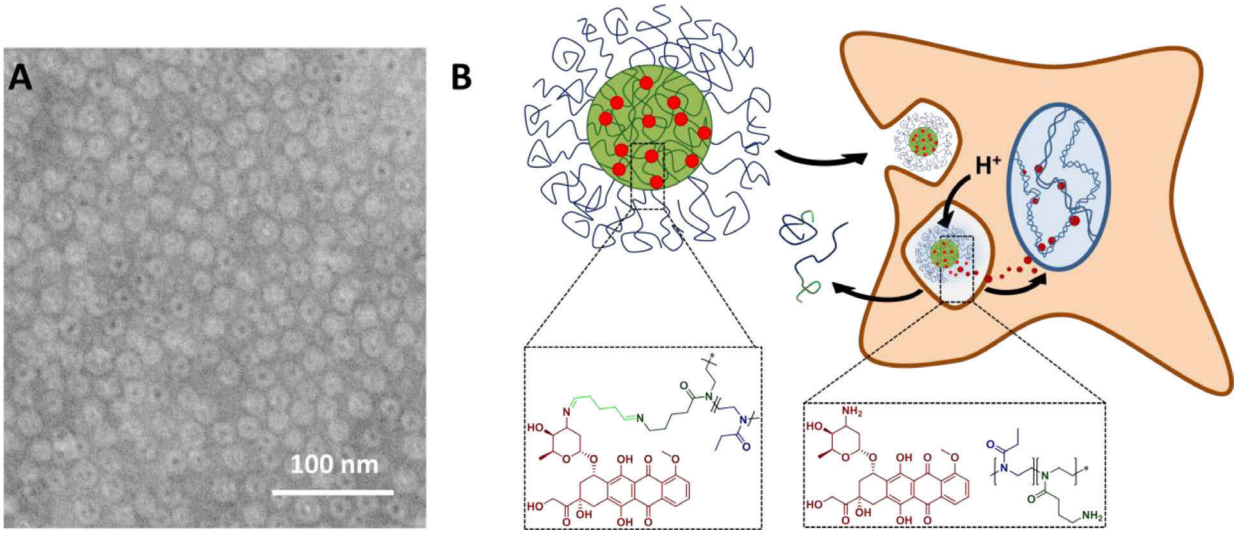

Figure 1: Schematic representation of nanogels obtained from P($EtOx_{98}$-*b*-$BocOx_{32}$) with a P(AmOx) core loaded with DOX and a P(EtOx) shell, cryo-TEM image of unlabeled DOX-nanogel 5 in water (scale bar represents 100 nm), and a schematic depiction of the drug delivery route of DOX.

Table 1: Analytical data of nanogels formed by the self-assembly of polymers 2 and 3

Sample	Precursor polymer	Capping agent	Size (DLS) [d, nm]	ζ [mV]	Content of capping agent [wt%]	Size (cryoTEM) [d, nm]
DOX-free nanogel	2	6AF	24	7	17	15
Unlabeled DOX-nanogel	2	DOX	26	18	5	20
Labeled DOX-nanogel	3	DOX	15	25	6	15

DLS and zeta potential values are determined in water. Sizes determined by DLS are derived from the number distribution.

environmental factors [36, 37]. The presence of amine groups within the core of the nanogel and other factors are likely to influence the fluorescence of DOX. In the case of the Alexafluor 660 labeled systems a high wavelength shoulder is visible in the emission spectrum indicating the presence of the near-IR dye. Upon excitation at λ_{ex} = 600 nm a pronounced fluorescence with a maximum at λ_{em} = 675 nm can be observed (Supplementary Figure 5).

To visualize the synthesized nanostructures, cryoTEM measurements were performed (Figure 1, Supplementary Figure 6). The images showed monodisperse spherical structures for all samples. For DOX-free and labeled DOX-nanogels an average diameter of 15 nm was obtained while the diameter of unlabeled DOX-nanogels was found to be 20 nm (Table 1, Supplementary Figure 6B and 6C). In addition, in the case of unlabeled DOX-nanogels a core-shell structure could be visualized showing a dark center and a lighter corona. The core is likely to be compact in water due to the presence of the hydrophobic DOX, whereas the shell is water swollen resulting in a lower contrast. For DOX-free nanogels and labeled DOX-nanogels this structure could not be visualized, which is possibly a result of the dense packing of nanostructures on the TEM grid. If the P(EtOx) shell is partially not visible due to overlap and lacking contrast this could explain the size discrepancy between the nanogels. The size was confirmed by dynamic light scattering (DLS) measurements (Table 1). Zeta potential measurements show positive values for all nanogels, which was expected due to the cationic nature of the micellar core. Fluorescein loaded nanogels show a lower zeta potential as compared to DOX loaded samples, which can be explained by the compensation of cationic charges by the anionic nature of fluorescein. This finding is in line with the increased loading of fluorescein quenched nanogels as compared to structures with DOX as a cargo.

The most important requirement for a drug carrier is the site specific release of the drug. As cargo molecules within the produced nanogels are attached *via* imine bonds, which are known to be reversible at pH values below 7, [39] a release within endosomal or lysosomal cellular compartments is likely as previously shown by M. Hruby and co-workers [40]. In order to investigate the stability of the nanogels at 4° C (storage temperature) and 37° C (human body temperature) at a pH value of 7.4, the z-average and the polydispersity index (PDI) as well as the number mean size value of the nanogels was determined using DLS measurements (Supplementary Figure 7). Nanogels were determined to be stable during the entire measurement time of two weeks, revealing no significant changes in size or PDI. Furthermore, it was necessary to determine the possibility of a drug release at a lysosomal pH value of 5. J. S. Basuki *et al.* previously investigated iron oxide nanoparticles that were loaded with DOX *via* pH sensitive imine bond *via* DLS measurements, revealing an increase in the particle size at a pH value of 5, caused by drug release [41]. Since glycine was determined to be essential for cancer cell proliferation and, consequently, is present within tumorous compartments, [42] DLS investigations of the labeled DOX-nanogels were conducted in phosphate buffered saline (PBS) and glycine was added representing a competitive amine to the imine bond (Supplementary Figure 8). While labeled DOX-nanogels did not reveal significant changes in size or PDI at a pH value of 7.4, both increase at a pH value of 5.0. Herein, it is noteworthy that after a second addition of glycine, this trend further increases. This might be beneficial for triggering the endosomal burst, as recently shown in gene transfection applications within our group [43]. In order to obtain additional qualitative information about the release of DOX from the labeled DOX-nanogel, diffusion order spectroscopy (DOSY) NMR measurements were also conducted (Supplementary Figures 9 and 10). Hereby, the diffusion coefficients of labeled DOX-nanogels in NaCl were compared to labeled DOX-nanogels in 150 mM PBS (pH = 5.0), which contained glycine. Pure DOX and glycine were evaluated for comparison. A stacking of the spectra suggests the release of DOX at pH 5.0, while no DOX release could be determined in NaCl (Supplementary Figure 9). Unfortunately, a quantification of the DOX release from the labeled DOX-nanogels was not possible by the applied methods.

In vitro cytotoxicity of nanogels

One major mechanism of DOX is the intercalation into the minor groove of DNA [3]. Therefore, the molecule

must penetrate the barrier of the nucleus to take effect. In order to verify whether DOX loaded nanogels are able to release DOX within cells, the cytotoxicity of labeled DOX-nanogels in comparison to free DOX and DOX-free nanogels was investigated (Figure 2, Supplementary Figure 11). The influence of the materials on the cell viability was probed using two different cell lines. L292 mouse fibroblasts are known to be sensitive to cytotoxic substances [44] and are used in the general assessment of biocompatibility (ISO 10993-5). Cytotoxicity tests were also performed with the human colorectal cancer cells HT-29, due to their ability to form tumors in nude mice and their usage for the nanogel *in vivo* studies that are described in later sections.

Cells were treated with nanogels or pure drug at varying concentrations for 24 h (Supplementary Figure 11) and 72 h (Figure 2), respectively. The amount of DOX loaded nanogels was chosen, so that the concentration of cargo drug matches the concentration of the free drug used for the tests. The concentration of DOX-free nanogels used, was identical to its DOX carrying equivalent in order to investigate the influence of the bare drug delivery system. DOX-free nanogels showed no adverse effects on both cell lines independent of incubation time or concentration. This was expected as P(EtOx) is considered to be biocompatible [13, 23, 24] and proves that neither cationic charges, nor potentially released 6AF influence the metabolism of the cells in a negative way. In contrast free DOX, as well as labeled DOX-nanogels, both show a time- and concentration-dependent decrease in cell viability for both cell lines. The effect is more pronounced for L929 mouse fibroblasts as they are more sensitive to cytotoxic effects. A 72 h treatment of L929 cells (Figure 2A) with labeled DOX-nanogels showed an increased cytotoxicity revealing an IC_{50} value of 0.043 µg mL^{-1} compared to a 24 h treatment (Supplementary Figure 11). Cytotoxicity of pure DOX was found to be lower, with an IC_{50} value of 0.547 µg mL^{-1} (72 h). This might be attributed to an enhanced internalization of the nanogels compared to the free drug [45]. For HT-29 cells (Figure 2B) this difference is less pronounced, with IC_{50} values of labeled DOX-nanogels of 0.752 µg mL^{-1} and pure DOX of 1.998 µg mL^{-1}, respectively. From the reduced viability of cells a release of DOX from the nanogels can be assumed, which is essential for the known toxic effect of the drug.

Cellular uptake and biocompatibility *in vitro*

To investigate whether the improved performance of nanogels is a result of an enhanced cellular uptake, flow cytometry measurements were performed after incubation with labeled DOX-nanogels and free DOX (Figure 3A and Supplementary Figure 12). HT-29 cells were used for the experiments as an *in vitro* cancer model, which was later used for xenograft mouse experiments. The fluorescence of DOX was quantified to determine the amount of DOX internalized within the cells. To elucidate the nature of uptake (energy dependent *vs.* energy independent) the experiments were performed at 37° C and 4° C [46], respectively. For an energy dependent uptake, a significant decrease of the amount of internalized drug would be expected as the metabolism of cells at 4° C is considerably slowed down. Incubation of HT-29 cells with labeled DOX-nanogels or pure DOX at 4° C reduced the cellular uptake compared to an incubation at 37° C. Therefore, cellular uptake seems to be energy-dependent, which would suggest an uptake by endocytosis. Additionally, cells treated with labeled DOX-nanogels possessed a higher fluorescence signal after 24 h treatment at 37° C compared to DOX

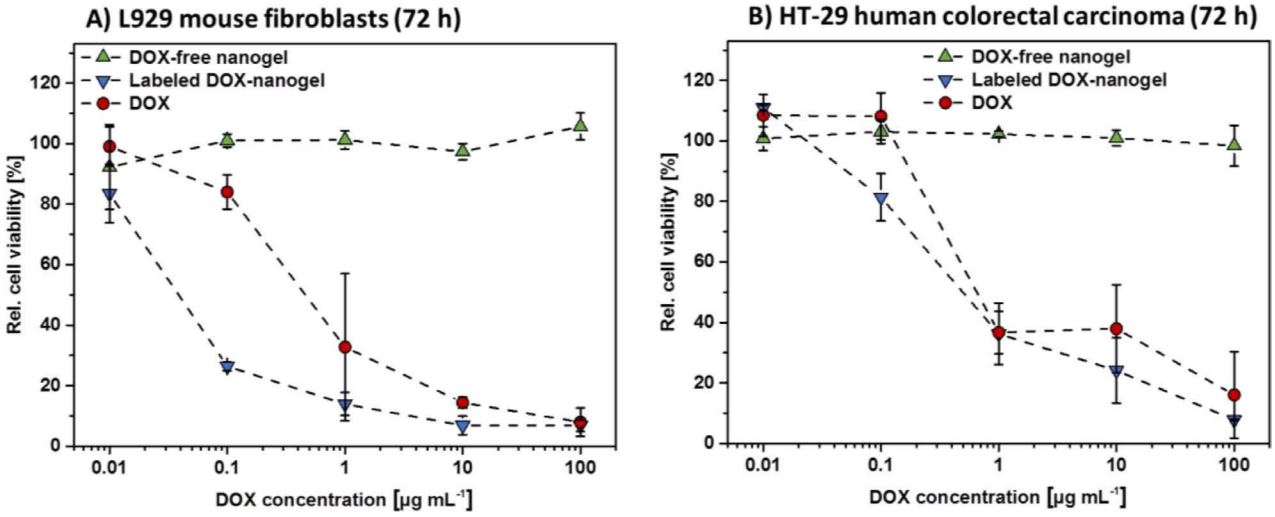

Figure 2: Cytotoxicity of DOX-free nanogels, labeled DOX-nanogels as well as free DOX were determined by XTT assay. L292 mouse fibroblasts (**A**) as well as HT-29 human colorectal carcinoma cells (**B**) were incubated for 72 h with testing substances. DOX-nanogels were used at a concentration where the amount of loaded drug resembles the amount of DOX used per data point (polymer concentration 17 times higher than DOX concentration). DOX-free nanogels were used at the same polymer concentration as DOX-nanogels. Data are expressed as mean ± SD of six determinations.

alone. These findings suggest a higher accumulation of the nanogels in the cells [45, 47] caused by a P-glycoprotein mediated efflux of the pure drug, mostly known from multi drug resistant breast cancer cells [48, 49].

Besides cellular uptake and intracellular drug release, a further requirement of a drug carrier that strives to target cancerous tissue by *i.e.* the EPR effect is a low level of unspecific interaction with *i.e.* healthy tissue or the components of the blood stream. For this reason P(EtOx) was chosen as a shell material as it is well-known that P(EtOx) exhibits stealth properties and shows a blood circulation behavior *in vivo* similar to PEG [27] One prerequisite for a prolonged circulation in the blood stream is the hemocompatibility of the compound comprising the absence of blood clotting as well as lysis of red blood cells. The biocompatibility of labeled DOX-nanogels was tested against sheep blood (Figure 3B and 3C). The compound induced no major aggregation of red blood cells as compared to the positive control branched poly(ethylene imine) (*b*PEI) (25 kDa) as demonstrated in Figure 3B. While the high cationic charge density of PEI results in blood clotting, the cationic charges of the nanogels are shielded within the core of the structure and cannot directly lead to a precipitation of erythrocytes. Also, hemolysis as measured by the absorbance intensity in the blood plasma caused by leakage of hemoglobin release from red blood cells supports the biocompatibility of the drug carrier. While nanogels show slight hemoglobin release of erythrocytes, the total amount as compared to the surfactant Triton-X100 which served as a positive control is well below 2%, which is generally considered as a threshold for hemolytic activity (according to the ASTM F756-00 standard).

To elucidate the uptake and intracellular activity of the nanogels further, their intracellular localization in L929 (Supplementary Figure 13) and HT-29 cells (Figure 4) was investigated using confocal laser scanning microscopy (CLSM). The nucleus was stained using Hoechst 33342 in order to examine its colocalization with DOX, which is indicative for release and activity of the drug. Lysosomal cellular compartments were stained using LysoTracker Green DND-26 and DOX was monitored *via* its fluorescence between λ_{em} = 600 to 650 nm. In addition, the polymer was tracked using the attached Alexafluor label measuring the emission between λ_{em} = 725 to 800 nm (Supplementary Figure 14). A first measurement was conducted after 6 h (Figure 4). Free DOX mainly shows a diffuse localization in the cytosol but is also to a certain extend present in the nucleus. Previous studies already reported a successful uptake and nucleus co-localization of DOX after 3 h incubation time, while the drug in polymersomes exhibited significantly longer times to enter the cell nucleus [47, 50]. In contrast, DOX-nanogels do not show a colocalization with the staining of the nucleus. For the labeled DOX- nanogels the overlap between red and green channel as well as the dotted structure of the signal suggests a lysosomal localization, which indicates an endocytic uptake mechanism [51] The presence of a polymer signal at the same position indicates that these signals represent intact nanogels that have not yet released the drug or been degraded.

Previous studies within our group already showed slower drug accumulation of the drug within the nucleus when using polymeric nanoparticles as drug delivery scaffolds [52]. For this reason, a second set of images was taken after 24 h incubation. After this time, the free drug is mostly localized in the nucleus of the cell. It can be assumed that DOX has either intercalated into the DNA in the nucleus or was excreted by the cells. However, also in the case of labeled DOX-nanogels a release of DOX into the nucleus was observed. The, in comparison to the DOX fluorescence, faint signal of the polymer suggests a partial degradation of the micelles. In addition, the signal is mostly associated with an extra nuclear localization. For longer incubation times it was increasingly difficult to locate intact cells for imaging due to the toxicity of the drug loaded system.

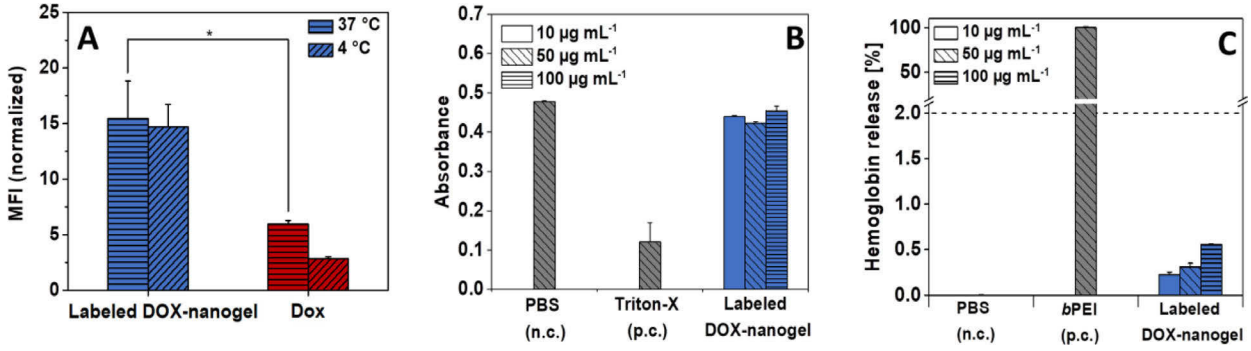

Figure 3: (**A**) Cellular uptake of DOX and labeled DOX-nanogels into HT-29 cells (0.01 mg mL^{-1}) in dependence on the incubation time and temperature. Statistical differences are displayed as $^{*}p < 0.05$ and according to a Student's *t*-test. For amount of fluorescent cells see Supplementary Figure 12. (**B**) Erythrocyte aggregation of DOX-nanogels compared to PBS (negative control) and branched poly(ethylene imine) (positive control) using sheep blood of three different donors. (**C**) Hemolytic activity of DOX-nanogels compared to PBS (negative control) and *b*PEI (positive control) using sheep blood of three different donors.

These results suggest that the uptake of nanogels is partially realized through endocytosis and that the material is degraded intracellularly, which leads to a release of the drug. Toxicity levels of the drug delivery system as well as co-localization studies indicate an accumulation of DOX in the nucleus after delivery to the cell. The kinetic as compared to the free drug is markedly slowed, which is probably associated to the release kinetic from the nanogel. An additional reason could be found in the dependence of the fluorescence of DOX on its environment. It is reported that the fluorescence signal of the drug strongly decreases upon intercalation with genetic material [36] and can be increased by incorporation in membranes or micelles [37]. Consequently, in the case of DOX associated nanogels, the fluorescence of the drug carrier in the cytosol is likely to outshine the intercalated drug. The similar toxicity of both, the free drug and the nanogel, however, suggests an efficient uptake and release of DOX within the cell.

In vivo biocompatibility and biodistribution

The conclusion that can be drawn from the *in vitro* results is that DOX loaded nanogels are relatively stable outside cells but will release the drug once taken up into the endosome, which can later on fuse with a lysosome due to pH sensitivity in acidic compartments. Furthermore, they represent ideal candidates to exploit the EPR effect, since they reveal optimal sizes of approximately 20 nm in diameter as well as the P(EtOx) shell, which will shield them to a certain extend from unspecific interactions. To test this hypothesis *in vivo* studies on male athymic nude mice (Crl:CD1-Foxn1^{nu}) with HT-29 originated tumors were conducted. In comparison to other studies with DOX loaded drug delivery systems [40] a relatively low DOX concentration was used in line with the concept of metronomic chemotherapy. In a first stage of the investigation the general biocompatibility was probed. Tumor-free nude mice were injected *via* tail vein with a single dose of labeled DOX-nanogels (corresponding to a DOX concentration of 0.3 or 1 mg kg^{-1}) or with the same volume of the 0.9 wt% NaCl solution as the negative control. Body weight was monitored for 2 weeks (Supplementary Figure 15). As expected, no negative influence on the development of body weight was detected and no obvious signs of toxicity (changes in physical activity or constitution) were observed for these low DOX

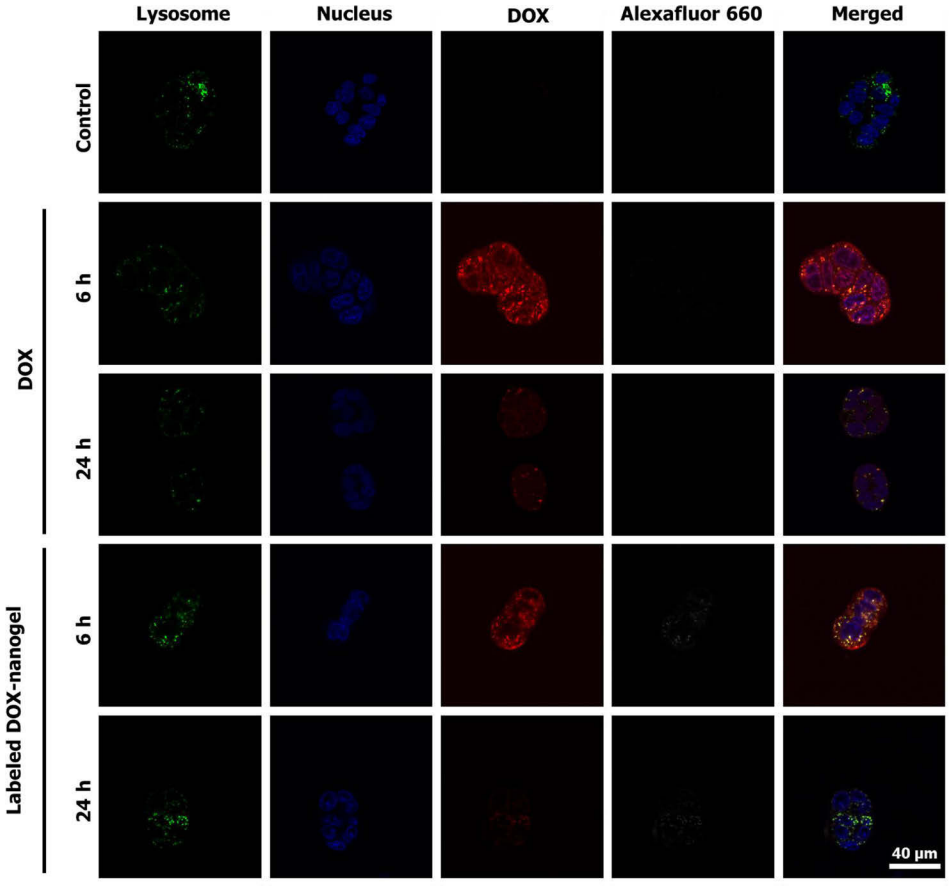

Figure 4: CLSM images of free DOX and labeled DOX-nanogels incubated with HT-29 colorectal carcinoma for 6 h or 24 h. Lysosomal cellular compartments were stained green using LysoTracker Green DND-26 and the nucleus was labeled with Hoechst 33342 (blue). The fluorescence of DOX is depicted in red and the Alexafluor label of the polymer is shown in white.

concentrations. For further analysis the 1 mg kg^{-1} DOX concentration was chosen.

It is already known that the biodistribution of drugs can be influenced by polymeric drug carriers, [53] *i.e.* when equipped with targeting units [54, 55]. Furthermore, the blood clearance and organ accumulation rates of POx-DOX conjugates were determined to be advantageous for cancer therapy, as the conjugates express high blood circulation times of more than 24 h ($t_{1/2}$ DOX = 4 min [56]) and tumor accumulation [40]. For this reason, the biodistribution of the drug carrier within the body was investigated using male nude mice, which received a subcutaneous injection of HT-29 cells (1×10^6 cells in 250 µL) into the flank. When the tumor reached 6 to 8 mm, mice were treated with a single dose of either labeled DOX-nanogels at 1 mg kg^{-1} (150 µl) or of a NaCl solution with the same volume. The mice were sacrificed after predetermined time points (6, 48, and 72 h) and several organs (heart, liver, and kidney) as well as the tumor were excised and prepared for cryo-sections. Sections of mentioned organs were cut to a thickness of 8 µm and embedded in a water-based mounting medium on glass slides. The obtained samples were investigated by CLSM in order to monitor the accumulation of DOX in different body compartments. Histological samples of the tumor clearly show an accumulation of DOX as evident by the inhomogeneous red fluorescence (Figure 5, Supplementary Figure 16). The fluorescence signal is most pronounced 6 h after the injection and is still detectable after 48 h, but to a lesser extent. This phenomenon is also known from other studies. M. Hruby and coworkers determined the radioactive intensity of a ^{125}I-labeled DOX carrier. Here, the mean radioactive intensity decreases significantly between 24 h and 72 h. Furthermore, the main amount of the carrier remains within the blood [40]. Since we used a comparable polymer system, a similar pharmacokinetic behavior might be favorable. Traces of DOX could also be observed in the liver in the form of small aggregates of about 1 µm size. The number of these aggregates increases over time, which points into the direction of either an accumulation in liver tissue or an excretion *via* the organ. Previously, a diminished accumulation of DOX loaded glycolchitosan nanoparticles within the heart could be determined [53]. Also in our study, only minor traces of DOX could be detected in the heart, which is promising, as cardiotoxicity is the most common side effect of DOX. No signal could be detected in the kidney indicating either a fast renal clearance of the nanogels or, more probably, no involvement of the kidney on the excretion of the nanogels. Small polymer-drug conjugates and nanoparticles with an average size below 5 nm are preferably renal excreted [57] and consequently accumulate within the kidney [40]. However, the utilized nanogels within this study possess an average diameter of around 20 nm and for this reason, an accumulation within the liver is more likely [57].

In vivo anti-tumor efficiency

To test the therapeutic efficiency of labeled DOX-nanogels, a xenograft mouse model was established by subcutaneous injection of HT-29 cells. When the tumor volume reached 100–200 mm^3 mice received 6 doses of

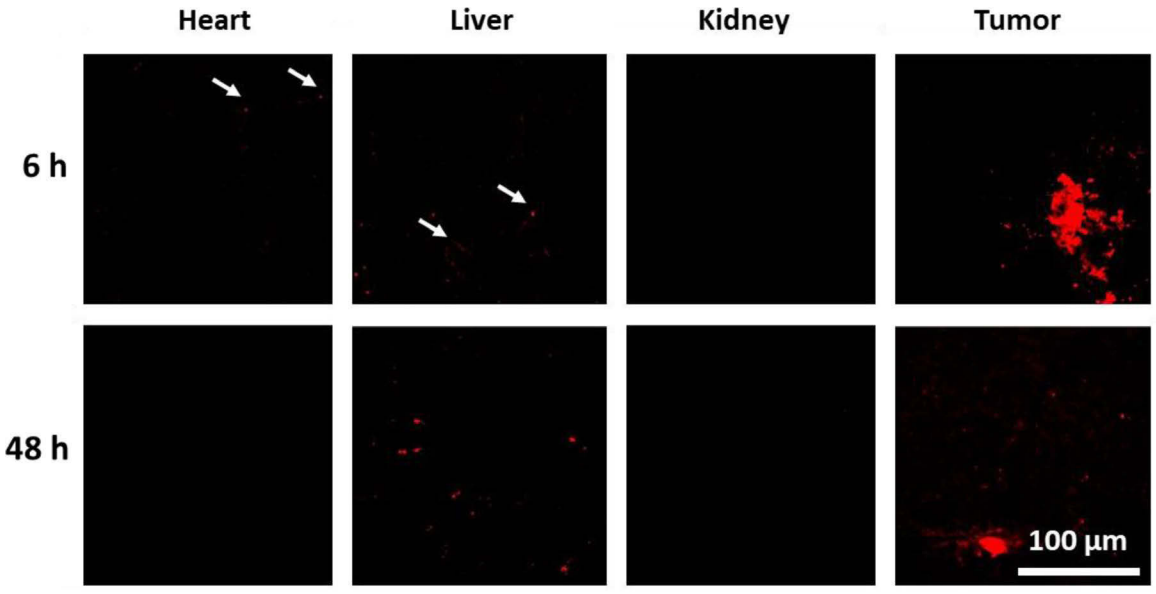

Figure 5: Confocal fluorescence images of histological samples derived from organs of mice that were treated with labeled DOX-nanogels at 1 mg kg^{-1}. Fluorescence of DOX is shown in red. See Supplementary Figure 16 for control sample and 72 h labeled DOX-nanogel sample. See Supplementary Figure 17 for transmitted light images.

drug or control every three days (day 0–15) according to a metronomic schedule. Mice were treated with saline (control), low dose of free DOX (1 mg kg^{-1}), DOX-free nanogels and labeled DOX-nanogels (corresponding to 1 mg kg^{-1} DOX.). The absolute tumor volume was monitored until it reached the termination condition of 1500 mm^3 (Supplementary Figure 18). No negative influence on the development of body weight was detected (Supplementary Figure 19). The individual time course of tumor development for each animal in the different treatment groups (n = 7–8) is shown in Figure 6A. The use of labeled DOX-nanogels reduced the tumor growth of mice compared to a treatment with NaCl, DOX-free nanogels or free DOX. These results are supported by the Kaplan–Meier survival of the HT-29 xenograft model (Figure 6B). Treatment with NaCl or DOX-free nanogels did not slow down the tumor growth, while the median survival time was 37 days for NaCl or 24 days for DOX-free nanogels, respectively. Administration of 1 mg kg^1 DOX also had no effect on tumor inhibition compared to control groups with a median survival time of 39 days (p = 0.202). This might be attributed to the low DOX concentration used in this study. However, even though pure DOX did not seem to be able to reduce tumor progression in the xenograft model, the labeled DOX-nanogels were highly effective. Mice treated with labeled DOX-nanogels had a significant prolonged median survival time of 73 days compared to the NaCl control (p = 0.002) or pure DOX (p = 0.031). This might be explained by the more direct impact of DOX-nanogels on tumor tissue due to the EPR effect. As DOX is shielded within the nanogel, protected by a P(EtOx) shell, a prolonged circulation time can be expected, as shown for linear P(EtOx) [27]. These findings are in agreement with a recently published study by O. Sedlacek *et al.*, prolonging the median survival time of DOX-POx conjugates from 19 to 36 days [40]. However, the utilized DOX dose within the mentioned study was 20 mg kg^1, while our nanogels already possess an effect at an administration of 1 mg kg^1. With an equal or higher toxicity after cellular uptake, as demonstrated by *in vitro* investigations the nanogels are able to interfere with tumor growth more efficiently than the free drug. Combined with their excellent biocompatibility the presented drug carriers proved to be a promising material for cancer therapy.

CONCLUSIONS

Within this report, a straightforward approach to POx based nanogels, covalently loaded with the anti-cancer drug DOX is presented. Nanogels were synthesized *via* cross-linking of a block copolymer micelle with a cationic poly(2-(4-aminobutyl)-2-oxazoline) core and a poly(2-ethyl-2-oxazoline) shell. Cross-linking as well as drug loading was accomplished by pH responsive imine chemistry. Moreover, the amine groups of the drug delivery system allowed the irreversible labeling with a near infra-red fluorescent dye. In *in vitro* studies DOX loaded POx based nanogels showed a toxicity profile comparable to the free drug, while unloaded drug carriers showed no toxicity. The blood compatibility of the drug delivery system was found to be suitable for the envisioned application, therefore the cellular uptake was investigated by flow cytometry and fluorescence microscopy. While the amount of internalized drug was enhanced when incorporated into a nanogel, the release of the drug into

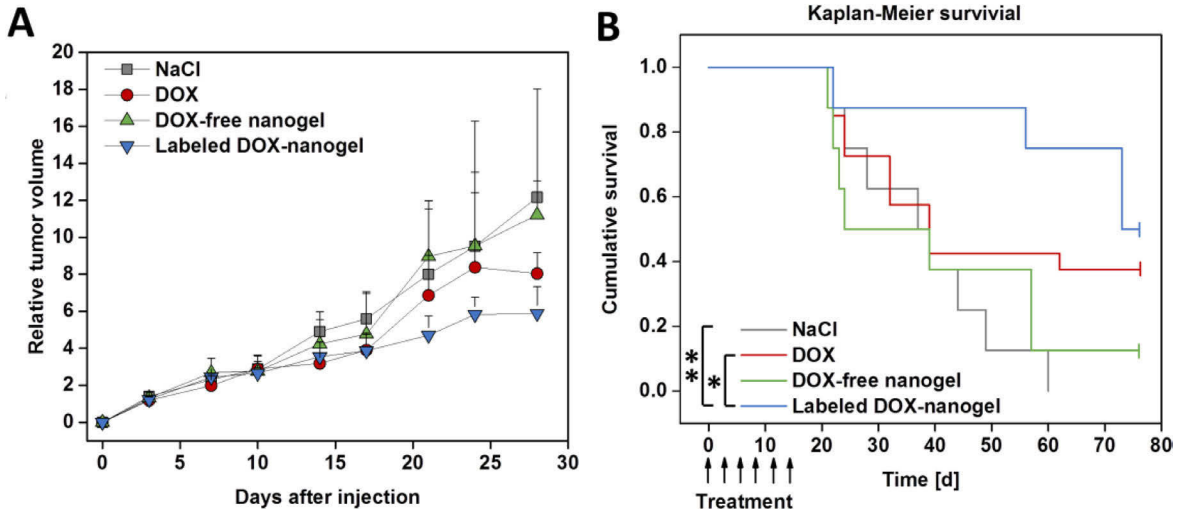

Figure 6: Anti-tumor activity of the DOX-nanogels was evaluated in a xenograft mouse model. Male nude mice received a subcutaneous injection of HT-29 cells into the flank. When tumors reached 100 to 200 mm^3 mice received 6 doses of 0.9 wt% NaCl, DOX (1 mg kg^{-1}), DOX-free nanogel and labeled DOX-nanogel (corresponding to 1 mg kg^{-1} DOX) *via* tail vein injection from day 0 to day 15. (**A**) Development of the relative tumor volume is illustrated over time. Results are indicated as median + semi interquartile range. (**B**) Survival of mice bearing HT-29 derived tumors presented as a Kaplan–Meier survival curve. The individual endpoint of each animal was achieved when the tumor volume reached 1500 mm^3. Statistical differences are displayed as $^*p < 0.05$ and $^{**}p < 0.01$ according to the log-rank test.

the nucleus was delayed compared to free DOX. This is beneficial as a lower amount of drug is required to yield the same effect. Furthermore, the nanogels were shown to be more tumor specific than DOX, which reduces side-effects during therapy. *In vivo* investigation on xenograft mouse models were conducted to assess the ability of the designed system to reduce tumor growth. In combination to the new nanogel-based drug delivery system a metronomic schedule of DOX treatment was applied. Initial studies on healthy mice showed no adverse effects of the DOX-free nanogels or low dosed labeled DOX-nanogels on body weight and behavior. The biodistribution was investigated by microscopy of organs of mice treated with labeled DOX-nanogels and showed a localization of DOX within tumorous tissue, most likely associated to the enhanced permeability and retention (EPR) effect. Finally, the therapeutic efficiency of the POx based drug delivery system was investigated in a survival study of xenograft mice. While the low doses of pure DOX did not show a significant reduction in tumor progression, the metronomic schedule of the labeled DOX-nanogels proved a significant tumor growth inhibition and increase in survival time. Future studies will focus on detailed investigations of the pharmacokinetics of the presented system as well as on studying the biocompatibility of higher drug doses.

MATERIALS AND METHODS

Material and instrumentation

Chemicals and solvents were purchased from Sigma-Aldrich, Merck, Fluka, and Acros. Hoechst 33342 trihydrochloride as well as LysoTracker® Green DND-26 were obtained from Life Technologies (Thermo Fisher, Germany). 2-Ethyl-2-oxazoline (EtOx) and methyl tosylate (MeOTos) were distilled to dryness prior to use. EtOx was dried using barium oxide before distillation. 2-(4-((*tert*-Butoxycarbonyl)amino)butyl)-2-oxazoline (BocOx) was synthesized as described in a previous publication [58]. Consumables for cell culture, like pipettes and cell culture plates (96 well) were obtained from Greiner Bio-one (Austria/ Germany). If not stated otherwise, cell culture media and supplements (L-Glutamin, antibiotics) were obtained from Biochrom (Merck Millipore, Germany).

The Initiator Sixty single-mode microwave synthesizer from Biotage, equipped with a non-invasive IR sensor (accuracy: 2%), was used for polymerizations under microwave irradiation. Microwave vials were heated overnight to 110° C and allowed to cool to room temperature under an argon atmosphere before use. All polymerizations were carried out under temperature control. Size-exclusion chromatography (SEC) measurements of the protected polymers were performed on a Shimadzu system equipped with a SCL-10A system controller, a LC-10AD pump, a RID-10A refractive index detector and a PSS SDV column with chloroform/triethylamine (NEt_3)/*iso*-propanol (94:4:2) as eluent. The column oven was set to 50° C. SEC of the deprotected statistical copolymers was performed on a Shimadzu system with a LC-10AD pump, a RID-10A refractive index detector, a system controller SCL-10A, a degasser DGU-14A, and a CTO-10A column oven using *N,N*-dimethyl acetamide (DMAc) with 2.1 g L^{-1} LiCl as the eluent and the column oven set to 50° C. Poly(styrene) (PS) samples were used as calibration standards for both solvent systems. Proton NMR spectroscopy (^{1}H NMR) measurements were performed at room temperature on a Bruker AC 300 and 400 MHz spectrometer, using $CDCl_3$ or *N,N*-dimethyl formamide (DMF)-D_7 as solvents. Diffusion-ordered spectroscopy (DOSY) NMR measurements were performed at room temperature on a Bruker AC 400 MHz spectrometer using D_2O as the deuterated solvent. The chemical shifts are given in ppm relative to the signal of the residual non-deuterated solvent.

Batch dynamic light scattering (DLS) was performed on a Zetasizer Nano ZS (Malvern Instruments, Herrenberg, Germany). All measurements were performed in folded capillary cells (DTS1071, Malvern Instruments, Herrenberg, Germany). After an equilibration time of 180 s, 3 × 30 s runs were carried out at 4° C, 25° C or 37° C (λ = 633 nm). If not stated explicitly, 25° C was used for measurements. The counts were detected at an angle of 173°. Each measurement was performed in triplicate. Apparent hydrodynamic radii, R_h, were calculated according to the Stokes–Einstein equation.

Laser Doppler velocimetry was used to measure the electrokinetic potential, also known as zeta potential. The measurements were performed on a Zetasizer Nano ZS (Malvern Instruments, Herrenberg, Germany) in folded capillary cells (DTS1071). For each measurement, 15 runs were carried out using the fast-field and slow-field reversal mode at 150 V. Each experiment was performed in triplicate at 25° C. The zeta potential (ζ) was calculated from the electrophoretic mobility (μ) according to the Henry Equation [59]. The Henry coefficient, f(ka), was calculated according to Ohshima [60].

cryoTEM investigations were conducted with a FEI Tecnai G^2 20 at 200 kV acceleration voltage. Specisms were vitrified by a Vitrobot Mark V system on Quantifoil grids (R2/2). The blotting time was 1 s with blotting force offset of 0. The amount of solution was 7 µL. Samples were plunge frozen in liquid ethane and stored under liquid nitrogen until transferred to the Gatan cryo-holder and brought into the microscope. Images were acquired with a 4k × 4k CCD Eagle camera.

Absorbance and fluorescence spectra were recorded using a Tecan Infinite M200 Pro micro plate reader (Crailsheim, Germany) by the use of black well plates with a flat and transparent bottom.

Block copolymer of 2-ethyl-2-oxazoline (EtOx) and 2-(4-((tert-butoxycarbonyl)amino)butyl)-2-oxazoline (BocOx) (P(EtOx-b-BocOx)), (1)

In a microwave vial, EtOx (757 µL, 7.5 mmol), MeTos (16.2 µL, 0.107 mmol) and acetonitrile (3.4 mL) were mixed under inert conditions. After heating in the microwave synthesizer at 140° C for 25 min the vial was introduced into a glove box with nitrogen atmosphere, a sample was taken for NMR and SEC measurements and BocOx (803 µL, 3.2 mmol) was added. The closed vial was heated again in the microwave synthesizer (140° C, 20 min). The solution was precipitated in cold (−80° C, 300 mL) diethyl ether. The white precipitate was filtered and dried in high vacuum (1.4 g, 92%).

^{1}H NMR ($CDCl_3$, 300 MHz) (6): δ = 7.66, (d, 8.1 Hz, 0.019 H, tosylate), 7.14 (d, 8.21 Hz, 0.019 H, tosylate), 3.45 (s, 4 H, backbone), 3.10 (s, 0.58 H, CH_2-CH_2-NH (BocOx)), 2.50–2.15 (m, 1.96 H, CH_2 (EtOx)/CH_2-CH_2-NHBoc), 1.62 (s, 0.52 H, CH_2-CH_2-CH_2 (BocOx)), 1.52 (s, 0.52 H, CH_2-CH_2-CH_2 (BocOx)), 1.42 (s, 2.3 H, CH_3 (BocOx)), 1.21 (s, 2.1 H, CH_3 (EtOx)) ppm.

SEC (eluent: $CHCl_3$/*iso*-propanol/NEt_3, PS-standard): M_n = 8,200 g mol^{-1}, M_w = 9.900 g mol^{-1}, Đ = 1.07.

Deprotection of P(EtOx-b-BocOx) (1) to yield (P(EtOx-b-AmOx), (2)

P(EtOx-*b*-BocOx) (1, 1.3 g) was dissolved in TFA (5 mL) and heated to 60° C for 1 h. After stirring for 12 h at room temperature, the mixture was diluted with 10 mL methanol and precipitated in 400 mL of cold (−80° C) diethyl ether. The precipitate was re-dissolved in methanol (100 mL) and stirred with Amberlyst A21 for 48 h. Subsequently, the solvent was removed, the polymer was dissolved in de-ionized water and freeze dried (−80° C, 0.003 mbar). The polymer was obtained as white powder (1.2 g, 92%).

^{1}H NMR (DMF-D_7, 300 MHz) (2): δ = 4.9 (s, 2.3 H, NH_2), 3.51 (s, 4 H, backbone), 3.07 (s, 0.49 H, CH_2-CH_2-NH_2), 2.44 (m, 2.1 H, CH_2 (EtOx)/CH_2-CH_2-CO (AmOx)), 1.9–1.54 (m, 0.96 H, CH_2-CH_2-CH_2-CH_2 (AmOx)), 1.2 (s, 2,3 H, CH_3 (EtOx)) ppm.

SEC (eluent: DMAc/LiCl, PS-standard): M_n = 13,900 g mol^{-1}, Đ = 1.11.

Labeling of P(EtOx-b-AmOx)(2) using Alexafluor 660, (3)

P(EtOx-*b*-AmOx) (2, 14 mg) was dissolved in DMF (5 mL) and Alexfluor 660® (1 mg, ~1 eq. per macromolecule) as well as triethyl amine (1 µL) were added under stirring. The solution was stirred at room temperature overnight and subsequently precipitated in cold diethyl ether, (300 mL, –80° C). The precipitated was filtered off, dissolved in water and transferred to a dialysis tube (6,000 to 8,000 g mol^{-1} cut off, Spectra/Por®). The polymer was dialysed against water until the solution outside the tube stayed colorless. After freeze drying, the product was obtained as deep blue powder (8 mg, 53%, degree of functionalization = 30%).

SEC (eluent: DMAc/LiCl, PS-standard): M_n = 14,600 g mol^{-1}, Đ = 1.11.

UV/Vis: λ_{Abs} = 660 nm, λ_{Em} (excitation at 600 nm) = 690 nm.

Self-assembly and cross-linking

To create nanostructures, the unlabeled block copolymer (2, 90 mg, 0.006 mmol) or a mixture of the polymers 2 and 3 (9:1, 90 mg, 0.006 mmol) were dissolved in $CHCl_3$, (5 mg mL^{-1}) and stirred for 3 h. Subsequently, glutaraldehyde (30 mg, 0.3 mmol, 1.5 eq. per amine) was added and the solution was stirred another 3 h. With proceeding reaction time the colour of the solution changed from colourless to yellow. To quench the excess of aldehyde functionalities, 6-amino fluorescein (50 mg) or DOX (50 mg) were added, respectively, and stirred for 12 h. Subsequently, the amount of solvent was reduced under an argon stream and the residual was precipitated in 100 mL cold diethyl ether (−80° C). To purify the self-assembled structures from residual capping agent and cross-linker, dialysis in MeOH/water (1:4) was applied using a membrane with a molar mass cut off of 3,500 g mol^{-1} (Roth Zellutrans). After the extraction was finished, the dialysis medium was changed to pure water and the aqueous solution was freeze dried to yield an orange or, in the case of DOX, a red powder.

Determination of dye loading content by absorbance/fluorescence

The absorbance/fluorescence of 6AF loaded nanostructures was investigated under alkaline conditions (1 mol L^{-1} NaOH in water) in diluted solution (0.1 mg mL^{-1}). The absorbance was determined at a wavelength of 490 nm and compared to a dilution series of 6AF in the same aqueous NaOH solution. To the 6AF stock solution a 100 fold excess of glutaraldehyde was added to ensure that only the imine species of 6AF is present. Emission was detected at an excitation wavelength of λ = 450 nm. Micellar samples as well as 6AF calibration exhibit an emission maximum at λ = 510 nm.

DOX conjugated samples were measured in water (0.1 mg mL^{-1}) and compared to a dilution series of DOX in water. All measurements were carried out in a 96 well-plate format with 200 µL per well and double determination for each measuring point. The read out was accomplished using a Tecan Infinite M200 Pro micro plate reader (Crailsheim, Germany).

Determination of the nanogel stability

Labeled DOX-nanogels were dissolved in 150 mM phosphate buffered saline (PBS) buffer (pH = 7.4) and measured by means of size (z-average and number mean) and uniformity (PDI) using DLS measurements as described above. Measurements were conducted at 4° C or 37° C, and nanogel solutions were stored at the respective temperature in between measurements.

Determination of the DOX release

Labeled DOX-nanogels were dissolved in 0.9 wt % NaCl or 150 mM phosphate buffered saline (PBS) buffer (pH = 5.0) containing 200 mM glycine. Qualitative DOX release was determined using DOSY NMR measurements as described above. A sample containing pure DOX dissolved in 0.9 wt % NaCl was used for comparison.

Determination of the cytotoxicity by XTT assay

Cytotoxicity studies were performed with the sensitive mouse fibroblast cell line L929, as recommended by ISO10993-5, and with the human colorectal adenocarcinoma cell line HT-29. The L929 cells were routinely cultured in Dulbecco's modified eagle's medium (DMEM) and HT-29 cells in RPMI 1640 supplemented with 10% fetal calf serum (FCS), 100 U mL^{-1} penicillin and 100 µg mL^{-1} streptomycin at 37° C in a humidified 5% (v/v) CO_2 atmosphere. Cells were seeded at 10^4 cells per well in a 96-well plate and incubated for 24 h, whereas no cells were seeded in the outer wells. Afterwards, the testing substances (nanogels or DOX) at indicated end concentrations were added to the cells and the plates were incubated for further 24 h. Subsequently, a XTT assay (Cell Proliferation Kit II, Roche Diagnostics) was performed according to supplier's information. After a further incubation of 4 h, the absorbance was measured at a wavelength of λ = 450 nm and a reference wavelength of λ = 630 nm with untreated cells on the same well plate serving as negative controls. The negative control was standardized as 0% of metabolism inhibition and referred as 100% viability. Cell viability below 70% was considered indicative of cytotoxicity. Data are expressed as mean ± SD of six determinations. The half maximal inhibitory concentration (IC_{50}) was calculated with the GraphPad Prism Software.

Blood compatibility measurements

To assess the hemolytic activity of the polymer solutions, blood from sheep, collected in heparinized-tubes (Institut für Versuchstierkunde und Tierschutz/Laboratory of Animal Science and Animal Welfare, Friedrich Schiller University Jena), was centrifuged at 4500 × g for 5 min, and the pellet was washed three times with cold 1.5 mmol L^{-1} phosphate buffered saline (PBS, pH 7.4). After dilution with PBS in a ratio of 1:7, aliquots of erythrocyte suspension were mixed 1:1 with the polymer solution and incubated in a water bath at 37° C for 60 min. After centrifugation at 2400 × g for 5 min the hemoglobin release into the supernatant was determined spectrophotometrically using a microplate reader (TECAN Infinite M200 PRO) at λ = 544 nm wavelength. Complete hemolysis (100%) was achieved using 1% Triton X-100 serving as positive control. Thereby, PBS served as negative control (0%). A value less than 2% hemolysis rate was taken as non-hemolytic. Experiments were run in triplicates and were performed with three different blood donors.

For the examination of the erythrocyte aggregation, erythrocytes were isolated as described above. An erythrocytes suspension was mixed with the same volume of polymer solution in a clear flat bottomed 96-well plate. The cells were incubated at 37° C for 2 h, and the absorbance was measured at λ = 645 nm in a microplate reader (TECAN Infinite M200 Pro). 25 kDa *b*PEI (50 µg mL^{-1}) was used as positive control and PBS treated cells served as negative control. Absorbance values of the test solutions lower than negative control were regarded as aggregation. Experiments are the result of triplicates and were performed with three different donor blood batches.

Confocal microscopy

For live CLSM analysis of cell uptake, HT-29 cells (0.2×10^6 cells mL^{-1}) were seeded in glass-bottomed, 4-chamber dishes (CELLVIEW, Greiner Bio-One) and cultured for 24 h. One hour prior to nanogel/ drug treatment, a media change with fresh culture media occurred. Cells were incubated with nanogel or DOX (10 µg mL^{-1}) for 6 h or 24 h, respectively. For examination of nanogel/ drug co-localization with cell organelles, the lysosomes were stained with LysoTracker Green® DND-26 and the cell nuclei were counterstained with Hoechst 33342. Live cell CLSM images were acquired using a Zeiss LSM 880, Elyra PS.1 system (Carl Zeiss, Germany) with excitation wavelengths/emission filters of 405nm/BP 405–480 nm for Hoechst 33342, 488 nm/ BP 505 to 530 nm for LysoTracker® Green DND-26 and 488 nm/BP 585 to 615 nm for DOX and 633 nm/BP 724 to 777 nm for Alexafluor 660®. Images were captured with a 1.4 NA Plan-Apochromat 63 × oil objective and in multitrack mode, enabling single excitation and emission of fluorescence dyes. Co-localization was visualized in overlay images of the multiple channels.

The imaging of histological tissue sections (heart, liver, kidney, tumor) were performed with excitation wavelengths/ emission filters of 488 nm/BP 580 to 615 nm and a 1.4 NA Plan-Apochromat 40 × oil objective.

Cellular uptake studies

The evaluation of the nanogel and free DOX uptake was performed by flow cytometry (FC) measured on a

Beckmann Coulter Cytomics FC-500 equipped with an Uniphase Argon ion laser (488 nm, 20 mW output) and analyzed with the Cytomics CXP software. In brief, HT-29 cells (0.2×10^6 cells mL^{-1} seeded in 24-well plates) were incubated for 6 h and 24 h with labeled labeled DOX-nanogel or free DOX (0.01 mg mL^{-1}) at 37° C or 4° C, respectively. In the case of the 4° C uptake study, cell culture media was supplemented with 15 mM HEPES (4-(2-hydroxyethyl)-1-piperazineethanesulfonic acid, Biochrom, Merck) as buffering agent. Afterwards, cells were harvested by trypsinization and trypan blue (1:10) was added to quench the outer fluorescence. 10^4 cells were measured by flow cytometry, whereby the number of all viable cells, showing signals at 575 nm, were gated. Cells incubated with culture medium only served as control. The experiments were performed at least three times independently.

Animals

Male athymic nude mice (Crl:CD1-Foxn1^{nu}), 6 to 8 weeks age, were purchased by Charles River and were kept in a standard pathogen-free barrier facility accredited by the Association for Assessment and Accreditation of Laboratory Animal Care. All experiments were approved by the local Institutional Animal Care and Use Committee (Jena, 02-011/15). Mice had free access to standard chow and tap water at all times. Body weight and tumor size (measured with a digital caliper) were monitored twice a week. Tumor volume was calculated with the formula $(L \times W^2)/2$, were L is the longest and W the shortest diameter (mm) of the tumor.

In vivo toxicity and biodistribution

Safety evaluation of the nanogels was carried out on healthy male nude mice without tumors, which were randomly assigned to 3 groups (4 mice per group). A single dose (150 µl) of saline (control) or nanogels corresponding to a DOX concentration of 0.3 and 1 mg kg^{-1} body weight were injected *via* tail vein. Body weight, animal constitution and physical activity were monitored for 2 weeks.

For biodistribution experiments HT-29 cells (1×10^6 in 250 µl) were injected subcutaneously into the flank of nude mice. Mice bearing tumors approximately 6–8 mm received a single dose (150 µl) of saline or nanogels with a DOX concentration of 1 mg kg^{-1} *via* tail vein injection. At 6, 48 and 72 h after injection mice were sacrificed and tumor, heart, liver and kidney were excised for further analysis, immediately frozen with liquid nitrogen and stored at –70° C prior to tissue sectioning. Single tissue sections (8 µm thickness) of organs and tumors were cut with a CM 1860 Crystat (Leica Biosystems, Wetzlar, Germany), air-dried on glass slides and embedded in a water-based mounting media (Aquatex, Merck).

Anti-tumor activity *in vivo*

The xenograft model was established by subcutaneous injection of HT-29 cells (1×10^6 in 250 µl) into the flank of male nude mice. When tumors reached a volume of 100–200 mm^3 mice were assigned to 4 treatment groups (10 mice per group) with no significant differences in body weight or tumor volume between the groups. Mice were injected with treatment solutions (saline, 1 mg kg^{-1} DOX, labeled DOX loaded nanogel (6) (corresponding to 1 mg kg^{-1} DOX), and Dox-free nanogel at the same concentration as nanogel 6) *via* tail vein injection on day 0, 3, 6, 9, 11 and 15. Mice were sacrificed when the tumor volume reached 1500 mm^3, which was determined as the individual end point of the survival curve. After sacrifice tumors were excised and weighed. Mice reaching any termination condition (maximum tumor volume, weight loss over 15%, infected wound or limited mobility) before the end of the treatment period were excluded from the survival study.

Statistical analysis

The values represent the mean ± SD (standard deviation). For uptake studies direct comparison of two different groups was done with two-tailed, non-paired Student's *t*-test. A value of $p < 0.05$ was considered as statistically significant. The body weight or tumor volume of the nude mice were tested regarding normal distribution and homogeneity of variances with the IBM SPSS software. Statistical differences were calculated according to a one-way ANOVA. Survival analysis was performed with SPSS and calculated with the Kaplan–Meier method. Significant differences were assessed with the log-rank test. A value of $p < 0.05$ was considered as statistically significant.

Author contributions

T. B. designed and performed the *in vitro* experiments. D. H., M. H., M. N. L. and R. T. designed the *in vivo* experiments. D. H., M. N. L. and R. T. performed the mouse experiments and analyzed the *in vivo* data. S. H. performed the TEM measurements. M. H., D. P., K. K. and U. S. S. designed the nanogels. M. H. synthesized and characterized the nanogels. D. H., M. N. L and M. H. wrote the manuscript, which was edited and approved by all authors.

ACKNOWLEDGMENTS

MNL and TB acknowledge the German Federal Ministry of Education and Research (BMBF, #13N13416 smart-dye-livery, #031A518B Vectura) for funding. CryoTEM investigations were performed at the cryoTEM facilities of the Jena Center for Soft Matter (JCSM). TEM facilities were funded by a grant of the DFG (German

Research Foundation) and the EFRE (European Fund for Regional Development). The LSM880 ELYRA PS.1 was further founded with a grant from the German Research Council (DFG). MH gratefully acknowledges the German Research Foundation (DFG, GZ: HA 7725/1-1) for funding.

CONFLICTS OF INTEREST

The authors declare no conflicts of interest.

REFERENCES

1. Gewirtz D. A critical evaluation of the mechanisms of action proposed for the antitumor effects of the anthracycline antibiotics adriamycin and daunorubicin. Biochem Pharmacol. 1999; 57:727–41.
2. Thorn CF, Oshiro C, Marsh S, Hernandez-Boussard T, McLeod H, Klein TE, Altman RB. Doxorubicin pathways: pharmacodynamics and adverse effects. Pharmacogenet. Genom. 2011; 21:440–6.
3. Yang F, Teves SS, Kemp CJ, Henikoff S. Doxorubicin, DNA torsion, and chromatin dynamics. BBA - Reviews on Cancer. 2014; 1845:84–9.
4. Lipshultz SE, Scully RE, Lipsitz SR, Sallan SE, Silverman LB, Miller TL, Barry EV, Asselin BL, Athale U, Clavell LA, Larsen E, Moghrabi A, Samson Y, et al. Assessment of dexrazoxane as a cardioprotectant in doxorubicin-treated children with high-risk acute lymphoblastic leukaemia: long-term follow-up of a prospective, randomised, multicentre trial. Lancet Oncol. 2010; 11:950–61.
5. He Z, Wan X, Schulz A, Bludau H, Dobrovolskaia MA, Stern ST, Montgomery SA, Yuan H, Li Z, Alakhova D, Sokolsky M, Darr DB, Perou CM, et al. A high capacity polymeric micelle of paclitaxel: Implication of high dose drug therapy to safety and *in vivo* anti-cancer activity. Biomaterials. 2016; 101:296–309.
6. Luxenhofer R, Han Y, Schulz A, Tong J, He Z, Kabanov AV, Jordan R. Poly(2-oxazoline)s as Polymer Therapeutics. Macromol Rapid Commun. 2012; 33:1613–31.
7. Bertrand N, Wu J, Xu X, Kamaly N, Farokhzad OC. Cancer nanotechnology: The impact of passive and active targeting in the era of modern cancer biology. Adv Drug Deliv Rev. 2014; 66:2–25.
8. Eckmann DM, Composto RJ, Tsourkas A, Muzykantov VR. Nanogel carrier design for targeted drug delivery. J Mater Chem B. 2014; 2:8085–97.
9. Pathak RK, Wen R, Kolishetti N, Dhar S. A prodrug of two approved drugs, cisplatin and chlorambucil, for chemo war against cancer. Mol Cancer Thera. 2017; 16:625–36.
10. Wen R, Banik B, Pathak RK, Kumar A, Kolishetti N, Dhar S. Nanotechnology inspired tools for mitochondrial dysfunction related diseases. Adv Drug Deliv Rev. 2016; 99:52–69.
11. Wen R, Dhar S. Turn up the cellular power generator with vitamin E analogue formulation. Chem Sci. 2016; 7:5559–67.
12. Sultana F, Imran-Ul-Haque M, Arafat M, Sharmin S. An Overview of Nanogel Drug Delivery System. J Appl Pharm Sci. 2013; 3:95–105.
13. Kronek J, Kroneková Z, Lustoň J, Paulovičová E, Paulovičová L, Mendrek B. *In vitro* bio-immunological and cytotoxicity studies of poly(2-oxazolines). J Mater Sci Mater Med. 2011; 22:1725–34.
14. Eskow Jaunarajs KL, Standaert DG, Viegas TX, Bentley MD, Fang Z, Dizman B, Yoon K, Weimer R, Ravenscroft P, Johnston TH, Hill MP, Brotchie JM, Moreadith RW. Rotigotine polyoxazoline conjugate SER-214 provides robust and sustained antiparkinsonian benefit. Mov Disord. 2013; 28:1675–82.
15. Wilson P, Chun Ke P, Davis TP, Kempe K. Poly(2-oxazoline)-based micro- and nanoparticles: A review. Eur Polym J. 2017; 88:486–515.
16. Chen F, Zhang J, Wang L, Wang Y, Chen M. Tumor pHe-triggered charge-reversal and redox-responsive nanoparticles for docetaxel delivery in hepatocellular carcinoma treatment. Nanoscale. 2015; 7:15763–79.
17. Dams ETM, Laverman P, Oyen WJG, Storm G, Scherphof GL, van der Meer JWM, Corstens FHM, Boerman OC. Accelerated Blood Clearance and Altered Biodistribution of Repeated Injections of Sterically Stabilized Liposomes. J Pharmacol Exp Ther. 2000; 292:1071–9.
18. Chanan-Khan A, Szebeni J, Savay S, Liebes L, Rafique NM, Alving CR, Muggia FM. Complement activation following first exposure to pegylated liposomal doxorubicin (Doxil®): possible role in hypersensitivity reactions. Ann Oncol. 2003; 14:1430–7.
19. Armstrong JK, Hempel G, Koling S, Chan LS, Fisher T, Meiselman HJ, Garratty G. Antibody against poly(ethylene glycol) adversely affects PEG-asparaginase therapy in acute lymphoblastic leukemia patients. Cancer. 2007; 110:103–11.
20. Rudmann DG, Alston JT, Hanson JC, Heidel S. High Molecular Weight Polyethylene Glycol Cellular Distribution and PEG-associated Cytoplasmic Vacuolation Is Molecular Weight Dependent and Does Not Require Conjugation to Proteins. Toxicol Pathol. 2013; 41:970–83.
21. Bendele A, Seely J, Richey C, Sennello G, Shopp G. Short Communication: Renal Tubular Vacuolation in Animals Treated with Polyethylene-Glycol-Conjugated Proteins. Toxicol Sci. 1998; 42:152–7.
22. Baumann A, Tuerck D, Prabhu S, Dickmann L, Sims J. Pharmacokinetics, metabolism and distribution of PEGs and PEGylated proteins: quo vadis? Drug Discov Today. 2014; 19:1623–31.
23. Luxenhofer R, Sahay G, Schulz A, Alakhova D, Bronich TK, Jordan R, Kabanov AV. Structure-property relationship

in cytotoxicity and cell uptake of poly(2-oxazoline) amphiphiles. J Controlled Release. 2011; 153:73–82.

24. Kronek J, Paulovičová E, Paulovičová L, Kroneková Z, Lustoň J. Immunomodulatory efficiency of poly(2-oxazolines). J Mater Sci Mater Med. 2012; 23:1457–64.
25. Zalipsky S, Hansen CB, Oaks JM, Allen TM. Evaluation of blood clearance rates and biodistribution of poly(2-oxazoline)-grafted liposomes. J Pharm Sci. 1996; 85:133–7.
26. Woodle MC, Engbers CM, Zalipsky S. New Amphipatic Polymer-Lipid Conjugates Forming Long-Circulating Reticuloendothelial System-Evading Liposomes. Bioconjugate Chem. 1994; 5:493–6.
27. Wyffels L, Verbrugghen T, Monnery BD, Glassner M, Stroobants S, Hoogenboom R, Staelens S. μPET imaging of the pharmacokinetic behavior of medium and high molar mass 89Zr-labeled poly(2-ethyl-2-oxazoline) in comparison to poly(ethylene glycol). J Controlled Release. 2016; 235:63–71.
28. Glassner M, Palmieri L, Monnery BD, Verbrugghen T, Deleye S, Stroobants S, Staelens S, wyffels L, Hoogenboom R. The Label Matters: μPET Imaging of the Biodistribution of Low Molar Mass 89Zr and 18F-Labeled Poly(2-ethyl-2-oxazoline). Biomacromolecules. 2016.
29. Guillerm B, Monge S, Lapinte V, Robin JJ. How to Modulate the Chemical Structure of Polyoxazolines by Appropriate Functionalization. Macromol Rapid Commun. 2012; 33:1600–12.
30. Hartlieb M, Kempe K, Schubert US. Covalently cross-linked poly(2-oxazoline) materials for biomedical applications - from hydrogels to self-assembled and templated structures. J Mater Chem B. 2015; 3:526–38.
31. Hartlieb M, Pretzel D, Wagner M, Hoeppener S, Bellstedt P, Gorlach M, Englert C, Kempe K, Schubert US. Core cross-linked nanogels based on the self-assembly of double hydrophilic poly(2-oxazoline) block copolymers. Journal of Materials Chemistry B. 2015; 3:1748–59.
32. Hartlieb M, Bus T, Kübel J, Pretzel D, Hoeppener S, Leiske MN, Kempe K, Dietzek B, Schubert US. Tailoring Cellular Uptake and Fluorescence of Poly(2-oxazoline)-Based Nanogels. Bioconjugate Chem. 2017; 28:1229–35.
33. Xin Y, Yuan J. Schiff`s base as a stimuli-responsive linker in polymer chemistry. Polym Chem. 2012; 3:3045–55.
34. Kareva I, Waxman DJ, Lakka Klement G. Metronomic chemotherapy: An attractive alternative to maximum tolerated dose therapy that can activate anti-tumor immunity and minimize therapeutic resistance. Cancer Lett. 2015; 358:100–6.
35. Romiti A, Cox MC, Sarcina I, Di Rocco R, D'Antonio C, Barucca V, Marchetti P. Metronomic chemotherapy for cancer treatment: a decade of clinical studies. Cancer Chemother Pharmacol. 2013; 72:13–33.
36. Fiallo M, Laigle A, Borrel MN, Garnier-Suillerot A. Accumulation of degradation products of doxorubicin and pirarubicin formed in cell culture medium within sensitive and resistant cells. Biochem Pharmacol. 1993; 45:659–65.
37. Mohan P, Rapoport N. Doxorubicin as a Molecular Nanotheranostic Agent: Effect of Doxorubicin Encapsulation in Micelles or Nanoemulsions on the Ultrasound-Mediated Intracellular Delivery and Nuclear Trafficking. Mol Pharm. 2010; 7:1959–73.
38. Hartlieb M, Pretzel D, Wagner M, Hoeppener S, Bellstedt P, Görlach M, Englert C, Kempe K, Schubert US. Core cross-linked nanogels based on the self-assembly of double hydrophilic poly(2-oxazoline) block copolymers. J Mater Chem B. 2015; 3:1748–1759.
39. Meyer CD, Joiner CS, Stoddart JF. Template-directed synthesis employing reversible imine bond formation. Chem Soc Rev. 2007; 36:1705–23.
40. Sedlacek O, Monnery BD, Mattova J, Kucka J, Panek J, Janouskova O, Hocherl A, Verbraeken B, Vergaelen M, Zadinova M, Hoogenboom R, Hruby M. Poly(2-ethyl-2-oxazoline) conjugates with doxorubicin for cancer therapy: *In vitro* and *in vivo* evaluation and direct comparison to poly [N-(2-hydroxypropyl)methacrylamide] analogues. Biomaterials. 2017; 146:1–12.
41. Basuki JS, Duong HT, Macmillan A, Erlich RB, Esser L, Akerfeldt MC, Whan RM, Kavallaris M, Boyer C, Davis TP. Using fluorescence lifetime imaging microscopy to monitor theranostic nanoparticle uptake and intracellular doxorubicin release. ACS nano. 2013; 7:10175–89.
42. Amelio I, Cutruzzolá F, Antonov A, Agostini M, Melino G. Serine and glycine metabolism in cancer. Trends Biochem Sci. 2014; 39:191–8.
43. Leiske MN, Sobotta FH, Hoeppener S, Brendel JC, Traeger A, Schubert US. How to tune the gene delivery and biocompatibility of poly(2-(4-aminobutyl)-2-oxazoline) by self and co assembly. Biomacromolecules. 2017. In press. DOI: 10.1021/acs.biomac.7b01535.
44. Thonemann B, Schmalz G, Hiller KA, Schweikl H. Responses of L929 mouse fibroblasts, primary and immortalized bovine dental papilla-derived cell lines to dental resin components. Dent Mater. 2002; 18:318–23.
45. Misra R, Sahoo SK. Intracellular trafficking of nuclear localization signal conjugated nanoparticles for cancer therapy. Eur J Pharm Sci. 2010; 39:152–63.
46. Cai S, Alhowyan AAB, Yang Q, Forrest WCM, Shnayder Y, Forrest ML. Cellular uptake and internalization of hyaluronan-based doxorubicin and cisplatin conjugates. J Drug Target. 2014; 22:648–57.
47. Yildirim T, Traeger A, Sungur P, Hoeppener S, Kellner C, Yildirim I, Pretzel D, Schubert S, Schubert US. Polymersomes with Endosomal pH-Induced Vesicle-to-Micelle Morphology Transition and a Potential Application for Controlled Doxorubicin Delivery. Biomacromolecules. 2017; 18:3280–90.
48. Kubota T, Furukawa T, Tanino H, Suto A, Otani Y, Watanabe M, Ikeda T, Kitajima M. Resistant mechanisms of

anthracyclines — pirarubicin might partly break through the P-glycoprotein-mediated drug-resistance of human breast cancer tissues. Breast Cancer. 2001; 8:333–8.

49. Mi Y, Lou L. ZD6474 reverses multidrug resistance by directly inhibiting the function of P-glycoprotein. Br J Cancer. 2007; 97:934–40.

50. Upadhyay KK, Bhatt AN, Mishra AK, Dwarakanath BS, Jain S, Schatz C, Le Meins JF, Farooque A, Chandraiah G, Jain AK, Misra A, Lecommandoux S. The intracellular drug delivery and anti tumor activity of doxorubicin loaded poly(γ-benzyl l-glutamate)-b-hyaluronan polymersomes. Biomaterials. 2010; 31:2882–92.

51. Upadhyay KK, Meins JFL, Misra A, Voisin P, Bouchaud V, Ibarboure E, Schatz C, Lecommandoux S. Biomimetic Doxorubicin Loaded Polymersomes from Hyaluronan-block-Poly(γ-benzyl glutamate) Copolymers. Biomacromolecules. 2009; 10:2802–8.

52. Yildirim T, Traeger A, Preussger E, Stumpf S, Fritzsche C, Hoeppener S, Schubert S, Schubert US. Dual Responsive Nanoparticles from a RAFT Copolymer Library for the Controlled Delivery of Doxorubicin. Macromolecules. 2016; 49:3856–68.

53. Hyung Park J, Kwon S, Lee M, Chung H, Kim JH, Kim YS, Park RW, Kim IS, Bong Seo S, Kwon IC, Young Jeong S. Self-assembled nanoparticles based on glycol chitosan bearing hydrophobic moieties as carriers for doxorubicin: *In vivo* biodistribution and anti-tumor activity. Biomaterials. 2006; 27:119–26.

54. Gao Y, Li Y, Li Y, Yuan L, Zhou Y, Li J, Zhao L, Zhang C, Li X, Liu Y. PSMA-mediated endosome escape-accelerating polymeric micelles for targeted therapy of prostate cancer and the real time tracing of their intracellular trafficking. Nanoscale. 2015; 7:597–612.

55. Qiu LY, Yan L, Zhang L, Jin YM, Zhao QH. Folate-modified poly(2-ethyl-2-oxazoline) as hydrophilic corona in polymeric micelles for enhanced intracellular doxorubicin delivery. Int J Pharm. 2013; 456:315–24.

56. Seymour LW, Ulbrich K, Strohalm J, Kopeček J, Duncan R. The pharmacokinetics of polymer-bound adriamycin. Biochem Pharmacol. 1990; 39:1125–31.

57. Wang J, Masehi-Lano JJ, Chung EJ. Peptide and antibody ligands for renal targeting: nanomedicine strategies for kidney disease. Biomater Sci. 2017; 5:1450–9.

58. Hartlieb M, Pretzel D, Kempe K, Fritzsche C, Paulus RM, Gottschaldt M, Schubert US. Cationic poly(2-oxazoline) hydrogels for reversible DNA binding. Soft Matter. 2013; 9:4693–704.

59. Delgado AV, Gonzalez-Caballero F, Hunter RJ, Koopal LK, Lyklema J. Measurement and interpretation of electrokinetic phenomena. J Colloid Interface Sci. 2007; 309:194–224.

60. Ohshima H. A Simple Expression for Henry‘s Function for the Retardation Effect in Electrophoresis of Spherical Colloidal Particles. J Colloid Interface Sci. 1994; 168:269–71.

Publication P5

Comparison of random and gradient amino functionalized poly(2-oxazoline)s: Can the transfection efficiency be tuned by the macromolecular structure?

D. Hertz[‡], M. N. Leiske[‡], T. Wloka, A. Traeger, M. Hartlieb, M. M. Kessels, S. Schubert, B. Qualmann, U. S. Schubert, *J. Polym. Sci., Part A: Polym. Chem.* **2018**, in press. DOI: 10.1002/pola.29000.

The paper as well as the supporting information (free of charge) is available online: doi.org/10.1002/pola.29000.

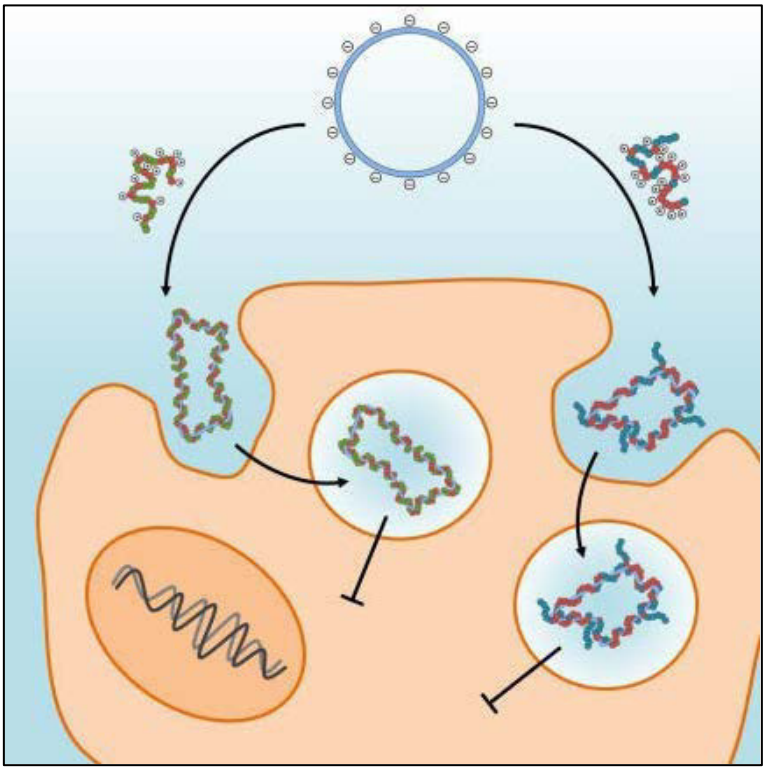

[‡]Equal contribution.

Comparison of random and gradient amino functionalized poly(2-oxazoline)s: Can the transfection efficiency be tuned by the macromolecular structure?

David Hertz,[a,b,#] Meike N. Leiske,[b,c,#] Thomas Wloka,[b,c] Anja Traeger,[b,c] Matthias Hartlieb,[b,c,¶] Michael M. Kessels,[a] Stephanie Schubert,[b,d] Britta Qualmann,[a,b,*] Ulrich S. Schubert[b,c,*]

[a]Institute for Biochemistry I, Jena University Hospital – Friedrich Schiller University Jena, Nonnenplan 2, 07743 Jena, Germany

[b]Jena Center for Soft Matter (JCSM), Friedrich Schiller University Jena, Philosophenweg 7, 07743 Jena, Germany

[c]Laboratory of Organic and Macromolecular Chemistry (IOMC), Friedrich Schiller University Jena, Humboldtstraße 10, 07743 Jena, Germany

[d]Institute of Pharmacy, Pharmaceutical Technology, Friedrich Schiller University Jena, Otto-Schott-Straße 41, 07745 Jena, Germany

[¶]Current address: Institute of Biomaterial Science, Helmholtz-Zentrum Geesthacht, Kantstr. 55, 14513 Teltow, Germany

[#]D. Hertz and M. N. Leiske contributed equally to this work.

Correspondence to: B. Qualmann and Ulrich S. Schubert (E-mail: *britta.qualmann@med.uni-jena.de; ulrich.schubert@uni-jena.de*)

The Supporting Information is available free of charge in the Wiley Online Library.

ABSTRACT

Poly(ethylene imine) can be considered as the gold standard for DNA delivery into cells *in vitro*, but severe cytotoxic side-effects and inapplicability for targeted approaches *in vivo* urgently call for the design of new gene carriers. Since poly(2-oxazoline)s (P(Ox)s) can be easily synthesized and modified, this polymer class might be ideal for the optimization of polymeric transfection processes. The utilization of 2-methyl-2-oxazoline (MeOx) and 2-ethyl-2-oxazoline (EtOx) is also known to be beneficial because these monomers were suggested to overcome solubility issues, mediate stealth behavior and, consequently, facilitate a reduction of cytotoxicity. A series of amino (AmOx) functionalized P(Ox) copolymers with either MeOx (gradient copolymers) or EtOx (random copolymers) was synthesized, deprotected and biochemically characterized regarding cytotoxicity, polyplex formation ability, cellular uptake and transfection efficiency.
Polymers with percentages of AmOx higher than 35 mol% showed stable polyplex formation but also an increase in cytotoxicity. All elucidated P(Ox)s revealed a poor transfection efficiency in both L929 and Hepa1-6 cell lines. However, the investigations contribute to the understanding of the influence of stealth units (MeOx and EtOx) and their distribution within the polymer chain on selected properties of polyplexes and describe characteristics of amino functionalized P(Ox)s in different cell lines.

KEYWORDS: Poly(2-oxazoline); DNA interaction; cell uptake; random and gradient copolymers; flow cytometry

INTRODUCTION

For the introduction of regulative RNAs such as small interfering RNA (siRNA) or short hairpin RNA (shRNA) into cells, delivery vectors represent attractive strategies enabling the treatment of *e.g.* cancer using gene therapy.[1-3] Since free genetic material is rapidly degraded *in vivo*,[4-7] efficient carriers preventing the degradation of nucleic acids are indispensable. These carriers require properties for the association with the plasma membrane of target cells and for internalization into the cytosol.[8] Beyond these requirements there are further intracellular hurdles, such as the escape from the endosomal pathway, trafficking through the cytosol, and, in the case of shRNA delivery, entry into the nucleus.[2, 9]

In general, carriers for nucleic acids complexation and transport are subdivided into viral and non-viral carriers.[10, 11] In contrast to viral carriers, which are highly efficient, but induce mutagenic and immunogenic responses,[12, 13] non-viral carriers, in particular cationic polymers, are safer, cheaper and simpler in production and storage.[14, 15] Furthermore, polymers can be easily modified and exhibit a high loading capacity of genetic material. One of the main disadvantages of polymers is the lower efficiency of transfection in comparison to viral carriers.[16] A reason for this problem is the disability of some polyplexes to escape from endosomal vesicles leading to a degradation of nucleic acids by lysosomal enzymes.[17] Polymers with efficient release from endosomes possess a pK_a value in the

physiological pH range showing buffer properties for acidic endosomal vesicles.[18] Additionally, a high transfection efficiency of polymeric vectors usually goes hand-in-hand with pronounced cytotoxicity.[19, 20] Consequently, the previously mentioned aspects are the major targets of research to improve non-viral carriers. Besides polyamides like poly(L-lysine) or poly(methacrylate)s[21, 22], PEI can be considered as the polymeric gold standard for DNA delivery into cells.[23] Both types of PEI, namely the linear (*l*-PEI) and the branched (*b*-PEI) form, possess high transfection efficiencies in various cell lines, but also severe cytotoxic effects and undesired non-specific interactions *in vitro* and *in vivo*.[19, 20] To reduce the cytotoxicity and enhance the delivery capacity, new carriers have to be designed. Since the well-defined *l*-PEI is synthesized by acidic or basic hydrolysis of (P(Ox)s),[24] commercially available *l*-PEI usually contain 5 to 10 mol% non-hydrolyzed P(EtOx) units.[25] P(EtOx) and P(MeOx) of various molar masses were already investigated *in vitro* in terms of biocompatibility, showing no harmful effects on cells in cytotoxicity assays or hemolysis.[26, 27] For this reason, it might be interesting to elucidate amino functionalized P(Ox)s with EtOx or MeOx in terms of transfection abilities and biocompatibility.

P(Ox)s can be produced *via* the cationic ring-opening polymerization (CROP) of 2-oxazolines, which was first described in the 1960's by four independent research groups.[28-31] The introduction of the microwave technique in 2004 reduced the reaction times from several days to minutes, by keeping the controlled character of the CROP and resulting in well-defined polymers.[32] The application of functional initiators or terminating agents results in α- and ω-functionalized P(Ox)s.[33-35] Furthermore, 2-oxazolines can be easily modified in the 2-position, leading to a high chemical versatility for structural modification through copolymerization. The utilization of the hydrophilic monomers MeOx and EtOx results in water-soluble polymers, which also mediate stealth behavior and facilitate the reduction of cytotoxicity.[33, 36] In 2015, our group showed advantages of amino functionalized P(Ox)s towards *l*-PEI, by using a library approach.[34] They synthesized allyl functionalized P(Ox) precursors, which were amino modified *via* thiol-ene click-reactions, to obtain different amino functionalized P(Ox)s. Some of the resulting polymers showed very good transfection efficiencies while maintaining a good biocompatibility. However, the use of proper protection groups enables the possibility to directly polymerize different monomers with a high variety of functional groups, such as aldehydes,[37, 38] carboxylic acids[39] and amino groups.[40, 41] The dependence of the polymerization constant (k_p) of 2-oxazolines on the substituent in 2-position has been recently summarized.[42] Due to the different k_p values reported, copolymerization of EtOx with the amino functionalized monomer 2-(4-((*tert*-butoxycarbonyl)amino)butyl)-2-oxazoline (BocOx) might result in another monomer distribution than a copolymerization of MeOx and BocOx.

Comparison of random and gradient copolymers regarding DNA complexation and cellular interaction are still largely unexplored. However, S. Filippov *et al.* could show that block and gradient copoly(2-oxazoline) micelles show a different behavior with a uniform density profile of the core in block copolymers and a higher density in the outer part of the core for gradient copolymers.[43] This could have a significant influence on polyplex formation and cell interaction, in particular with immune cells, regarding a higher shielding capacity in block copolymers in comparison with gradient polymers.

In the present study, a series of amino functionalized P(Ox) copolymers with either MeOx or EtOx representing the stealth unit and different amounts of the Boc-protected amino functionalized comonomer BocOx was synthesized, deprotected and fully characterized. Polyplex formation using plasmid DNA (pDNA) in a wide range of nitrogen-to-phosphate group (N/P) ratios as well as the structure, stability, and cytotoxicity of

polyplexes were studied. In addition, polyplex uptake and transfection efficiency were determined by flow cytometry and confocal laser scanning microscopy (CLSM).

EXPERIMENTAL

Materials and Instrumentation

EtOx, MeOx and methyl tosylate (MeTos) were purchased from Sigma-Aldrich and were distilled to dryness over calcium hydride (VWR) under argon atmosphere prior to usage. Triethylamine (TEA, Sigma-Aldrich) was distilled under argon atmosphere prior to usage. Acetonitrile was obtained from a solvent purification system (MB-SPS-800, MBraun) and stored under argon. All other solvents used were obtained from standard suppliers. Trifluoroacetic acid (TFA, Sigma-Aldrich), Amberlyst® A21 (Sigma-Aldrich), ethidium bromide (EtBr) solution (10 mg mL^{-1}, Carl Roth), YOYO-1 iodide (Thermo Fisher), LysoTracker Red DND-99 (Thermo Fisher) and Hoechst 33342 trihydrochloride (Thermo Fisher) were used as obtained. Cell culture media and antibiotics were obtained from Biochrom. Plasmid pRNAT-H1.1 (Genscript) was isolated with the Midi Plasmid Kit (Qiagen). Cell Proliferation Kit I (MTT), heparin sodium salt and trypan blue solution (0.4%) were purchased from Sigma-Aldrich.

l-PEI and BocOx were synthesized according to literature procedures.[25, 33, 44]

For the general characterization of *l*-PEI, please refer to T. Bus *et al*..[33]

Polymerization reactions of 2-oxazolines were performed under microwave irradiation, using an Initiator Sixty single-mode microwave synthesizer from Biotage, equipped with a noninvasive IR sensor (accuracy: 2%). Microwave vials were stored overnight at 100 °C under vacuum and allowed to cool to room temperature (RT) under argon before usage. Polymerizations were performed under temperature control. According to the polymer characteristics, size exclusion chromatography (SEC) measurements of the polymers were performed on different systems and noted in the respective part.

SEC measurements of the polymerization kinetics were performed on an Agilent 1200 series system, equipped with a PSS degasser, a G1329A pump, a PSS GRAM guard/30/1000 Å with 10 µm particle size and a G1362 refractive index (RI) detector. Dimethylacetamide (DMAc) containing 0.21% LiCl served as eluent. The column oven was set to 40 °C at a flow rate of 1 mL min^{-1} and poly(styrene) (PS, 400 to 1,000,000 g mol^{-1}) served as the calibration.

SEC of the Boc-protected copolymer precursors was conducted on a Shimadzu system equipped with a SCL-10A VP controller, GDU-14A degasser and a LC-10AD VP pump, a PSS GRAM guard/30/1000 Å with 10 µm particle size and a RID-10A RI detector. DMAc containing 0.21% LiCl served as eluent. The column oven was set to 40 °C using a flow rate of 1 mL min^{-1} and PS (400 to 1,000,000 g mol^{-1}) served as the calibration.

SEC of the Boc-protected P($EtOx_3$-*b*-$BocOx_{157}$) was performed on a Shimadzu system equipped with a CBM-20A controller, GDU-14A degasser and a LC-10AD VP pump, a PSS SDV guard/linear S column with 5 µm particle size and a RID-10A RI detector. $CHCl_3$-*iso*-propanol (*i*-PrOH)-NEt_3 (94:2:4) served as eluent. The column oven was set to 40 °C using a flow rate of 1 mL min^{-1}. PS (400 to 100,000 g mol^{-1}) served as the calibration.

SEC of the deprotected, amino functionalized polymers was conducted on a Jasco system equipped with a DG-980-50 degasser and a PU-980 pump, PSS SUPREMA-MAX guard/300 Å column with 10 µm particle size and a RI-930 RI detector. 0.3% (v/v) TFA containing 0.1 M NaCl served as aqueous eluent. The column oven was set to 30 °C using a flow rate of 1 mL min^{-1}. Poly(2-vinylpyridine) (P2VP, 1,300 to 81,000 g mol^{-1}) served as the calibration.

Proton NMR spectroscopy (^{1}H-NMR) was performed at RT using a Bruker Avance I 300 MHz spectrometer, utilizing either $CDCl_3$ or D_2O as solvent. The chemical shifts are given in ppm relative to the signal from the residual non-deuterated solvent.

Gas chromatography (GC) was performed on a Shimadzu system (GC-2010 plus) equipped with a flame ionization detector, AOC-20s autosampler, AOC-20i injector and a PerkinElmer Elite-5MS column using helium as carrier gas. The stationary phase consists of 5% diphenyl and 95% dimethyl polysiloxane.

Lyophilization of the polymers was conducted using an Alpha 1-2 LDplus freeze dryer from Martin Christ Gefriertrocknungsanlagen GmbH.

For the characterization of polyplexes and biocompatibility assays, a SpectraMax microplate reader (Molecular Devices) was used.

Flow cytometry was conducted on a Cytomics FC 500 (Beckman Coulter).

CLSM was performed with a LSM880, Elyra PS.1 system (Zeiss) using the following excitation wavelengths/laser lines 405 nm (for Hoechst 33342), 488 nm (for YOYO-1) and 561 nm (for LysoTracker Red DND-99).

Batch dynamic light scattering (DLS) was performed on a Zetasizer Nano ZS (Malvern Instruments). All measurements were performed in folded capillary cells (DTS1070 Malvern Instruments). After an equilibration time of 180 s, 3 × 30 s runs were carried out at 25 °C (λ_{Ex} = 633 nm). Scattered light was detected at an angle of 173°. The mean particle size was approximated as the effective (z-average) diameter and the width of the distribution as the polydispersity index of the particles (PDI) obtained by the cumulants method assuming a spherical shape. Each measurement was performed in triplicates.

Electrophoretic light scattering (ELS) was used to measure the zeta potential (ζ). The measurement was also performed on the Zetasizer Nano ZS by applying laser Doppler velocimetry. For each measurement, 20 runs were carried out using the slow-field reversal and the fast-field reversal mode at 150 V. Each experiment was performed in triplicates at 25 °C. The zeta potential was calculated from the electrophoretic mobility (μ) according to the Henry equation. Henry coefficient f(ka) was calculated according to Ohshima.[45]

For the acid/base titration, the copolymers were dissolved in deionized water, reaching a final concentration of 10 mg mL^{-1} and 10 µL concentrated HCl (12 M) were added. The titration was performed against 0.1 M NaOH using a 765 Dosimat (Metrohm), a digital pH/mV-thermometer GMH 3530 (Greisinger electronic), and the EBS9 M Recorder software. Recorded curves were smoothed using 5-point FFT-fitting in OriginPro 2015G. The resulting curve was derivated two times to determine the pK_a value of the copolymers.

Synthesis and Characterization

Kinetic Studies of Copolymerizations

The general procedure for all kinetic investigations is as follows:

Under inert conditions, a solution of MeTos and MeOx (respectively EtOx) in acetonitrile (c_{MeTos} = 0.013 mol L^{-1}, [M]/[I] = 3) was prepared in a microwave vial and heated in a microwave synthesizer (140 °C, 102 min, absorption level high). Subsequently, distinct ratios of BocOx and MeOx or EtOx ($n_{MeOx/EtOx}$:n_{BocOx}; 80:20, 60:40, 40:60, 20:80, [M]/[I] = 147) were added and the solution was aliquoted into microwave vials and heated in a microwave synthesizer (140 °C, varying reaction times, absorption level very high). After polymerization, the conversions of the monomers were determined utilizing GC measurements, using the solvent as an internal standard. The polymerization constants (k_p) of the monomers were determined using equations (1) and (2) assuming that the slope of the linear fit of $\ln([M]_0/[M]_t) = f(t)$ complies with k_{eff}.

$$\ln M_0 - \ln M_t = k_{eff} \cdot t \quad (1)$$

$$k_{eff} = k_p[I] \quad (2)$$

The reactivity ratios of both monomers were calculated for four different monomer ratios at 30 mol% BocOx (for the EtOx kinetics) respectively 30 mol% MeOx (for the MeOx

kinetics) conversion (determined by GC) using non-linear least square fitting[46] (equation (3)):

$$F_1 = \frac{(r_1-1)f_1^2+f_1}{(r_1+r_2-2)f_1^2+2(1-r_2)f_1+r_2} \quad (3)$$

F_1 = instantaneous mole fraction; f_1 = mole fraction of monomer EtOx/MeOx; f_2 = mole fraction of monomer BocOx; r_1 = reactivity ratio of MeOx/EtOx; r_2 = reactivity ratio of BocOx.

Synthesis of Boc-protected P(Ox)s

The synthesis of P(Ox)s was accomplished as previously described.[44]
Briefly, it is explained for P(EtOx$_{150}$-*r*-BocOx$_{33}$) (P(E$_{150}$B$_{33}$)). In a microwave vial, MeTos (9.3 mg, 0.05 mmol), EtOx (15.1 mg, 0.15 mmol) and acetonitrile (2.87 g) were mixed under inert conditions and heated in the microwave to 140 °C for 93 min. Subsequently, the vial was opened under an inert atmosphere, and EtOx (778.2 mg, 7.85 mmol) and BocOx (484.6 mg, 2.00 mmol) were added. In the case of the homopolymers, only BocOx was added. The reaction mixture was heated in the microwave at 140 °C for another 44 min. The resulting polymer was precipitated in ice-cold diethyl ether and the solid was re-dissolved in CH_2Cl_2. The solvent was evaporated under reduced pressure to obtain the product as a white solid.

^{1}H-NMR ($CDCl_3$, 300 MHz): δ = 3.48 (s, 4 H, backbone), 3.12 (m, 0.5 H, CH_2-CH_2-NH (BocOx)), 2.38 (m, 1.91 H, CH_2 (EtOx)), 1.43 – 1.65 (m, 2.4 H, CH_2-CH_2-CO (BocOx) + CH_2-CH_2-CH_2-CH_2 (BocOx)), 1.37 (s, 2.4 H, CH_3 (EtOx)) ppm.

SEC (eluent: DMAc, 0.21% LiCl, PS-cal.): M_n = 19,100 g mol^{-1}; M_w = 22,200 g mol^{-1}; Đ = 1.16.

Deprotection of Boc-protected P(Ox)s to Yield Primary Amino Functionalized P(Ox)s

The deprotection of P(E$_{150}$B$_{33}$) to yield P(EtOx$_{150}$-*r*-AmOx$_{33}$) (P(E$_{150}$A$_{33}$)) is exemplarily described.

P(E$_{150}$B$_{33}$) (1.0 g) was dissolved in 5 mL TFA and stirred at RT overnight. Subsequently, it was diluted using 10 mL methanol and precipitated in ice-cold diethyl ether. The resulting solid was filtered off and re-dissolved in methanol. Amberlyst® A21 was added and the polymer solution was stirred at 100 rpm at RT overnight. Then, the Amberlyst® A21 was filtered off and the solvent was evaporated under reduced pressure. The polymer was re-dissolved in deionized water and lyophilized to obtain the product as a white powder.

^{1}H-NMR (D_2O, 300 MHz): δ = 3.39 (s, 4 H, backbone), 2.87 (0.4 H, CH_2-CH_2-NH_2 (AmOx)), 2.23 (s, 2 H, CH_2 (EtOx) + CH_2-CH_2-CO (EtOx + AmOx)), 1.50 (s, 0.8 H, CH_2-CH_2-CH_2-CH_2 (AmOx)), 0.92 (s, 2.4 H, CH_3 (EtOx)) ppm.

SEC (eluent: 0.3% TFA + 0.1 M NaCl, P2VP-cal.): M_n = 8,000 g mol^{-1}; M_w = 11,200 g mol^{-1}; Đ = 1.41.

Polyplex Formation

Polyplexes were prepared by mixing stock solutions of 15 µg mL^{-1} pDNA and different amounts of polymers to obtain various N/P ratios in HBG buffer (20 mM 4-(2-hydroxyethyl)piperazine-1-ethanesulfonic acid (HEPES) and 5% (w/v) glucose, pH 7.2). The solutions were vortexed for 10 sec at maximum speed (2800 rpm) and incubated at RT for 15 min to ensure complex formation.

EtBr Quenching Assay (EBA)

Formation of polyplexes with pDNA was investigated by quenching of EtBr fluorescence as described previously.[47] Briefly, pDNA (15 µg mL^{-1}) in a total volume of 100 µL HBG buffer was incubated with EtBr (10 µg mL^{-1}) for 10 min at RT. Subsequently, polyplexes with increasing concentrations of each polymer (calculated to N/P ratios) were formed in black 96-well plates (Nunc, Thermo Fisher) and incubated at RT for 15 min. The fluorescence of the samples was measured at λ_{Ex} = 525 nm/λ_{Em} = 605 nm using a microplate

reader. A sample containing only pDNA and EtBr was used to calibrate the device to 100% fluorescence against a background of 10 µg mL^{-1} of EtBr in HBG solution. The percentage of dye displaced upon polyplex formation was calculated using equation (4).

$$\text{RFU}\,[\%] = \frac{F_{sample} - F_0}{F_{pDNA} - F_0} \cdot 100 \qquad (4)$$

Here, RFU is the relative fluorescence units and F_{sample}, F_0, and F_{pDNA} are the fluorescence intensities of a given sample, EtBr in HBG alone, and EtBr intercalated into pDNA alone. Experiments were conducted in triplicates.

Heparin Dissociation Assay

To investigate the release of pDNA from polyplexes, the heparin dissociation assay was performed. Polyplexes with an N/P ratio of 30 were formed as described above in a total volume of 100 µL HBG buffer containing EtBr (10 µg mL^{-1}). After incubation in the dark at RT for 15 min, the polyplexes were transferred into a black 96-well plate containing heparin in increasing concentrations. The solution was mixed and incubated for further 30 min at 37 °C in the dark. The fluorescence of EtBr was measured at λ_{Ex} = 525 nm/λ_{Em} = 605 nm utilizing a microplate reader. The percentage of intercalated EtBr was calculated as described before. The experiments were conducted in triplicates.

Cell Culture

Mouse liver cell line Hepa1-6 (CRL-1830™, ATCC) and mouse fibroblast cell line L929 (CCL-1™, ATCC) were cultured in growth medium containing Dulbecco's modified eagle's medium (DMEM, Lonza) supplemented with 10% fetal calf serum (FCS), 100 U mL^{-1} penicillin and 100 µg mL^{-1} streptomycin at 37 °C in a humidified 5% (v/v) CO_2 atmosphere.

Cytotoxicity MTT Assay

The cytotoxicity of the investigated polymers was measured by MTT assay using the cell lines Hepa1-6 and L929. Cells were cultured in a 96-well plate for 24 h as described above. The polymers to be tested were added to the cells in a concentration range of 1 to 500 µg mL^{-1} for 24 h. Subsequently, 10 µL aliquots of the MTT solution were added to each well and the plates were further incubated for 4 h at 37 °C in a humidified 5% (v/v) CO_2 atmosphere. The formed formazan crystals were solubilized by addition of 10% sodium dodecyl sulfate (SDS) in 0.01 M HCl. The solubilized formazan product was spectro-photometrically quantified using a microplate reader at λ_{Ex1} = 550 nm and the reference at λ_{Ex2} = 690 nm. The relative cell viability was calculated using equation (5):

$$\text{Rel. cell viab.}\,[\%] = \frac{(\lambda_{Ex1} - \lambda_{Ex2})_{sample}}{(\lambda_{Ex1} - \lambda_{Ex2})_{control}} \cdot 100 \qquad (5)$$

Data are expressed as mean and standard deviation (S.D.) of three measurements. Furthermore, the 50% cytotoxic concentration (CC_{50}) was determined for comparison of the gradient and random polymers in both cell lines.

Polyplex Uptake

For uptake studies, cells were seeded at a density of 2×10^5 cells mL^{-1} in 24-*well* plates (500 µl) and cultured for 24 h. One hour prior to the addition of the polyplexes at concentrations described in Table 1, the medium was changed to DMEM with or without FCS.
The polyplexes were formed and 50 µL polyplexes in HBG buffer were added to the cells. The plates were incubated for 2 or 4 h at 37 °C in a humidified 5% (v/v) CO_2 atmosphere. For kinetic studies of polyplex uptake, pDNA was labeled with YOYO-1 prior to polyplex preparation. For this reason, 0.02 µL of 1 M YOYO-1 solution was mixed with 1 µg pDNA in HBG buffer and incubated for 20 min at 4 °C protected from light.

TABLE 1 Corresponding concentrations of all tested polymers with an N/P ratio of 30.

Polymer system	Concentration [µg mL^{-1}]
P($M_{97}A_{55}$)	9.79
P($M_{73}A_{89}$)	9.47
P($M_{29}A_{166}$)	9.10
P($E_{77}A_{55}$)	10.41
P($E_{57}A_{139}$)	9.56
P($E_{31}A_{163}$)	9.27
P(E_3A_{157})	8.99
l-PEI	5.43

Subsequently, polymers were added at an N/P ratio of 30 and the polyplexes were formed as described before (Table 1). After 2 or 4 h of polyplex incubation the cells were washed to remove extracellular polyplexes.

To determine the relative uptake of the polyplexes, 10,000 cells were measured by flow cytometry and the amounts of viable cells showing YOYO-1 signal were gated. Uptake of pDNA with YOYO-1 alone was used as control to define the gate. Dead cells were identified *via* SSC/FSC signal. The experiments were performed at least three times independently.

For live cell imaging, Hepa1-6 cells (5×10^5 cells mL^{-1}) were seeded in glass-bottomed, 4-chamber dishes (CELLview™, Greiner Bio One) and cultured for 24 h. One hour prior to polymer addition, the cells were rinsed with PBS and the media were changed to DMEM without FCS. Polyplexes were prepared with an N/P ratio of 30 as described above (Table 1) and added to the cells (50 µL per well) for 4 h. Subsequently, the cells were washed with PBS and incubated for 5 min with a mixture of DMEM and PBS supplemented with LysoTracker Red DND-99 (1:1000) and Hoechst 33342 (1:1000; 10 mg mL^{-1}) for lysosomes as well as nucleus staining, respectively. A 1:10 diluted trypan blue solution was added to the medium immediately before imaging to quench polyplexes not taken up by the cells. The living cells were imaged with a LSM880, Elyra PS.1 system. For the quantification of the amount of YOYO-1 and/or LysoTracker Red DND-99 positive organelles per cell the software ImageJ and the plugin Coloc2 (version 3.0.0) were used. Since cell borders could not be defined due to overlap of the cells, the average numbers of YOYO-1 and LysoTracker Red DND-99 positive organelles per cell (defined by the number of Hoechst 33342 positive nuclei) per area of 112.5 µm × 112.5 µm were determined. Cut-off was set to 5 to 1000 pixel units for all organelles.

Transfection Efficiencies in Adherent Cells

Hepa1-6 and L929 cells were cultured as described above. For transfection, the cells were seeded at a density of 10^5 cells mL^{-1} in 24-well plates (500 µl) and incubated for 24 h. One hour prior to transfection, the cells were washed with phosphate buffer saline (PBS) and supplemented with DMEM with or without FCS. Polyplexes with an N/P ratio of 30 were prepared as described above and were added to the cells (50 µL per well). The corresponding concentrations for all tested polymers with an N/P ratio of 30 are shown in Table 1.

After an incubation time of 4 h at 37 °C, the supernatant was replaced by fresh medium, and the cells were further incubated for 44 h. For analysis *via* flow cytometry, the cells were harvested by trypsinization and 10,000 cells were analyzed by flow cytometry. For determination of the viability, dead cells were identified *via* side scatter/forward scatter (SSC/FSC) signal as described previously.[48] Viable cells expressing GFP were gated for analysis of the transfection efficiency. Transfection with pDNA alone was used as control to define the gate. The experiments were performed at least three times independently.

Statistical Analysis

The quantification of YOYO-1 and LysoTracker Red DND-99 positive organelles was performed for normal distribution by Shapiro-Wilk normality test. As the values did not follow normal distributions, data were analyzed by non-parametric Kruskal-Wallis test with Dunn's

post-test to examine the significance of the differences.

RESULTS AND DISCUSSION

Polymer Synthesis

In order to obtain polymers, which are capable of transfecting genetic material, while maintaining a good biocompatibility, a series of different P(Ox) copolymers with a varying amino content was synthesized. Previously, we reported the copolymerization of EtOx and BocOx.[44] However, detailed kinetic investigations on the copolymerization of varying ratios of EtOx and BocOx, respectively MeOx and BocOx have not been part of the previous publication.

For this reason, we performed kinetics to gain information about the monomer distribution within the polymer chains (Figure 1, Figures S1 to S8). All samples were characterized using SEC, ^{1}H-NMR spectroscopy and GC measurements. The monomer conversions after certain reaction times could be determined by the utilization of GC measurements. The polymerization constants (k_p) of the different monomers were calculated using equations (1) and (2).[49]

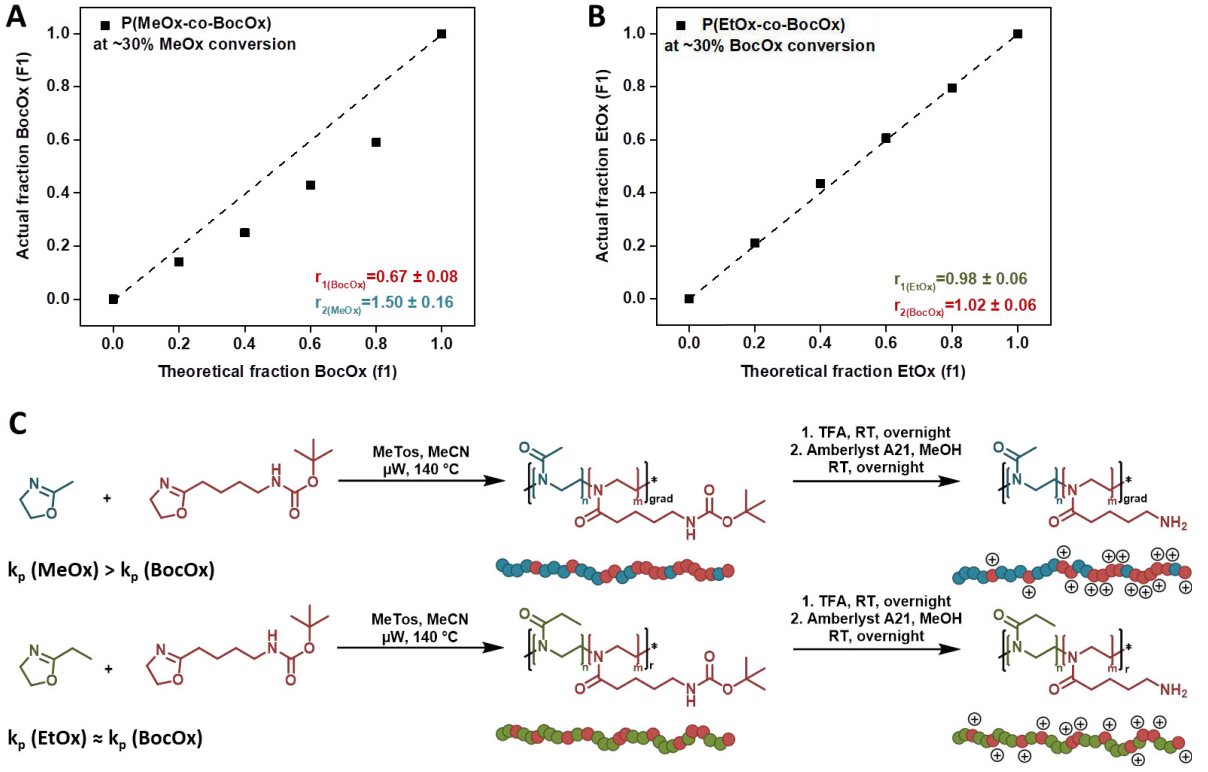

FIGURE 1 A: Relation between the fraction of BocOx in the monomer feed (f1) and the incorporated fraction of BocOx in the copolymerization (F1) determined *via* GC measurements at ~30 mol% MeOx conversion ($\ln(M_0/M_t) = 0.36$). B: Relation between the fraction of EtOx in the monomer feed (f1) and the incorporated fraction of EtOx in the copolymerization (F1) determined *via* GC-measurements at ~30 mol% BocOx conversion ($\ln(M_0/M_t) = 0.36$). C: Schematic representation of the copolymerization of MeOx (cyan) and BocOx (red) as well as EtOx (green) and BocOx (red). The monomers are copolymerized by the living CROP and subsequently deprotected under acidic conditions to obtain copolymers that are either gradient (P(MeOx$_n$-*grad*-BocOx$_m$)) or randomly (P(EtOx$_n$-*r*-BocOx$_m$)) distributed. Reactivity ratios were calculated according to equation 3. µW – microwave.

TABLE 2 Key properties of the synthesized P(Ox)s determined by ^{1}H-NMR spectroscopy (300 MHz) in indicated solvents.

Sample	Polymer	DP	mol% MeOx or EtOx	mol% BocOx or AmOx	M_n [g mol^{-1}]
$P(M_{130}B_{31})$	$P(MeOx_{130}$-*grad*-$BocOx_{31})^a$	161	81[d]	19[d]	18,600
$P(M_{97}B_{55})$	$P(MeOx_{97}$-*grad*-$BocOx_{55})^a$	152	64[d]	36[d]	21,600
$P(M_{73}B_{89})$	$P(MeOx_{73}$-*grad*-$BocOx_{89})^a$	162	45[d]	55[d]	27,700
$P(M_{29}B_{166})$	$P(MeOx_{29}$-*grad*-$BocOx_{166})^a$	195	15[d]	85[d]	41,400
$P(M_{130}A_{31})$	$P(MeOx_{130}$-*grad*-$AmOx_{31})^b$	161[c]	81	19	15,500
$P(M_{97}A_{55})$	$P(MeOx_{97}$-*grad*-$AmOx_{55})^b$	152[c]	64	36	16,100
$P(M_{73}A_{89})$	$P(MeOx_{73}$-*grad*-$AmOx_{89})^b$	162[c]	45	55	18,900
$P(M_{29}A_{166})$	$P(MeOx_{29}$-*grad*-$AmOx_{166})^b$	195[c]	15	85	24,900
$P(E_{150}B_{33})$	$P(EtOx_{150}$-*r*-$BocOx_{33})^a$	183	82[d]	18[d]	22,800
$P(E_{77}B_{55})$	$P(EtOx_{77}$-*r*-$BocOx_{55})^a$	132	58[d]	42[d]	20,900
$P(E_{57}B_{139})$	$P(EtOx_{57}$-*r*-$BocOx_{139})^a$	196	29[d]	71[d]	39,300
$P(E_{31}B_{163})$	$P(EtOx_{31}$-*r*-$BocOx_{163})^a$	194	16[d]	84[d]	42,500
$P(E_{150}A_{33})$	$P(EtOx_{150}$-*r*-$AmOx_{33})^b$	183[c]	82	18	19,600
$P(E_{77}A_{55})$	$P(EtOx_{77}$-*r*-$AmOx_{55})^b$	132[c]	58	42	15,500
$P(E_{57}A_{139})$	$P(EtOx_{57}$-*r*-$AmOx_{139})^b$	196[c]	29	71	25,400
$P(E_{31}A_{163})$	$P(EtOx_{31}$-*r*-$AmOx_{163})^b$	194[c]	16	84	26,300
$P(E_3B_{157})$	$P(EtOx_3$-*b*-$BocOx_{157})^a$	160	2[d]	98[d]	38,300
$P(E_3A_{157})$	$P(EtOx_3$-*b*-$AmOx_{157})^b$	160[c]	2	98	22,600

[a]$CDCl_3$; [b]CD_3OD; [c]calculated from Boc-protected precursor; [d]calculated from deprotected copolymer.

Within the investigated monomer ratios, EtOx and BocOx exhibited similar k_p values ($k_{p(EtOx)}$ = 47.2 ± 11.0 L mol^{-1} s^{-1}; $k_{p(BocOx)}$ = 44.0 ± 13.3 L mol^{-1} s^{-1}), while MeOx polymerized faster than BocOx ($k_{p(MeOx)}$ = 75.4 ± 2.8 L mol^{-1} s^{-1}; $k_{p(BocOx)}$ = 50.7 ± 4.0 L mol^{-1} s^{-1}).

This complies with previously published k_p values of the homopolymerizations of the investigated monomers.[42] To gain an insight into the monomer distribution within the polymer chain, the calculation of the reactivity ratios is indispensable and was performed using equation (3).[46, 49, 50] The reactivity ratios of EtOx and BocOx were found to be similar (r_{BocOx} = 1.02 ≈ 1 ≈ r_{EtOx} = 0.98), suggesting the formation of random copolymers.[51] On the other hand, copolymerization of MeOx and BocOx resulted in slight gradient copolymers (r_{MeOx} = 1.50 > 1 > r_{BocOx} = 0.67).

Regarding the SEC measurements, the polymers showed a linear increase in the molar mass and low dispersities (Đ ≤ 1.2) up to high conversions. Only polymers with high BocOx amounts revealed small high molar mass shoulders, suggesting side reactions at high BocOx conversions of more than 90 mol%, which are probably caused by the amino side chain. However, these side reactions can be minimized by aiming for a slightly lower conversion during the preparation of copolymers.

The investigations of cytotoxicity, polyplex stability and cellular uptake efficiency within this study enable a comparison of gradient (MeOx) and random (EtOx) copolymers by variation of the non-charged comonomers. Differences regarding the polyplex performance might be found in terms of cytotoxicity provoked by an enhanced shielding by gradient copolymers compared to random polymers. Furthermore, differences in the cellular uptake could also be caused by the shielding of the non-ionic comonomer. These two crucial factors might be important for a successful transfection efficiency of the investigated polyplexes.

TABLE 3 Size and surface charge (zeta potential, ζ) of polyplexes at an N/P ratio of 15 measured in HBG or 150 mM NaCl determined by DLS and ELS (n=3).

	HBG			NaCl	
Polymer system	z-average [d, nm]	PDI	ζ [mV]	z-average [d, nm]	PDI
$P(M_{97}A_{55})$	209 ± 17	0.396 ± 0.063	29.2 ± 6.0	210 ± 10	0.107 ± 0.025
$P(M_{73}A_{89})$	164 ± 6	0.356 ± 0.076	27.6 ± 2.2	138 ± 6	0.060 ± 0.031
$P(M_{29}A_{166})$	194 ± 12	0.527 ± 0.117	34.2 ± 6.3	n.d.	n.d.
$P(E_{77}A_{55})$	158 ± 8	0.342 ± 0.069	26.9 ± 1.6	1,360 ± 167	0.532 ± 0.123
$P(E_{57}A_{139})$	210 ± 58	0.468 ± 0.139	33.7 ± 2.8	730 ± 243	0.336 ± 0.074
$P(E_{31}A_{163})$	207 ± 37	0.581 ± 0.143	27.5 ± 3.8	n.d.	n.d.
$P(E_3A_{157})$	187 ± 41	0.546 ± 0.164	36.4 ± 4.2	1,443 ± 171	0.316 ± 0.074
l-PEI	306 ± 126	0.528 ± 0.078	37.1 ± 1.9	1,310 ± 174	0.285 ± 0.025

n.d.: not determined

All Boc-protected polymeric precursors were analyzed using ^{1}H-NMR spectroscopy to obtain information about the DP and the monomer ratios (Table 2, Figures S9 to S13) as well as by SEC to gain an insight about the dispersity of the polymers (Table S1, Figures S14 to S16).

The total DP of the Boc-protected P(Ox) precursors was between 150 and 200 for all polymers while the BocOx content was approximately 20, 40, 60 or 80 mol% (Table 2, column 5). All copolymers were deprotected under acidic conditions to yield the final amino functionalized copolymers with either MeOx ($P(M_nA_m)$) or EtOx ($P(E_nA_m)$) to evaluate the influence of the neutral comonomer on transfection as well as cytotoxicity. After deprotection, SEC measurements under aqueous conditions were performed to validate the absence of degradation (Table S1, Figures S14 to S16).

Characterization of the Polyplexes

After successful synthesis and characterization of a series of cationic P(Ox)s, they were investigated regarding their polyplex formation and dissociation abilities. For the characterization of all indicated polyplexes, EBA at different N/P ratios and heparin dissociation assays at an N/P of 30 were performed. These assays are based on the ability of EtBr to intercalate into DNA leading to an increase in fluorescence. A displacement of EtBr by interaction of polymers with DNA reduces the fluorescence indicating polyplex formation.[52]

As expected, the complexation of the tested polymers with pDNA was stronger with increasing percentages of AmOx (Figures 2A and 2B). To form stable polyplexes, polymers needed AmOx percentages higher than 35 mol%. Polymers with less than 35 mol% AmOx ($P(M_{130}A_{31})$ and $P(E_{150}A_{33})$) did not form stable polyplexes and were, therefore, excluded from further investigations. The pDNA complexation ability of the polymer consisting of 98 mol% AmOx ($P(E_3A_{157})$) was comparable to *l*-PEI (Figure 2B), which is commonly used within our group as an internal reference.[33, 53] This supports the assumption that the investigated P(Ox)s with primary amines contribute in a similar way to the polyplex formation like *l*-PEI does. The polyplex formation was found to be dependent on the AmOx amount within the polymers, however, not on the utilized non-ionic monomers MeOx or EtOx (Figure 2C).

For most of the investigated polymers, an N/P ratio of 30 was required to reach a plateau, where no further decrease of the RFU was seen. For this reason, heparin dissociation assays were performed at an N/P ratio of 30.

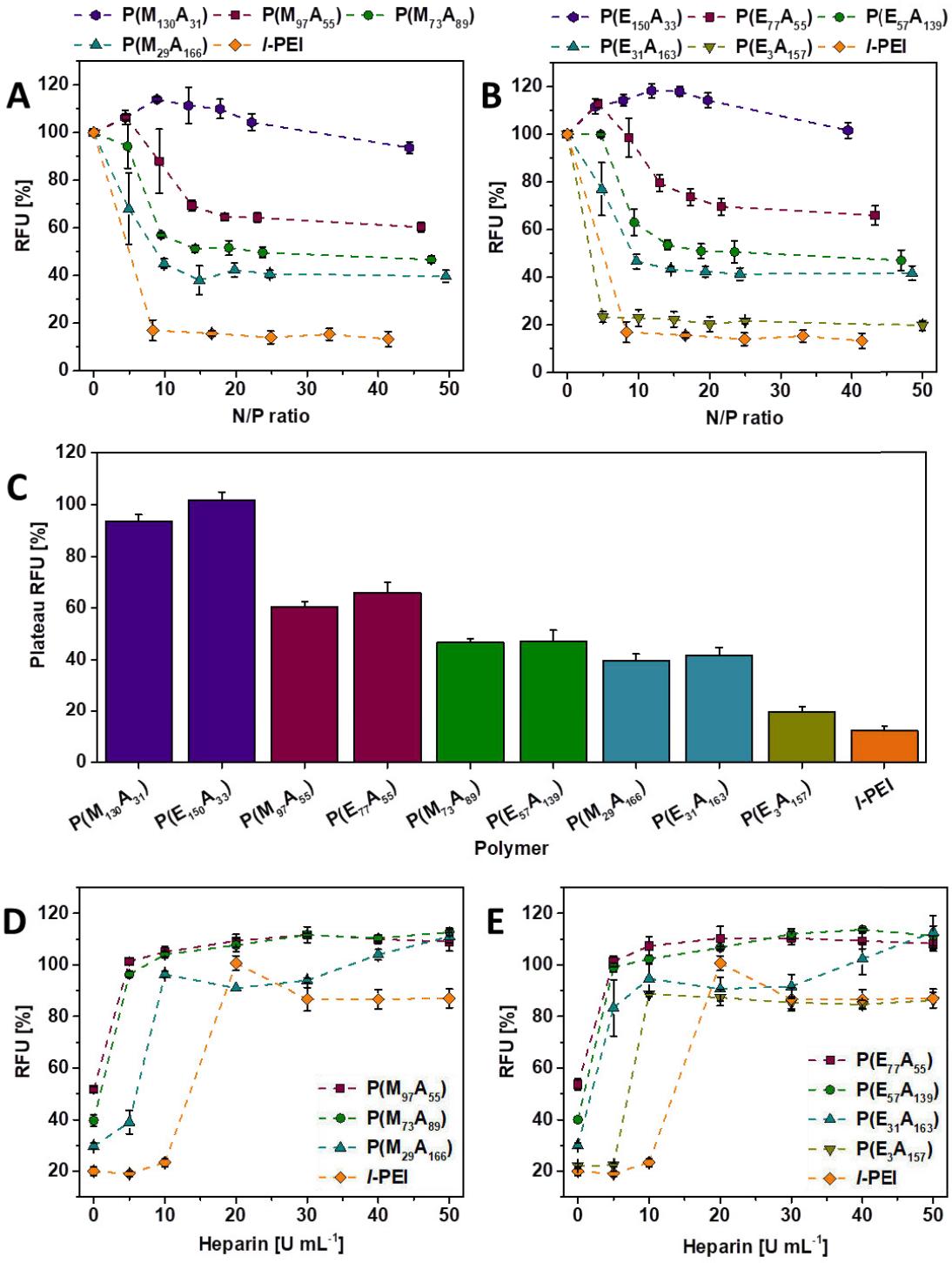

FIGURE 2 Comparison of polyplex formation and stability with pDNA using $P(M_nA_m)$ and $P(E_nA_m)$ as well as *l*-PEI as control. A and B: DNA complexation affinity determined by EBA of all polymers at indicated N/P ratios. C: EBA plateau of indicated polymers in comparison to *l*-PEI. D and E: Heparin dissociation assay of polyplexes formed at an N/P ratio of 30. Values represent the mean and S.D. (n=3). A sample of mixed pDNA and EtBr served as the control for 100% fluorescence. RFU – relative fluorescence units.

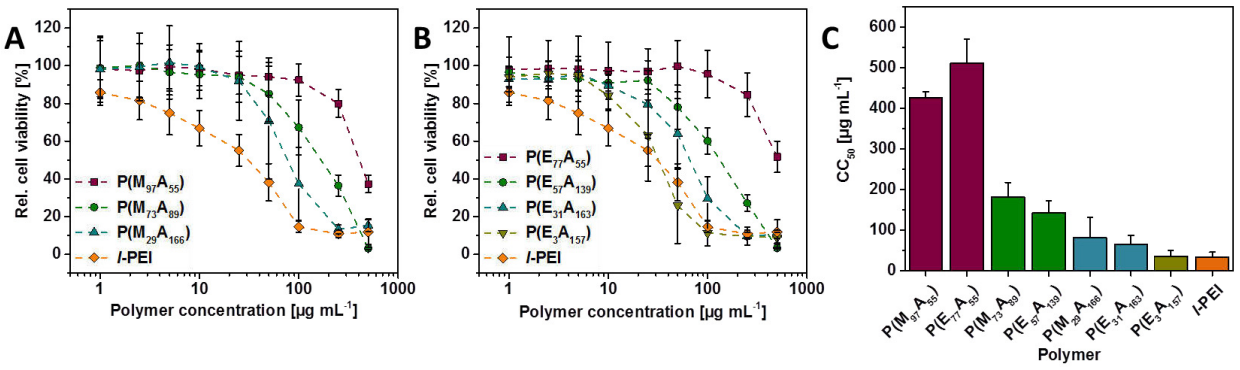

FIGURE 3 Cytotoxicity of indicated polymers after 24 h as determined by MTT assays. A and B: Relative cell viability of Hepa1-6 cells after treatment with polymers using different polymer concentrations. C: CC_{50} of indicated polymers in Hepa1-6 cells. Values represent the mean and S.D. (n=3).

All tested polymers revealed a lower stability in the presence of heparin in comparison to *l*-PEI (Figures 2D and 2E), which was expected due to the lower cationic charge density of the polymers as already shown before.[34]

For an efficient uptake of polymeric nanocarriers into cells *via* endocytic pathways, size and charge of the complexes are crucially important. Therefore, DLS and ELS were used for determination of the physicochemical properties. A critical diameter up to 200 nm is recommended for an efficient delivery.[54] The polyplexes formed with all investigated polymers with an N/P ratio of 15 exhibited a z-average diameter of 150 to 210 nm in HBG preferred for efficient uptake (Table 3). Nevertheless, PDI values between 0.3 and 0.6 were observed, which corresponded to formation of aggregates also shown in Table S2.

Interestingly, polyplex formations in 150 mM NaCl showed small polyplexes with a low PDI for $P(M_nA_m)$ whereas for $P(E_nA_m)$ mostly aggregates larger than 700 nm with a high PDI could be detected (Table 3). The influence of N/P ratio and transfection medium for *l*-PEI was recently shown and are in good accordance to our results.[55]

An explanation for these differences might be the architecture of the investigated polymers. $P(M_nA_m)$ are gradient polymers while the monomers are randomly distributed in $P(E_nA_m)$. During polyplex formation, the cationic units of the polymers interact with the negatively charged phosphate backbone of the pDNA. By using gradient copolymers, the cationic pseudo-block can interact with one pDNA, while the stealth moiety shields the polyplex from aggregation. The influence of salt concentrations on PEI solutions was also reported previously and is in line with our results.[56]

Biocompatibility of the Polymers

After successful DNA complexation and dissociation experiments, the cytotoxicity of all relevant polymers was investigated in the biomedical relevant mouse liver cell line Hepa1-6. Additionally, the fibroblast cell line L929 was used for comparison because of its high endocytosis rate and sensitivity to cytotoxic effects[20, 57, 58] as recommended by ISO10993-5. All polymers were compared to *l*-PEI. As shown in Figure 3 and Figure S17, cytotoxicity correlated well with the amount of AmOx in the polymer.[33, 34, 53] Furthermore, the polymers did not reveal a dependency on the used hydrophilic monomer. $P(M_{29}A_{166})$ and $P(E_{31}A_{163})$ as well as a sample with very high AmOx content ($P(E_3A_{157})$) caused cytotoxicity similar to *l*-PEI. The CC_{50} values determined demonstrated that the cytotoxicity data measured were consistent in both cell lines analyzed.

Uptake Efficiency of the Polyplexes

The proposed pathway for transfection involves endocytosis of polyplexes, endosomal release of pDNA into the cytosol followed by its transport into the nucleus.[23] To clarify the general potential of the polyplexes in terms of transfection, the cellular uptake efficiency of all relevant polyplexes consisting of the mentioned polymers and YOYO-1 labeled pDNA was investigated using flow cytometry (Figure 4 and S18). Hereby, we compared the Hepa1-6 cell-line directly with the L929 mouse fibroblast cell line. Cellular uptake was studied in serum free medium (Figure 4A and B, Figure S18 A and B) to evaluate the general ability of polyplexes to be internalized by cells, whereas the FCS containing complete medium (Figure 4C and D, Figure S18C and D) is supposed to be of higher relevancy for future applications. By the utilization of a flow cytometer, it is possible to determine the portion of cells, which internalized polyplexes as well as the mean fluorescence intensity (MFI) of the cells, which provides rough information about the amount of polyplex per cells (Figure 4B and D, Figure S18B and D). By comparing the results obtained, it was obvious that the uptake efficiency of polyplexes into L929 cells was in general higher than into Hepa1-6 cells, which is supported by other literature reports.[57, 58]

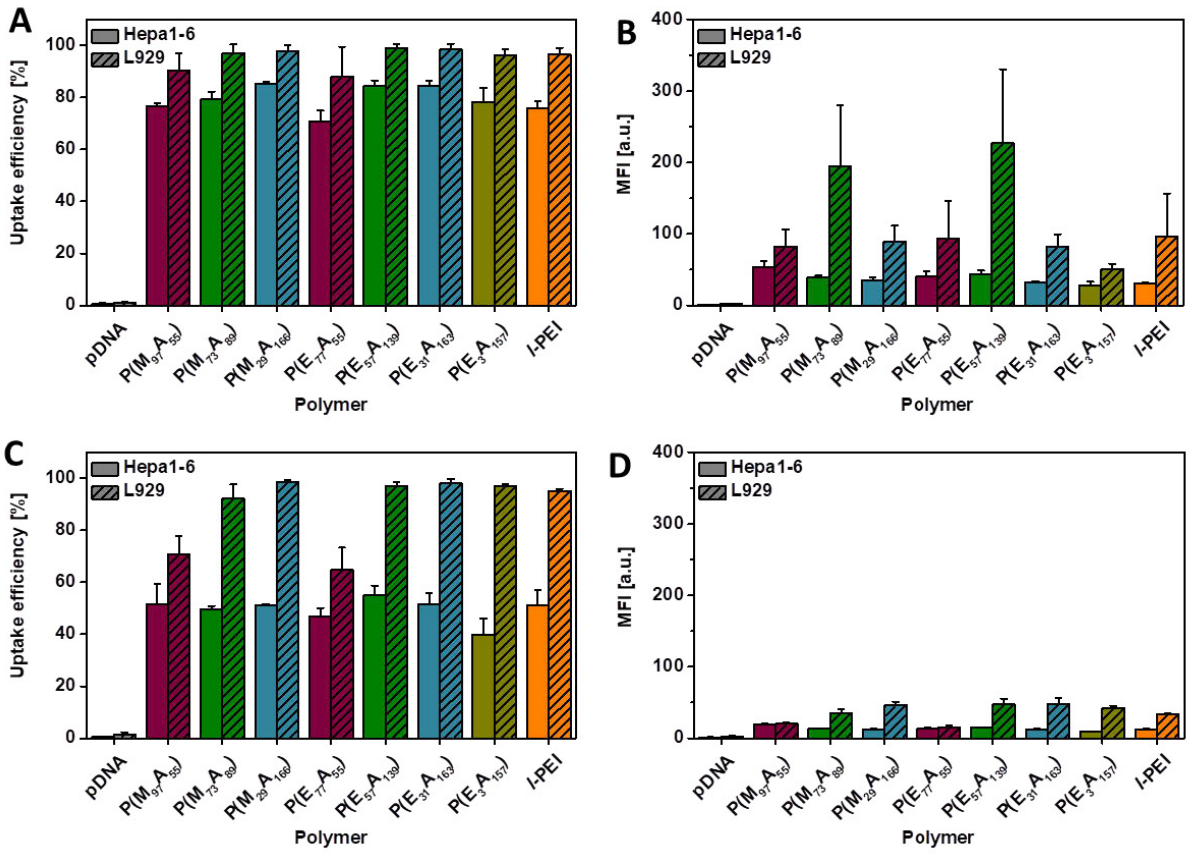

FIGURE 4 Cellular uptake studies of indicated polyplexes at an N/P ratio of 30 using YOYO-1 labeled pDNA. Hepa1-6 and L929 cells were treated with polyplexes 2 h in medium with (complete, C and D) or without FCS (serum free, A and B) and uptake efficiency (A and C) as well as MFI (B and D) were analyzed *via* flow cytometry. Values represent the mean and S.D. (n=3). For values after 4 h incubation see Figure S18.

Possible explanations for the observed cell type dependency of the uptake and transfection efficiency are different membrane characteristics, intracellular transport mechanisms and DNA-degrading enzymes due to discriminative expression patterns.[59] Polyplexes with AmOx amounts of 35 mol% were internalized less well in both cell lines due to the presence of fewer cationic charges.[60] Having a closer look at the cells, which were cultivated in serum free medium, L929 cells revealed an uptake efficiency of nearly 100% even after 2 h of incubation, while efficiency was slightly less (80 to 90%) for Hepa1-6 cells (Figure 4A).

After 4 h incubation exclusively the MFI per cell in both cell lines further increased suggesting an increased polyplex uptake by several cells, which could have a positive effect on transfection efficiency (Figure S18B). No differences between the P(Ox)s and *l*-PEI were observed.

Interestingly, the uptake efficiency significantly decreased when using 10% FCS containing (complete) medium in combination with Hepa1-6 cells. While the differences between the two media were negligible within the L929 cell line, in Hepa1-6 cells, we observed an uptake efficiency in complete medium of only 50% after 2 h (Figure 4C) and 50 to 70% after 4 h (Figure S18C). This phenomenon might be explained by the interaction of the polyplexes with serum proteins.[61] It is noteworthy that similar results were obtained for *l*-PEI, possibly due to high charge densities within all polyplexes. As there were no difference between the investigated polymers and *l*-PEI the influence of P(MeOx) and P(EtOx) on polyplex uptake is only of minor importance.

Transfection Efficiency

The previous results indicated that the tested polymers fulfill the prerequisites to be investigated as non-viral gene-delivery agents. As a consequence, they were analyzed regarding transfection efficiency using Hepa1-6 and L929 cells and pDNA encoding green fluorescent protein (GFP) as visual reporter. The transfection efficiency was analyzed by flow cytometry counting all viable cells (SSC/FSC), which successfully expressed GFP (Figures 5 and S18). For all tested polymers, an N/P ratio of 30 was used to form stable polyplexes. In a first step, we determined the optimal time point for the detection of the GFP expression using *l*-PEI. After 48 h of transfection in both cell lines (Hepa1-6 and L929) the number of GFP expressing cells doubled, and an increase of the MFI was detected compared to measurements after 24 h (Figure S19). In comparison to L929 cells, Hepa1-6 cells revealed a lower GFP expression. It is well-known that various transfection reagents show different transfection efficiencies in various cell lines and especially L929 cells display high uptake and transfection efficiencies.[57, 58, 62] Similar to differences in the uptake efficiency also the transfection efficiency is dependent on the discriminative expression pattern leading to variations in membrane topology, intracellular transport and enzymes for DNA degradation.[59]

Furthermore, as serum proteins influenced the uptake efficiency, we also investigated the transfection efficiency of *l*-PEI based polyplexes in growth media supplemented with 10% FCS in comparison to media without serum. In L929 cells, serum containing medium decreased the transfection efficiency by 50% after 24 h and 48 h. Nevertheless, GFP expression was detectable after 48 h in 40% of all cells. Hepa1-6 cells showed a stronger impact upon presence of serum with no transfection efficiencies higher than 5%, neither after 24 h nor 48 h (Figure S19).

Based on these results and with the knowledge that stealth moieties are able to reduce the interaction with serum proteins, we investigated transfection after 48 h in medium with (complete) or without serum (serum free).

Figure 5 shows the results of the transfection efficiencies of all investigated P(Ox)s comparing Hepa1-6 and L929 cells in medium with (complete, Figure 5A and B) or without FCS (serum free, Figure 5C and D). None of the elucidated P(Ox)s was able to transfect Hepa1-6

cells after 48 h of incubation (transfection efficiency < 1%), even in medium without FCS. Analysis of L929 cells, which are more easily transfected with *l*-PEI (Figure S19), led to similar results indicating a more general problem concerning the investigated P(Ox)s. One possible explanation could account for the observed lack of GFP reporter expression, namely the inability of the polyplexes to release pDNA from the endosomal pathway into the cytosol. For the release, the endosomal membranes have to be disrupted which depends on the so-called "proton sponge effect".[63]

Afterwards, the polyplexes undergo endosomal escape and the genetic material can enter the cell nucleus. Amino functionalized polymers can have a buffer capacity within the physiological pH value of 7.4, enhancing the endosomal release. For this reason, pK_a values of different amino functionalized P(Ox)s, which show favorable biochemical characteristics, were elucidated (Table 4, Figure S20 to S24).

The tested P(Ox)s had a pK_a value between 9 and 10. Since these values are out of the range of physiological pH values, there seems to be no buffer capacity of the polymers in the physiological relevant pH range, possibly improving the endosomal release of polyplexes within the cells.

In comparison, J.-B. Behr showed that the protonation of PEI increases from 20% to 45% when decreasing the pH value from 7 to 5.[63] This difference within the observed pK_a values might lead to a prevention of the endosomal release of the herein investigated polyplexes. To clarify the location of the polyplexes within the cell and to address a potential inability of the polyplexes to release pDNA from endosomes into the cytosol, analyses of the fate of the polyplexes by CLSM were performed (Figure 6). To investigate only intracellular polyplexes trypan blue was used to quench extracellular polyplexes. Like *l*-PEI, the newly investigated polymers also showed uptake into the cells.

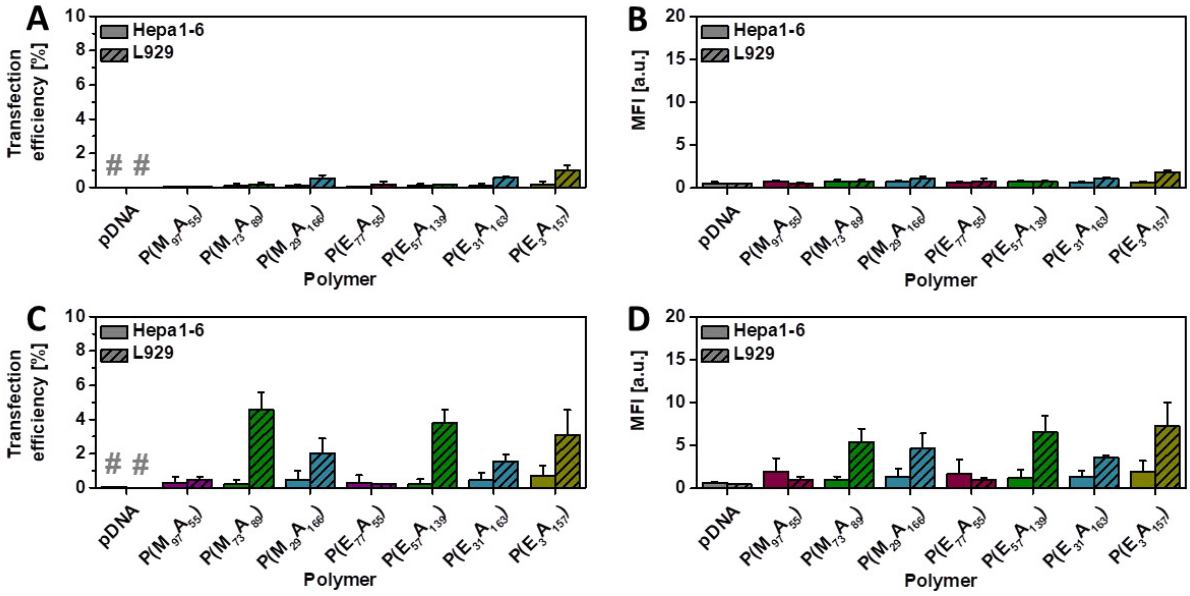

FIGURE 5 Transfection efficiencies (A and C) and MFI (B and D) of indicated polyplexes at an N/P ratio of 30 after 48 h of transfection analyzed by GFP expression *via* flow cytometry. Adherent Hepa1-6 and L929 cells were transfected in medium with (complete, A and B) or without FCS (serum free, C and D). Values represent the mean and S.D. (n=3). Transfection efficiencies of *l*-PEI can be found in Figure S19. Hashes represent the position of control values in A and C.

TABLE 4 pK_a values of different P(Ox)s determined by titration of acidified solutions with 0.1 M NaOH. pK_a values were calculated from 1st derivation (Figures S20 to S24).

Polymer	pK_a value
$P(M_{97}A_{55})$	9.9
$P(M_{73}A_{89})$	9.6
$P(E_{77}A_{55})$	9.5
$P(E_{57}A_{139})$	9.4
$P(E_3A_{157})$	9.5
PEI	7.9 to 9.6[64]

Since polyplexes have to escape the endolysosomal system for transfection, a strong colocalization with the specific lysosomal marker LysoTracker Red DND-99 indicates a prevention of mentioned release. As shown in Figure 7, polymers containing EtOx as the non-ionic comonomer possessed a significant increase in YOYO-1 and LysoTracker Red DND-99 positive organelles per cell in comparison to *l*-PEI (Figure 7A). In contrast to that, the MeOx based copolymer did not show a significant increase of dye positive organelles. A closer look further revealed an increased amount of YOYO-1 positive organelles for P(Ox)s analyzed in comparison to *l*-PEI (Figure 7B). For this reason, it is assumed that MeOx containing copolymers were partially retained in other vesicular organelles of the endolysosomal system, which were not acidified after 4 h of incubation. The significant increase in these YOYO-1 positive organelles suggests strong defects in polyplex release into the cytosol, consequently a prevention of transfection.

Previous investigations on amino functionalized P(Ox)s revealed significantly higher transfection efficiencies.[33, 34, 41, 53] We could show that the transfection efficiency of AmOx can be enhanced by the preparation and self-assembly of amphiphilic 2-nonyl-2-oxazoline containing block copolymers.[53] Hereby, the hydrophobicity could increase the interaction of the polyplexes with the lysosomal membrane, or the assembly of the polymers might trigger the endosomal release. In addition to the investigated micelles, MeOx or EtOx containing, hydrophilic copolymers exhibited an enhanced transfection efficiency compared to the herein investigated system.[33, 34] However, the amino functionalities were introduced *via* thiol-ene reaction after the polymerization, resulting in copolymers with a thio-ether containing spacer within the amino functional side chain.

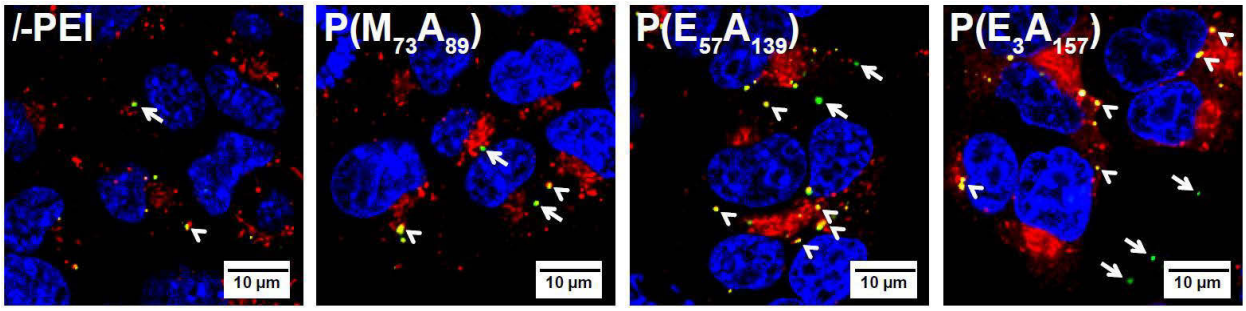

FIGURE 6 CLSM images of Hepa1-6 cells. Cells were incubated with *l*-PEI, $P(M_{73}A_{89})$, $P(E_{57}A_{139})$, or $P(E_3A_{157})$ based polyplexes at an N/P of 30 in medium without FCS at 37 °C for 4 h. The cell nucleus is stained with Hoechst 33342 (blue), lysosomes are stained with LysoTracker Red DND-99 (red) and pDNA with YOYO-1 (green). Trypan blue was used to quench extracellular polyplexes. While only few YOYO-1 (green dots, highlighted by white arrows) or YOYO-1 and LysoTracker Red DND-99 positive organelles (yellow dots, highlighted by white arrowheads) were detected after incubation with *l*-PEI based polyplexes, incubation with polyplexes of $P(M_{73}A_{89})$, $P(E_{57}A_{139})$ and $P(E_3A_{157})$ resulted in an increase in YOYO-1 positive organelles indicating defects in the endolysosomal release of the polyplexes.

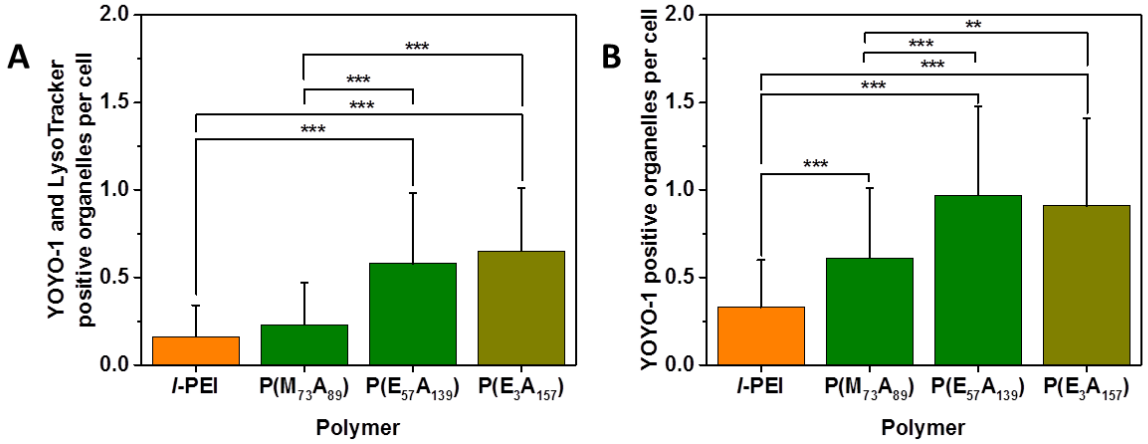

FIGURE 7 Quantification of YOYO-1 and LysoTracker Red DND-99 positive (A) and YOYO-1 positive organelles alone (B) in Hepa1-6 after incubation with indicated polymers at an N/P ratio of 30 for 4 h. Values represent the mean and S.D. (n = 3, 20 pictures per assay). Statistical significance was analyzed by non-parametric Kruskal-Wallis test with Dunn's post-test. ** = $p < 0.01$; *** = $p < 0.001$.

Additionally, the resulting alkyl spacer was longer compared to the current study. For this reason, either the heteroatom or the hydrophobicity of the side chain might have an influence on the transfection efficiency of the polymers. For this reason, different modifications of amino functionalized P(Ox)s, such as PEI or imidazole units for the utilization of the "proton sponge effect" as well as (cleavable) linkers (*e.g.* disulfides) might help to release polyplexes from lysosomes and finally promote the dissociation of the DNA from the polyplexes. Even though there are already some examples from literature how to enhance the transfection efficiency and biocompatibility of cationic polymers, detailed investigations on the influence of small modifications within the polymer chain are of most interest for the preparation of ideal polymer-based vehicles.

CONCLUSIONS

Here, we described the characterization of a series of amino functionalized P(Ox)s with P(MeOx) or P(EtOx) as stealth units. We could show that both hydrophilic monomers have different polymerization constants leading to a gradient distribution within MeOx and a random distribution within EtOx copolymers. Neither P(MeOx) nor P(EtOx) nor the monomer distribution within the polymer chain revealed a significant influence on the properties of the investigated polymers. The percentage of AmOx played an important role in DNA interaction and cytotoxicity. Regarding DNA binding and dissociation as well as cytotoxicity, usage of $P(E_3A_{157})$ gave results comparable to *l*-PEI, one of the most often used non-viral cationic carriers for transfection. Polymers with more than 35 mol% AmOx formed stable polyplexes with diameters in the range for efficient cellular uptake (d = 150 to 200 nm). Despite the fact that with these properties most of the polyplexes showed efficient uptake into cells, there was almost no transfection seen in Hepa1-6 and L929 cells even after 48 h of transfection. Microscopic investigations revealed that all tested P(Ox) polyplexes were taken up into cells but exhibited no release from lysosomes into the cytosol due to a missing buffer capacity of the polymers, which is required for the lysosomal release. In addition, Hepa1-6 cells showed in general reduced transfection efficiency in comparison to L929 cells.

Therefore, the investigated polymers are usable for the purification of genetic material[44, 65, 66] or drug delivery applications,[67, 68] however, not for

gene delivery by using the investigated conditions. Future studies might concentrate on alternative copolymers with differences in the hydrophobicity and buffer capacity to identify ideal carriers for genetic material, which can ensure biocompatibility while expressing higher transfection efficiencies.

Based on the different uptake efficiencies in the investigated cell lines targeting moieties can also increase the uptake and possibly transfection efficiency. Since gradient polymers show higher polyplex stability in physiological sodium chloride solution we would recommend to prefer this polymer structure over random polymers.

ACKNOWLEDGEMENTS

This project was funded by the Thüringer Ministerium für Wirtschaft, Wissenschaft und Digitale Gesellschaft (ProExzellenz II, NanoPolar) to BQ and USS. The funding of the collaborative research center PolyTarget (SFB 1278-C03) by the Deutsche Forschungsgemeinschaft (DFG) is highly acknowledged. MNL acknowledges the German Federal Ministry of Education and Research (BMBF, #13N13416 smart-dye-livery) for funding. AT acknowledges the Carl Zeiss Foundation as well as the BMBF (#13XP5034A, PolyBioMik) for funding. The authors gratefully acknowledge the members of the IOMC Fabian H. Sobotta for the synthesis and characterization of P(E_3A_{157}) and Anne-Kristin Trützschler for the supply of *l*-PEI.

REFERENCES AND NOTES

1 C. Zhang; R. Jin; P. Zhao; C. Lin, *Acta Biomater.* **2015,** *22*, 120.
2 D. W. Pack; A. S. Hoffman; S. Pun; P. S. Stayton, *Nat. Rev. Drug Discov.* **2005,** *4*, (7), 581.
3 H. J. Kim; A. Kim; K. Miyata; K. Kataoka, *Adv. Drug Deliv. Rev.* **2016,** *104*, 61.
4 K. Kawabata; Y. Takakura; M. Hashida, *Pharm. Res.* **1995,** *12*, (6), 825.
5 J. Hisazumi; N. Kobayashi; M. Nishikawa; Y. Takakura, *Pharm. Res.* **2004,** *21*, (7), 1223.
6 R. M. Schiffelers; A. Ansari; J. Xu; Q. Zhou; Q. Tang; G. Storm; G. Molema; P. Y. Lu; P. V. Scaria; M. C. Woodle, *Nucleic Acids Res.* **2004,** *32*, (19), e149.
7 Y. Fujiwara; A. Furuta; H. Kikuchi; S. Aizawa; Y. Hatanaka; C. Konya; K. Uchida; A. Yoshimura; Y. Tamai; K. Wada; T. Kabuta, *Autophagy* **2013,** *9*, (3), 403.
8 M. Mees; E. Haladjova; D. Momekova; G. Momekov; P. S. Shestakova; C. B. Tsvetanov; R. Hoogenboom; S. Rangelov, *Biomacromolecules* **2016,** *17*, (11), 3580.
9 D. Luo; W. M. Saltzman, *Nat. Biotech.* **2000,** *18*, (1), 33.
10 N. Nayerossadat; T. Maedeh; P. A. Ali, *Adv. Biomed. Res.* **2012,** *1*, 27.
11 A. El-Aneed, *J. Control. Release* **2004,** *94*, (1), 1.
12 T. Friedmann; R. Roblin, *Science* **1972,** *175*, (4025), 949.
13 Y. Huang; X. Liu; L. Dong; Z. Liu; X. He; W. Liu, *Pain Res. Treat.* **2011,** *2011*, 8.
14 S. Zhang; B. Zhao; H. Jiang; B. Wang; B. Ma, *J. Control. Release* **2007,** *123*, (1), 1.
15 A. G. Schatzlein, *Anti-Cancer Drugs* **2001,** *12*, (4), 275.
16 M. A. Mintzer; E. E. Simanek, *Chem. Rev.* **2008,** *109*, (2), 259.
17 R. Wattiaux; N. Laurent; S. Wattiaux-De Coninck; M. Jadot, *Adv. Drug Deliv. Rev.* **2000,** *41*, (2), 201.
18 A. Akinc; R. Langer, *Biotechnol. Bioeng.* **2002,** *78*, (5), 503.
19 D. Fischer; T. Bieber; Y. Li; H.-P. Elsässer; T. Kissel, *Pharm. Res.* **1999,** *16*, (8), 1273.
20 D. Fischer; Y. Li; B. Ahlemeyer; J. Krieglstein; T. Kissel, *Biomaterials* **2003,** *24*, (7), 1121.
21 S. C. De Smedt; J. Demeester; W. E. Hennink, *Pharm. Res.* **2000,** *17*, (2), 113.
22 M. E. Favretto; A. Krieg; S. Schubert; U. S. Schubert; R. Brock, *J. Control. Release* **2015,** *209*, 1.
23 O. Boussif; F. Lezoualc'h; M. A. Zanta; M. D. Mergny; D. Scherman; B. Demeneix; J. P. Behr, *Proc. Natl. Acad. Sci. U S A* **1995,** *92*, (16), 7297.
24 M. Jager; S. Schubert; S. Ochrimenko; D. Fischer; U. S. Schubert, *Chem. Soc. Rev.* **2012,** *41*, (13), 4755.

25 L. Tauhardt; K. Kempe; K. Knop; E. Altuntaş; M. Jäger; S. Schubert; D. Fischer; U. S. Schubert, *Macromol. Chem. Phys.* **2011,** *212*, (17), 1918.
26 M. Bauer; C. Lautenschlaeger; K. Kempe; L. Tauhardt; U. S. Schubert; D. Fischer, *Macromol. Biosci.* **2012,** *12*, (7), 986.
27 M. Bauer; S. Schroeder; L. Tauhardt; K. Kempe; U. S. Schubert; D. Fischer, *J. Polym. Sci. A: Polym. Chem.* **2013,** *51*, (8), 1816.
28 T. G. Bassiri; A. Levy; M. Litt, *J. Polym. Sci. B: Polym. Lett.* **1967,** *5*, (9), 871.
29 T. Kagiya; S. Narisawa; T. Maeda; K. Fukui, *J. Polym. Sci. B: Polym. Lett.* **1966,** *4*, (7), 441.
30 W. Seeliger; E. Aufderhaar; W. Diepers; R. Feinauer; R. Nehring; W. Thier; H. Hellmann, *Angew. Chem. Int. Ed. Eng.* **1966,** *5*, (10), 875.
31 D. A. Tomalia; D. P. Sheetz, *J. Polym. Sci. A: Polym. Chem.* **1966,** *4*, (9), 2253.
32 F. Wiesbrock; R. Hoogenboom; C. H. Abeln; U. S. Schubert, *Macromol. Rapid Commun.* **2004,** *25*, (22), 1895.
33 T. Bus; C. Englert; M. Reifarth; P. Borchers; M. Hartlieb; A. Vollrath; S. Hoeppener; A. Traeger; U. S. Schubert, *J. Mater. Chem. B* **2017,** *5*, (6), 1258.
34 A. C. Rinkenauer; L. Tauhardt; F. Wendler; K. Kempe; M. Gottschaldt; A. Traeger; U. S. Schubert, *Macromol. Biosci.* **2015,** *15*, (3), 414.
35 B. Guillerm; S. Monge; V. Lapinte; J. J. Robin, *Macromol. Rapid Commun.* **2012,** *33*, (19), 1600.
36 M. Bauer; C. Lautenschlaeger; K. Kempe; L. Tauhardt; U. S. Schubert; D. Fischer, *Macromol. Biosci.* **2012,** *12*, (7), 986.
37 C. Taubmann; R. Luxenhofer; S. Cesana; R. Jordan, *Macromol. Biosci.* **2005,** *5*, (7), 603.
38 C. Legros; M.-C. De Pauw-Gillet; K. C. Tam; S. Lecommandoux; D. Taton, *Eur. Polym. J.* **2015,** *62*, (Supplement C), 322.
39 P. J. M. Bouten; D. Hertsen; M. Vergaelen; B. D. Monnery; M. A. Boerman; H. Goossens; S. Catak; J. C. M. van Hest; V. Van Speybroeck; R. Hoogenboom, *Polym. Chem.* **2015,** *6*, (4), 514.
40 S. Cesana; J. Auernheimer; R. Jordan; H. Kessler; O. Nuyken, *Macromol. Chem. Phys.* **2006,** *207*, (2), 183.
41 Z. He; L. Miao; R. Jordan; D. S-Manickam; R. Luxenhofer; A. V. Kabanov, *Macromolecular Bioscience* **2015**, *15*, (7), 1004.
42 M. Glassner; M. Vergaelen; R. Hoogenboom, *Polym. Int.* **2017**, *67*, (1), 32.
43 S. K. Filippov; B. Verbraeken; P. V. Konarev; D. I. Svergun; B. Angelov; N. S. Vishnevetskaya; C. M. Papadakis; S. Rogers; A. Radulescu; T. Courtin, *J. Phys. Chem. Lett.* **2017,** *8*, (16), 3800.
44 M. Hartlieb; D. Pretzel; K. Kempe; C. Fritzsche; R. M. Paulus; M. Gottschaldt; U. S. Schubert, *Soft Matter* **2013,** *9*, (18), 4693.
45 H. Ohshima, *J. Colloid Interface Sci.* **1994,** *168*, (1), 269.
46 V. E. Meyer; G. G. Lowry, *J. Polym. Sci. Part A: Gen. Pap.* **1965,** *3*, (8), 2843.
47 C. Englert; A.-K. Trützschler; M. Raasch; T. Bus; P. Borchers; A. S. Mosig; A. Traeger; U. S. Schubert, *J. Control. Release* **2016,** *241*, 1.
48 A. Vollrath; A. Schallon; C. Pietsch; S. Schubert; T. Nomoto; Y. Matsumoto; K. Kataoka; U. S. Schubert, *Soft Matter* **2013,** *9*, (1), 99.
49 M. N. Leiske; M. Hartlieb; F. H. Sobotta; R. M. Paulus; H. Gorls; P. Bellstedt; U. S. Schubert, *Polymer Chemistry* **2016,** *7*, (30), 4924.
50 S. M. Shawki; A. E. Hamielec, *J. Appl. Polym. Sci.* **1979,** *23*, (11), 3155.
51 K. Kempe; S. Jacobs; H. M. L. Lambermont-Thijs; M. M. W. M. Fijten; R. Hoogenboom; U. S. Schubert, *Macromolecules* **2010,** *43*, (9), 4098.
52 R. Mehta; R. Kumari; P. Das; A. K. Bhowmick, *J. Mater. Chem. B* **2014,** *2*, (37), 6236.
53 M. N. Leiske; F. H. Sobotta; S. Hoeppener; J. C. Brendel; A. Traeger; U. S. Schubert, *Biomacromolecules* **2017**.
54 R. Luxenhofer; G. Sahay; A. Schulz; D. Alakhova; T. K. Bronich; R. Jordan; A. V. Kabanov, *J Control Release* **2011,** *153*, (1), 73.
55 D. Pezzoli; E. Giupponi; D. Mantovani; G. Candiani, *Sci. Rep.* **2017,** *7*, 44134.
56 K. A. Curtis; D. Miller; P. Millard; S. Basu; F. Horkay; P. L. Chandran, *PLOS ONE* **2016,** *11*, (9), e0158147.
57 A. Rémy-Kristensen; J.-P. Clamme; C. Vuilleumier; J.-G. Kuhry; Y. Mély, *BBA - Biomembranes* **2001,** *1514*, (1), 21.

58 N. Zhao; S. Roesler; T. Kissel, *Int. J. Pharm.* **2011,** *411*, (1), 197.
59 E. V. B. van Gaal; R. van Eijk; R. S. Oosting; R. J. Kok; W. E. Hennink; D. J. A. Crommelin; E. Mastrobattista, *J. Control. Release* **2011,** *154*, (3), 218.
60 A. C. Rinkenauer; L. Tauhardt; F. Wendler; K. Kempe; M. Gottschaldt; A. Traeger; U. S. Schubert, *Macromol. Biosci.* **2015,** *15*, (3), 414.
61 S. Tenzer; D. Docter; J. Kuharev; A. Musyanovych; V. Fetz; R. Hecht; F. Schlenk; D. Fischer; K. Kiouptsi; C. Reinhardt; K. Landfester; H. Schild; M. Maskos; S. K. Knauer; R. H. Stauber, *Nat. Nanotechnol.* **2013,** *8*, 772.
62 S. Yamano; J. Dai; A. M. Moursi, *Molecular Biotechnology* **2010,** *46*, (3), 287.
63 J.-P. Behr, *Chimia* **1997,** *51*, (1-2), 34.
64 J. J. Virgen-Ortiz; J. C. S. dos Santos; A. Berenguer-Murcia; O. Barbosa; R. C. Rodrigues; R. Fernandez-Lafuente, *J. Mater. Chem. B* **2017,** *5*, (36), 7461.
65 M. N. Leiske; M. Hartlieb; C. Paulenz; D. Pretzel; M. Hentschel; C. Englert; M. Gottschaldt; U. S. Schubert, *Adv. Func. Mater.* **2015,** *25*, (16), 2458.
66 M. Hartlieb; D. Pretzel; C. Englert; M. Hentschel; K. Kempe; M. Gottschaldt; U. S. Schubert, *Biomacromolecules* **2014,** *15*, (6), 1970.
67 T. Lühmann; M. Schmidt; M. N. Leiske; V. Spieler; T. C. Majdanski; M. Grube; M. Hartlieb; I. Nischang; S. Schubert; U. S. Schubert; L. Meinel, *ACS Biomater. Sci. Eng.* **2016**.
68 M. Hartlieb; T. Bus; J. Kübel; D. Pretzel; S. Hoeppener; M. N. Leiske; K. Kempe; B. Dietzek; U. S. Schubert, *Bioconjugate Chem.* **2017,** *28*, (4), 1229.

GRAPHICAL ABSTRACT

David Hertz,[a,b,#] Meike N. Leiske,[b,c,#] Thomas Wloka,[b,c] Anja Traeger,[b,c] Matthias Hartlieb,[b,c,¶] Michael M. Kessels,[a] Stephanie Schubert,[b,d] Britta Qualmann,[a,b,*] Ulrich S. Schubert[b,c,*]

Comparison of random and gradient amino functionalized poly(2-oxazoline)s: Can the transfection efficiency be tuned by the macromolecular structure?

Gradient and random water-soluble copolymers consisting of either 2-methyl-2-oxazoline (MeOx) and 2-aminobutyl-2-oxazoline (AmOx) (gradient copolymers) or 2-ethyl-2-oxazoline (EtOx) and AmOx (random copolymers) are prepared using the cationic ring-opening technique. Polymers with different AmOx contents are characterized and compared regarding their polyplex formation and dissociation ability as well as cytotoxicity, cellular uptake and transfection efficiency. The study compared L929 mouse fibroblasts with Hepa1-6 murine liver cells in different cultivation media.

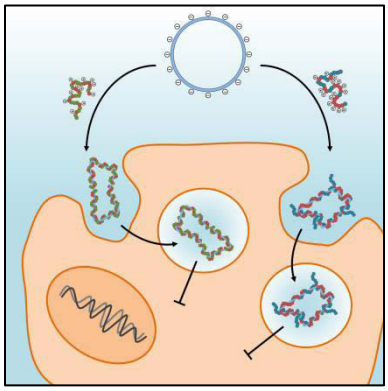

Publication P6

Evolution of poly(2-oxazoline)s from in vitro and in vivo studies to clinical trials

M. N. Leiske, M. Hartlieb, A. Traeger, U. S. Schubert, *submitted*.

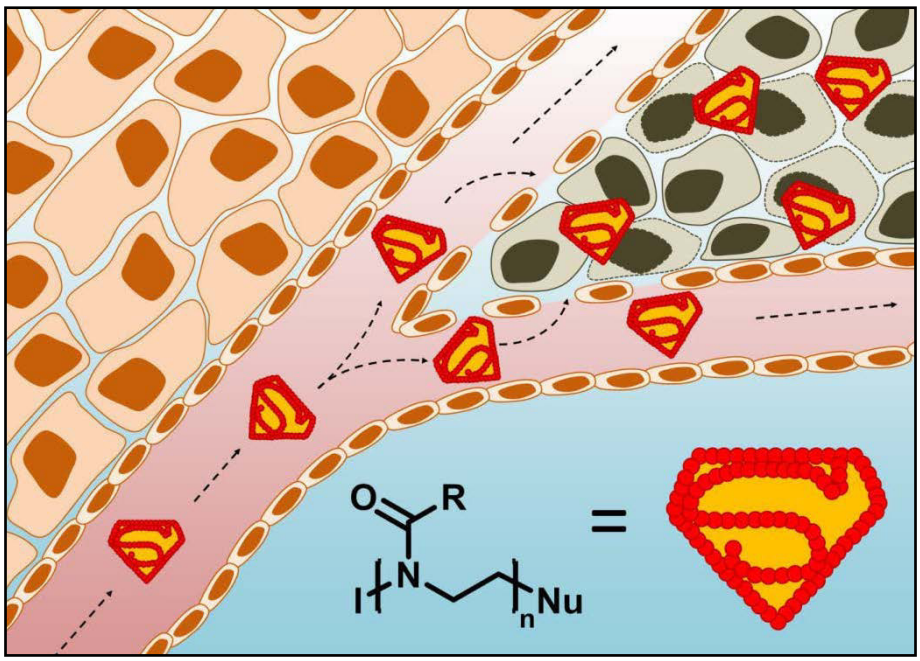

Evolution of poly(2-oxazoline)s from *in vitro* and *in vivo* studies to clinical trials

Meike N. Leiske,[a,b] Matthias Hartlieb,[a,b,†] Anja Traeger,[a,b] Ulrich S. Schubert[a,b,*]

[a.] *Jena Center for Soft Matter (JCSM), Friedrich Schiller University Jena, Philosophenweg 7, 07743 Jena, Germany.*
[b.] *Laboratory of Organic and Macromolecular Chemistry (IOMC), Friedrich Schiller University Jena, Humboldtstraße 10, 07743 Jena, Germany.*
[c.] *† Current address: Institute of Biomaterial Science, Helmholtz-Zentrum Geesthacht, Kantstr. 55, 14513 Teltow, Germany.*

Research on poly(2-oxazoline)s (P(Ox)s) has significantly evolved over the last decades. Whereas mainly synthesis and characterization were studied first, focus is increasingly shifting towrads biomedical applications of the polymer class, also catalyzed by the drawbacks of commonly used polymers, such as poly(ethylene glycol) (PEG). The cationic ring-opening polymerization enables the copolymerization of various functional monomers, as well as modifications at the α- and ω-terminus. This variety of functional groups is supposed to be beneficial for self-assembly processes, drug conjugation or polyplex formation. Copolymers with 2-ethyl-2-oxazoline (EtOx) or 2-methyl-2-oxazoline (MeOx) repeating units were found to show stealth ability and, consequently, provide an enhanced biocompatibility and elongated blood circulation times. For these reasons, P(Ox)s are progressively used for *in vivo* studies and clinical trials to find safe pharmaceuticals. Hence, the synthetic approaches leading to biomedical relevant P(Ox)s, their biocompatiblity, as well as findings from *in vivo* studies using P(Ox)s is summarized and evaluated within this review.

Key learning points

- P(Ox) synthesis and important polymer characteristics for *in vivo* studies
- Important P(Ox) architectures for *in vivo* studies
- Influence of P(Ox)s on the blood circulation time and the biodistribution of drugs
- Controlled drug release by P(Ox) conjugates
- Developments in cancer therapy

Introduction

The first synthetic polymer-based medicines in clinical practice were developed only three decades ago and the first product approval occurred in 1990.[1] In the 1990s, R. Duncan coined the term “polymer therapeutics”, which means that the polymer can either act as the bioactive itself or as a part of the covalent conjugate, *e.g.* polymer-drug conjugates and polymer-protein conjugates.[2] Furthermore, self-assembled systems, such as polymeric micelles and multi-component polyplexes, which are known as non-viral vectors, are of great importance.[1] In general, biodegradable structures are preferred since the body needs to be able to deal with the polymers after they fulfilled their purpose; however, none of them should lead to undesired toxicity or an immunogenic response before and after biodegradation.[3, 4]

The currently most prominent example in this context is poly(ethylene glycol) (PEG), which is already in use for several applications against various diseases, *e.g.* multiple sclerosis (Copaxone®), hepatitis C (PEGIntron®) or anaemia (Macugen®, Puricase®).[5] However, many advantages and disadvantages of

PEG have become apparent, as reviewed by Knop *et al.*.[6] On the one hand, PEG can be synthesized with a tailored molar mass and narrow dispersity (Đ < 1.2). The resulting polymers are both, soluble in water and organic solvents, which enables post-polymerization functionalization reactions, as well as the conjugation and solubilization of hydrophobic drugs. The polymer itself shows a stealth effect and has a low intrinsic toxicity. On the other hand, PEG has certain disadvantages, *i.e.* in terms of its production using highly toxic and explosive ethylene oxide. Furthermore, toxic by-products can be formed during the polymerization. Additional issues concern their storage stability as well as allergic and hypersensitivity reactions, complement activation, the accelerated blood clearance (ABS) phenomenom and, last but not least, the existence of anti-PEG antibodies in up to 25% of the human population.[6, 7]

For these reasons, researchers are continuously searching for alternatives to PEG. Examples are poly(amino acid)s, poly(glycerol), and poly(2-oxazoline)s (P(Ox)s), in particular 2-ethyl-2-oxazoline (EtOx) and 2-methyl-2-oxazoline (MeOx).[6, 8] P(Ox)s are pseudo peptides that were first synthesized *via* cationic ring-opening polymerization (CROP) in the 1960s. The polymerization technique enables the reproducible synthesis of tailored macromolecules with a narrow dispersity (Đ < 1.2),[9] which is of critical importance for clinical applications.

A crucial drawback in the synthesis of P(Ox)s in the 20th century were the long reaction times. This has been overcome in 2004, when F. Wiesbrock *et al*. combined microwave assisted heating with CROP, reducing the reaction times from weeks to minutes.[10] Since then, many new functionalization strategies have been successfully established for the synthesis of functional P(Ox)s.[11, 12] This variety of possible structures[13] and, therefore, accessible nano and micro architectures[14] has shifted the point of interest from synthetic aspects to biomedical applications, as evident by the increasing amount of publications of P(Ox)s related to *in vitro* or i*n vivo* applications (Figure 1).

The aim of this review is to conclude the most important characteristics of P(Ox)s and their various possible applications regarding biomedical science in different fields of interest, namely drug delivery or gene delivery, *e.g.* for cancer research or Parkinson's disease. By now, there are already some excellent reviews about the biocompatibility and the variety of possible nanostructures in *in vitro* systems.[2, 8, 13-15] However, since the biomedical research on P(Ox)s has, by the conduction of the first clinical trial, reached a new level utilizing these polymers, this review will focus on the progress of *in vivo* studies using P(Ox)s.

As the reproducible and versatile synthesis of P(Ox)s is one of their major advantages, we will provide a short introduction on the possibilities of P(Ox) synthesis and polymer modification and cover the most promising *in vitro* studies before discussing important milestones within the field of *in vivo* experiments using P(Ox)s as a promising polymer class, which has already made its way to the first clinical trial.

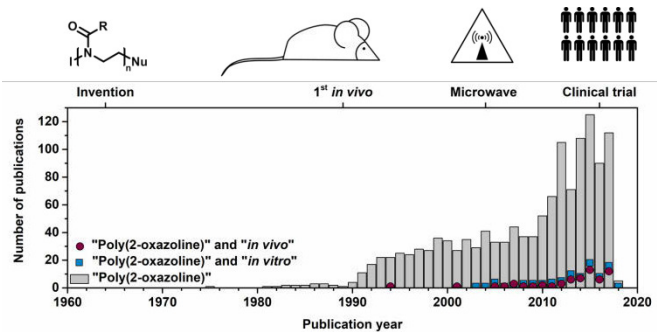

Figure 1. Publications in the research area of poly(2-oxazoline)s and the subareas *in vitro* and *in vivo* regarding www.webofknowledge.com on 23rd of January 2018.

Synthesis of P(Ox)s and P(Ox)-based materials

P(Ox)s are pseudo peptides, meaning that their polymer backbone is stable against the degradation by enzymatic degradation within cellular compartments. In general, they are synthesized *via* the CROP of 2-oxazolines, enabling the introduction of specific functional groups at different positions of the polymers as well as copolymerization of different monomers (Scheme 1).

Using functional initiators represents one opportunity for the introduction of different α-end groups.[10] In particular, alkyl functionalities are used; however also amines[16] and carboxyl groups[17, 18], which are of great interest for post polymerization modification, are utilized. The introduction of ω-functionalities can be realized by the utilization of different nucleophiles as terminating agents to introduce, *e.g.*, hydroxyl[17, 19, 20] or carboxyl groups, amino groups[21, 22] or large hydrophobic end groups,[19, 23, 24] which are important to obtain liposomes with P(Ox) modifications on the shell.

The possibility and simplicity to install functional side-chain are the most important features and major advantages compared to PEG.[11] By variation of the ratios or distribution of functional groups the polymer characteristics can be further adjusted.

MeOx and EtOx are commercially available monomers, and, at physiological conditions poly(2-methyl-2-oxazoline) (P(MeOx)) and poly(2-ethyl-2-oxazoline) (P(EtOx)) are water soluble and show a decreased unspecific interaction with proteins as well as cellular uptake, which is favorable for most biomedical applications. By copolymerization with other monomers, functional or hydrophobic groups can be easily introduced.

In particular, alkynes,[25] azides,[10] alkenyls,[10] carboxyl groups,[26] aldehydes[27] or amino groups[28] are interesting candidates for self-assembly,[22] further modification,[26] or drug attachment.[25] These functional groups can then be used for labeling,[29] cross-linking,[30] attachment of ligands or drug-,[25, 31] gene-,[2] and protein-conjugation.[2, 32]

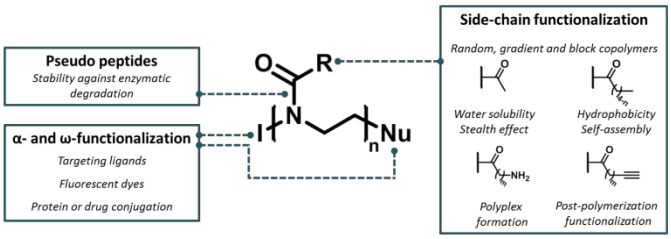

Scheme 1. Schematic representation of P(Ox)s and their possibilities of modification useful for biomedical applications.

Furthermore, the introduction of hydrophobic side-chains leads to the feasibility of self-assembly in aqueous media, as well as serum or cell compartments.[33]

The great structural diversity of P(Ox)s makes them a promising starting material for various biomedical applications. However, before we can focus on the exciting aspects of the interaction of P(Ox) with cells and organisms an intermediate stop at POx-based materials is necessary. The versatility of P(Ox) does not halt the level of chemical functionality and the nano or micro structure heavily influences the interaction of polymer therapeutics with biological systems.

Nanomaterials based on P(Ox)s

The living CROP offers a high level of control over the macromolecular structure and enables the synthesis of various polymeric architectures such as star-shaped copolymers, bottle brushes or block copolymers by sequential monomer addition.[2] Exploiting the variations in reactivity ratios of different monomers (*i.e.* EtOx and 2-phenyl-2-oxazoline), gradient copolymers can be produced in a one pot fashion.[13, 14] These segmented polymers can, in turn, self-assemble (Scheme 2) into nanostructures such as micelles, polymersomes or nanoparticles, whereas a hydrophobic monomer (commonly 2-butyl- or 2-nonyl-2-oxazoline) is used to constitute the water insoluble domain and hydrophilic monomers, *e.g.* EtOx or MeOx, are utilized to create the hydrophilic segment. The block ratio usually determines which sub structure is formed with longer hydrophobic domains favoring nanoparticles as well as polymersomes and shorter hydrophobic segments forming micelles. This nanoscopic phase separation can be utilized to encapsulate *i.e.* drug molecules or dyes,[22, 34] either passively by an absorption of the small molecule into the hydrophobic phase of the material or by attachment to functional subunits of the polymer. The hydrophilic shell acts as shielding towards unspecific interaction with biological matter and prevents *i.e.* undesired protein interaction, just as a PEG shell would.[4, 23, 35, 36]

As described in the previous chapter, the functional diversity able to be integrated into POx is vast and this versatility can be used to create cross linked materials using side chain and end functionalities.[13] Based on the initial solution behavior of the polymer or the processing mechanism, the resulting materials can take the form of nanogels,[13] capsules,[37] or hydrogels[13] able to be used for a multitude of applications from drug delivery,[26] gene delivery,[28] gene purification[29] and tissue engineering,[38] or as nano reaction compartment[39].

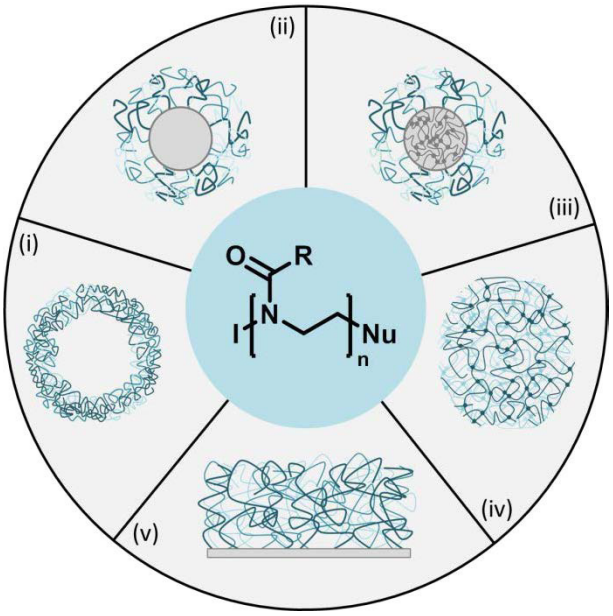

Scheme 2. Schematic representation of different self-assembled P(Ox) structures: (i) Nanocapsules,[37] (ii) micelles,[21] (iii) nanogels,[13] (iv) hydrogels,[13] and (v) surface coatings.[40]

Cross-linking can be accomplished in a covalent fashion or by physical interactions.[13]

Due to the excellent stealth abilities of derivatives such as P(MeOx) and P(EtOx), these polymers can also be used to generate anti- or low-fouling coatings able to prevent or reduce the attachment of microorganisms by generating a hydrophilic, highly hydrated layer.[40] This feature can be used to coat surfaces of, *i.e.*, implants or sensors to prevent undesired biofilm formation. For a deeper insight into the structural diversity of POx the reader is referred to several excellent reviews in the field.[14 9, 15]

***In vitro* studies of P(Ox)s and P(Ox)-based materials**

To evaluate the potential of P(Ox)s for biomedical applications, *in vitro* investigations, in particular cell tests, are mandatory. Studies done before 2012 can be found elsewhere.[2]

To ensure suitability for further *in vivo* studies or clinical trials, all polymer therapeutics need to be preliminary tested for cell viability regarding their hemolytic activity, erythrocyte aggregation as well as cytotoxicity (Scheme 3).

Hemolysis assays elucidating P(EtOx)[41] or P(MeOx)[42] homopolymers of various molar masses and nanogels with an EtOx shell[30] revealed no hemolytic activity caused by the polymers. Similar results were observed in terms of erythrocyte aggregation in the presence of P(EtOx)[41] or P(MeOx).[42] In addition to these blood compatibility experiments, general cell viability determinations are of great interest within the context of *in vivo* investigations. Using standardized *in vitro* cytotoxicity assays, P(MeOx)[42] and P(EtOx)[41] did not influence the cell viability, however, in long-term experiments both of the polymers slightly decreased the cell viability in dependence on the molar mass, polymer concentration and incubation time. In addition to the homopolymers, also polymeric micelles with either a poly(lactide)[43] or a hydrophobic 2-butyl-2-oxazoline[33] core were determined to be non-toxic. Since it is possible that

P(Ox)s are partially hydrolyzed within an organism, also the evaluation of partially hydrolyzed P(Ox)s is relevant and revealed a dependence of the cytotoxicity on the degree of hydrolysis.[44]

Additionally to a high biocompatibility, applications in drug or gene delivery require moderate cellular uptake and an efficient release of the active pharmaceutical ingredient (API) or the genetic material. In general, the cellular uptake of polymer carriers with an EtOx shell was found to be slower than that of pure drugs,[16, 18, 32, 45] which might be advantageous in terms of blood circulation times and pharmacokinetics. The cellular uptake of EtOx shielded nanogels was determined to be dependent on the amount of cationic charges within the core.[30] Furthermore, cell specificity of the carriers could be increased by the utilization of special targeting units.[16, 17]

In vivo performance of P(Ox)s and P(Ox)s based materials

In vitro experiments have shown demonstrated that P(EtOx) and P(MeOx) are generally biocompatible polymers, meaning that they do not induce cytotoxicity, hemolytic activity or cell aggregation up to polymer concentrations of 10 mg mL^{-1}. However, these experiments can only provide a first impression about the therapeutic efficiency of the polymeric carrier systems.

In vivo, several attributes of drugs can be altered by using polymers (Scheme 4): (i) Many drugs are not (well) water soluble. The conjugation to or encapsulation into polymeric delivery systems that can be solubilized or suspended in water is a common way to resolve this issue. (ii) Polymeric carriers can enhance the blood circulation time of drugs, *i.e.* by the prevention of phagocytosis or undesired protein interaction. Furthermore, small molecules usually undergo renal excretion. The conjugation to polymers, and polymer based carrier systems having a significantly higher hydrodynamic volume can reduce the blood clearance of the drugs and, consequently, increase their blood circulation times. (iii) In contrast to *in vitro* cell culturing, various different tissue and cell types expressing different receptors and markers can be encountered by a drug delivery system within an organism. Polymer carriers can be equipped with targeting ligands to enhance the cell specificity of the drugs.

P(Ox)s have the possibility to fulfill all these requirements for a successful drug delivery system. Due to their preparation route, it is possible to introduce the stealth monomers EtOx and MeOx into the polymer chain to enhance the blood circulation time.[32] Furthermore, by using functional α-, ω- or side-chain functionalities, they can be equipped by various different targeting moieties to achieve tissue specificity.[16] For this reason, *in vivo* experiments regarding their blood circulation times, cellular uptake and the following therapeutic efficiency are in the current focus of research.

Biodistribution and biocompatibility

One of the most important properties of a polymeric material in therapeutic context is its ability to circulate in the bloodstream for a prolonged time in order to accumulate on the target site. On that account, stealth abilities are beneficial to reduce phagocytosis, protein interaction and undesired cellular uptake.

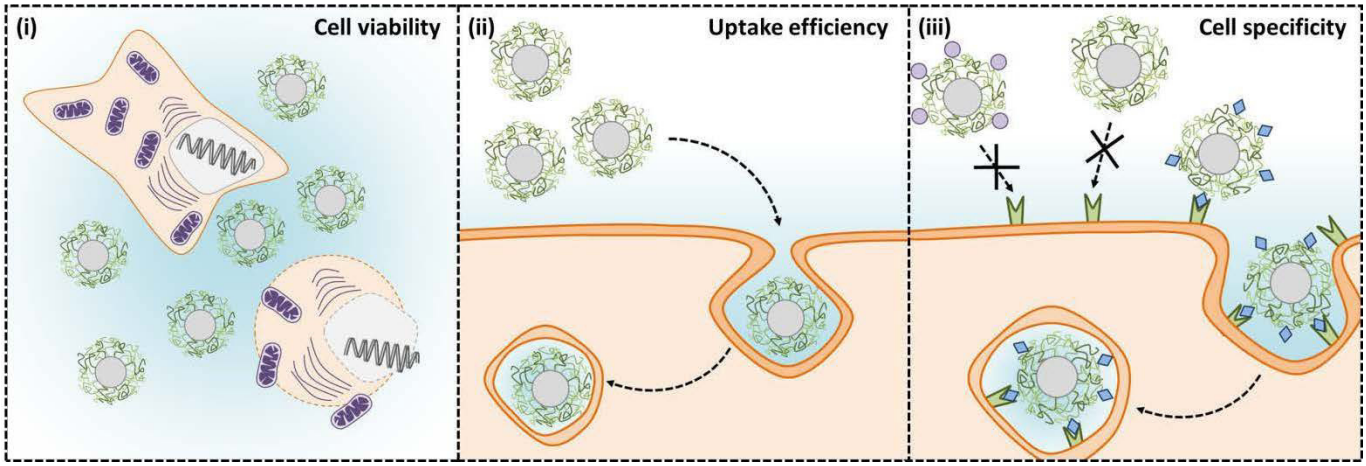

Scheme 3. Possibilities of in vitro studies in terms of biochemical polymer or carrier systems: (i) Cell viability determination by cytotoxicity, hemoglobin release or cell aggregation measurements, (ii) comparison of uptake efficiency of drugs, polymers and carrier systems, (iii) utilization of different cell lines for the determination of cell specificity.

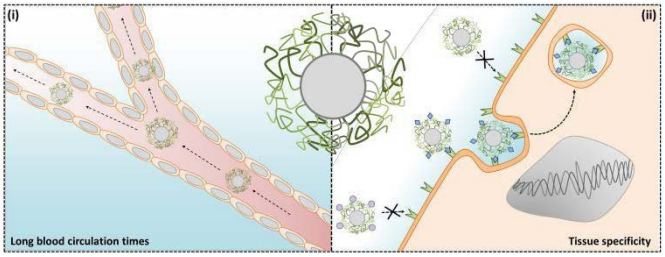

Scheme 3. Favorable attributes of polymeric nanocarriers for drug delivery. (i) Long blood circulation times, and (ii) tissue specificity, *i.e.* targeted cellular uptake.

The biodistribution of P(Ox) was investigated by different groups (Table 1) using radioactively labeled polymers utilizing various tracer elements (^{125}Iodine,[3, 23] ^{89}Zirkonium,[4, 36] ^{18}Fluorine[36] or ^{111}Indium[46]). By measuring the tissue related radioactivity, organ accumulations and blood circulation times could be determined. P. Goddard *et al*. evaluated the dependency of the blood circulation time and organ accumulation on the molar mass of the polymer exemplary for copolymers consisting of MeOx and 2-(4-hydroxy-phenyl)-2-oxazoline (HOPeOx) with similar monomer ratios, but varying polymer length.[3]

From the results it is obvious that the blood circulation time of the polymer is dependent on its molar mass. After 48 h of treatment with the 29 kDa polymer, the mean radioactivity of the blood is still three times higher than after treatment with a 15 kDa polymer. By comparing the mean radioactivity of the different tissues, no significant variety is observable, leading to the conclusion that smaller P(Ox)s are excreted faster.[4]

It was however demonstrated by M. Glassner *et al.* that the radiolabel itself can have a significant influence on the biodistribution.[36] *In vivo* and *ex vivo* experiments of the polymers revealed a clear dependence of 5 kDa P(EtOx) biodistribution on the radiolabel being used. ^{89}Zr-labeled polymers showed an increased uptake into the kidneys, liver and heart after 1 h and 4 h, whereas initially after polymer injection the kidney uptake was increased when using the ^{18}F label (Figure 2). This finding demonstrated that even small end-groups can have a tremendous effect on the performance of a polymeric carrier *in vivo* and have to be considered carefully.

As PEG represents the gold standard for stealth polymers, different research groups compared water soluble P(Ox)s with PEG. Herein, the pure polymers[4, 46] as well as polymer shielded liposomes were elucidated.[23, 35]

L. Wyffels *et al.* synthesized well-defined P(Ox)s ($Đ \leq 1.1$) in a molar mass range of 20 to 110 kDa and compared the tissue distribution of PEG and P(EtOx) of various molar masses using ^{89}Zr radiolabeling. Their results showed an increased blood circulation time for polymers of at least 40 kDa. Furthermore, with increasing molar mass, the differences between P(EtOx) and PEG in tissue distribution decreased, leading to a similar behavior and good comparability of polymers when the overall molar mass (not the degree of polymerization) is similar.

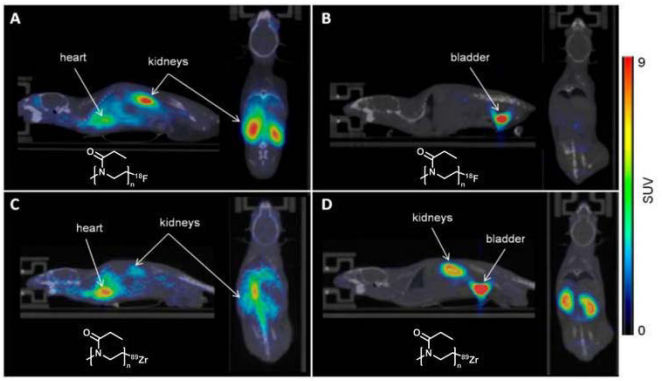

Figure 2. Representative μPET/CT images of C57BL/6 mice injected with [^{18}F]-PEtOx (A and B) or [^{89}Zr]-Df-PEtOx (C and D) at 1 min (A and C) or 60 min (B and D) p.i. Reprinted from Ref.[36] with permission from the American Chemical Society.

Furthermore, S. Zalipsky *et al.* compared pure liposomes with PEG and P(Ox) grafted liposomes. These were compared regarding their elimination from blood after certain time points. By comparing the blood clearance rates of the liposomes, PEG and P(MeOx) grafted liposomes show similar circulation times, whereas P(EtOx) grafted liposomes were excreted faster.

Neither of the conducted studies showed any evidences of toxicity or immune response. Hence, the experiments using P(Ox) revealed that they have a similar biodistribution and blood clearance rate as PEG and are biocompatible, making them ideal candidates for the usage as drug carriers. Furthermore, the adjustment of the molar mass of the polymers and the choice of the monomers can influence the blood circulation time as well as the organ accumulations.

P(Ox) based drug conjugates and delivery systems

Short blood circulation times of drugs represent one of the major obstacles in therapeutic applications. By the covalent conjugation of biocompatible, stealth polymers such as PEG (PEGylation) these can be increased and, furthermore, the unspecific interactions with proteins in the blood plasma can be prohibited (stealth effect).[41] Similar to this principle it is possible to increase the half-life time of drugs by conjugation to P(Ox).[25, 32, 47] In particular, drugs that do not exhibit prolonged blood circulation or show high plasma stability benefit from this approach. As already mentioned, the living CROP of 2-oxazolines offers various opportunities of polymer functionalization.[10] Consequently, the conjugation of single APIs to the α- or ω-chain end of the macromolecules is possible.[32, 47] By using this technique, only one API per polymer chain can be attached, leading to reproducible pharmacokinetics.

Table 1. Overview of publications using P(Ox)s in terms of biocompatibility and pharmacokinetics.

Author	Year	Polymer	Purpose	Drug	Nanostructure
Goddard *et al.*[3]	1989	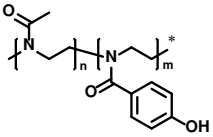	Biodistribution and blood clearance	None	None
Zalipsky *et al.*[23]	1996	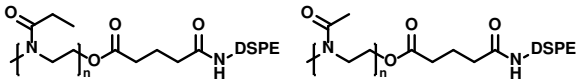	Blood clearance	None	Liposome
Gaertner *et al.*[46]	2007	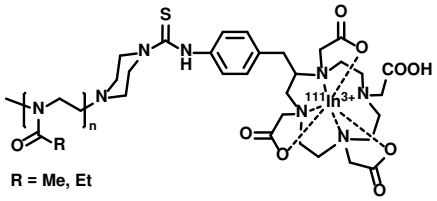	Biodistribution	None	None
Mero *et al.*[47]	2012	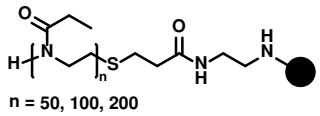	Physicochemical properties and aggregation potential	Granulocyte colony stimulating factor	Conjugate
Tong *et al.*[32]	2013	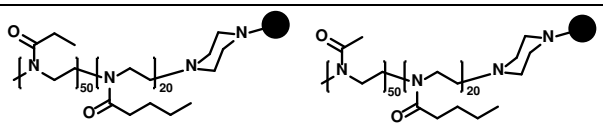	Crossing the BBB, Enhancement of blood circulation times	Superoxide dismutase I	Conjugate
Eskow Jaunarajs *et al.*[25]	2013	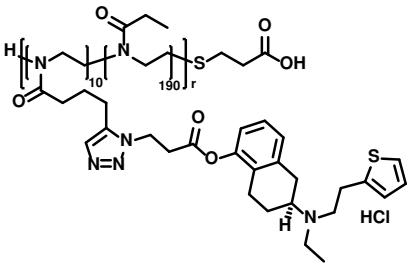	Parkinson's Disease	Rotigotine	Conjugate
Wyffels *et al.*[4]	2016	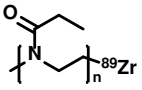	None	None	None
Glassner *et al.*[36]	2017	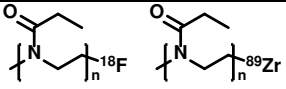	None	None	None

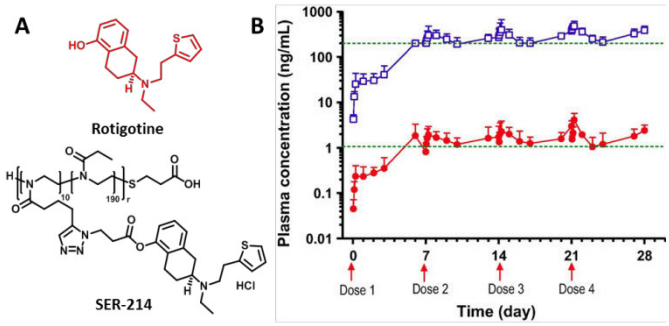

Figure 3. A) Schematic representation of the chemical structures of rotigotine and SER-214. B) Plasma levels of release rotigotine (red dots) and total releasable rotigotine (blue squares) in MPTP-lesioned monkeys (n = 3, ± SD) following four weekly subcutaneous injections of SER-214 at a dose of 1 mg kg^{-1} (rotigotine equivalents). Reprinted from Ref.[31] with permission from Elsevier.

A. Mero *et al.* conjugated the granulocyte stimulating factor G (CSF-G) to $P(EtOx)_n$ with varying molar masses.[47] The conjugates of 10 and 20 kDa P(EtOx) were compared with native CSF-G *in vivo*, resulting in a higher pharmacodynamics area under the curve (AUC) for neutrophils and leucocytes. The improvement of the AUC furthermore increased with the molar mass of the used polymers. Consequently, the biological activity of the conjugates could be demonstrated successfully.

In addition to drug conjugation *via* end functionalities, the conjugation to functional side-chains of P(Ox)s might be beneficial. The living CROP enables the possibility to create tailored copolymers, where monomer units can be distributed randomly, statistically or block-like within the polymer chain.[11] By adjusting the monomer ratio, a defined amount of functional groups can be introduced and used for multiple API conjugation. K. L. Eskow Jaunarajs *et al*. applied randomly distributed copolymers for the conjugation of a rotigotine derivative *via* azide-alkyne click chemistry.[25] Conjugates were equipped with an esterase labile linker (Figure 3A) to ensure the release of the drug.

After adjustment of the monomer composition within the polymer as well as the injected dose, a steady plasma drug concentration could be obtained over several days (Figure 3B),[31] which is advantageous for the treatment of Parkinson's disease (PD). Within an *in vivo* study using macaque monkeys, the authors compared the impact of SER-214 and L-3,4-dihydroxyphenylalanine (L-DOPA), which is clinically used for the treatment of PD, however with the side-effect of dyskinesia due to fluctuating plasma concentrations. By the weekly treatment with 1 mg kg^{-1} of SER-214, dyskinesia could be prevented completely, whereas doses of 15 mg kg^{-1} that were administered twice daily could not prevent the side-effect in 50% of the animals.[31] The pioneering results of the *in vivo* studies using SER-214 for the treatment of PD paved the way for the first clinical trial using P(Ox)s as polymeric carriers. In phase I, the human subjects received weekly doses and expressed stable plasma drug concentrations, caused by a continuous rotigotine release. These first positive results initiated a soon phase II trial.

In summary, water soluble P(Ox)s have blood clearance and biodistribution properties similar to PEG. Furthermore, their tissue accumulation is dependent on their molar mass and can also be altered by end-functionalization, *e.g.* by radio-labeling. Conjugation of APIs can influence the pharmacokinetics of the drug in a beneficial manner. For this reason, they might represent interesting candidates for the improvement of cancer therapy.

Cancer treatment

Cytostatic agents, which are commonly used in cancer therapy, are usually not tissue specific and are, consequently, responsible for various (severe) side-effects. This disadvantage might be prevented by efficient drug encapsulation or conjugation to polymeric drug carriers.[5] Furthermore, as shown in the last chapter, the pharmacokinetics can be altered and specific targeting units can be added to the drug carriers to achieve a tailored cellular uptake. It is envisioned that an ideal drug delivery system is able to deliver the drug to the target site and, in turn, to reduce unspecific cellular uptake as well as side-effects. Various self-assembled system using P(Ox) as a component were investigated for the delivery of different anti-cancer drugs *in vivo* (Table 2).

Overcoming the unwanted side-effects could already be partially achieved, *e.g.*, by PEGylation.[6] Conjugates consisting of a drug and the water soluble stealth polymer PEG enhanced the blood circulation times while reducing unwanted protein-interactions and cellular uptake. P(Ox)s exhibit similar beneficial characteristics, while possessing less unwanted side-effects such as toxic by-products during synthesis.[6] For these reasons, conjugation of anti-cancer drugs to P(Ox)s might improve their performance in terms of tumor inhibition potential.

A promising approach might be the conjunction of the drug to the polymer using a pH-sensitive hydrazone linker to ensure a stability of the conjugates in the blood stream, while the drug can be cleaved off in the acidic compartments of the (cancer) cells.[18, 26] The covalent binding of DOX *via* pH labile Schiff base within the cross-linked core of P(Ox)s nanogels could be utilized for efficient cancer therapy at were low doses of 1 mg kg^{-1}.[48] Another auspicious strategy might be the encapsulation of the drugs into P(Ox) based micelles[16, 18, 20] or modified liposomes.[24, 49] The defined self-assembly of the polymers offers hereby the opportunity to adjust the size of the drug carrier as well as the introduction of targeting units.

Polymeric nanostructures, which consist of a biodegradable (polyester) core and a P(Ox) shell, able to shield the material by the stealth moieties were prepared and investigated *in vivo*.[1, 16, 17, 20, 43, 45, 50] Furthermore, micelles, which only consist of P(Ox)s, were synthesized and characterized regarding their *in vivo* properties. Hereby, 2-oxazolines with hydrophobic side chains, *e.g.* BuOx, were used to form a hydrophobic micellar core [22, 33] exhibiting drug encapsulation efficiencies of 1:1 or even more,[21, 22, 33] leading to an increased drug solubility.[33]

Z. He *et al.* used 3rd generation toxoids, namely paclitaxel and docetaxel, encapsulated in P(Ox) micelles with a diameter below 100 nm.[21] They reached a drug incorporation ratio of nearly 1:1, comparing the weight of the drug and the polymer. After *in vitro* testing, *in vivo* studies were performed by comparing the tumor growth inhibition of the drug loaded polymeric micelles, Abraxane and Taxol®. Taxol® and P(Ox)-based micelles revealed a significant tumor growth inhibition while the survival time using the clinical approved formulation

of paclitaxel in an albumin nanoparticle (nab-paclitaxel, Abraxane) was worse (Figure 4). In 2014, H. Xu et al. used bifunctional liposomes consisting of cholesterol methyl carbonate conjugated to P(EtOx) for doxorubicin (DOX) delivery.[24] In vivo experiments resulted in elongated blood circulation times of the P(EtOx) modified liposomes when compared with their non-modified equivalents.

By using functional initiators or terminating agents, the introduction of functional α- or ω-end groups is possible.[10] Consequently, the polymeric nanostructures, such as micelles, can be modified by the conjugation of targeting units, which are cell specific.[16, 17, 43]

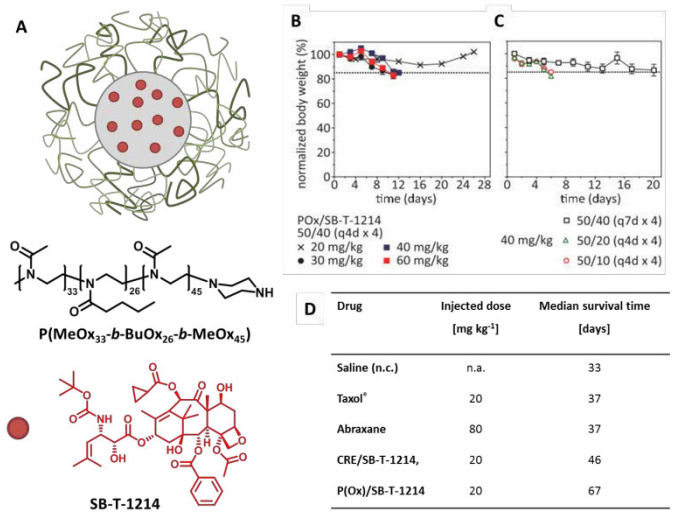

D

Drug	Injected dose [mg kg^{-1}]	Median survival time [days]
Saline (n.c.)	n.a.	33
Taxol®	20	37
Abraxane	80	37
CRE/SB-T-1214,	20	46
P(Ox)/SB-T-1214	20	67

Figure 4. Establishment of the safe dose of SB-T-1214 in nude mice. A) Schematic representation of micelles consisting of P(MeOx33-b-BuOx26-b-MeOx45) and the drug SB-T-1214. B) MTD of P(Ox)/SB-T-1214 = 50/40 formulation using a q4d × 4 treatment regimen in escalating doses from 20 to 60 mg/kg. C) MTD of P(Ox)/SB-T-1214 = 50/20 and 50/10 using a q4d × 4 regimen or 50/40, 40 mg/kg using a q7d × 4 regimen. D) Median survival time of mice after treatment with different formulations. Reprinted from Ref.[21] with permission from Elsevier.

Y. Gao *et al.* used paclitaxel loaded pH-sensitive polymeric micelles, which were decorated with a prostate specific membrane antigen antibody (YPSMA-1, Y). The micelles consisted of P(EtOx-*b*-LA) and aimed to target prostate cancer cells *via* the prostate specific membrane antigen (PSMA).[17]

In the 22Rv-1 tumor model, nearly a complete tumor growth inhibition could by observed by using PTX/PM-Y micelles, verifying the assumption of a targeted uptake by the PSMA positive prostate cancer cells and also demonstrating that P(EtOx) has sufficient shielding abilities to enable such an effect. L.-Y. Qiu *et al.* used folate modified to enhance the intracellular DOX delivery.[16] By comparing the results, folate modified nanostructures revealed the best tumor growth inhibition (Figure 5A) as well as a continuous increase in the body weight of the mice, while DOX treated animals lost bodyweight directly after drug administration (Figure 5B). Y. Gao *et al.* conjugated cyclic Arg-Gly-Asp-Tyr-Lys (cRGDyK, R) to P(EtOx-*b*-LA) to obtain pH-sensitive polymeric micelles to target the delivery of paclitaxel (PTX) to cure prostate cancer.[43] The micelles were evaluated *in vivo* regarding the biodistribution and tumor growth inhibition using the PC-3 tumor model (Figure 6).

Micelles, which were decorated with cRGDyK and loaded with 1,1'-dioctadecyl-3,3,3',3'-tetramethylindotricarbocyanine iodide (DiR) had an enhanced tumor uptake and a notable tumor inhibition (Figure 8). Compared with both, Taxol® and PTX/PM, PTX/PM-R exhibited the best tumor growth inhibition, which can be explained by the targeting.

Nevertheless, also PTX/PM were significantly better than Taxol® indicating that target specifity and pH-sensitivity could provide a synergistic effect. The small diameter of 28 nm of the drug loaded polymeric micelles might also have been beneficial for the EPR effect.[17] These experiments by various researchers showed an elongated blood circulation time[22, 49, 50] as well as an enhanced biocompatibility[22, 45] while the cytostatic effect on the cancer tissue could be kept similar to the pure drug or even improved.[16, 17, 21, 33, 43, 50]

The preparation of micelles also offers the opportunity to conduct a co-delivery of different tumor-suppressing substances.[45, 50] M.-J. Shieh *et al.* prepared micelles consisting of P(EtOx-*b*-LA) containing 10wt% meta-tetra(hydroxylphenyl)chlorin) (m-THPC), which represents a photosensitizer used for photodynamic therapy (PDT) Photodynamic therapy (PDT), however, causing phototoxicity.[45] By using polymeric micelles combined long lag times before light treatment, the photosensitivity could be reduced significantly, while enhancing the tumor growth inhibition.

Table 2. Overview on the publications using P(Ox)s for cancer curing.

Author	Year	Polymer	Drug	Nanostructure
Luxenhofer *et al.*[33]	2010	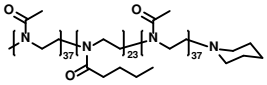	Paclitaxel	Micelles
Shieh *et al.*[45]	2010	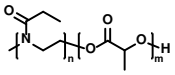	m-THPC	Micelles
Qiu *et al.*[16]	2013	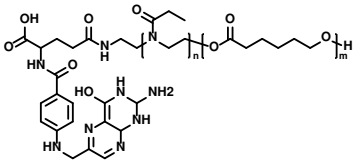	Doxorubicin	Micelles, conjugate
Xu *et al.*[24]	2014	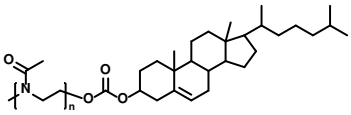	Doxorubicin	Modified liposomes
Gao *et al.*[17, 43]	2015	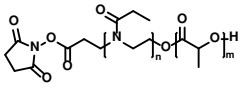	Paclitaxel	Micelles
Li *et al.*[18]	2015	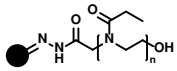	Doxorubicin	Micelles, conjugate
Zhao *et al.*[20]	2015	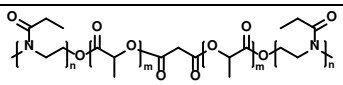	Doxorubicin and P-glycoprotein inhibitor	Micelles
He *et al.*	2015[21] 2016[22]	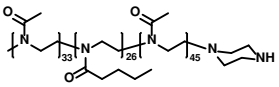	Taxoids, Paclitaxel	Micelles
Sedlacek *et al.*[26]	2017	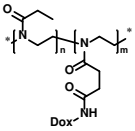	Doxorubicin	Conjugate
P. Zhang *et al.*[50]	2017	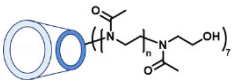	Cabazitaxel	Micelle
D. Hoelzer, M. N. Leiske *et. al.*[48]	2018	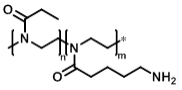	Doxorubicin	Core cross-linked nanogel

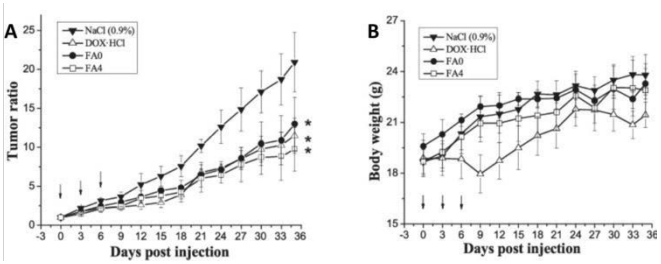

Figure 5. A) The increase ratio of tumor volume and B) body weight of mice treated with NaCl (0.9%), free DOX, FA0 and FA4. The black arrows indicate the days when the formulations are administrated. Each data point was calculated from four parallel experiments and was denoted as mean ± SD. *P < 0.05, compared with NaCl (0.9%). Reprinted from Ref. [16] with permission from Elsevier.

In summary, it can be stated that the used of P(Ox)s in terms of cancer drug conjugation was beneficial in all cases. Experiments demonstrated enhanced biocompatibility combined with improved anti-tumor efficiencies compared to the commercial available substances. Furthermore, the possibility to introduce targeting units to the polymeric drug carriers makes them attractive candidates for clinical developments.

Conclusion and outlook

P(Ox)s represent an interesting class of polymers with striking characteristics that can be introduced *via* the living CROP. The possibility to insert multiple functionalities as well as copolymerization in a tailored way leads to many options of drug conjugation as well as the introduction of targeting units. *In vivo* experiments of different research groups have shown their biocompatibility and their potential to be utilized in curative medicine.

Furthermore, a clinical trial using SER-214 for the treatment of Parkinson's disease is running. For these reasons, P(Ox)s are interesting for many biomedical applications, which have the potential to being used in many other application fields in nanomedicine. Prospectively, after the first successful clinical trial, the way ought to be paved for further clinical applications. Additionally, this might lead to a continuing increase of the research interest in the translation of P(Ox)s based materials to a biomedical setting.

Conflicts of interest

There are no conflicts to declare.

Acknowledgements

The authors highly acknowledge the German Federal Ministry of Education and Research (BMBF, #13N13416, smart-dye-livery). AT acknowledges the Carl Zeiss Foundation as well as the BMBF (#13XP5034A, PolyBioMik) for funding.

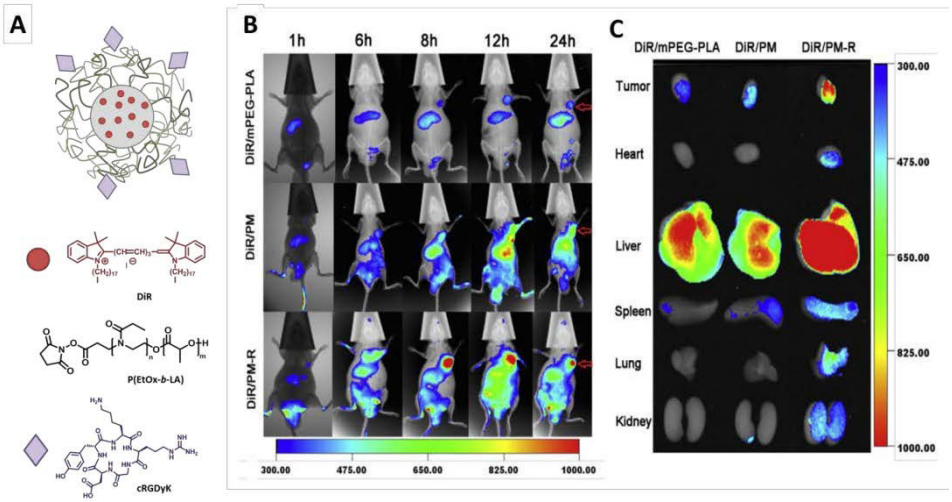

Figure 6. A: Schematic representation of the nanostructures. B: *In vivo* whole body imaging of PC-3 tumor bearing nude mice after DiR/mPEG PM, DiR/PM and DiR/PM-R administration at different time point at the same DiR dose of 20 μg kg^{-1}, respectively. C: The *ex vivo* images of tumors and organic tumor bearing mice sacrificed at 24 h. Intensity levels of DiR were depicted in the figure. Reprinted from Ref. [43] with permission from Elsevier.

Notes and references

1. R. Gaspar and R. Duncan, *Adv. Drug Deliv. Rev.*, 2009, **61**, 1220-1231.
2. R. Luxenhofer, Y. Han, A. Schulz, J. Tong, Z. He, A. V. Kabanov and R. Jordan, *Macromol. Rapid Commun.*, 2012, **33**, 1613-1631.
3. L. E. H. Peter Goddard, Janet Brown and Laurence J. Brookman *J. Controlled Release*, 1989, **10**, 5 - 16.
4. L. wyffels, T. Verbrugghen, B. D. Monnery, M. Glassner, S. Stroobants, R. Hoogenboom and S. Staelens, *J. Controlled Release*, 2016, **235**, 63-71.
5. R. Duncan and R. Gaspar, *Mol. Pharm.*, 2011, **8**, 2101-2141.
6. K. Knop, R. Hoogenboom, D. Fischer and U. S. Schubert, *Angew. Chem. Int. Ed.*, 2010, **49**, 6288-6308.
7. R. P. Garay, R. El-Gewely, J. K. Armstrong, G. Garratty and P. Richette, *Expert Opin. Drug Deliv.*, 2012, **9**, 1319-1323.
8. M. Barz, R. Luxenhofer, R. Zentel and M. J. Vicent, *Polym. Chem.*, 2011, **2**, 1900-1918.
9. B. Verbraeken, B. D. Monnery, K. Lava and R. Hoogenboom, *Eur. Polym. J.*, 2017, **88**, 451-469.
10. B. Guillerm, S. Monge, V. Lapinte and J.-J. Robin, *Macromol. Rapid Commun.*, 2012, **33**, 1600-1612.
11. M. Glassner, M. Vergaelen and R. Hoogenboom, *Polym. Int.*, 2018, **67**, 32-45.

12. H. Schlaad, C. Diehl, A. Gress, M. Meyer, A. L. Demirel, Y. Nur and A. Bertin, *Macromol. Rapid Commun.*, 2010, **31**, 511-525.
13. M. Hartlieb, K. Kempe and U. S. Schubert, *J. Mat. Chem. B*, 2015, **3**, 526-538.
14. P. Wilson, P. C. Ke, T. P. Davis and K. Kempe, *Eur. Polym. J.*, 2016, **88**, 486-515.
15. K. Lava, B. Verbraeken and R. Hoogenboom, *Eur. Polym. J.*, 2015, **65**, 98-111.
16. L.-Y. Qiu, L. Yan, L. Zhang, Y.-M. Jin and Q.-H. Zhao, *Int. J. Pharm.*, 2013, **456**, 315-324.
17. Y. Gao, Y. Li, Y. Li, L. Yuan, Y. Zhou, J. Li, L. Zhao, C. Zhang, X. Li and Y. Liu, *Nanoscale*, 2015, **7**, 597-612.
18. J. Li, Y. Zhou, C. Li, D. Wang, Y. Gao, C. Zhang, L. Zhao, Y. Li, Y. Liu and X. Li, *Bioconjugate Chem.*, 2015, **26**, 110-119.
19. P. H. Kierstead, H. Okochi, V. J. Venditto, T. C. Chuong, S. Kivimae, J. M. J. Fréchet and F. C. Szoka, *J. Controlled Release*, 2015, **213**, 1-9.
20. Y. Zhao, Y. Zhou, D. Wang, Y. Gao, J. Li, S. Ma, L. Zhao, C. Zhang, Y. Liu and X. Li, *Acta Biomater.*, 2015, **17**, 182-192.
21. Z. He, A. Schulz, X. Wan, J. Seitz, H. Bludau, D. Y. Alakhova, D. B. Darr, C. M. Perou, R. Jordan, I. Ojima, A. V. Kabanov and R. Luxenhofer, *J. Controlled Release*, 2015, **208**, 67-75.
22. Z. He, X. Wan, A. Schulz, H. Bludau, M. A. Dobrovolskaia, S. T. Stern, S. A. Montgomery, H. Yuan, Z. Li, D. Alakhova, M. Sokolsky, D. B. Darr, C. M. Perou, R. Jordan, R. Luxenhofer and A. V. Kabanov, *Biomaterials*, 2016, **101**, 296-309.
23. S. Zalipsky, C. B. Hansen, J. M. Oaks and T. M. Allen, *J. Pharm. Sci.*, 1996, **85**, 133-137.
24. H. Xu, W. Zhang, Y. Li, F. F. Ye, P. P. Yin, X. Yu, M. N. Hu, Y. S. Fu, C. Wang and D. J. Shang, *Pharm. Res.*, 2014, **31**, 3038-3050.
25. K. L. Eskow Jaunarajs, D. G. Standaert, T. X. Viegas, M. D. Bentley, Z. Fang, B. Dizman, K. Yoon, R. Weimer, P. Ravenscroft, T. H. Johnston, M. P. Hill, J. M. Brotchie and R. W. Moreadith, *Mov. Disord.*, 2013, **28**, 1675-1682.
26. O. Sedlacek, B. D. Monnery, J. Mattova, J. Kucka, J. Panek, O. Janouskova, A. Hocherl, B. Verbraeken, M. Vergaelen, M. Zadinova, R. Hoogenboom and M. Hruby, *Biomaterials*, 2017, **146**, 1-12.
27. C. Legros, M.-C. De Pauw-Gillet, K. C. Tam, S. Lecommandoux and D. Taton, *Eur. Polym. J.*, 2015, **62**, 322-330.
28. Z. He, L. Miao, R. Jordan, D. S-Manickam, R. Luxenhofer and A. V. Kabanov, *Macromol. Biosci.*, 2015, **15**, 1004-1020.
29. M. N. Leiske, M. Hartlieb, C. Paulenz, D. Pretzel, M. Hentschel, C. Englert, M. Gottschaldt and U. S. Schubert, *Adv. Funct. Mater.*, 2015, **25**, 2458-2466.
30. M. Hartlieb, T. Bus, J. Kübel, D. Pretzel, S. Hoeppener, M. N. Leiske, K. Kempe, B. Dietzek and U. S. Schubert, *Bioconjugate Chem.*, 2017, **28**, 1229-1235.
31. R. W. Moreadith, T. X. Viegas, M. D. Bentley, J. M. Harris, Z. Fang, K. Yoon, B. izman, R. Weimer, B. P. Rae, X. Li, C. Rader, D. Standaert and W. Olanow, *Eur. Polym. J.*, 2016.
32. J. Tong, X. Yi, R. Luxenhofer, W. A. Banks, R. Jordan, M. C. Zimmerman and A. V. Kabanov, *Mol. Pharm.*, 2013, **10**, 360-377.
33. R. Luxenhofer, A. Schulz, C. Roques, S. Li, T. K. Bronich, E. V. Batrakova, R. Jordan and A. V. Kabanov, *Biomaterials*, 2010, **31**, 4972-4979.
34. Y. Seo, A. Schulz, Y. Han, Z. He, H. Bludau, X. Wan, J. Tong, T. K. Bronich, M. Sokolsky, R. Luxenhofer, R. Jordan and A. V. Kabanov, *Polym. Adv. Technol.*, 2015, **26**, 837-850.
35. M. C. Woodle, C. M. Engbers and S. Zalipsky, *Bioconjugate Chem.*, 1994, **5**, 493-496.
36. M. Glassner, L. Palmieri, B. D. Monnery, T. Verbrugghen, S. Deleye, S. Stroobants, S. Staelens, L. wyffels and R. Hoogenboom, *Biomacromolecules*, 2017, **18**, 96-102.
37. K. Kempe, S. L. Ng, K. F. Noi, M. Müllner, S. T. Gunawan and F. Caruso, *ACS Macro Lett.*, 2013, **2**, 1069-1072.
38. T. R. Dargaville, B. G. Hollier, A. Shokoohmand and R. Hoogenboom, *Cell Adh. Migr.*, 2014, **8**, 88-93.
39. Y. Liu, Y. Wang, Y. Wang, J. Lu, V. Piñón and M. Weck, *J. Am. Chem. Soc.*, 2011, **133**, 14260-14263.
40. L. Tauhardt, K. Kempe, M. Gottschaldt and U. S. Schubert, *Chem. Soc. Rev.*, 2013, **42**, 7998-8011.
41. M. Bauer, C. Lautenschlaeger, K. Kempe, L. Tauhardt, U. S. Schubert and D. Fischer, *Macromol. Biosci.*, 2012, **12**, 986-998.
42. M. Bauer, S. Schroeder, L. Tauhardt, K. Kempe, U. S. Schubert and D. Fischer, *J. Polym. Sci. A: Polym. Chem.*, 2013, **51**, 1816-1821.
43. Y. Gao, Y. Zhou, L. Zhao, C. Zhang, Y. Li, J. Li, X. Li and Y. Liu, *Acta Biomater.*, 2015, **23**, 127-135.
44. R. Shah, Z. Kronekova, A. Zahoranová, L. Roller, N. Saha, P. Saha and J. Kronek, *J. Mater. Sci. Mater. Med.*, 2015, **26**, 157.
45. M.-J. Shieh, C.-L. Peng, W.-L. Chiang, C.-H. Wang, C.-Y. Hsu, S.-J. J. Wang and P.-S. Lai, *Mol. Pharm.*, 2010, **7**, 1244-1253.
46. F. C. Gaertner, R. Luxenhofer, B. Blechert, R. Jordan and M. Essler, *J. Controlled Release*, 2007, **119**, 291-300.
47. A. Mero, Z. Fang, G. Pasut, F. M. Veronese and T. X. Viegas, *J. Controlled Release*, 2012, **159**, 353-361.
48. D. Hoelzer, M. N. Leiske, M. Hartlieb, T. Bus, D. Pretzel, S. Hoeppener, K. Kempe, R. Thierbach and U. S. Schubert, *Oncotarget*, 2018, **Submitted**.
49. H. Xu, M. Hu, X. Yu, Y. Li, Y. Fu, X. Zhou, D. Zhang and J. Li, *Eur. J. Pharm. Biopharm.*, 2015, **91**, 66-74.
50. P. Zhang, X. Qian, Z. Zhang, C. Li, C. Xie, W. Wu and X. Jiang, *ACS Appl. Mater. Interfaces*, 2017, **9**, 5768-5777.

Publication P7

Site-specific POxylation of interleukin-4

T. Luehmann, M. Schmidt, M. N. Leiske, V. Spieler, T. C. Majdanski, M. Grube, M. Hartlieb, I. Nischang, S. Schubert, U.S. Schubert, L. Meinel,
ACS Biomater. Sci. Eng. **2017**, *3*, 304 - 312.

The paper as well as the supporting information (free of charge) is available online: doi.org/10.1021/acsbiomaterials.6b00578.

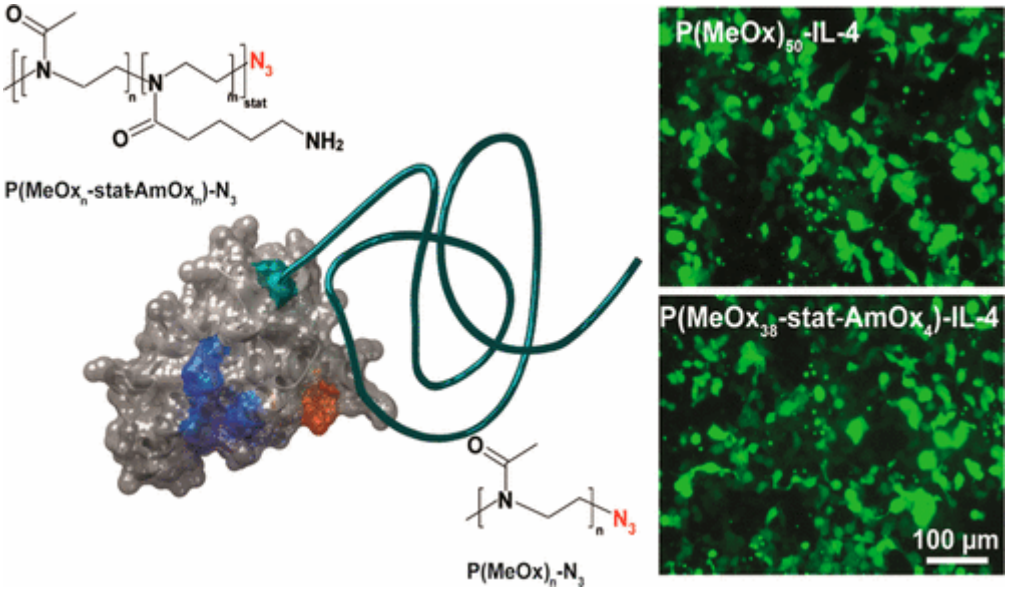

ACS Biomaterials SCIENCE & ENGINEERING

Article

pubs.acs.org/journal/abseba

Site-Specific POxylation of Interleukin-4

Tessa Lühmann,[†] Marcel Schmidt,[†] Meike N. Leiske,[‡,§] Valerie Spieler,[†] Tobias C. Majdanski,[‡,§] Mandy Grube,[‡,§] Matthias Hartlieb,[‡,§,#] Ivo Nischang,[‡,§] Stephanie Schubert,[§,∥] Ulrich S. Schubert,[‡,§] and Lorenz Meinel*[,†]

[†]Institute of Pharmacy and Food Chemistry, University of Würzburg, Am Hubland, DE-97074 Würzburg, Germany

[‡]Institute of Organic and Macromolecular Chemistry [IOMC], Friedrich Schiller University Jena, Humboldtstrasse 10, DE-07743 Jena, Germany

[§]Jena Center for Soft Matter (JCSM), Friedrich Schiller University Jena, Philosophenweg 7, DE-07743 Jena, Germany

[∥]Department of Pharmaceutical Technology, Friedrich Schiller University Jena, Otto-Schott-Strasse 41, DE-07747 Jena, Germany

Supporting Information

ABSTRACT: Polymer conjugated biologics form a multibillion dollar market, dominated by poly(ethylene glycol) (PEG). Recent reports linked PEGs to immunological concerns, fueling the need for alternative polymers. Therefore, we are presenting a strategy replacing PEG by poly(2-oxazoline) (POx) polymers using genetically engineered interleukin-4 (IL-4) featuring an unnatural amino acid for site-specific conjugation through bioorthogonal copper-catalyzed azide alkyne cycloaddition (CuAAC). Conjugation yields of IL-4-PEG were poor and did not respond to an increase in the copper catalyst. In contrast, POxylated IL-4 conjugates resulted in homogeneous conjugate outcome, as demonstrated electrophoretically by size exclusion chromatography and analytical ultracentrifugation. Furthermore, POxylation did not impair thermal and chemical stability, and preserved wild-type IL-4 activity for the conjugates as demonstrated by TF-1 cell proliferation and STAT-6 phosphorylation in HEK293T cells, respectively. In conclusion, POxylation provides an interesting alternative to PEGylation with superior outcome for the synthesis yield by CuAAC and resulting in conjugates with excellent thermal and chemical stress profiles as well as biological performances.

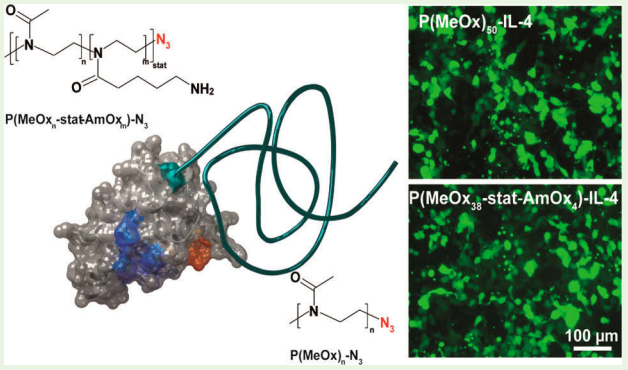

KEYWORDS: *cytokine engineering, 2-methyl-2-oxazoline, genetic code expansion, CuAAC (copper(I) catalyzed azide alkyne cycloaddition), bioconjugation*

INTRODUCTION

Many low-molar-mass biologics (5−50 kDa), including enzymes, growth factors and cytokines are efficiently excreted via the kidney and sinusoidal lining cells. Protein conjugation using hydrophilic polymers increases the circulation half-life, dominated by poly(ethylene glycols) (PEGs).[1] The PEGylated biologic conjugates are hydrophilic, thereby decreasing interaction with blood and cellular components while increasing biocompatibility through the "stealth effect".[2,3] However, in spite of these stealth properties, recent reports linked complement activation to PEG attached to liposomes, leading to accelerated blood clearance after the second injection, which was finally assigned to anti-PEG neutralizing antibodies.[4−8] Additionally, PEGylation may reduce receptor affinities which is through PEG binding of water introducing steric hindrance for interaction with cell surfaces.[9] As a promising alternative to PEG, poly(2-oxazoline)s (POx) have attained increasing attention and are intensively studied for biomedical applications ranging from antifouling polymer coatings[10,11] to the delivery of hydrophobic drugs, proteins, and genetic materials.[12−17] Small side chain derivatives of POx are known to be biocompatible[18] and possess a stealth effect similar to PEG.[19,20] Moreover, a recent clinical study detailed the potential of site-directed modification of rotigotine with POx, establishing successful "first in man" use of POx−drug conjugates.[21]

Conjugation of POx to proteins has been performed with unspecific coupling chemistries, for example linking the POx to amino- or carboxyl-groups of the biologic through (1-ethyl-3-(3-(dimethylamino)propyl)carbodiimide) (EDC)/*N*-hydroxysuccinimide (NHS) synthesis or, more selectively, enzymatically to glutamine residues[15,22−24,16] and by thiol reactive iodacetamide.[21] Unspecific coupling leads into product heterogeneity introducing challenges to pharmaceutical development including, for example, yield or analytical characterization.[25,26]

Received: September 22, 2016
Accepted: December 12, 2016
Published: December 12, 2016

DOI: 10.1021/acsbiomaterials.6b00578
ACS Biomater. Sci. Eng. XXXX, XXX, XXX−XXX

Furthermore, unspecific chemistries, leading to heterogeneous product outcome, drive another challenge—immunogenicity.[27] Through heterogeneity, more species (thereby more conformational variants) are presented to the patient's immune system thereby exposing the immune system to a number of altered epitopes as compared to the wild type, arguably more effectively supporting antibody formation against the biologic. These considerations fuel the need for alternatives, leading to homogeneous product outcome. We are approaching this by genetically introducing unnatural groups into the biologics backbone at one predefined site, providing a distinctive functional group. Only at that introduced group will decoration occur, removing the heterogeneity of the majority of coupling strategies pursued today.[26,28−30] To this end, we recently reported on genetic code expansion integrating pyrrolysine derivatives, e.g., N-propargyl-L-lysine (Plk), through recombinant protein expression for site-specific modification of growth factors,[31] fluorescent proteins,[32] as well as for cytokines[33] and use for the surface decoration of glyco-engineered cells[34] or bioresponsive drug delivery[35] through bio-orthogonal copper catalyzed azide alkyne cycloaddition (CuAAC). In this study, we pursue the production of site-specifically decorated polymer-interleukin-4 (IL-4) conjugates with the ultimate goal for unprecedented homogeneity in IL-4 conjugate outcome and maintained potency as compared to the wild type (wt) IL-4. IL-4 is a small and (at physiological conditions) positively charged 15 kDa-cytokine, triggering macrophage (Mφ) polarization along the M2 lineage with possible application in Mφ associated diseases.[36] In light of the favorable protein-repellent property and good biocompatibility, hydrophilic POx-based polymers of different molar masses (2.5, 4, 10 kDa) and architecture, including an azide group for cycloaddition, were synthesized to approach site-specific conjugation of Plk-IL-4 with the polymer. Conjugation with PEG resulted in poor yield, whereas POx polymers were effectively conjugated as a function of the polymers' weight-average molar mass M_W. The IL-4 conjugate products were detailed with respect to bioactivity, secondary structure, as well as thermal and chemical stability.

2. MATERIALS AND METHODS

DMEM, RPMI-1640 medium, L-glutamine, L-alanyl-L-glutamine, sodium pyruvate, bovine serum albumin solution 7.5%, lipid medium supplement, copper(II) sulfate, sodium L-ascorbate, and tris(3-hydroxypropyltriazolylmethyl) amine (THPTA) were purchased from Sigma-Aldrich (Schnelldorf, Germany). Penicillin G and streptomycin solution (Pen/Strep) were purchased from Biochrom AG (Berlin, Germany). Fetal bovine serum (FBS) was from GIBCO life technologies (Carlsbad, USA). HiTrap SP XL and HiTrap SP HP ÄKTA columns were from GE Healthcare (Buckinghamshire, GB). Vivaspin centrifugal concentrators were from Sartorius AG (Göttingen, Germany) and HyperSep C18 desalting columns were from Thermo Scientific (Waltham, USA). WST-1 was purchased from Roche (Basel, Switzerland). All other chemicals used were at least of pharmaceutical grade and were purchased from Sigma-Aldrich and Merck (unless noted otherwise). Solvents were obtained by Sigma-Aldrich, VWR, Linde, and Arcos Organics.

2.1. Polymer Synthesis and Characterization. A detailed overview about synthetic procedures and characterization is given in the Supporting Information.

2.2. Chemical Synthesis of Propargyl-L-lysine (Plk). Propargyl-L-lysine (Plk) was prepared as HCl-salt following procedures described by Milles et al.[37] ^{1}H NMR spectra were acquired on a Bruker Advance 400 MHz spectrometer for confirmation of the product.[31]

2.3. Expression of Plk-IL-4 and wt-IL-4. Plk-IL-4 and wt-IL-4 were expressed as described previously.[33] Briefly, *E.coli* BL21 DE3, encoding for TAG(42)-IL-4 and for the PylRS/tRNA^{CUA} pair, were cultured at 37 °C and the Plk substrate was added at a final concentration of 2 mM at OD_{600} = 0.3 in standard TB (Terrific Broth) medium. For wt-IL-4 expression, BL21 (DE3) cells, encoding for wt-IL-4, were used. Protein expression was subsequently induced with 1 mM IPTG at OD_{600} = 0.6 at 37 °C. After 6 h, the bacterial cells were harvested and the pellet was solubilized after sonification and centrifugation with lysis buffer, containing 5 M guanidine-HCl and 2 mM reduced and 0.2 mM oxidized glutathione. This solution was subsequently refolded using a glutathione redox buffer system as described.[38] After centrifugation, the supernatant containing Plk-IL-4 was purified by ion exchange affinity chromatography using a FPLC system (GE Healthcare Äkta Purifier, Life sciences, Freiburg, Germany). After purification, fractions containing IL-4 proteins were extensively dialyzed against PBS and stored at −80 °C. Wt-IL-4 and Plk-IL-4 concentrations were determined by UV-absorbance at 280 nm, using a molar extinction coefficient of 8860 M^{-1} cm^{-1}.[39]

2.4. Copper-Catalyzed Azide−Alkyne Huisgen Cycloaddition (CuAAC). Twenty-five μM Plk-IL-4 and a 50-fold molar excess of each polymer was used. The click reaction was performed in the presence of 2.5 mM L-ascorbic acid, 500 μM THPTA, and 100 μM $CuSO_4$ or in the presence of 2.5 mM L-ascorbic acid, 1 mM THPTA, and 1 mM $CuSO_4$ in PBS (137 mM NaCl, 2.7 mM KCl, 4.3 mM Na_2HPO_4,1.47 mM KH_2PO_4, pH 7.4). $CuSO_4$ and THPTA was premixed and incubated with L-ascorbic acid under air exclusion for 10 min to quench occurring reactive oxygene species (ROS) as detailed before.[34] The click reaction was performed at room temperature overnight and the reaction was stopped by the addition of 5 mM EDTA. The proteins and conjugates were subsequently analyzed by SDS-PAGE and MALDI-MS analysis or used for further purification.

2.5. MALDI-MS. The samples were desalted using ZipTipC18-tips following the manufacturer's instructions. Matrix-assisted laser desorption ionization (MALDI-MS) spectra were acquired in the linear positive mode by using an Autoflex II LRF instrument (Billerica, USA). Mass spectra were calibrated externally with a protein standard I from Bruker Daltonics Inc. (Billerica, USA), containing insulin, ubiquitin, myoglobin, and cytochrome C.

2.6. SDS-PAGE. Expressed proteins and proteins used in click reactions were analyzed by standard Tris-glycine SDS-PAGE as outlined before.[40] Gels were stained with Coomassie Brilliant Blue G250 and photographed using a FluorChem FC2 imaging system (Protein Simple, Santa Clara, CA).

2.7. RP-HPLC and SEC Analysis. Protein purity was assessed on a RP-HPLC system using a VWR Hitachi LaChrom HPLC system (Darmstadt, Germany). Protein samples and polymers were applied to a ZORBAX Eclipse XDB-C18 column (150 mm * 4.6 mm, particle size = 5 μm (Agilent, Santa Clara, CA)), equilibrated by water containing 0.1% TFA and acetonitrile (ACN) containing 0.1% TFA (90:10 v/v). Polymers, wt-IL-4 and IL-4 conjugates were eluted by a linear gradient of 10−60% ACN containing 0.1% TFA with a gradient of 1% ACN/min and a flow rate of 1 mL/min. Column temperature was kept at 24 °C and UV-absorbance was monitored at λ = 214 nm and λ = 280 nm, respectively.

After desalting using HyperSep C18 columns, IL-4-conjugates were eluated with 45% MeCN, containing 0.1% TFA (v/v). For SEC analysis, approximately 10 μg protein sample was applied to an equilibrated BioSep-SEC s2000 column (300 * 4.6 mm, particle size = 5 μm, pore size = 145 Å (Phenomenex, Torrance, USA)). Polymers, wt-IL-4 and IL-4 conjugates were analyzed in 45% MeCN, containing 0.1% TFA (v/v) at a flow rate of 1 mL/min according to the manufacturer's instructions for small peptides and proteins. UV-absorbance was monitored at λ = 220 nm. Data analysis, including nonlinear curve fitting and parameter determination (EC_{50}-value range within the 95% confidence interval), was performed with the software GraphPad Prism 7 (San Diego, California, USA).

2.8. Analytical Ultracentrifugation (AUC). Sedimentation velocity experiments were performed using a ProteomeLab XL-I analytical ultracentrifuge (Beckman Coulter Instruments, Brea, CA) with an An-60Ti four-hole rotor using double-sector aluminum centerpieces with a 12 mm optical path length. Interference optics detection

DOI: 10.1021/acsbiomaterials.6b00578
ACS Biomater. Sci. Eng. XXXX, XXX, XXX−XXX

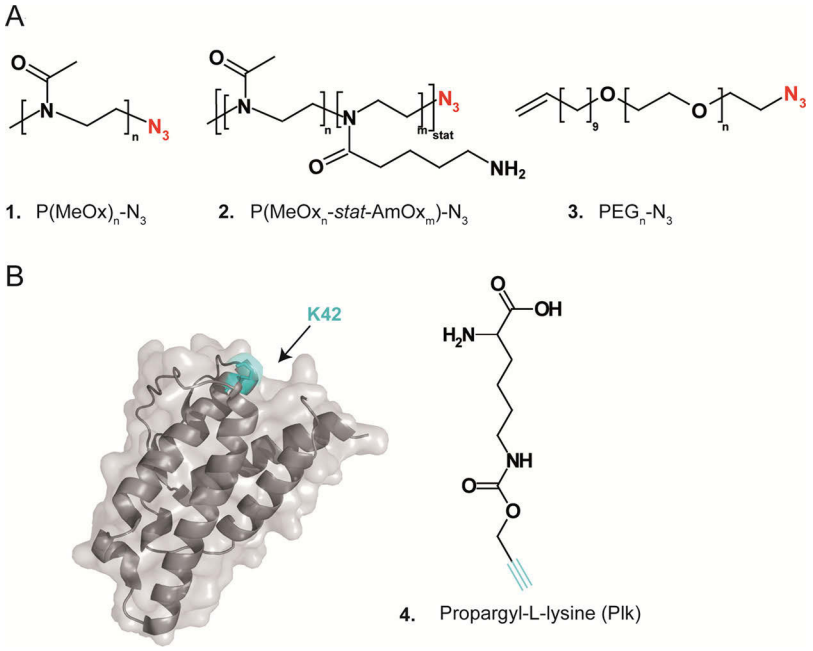

Figure 1. (A) Structure of polymers and copolymers. (B) Crystal structure of IL-4. Pdb =2B8U[1]. The introduction site of the uAA (cyan) is highlighted. Structure of the uAA propargyl-L-lysine (Plk) (**4**).

was used for observation of the sedimentation boundary in respect to time. All experiments were performed at a rotor speed of 50.000 rpm for 24 h and at a temperature of 20 °C. The cells were filled with 410 μL of the sample in PBS and with 440 μL of the solvent PBS as the reference. Sedimentation velocity data were analyzed with SEDFIT (version 15.01b) and the c(s) model with a maximum entropy regularization procedure. This model accounts for a numerical solution of the sedimentation velocity profiles and provides respective distributions of sedimentation coefficients. Density and viscosity of the solvent used for the modeling procedure were estimated as follows. The density of PBS was determined to 1.0056 g cm^{-3} at a temperature of 20 °C with a density meter DMA 4100 (Anton Paar, Graz, Austria). The dynamic viscosity of PBS was measured as 1.03 mPas with an AMVn Automated Micro Viscometer also from Anton Paar. The value of the partial specific volume (0.73 cm^3 g^{-1}) of the polymer−protein conjugate could only be assumed from typical values of proteins[41] and the literature concerning a related protein.[42] For the polymer, an average value based on previous measurements of P(MeOx) (0.8 cm^3 g^{-1}) was used.

2.9. Cell Culture. TF-1 cells (ATCC-Number CRL-2003, ATCC, and Manassas, VA) were harvested from exponentially growing suspensions. The cells were maintained in 75 cm^2 culture flasks in growth medium (RPMI-1640 medium, supplemented with 10% heat-inactivated FBS, 1% Pen/Strep solution, 4.5 g/L D-glucose, 2 mM L-glutamine, 2 mM L-alanyl-L-glutamine, 1 mM sodium pyruvate, and 2 ng/mL human GM-CSF) at 37 °C and 5% CO_2. HEK 293T cells (ATCC-Number CRL-1573, ATCC, Manassas, VA) were harvested from exponentially growing subconfluent monolayers in growth medium (DMEM containing 10% heat-inactivated FBS and 1% Pen/Strep solution) at 37 °C and 5% CO_2.

2.10. WST-Proliferation Assay. TF-1 cells were seeded in a 96-well plate format (50 000 cells/well) in WST-1 assay medium (RPMI-1640 medium, supplemented with 10% FBS, 1% Pen/Strep, 0.5% BSA), supplemented with dilution series of wt-IL-4, Plk-IL-4 and polymer conjugated IL-4 variants ranging from 0.001 to 2 nM. After stimulation for 48 h, the cells were incubated with WST-1 for 4 h at 37 °C according to the manufacturer's instructions. The absorbance of the soluble formazan product was determined at λ = 450 nm using a Spectramax 250 microplate reader (Molecular Devices, Sunnyvale).

2.11. Enhanced Yellow Fluorescent Protein and Secreted Alkaline Phosphatase Reporter Gene Assays in HEK293T cells. For the enhanced yellow fluorescent protein (eYFP) reporter gene assay, 15.000 HEK 293T cells were cotransfected in 24 well plates with 1 μg of the plasmids pHW0040 (P_{STAT6}−eYFP) and 1 μg of the constitutive STAT6 expression vector pSTAT6 (Genebank accession N-BC075852.1) as described before.[33] After exchange of the transfection medium against growth medium, supplemented with 1.3 nM of wt-IL-4, Plk-IL-4, and polymer-conjugated IL-4 variants, respectively, HEK 293T cells were stimulated for 48 h at 37 °C and 5% CO_2. eYFP expression was detected with an Axiovert 200 M inverted microscope (Zeiss, Oberkochen, Germany). For the secreted alkaline phosphatase (SEAP) reporter gene assay 4000 HEK 293T cells were cotransfected in 96 well plates with 0.2 μg of the plasmid pHW003 (P_{STAT6}−SEAP) and 0.2 μg of the constitutive STAT6 expression plasmid pSTAT6 (Genebank accession N- BC075852.1). After exchange of the transfection against growth medium supplemented with 1.3 nM wt-IL-4 or polymer-conjugated-IL-4, respectively, the cells were stimulated for 48 h at 37 °C and 5% CO_2. Twenty microliters of the medium supernatant was then incubated with 200 μL of Quanti-BlueTM alkaline phosphatase detection medium and SEAP activity was monitored at 650 nm using a Spectramax 250 microplate reader (Molecular Devices, Sunnyvale, CA). Detailed information about STAT-6 gene reporter plasmids is given elsewhere.[43]

2.12. Chemical Unfolding and Fluorescence Emission Spectroscopy. Unfolding of Plk-IL- 4, wt-IL- 4 ,and polymer-IL-4 conjugates in dependency to the denaturant urea was analyzed as previously described.[44] A stock solution of IL-4 variants was diluted to a final concentration of 10 μM in the presence of increasing concentrations of urea, ranging from 0−9 M, in 20 mM phosphate buffer, pH 7.4. Fresh stock solutions of urea were prepared gravimetrically in 20 mM phosphate buffer and its final concentration were as described before.[45] Samples of Plk-IL- 4, wt-IL-4, and polymer-IL-4 conjugates were incubated at room temperature for 20 h before analysis on a LS 50 B fluorescence spectrophotometer (PerkinElmer, Waltham, USA). Fluorescence emission spectra were obtained using at λ = 280 nm as excitation wavelength and λ = 380 nm as emission wavelength and a scan speed of 240 nm/min in a quartz cuvette. All obtained spectra were baseline corrected against urea containing buffer fluorescence intensities.

2.13. Circular Dichroism Spectroscopy. IL-4 samples were dialyzed against 20 mM sodium phosphate buffer with a pH of 7.0, with the identical buffer serving as a blank. Circular dichroism (CD) spectra were recorded at different temperatures or during increasing temperature with a J715 spectropolarimeter (JASCO Labor- and

DOI: 10.1021/acsbiomaterials.6b00578
ACS Biomater. Sci. Eng. XXXX, XXX, XXX−XXX

Datentechnik GmbH, Groß-Umstadt, Germany) with protein solutions with a final concentration of 0.2 mg mL^{-1} in a 2 mm path length cell with the following scan parameters: 100 mdeg sensitivity, 0.1 nm step resolution, 50 nm min^{-1} scan speed, 2 s time constant. Three accumulations per scan were averaged. Thermal unfolding curves of IL-4 samples were similarly performed by monitoring the change in ellipticity at λ = 222 nm. Data processing included solvent background correction and adjustment for path length and concentration.

Table 1. List of Polymers with *n* and *m* = Number of Repeating Monomer Units (see Figure 1)

	molar mass (g mol^{-1})		
polymer	~2500	~4000	~10 000
1, $P(MeOx)_n$-N_3	n = 30	n = 50	n = 108
2, $P(MeOx_n$-*stat*-$AmOx_m)$-N_3		n = 41; m = 2	
		n = 38; m = 4	
		n = 32; m = 8	
3, PEG_n-N_3	n = 57	n = 91	

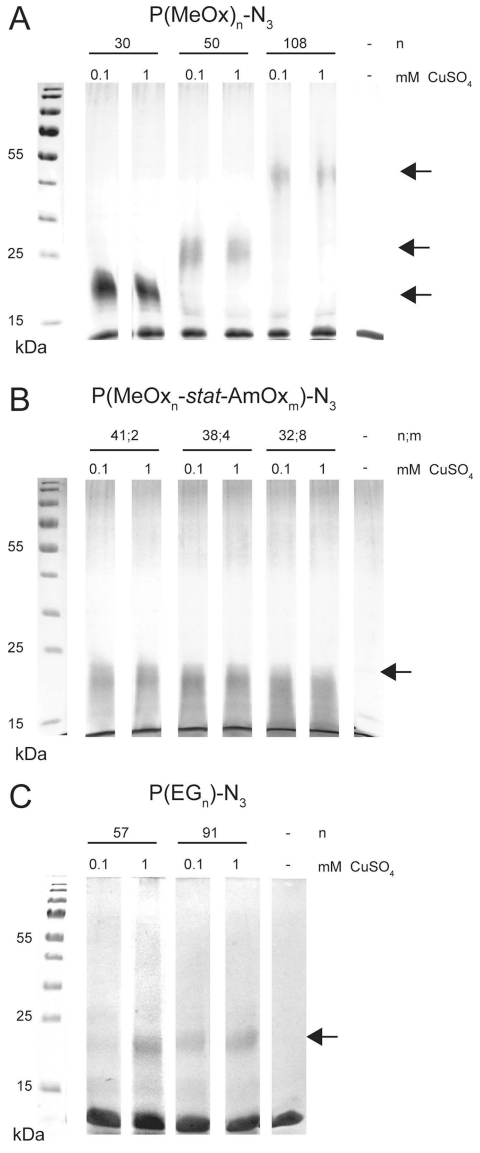

Figure 2. (A) CuAAC reactions between Plk-IL-4 and $P(MeOx)_n$-N_3 polymers. (B) CuAAC reactions between Plk-IL-4 and $P(MeOx_n$-*stat*-$AmOx_m)$ -N_3 polymers. (C) CuAAC reactions between Plk-IL-4 and $P(EG)_n$-N_3 polymers as analyzed by reduced SDS-PAGE. Plk-IL-4 is shown as control. Arrows indicate polymer conjugated IL-4 species.

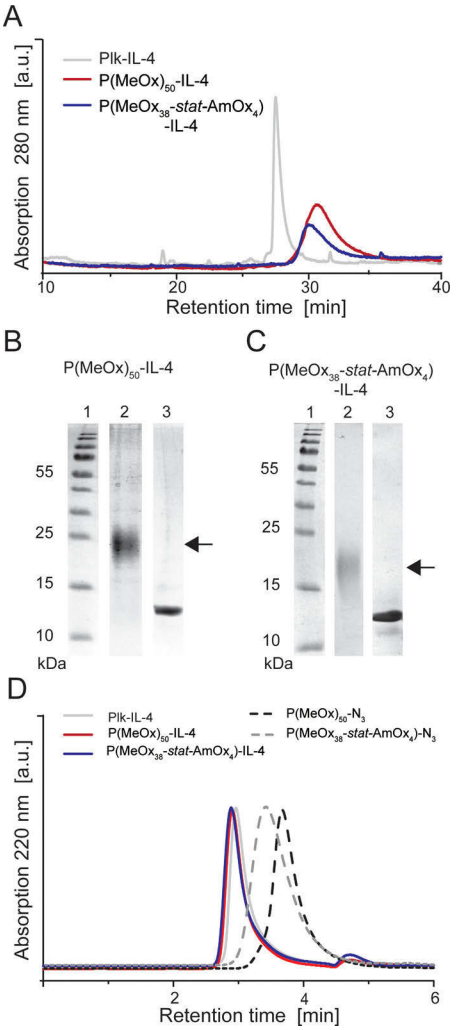

Figure 3. (A) RP-HPLC analysis of Plk-IL-4 and purified $P(MeOx)_{50}$-IL-4 and purified $P(MeOx_{38}$-*stat*-$AmOx_4)$-IL-4. (B) Reducing SDS-PAGE of $P(MeOx)_{50}$-IL-4 in comparison to Plk-IL-4. (C) Reducing SDS-PAGE of $P(MeOx_{38}$-*stat*-$AmOx_4)$-IL-4 in comparison to Plk-IL-4. (D) SEC analysis of IL-4 polymer conjugates in comparison to Plk-IL-4 and unconjugated polymers.

2.14. Statistics. Data were analyzed using ANOVA with the Tukey-Kramer test for post hoc comparison. Results were considered statistically significant at $p \leq 0.05$(*) and are displayed as mean with standard deviation (SD).

3. RESULTS AND DISCUSSION

3.1. Polymer Synthesis and Characterization. Azide functionalized hydrophilic polymers composed of 2-methyl-2-oxazoline (MeOx) were produced by cationic ring-opening polymerization as previously described[46,47] (Figure 1A, **1**). Additionally, statistical copolymers composed of MeOx in combination with aminobutyl-2-oxazoline (AmOx)[48]—free primary amine groups at the polymer side chains that can be used for additional decoration purposes including the coupling of targeting motifs—were synthesized with a terminally located azide group (for CuAAC with Plk-IL-4) (Figure 1A, **2**). PEG polymers were functionalized with azide groups following polymerization (Figure 1A, **3**).

The composition of the used polymers is described (Table 1) and polymerization procedures and characterization including ^{1}H NMR, MALDI-MS and SEC data are provided in Figures S1− S11.

DOI: 10.1021/acsbiomaterials.6b00578
ACS Biomater. Sci. Eng. XXXX, XXX, XXX−XXX

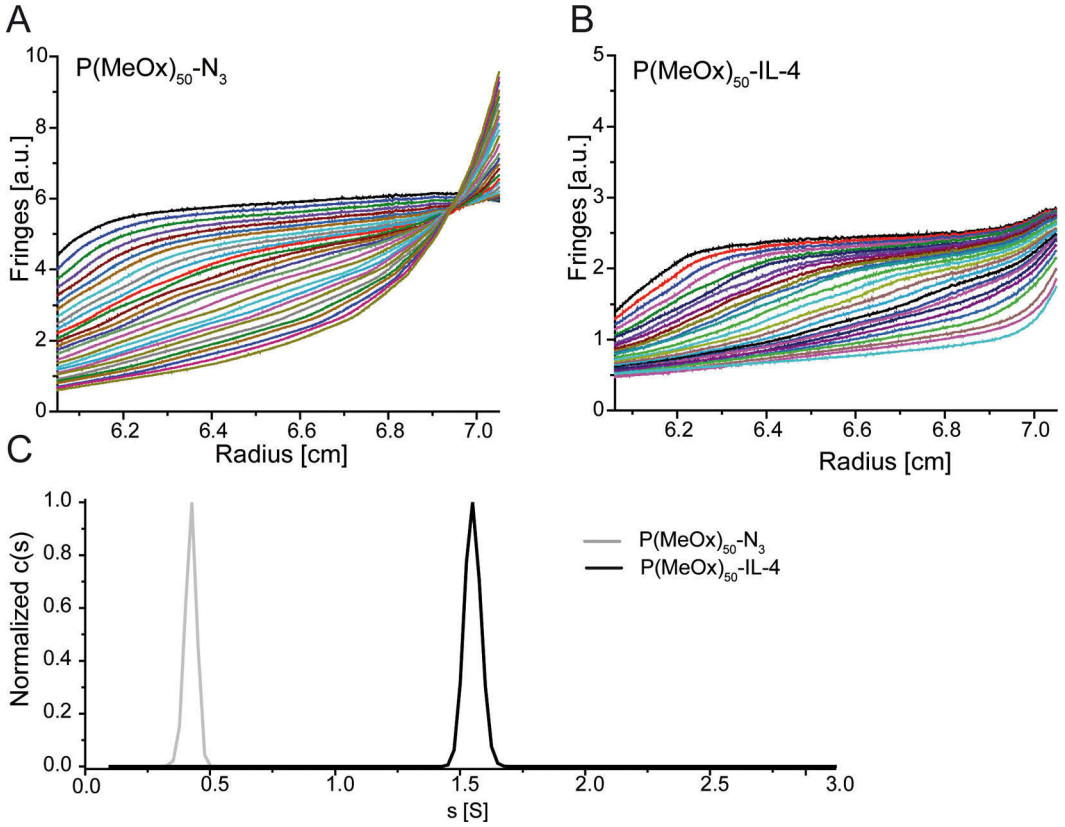

Figure 4. Results from analytical ultracentrifugation showing (A) the sedimentation fronts of the polymer $P(MeOx)_{50}$-N_3 (c = 0.1% (w/w)), (B) the conjugate $P(MeOx)_{50}$-IL-4 (c = 0.04% (w/w)), and (C) the normalized differential distribution of sedimentation coefficients c(s) of the polymer $P(MeOx)_{50}$-N_3 in gray and of the $P(MeOx)_{50}$-IL-4 in black.

3.2. Expression and Chemical Functionalization of Plk-IL-4 with $P(MeOx)_n$-N_3, $P(MeOx_n$ -*stat*-$AmOx_m)$-N_3, and PEG_n-N_3 by CuAAC. IL-4 with an unnatural amino acid (uAA) Plk (**4**) integrated at position #42 (K42/Plk42) was engineered in *E. coli* by amber codon suppression[31] (Figure 1B; IL-4 receptor signaling tolerates K42/Plk exchange[33]). At first, we studied the efficiency of the click reaction chemistry of Plk-IL-4 and the azide functionalized polymers on small scale using copper(II) sulfate with sodium L-ascorbate and the water-soluble base tris(3-hydroxypropyltriazolyl-methyl) amine (THPTA).[31,34,49] Two different copper(II) sulfate concentration were compared (100 μM and 1 mM). The electrophoretic mobility of unconjugated Plk-IL-4 (15 kDa) and conjugated Plk-IL-4 was qualitatively assessed by gel electrophoresis followed by Coomassie staining (Figure 2).

Qualitatively, the conjugation yield was highest with the low molecular weight $P(MeOx)_{30}$-N_3 (Figure 2A, lanes 1 and 2), followed by the higher molar mass $P(MeOx)_{50}$-N_3 and $P(MeOx)_{108}$-N_3 (Figure 2A, lanes 3−7), respectively. The copper(II) sulfate concentration (100 μM versus 1 mM) had no impact on the unconjugated Plk-IL-4 (e.g., aggregation could have been expected) or conjugation outcome. Conjugation of Plk-IL-4 with $P(MeOx_n$-*stat*-$AmOx_m)$-N_3-polymers bearing different amino group contents resulted in broader bands as compared to the amine-free polymers reflecting that additional charges might influence SDS complexation[50] and gel migration behavior[51] of the $P(MeOx_n$-*stat*-$AmOx_m)$-IL-4 conjugates (Figure 2 **B**). Contrasting the excellent reaction with MeOx homopolymers, conjugation efficiencies of Plk-IL4 with $P(EG)_n$-N_3 were poor, resulting in small amounts of the conjugated species running at ∼20 kDa (Figure 2C). We speculate that polyethers, in spite of the fact that this chemistry is frequently used for similar conjugation purposes,[49] interact noncovalently with the copper(I) catalyst, reducing the conjugation yield and in analogy to previous reports, linking impaired copper electrodeposition to the presence of PEG during electroplating.[52] The unsuccessful conjugation of PEG-N_3 could also be related to its hydrophobic end-group, possibly leading into polymer aggregation[53] or nonspecific interactions[54] with the Plk-IL-4. We could not overcome this limitation even when providing the catalyst at 10-fold concentration (from 100 μM to 1 mM; Figure 2). Therefore, copper-free bioorthogonal chemistries should be preferred for site-specific PEGylation of proteins.[55]

MeOx based polymers with similar molar masses (∼4 kDa) but different architecture, namely, $P(MeOx)_{50}$-N_3 and $P(MeOx_{38}$-*stat*-$AmOx_4)$-N_3 but not PEG, were selected for bioconjugation to Plk-IL-4 on a larger scale. Large-scale production was followed by cationic ion exchange chromatography for purification and further characterization of the conjugates.

3.3. Characterization of IL-4 Conjugates. Following upscaling, IL-4 bioconjugates $P(MeOx)_{50}$-IL-4 and $P(MeOx_{38}$-*stat*-$AmOx_4)$-IL-4 were purified from unreacted educts (Figure 3).

The conjugates eluted at 30.6 and 30.8 min, respectively (Figure 3A). This result was confirmed by gel electrophoresis, with unconjugated IL-4 (15 kDa) being absent (Figure 3B, C) and new bands at approximately 20 kDa for ($P(MeOx)_{50}$-IL-4 (Figure 3B) and for $P(MeOx_{38}$-*stat*-$AmOx_4)$-IL-4 (Figure 3C), corresponding to the monoconjugated IL-4 species, respectively. We deployed MALDI-MS analysis, which corroborated

DOI: 10.1021/acsbiomaterials.6b00578
ACS Biomater. Sci. Eng. XXXX, XXX, XXX−XXX

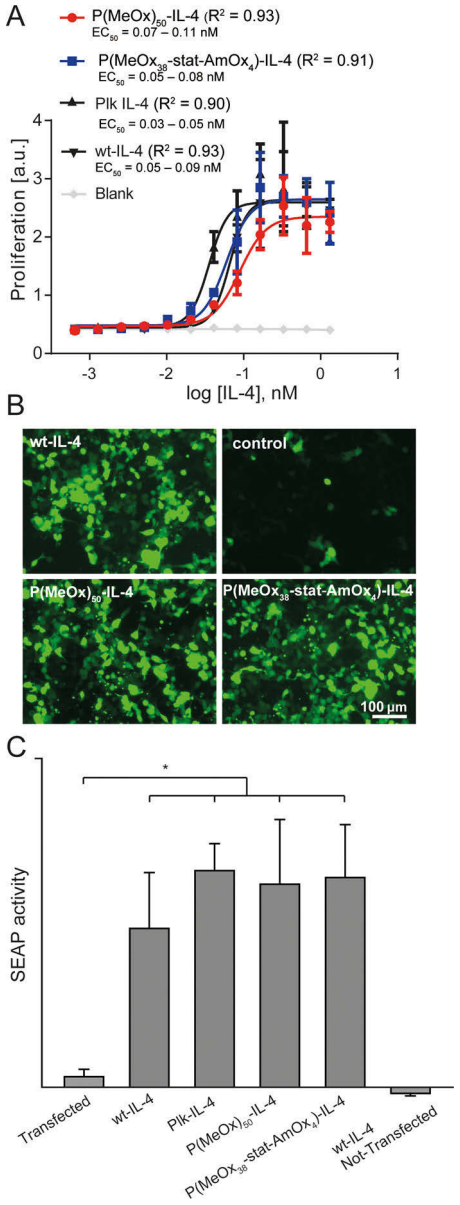

Figure 5. (A) TF-1 proliferation assay of wt-IL-4, Plk-IL-4, and polymer conjugated IL-4 derivatives (mean ± standard deviation, n = 3). R^2 values of the nonlinear fitting as well as the 95% confidence intervals of the estimated EC_{50} values are given. (B) eYFP reporter gene assay of HEK 293 T cells transfected with pSTAT6−eYFP and pSTAT6 after stimulation with 1.3 nM wt-IL-4, Plk-IL-4, and polymer conjugated IL-4 species. The control shows transfected but unstimulated cells. (C) SEAP reporter gene assay of HEK293 T cells transfected with pSTAT6-SEAP and pSTAT6 after stimulation with 1.3 nM wt-IL-4, Plk-IL-4 and polymer conjugated IL-4 species. Asterisks indicate statistically significant differences among groups ($p \leq 0.05$ (*), n = 5).

these findings. ($P(MeOx)_{50}$-IL-4 revealed an average centered mass of 20 000 Da (Figure S12).

Conjugation of the statistical copolymer $P(MeOx_{38}$-*stat*-$AmOx_4)-N_3$ resulted in an average centered mass of 19.1 kDa and a broad peak reflecting the statistical mass distribution of the $P(MeOx_{38}$-*stat*-$AmOx_4)$ conjugated to IL-4 (Figure S13).

The homogeneity of the IL-4-conjugates was further corroborated by SEC and AUC experiments. Both bioconjugates ($P(MeOx)_{50}$-IL-4 and the statistical copolymer $P(MeOx_{38}$-*stat*-$AmOx_4)$-IL-4) were indistinguishable by SEC (r.t.: $P(MeOx)_{50}$-IL-4 = 2.90 min; r.t.: $P(MeOx_{38}$-*stat*-$AmOx_4)$-IL-4 = 2.88 min) and similar to unmodified Plk-IL-4 (r.t. = 2.96 min; Figure 3D), whereas the (unreacted) polymers eluted at later retention times (r.t.: $P(MeOx)_{50}$-N_3 = 3.67 min; r.t.: $P(MeOx_{38}$-*stat*-$AmOx_4)$-N_3 = 3.42 min) reflecting their lower molar mass as compared to the conjugates. The presence of one single peak for both IL-4 bioconjugates suggested homogeneous product outcome through CuAAC coupling without detectable oligomers.

The SEC findings were further detailed by AUC and the monodisperse $P(MeOx)_{50}$-N_3. $P(MeOx)_{50}$-N_3 had an approximate molar mass of 3700 g mol^{-1} with a diffuse sedimentation profile and significant back-diffusion (Figure 4A). The resulting distribution of the sedimentation coefficient (Figure 4C, gray line) was narrow and indicated one single population of species, i.e. homogeneity of the polymer's molar mass. $P(MeOx)_{50}$-IL-4 conjugates had less diffuse sedimentation profiles as compared to the unconjugated $P(MeOx)_{50}$-N_3 polymer, reflecting the conjugate's higher molar mass (Figure 4B). However, $P(MeOx)_{50}$-IL-4 conjugates sedimented with a single population of species, indicating the absence of the unconjugated $P(MeOx)_{50}$ on the one hand or higher oligomeric species on the other hand (Figure 4C, black line). Therefore, these conjugation protocols lead to homogeneous conjugation outcome.

3.4. In Vitro Activity of IL-4 Conjugates. IL-4 signals through two different receptor complexes both of which comprising IL-4Rα and γc (type I receptor; preferentially expressed on cells of hematopoietic origin) or IL13Rα1 (type II receptor; preferentially on nonhematopoietic cells). Interaction of IL-4 with the IL-4Rα subunit has picomolar affinity (K_D = 100 pM)[56] (step 1) followed by ligand-mediated receptor heterodimerization (step 2) to recruit the low affinity receptors γc (type I receptor) or IL13Rα1 (type II receptor). Proliferation of TF-1 suspension cells (hematopoietic cells expressing both the type I and the type II IL-4 receptor) was detailed in response to IL-4 concentration (Figure 5A).

Bioactivity of IL-4 conjugates was alike the wt-IL-4, indicating fully retained IL-4 bioactivity following POxylation. A weak reduction in bioactivity was observed for P(MeOx)50-IL-4 in contrast to Plk-IL-4 (but not wt-IL-4). This data set was corroborated by analyzing STAT-6 phosphorylation, thereby reporting on IL-4 receptor activation (Figure 5B, C). Kidney derived HEK293T cells (nonhematopoietic and expressing the type II receptor) were cotransfected with a STAT-6 expression vector reporting either for eYFP or for SEAP expression as previously described.[57] Treatment with both IL-4 conjugates resulted in similarly strong STAT-6 phosphorylation as compared to wt-IL-4 and significant weaker responses in unstimulated but transfected control cells (Figure 5C). These results suggested that both chemically modified IL-4 conjugates conserved wt-IL-4-activity in cells of hematopoietic and nonhematopoietic origin.

3.5. Stability of IL-4 Conjugates. The stability of IL-4 was studied through fluorescence emission taking advantage of a single tryptophan (W91) buried within the correctly folded IL-4 (not fluorescent) and being surface exposed after unfolding (fluorescent; Figure 6A).

Chemically induced IL-4 unfolding was studied with increasing urea concentrations. Identical curves were recorded for $P(MeOx)_{50}$-IL-4 and of $P(MeOx_{38}$-*stat*-$AmOx_4)$-IL-4 as compared to unconjugated wt-IL-4 and Plk-IL-4, respectively. Both IL-4 conjugates maintained their structural integrity after stressing with up to 6 M of the denaturant urea, highlighting their excellent chemical stability. This data was corroborated by exposing the groups to thermal stress tying to previous reports

DOI: 10.1021/acsbiomaterials.6b00578
ACS Biomater. Sci. Eng. XXXX, XXX, XXX−XXX

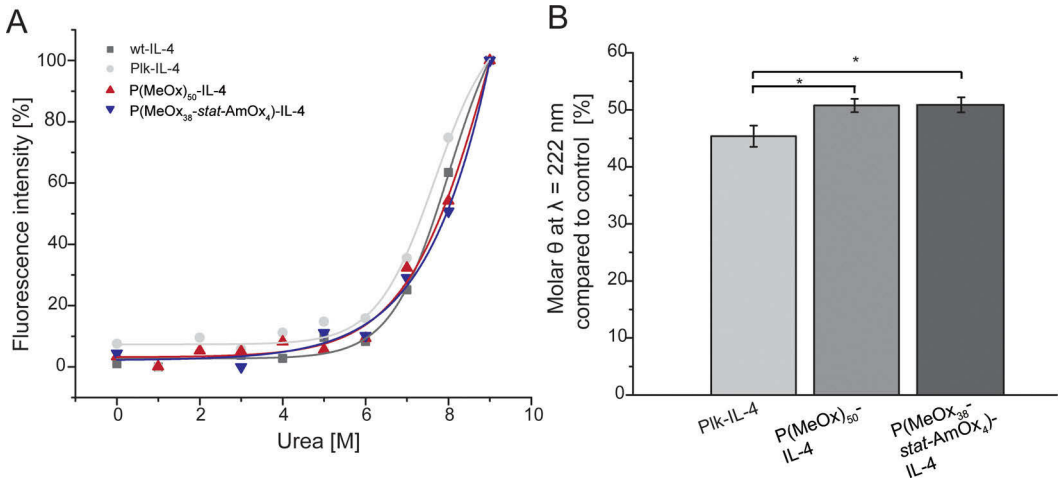

Figure 6. (A) Chemical unfolding curves of wt-IL-4, Plk-IL-4 and polymer conjugated IL-4 species as determined by tryptophan emission fluorescence at λ = 380 nm. (B) Molar ellipticity [Θ] recovery after protein stressing at 100 °C of polymer conjugated IL-4 species and Plk-IL-4 as analyzed at λ = 222 nm. Asterisks indicate statistically significant differences among groups ($p \leq 0.05$ (*), n = 3).

on the thermal stability of POxylated virus particles.[58] Moreover, other hydrophilic polymers such as trehalose side chain polymers induced enhanced stability of lysozyme conjugates to environmental stress factors compared to unconjugated polymers added to the enzyme,[59] providing insights into an superior effect of covalent conjugation for protein stabilization.

Unfolding with temperature was recorded through variable temperature circular dichroism (CD; Figure 6B). CD pattern of IL-4 conjugates and Plk-IL-4 were recorded at temperature of maximal stability (T_s = 20.8 °C)[44] before, during, and after thermal stressing (100 °C; Figure S14A, B). The IL-4 conjugates had equal helicity (minima at λ = 208 nm and λ = 222 nm; maximum at λ = 193 nm) as unconjugated Plk-IL-4 at 20 °C, indicating that the polymer modification on the IL-4 surface did not interfere with IL-4 folding. Under thermal stress (100 °C), the overall levels of helical content were reduced in all groups (Figure S14B). Following cooling to 20 °C of these samples (Figures S14C), refolding of P(MeOx)$_{50}$-IL-4 and of P(MeOx$_{38}$-*stat*-AmOx$_4$)-IL-4 resulted in 50.8% ± 1.2 and 50.9% ± 1.3 of recovered helical content, respectively (with respect to the molar ellipticity (at λ = 222 nm) of untreated IL-4 samples set as 100%; Figure 6B). In contrast, unconjugated, thermally stressed Plk-IL-4 attained at significantly reduced helical content of 45.4% ± 1.9 at 20 °C, reflecting facilitated refolding upon thermal stress for the conjugated variants as compared to unconjugated IL-4.

We than recorded thermal unfolding profiles of P(MeOx)$_{50}$-IL-4, of P(MeOx$_{38}$-*stat*-AmOx$_4$)-IL-4 and of Plk-IL-4 from 45 to 100 °C as a function of the CD signal at λ = 222 nm (Figure S15).

The transition temperatures of unfolding (T_m) were calculated from the inflection points of the nonlinear fitted curves with Plk-IL-4 unfolding at 83.2 °C (in line with previously reported 83.8 °C[44]), and P(MeOx)$_{50}$-IL-4 and P(MeOx$_{38}$-*stat*-AmOx$_4$)-IL-4 at 83.4 and 83.9 °C, respectively. These studies demonstrated the excellent stability properties of POxylated IL-4 with respect to both chemical and thermal stresses.

CONCLUSIONS

In summary, we presented a modular design strategy for polymer conjugation of the immune modulating cytokine IL-4 by using bio-orthogonal copper-catalyzed click chemistry. Hydrophilic poly-2-oxazolines were effectively coupled to Plk-IL-4, contrasting the unsatisfying outcome when using PEG instead. Future work is required addressing the in vivo potential of POxylated IL-4-conjugates in terms of pharmacokinetic, safety, and pharmacodynamic performances, respectively. Promising outcome on conjugate stability following chemical and thermal stresses, suggests interesting features in terms of storage stability of future conjugates, potentially facilitating manufacture and shipment of future drug products formats. Further stability studies with other biologics are required before final conclusions can be drawn on this potential advantage of POxylated conjugates. In the light of the need for PEG-alternatives as of observed immunological challenges in some but not all patients, the developed P(MeOx)$_n$-IL-4 conjugates are interesting images for future (pre)-clinical testing, with fully retained stability and in vitro biological performances as compared to wt-IL-4. Furthermore, the demonstrated successes with conjugates holding an additional amine functional group provide further handle for future conjugates, e.g., the facilitated decoration with targeting motifs or other ligands at the polymer. From a developmental perspective this would provide various advantages, particularly the separate production of a target motif-decorated polymer, which in return is site-specifically clicked to the Plk-biologic. These approaches using copper-catalyzed synthesis for protein−polymer conjugation provide a blue print leading to homogeneous, high-quality polymer−conjugate outcome.

ASSOCIATED CONTENT

Supporting Information

The Supporting Information is available free of charge on the ACS Publications website at DOI: 10.1021/acsbiomaterials.6b00578.

Detailed information about polymer synthesis and characterization, and Figures S1−S15 (PDF)

AUTHOR INFORMATION

Corresponding Author

*E-mail: lorenz.meinel@uni-wuerzburg.de. Tel.: +49 931 318 54 71. Fax: +49 931 318 46 08.

ORCID

Lorenz Meinel: 0000-0002-7549-7627

DOI: 10.1021/acsbiomaterials.6b00578
ACS Biomater. Sci. Eng. XXXX, XXX, XXX−XXX

Present Address

[#]M.H. is currently at Department of Chemistry, University of Warwick, Gibbet Hill Road, Coventry CV4 7AL, UK.

Notes

The authors declare no competing financial interest.

■ ACKNOWLEDGMENTS

Support by DFG (grant ME 3920/3-1 'Macrophage plasticity deployed for efficient bone (re-) generation'), the Sino-German center, and the Bundesministerium für Bildung und Forschung (Germany) (13N13454) are gratefully acknowledged. We also acknowledge funding from the Carl-Zeiss Foundation (JCSM Strukturantrag) and the Thüringer Ministerium für Wirtschaft, Wissenschaft, und Digitale Gesellschaft (TMWWDG, Pro-Exzellenz II, NanoPolar). M.H. gratefully acknowledges the German Research Foundation (DFG, GZ: HA 7725/1-1) for funding. M.N.L. gratefully acknowledges the Bundesministerium für Bildung und Forschung (Germany) (project: smart-dye-livery, 081220/127) for funding. The authors thank Annett Urbanek for MALDI-MS measurements. We thankfully acknowledge the kind support by Caroline Kisker (University of Würzburg) and her group with the CD measurements.

■ REFERENCES

(1) Alconcel, S. N. S.; Baas, A. S.; Maynard, H. D. FDA-approved poly(ethylene glycol)-protein conjugate drugs. *Polym Chem* **2011**, *2* (7), 1442−1448.

(2) Knop, K.; Hoogenboom, R.; Fischer, D.; Schubert, U. S. Poly(ethylene glycol) in Drug Delivery: Pros and Cons as Well as Potential Alternatives. *Angew. Chem., Int. Ed.* **2010**, *49* (36), 6288−6308.

(3) Schottler, S.; Becker, G.; Winzen, S.; Steinbach, T.; Mohr, K.; Landfester, K.; Mailander, V.; Wurm, F. R. Protein adsorption is required for stealth effect of poly(ethylene glycol)- and poly-(phosphoester)-coated nanocarriers. *Nat. Nanotechnol.* **2016**, *11* (4), 372−377.

(4) Chanan-Khan, A.; Szebeni, J.; Savay, S.; Liebes, L.; Rafique, N. M.; Alving, C. R.; Muggia, F. M. Complement activation following first exposure to pegylated liposomal doxorubicin (Doxil): possible role in hypersensitivity reactions. *Ann. Oncol* **2003**, *14* (9), 1430−1437.

(5) Sroda, K.; Rydlewski, J.; Langner, M.; Kozubek, A.; Grzybek, M.; Sikorski, A. F. Repeated injections of PEG-PE liposomes generate anti-PEG antibodies. *Cell Mol. Biol. Lett.* **2005**, *10* (1), 37−47.

(6) Dams, E. T. M.; Laverman, P.; Oyen, W. J. G.; Storm, G.; Scherphof, G. L.; Van der Meer, J. W. M.; Corstens, F. H. M.; Boerman, O. C. Accelerated blood clearance and altered biodistribution of repeated injections of sterically stabilized liposomes. *J. Pharmacol. Exp. Ther.* **2000**, *292* (3), 1071−1079.

(7) Tagami, T.; Nakamura, K.; Shimizu, T.; Ishida, T.; Kiwada, H. The relationship between PEGylated siRNA-lipoplex and anti-PEG IgM on the induction of accelerated blood clearance (ABC) phenomenon. *Yakugaku Zasshi* **2008**, *128*, 109−110.

(8) Ishida, T.; Kiwada, H. Accelerated blood clearance (ABC) phenomenon upon repeated injection of PEGylated liposomes. *Int. J. Pharm.* **2008**, *354* (1−2), 56−62.

(9) Veronese, F. M. Peptide and protein PEGylation: a review of problems and solutions. *Biomaterials* **2001**, *22* (5), 405−17.

(10) Pidhatika, B.; M?ller, J.; Benetti, E. M.; Konradi, R.; Rakhmatullina, E.; Muhlebach, A.; Zimmermann, R.; Werner, C.; Vogel, V.; Textor, M. The role of the interplay between polymer architecture and bacterial surface properties on the microbial adhesion to polyoxazoline-based ultrathin films. *Biomaterials* **2010**, *31* (36), 9462−9472.

(11) Chen, Y.; Pidhatika, B.; von Erlach, T.; Konradi, R.; Textor, M.; Hall, H.; Luhmann, T. Comparative assessment of the stability of nonfouling poly(2-methyl-2-oxazoline) and poly(ethylene glycol) surface films: an in vitro cell culture study. *Biointerphases* **2014**, *9* (3), 031003.

(12) Sedlacek, O.; Hruby, M.; Studenovsky, M.; Vetvicka, D.; Svoboda, J.; Kankova, D.; Kovar, J.; Ulbrich, K. Polymer conjugates of acridine-type anticancer drugs with pH-controlled activation. *Bioorg. Med. Chem.* **2012**, *20* (13), 4056−63.

(13) von Erlach, T.; Zwicker, S.; Pidhatika, B.; Konradi, R.; Textor, M.; Hall, H.; Luhmann, T. Formation and characterization of DNA-polymer-condensates based on poly(2-methyl-2-oxazoline) grafted poly(L-lysine) for non-viral delivery of therapeutic DNA. *Biomaterials* **2011**, *32* (22), 5291−303.

(14) Rinkenauer, A. C.; Tauhardt, L.; Wendler, F.; Kempe, K.; Gottschaldt, M.; Traeger, A.; Schubert, U. S. A cationic poly(2-oxazoline) with high in vitro transfection efficiency identified by a library approach. *Macromol. Biosci.* **2015**, *15* (3), 414−25.

(15) Tong, J.; Luxenhofer, R.; Yi, X.; Jordan, R.; Kabanov, A. V. Protein modification with amphiphilic block copoly(2-oxazoline)s as a new platform for enhanced cellular delivery. *Mol. Pharmaceutics* **2010**, *7* (4), 984−92.

(16) Mero, A.; Fang, Z. H.; Pasut, G.; Veronese, F. M.; Viegas, T. X. Selective conjugation of poly(2-ethyl 2-oxazoline) to granulocyte colony stimulating factor. *J. Controlled Release* **2012**, *159* (3), 353−361.

(17) He, Z. J.; Wan, X. M.; Schulz, A.; Bludau, H.; Dobrovolskaia, M. A.; Stern, S. T.; Montgomery, S. A.; Yuan, H.; Li, Z. B.; Alakhova, D.; Sokolsky, M.; Darr, D. B.; Perou, C. M.; Jordan, R.; Luxenhofer, R.; Kabanov, A. V. A high capacity polymeric micelle of paclitaxel: Implication of high dose drug therapy to safety and in vivo anti-cancer activity. *Biomaterials* **2016**, *101*, 296−309.

(18) Luxenhofer, R.; Sahay, G.; Schulz, A.; Alakhova, D.; Bronich, T. K.; Jordan, R.; Kabanov, A. V. Structure-property relationship in cytotoxicity and cell uptake of poly(2-oxazoline) amphiphiles. *J. Controlled Release* **2011**, *153* (1), 73−82.

(19) Zalipsky, S.; Hansen, C. B.; Oaks, J. M.; Allen, T. M. Evaluation of blood clearance rates and biodistribution of poly(2-oxazoline)-grafted liposomes. *J. Pharm. Sci.* **1996**, *85* (2), 133−137.

(20) Platen, M.; Mathieu, E.; Luck, S.; Schubel, R.; Jordan, R.; Pautot, S. Poly(2-oxazoline)-Based Microgel Particles for Neuronal Cell Culture. *Biomacromolecules* **2015**, *16* (5), 1516−24.

(21) Moreadith, R. W.; Viegas, T. X.; Bentley, M. D.; Harris, J. M.; Fang, Z.; Yoon, K.; Dizman, B.; Weimer, R.; Rae, B. P.; Li, X.; Rader, C.; Standaert, D.; Olanow, W., Clinical development of a poly(2-oxazoline) (POZ) polymer therapeutic for the treatment of Parkinson's disease − Proof of concept of POZ as a versatile polymer platform for drug development in multiple therapeutic indications. *Eur. Polym. J.*.**2016**10.1016/j.eurpolymj.2016.09.052

(22) Viegas, T. X.; Bentley, M. D.; Harris, J. M.; Fang, Z. F.; Yoon, K.; Dizman, B.; Weimer, R.; Mero, A.; Pasut, G.; Veronese, F. M. Polyoxazoline: Chemistry, Properties, and Applications in Drug Delivery. *Bioconjugate Chem.* **2011**, *22* (5), 976−986.

(23) Mero, A.; Pasut, G.; Via, L. D.; Fijten, M. W. M.; Schubert, U. S.; Hoogenboom, R.; Veronese, F. M. Synthesis and characterization of poly(2-ethyl 2-oxazoline)-conjugates with proteins and drugs: Suitable alternatives to PEG-conjugates? *J. Controlled Release* **2008**, *125* (2), 87−95.

(24) Glassner, M.; Maji, S.; de la Rosa, V. R.; Vanparijs, N.; Ryskulova, K.; De Geest, B. G.; Hoogenboom, R. Solvent-free mechanochemical synthesis of a bicyclononyne tosylate: a fast route towards bioorthogonal clickable poly(2-oxazoline)s. *Polym. Chem.* **2015**, *6* (48), 8354−8359.

(25) Totaro, K. A.; Liao, X.; Bhattacharya, K.; Finneman, J. I.; Sperry, J. B.; Massa, M. A.; Thorn, J.; Ho, S. V.; Pentelute, B. L. Systematic Investigation of EDC/sNHS-Mediated Bioconjugation Reactions for Carboxylated Peptide Substrates. *Bioconjugate Chem.* **2016**, *27*, 994.

(26) Agarwal, P.; Bertozzi, C. R. Site-specific antibody-drug conjugates: the nexus of bioorthogonal chemistry, protein engineering, and drug development. *Bioconjugate Chem.* **2015**, *26* (2), 176−92.

DOI: 10.1021/acsbiomaterials.6b00578
ACS Biomater. Sci. Eng. XXXX, XXX, XXX−XXX

(27) Caliceti, P.; Veronese, F. M. Pharmacokinetic and biodistribution properties of poly(ethylene glycol)-protein conjugates. *Adv. Drug Delivery Rev.* **2003**, *55* (10), 1261−1277.
(28) Aravind, S.; Paul, W.; Vasudev, S. C.; Sharma, C. P. Polyethylene glycol (PEG) modified bovine pericardium as a biomaterial: a comparative study on immunogenicity. *J. Biomater Appl.* **1998**, *13* (2), 158−165.
(29) Luhmann, T.; Meinel, L. Nanotransporters for drug delivery. *Curr. Opin. Biotechnol.* **2016**, *39*, 35−40.
(30) Zhao, H.; Heusler, E.; Jones, G.; Li, L.; Werner, V.; Germershaus, O.; Ritzer, J.; Luehmann, T.; Meinel, L. Decoration of silk fibroin by click chemistry for biomedical application. *J. Struct. Biol.* **2014**, *186* (3), 420−30.
(31) Luhmann, T.; Jones, G.; Gutmann, M.; Rybak, J. C.; Nickel, J.; Rubini, M.; Meinel, L. Bio-orthogonal Immobilization of Fibroblast Growth Factor 2 for Spatial Controlled Cell Proliferation. *ACS Biomater. Sci. Eng.* **2015**, *1* (9), 740−746.
(32) Wandrey, G.; Wurzel, J.; Hoffmann, K.; Ladner, T.; Büchs, J.; Meinel, L.; Lühmann, T. Probing unnatural amino acid integration into enhanced green fluorescent protein by genetic code expansion with a high-throughput screening platform. *J. Biol. Eng.* **2016**, *10* (1), 11.
(33) Luhmann, T.; Spieler, V.; Werner, V.; Ludwig, M. G.; Fiebig, J.; Muller, T.; Meinel, L. Interleukin-4 clicked surfaces drive M2 macrophage polarization. *ChemBioChem* **2016**, *17*, 2123.
(34) Gutmann, M.; Memmel, E.; Braun, A. C.; Seibel, J.; Meinel, L.; Luhmann, T. Biocompatible Azide-Alkyne "Click" Reactions for Surface Decoration of Glyco-Engineered Cells. *ChemBioChem* **2016**, *17* (9), 866−75.
(35) Braun, A. C.; Gutmann, M.; Ebert, R.; Jakob, F.; Gieseler, H.; Luehmann, T.; Meinel, L. Matrix metalloproteinase responsive delivery of myostatin inhibitors. *Pharm. Res.* **2016**, DOI: 10.1007/s11095-016-2038-6.
(36) Chazaud, B. Macrophages: supportive cells for tissue repair and regeneration. *Immunobiology* **2014**, *219* (3), 172−8.
(37) Milles, S.; Tyagi, S.; Banterle, N.; Koehler, C.; VanDelinder, V.; Plass, T.; Neal, A. P.; Lemke, E. A. Click strategies for single-molecule protein fluorescence. *J. Am. Chem. Soc.* **2012**, *134* (11), 5187−95.
(38) van Kimmenade, A.; Bond, M. W.; Schumacher, J. H.; Laquoi, C.; Kastelein, R. A. Expression, renaturation and purification of recombinant human interleukin 4 from Escherichia coli. *Eur. J. Biochem.* **1988**, *173* (1), 109−14.
(39) Wang, Y.; Shen, B. J.; Sebald, W. A mixed-charge pair in human interleukin 4 dominates high-affinity interaction with the receptor alpha chain. *Proc. Natl. Acad. Sci. U. S. A.* **1997**, *94* (5), 1657−62.
(40) Germershaus, O.; Schultz, I.; Luhmann, T.; Beck-Broichsitter, M.; Hogger, P.; Meinel, L. Insulin-like growth factor-I aerosol formulations for pulmonary delivery. *Eur. J. Pharm. Biopharm.* **2013**, *85* (1), 61−8.
(41) Johnson, M. L.; Brand, L. *Numerical Computer Methods, Part C*; Methods in Enzymology; Academic Press: New York, 2000; Vol. *321*.
(42) Wingfield, P.; Payton, M.; Tavernier, J.; Barnes, M.; Shaw, A.; Rose, K.; Simona, M. G.; Demczuk, S.; Williamson, K.; Dayer, J. M. Purification and characterization of human interleukin-1 beta expressed in recombinant Escherichia coli. *Eur. J. Biochem.* **1986**, *160* (3), 491−7.
(43) Christen, E. H.; Karlsson, M.; Kampf, M. M.; Schoenmakers, R.; Gubeli, R. J.; Wischhusen, H. M.; Friedrich, C.; Fussenegger, M.; Weber, W. Conditional DNA-Protein Interactions Confer Stimulus-Sensing Properties to Biohybrid Materials. *Adv. Funct. Mater.* **2011**, *21* (15), 2861−2867.
(44) Vaz, D. C.; Rodrigues, J. R.; Sebald, W.; Dobson, C. M.; Brito, R. M. M. Enthalpic and entropic contributions mediate the role of disulfide bonds on the conformational stability of interleukin-4. *Protein Sci.* **2006**, *15* (1), 33−44.
(45) Pace, C. N.; Shirley, B. A.; Thomson, J. A.; Measuring the conformational stability of a protein. In *Protein Structure: A Practical Approach*; Oxford University Press: New York, 1997; 299−321.
(46) Volet, G.; Lav, T. X.; Babinot, J.; Amiel, C. Click-Chemistry: An Alternative Way to Functionalize Poly(2-methyl-2-oxazoline). *Macromol. Chem. Phys.* **2011**, *212* (2), 118−124.
(47) Kempe, K.; Hoogenboom, R.; Jaeger, M.; Schubert, U. S. Three-Fold Metal-Free Efficient ("Click") Reactions onto a Multifunctional Poly(2-oxazoline) Designer Scaffold. *Macromolecules* **2011**, *44* (16), 6424−6432.
(48) Hartlieb, M.; Pretzel, D.; Englert, C.; Hentschel, M.; Kempe, K.; Gottschaldt, M.; Schubert, U. S. Matrix supported poly(2-oxazoline)-based hydrogels for DNA catch and release. *Biomacromolecules* **2014**, *15* (6), 1970−8.
(49) Presolski, S. I.; Hong, V. P.; Finn, M. G. Copper-Catalyzed Azide-Alkyne Click Chemistry for Bioconjugation. *Curr. Protoc. Chem. Biol.* **2011**, *3* (4), 153−162.
(50) Zheng, C.; Ma, G.; Su, Z. Native PAGE eliminates the problem of PEG-SDS interaction in SDS-PAGE and provides an alternative to HPLC in characterization of protein PEGylation. *Electrophoresis* **2007**, *28* (16), 2801−7.
(51) Park, E. J.; Kim, M. S.; Lee, H. S.; Lee, K. C.; Na, D. H. Differences in electrophoretic behavior between linear and branched PEG-conjugated proteins. *Electrophoresis* **2015**, *36* (6), 918−923.
(52) Hebert, K. R.; Adhikari, S.; Houser, J. E. Chemical mechanism of suppression of copper electrodeposition by poly (ethylene glycol). *J. Electrochem. Soc.* **2005**, *152* (5), C324−C329.
(53) Israelachvili, J. The different faces of poly(ethylene glycol). *Proc. Natl. Acad. Sci. U. S. A.* **1997**, *94* (16), 8378−9.
(54) Sheth, S. R.; Leckband, D. Measurements of attractive forces between proteins and end-grafted poly(ethylene glycol) chains. *Proc. Natl. Acad. Sci. U. S. A.* **1997**, *94* (16), 8399−8404.
(55) Cho, H.; Daniel, T.; Buechler, Y. J.; Litzinger, D. C.; Maio, Z.; Putnam, A. M.; Kraynov, V. S.; Sim, B. C.; Bussell, S.; Javahishvili, T.; Kaphle, S.; Viramontes, G.; Ong, M.; Chu, S.; GC, B.; Lieu, R.; Knudsen, N.; Castiglioni, P.; Norman, T. C.; Axelrod, D. W.; Hoffman, A. R.; Schultz, P. G.; DiMarchi, R. D.; Kimmel, B. E. Optimized clinical performance of growth hormone with an expanded genetic code. *Proc. Natl. Acad. Sci. U. S. A.* **2011**, *108* (22), 9060−9065.
(56) Duppatla, V.; Gjorgjevikj, M.; Schmitz, W.; Hermanns, H. M.; Schafer, C. M.; Kottmair, M.; Muller, T.; Sebald, W. IL-4 analogues with site-specific chemical modification at position 121 inhibit IL-4 and IL-13 biological activities. *Bioconjugate Chem.* **2014**, *25* (1), 52−62.
(57) Lienemann, P. S.; Karlsson, M.; Sala, A.; Wischhusen, H. M.; Weber, F. E.; Zimmermann, R.; Weber, W.; Lutolf, M. P.; Ehrbar, M. A versatile approach to engineering biomolecule-presenting cellular microenvironments. *Adv. Healthcare Mater.* **2013**, *2* (2), 292−6.
(58) Manzenrieder, F.; Luxenhofer, R.; Retzlaff, M.; Jordan, R.; Finn, M. G. Stabilization of Virus-like Particles with Poly(2-oxazoline)s. *Angew. Chem., Int. Ed.* **2011**, *50* (11), 2601−2605.
(59) Mancini, R. J.; Lee, J.; Maynard, H. D. Trehalose Glycopolymers for Stabilization of Protein Conjugates to Environmental Stressors. *J. Am. Chem. Soc.* **2012**, *134* (20), 8474−8479.

DOI: 10.1021/acsbiomaterials.6b00578
ACS Biomater. Sci. Eng. XXXX, XXX, XXX−XXX

Publication P8

Tailoring cellular uptake and fluorescence of poly(2-oxazoline)-based nanogels

M. Hartlieb, T. Bus, J. Kübel, D. Pretzel, S. Hoeppener, M. N. Leiske, K. Kempe, B. Dietzek, U. S. Schubert, *Bioconjugate Chem.* **2017**, *28*, 1229 - 1235.

The paper as well as the supporting information (free of charge) is available online: doi.org/10.1021/acs.bioconjchem.7b00067.

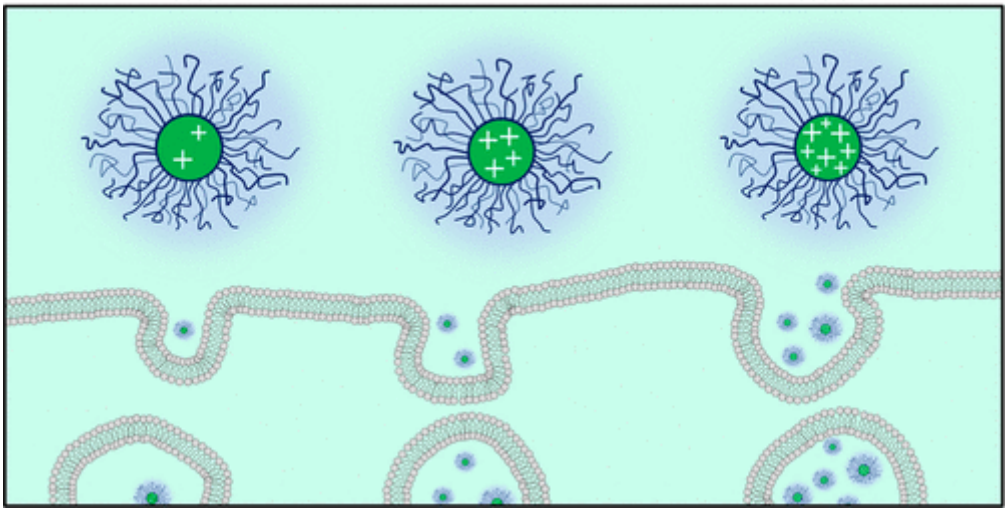

Bioconjugate Chemistry

Article

pubs.acs.org/bc

Tailoring Cellular Uptake and Fluorescence of Poly(2-oxazoline)-Based Nanogels

Matthias Hartlieb,[†,‡,#,¶] Tanja Bus,[†,‡,#] Joachim Kübel,[§,∥,⊥] David Pretzel,[†,‡] Stephanie Hoeppener,[†,‡] Meike N. Leiske,[†,‡] Kristian Kempe,[†,‡,¶] Benjamin Dietzek,[§,∥] and Ulrich S. Schubert*[,†,‡]

[†]Laboratory of Organic and Macromolecular Chemistry (IOMC), Friedrich Schiller University Jena, Humboldtstrasse 10, 07743, Jena, Germany

[‡]Jena Center for Soft Matter (JCSM), Friedrich Schiller University Jena, Philosophenweg 7, 07743, Jena, Germany

[§]Institute of Physical Chemistry (IPC) and Abbe Center of Photonics, Friedrich Schiller University Jena, Helmholtzweg 4, 07743 Jena, Germany

[∥]Leibniz Institute of Photonic Technology (IPHT), Albert-Einstein-Str. 9, 07745 Jena, Germany

Supporting Information

ABSTRACT: Controlling the size and charge of nanometer-sized objects is of upmost importance for their interactions with cells. We herein present the synthesis of poly(2-oxazoline) based nanogels comprising a hydrophilic shell and an amine containing core compartment. Amine groups were cross-linked using glutaraldehyde resulting in imine based nanogels. As a drug model, amino fluorescein was covalently immobilized within the core, quenching excessive aldehyde functions. By varying the amount of cross-linker, the zeta potential and, hence, the cellular uptake could be adjusted. The fluorescence of the nanogels was found to be dependent on the cross-linking density. Finally, the hemocompatibility of the described systems was studied by hemolysis and erythrocyte aggregation assays. While cellular uptake was shown to be dependent on the zeta potential of the nanogel, no harmful effects to red blood cells was observed, rendering the present system as an interesting toolbox for the production of nanomaterials with a defined biological interaction profile.

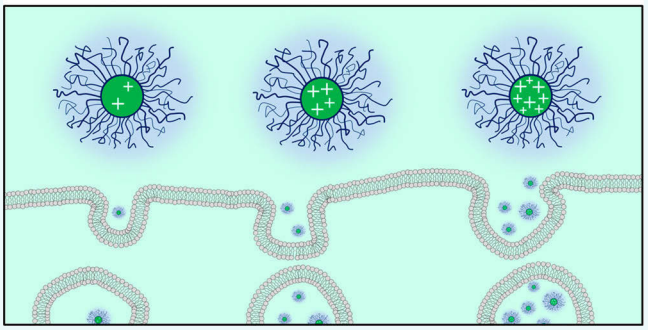

INTRODUCTION

Nanomedicine, the use of nanoscopic objects for biomedical applications such as diagnostics or treatment of diseases, has attracted increasing interest in recent years.[1,2] By using (polymeric) carriers, it is possible to solubilize, protect, and deliver drug molecules to the desired site of action in the body. Nanogels, such as (reversibly) cross-linked polymer micelles,[3] are particularly valuable in this context as, if the chemistry is chosen appropriately, premature drug release or disassembly can be reduced.[4] In the nanomedicine based treatment of cancer, the enhanced permeability and retention (EPR) effect is used to generate a tumor specific accumulation of the drug.[5] The concept exploits the leaky nature of tumor tissue and the passive accumulation of nanosized objects within those cavities. However, in order to take advantage of the EPR effect, a drug carrier has to exhibit long blood circulation times and a low level of unspecific cellular interactions. Many parameters such as size, shape, hydrophilicity or charge influence the cellular uptake,[6,7] and with regard to new nanomedicines, the ability to tailor the cellular interaction in an easy way is highly beneficial. It was shown that a positively charged surface significantly increases the uptake of nanoparticles.[6,8−12] This effect is also used in gene therapy approaches in terms of a complexation of negatively charged genetic material by positively charged polymers in order to penetrate cellular membranes.[13] However, a positively charged surface usually also increases the cytotoxicity induced by the system.[14,15] In addition, in the context of the EPR effect, a hydrophilic, low fouling surface is indispensable to maintain low protein adsorption levels. Poly(2-oxazoline)s (POx) display a promising material in a biomedical context, as certain derivatives bearing small side chains, like poly(2-methyl-2-oxazoline) (PMeOx) or poly(2-ethyl-2-oxazoline) (PEtOx), show excellent biocompatibility.[16−18] Indeed, their performance in biological applications is often compared to poly(ethylene glycol) (PEG), since they also show a stealth effect.[19,20] Recent studies show that in terms of circulation time in the bloodstream and unspecific accumulation in the body, PEtOx is even more advantageous than PEG.[21] Their versatile functionalization chemistry displays another advantage.[22] There are sparse examples of POx based nanogels using PEtOx or PMeOx as a polymer shell[23,24] and only a few were utilized for biomedical applications.[25,26]

Received: February 7, 2017
Revised: February 9, 2017
Published: February 16, 2017

DOI: 10.1021/acs.bioconjchem.7b00067
Bioconjugate Chem. 2017, 28, 1229−1235

Recently, we reported the synthesis of nanogels based on the self-assembly of POx block copolymers consisting of an amine-containing, cationic block (poly(4-amino-butyl-2-oxazoline (PAmOx))[27] and a hydrophilic PEtOx segment.[26] The nanogels maintained low toxicity levels while possessing a positive zeta potential. Within the present contribution, the influence of the cross-linking process on the properties of nanogels, in particular, on the cellular uptake, is investigated.

RESULTS AND DISCUSSION

A highly defined POx-based diblock copolymer P($EtOx_{98}$-*b*-$BocOx_{32}$), **1**, $Đ$ = 1.07, Table 1, was synthesized via cationic ring opening polymerization by sequential monomer addition. The Boc-group was abstracted using trifluoroacetic acid to yield P($EtOx_{98}$-*b*-$AmOx_{32}$), **2** with a dispersity of 1.07. To produce nanogels this polymer was dissolved in chloroform, which leads to the formation of micellar structures comprising an PAmOx core. The charged nature of the amine groups leads to a phase segregation of the PAmOx block while PEtOx is readily soluble in chloroform, stabilizing the micelle.

Table 1. Composition and Analytical Data of the POx Block Copolymers

		NMR	SEC	
sample	composition (NMR)	M_n (g mol^{-1})	M_n (g mol^{-1})	$Đ$
1[a]	P($EtOx_{98}$-*b*-$BocOx_{32}$)	17 500	8 200	1.07
2[b]	P($EtOx_{98}$-*b*-$AmOx_{32}$)	14 200	13 900	1.11

[a]SEC measurement in $CHCl_3$. [b]SEC Measurement in DMAc.

Cross-linking was applied using glutaraldehyde (GA) resulting in the formation of nanogels cross-linked by imine bonds, which are pH responsive.[28] To quench the gelation and to obtain systems that are stable within an aqueous environment, 6-amino fluorescein (6AF) was used. The free amino group of 6AF reacts with residual aldehyde groups of the cross-linker resulting in a reversible covalent attachment to the nanogel (Scheme 1). In order to use these systems in drug delivery applications, the interaction of the produced nanogels with cells is of utmost importance. Therefore, the content of cross-linker was varied to alter the charge of the resulting nanogels (**3** to **7**). A higher degree of cross-linking and, consequently, a lower amount of free amine groups should result in a reduced zeta potential and, henceforth, in a reduction of the cellular uptake. The content of GA was varied between 1 and 3 equiv. (per 2 amine groups) (Table 2).

As displayed in Figure 1, an increase of GA leads to a reduction of the zeta potential from ζ = 28 mV for equimolar cross-linking to ζ = 7 mV for a 3-fold excess of GA. Moreover, an increase in size, as detected by DLS, can be observed for compounds **3** to **7**. These findings seem best explained by increased amounts of water present during gelation. GA was applied in a 70 wt % aqueous solution and during the cross-linking reaction water is produced as a byproduct. The additional water will accumulate within the hydrophilic core compartment of the micelle and swell the nanostructure prior to or during cross-linking resulting in larger nanogel sizes. This assumption is supported by cryoTEM measurements showing an increase in size with an increasing cross-linking density (Figure 2).

Table 2. Characterization of POx Nanogels in an Aqueous Environment

sample	cross-linker (equiv per 2 NH_2)	size[a] (nm, r)	ζ (mV)	content of 6AF (wt %)	size[b] (r, nm)
3	1	13	28	17	12
4	1.5	17	13	27	13
5	2	20	10	20	14
6	2.5	22	8	24	15
7	3	24	7	17	15

[a]Determined by DLS. [b]determined by cryo-TEM.

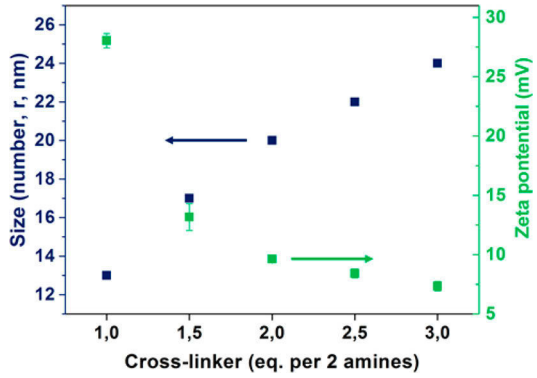

Figure 1. Dependency of zeta potential, as well as size by DLS on the cross-linking density of POx nanogels.

The obtained values are, however, smaller compared to DLS data indicating a falsification of the DLS derived values possibly caused by the presence of a small fraction of agglomerates. A third parameter investigated, depending on the cross-linking density, was the dye-loading of the resulting systems by evaluating their absorption and fluorescence. Based on its absorbance, the amount of 6AF conjugated to the nanogels can be estimated to values between 17 and 27 wt %, without an obvious dependence on the degree of cross-linking. However, determined by fluorescence intensity, a steady increase in the amount of dye could be monitored up to values which would correspond to a loading efficiency above 100 wt % when

Scheme 1. Schematic Representation of the Synthesis and Self-Assembly of P(EtOx-*b*-AmOx) in Chloroform to Form Micelles with a Cationic Core and a PEtOx Shell, as Well as the Subsequent Cross-Linking and 6AF Conjugation to Obtain Dye-Loaded Nanogels

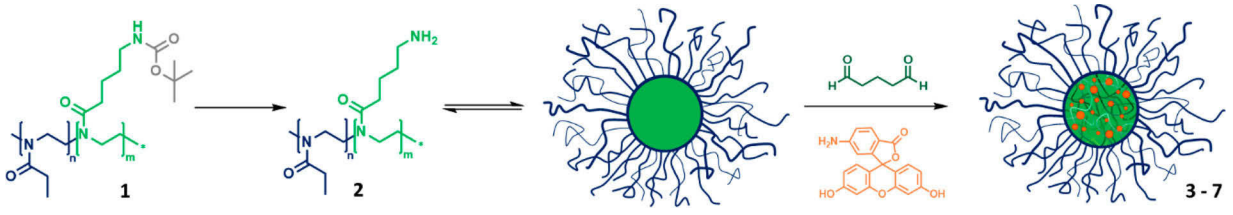

DOI: 10.1021/acs.bioconjchem.7b00067
Bioconjugate Chem. 2017, 28, 1229−1235

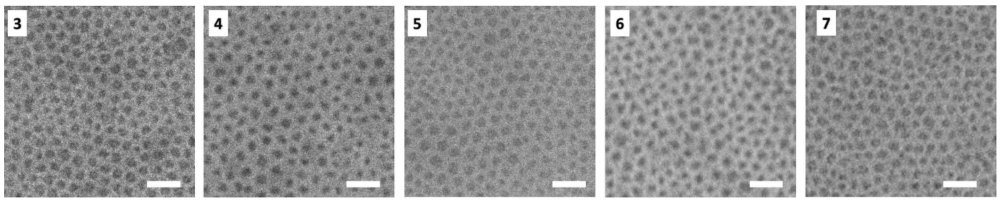

Figure 2. CryoTEM images of nanogels (**3** to **7**) in water. Scale bars represent 100 nm.

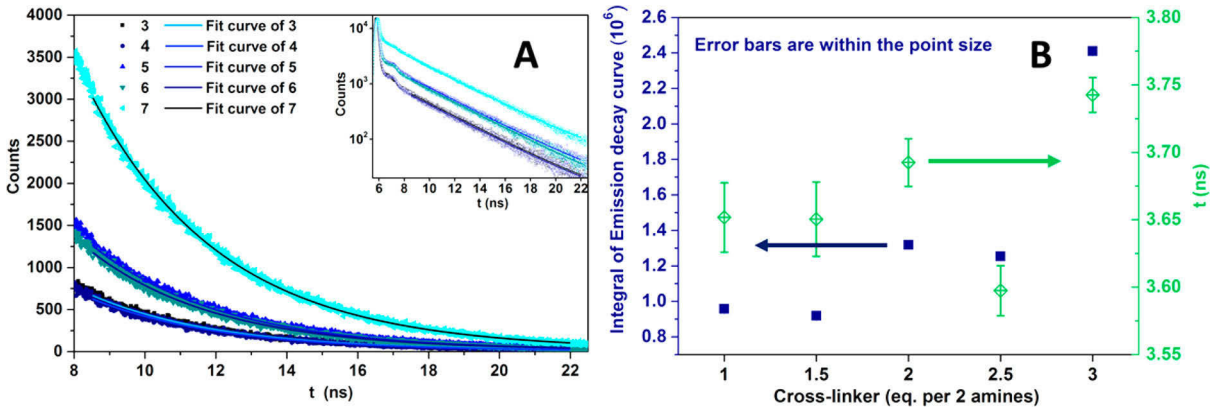

Figure 3. Fluorescence lifetime measurements of POx nanogels with varying degrees of cross-linking. (A) Fluorescence decay curves. (B) Fluorescence life times and decay integrals of nanogels **3** to **7**.

compared to a calibration of free 6AF, indicating a boost in fluorescence intensity by varying the core composition (Figure S1). To study this effect in detail, fluorescence lifetime measurements were conducted (Figure 3).

The investigations revealed an increase in fluorescence lifetime with increasing degree of cross-linking except for 2.5 equiv. of GA. Also, the integrals of the decay curves, which serve as a measure of the fluorescence quantum yield, increase within the series. As depicted in Figure S1, the absolute amount of dye within the nanogels is relatively constant between 17 and 27 wt %. It is described for fluorescein and its derivatives that electrostatic interactions between the dye and a cationic (surfactant) micelle are able to stabilize the anionic form of the molecule which leads to an increase in fluorescence lifetime and quantum yield.[29] However, the cationic character decreases with a higher degree of cross-linking and can, therefore, be held responsible for a general boost of fluorescence compared to pure 6AF, but not for the increasing lifetimes within the series.

Also, the dye−dye distance can be estimated as roughly constant. Therefore, dye−dye interactions such as excimer formation are unlikely to be responsible for the observed effects. Presumably, increasing the amount of cross-linker will increase the stiffness of the core. Thus, the increases in quantum yield and emission lifetime could be explained by frozen degrees of freedom, resulting in a reduced rate constant for nonradiative decay processes.[30,31] This is supported by proton NMR measurements of the nanogels (Figure S2). In contrast to the precursor polymer, only signals of the PEtOx constituting the shell are visible, while PAmOx signals are absent. This indicates a restriction of degrees of freedom of the block forming the core compartment of the micellar structure and supports the hypothetic cause for the increase in quantum yield.

In order to determine the influence of the varying cross-linking density on the cellular uptake, flow cytometry investigations were performed using L929 mouse fibroblasts (Figure 4). The decrease in mean fluorescence with an increasing cross-linking degree within the series of nanogels demonstrates the influence of the zeta potential on the internalization for all concentrations investigated. Moreover, time dependent uptake experiments visualize this behavior. The

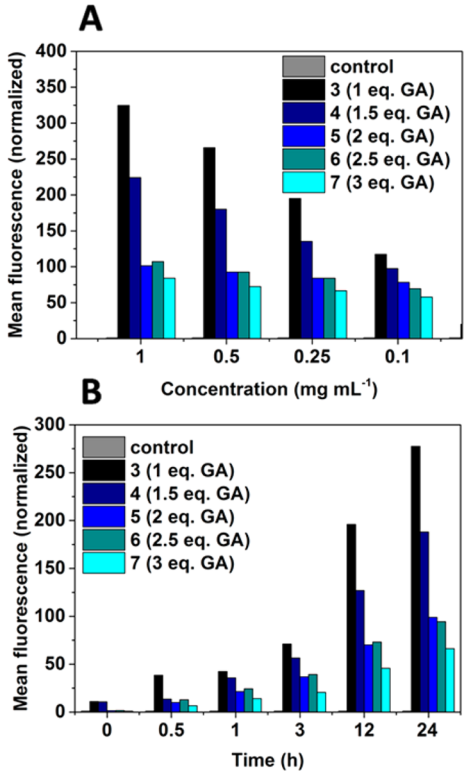

Figure 4. Cellular internalization of nanogels **3** to **7** dependent on the concentration (A) after 24 h incubation at 37 °C or at varying incubation times (B) at a concentration of 0.5 mg mL^{-1} at 37 °C.

DOI: 10.1021/acs.bioconjchem.7b00067
Bioconjugate Chem. 2017, 28, 1229−1235

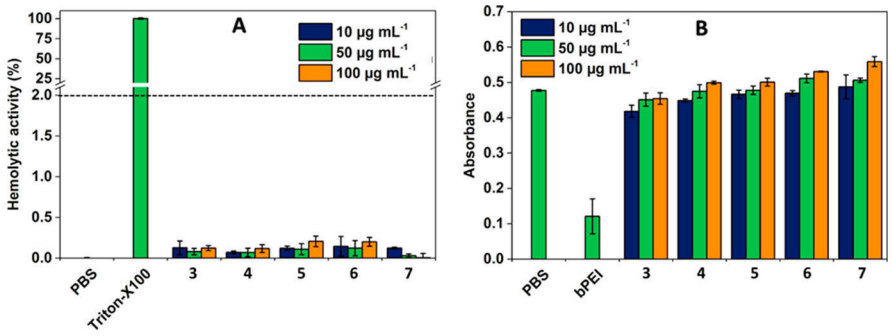

Figure 5. Induction of hemolysis (A) as well as erythrocyte aggregation (B) by 6AF loaded nanogels (**3** to **7**) in a concentration range between 10 and 100 μg mL^{-1} using sheep blood of three different donor batches.

difference in the fluorescence intensity between the nanogels was considered by referencing to the absolute fluorescence intensity of the measurement. This finding is in agreement with literature reports where objects having a positive net charge are described to be taken up more efficiently as compared to neutral or anionic structures.[32] The reported investigation shows that the cellular uptake, which displays a crucial factor for the utilization as a drug delivery agent, can be fine-tuned for the presented nanogel systems.

In order to investigate the nature of the cellular internalization, uptake studies at 4 °C were performed (Figure S3). The diminished uptake at low temperatures suggests an energy dependent internalization via endocytosis as expected for objects in such a size range.[7,33]

Besides cellular uptake, the biocompatibility of the drug carriers represents an essential parameter. It was reported that an increase in zeta potential of nanoparticles negatively affects the cell viability.[14,15] Nanogel **3**, investigated in a previous study, possesses the highest zeta potential (ζ = +28 mV) within the series and is, therefore, expected to induce the highest toxicity, although the system did not interfere with the metabolism of L929 mouse fibroblasts in a negative way up to a concentration of 5 mg mL^{-1}.[26] While this is a promising indication regarding the biocompatibility of the material, the most important environment a drug delivery system is facing is the bloodstream. Long circulation times, leading to a passive targeting, require a low level of interaction with the components of the blood. An interaction with erythrocytes resulting in clotting or disruption is highly undesired. The hemolytic activity of 6AF loaded nanogels was studied depending on the applied concentration (Figure 5A). All nanogels in a concentration range between 10 and 100 μg mL^{-1} resulted in hemolytic activity values well below 2%, which is defined as the threshold for a hemolysis (according to the ASTM F756−00 standard).

Furthermore, the erythrocyte aggregation was investigated and found to be negligible in the given concentration range with absorbance values comparable with the negative control (Figure 5B, Figure S4).

These findings are remarkable, since positively charged nanomaterials are expected to feature a decreased blood compatibility. In contrast to nanoparticle systems with an altered surface chemistry, the charge of the nanogels presented herein results from amine groups within the core of the micellar structure, whereas the periphery is covered with noncharged PEtOx chains. While this setup enables tailoring of the cellular interaction, as shown by the cellular uptake studies, the biocompatibility of the nanogels is maintained in all cases.

CONCLUSION

Within this contribution, we present a straightforward synthetic route to poly(2-oxazoline)-based polymeric nanogels with a tailored cellular uptake. The gels are produced by phase segregation of a diblock copolymer, containing a cationic and a neutral block forming micellar structures in chloroform. Cross-linking is conducted using glutaraldehyde and the fluorescent dye 6-amino fluorescein is loaded covalently. By changing the cross-linking density, it is possible to alter the properties of the nanogels in terms of fluorescence intensity and zeta potential. Hence, it is possible to adjust their cellular uptake as shown by flow cytometry measurements. Due to the unique nature of the nanogels, which carry the charged units within the core of the micellar structure, the biocompatibility is not affected by the variation in charge as demonstrated by hemocompatibility experiments. Therefore, the herein presented material displays a versatile toolbox for the production of drug delivery vehicles. Further studies will focus on the extension of the concept to in vivo investigations as well as on the loading of anticancer drugs such as doxorubicin, and the utilization of drug loaded nanogels in vitro and in vivo.

EXPERIMENTAL SECTION

Material and Instrumentation. Chemicals and solvents were purchased from Sigma-Aldrich, Merck, Fluka, and Acros. 2-Ethyl-2-oxazoline (EtOx) and methyl tosylate (MeOTos) were distilled to dryness prior to use. EtOx was dried using barium oxide before distillation. 2-(4-((*tert*-Butoxycarbonyl)-amino)butyl)-2-oxazoline (BocOx) was synthesized as described in a previous publication.[27] If not stated otherwise, cell culture media and supplements (L-Glutamin, antibiotics) were obtained from Biochrom (Merck Millipore, Germany).

The Initiator Sixty single-mode microwave synthesizer from Biotage, equipped with a noninvasive IR sensor (accuracy: 2%), was used for polymerizations under microwave irradiation. Microwave vials were heated overnight to 110 °C and allowed to cool to room temperature under an argon atmosphere before use. All polymerizations were carried out under temperature control. Size-exclusion chromatography (SEC) measurements of the protected polymers were performed on a Shimadzu system equipped with a SCL-10A system controller, a LC-10AD pump, a RID-10A refractive index detector, and a PSS SDV column with chloroform/triethylamine (NEt_3)/*iso*-propanol (94:4:2) as eluent. The column oven was set to 50 °C. SEC of the deprotected statistical copolymers was performed on a Shimadzu system with a LC-10AD pump, a RID-10A refractive index detector, a system controller SCL-10A, a degasser DGU-14A, and a CTO-10A column oven using *N,N*-

DOI: 10.1021/acs.bioconjchem.7b00067
Bioconjugate Chem. 2017, 28, 1229−1235

dimethylacetamide (DMAc) with 2.1 g L^{-1} LiCl as the eluent and the column oven set to 50 °C. Poly(styrene) (PS) samples were used as calibration standards for both solvent systems. Proton NMR spectroscopy (^{1}H NMR) measurements were performed at room temperature on a Bruker AC 300 and 400 MHz spectrometer, using $CDCl_3$ or *N,N*-dimethylformamide (DMF)-D_7 as solvents. The chemical shifts are given in ppm relative to the signal of the residual nondeuterated solvent.

Batch dynamic light scattering (DLS) was performed on a Zetasizer Nano ZS (Malvern Instruments, Herrenberg, Germany). All measurements were performed in folded capillary cells (DTS1071, Malvern Instruments, Herrenberg, Germany). After an equilibration time of 180 s, 3 × 30 s runs were carried out at 25 °C (λ = 633 nm). The counts were detected at an angle of 173°. Each measurement was performed in triplicate. Apparent hydrodynamic radii, R_h, were calculated according to the Stokes−Einstein equation.

Laser Doppler velocimetry was used to measure the electrokinetic potential, also known as zeta potential. The measurements were performed on a Zetasizer Nano ZS (Malvern Instruments, Herrenberg, Germany) in folded capillary cells (DTS1071). For each measurement, 15 runs were carried out using the fast-field and slow-field reversal mode at 150 V. Each experiment was performed in triplicate at 25 °C. The zeta potential (ζ) was calculated from the electrophoretic mobility (μ) according to the Henry equation.[34] The Henry coefficient, f(ka), was calculated according to Ohshima.[35]

CryoTEM investigations were conducted utilizing a FEI Tecnai G^2 20 at 200 kV acceleration voltage. Specisms were vitrified by a Vitrobot Mark V system on Quantifoil grids (R2/2). The blotting time was 1 s with blotting force offset of 0. The amount of solution was 7 μL. Samples were plunge frozen in liquid ethane and stored under liquid nitrogen until transferred to the Gatan cryo-holder and brought into the microscope. Images were acquired with a 4k × 4k CCD Eagle camera.

Absorbance and fluorescence spectra as well as hemolysis and erythrocyte aggregation assays were recorded using a Tecan M200 Pro fluorescence microplate reader (Crailsheim, Germany) by the use of black well plates with a flat and transparent bottom.

The cellular uptake studies of nanogels were performed with a Beckmann Coulter Cytomics FC-500 equipped with a Uniphase Argon ion laser (488 nm, 20 mW output) and analyzed with the Cytomics CXP software.

Block Copolymer of 2-Ethyl-2-oxazoline (EtOx) and 2-(4-((*tert*-Butoxycarbonyl)amino)butyl)-2-oxazoline (BocOx) (P(EtOx-*b*-BocOx)), (1). In a microwave vial, EtOx (757 μL, 7.5 mmol), MeOTos (16.2 μL, 0.107 mmol) and acetonitrile (3.4 mL) were mixed under inert conditions. After heating in the microwave synthesizer at 140 °C for 25 min the vial was introduced into a glovebox with nitrogen atmosphere and BocOx (803 μL, 3.2 mmol) was added. The closed vial was heated again in the microwave synthesizer (140 °C, 20 min). The solution was precipitated in cold (−80 °C, 300 mL) diethyl ether. The white precipitate was filtered and dried in high vacuum (1.4 g, 92%).

^{1}H NMR ($CDCl_3$, 300 MHz): δ = 7.66, (d, 8.1 Hz, 0.019 H, tosylate), 7.14 (d, 8.21 Hz, 0.019 H, tosylate), 3.45 (s, 4 H, backbone), 3.10 (s, 0.58 H, CH_2−CH_2−NH (BocOx)), 2.50−2.15 (m, 1.96 H, CH_2 (EtOx)/CH_2−CH_2−NHBoc), 1.62 (s, 0.52 H, CH_2−CH_2−CH_2 (BocOx)), 1.52 (s, 0.52 H, CH_2−CH_2 (BocOx)), 1.42 (s, 2.3 H, CH_3 (BocOx)), 1.21 (s, 2.1 H, CH_3 (EtOx)) ppm.

SEC (eluent: $CHCl_3$/*iso*-propanol/NEt_3, PS-standard): M_n = 8200 g mol^{-1}, $Đ$ = 1.07.

Deprotection of P(EtOx-*b*-BocOx) (1) to yield (P(EtOx-*b*-AmOx), (2). P(EtOx-*b*-BocOx) (**1**, 1.3 g) was dissolved in TFA (5 mL) and heated to 60 °C for 1 h. After stirring for 12 h at room temperature, the mixture was diluted with 10 mL methanol and precipitated in 400 mL of cold (−80 °C) diethyl ether. The precipitate was redissolved in methanol (100 mL) and stirred with Amberlyst A21 for 48 h. Subsequently, the solvent was removed, the polymer was dissolved in deionized water and freeze-dried (−80 °C, 0.003 mbar). The polymer was obtained as white powder (1.2 g, 92%).

^{1}H NMR (DMF-D_7, 300 MHz): δ = 4.9 (s, 2.3 H, NH_2), 3.51 (s, 4 H, backbone), 3.07 (s, 0.49 H, CH_2−CH_2−NH_2), 2.44 (m, 2.1 H, CH_2 (EtOx)/CH_2−CH_2−CO (AmOx)), 1.9−1.54 (m, 0.96 H, CH_2−CH_2−CH_2−CH_2 (AmOx)), 1.2 (s, 2,3 H, CH_3 (EtOx)) ppm.

SEC (eluent: DMAc/LiCl, PS-standard): M_n = 13 900 g mol^{-1}, $Đ$ = 1.11.

General Procedure for Self-Assembly and Cross-Linking (3−7). To create nanostructures, block copolymer (**2**, 90 mg, 0.006 mmol) was dissolved in $CHCl_3$, (5 mg mL^{-1}) and stirred for 3 h. Subsequently, glutaraldehyde (30 mg, 0.3 mmol, 1.5 equiv per amine (**4**)) was added and the solution was stirred another 3 h. With proceeding reaction time the color of the solution changed from colorless to yellow. To quench the excess of aldehyde functionalities, 6-amino fluorescein (50 mg) was added and the mixture was stirred for 12 h. Subsequently, the amount of solvent was reduced under an argon stream and the residual was precipitated in 100 mL cold diethyl ether (−80 °C). To purify the self-assembled structures from residual capping agent and cross-linker, dialysis in MeOH/water (1:4) was applied using a membrane with a molar mass cut off of 3500 g mol^{-1} (Roth Zellutrans). After the extraction was finished, the dialysis medium was changed to pure water and the aqueous solution was freeze-dried to yield an orange powder.

Determination of Dye Loading Content by Absorbance/Fluorescence. The absorbance/fluorescence of 6AF loaded nanostructures was investigated under alkaline conditions (1 mol L^{-1} NaOH in water) in diluted solution (0.1 mg mL^{-1}). The absorbance was determined at a wavelength of 490 nm and compared to a sequential dilution series of 6AF in the same aqueous NaOH solution. A 100-fold excess of glutaraldehyde was added to the control to ensure that only the imine species of 6AF is present. Emission was detected at an excitation wavelength of 450 nm. Nanogels as well as 6AF calibration exhibit an emission maximum at 510 nm. The readout was accomplished using a Tecan M200 Pro fluorescence microplate reader (Crailsheim, Germany).

Fluorescence Lifetime Measurements. The emission decay curves were obtained by time-correlated-single-photon-counting. After excitation with a frequency-doubled Ti-sapphire laser adjusted to 870 nm (Tsunami, Newport Spectra-Physics GmbH, pulse-to-pulse repetition rate 400 kHz after passing a pulse selector, model 3980, Newport Spectra-Physics GmbH), i.e., at λ_{ex} = 435 nm, the luminescence of the sample was collected in a 90°-geometry and detected with a Becker & Hickl PMC-100-4 photon-counting module. A long-pass filter (455 nm) is inserted in the detection beam path. The samples were adjusted to yield optical densities <0.03 at the excitation

DOI: 10.1021/acs.bioconjchem.7b00067
Bioconjugate Chem. 2017, 28, 1229−1235

wavelength in aqueous NaOH (0.1 mol L^{-1}). The measurements were accumulated at count rates <3% of the rep.-rate until 15 000 counts in the maximum were reached.

Blood Compatibility Measurements. To assess the hemolytic activity of the polymer solutions, blood from sheep collected in heparinized tubes (Institute of Laboratory Animal Science and Animal Welfare, Friedrich Schiller University Jena) was centrifuged at 4500 × *g* for 5 min, and the pellet was washed three times with cold 1.5 mmol L^{-1} phosphate buffered saline (PBS, pH 7.4). After dilution with PBS in a ratio of 1:7, aliquots of erythrocyte suspension were mixed 1:1 with the polymer solution and incubated in a water bath at 37 °C for 60 min. After centrifugation at 2400 × *g* for 5 min the hemoglobin release was determined by measuring the absorbance of the supernatant with a microplate reader at 544 nm wavelength. Complete hemolysis (100%) was achieved using 1% Triton X-100 serving as positive control. Thereby, PBS served as negative control (0%). A value less than 2% hemolysis rate was taken as nonhemolytic. Experiments were run in triplicate and were performed with three different batches of donor blood.

The hemolytic activity of the polycations was calculated as follows (eq 1):

$$\%\text{Hemolysis} = 100 \times \frac{(A_{\text{Sample}} - A_{\text{Negative control}})}{A_{\text{Positive control}}} \quad (1)$$

For the examination of the erythrocyte aggregation, the erythrocyte suspension was mixed with the same volume of polymer solution in a clear flat-bottomed 96-well plate. The cells were incubated at 37 °C for 2 h, and the absorbance was measured at 645 nm in a microplate reader. 25 kDa bPEI (50 μg mL^{-1}) was used as positive control, and as negative control, cells were treated with PBS. Absorbance values of the test solutions lower than negative control were regarded as aggregation. Experiments are the result of triplicates and were performed with three different donor blood batches.

Investigation of the Cellular Uptake. The evaluation of the nanogel uptake was performed with the cell line L929 (CCL-1, ATCC). In general, the cells were cultured in Dulbecco's modified Eagle's medium (DMEM) supplemented with 10% fetal calf serum (FCS), 100 U mL^{-1} penicillin and 100 μg mL^{-1} streptomycin at 37 °C in a humidified 5% CO_2 atmosphere. For the uptake studies, cells were seeded at 10^5 cells per mL in a 24-well plate and incubated for 24 h.

For the time-dependent uptake studies, cells were incubated with nanogels at a concentration of 0.5 mg mL^{-1} for 30 min to 24 h, whereas the concentration-dependent uptake was investigated over an incubation time of 24 h using nanogel concentrations in the range between 0.1 and 1 mg mL^{-1}. Cells incubated with culture medium only served as control. For uptake studies at low temperature, the cells were incubated with nanogels (0.5 mg mL^{-1}) for 4 h at 4 and 37 °C, respectively, and the internalization was monitored using FC analysis as described above.

■ ASSOCIATED CONTENT

Supporting Information

The Supporting Information is available free of charge on the ACS Publications website at DOI: 10.1021/acs.bioconjchem.7b00067.

Details on nanogel characterization regarding fluorescence, cellular uptake and biocompatibility (PDF)

■ AUTHOR INFORMATION

Corresponding Author

*E-mail: ulrich.schubert@uni-jena.de.

ORCID

Ulrich S. Schubert: 0000-0003-4978-4670

Present Addresses

[¶]Department of Chemistry, University of Warwick, Gibbet Hill Road, Coventry, CV4 7AL, United Kingdom.

[⊥]Department of Chemistry and Molecular Biology University of Gothenburg 40530 Gothenburg, Sweden.

Author Contributions

[#]Matthias Hartlieb and Tanja Bus contributed equally.

Notes

The authors declare no competing financial interest.

■ ACKNOWLEDGMENTS

T.B. acknowledges the German Federal Ministry of Education & Research (BMBF, #031A518B Vectura). CryoTEM investigations were performed at the cryoTEM facilities of the Jena Center for Soft Matter (JCSM). TEM facilities were funded by a grant of the DFG (German Research Foundation) and the EFRE (European Fund for Regional Development). MH gratefully acknowledges the German Research Foundation (DFG, GZ: HA 7725/1-1) for funding. U.S.S. and M.N.L. acknowledge German Federal Ministry of Education & Research (BMBF, #13NI3417, smart-dye-livery).

■ REFERENCES

(1) Duncan, R., and Vicent, M. J. (2013) Polymer therapeutics-prospects for 21st century: The end of the beginning. *Adv. Drug Delivery Rev. 65*, 60−70.

(2) Duncan, R., and Gaspar, R. (2011) Nanomedicine(s) under the Microscope. *Mol. Pharmaceutics 8*, 2101−2141.

(3) van Nostrum, C. F. (2011) Covalently cross-linked amphiphilic block copolymer micelles. *Soft Matter 7*, 3246−3259.

(4) Talelli, M., Rijcken, C. J. F., Hennink, W. E., and Lammers, T. (2012) Polymeric micelles for cancer therapy: 3 C's to enhance efficacy. *Curr. Opin. Solid State Mater. Sci. 16*, 302−309.

(5) Maeda, H., Greish, K., and Fang, J. (2006) The EPR effect and polymeric drugs: A paradigm shift for cancer chemotherapy in the 21st century, in *Polymer Therapeutics II* (Satchi-Fainaro, R., and Duncan, R., Eds.) pp 103−121, Springer, Berlin Heidelberg.

(6) Zhu, M., Nie, G., Meng, H., Xia, T., Nel, A., and Zhao, Y. (2013) Physicochemical Properties Determine Nanomaterial Cellular Uptake, Transport, and Fate. *Acc. Chem. Res. 46*, 622−631.

(7) Albanese, A., Tang, P. S., and Chan, W. C. W. (2012) The Effect of Nanoparticle Size, Shape, and Surface Chemistry on Biological Systems. *Annu. Rev. Biomed. Eng. 14*, 1−16.

(8) Adjei, I. M., Sharma, B., and Labhasetwar, V. (2014) Nanoparticles: Cellular Uptake and Cytotoxicity, in *Nanomaterial: Impacts on Cell Biology and Medicine* (Capco, G. D., and Chen, Y., Eds.) pp 73−91, Springer, Netherlands, Dordrecht.

(9) Cho, E. C., Xie, J., Wurm, P. A., and Xia, Y. (2009) Understanding the Role of Surface Charges in Cellular Adsorption versus Internalization by Selectively Removing Gold Nanoparticles on the Cell Surface with a I2/KI Etchant. *Nano Lett. 9*, 1080−1084.

(10) Hauck, T. S., Ghazani, A. A., and Chan, W. C. W. (2008) Assessing the Effect of Surface Chemistry on Gold Nanorod Uptake, Toxicity, and Gene Expression in Mammalian Cells. *Small 4*, 153−159.

(11) Yue, Z.-G., Wei, W., Lv, P.-P., Yue, H., Wang, L.-Y., Su, Z.-G., and Ma, G.-H. (2011) Surface Charge Affects Cellular Uptake and Intracellular Trafficking of Chitosan-Based Nanoparticles. *Biomacromolecules 12*, 2440−2446.

DOI: 10.1021/acs.bioconjchem.7b00067
Bioconjugate Chem. 2017, 28, 1229−1235

(12) He, C., Hu, Y., Yin, L., Tang, C., and Yin, C. (2010) Effects of particle size and surface charge on cellular uptake and biodistribution of polymeric nanoparticles. *Biomaterials 31*, 3657−3666.
(13) Rinkenauer, A. C., Schubert, S., Traeger, A., and Schubert, U. S. (2015) The influence of polymer architecture on in vitro pDNA transfection. *J. Mater. Chem. B 3*, 7477−7493.
(14) Fröhlich, E. (2012) The role of surface charge in cellular uptake and cytotoxicity of medical nanoparticles. *Int. J. Nanomed. 7*, 5577−5591.
(15) Xia, T., Kovochich, M., Liong, M., Meng, H., Kabehie, S., George, S., Zink, J. I., and Nel, A. E. (2009) Polyethyleneimine Coating Enhances the Cellular Uptake of Mesoporous Silica Nanoparticles and Allows Safe Delivery of siRNA and DNA Constructs. *ACS Nano 3*, 3273−3286.
(16) Kronek, J., Kroneková, Z., Lustoň, J., Paulovičová, E., Paulovičová, L., and Mendrek, B. (2011) In vitro bio-immunological and cytotoxicity studies of poly(2-oxazolines). *J. Mater. Sci.: Mater. Med. 22*, 1725−1734.
(17) Luxenhofer, R., Sahay, G., Schulz, A., Alakhova, D., Bronich, T. K., Jordan, R., and Kabanov, A. V. (2011) Structure-property relationship in cytotoxicity and cell uptake of poly(2-oxazoline) amphiphiles. *J. Controlled Release 153*, 73−82.
(18) Kronek, J., Paulovičová, E., Paulovičová, L., Kroneková, Z., and Lustoň, J. (2012) Immunomodulatory efficiency of poly(2-oxazolines). *J. Mater. Sci.: Mater. Med. 23*, 1457−1464.
(19) Woodle, M. C., Engbers, C. M., and Zalipsky, S. (1994) New Amphipatic Polymer-Lipid Conjugates Forming Long-Circulating Reticuloendothelial System-Evading Liposomes. *Bioconjugate Chem. 5*, 493−496.
(20) Zalipsky, S., Hansen, C. B., Oaks, J. M., and Allen, T. M. (1996) Evaluation of blood clearance rates and biodistribution of poly(2-oxazoline)-grafted liposomes. *J. Pharm. Sci. 85*, 133−137.
(21) Wyffels, L., Verbrugghen, T., Monnery, B. D., Glassner, M., Stroobants, S., Hoogenboom, R., and Staelens, S. (2016) μPET imaging of the pharmacokinetic behavior of medium and high molar mass 89Zr-labeled poly(2-ethyl-2-oxazoline) in comparison to poly(ethylene glycol). *J. Controlled Release 235*, 63−71.
(22) Guillerm, B., Monge, S., Lapinte, V., and Robin, J.-J. (2012) How to modulate the chemical structure of polyoxazolines by appropriate functionalization. *Macromol. Rapid Commun. 33*, 1600−1612.
(23) Wilson, P., Ke, P. C., Davis, T. P., and Kempe, K. (2016) Poly(2-oxazoline)-based micro- and nanoparticles: A review. *Eur. Polym. J.*, 1 DOI: 10.1016/j.eurpolymj.2016.09.011.
(24) Hartlieb, M., Kempe, K., and Schubert, U. S. (2015) Covalently cross-linked poly(2-oxazoline) materials for biomedical applications - from hydrogels to self-assembled and templated structures. *J. Mater. Chem. B 3*, 526−538.
(25) Legros, C., Wirotius, A.-L., De Pauw-Gillet, M.-C., Tam, K. C., Taton, D., and Lecommandoux, S. (2015) Poly(2-oxazoline)-Based Nanogels as Biocompatible Pseudopolypeptide Nanoparticles. *Biomacromolecules 16*, 183−191.
(26) Hartlieb, M., Pretzel, D., Wagner, M., Hoeppener, S., Bellstedt, P., Gorlach, M., Englert, C., Kempe, K., and Schubert, U. S. (2015) Core cross-linked nanogels based on the self-assembly of double hydrophilic poly(2-oxazoline) block copolymers. *J. Mater. Chem. B 3*, 1748−1759.
(27) Hartlieb, M., Pretzel, D., Kempe, K., Fritzsche, C., Paulus, R. M., Gottschaldt, M., and Schubert, U. S. (2013) Cationic poly(2-oxazoline) hydrogels for reversible DNA binding. *Soft Matter 9*, 4693−4704.
(28) Jackson, A. W., and Fulton, D. A. (2012) Triggering Polymeric Nanoparticle Disassembly through the Simultaneous Application of Two Different Stimuli. *Macromolecules 45*, 2699−2708.
(29) Song, A., Zhang, J., Zhang, M., Shen, T., and Tang, J. a. (2000) Spectral properties and structure of fluorescein and its alkyl derivatives in micelles. *Colloids Surf., A 167*, 253−262.
(30) Humphry-Baker, R., Graetzel, M., and Steiger, R. (1980) Drastic fluorescence enhancement and photochemical stabilization of cyanine dyes through micellar systems. *J. Am. Chem. Soc. 102*, 847−848.
(31) Wu, W.-C., Chen, C.-Y., Tian, Y., Jang, S.-H., Hong, Y., Liu, Y., Hu, R., Tang, B. Z., Lee, Y.-T., Chen, C.-T., et al. (2010) Enhancement of Aggregation-Induced Emission in Dye-Encapsulating Polymeric Micelles for Bioimaging. *Adv. Funct. Mater. 20*, 1413−1423.
(32) Verma, A., and Stellacci, F. (2010) Effect of Surface Properties on Nanoparticle−Cell Interactions. *Small 6*, 12−21.
(33) Rejman, J., Oberle, V., Zuhorn, I. S., and Hoekstra, D. (2004) Size-dependent internalization of particles via the pathways of clathrin- and caveolae-mediated endocytosis. *Biochem. J. 377*, 159−169.
(34) Delgado, A. V., Gonzalez-Caballero, F., Hunter, R. J., Koopal, L. K., and Lyklema, J. (2007) Measurement and interpretation of electrokinetic phenomena. *J. Colloid Interface Sci. 309*, 194−224.
(35) Ohshima, H. (1994) A Simple Expression for Henry's Function for the Retardation Effect in Electrophoresis of Spherical Colloidal Particles. *J. Colloid Interface Sci. 168*, 269−271.

DOI: 10.1021/acs.bioconjchem.7b00067
Bioconjugate Chem. 2017, 28, 1229−1235